

IEA Heat Pump Programme

Annex 27

Selected Issues on CO₂ in Compression Systems

Final Report

Operating Agent: Norway



IEA Heat Pump Programme Report

Report no. HPP-AN27-2
ISBN 91-85303-01-X

2004

Published by

IEA Heat Pump Centre
Box 857, SE-501 15 Borås
Sweden
Phone: +46 33 16 55 12
Fax: +46 33 13 19 79

Legal Notice

Neither the IEA Heat Pump Centre nor any person acting on its behalf: (a) makes any warranty or representation, express or implied, with respect to the information contained in this report; or (b) assumes liabilities with respect to the use of, or damages, resulting from the use of this information. Reference herein to any specific commercial product, process, or service by trade name, trademark, manufacturer, or otherwise, does not necessarily constitute or imply its endorsement recommendation or favouring. The views and opinions of authors expressed herein do not necessarily state or reflect those of the IEA Heat Pump Centre, or any of its employees. The information herein is presented in the authors' own words.

© IEA Heat Pump Centre

All rights reserved. No part of this publication may be reproduced, stored in a retrieval system, or transmitted in any form or by any means, electronic, mechanical, photocopying, recording or otherwise, without prior permission of the IEA Heat Pump Centre, Borås, Sweden.

Production

IEA Heat Pump Centre, Borås, Sweden

ISBN 91-85303-01-X
Report No. HPP-AN27-2

The IEA

The IEA was established in 1974 within the framework of the Organization for Economic Cooperation and Development (OECD) to implement an International Energy Programme. A basic aim of the IEA is to foster cooperation among the IEA participating countries to increase energy security through energy conservation, development of alternative energy sources, new energy technology and research and development (R&D). This is achieved, in part, through a programme of energy technology and R&D collaboration, currently within the framework of over 40 Implementing Agreements.

The IEA Heat Pump Programme

The Implementing Agreement for a Programme of Research, Development, Demonstration and Promotion of Heat Pumping Technologies (IA) forms the legal basis for the IEA Heat Pump Programme. Signatories of the IA are either governments or organizations designated by their respective governments to conduct programmes in the field of energy conservation.

Under the IA collaborative tasks or “Annexes” in the field of heat pumps are undertaken. These tasks are conducted on a cost-sharing and/or task-sharing basis by the participating countries. An Annex is in general coordinated by one country which acts as the Operating Agent (manager). Annexes have specific topics and workplans and operate for a specified period, usually several years. The objectives vary from information exchange to the development and implementation of technology. This report presents the results of one Annex. The Programme is governed by an Executive Committee, which monitors existing projects and identifies new areas where collaborative effort may be beneficial.

The IEA Heat Pump Centre

A central role within the IEA Heat Pump Programme is played by the IEA Heat Pump Centre (HPC). Consistent with the overall objective of the IA the HPC seeks to advance and disseminate knowledge about heat pumps, and promote their use wherever appropriate. Activities of the HPC include the production of a quarterly newsletter and the webpage, the organization of workshops, an inquiry service and a promotion programme. The HPC also publishes selected results from other Annexes, and this publication is one result of this activity.

For further information about the IEA Heat Pump Programme and for inquiries on heat pump issues in general contact the IEA Heat Pump Centre at the following address:

IEA Heat Pump Centre
Box 857
SE-501 15 BORÅS
Sweden
Phone: +46 33 16 55 12
Fax: +46 33 13 19 79

IEA-HPP ANNEX 27

Carbon Dioxide (CO₂) has shown promising results as an alternative working fluid compared to the CFCs, HFCs and HCFCs. CO₂ provides an environmental friendly alternative in a number of heat pump applications, in automobile air conditioning, and as a secondary fluid in refrigeration systems. The physical and the thermodynamic properties of CO₂ differ considerably from the more conventional working fluids and offer new possibilities as well as design challenges for systems and components.

On this background IEA Heat Pump Programme's Annex 27 was established. The main objective of the Annex has been to bring the CO₂ heat pump technology closer to commercialization, by addressing critical issues of both basic and applied character.

The scope of the work under this Annex includes *compression heat pump, refrigeration and air-conditioning systems and components*, with the main emphasis on heat pumps, using CO₂ as working fluid. The term "compression heat pump" covers vapor compression circuits with phase change. The term "system" includes all the components used in a heating/cooling system from the heat pump to the inside unit, controls included.

Results from 12 different research projects together with an extensive literature survey are presented. The projects are carried out as independent research projects, and the findings and the results are the sole responsibility of the authors. The following projects are presented:

- Feasibility of transcritical CO₂ systems for mobile space conditioning applications
- Use of CO₂- and propane thermosyphons in combination with compact cooler in domestic freezer
- Heat transfer of carbon dioxide in an evaporator
- Correlating the heat transfer coefficient during in-tube cooling of turbulent supercritical CO₂
- Heat transfer and pressure drop characteristics of super-critical CO₂ in microchannel tubes under cooling
- Flow vaporization of CO₂ in microchannel tubes
- Two-phase flow patterns during microchannel vaporization of CO₂ at near-critical pressures
- Small oil-free piston type compressor
- Some safety aspects of CO₂ vapor compression systems
- Boiling liquid expanding vapor explosions (BLEVE) in CO₂ vessels: initial experiments
- Experimental study on boiling liquid expansion in a CO₂ vessel
- CO₂ as secondary refrigerant (Sweden)

Participating countries were: Japan, Norway, Sweden, Switzerland, and USA. The report, which during the first two years is available for Annex 27 member countries only, can be obtained from the Heat Pump Center (<http://www.heatpumpcentre.org>).

Keywords: Natural working fluids, Carbon dioxide, heat pumping equipment, IEA

Table of Contents

1	Preface	1
2	Summary	2
3	Aim and Scope of the Annex	8
4	Contributing Research Teams	9
5	Literature Overview	10
6	Annex Projects	66
6.1	Systems	
6.1.1	Feasibility of transcritical CO ₂ systems for mobile space conditioning applications (USA)	67
6.1.2	Use of CO ₂ - and propane thermosyphons in combination with compact cooler in domestic freezer (Sweden)	108
6.2	Heat Transfer	
6.2.1	Heat transfer of carbon dioxide in an evaporator (Japan)	117
6.2.2	Correlating the heat transfer coefficient during in-tube cooling of turbulent supercritical carbon dioxide (USA)	129
6.2.3	Heat transfer and pressure drop characteristics of supercritical carbon dioxide in microchannel tubes under cooling (Norway)	145
6.2.4	Flow vaporization of CO ₂ in microchannel tubes (Norway)	154
6.2.5	Two-phase flow patterns during microchannel vaporization of CO ₂ at near-critical pressures (Norway)	163
6.3	Compressors/machinery	
6.3.1	Small oil-free piston type compressor (Switzerland)	173
6.4	Safety Issues	
6.4.1	Some safety aspects of CO ₂ vapor compression systems (Norway)	192
6.4.2	Boiling liquid expanding vapor explosions (BLEVE) in CO ₂ vessels: initial experiments (Norway)	207
6.4.3	Experimental study on boiling liquid expansion in a CO ₂ vessel (Norway)	215
6.5	Other Issues	
6.5.1	CO ₂ as secondary refrigerant (Sweden)	223

1 Preface

Carbon Dioxide (CO₂) has shown promising results as an alternative working fluid compared to the CFCs, HFCs and HCFCs. CO₂ provides an environmental friendly alternative in certain heat pump applications, in automobile air conditioning, and as secondary fluid in refrigeration systems. The physical and the thermodynamic properties of CO₂ differ considerably from the more conventional working fluids and offer new possibilities as well as design challenges for systems and components.

To meet these challenges, five participants under the IEA Heat Pump Programme, joined forces in the collaborative project Annex 27: *Selected Issues on CO₂ as Working Fluid in Compression Systems*. The aim of the Annex was to bring the CO₂ technology closer to commercialisation by filling in some remaining gaps in the technology and to expand the knowledge of the use of this natural working fluid in heat pumps, air conditioning and refrigeration systems.

The prospects for the CO₂-technology are positive. The first commercial pilot plant CO₂ heat pump water heater was built and installed in Norway in 1999. In addition, Denso Corporation has, in cooperation with Tokyo Electric Power Co. (TEPCO), developed a residential CO₂ heat pump water heater already on the market for some time in Japan. Furthermore, Toyota has introduced a CO₂ air conditioning system in their hybrid automobiles from 2003.

As part of Annex 27, a workshop (in Trondheim, Norway) was organised in co-operation with the IEA Heat Pump Centre. The workshop provided a broad overview of the latest developments, and stimulated exchange of knowledge and views between industry parties, researchers and policy makers on the issue of the application of CO₂. The results from the workshop are published in a separate report *HPP-AN27-1, Workshop Proceedings, Selected Issues on CO₂ as Working Fluid in Compression Systems, November 2000*.

The present document constitutes the final report of the work carried out under Annex 27. Results from 12 different research projects together with an extensive literature survey are presented. Even though several issues still remains to be solved in connection with the CO₂ technology, it is our hope that the present report will make a contribution in bringing the technology as such, a few steps forward.

SINTEF Energy Research

January 2004

2 Summary

This report consists of a literature survey and a series of individual papers on different issues related to CO₂ technology applied to refrigeration, air-conditioning, and heat pumps. The intention with the literature survey is to provide a status report on the subject area, whereas the papers addresses specific challenges related to different CO₂ technology issues. The papers present the findings of the individual research teams, who are solely responsible for the contents.

The following is a summary of the findings from the projects included in this report.

LITERATURE SURVEY

The literature survey presents recent developments and state-of-the-art for transcritical CO₂ cycle technology in various refrigeration, air-conditioning, and heat pump applications. The focus is on fundamental process and system design issues, including discussions of properties and characteristics of CO₂, cycle fundamentals, methods of high-side pressure control, thermodynamic losses, cycle modifications, component and system design, safety factors, and promising applications. Advanced cycle design options are also introduced suggesting possible performance improvements of the basic cycle.

SYSTEMS

Feasibility of transcritical CO₂ systems for mobile space conditioning applications

This project explores the feasibility of transcritical CO₂ systems for mobile space conditioning. Focus areas are: 1) combining validated component sub-models into a system simulation model; 2) validating the system model; and 3) using the validated model to design a truly reversible transcritical CO₂ heat pump systems.

Use of CO₂- and propane thermosyphons in combination with compact cooler in domestic freezer

This project is an evaluation of the use of a compact cooler in a standard freezer. Previous attempts using secondary, liquid loops on the cold and the hot side have been done in an earlier project but there were problems keeping an acceptable efficiency because of the energy demand of the pumps in these loops. The objective of this project is to design systems for both evaporator and condenser that are driven by density difference, so called thermosyphons. The intention is that at least the cold side should have CO₂ as refrigerant. The appliance for this test was a standard freezer. Before the modifications were made, the cabinet was tested according to the standard test procedure to receive reference values. After testing was finished, all of the standard equipment except the cabinet was removed, things as: compressor, condenser, evaporator and all shelves. The cabinet was finally turned upside down. Two thermosyphon systems were designed. The first system is for cooling the compact cooler's warm side. This cooling system uses propane as refrigerant. The

other thermosyphon system is used for heat extraction from the cabinet. It uses CO₂ as refrigerant. The tests show at first that the output capacity of the cooler is smaller than expected. Only 70 % of expected output could be reached and that was not sufficient to reach the desired cabinet temperature of -18°C. A lowest cabinet temperature of -11°C was reached, while the saturation temperature in the CO₂ thermosyphon was -18°C and the surface temperature of the compact cooler was -37°C. The tests definitely show a potential to use the compact cooler as a replacement for the standard compressor system. Both thermosyphon systems are only prototypes and much more can be done to reduce the temperature differences.

HEAT TRANSFER

Heat transfer of carbon dioxide in an evaporator

An experimental apparatus for carbon dioxide was constructed for measurement of boiling heat transfer characteristics inside horizontal tubes. The test sections were horizontally placed smooth tubes of which inner diameter was 0.7, 1.0, 2.0 and 4.0 mm. Experimental conditions were as following; evaporating temperature was 15°C, quality was from 0.1 to 0.9, heat flux was between 9 and 36 kW/m² and mass flux was between 360 and 1440 kg/m²s. The heat flux mainly affected the heat transfer, and mass velocity mainly affected the quality at onset of dry-out. The experimental results of boiling heat transfer and pressure drop in tubes were compared with those of fluorocarbons, but they were not fitted very much. Then a new correlation of heat transfer coefficient was proposed.

Correlating the heat transfer coefficient during in-tube cooling of turbulent supercritical carbon dioxide

An extensive study of the heat transfer and pressure drop characteristics of supercritical carbon dioxide during in-tube cooling was carried out as part of ASHRAE RP-913. Within this study, a new correlation to predict the heat transfer coefficient of supercritical carbon dioxide during in-tube cooling was developed based on the numerical predictions and experimental data. The new correlation is presented in this paper. It is based on a mean Nusselt number that is calculated using the Gnielinsky correlation, which is determined using the thermophysical properties at the wall and the bulk temperatures, respectively. It was seen that the majority of the numerical and experimental values predicted by the new correlation were within ±20%.

Heat transfer and pressure drop characteristics of super-critical carbon dioxide in microchannel tubes under cooling

This paper provides heat transfer and pressure drop data for carbon dioxide (CO₂) at supercritical pressures in a multiport extruded (MPE) aluminium tube. The tube had 25 circular ports/channels with 0.79 mm inner diameter. Data are presented for the following range of variables: Mass flux 600 - 1200 kg/(m²s), pressure 81 - 101 bar and heat flux 10 – 20 kW/m². The temperature range investigated was 15 to 70°C. The measured heat transfer coefficients were in the range of 5,000 to 17,500 W/(m²K) and the measured pressure drop in the range of 0.05 to 0.32 bar corresponding to a

mean pressure gradient of 10,000 to 64,000 Pa/m. In addition, the measured values were compared to correlations available in literature. Gnielinski's correlation for the single-phase heat transfer coefficient and Colebrook & White's correlation for the pressure drop showed a satisfactory correspondence. An accompanying paper presents the results of two-phase heat transfer and pressure drop experiments.

Flow vaporization of CO₂ in microchannel tubes

Flow vaporization heat transfer coefficient and pressure drop of carbon dioxide was measured in an extruded microchannel tube with 25 flow channels of 0.8 mm inner diameter and 0.5 m length. The test tube was heated by a water jacket, and the internal heat transfer coefficient was derived based on measured overall heat transfer and a regression-based expression for water-side heat transfer. Test principles are discussed and special emphasis is given to measurement uncertainties, including the propagation of uncertainty through the water-side regression. Studies of two-phase flow pattern were conducted in a separate test rig, using a 0.98 mm heated glass tube and a high-speed digital camera. Heat transfer and pressure drop measurements were conducted at varying vapor fraction for temperatures 0-25°C, mass flux 190-570 kg/(m²s), and heat flux 5-20 kW/m²k. Heat transfer results show significant influence of dryout, particularly at high mass flux and high temperature. Nucleate boiling dominates prior to dryout. Two-phase flow observations show increasing entrainment at higher mass flux, and a dominance of annular flow. Heat transfer data can be correlated reasonably well with a combination of models for nucleate boiling, convective evaporation, dryout incipience, and post-dryout heat transfer.

Two-phase flow patterns during microchannel vaporization of CO₂ at near-critical pressures

Carbon dioxide (CO₂) is receiving renewed interest as a refrigerant, in many cases based on systems with microchannel heat exchangers that have high pressure capability, efficient heat transfer, and compact design. A good understanding of two-phase flow of evaporating CO₂ in microchannels is needed to analyze and predict heat transfer. A special test rig was built in order to observe two-phase flow patterns, using a horizontal quartz glass tube with inner diameter 0.98 mm, externally coated by a transparent resistive film. Heat flux was obtained by applying DC power to the film, and flow patterns were recorded at 4,000 or 8,000 frames per second by a digital video camera. Flow patterns were recorded for temperatures 20°C and 0°C, and for mass flux ranging from 100 to 580 kg/(m²s). The observations showed a dominance of intermittent (slug) flow at low x , and wavy annular flow with entrainment of droplets at higher x . At high mass flux, the annular/entrained flow pattern could be described as dispersed. The aggravated dryout problem reported from heat transfer experiments at high mass flux could be explained by increased entrainment. Stratified flow was not observed in the tests with heat load. Bubble formation and growth could be observed in the liquid film, and the presence of bubbles gave differences in flow pattern compared to adiabatic flow. The flow pattern observations did not fit generalized maps or transition lines showed in the literature.

COMPRESSORS/MACHINERY

Small oil-free piston type compressor

The objective of this project was to prove the feasibility of a small oil-free semi hermetic piston type CO₂ compressor for supercritical heat pump applications with large temperature spans. These processes involve high pressures like 35 bar suction pressure and 80 to 150 bar delivery pressure. The compressor design is based on two key elements, which are: clearance seal piston/cylinder combination and PEEK-plate valves with flat valve springs. The feasibility study covers: design and manufacturing of a functional model, performance tests over the full range of speed and pressure, and manufacturing cost estimate for a modified serial model design. The compressor was designed for domestic water heating applications and has therefore no external cooling. The cooling of the motor is effected by the suction CO₂ gas flow through the motor, crankcase and cylinder head to the suction valves.

The tests confirmed the feasibility of the technology for the use in small oil-free compressors. The compressor, which has a scotch yoke drive, operates very quietly and without vibrations. It is able to handle outlet pressures up to 150 bar and outlet temperatures up to 200°C. Two kinds of cylinder heads from stainless steel and from plastic were tested in order to find out the influence of heat exchange and heat conduction. The stainless steel cylinder heads conduct a lot of heat to the compressor housing, which results in a considerable preheating of the suction gas. The process of preheating and compression follows different courses for the two cylinder head materials. However, the characteristic values of compression are practically the same for both. The isentropic efficiency is comparable to the efficiency of oil-lubricated compressors on the market, despite the very small cylinder volume of 1.25 cm³. The volumetric efficiency is rather low due to the large design-related dead volume of 18%. This CO₂ compressor technology is a possible alternative to oil lubricated compression systems in: automotive air conditioning (heating and cooling), domestic water heating, and applications in the food industry where oil-free compression is a must. Precondition for most of the applications however are competitive costs in comparison to oil-lubricated systems. In order to reach this target further development steps will be needed.

SAFETY ISSUES

Some safety aspects of CO₂ vapor compression systems

Since CO₂ is a non-toxic and non-flammable refrigerant, the major safety issues for CO₂ systems are related to the high operating pressure. In case of a component rupture, the explosion energy (stored energy) may characterise the extent of potential damage. The explosion energy can be estimated based on component (refrigerant-side) volumes, pressures and refrigerant property data. The explosion (stored) energies of baseline systems and CO₂ systems are calculated and compared. Results show that the explosion energies are not as different as the large difference in pressure would indicate. It has been suggested that a Boiling Liquid Expanding Vapour Explosion (BLEVE) may occur when a vessel containing pressurised liquid or supercritical fluid is rapidly depressurised, e.g. due to a crack or a rupture. The overpressure from a BLEVE may be high enough to rupture the whole vessel, with a

resulting blast wave and risk of flying fragments. Some tests on CO₂ have been conducted at varying initial conditions and liquid fill levels, and with varying vent areas. No significant overpressure peaks above the initial pressure has been observed in the current test programme.

Boiling liquid expanding vapor explosions (BLEVE) in CO₂ vessels: initial experiments

A Boiling Liquid Expanding Vapour Explosion (BLEVE) may occur when a vessel containing pressurised liquid or supercritical fluid is rapidly depressurised, e.g. due to a crack or a rupture. The sudden depressurisation leads to instant vaporisation that may give a transient overpressure peak. In some cases the overpressure can be high enough to rupture the whole vessel, with a resulting blast wave and risk of flying fragments. An experimental study at NTNU/SINTEF aims at improving the understanding of BLEVE in CO₂ systems. A test vessel has been built in order to measure transient pressures during initial depressurisation and possible subsequent overpressure peak(s). Some tests have been conducted at varying initial conditions and liquid fill levels, and with varying vent areas. The paper shows typical transient pressure recordings, and provides a discussion of practical relevance of the results. A maximum overpressure peak of 3 bar above the initial pressure has been observed in the current test programme.

Experimental study on boiling liquid expansion in a CO₂ vessel

Theory predicts that a Boiling Liquid Expanding Vapour Explosion (BLEVE) or Boiling Liquid Collapsed Bubble Explosion (BLCBE) may occur when a vessel containing pressurised saturated liquid is rapidly depressurised, e.g. due to a crack or initial rupture. The sudden depressurisation leads to explosive vaporisation and a transient overpressure peak that may burst the vessel. The paper provides results from an experimental study aimed at clarifying the possible occurrence of BLEVE/BLCBE in CO₂ systems. A test vessel was built and instrumented in order to measure transient pressures during initial depressurisation, and to record possible subsequent overpressure peak(s). A test program was conducted at varying initial conditions and liquid fill levels, and with varying vent areas. The paper shows typical transient pressure recordings, and provides a discussion of practical relevance of the results. No signs of BLEVE/BLCBE were recorded during this study.

OTHER ISSUES

CO₂ as secondary refrigerant

The operation and analysis of the existing plants proved that CO₂ could be successfully used as an alternative for the artificial refrigerants within the application of refrigeration in supermarkets. In addition to the obvious environmental advantages by using such systems, an extra economical gain was observed during the installation and running of the plants.

The power consumption in the CO₂ secondary system is very close to that of the DX-system with the same refrigerant in the primary loop. The secondary system allows

the use of refrigerants that cannot be used in a DX-system. Ammonia and propane cannot be used in DX-systems for safety reasons, but can be used in secondary systems, and the calculations show that the power consumption of such systems is less than that of the R404A DX-system. In the power consumption calculations the focus was on plants with conventional technologies, which are converted to a CO₂ secondary system. If the plant was originally constructed with a CO₂ secondary system then smaller pipes could be used for the return and liquid lines, which would compensate for the cost of the additional equipment in the secondary loop and the safety devices needed for the use of ammonia or propane. The power needed for the CO₂ pump is very small compared to the compressor power. From the analysis of the safety calculations' results, it is clear that using CO₂ in supermarket refrigeration does not enclose health risks for the customers and the workers in the shopping area. Yet, CO₂ detectors are recommended installed in the shopping area, especially in places where CO₂ leakage is probable and high local concentrations of CO₂ is expected. We would like to point out that even if the CO₂ charge and the size of the supermarket's shopping area and machine room are identical to the modelled case in this report, the individual case of every supermarket must be considered separately, taking into consideration the geometrical variations and the location of the distribution lines. Apparently, safety requirements such as proper ventilation and alarm system are a must in the machine room.

In the future all three CO₂ systems (secondary, cascade, and trans-critical systems) will exist, each finding its niche.

3 Aim and Scope of the Annex

The main objective of this Annex has been to bring the CO₂ heat pump technology closer to commercialisation, by addressing critical issues of both basic and applied character.

The scope of the work under this Annex includes *compression heat pump, refrigeration and air-conditioning systems and components*, with the main emphasis on heat pumps, using CO₂ as working fluid. The term “compression heat pump” covers vapour compression circuits with phase change. The term “system” includes all the components used in a heating/cooling system from the heat pump to the inside unit, control included.

The work is carried out as a common study with both task sharing and cost-sharing activities. The cost-sharing activities will be financed by annual contributions from the Annex Participants. Participants shall share the co-ordinated work necessary to carry out this Task

4 Contributing Research Teams

Participating countries in Annex 27 have been:

- Japan
- Norway (Operating Agent)
- Sweden
- Switzerland
- UK
- USA

Owing to financial difficulties, UK found it necessary to withdraw from the Annex before completion, and has consequently no contribution in the final report.

The following research teams from each country have contributed input to the Annex and the final report:

Japan:

- Contributing organization:
 - The University of Tokyo
- Principal investigator:
 - Professor Eiji HIHARA

Norway:

- Contributing organizations:
 - Norwegian University of Science and Technology
 - SINTEF Energy Research
- Principal investigator:
 - Professor Jostein PETTERSEN

Sweden

- Contributing organization:
 - Royal Institute of Technology
- Principal investigator:
 - Professor Björn PALM

Switzerland

- Contributing organization:
 - Zurich University of Applied Sciences
- Principal investigator:
 - Dr. Heinz BAUMANN

USA

- Contributing organizations:
 - University of Illinois at Urbana-Champaign, ACRC
 - Purdue University
- Principal investigators:
 - Professor Clark W. BULLARD
 - Professor Eckhard A. GROLL

5 Literature Overview

Available online at www.sciencedirect.com
**PROGRESS IN
ENERGY AND
COMBUSTION SCIENCE**

Progress in Energy and Combustion Science 30 (2004) 119–174

www.elsevier.com/locate/pecs

Fundamental process and system design issues in CO₂ vapor compression systems

Man-Hoe Kim^{a,*}, Jostein Pettersen^b, Clark W. Bullard^c^a*Department of Mechanical Engineering, Korea Advanced Institute of Science and Technology, Science Town, Daejeon 305-701, South Korea*^b*Department of Energy and Process Engineering, Norwegian University of Science and Technology, NO-7491 Trondheim, Norway*^c*Department of Mechanical and Industrial Engineering, University of Illinois at Urbana-Champaign,
1206 West Green Street, Urbana, IL 61801, USA*

Received 25 February 2003; accepted 15 September 2003

Abstract

This paper presents recent developments and state of the art for transcritical CO₂ cycle technology in various refrigeration, air-conditioning and heat pump applications. The focus will be on fundamental process and system design issues, including discussions of properties and characteristics of CO₂, cycle fundamentals, methods of high-side pressure control, thermodynamic losses, cycle modifications, component/system design, safety factors, and promising application areas. The article provides a critical review of literature, and discusses important trends and characteristics in the development of CO₂ technology in refrigeration, air-conditioning and heat pump applications. Advanced cycle design options are also introduced suggesting possible performance improvements of the basic cycle.

© 2003 Published by Elsevier Ltd.

Keywords: Natural refrigerant; CO₂ (R-744); Transcritical cycle; Vapor compression system; COP; Air-conditioning; Heat pump; Compressor; Heat exchanger

Contents

1. Introduction	120
1.1. Background	120
1.2. The history and reinvention of CO ₂	122
1.3. Structure of paper	123
2. Properties of CO ₂	123
2.1. Thermodynamic properties	124
2.2. Transport properties	127
3. Transcritical vapor compression cycle	128
3.1. Fundamentals of transcritical cycle	128
3.2. Methods of high-side pressure control	129
3.2.1. Systems with high-side charge control	129
3.2.2. Systems with high-side volume control	130
3.3. Thermodynamic losses	131
3.4. Transcritical cycles in heat pumps and systems with heat recovery	131
3.4.1. Temperature glide in heat rejection	131
3.4.2. Heating capacity and COP characteristics	131
3.5. Approach temperature and its importance	132

* Corresponding author. Tel.: +82-42-869-3089; fax: +82-42-869-3210.

E-mail address: kimmh@asme.org (M.-H. Kim).

3.6. Analysis of transcritical system energy efficiency	132
4. Modified cycles	133
4.1. Internal heat exchange cycle	133
4.2. Expansion with work recovery	134
4.3. Two-stage cycle	135
4.4. Flash gas bypass	136
5. Heat transfer and fluid flow	137
5.1. Supercritical-flow heat transfer and pressure drop	137
5.2. Flow vaporization heat transfer and pressure drop	138
5.3. Two-phase flow patterns	138
6. Issues related to high operating pressure	139
6.1. High pressure compression	139
6.2. High pressure heat transfer	139
6.3. Compactness of equipment	139
6.4. High-pressure safety issues	140
6.4.1. Explosion energy	140
6.4.2. Boiling liquid explosion	141
7. Component design	142
7.1. Compressors	142
7.2. Heat exchangers	144
7.2.1. Gas coolers	146
7.2.2. Evaporators	148
7.2.3. Internal heat exchangers	149
7.3. Other components	150
7.3.1. Lubricants	150
7.3.2. Elastomers	150
7.3.3. Valves and controls	150
8. Application areas	150
8.1. Automotive air conditioning	151
8.2. Automotive heating	154
8.3. Residential cooling	155
8.4. Residential heating	156
8.4.1. Direct air heating	157
8.4.2. Hydronic heating	159
8.5. Water heating	160
8.6. Environmental control units	162
8.7. Transport refrigeration	163
8.8. Commercial refrigeration	163
8.9. Dryers	164
9. Concluding remarks	165
Acknowledgements	169
Pressure–enthalpy diagram and saturation properties for CO ₂	169
References	169

1. Introduction

1.1. Background

Over the last decades, the refrigeration, air conditioning and heat pump industry has been forced through major changes caused by restrictions on refrigerants. The change-over to ‘ozone-friendly’ chlorine-free substances is not finished yet, as the HCFC fluids still need to be replaced, mostly involving R-22 in air-conditioning and heat pump

applications. The HFC refrigerants that were once expected to be acceptable permanent replacement fluids are now on the list of regulated substances due to their impact on climate change [1], and there is growing concern about future use. The global warming potential (GWP) is an index that relates the potency of a greenhouse gas to the CO₂ emission over a 100-year period. As shown in Table 1, the GWPs of the HFCs (R-134a, R-407C, R-410A) are in the order of 1300–1900 related to CO₂ with GWP = 1, and the HFCs are included in the greenhouse gases covered by

Nomenclature		T_{eai}	evaporator air inlet temperature, °C
COP	coefficient of performance	T_{ex}	refrigerant temperature at the exit of gas cooler, °C
c_p	specific heat, kJ/kg K	T_0	evaporating temperature, °C
F_c	compressor torque, N m	TEWI	total equivalent warming impact
G	mass flux, kg/m ² s	V	volume, m ³
GWP	global warming potential	V_c	outdoor air flow rate, m ³ /min
h	enthalpy, kJ/kg	V_e	indoor air flow rate, m ³ /min
HPF	heating performance factor	ν	specific volume, m ³ /kg
HSPF	heating seasonal performance factor	w	specific compressor work, kJ/kg
HX	heat exchanger	x	quality
IHX	internal heat exchanger (suction-line liquid-line heat exchanger)	ε	effectiveness
L	internal heat exchanger length, m	η_{is}	isentropic efficiency
LMTD	log mean temperature difference, °C or K	κ	thermal conductivity, W/m K
m	refrigerant charge, kg	λ	volumetric efficiency
m_r	refrigerant mass flow rate, g/s	μ	viscosity, kg/m s
NTU	number of transfer unit	π	pressure ratio
ODP	ozone depletion potential	ρ	density, kg/m ³
P	pressure, bar or MPa	σ	surface tension, N/m
p_m	mean effective pressure, bar	<i>Subscripts</i>	
Pr	Prandtl number	f	liquid
Q	capacity, kW	g	vapor
q	heat flux, kW/m ²	max	maximum
q_0	specific refrigeration capacity, kW/kg	opt	optimum
q_v	volumetric refrigeration capacity, kJ/m ³	pseudo	pseudocritical state
RH	relative humidity, %	ref	reference point
s	entropy, kJ/kg K		
SPF	seasonal performance factor		
T	temperature, °C or K		

Table 1
Characteristics of some refrigerants

	R-12	R-22	R-134a	R-407C ^a	R-410A ^b	R-717	R-290	R-744
ODP/GWP ^c	1/8500	0.05/1700	0/1300	0/1600	0/1900	0/0	0/3	0/1
Flammability/toxicity	N/N	N/N	N/N	N/N	N/N	Y/Y	Y/N	N/N
Molecular mass (kg/kmol)	120.9	86.5	102.0	86.2	72.6	17.0	44.1	44.0
Normal boiling point ^d (°C)	−29.8	−40.8	−26.2	−43.8	−52.6	−33.3	−42.1	−78.4
Critical pressure (MPa)	4.11	4.97	4.07	4.64	4.79	11.42	4.25	7.38
Critical temperature (°C)	112.0	96.0	101.1	86.1	70.2	133.0	96.7	31.1
Reduced pressure ^e	0.07	0.10	0.07	0.11	0.16	0.04	0.11	0.47
Reduced temperature ^f	0.71	0.74	0.73	0.76	0.79	0.67	0.74	0.90
Refrigeration capacity ^g (kJ/m ³)	2734	4356	2868	4029	6763	4382	3907	22545
First commercial use as a refrigerant [14]	1931	1936	1990	1998	1998	1859	?	1869

^a Ternary mixture of R-32/125/134a (23/25/52, %).

^b Binary mixture of R-32/125 (50/50, %).

^c Global warming potential in relation to 100 years integration time, from the Intergovernmental Panel on Climate Change (IPCC).

^d ASRAE handbook 2001 fundamentals.

^e Ratio of saturation pressure at 0 °C to critical pressure.

^f Ratio of 273.15 K (0 °C) to critical temperature in Kelvin.

^g Volumetric refrigeration capacity at 0 °C.

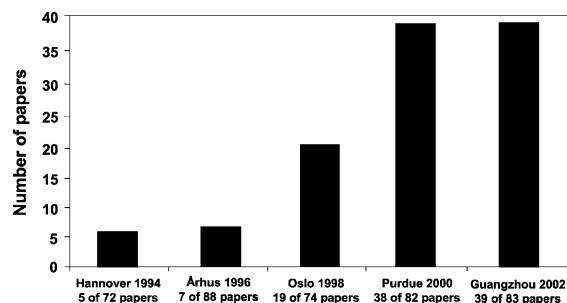


Fig. 1. Number of papers on CO₂ as a primary refrigerant presented at the IIR-Gustav Lorentzen Conference on Natural Working Fluids.

the Kyoto Protocol. The Kyoto protocol is not yet in force since the number of countries that have ratified it is not sufficient, but the spirit of Kyoto is certainly gaining impetus and something will be achieved at a reasonable level whether it is ratified or not [2]. The focus on greenhouse effect of fluorinated compounds has led to a proposed gradual phase-out of refrigerant R-134a in mobile air conditioning in EU, starting from 2008.

In this situation it is hardly surprising that the industry is looking for completely different long-term solutions. Instead of continuing the search for new chemicals, there is an increasing interest in technology based on ecologically safe 'natural' refrigerants, i.e. fluids like water, air, noble gases, hydrocarbons, ammonia and carbon dioxide. Among these, carbon dioxide (CO₂, R-744) is the only non-flammable and non-toxic¹ fluid that can also operate in a vapor compression cycle below 0 °C. Thus, CO₂ has the potential to offer environmental and personal safety in a system based on the well-proven and cost-efficient Evans–Perkins cycle.

During the 10 years since the refrigerant CO₂ was 'rediscovered' [3], there has been a considerable increase in the interest and development activity internationally. The number of papers on CO₂ as a primary refrigerant presented at the biennial IIR Conference on Natural Working Fluids has increased markedly since 1994 as shown in Fig. 1.

1.2. The history and reinvention of CO₂

CO₂ is an 'old' refrigerant, and it is therefore natural to start the paper by briefly looking back on the history of 'carbonic' systems. This section outlines the early history, including some views on why the use declined after World War II. The recent revival of CO₂ is also discussed.

During the first decades of the 20th century, CO₂ was widely used as a refrigerant, mainly in marine systems but also in air conditioning and stationary refrigeration applications. Alexander Twining appears to be the first to

¹ There are physiological effects from breathing air with high concentrations of CO₂. A maximum acceptable concentration of about 4–5% by volume seems to be a reasonable limit.

propose CO₂ as a refrigerant in his 1850 British Patent [4], but the first CO₂ system was not built until the late 1860s by the American Thaddeus S.C. Lowe [5]. Lowe, who received a British Patent in 1867, did not develop his ideas further [6]. In Europe, Carl Linde built the first CO₂ machine in 1881 [7]. Franz Windhausen of Germany advanced the technology considerably, and was awarded a British Patent in 1886. The company J. & E. Hall in Britain purchased the patent rights in 1887, and after having further improved the technology, Hall commenced manufacture in about 1890 [6]. Hall made the first two-stage CO₂ machine in 1889 [5]. The primary application was in marine refrigeration, a field where CO₂ dominated as a refrigerant until 1950–1960 as shown in Fig. 2 [8].

In Europe, CO₂ machines were often the only choice due to legal restrictions on the use of toxic or flammable refrigerants like NH₃ and SO₂ [9]. In the United States, CO₂ was used in refrigerating systems from about 1890 and in comfort cooling from about 1900 [6]. The refrigeration applications included small cold storage systems, display counters, food markets, kitchen and restaurant systems, while comfort-cooling systems were installed for instance in passenger ships, hospitals, theatres and restaurants. Most of these systems used calcium chloride solutions as a secondary refrigerant. Compressors were slow-running double- or single-acting crosshead machines with atmospheric crankcase pressure, and expansion valves were usually of the manual-control type. Condensers were often water-cooled double-pipe units [4].

The safety compared to refrigerants like NH₃ and SO₂ gave CO₂ a preference on board of ships and in public buildings. The commonly reported disadvantages of CO₂ were loss of capacity and low COP at high heat rejection temperature, compared to other common refrigerants. Especially in warm climates, this gave CO₂ a disadvantage. Refrigerant containment at high pressure was difficult with the sealing technology available at that time. By operation at supercritical high-side pressure or by various two-stage arrangements, the capacity and efficiency loss could be reduced. The so-called multiple-effect compression,

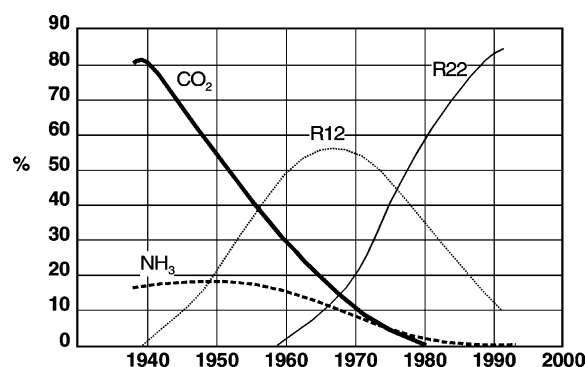


Fig. 2. Percentage use of main primary refrigerants in existing marine cargo installations classed by Lloyd's Register [8].

as devised by Voorhees in 1905 [10], is one example of the improvements that were made. When supercritical high-side operation was needed, this was obtained by charging more refrigerant into the system.

As the CFC fluids were introduced in the 1930s and 1940s, these ‘safety refrigerants’ eventually replaced the old working fluids in most applications. Although the major argument in their favor was improved safety compared to fluids like ammonia and sulfur dioxide, CO₂ was also displaced by this transition to CFC. There is no single reason why the use of CO₂ declined, but a number of factors probably contributed. These factors included high-pressure containment problems, capacity and efficiency loss at high temperature (aggravated by the need to use air cooling instead of water), aggressive marketing of CFC products, low-cost tube assembly in competing systems, and a failure of CO₂ system manufacturers to improve and modernize the design of systems and machinery.

With the CFC problem becoming a pressing issue in the late 1980s, the whole industry was searching for viable refrigerant alternatives. In Norway, Professor Gustav Lorentzen believed that the old refrigerant CO₂ could have a renaissance. In a 1989 international patent application [11], he devised a ‘transcritical’ CO₂ cycle system, where the high-side pressure was controlled by the throttling valve. One of the intended applications for this system was automobile air-conditioning, a sector that dominated the global CFC refrigerant emissions, and also an application where a non-toxic and non-flammable refrigerant was needed. The potential for more compact components due to high pressure was also an interesting feature.

In 1992, Lorentzen and Pettersen [3] published the first experimental results on a prototype CO₂ system for automobile air conditioning. A comparison was made between a state-of-the-art R-12 system and a laboratory prototype CO₂ system with equal heat exchanger dimensions and design-point capacity. Although simple cycle calculations indicated that the CO₂ system efficiency would be inferior, a number of practical factors made the actual efficiencies of the two systems equal.

Based on these and other results, the interest in CO₂ as a refrigerant increased considerably throughout the nineties, in spite of resistance from the fluorocarbon industry [12] and conservative parts of the automotive industry [13]. A number of development and co-operation projects were initiated by the industry and the research sector, including the European industry consortium project ‘RACE’ on car air conditioning, the European ‘COHEPS’ project on CO₂ heat pumps, and the CO₂ activities within the international IEA (International Energy Agency) Annexes on Natural Working Fluids and Selected Issues in CO₂ systems.

1.3. Structure of paper

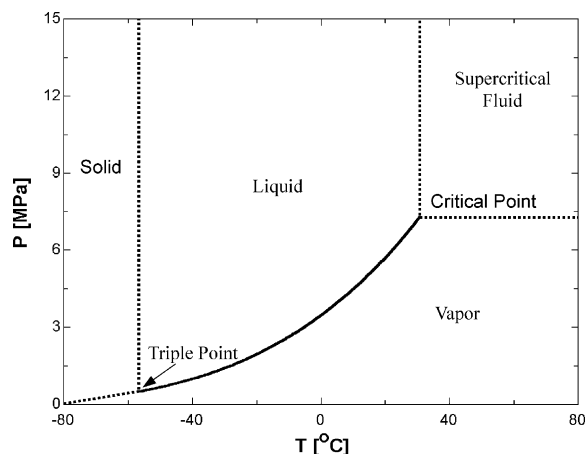
This article provides a critical review of transcritical CO₂ cycle technology in various refrigeration, air-conditioning

and heat pump applications. Recent research results in the world are introduced suggesting the possible applications for the particular purpose and the barriers that should be overcome before commercialization.

The history and reinvention of CO₂ have been introduced in Section 1 since it is not a new refrigerant. The thermodynamic and transport properties of CO₂ are quite different from all the conventional refrigerants and are important for the system design, especially for cycle simulation, heat transfer and pressure drop calculations. Section 2 presents the properties of CO₂ and its comparison with other refrigerants. Section 3 discusses some peculiarities of transcritical cycles and systems. A large number of cycle modifications are possible, including staging of compression and expansion, splitting of flows, use of internal heat exchange, and work-generating expansion instead of throttling. Some of these options are discussed in Section 4. Section 5 presents the heat transfer and pressure drop issues in CO₂ systems, which focus on supercritical flow and flow vaporization. Section 6 deals with issues and design characteristics related to high operating pressure. Operating pressures in CO₂ systems are typically 5–10 times higher than with conventional refrigerants, and this gives several effects that influence the design of components and their performance. In addition, high pressure may create perceived safety problems unless the underlying issues are addressed properly. Section 7 presents component design issues for CO₂ system and those barriers that should be overcome before commercialization. Section 8 introduces some possible applications for the particular purpose such as mobile and residential air conditioning and heat pump applications, environmental control unit, heat pump water heaters which are available in the market, dehumidifier, commercial refrigeration, and heat recovery system. Future research challenges and concluding remarks are summarized in Section 9.

2. Properties of CO₂

The refrigerant properties are important for the design of the heat pump system and its components. The properties of CO₂ are well known and they are quite different from all the conventional refrigerants. Table 1 compares the characteristics and properties of CO₂ with other refrigerants [14,15]. CO₂ is a non-flammable natural refrigerant with no Ozone Depletion Potential and a negligible GWP. Its vapor pressure is much higher and its volumetric refrigeration capacity (22,545 kJ/m³ at 0 °C) is 3–10 times larger than CFC, HCFC, HFC and HC refrigerants. The critical pressure and temperature of CO₂ are 7.38 MPa (73.8 bar) and 31.1 °C, respectively, and it is not possible to transfer heat to the ambient above this critical temperature by condensation as in the conventional vapor compression cycle. This heat transfer process (gas cooling) above the

Fig. 3. Phase diagram of CO₂.

critical point results in the transcritical cycle, i.e. with subcritical low-side and supercritical high-side pressure (for a single-stage cycle). The high-side pressure and temperature in the supercritical region are not coupled and can be regulated independently to get the optimum operating condition. As may be observed from the phase diagram of CO₂ (Fig. 3), the temperature and pressure for the triple point are -56.6°C and 0.52 MPa, respectively, and the saturation pressure at 0°C is 3.5 MPa. The reduced pressure at 0°C for CO₂ is 0.47 (Table 1), which is much higher than those for the conventional fluids. Owing to the low critical temperature and high-reduced pressure of CO₂, the low-side conditions will be much closer to the critical point than with conventional refrigerants.

Regarding transport properties (viscosity and thermal conductivity), the work by Vesovic et al. [16] is a key reference. However, improved viscosity data were published by Fenghour et al. [17]. While the earlier viscosity data were based on partly inconsistent experimental liquid viscosity data and used separate gas-phase and liquid-phase equations, the 1998 publication used new experimental data and represented the viscosity for the whole thermodynamic surface with one equation.

Rieberer [14] developed the property database CO2REF for CO₂, which covers both the sub- and super-critical regions. The thermodynamic and transport properties based on CO2REF were in good agreement with those from VDI [18] in spite of using different equations of state. ASHRAE [19] also presented tabular data for the thermophysical properties of CO₂, which covered from the triple point to the critical point (Appendix A). Pettersen [20] presented some properties of CO₂ using the program library CO2lib developed at NTNU/SINTEF, and he focused on the effect of properties on evaporating characteristics. Liley and Desai [21] also presented thermophysical properties (specific heat, thermal conductivity, viscosity, speed of sound, and surface tension) of CO₂ in tabular form. The following sections will

discuss the thermodynamic and transport properties of CO₂, compared to other refrigerants. Unless stated otherwise, all thermophysical properties were calculated using EES (Engineering Equation Solver), which uses the high-accuracy equation of state [22].

2.1. Thermodynamic properties

Span and Wagner [23] reviewed the available data on thermodynamic properties of CO₂ and presented a new equation of state in the form of a fundamental equation explicit in the Helmholtz free energy. In the technically most important region up to pressures of 30 MPa and up to temperatures of 523 K, the estimated uncertainty of the equation ranges from ± 0.03 to $\pm 0.05\%$ in the density, ± 0.03 to $\pm 1\%$ in the speed of sound, and $+0.15$ to $\pm 1.5\%$ in the isobaric specific heat. Special interest was focused on the description of the critical region and the extrapolation behavior of the formulation. Note that thermodynamic properties of CO₂ in EES [22] are provided using

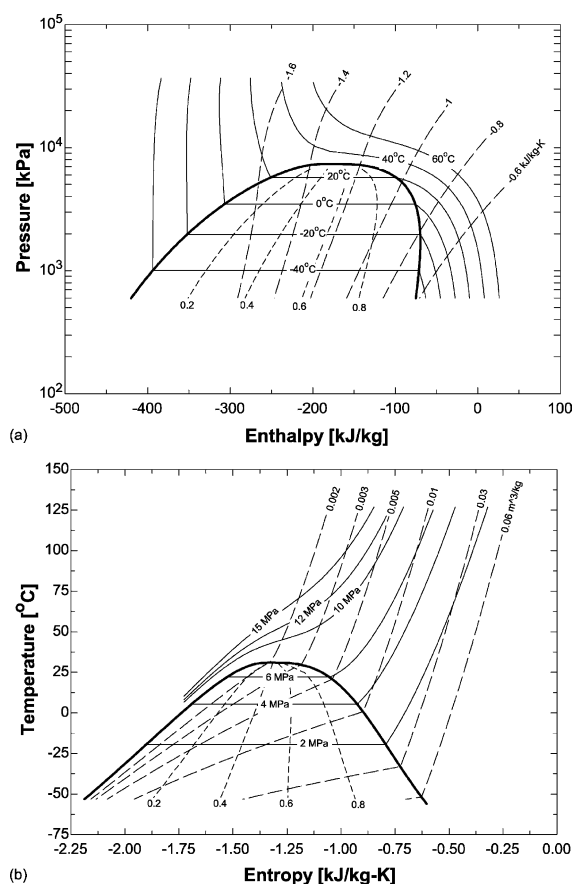
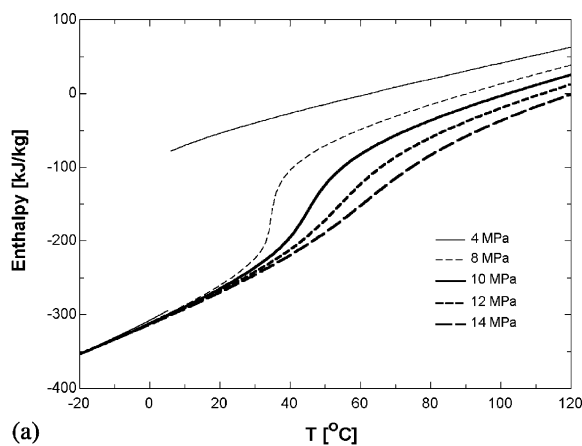


Fig. 4. Pressure–enthalpy and temperature–entropy diagrams of CO₂. (a) Pressure–enthalpy diagram, (b) Temperature–entropy diagram.

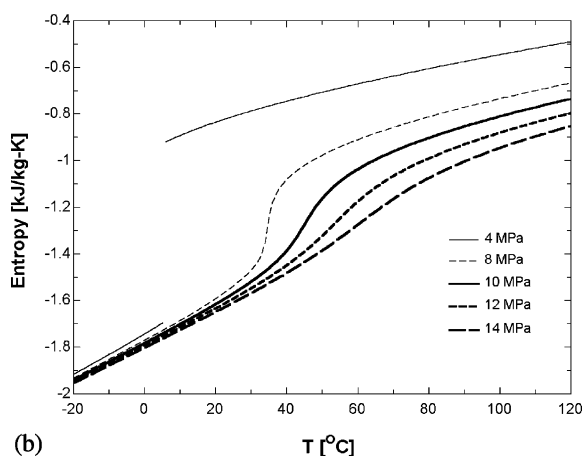
the fundamental equation of state developed by Span and Wagner [23].

Fig. 4 presents pressure–enthalpy and temperature–entropy diagrams of CO₂ and more detailed charts can be found elsewhere [14,19] (Appendix A). Fig. 5 shows enthalpy and entropy changes in gas cooling process at constant pressures. In the supercritical region, the enthalpy and entropy decrease with temperature with more abrupt changes near the critical point. The pressure influences the enthalpy and entropy above the critical temperature, while the effect of pressure is small below the critical temperature as the pressure drops may be allowed to be higher.

Figs. 6 and 7 present vapor pressure and slope of the saturation temperature curve of CO₂ compared to other fluids. The vapor pressure of CO₂ is much higher than other refrigerants, and its higher steepness near the critical point gives a smaller temperature change for a given pressure change. Thus, the temperature change associated with pressure drop in the evaporator will become smaller. For example, at 0 °C, the temperature change of



(a)



(b)

Fig. 5. Enthalpy and entropy changes of CO₂ in gas cooling process. (a) Enthalpy change, (b) entropy change.

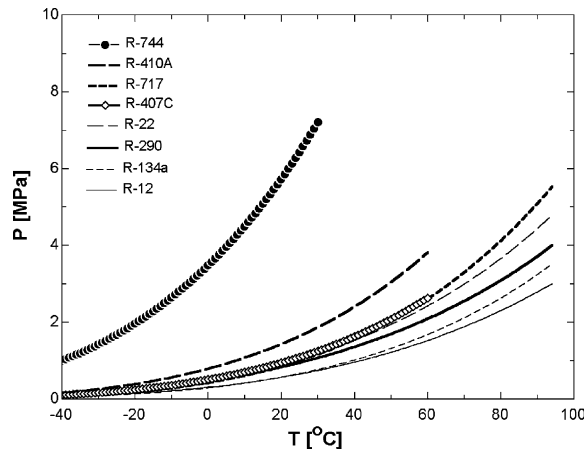


Fig. 6. Vapor pressure for refrigerants.

CO₂ for 1 kPa pressure drop is about 0.01 K. On the other hand, the same pressure drop with R-410A and R-134a give the temperature changes of 0.04 and 0.10 K, respectively, i.e. about 4–10 times higher, as shown in Fig. 7.

The high vapor pressure and closeness to the critical point result in quite different characteristics of liquid and vapor density of CO₂ compared to other refrigerants. The high vapor density may have significant effects on two-phase flow patterns where differences in phase density determine phase separation characteristics, and vapor density influences the flow momentum of the vapor phase and shear force between vapor and liquid phase [20]. Figs. 8 and 9 show density of CO₂ at varying temperature and the ratio of liquid to vapor density for several refrigerants. The density of CO₂ changes rapidly with temperature near the critical point, and the density ratio of CO₂ is much smaller than other refrigerants. At 0 °C, for instance, the ratio of liquid (927 kg/m³) to vapor density (98 kg/m³) of CO₂ is around 10, whereas R-410A and R-134a have the density ratios of 65 and 89, respectively. The vapor densities of R-410A and R-134a are 31 and 14 kg/m³, which are 32

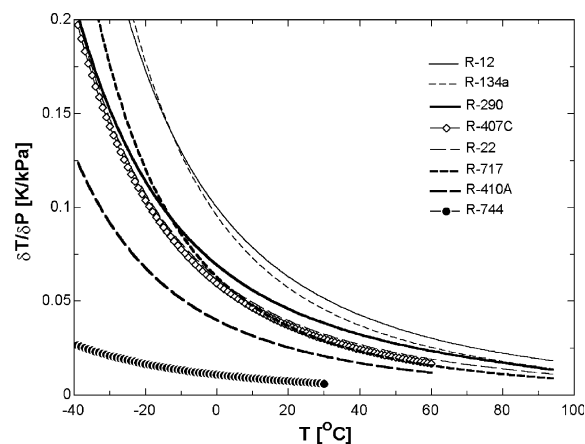
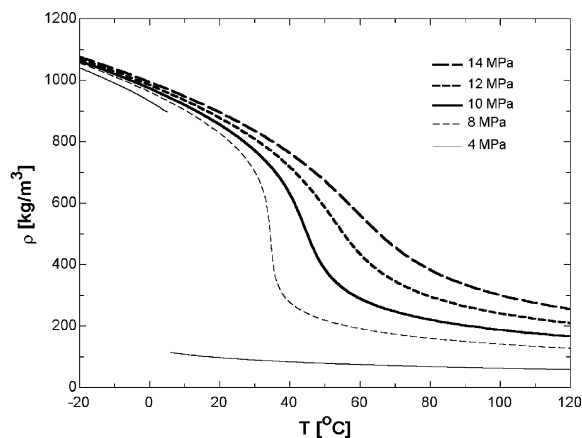


Fig. 7. Slope of saturation pressure curve dT/dP for refrigerants.

Fig. 8. Density of CO₂.

and 14% of the CO₂ vapor density, respectively. The low-density ratio of CO₂ may give more homogenous two-phase flow than with other refrigerants [24]. The liquid to vapor density ratio plays an important role in an evaporator since it determines the flow pattern and thus the heat transfer coefficient [20].

The higher vapor density gives the high volumetric refrigeration capacity of CO₂, which is defined as product of vapor density and latent heat of evaporation. The volumetric refrigeration capacity of CO₂ increases with temperature, has a maximum at 22 °C, and then decreases again. By definition it is zero at the critical point as shown in Fig. 10.

Surface tension of the refrigerants influences nucleate boiling and two-phase flow characteristics. A small surface tension reduces the superheat required for nucleation and growth of vapor bubbles, which may positively affect heat transfer. Wetting characteristics of the liquid is affected by surface tension, thus influencing evaporation heat transfer. Reduced liquid surface stability with small surface tension may affect heat transfer

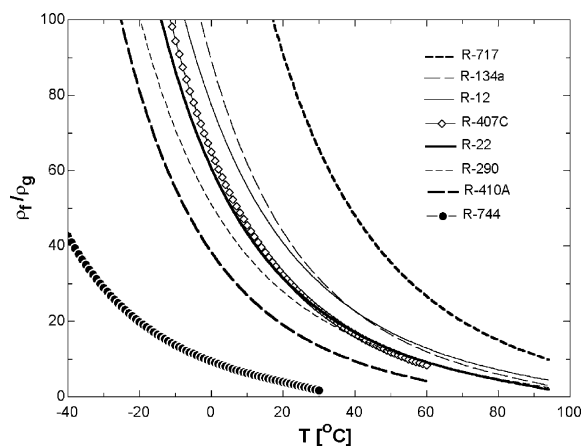


Fig. 9. Ratio of liquid to vapor density at saturation for refrigerants.

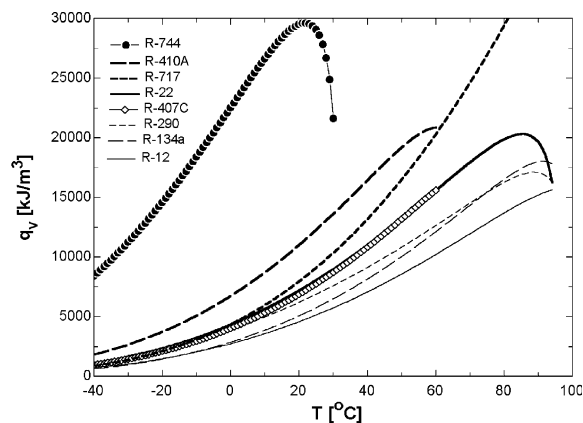


Fig. 10. Volumetric refrigeration capacity for refrigerants.

negatively due to increased droplet formation and entrainment [20]. Fig. 11 presents surface tension of saturated CO₂ liquid at varying temperatures, compared to other fluids. The surface tension of the refrigerants decreases with temperature and becomes zero at the critical point. As shown in Fig. 11, the surface tension of CO₂ is smaller than those of other fluids. For instance at 0 °C it is 0.0044 N/m, which is 2.5 times smaller than that of R-134a at the same temperature. Surface tension data for CO₂ can be estimated based on the publication of Rathjen and Straub [25], and speed-of-sound data were derived by Estrada-Alexanders and Trusler [26].

One of the most important characteristics of supercritical fluids near the critical point is that their properties change rapidly with temperature in an isobaric process, especially near the pseudocritical points (the temperature at which the specific heat becomes a maximum for a given pressure). This may be clearly seen from Figs. 12 and 13, where the isobaric specific heat and pseudocritical temperature are depicted. It should be noted that the ϵ -NTU or LMTD method requires that the specific heat be constant over the test section. Thus when the data are analyzed using

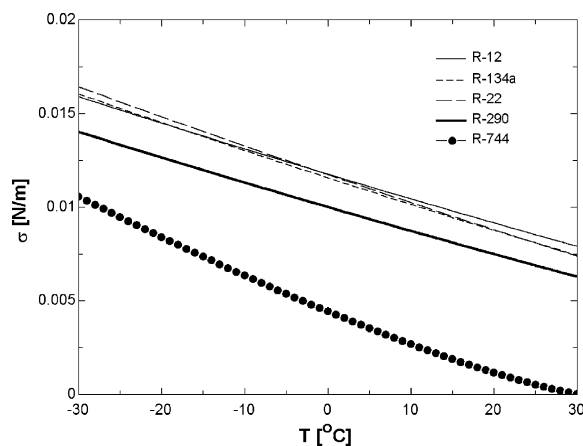
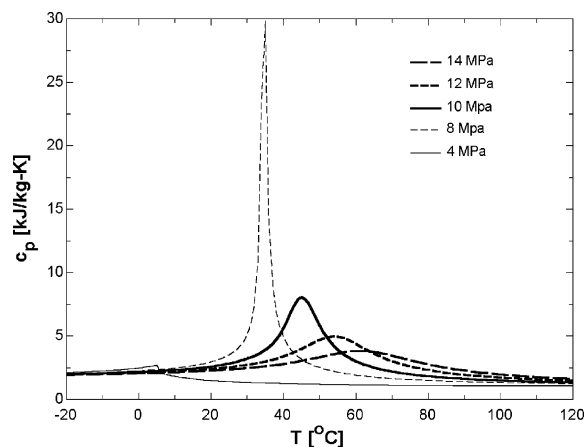


Fig. 11. Surface tension for refrigerants.

Fig. 12. Isobaric specific heat of CO₂.

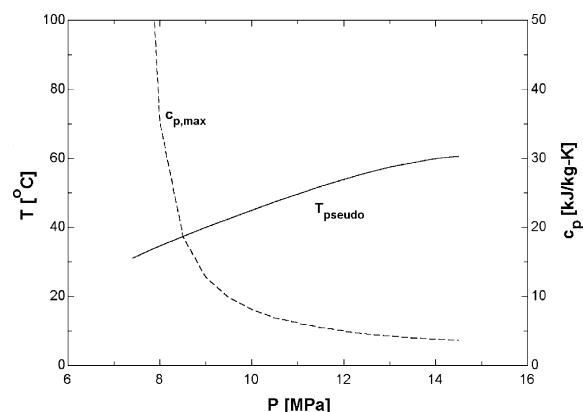
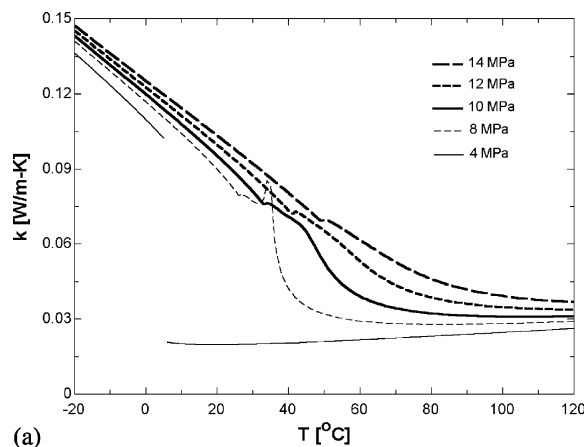
the ε -NTU or LMTD method, it should be carefully investigated whether the specific heat is constant. The pseudocritical temperature of CO₂ was calculated using the following algebraic equation [27]

$$T_{\text{pseudo}} = -122.6 + 6.124P - 0.1657P^2 + 0.1773P^{2.5} - 0.0005608P^3, \quad 75 \leq P \leq 140 \quad (1)$$

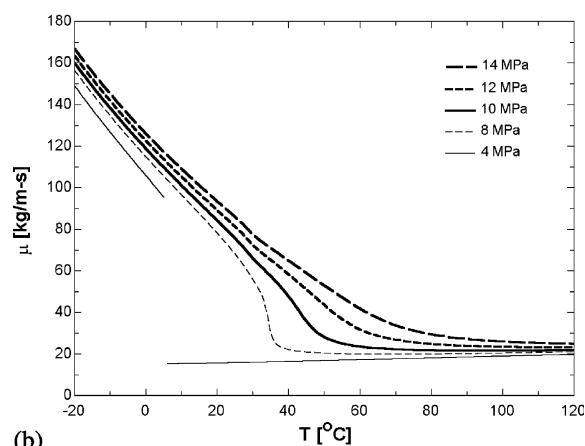
where the temperature (T_{pseudo}) and pressure (P) are in °C and bar, respectively.

2.2. Transport properties

The transport properties of refrigerants play an important role in heat transfer and pressure drop characteristics. Fig. 14 shows the transport properties, which are thermal conductivity and viscosity at subcritical and supercritical pressures at varying temperatures. A high thermal conductivity is essential for heat transfer coefficients both in single-phase and two-phase flow. Viscosity, particularly of the liquid

Fig. 13. Pseudocritical temperature and maximum isobaric specific heat of CO₂.

(a)

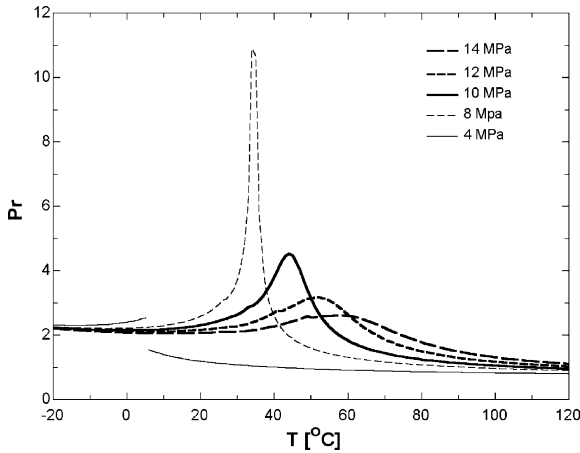


(b)

Fig. 14. Transport properties of CO₂. (a) Thermal conductivity, (b) viscosity.

phase, and the ratio of liquid to vapor viscosity, are important parameters for the fluid flow behaviors, convection characteristics and two-phase heat transfer and pressure drop. The thermal conductivities of saturated CO₂ liquid and vapor at 0 °C are 20 and 60% higher than of R-134a liquid and vapor, respectively, while the viscosity of CO₂ liquid is only 40% of R-134a liquid viscosity, and the vapor viscosities of the two fluids are comparable [20].

The Prandtl number is an important parameter for the heat transfer coefficient. Fig. 15 depicts the Prandtl number of supercritical and liquid/vapor CO₂ at varying temperatures. It has a maximum at the pseudocritical temperature associated with the corresponding specific heat, and the maximum value decreases with pressure. The effect of the temperature on the Prandtl number depends on pressure. The Prandtl number becomes higher with pressure for $T >$ about 60 °C in the supercritical region, whereas it decreases with pressure when temperature is smaller than about 20 °C. This results in a strongly varying local heat transfer coefficient depending on temperature and pressure [14]. In summary, the thermodynamic and transport properties of

Fig. 15. Prandtl number of CO₂.

CO₂ seem to be favorable in terms of heat transfer and pressure drop, compared to other typical refrigerants.

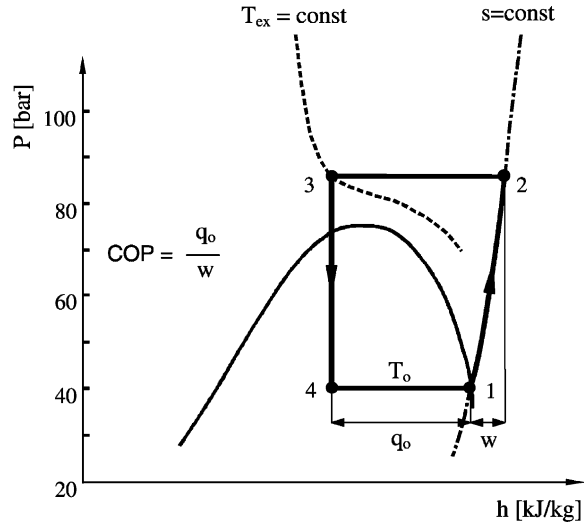
3. Transcritical vapor compression cycle

Compared to conventional refrigerants, the most remarkable property of CO₂ is the low critical temperature of 31.1 °C. Vapor compression systems with CO₂ operating at normal refrigeration, heat pump and air-conditioning temperatures will therefore work close to and even partly above the critical pressure of 7.38 MPa. Heat rejection will in most cases take place at supercritical pressure, causing the pressure levels in the system to be high, and the cycle to be ‘transcritical’, i.e. with subcritical low-side and supercritical high-side pressure (for a single-stage cycle). Some peculiarities of transcritical cycles and systems are discussed in the following text.

3.1. Fundamentals of transcritical cycle

During operation at high ambient air temperatures the CO₂ system will operate in a *transcritical* cycle most of the time. Heat rejection then takes place by cooling the compressed fluid at supercritical high-side pressure. The low-side conditions remain subcritical, however, as shown in Fig. 16.

At supercritical pressure, no saturation condition exists and the pressure is independent of the temperature. In conventional subcritical cycles, the specific enthalpy in point 3 is mainly a function of temperature, but at supercritical high-side conditions the pressure also has a marked influence on enthalpy. This effect may be observed as non-vertical or S-shaped isotherms in the supercritical and near-critical region. An important consequence of this is that it is necessary to control the high-side pressure, since the pressure at the throttling valve inlet will determine specific

Fig. 16. Transcritical cycle in the CO₂ pressure–enthalpy diagram.

refrigeration capacity. As in conventional systems, the compressor work and thereby also the COP will depend on the discharge pressure. However, while the COP tends to drop with increasing pressure in conventional cycles, the behavior is quite different in a transcritical cycle, as will be shown in the following [28].

Fig. 17 shows the theoretical influence from varying high-side pressure on specific refrigerating capacity (q_0), specific compressor work (w) and cooling COP. The refrigerant outlet temperature from the gas cooler (T_{ex}) is assumed to be constant. In practice, this temperature will be some degrees higher than the coolant inlet temperature. The curves are based on ideal cycle calculations, with evaporating temperature ($T_0 = 5$ °C) and a minimum heat rejection temperature (T_{ex}) of 35 °C (left), and 50 °C (right). Note that all curves are normalized (Fig. 17).

As the high-side pressure is increased, the COP reaches a maximum above which the added capacity no longer fully compensates for the additional work of compression. In Fig. 16, it may be observed that the T_{ex} -isotherm becomes steeper as the pressure increases, thereby reducing the capacity enhancement from a given pressure increment. In contrast, the isentropic (compression) line shows a nearly linear shape. Differentiation of cooling $COP = (h_1 - h_3)/(h_2 - h_1)$ with respect to the high-side pressure gives maximum COP for $\partial COP/\partial p = 0$ at a pressure (p) defined by Inokuty [29]

$$\left(\frac{\partial h_3}{\partial p}\right)_T = -COP \left(\frac{\partial h_2}{\partial p}\right)_s \quad (2)$$

That is, the ‘optimum’ pressure is reached when the marginal increase in capacity equals COP times the marginal increase in work. The enthalpy h_1 is constant. Curves in Fig. 17 are normalized by the values for COP, q_0 and w at the optimum high-side pressure. At $T_{ex} = 35$ °C

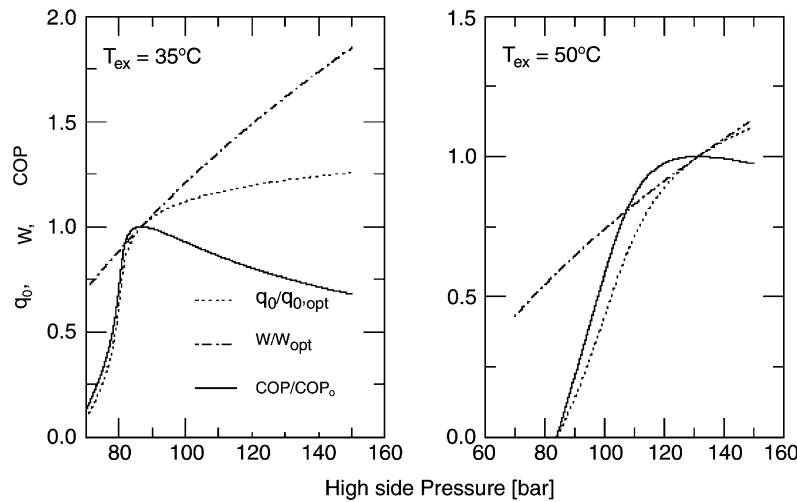


Fig. 17. Influence of varying high-side pressure on specific refrigerating capacity (q_0), specific compressor work (w) and COP in a transcritical CO₂ cycle. The results are based on isentropic compression, evaporating temperature ($T_0 = 5^\circ\text{C}$) and a refrigerant outlet temperature (T_{ex}) from the gas cooler of 35°C (left) and 50°C (right).

the theoretical maximum COP is reached at a pressure of 8.7 MPa (87 bar), while at 50°C , the optimum is at 13.1 MPa (131 bar). In practice, the cooling capacity (q) curve will also go through a maximum, as compressor volumetric capacity drops off at higher discharge pressures. In most situations there will also be a capacity-maximum, usually at a somewhat higher pressure than the COP-maximum.

High-side pressure regulation can be applied to maintain the COP at its maximum and/or to regulate the cooling or heating capacity. The optimum pressure increases steadily and almost linearly as T_{ex} is raised, and the influence from varying evaporating temperature is quite small.

3.2. Methods of high-side pressure control

The high-side pressure in a CO₂ system may be either subcritical or supercritical. In case of subcritical operation, the system will behave as conventional systems, with high-side pressure determined by condensing temperature. In case of supercritical operation, however, the pressure in the high side is determined by the relationship between refrigerant charge (mass), inside volume and temperature. Refrigerant properties can be described by an equation of state in the following form:

$$p = p(v, T) = p\left(\frac{V}{m}, T\right) \quad (3)$$

As a result, there are three fundamentally different ways of controlling pressure [30]:

- Varying the refrigerant charge (m) in the high side of the circuit,
- Varying the inside volume (V) of the high-side, and

- Allowing the refrigerant temperature (T) to control the pressure.

While the first two options give possibilities for active pressure control, the last method is actually a passive scheme where the refrigerant charge/volume conditions are adapted to give the desired change in pressure when temperature varies. Thus, in case of leakage, the temperature/pressure relation will change when using a passive scheme and this may give loss of capacity and COP.

Even though high-side conditions are supercritical a large part of the time, the circuit and control system must also be designed for subcritical (condensing) high-side conditions as well, since this type of operation will be encountered when heat rejection temperatures are moderate or low.

3.2.1. Systems with high-side charge control

In systems where the high-side pressure is controlled by varying the high-side refrigerant charge, the circuit must include means for controlling the momentary mass of refrigerant located between the compressor outlet and the expansion valve inlet. Assuming that the total refrigerant charge in the circuit is constant, a refrigerant buffer must be provided so that the high-side charge can be varied without flooding or drying up the evaporator. Several buffer volume locations and control concepts are possible. The various solutions can be divided into low-pressure and intermediate-pressure buffer systems.

Low pressure buffer systems. Systems with low-pressure buffers include circuits with low-pressure receiver on the evaporator outlet, and systems with liquid separator using gravity, pump or possibly ejector circulation. A system with low-pressure receiver on the evaporator outlet is shown in Fig. 18 [11]. High-side pressure is controlled by

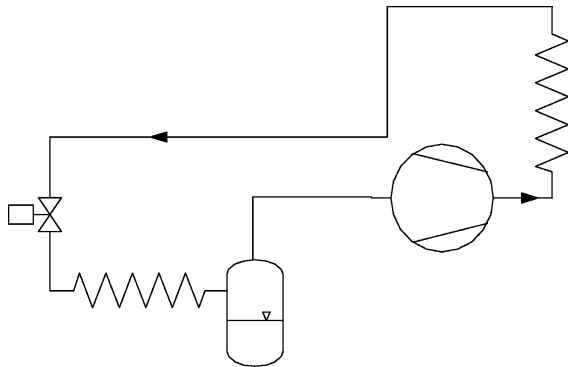


Fig. 18. System with low-pressure receiver.

adjusting the expansion valve, temporarily changing the balance between compressor mass flow rate and valve flow rate. By reducing the valve opening, a temporary reduction in the valve mass flow rate gives refrigerant accumulation in the high side, and the pressure rises until a new balance point between valve flow rate and compressor flow rate is found. The vapor fraction at the evaporator outlet may temporarily rise while pressure is rising, and the additional high-side charge is transferred from the low-side buffer. Conversely, increased valve opening will reduce the high-side charge and pressure, and the excess high-side charge is deposited as liquid in the buffer. In practice, such systems will in most cases need a liquid bleed from the receiver in order to return lubricant to the compressor and to maintain the evaporator outlet slightly wet. The liquid surplus may be an advantage when the high-side pressure is raised, to avoid drying up the evaporator. By installing an internal (suction line) heat exchanger, the liquid is evaporated before the compressor inlet, and the COP is improved at high heat rejection temperature. The use of internal heat exchange is discussed elsewhere in the paper.

Systems with medium-pressure buffer. Fig. 19 shows a system where the buffer is kept at an intermediate pressure [11]. An in-line receiver is located between

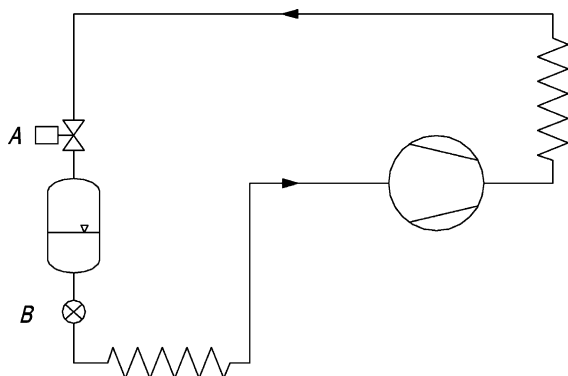


Fig. 19. System with in-line medium-pressure receiver.

a pressure-regulating valve (A), that controls the high-side pressure, and an electronic or thermostatic expansion valve (B), that regulates liquid flow to the evaporator. The receiver pressure may either be supercritical or subcritical.

In case of subcritical receiver pressure, the outlet from the pressure-regulating valve (A) will be on the saturation line during steady-state operation. The receiver pressure will adjust itself to this point, since vapor cannot escape. Adjustment of the valve opening temporarily moves the end-point of the throttling away from the saturation line, and the resulting imbalance between the mass flow rates through the two valves gives a transfer of mass to or from the receiver, thereby affecting high-side charge and pressure.

In case of supercritical receiver pressure, the refrigerant mass in the buffer is regulated by changing the buffer pressure, thereby modifying the density of the compressed fluid. The pressure can be controlled between the compressor discharge pressure and the critical pressure. A large receiver volume may be necessary in order to obtain the necessary range of high-side charge variation.

Another system with intermediate-pressure buffer is shown in Fig. 20 [11]. Here, the receiver is located in parallel to the flow circuit, connected to the high and low sides by valves. These two valves and the expansion valve are operated to control high-side charge and pressure.

3.2.2. Systems with high-side volume control

Instead of varying the mass, the pressure in the high side can be regulated by adjusting the internal volume of the high-side part of the circuit. For a given volume change, the largest pressure variation will be obtained at the lowest possible temperature (highest density). This makes the gas cooler refrigerant outlet the ideal location for a volume-control device. This device may be constructed in a number of ways, including bellows arrangement inside a pressure vessel or a cylinder where the displacement of a piston defines the refrigerant-side volume. The buffer design must consider factors like lubricant trapping and means for

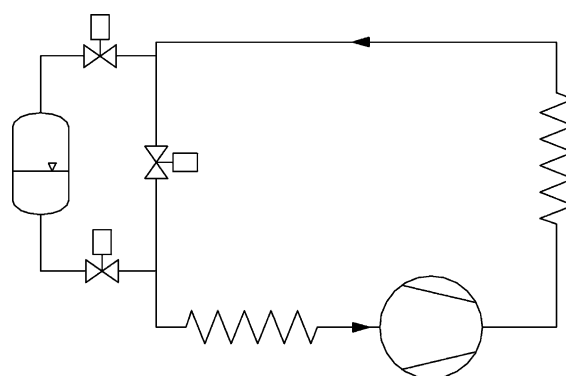


Fig. 20. System with medium-pressure receiver.

control of the volume through mechanical or hydraulic actuation.

3.3. Thermodynamic losses

Assuming given evaporating temperature and given minimum heat rejection temperature, the transcritical cycle suffers from larger thermodynamic losses than an 'ordinary' Evans–Perkins cycle with condensation, Fig. 21. Owing to the higher average temperature of heat rejection, and the larger throttling loss, the theoretical cycle work for CO₂ increases compared to a conventional refrigerant as R-134a as indicated. The throttling loss in a refrigerating cycle is given by temperatures before and after the throttling device, and by refrigerant properties. With temperatures given, the refrigerant properties become essential. Given the high liquid specific heat and low evaporation enthalpy of CO₂ near the critical point, the loss in refrigeration capacity (and the equal increase in compressor power) becomes large.

In reality though, as discussed in subsequent sections, the minimum heat rejection temperature will be lower in the CO₂ cycle when heat sink inlet temperature and heat exchanger size is given. In addition, the evaporating temperature tends to be higher for a given duty, heat source temperature, and heat exchanger size. Finally, the compressor losses, which are not shown in Fig. 21, tend to be lower in CO₂ machines.

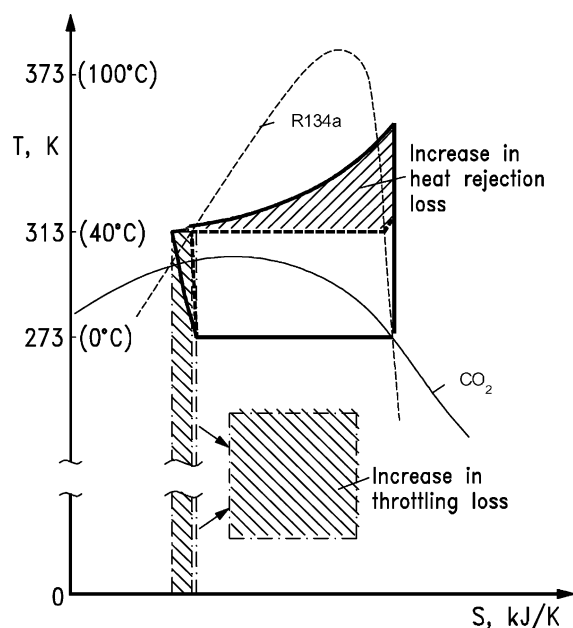


Fig. 21. Comparison of thermodynamic cycles for R-134a and CO₂ in temperature–entropy diagrams, showing additional thermodynamic losses for the CO₂ cycle when assuming equal evaporating temperature and equal minimum heat rejection temperature.

3.4. Transcritical cycles in heat pumps and systems with heat recovery

3.4.1. Temperature glide in heat rejection

As may be observed from Fig. 21, heat is rejected from the CO₂ cycle at gliding temperature, as the supercritical-pressure single-phase refrigerant is cooled. The temperature profile of the cooled refrigerant thus matches the heating-up curve of water or air to be heated, thus giving reduced thermodynamic losses in water- or air heating. This feature may be utilized in heat pumps for tap water heating and/or hydronic heating systems, and may also give advantages in heat recovery from refrigeration or air conditioning systems. In applications where the rejected heat is not of interest, the gliding temperature is not an advantage, since the average temperature of heat rejection becomes higher than necessary.

In water heating applications, the inlet temperature is often quite low, and the CO₂ temperature glide during heat rejection in a 'triangular' process with low inlet temperature is ideal for heating of service water from around 10 to 70–80 °C. By proper counterflow heat exchanger design and by adjustment of the high-side pressure, varying temperature requirements can be met. Application examples will be described in the following text.

3.4.2. Heating capacity and COP characteristics

In heat pump operation, the CO₂ system obtains a maximum COP at a certain high-side pressure, as explained above. By raising the pressure above this level, the heating capacity may be increased or maintained as the evaporating temperature is reduced. Despite the reduced COP, the overall efficiency of heating may then be increased in bivalent systems due to reduced supplementary heat. Another peculiarity of the CO₂ cycle is the smaller influence on heating capacity and COP by varying evaporating temperature, which enables the CO₂ system to maintain a high heating capacity at low ambient temperature. Both of these principles are illustrated for ideal cycles in Fig. 22, showing relative changes in heating capacity and heating COP with varying evaporating temperature and CO₂ high-side pressure [31]. Similar tendencies can also be observed for cooling capacity and cooling COP.

Even at the optimum pressure (opt), the CO₂ heat pump output is decreased less than with the other refrigerants as the evaporating temperature is reduced. At –15 °C, the capacity ratio CO₂/fluorocarbon is about 1.5, and the relative reduction in COP is smaller with CO₂ than with the other fluids. This diagram is intended to illustrate the effects of differences in thermodynamic properties on cycle behavior, and not to demonstrate the performance level of CO₂ compared to other refrigerants. By raising the high-side pressure, a further increase in heat pump capacity can be obtained. The actual operation with capacity-boosting will depend on factors like maximum allowable

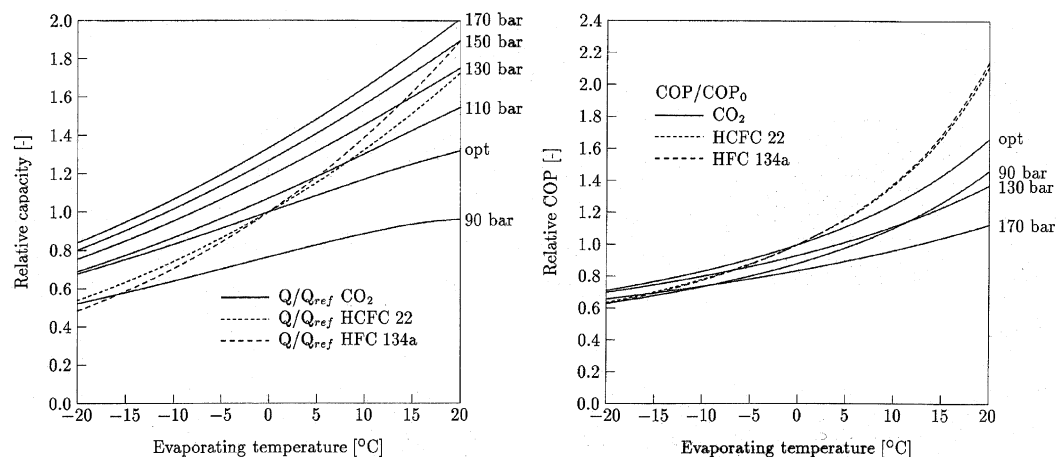


Fig. 22. Relative change in heating capacity (left) and heating COP (right) for R-22, R-134a and CO₂ at varying evaporating temperature, for a condenser/gas cooler exit temperature of 40 °C. Reference point: 0 °C evaporating temperature. Results for CO₂ are shown at COP-optimum high-side pressure, and with relative data for other high-side pressures. Based on ideal cycle calculations without subcooling or superheating.

pressure, maximum motor load, and compressor discharge temperature limitations.

3.5. Approach temperature and its importance

In applications where the rejected heat is not needed, the thermodynamic losses in heat transfer can be limited by allowing the CO₂ exit temperature from the gas cooler to approach the air- or cooling water inlet temperature as closely as possible. Heat exchanger design calculations and practical experience show that it is possible to obtain a temperature approach of a few degrees, even in air-cooled coils. Assuming that the mean temperature difference is approximately equal for a given heat exchanger size, the temperature approach must necessarily be lower when heat is rejected over a temperature glide than when it is rejected at constant temperature.

Owing to the relatively high throttling loss and the gliding heat rejection temperature, the cooling COP for a CO₂ system is very sensitive to the gas cooler refrigerant exit temperature. Fig. 23 shows the relative change in ideal cycle COP at varying condenser/gas cooler outlet temperature, normalized by the COP at 40 °C [31]. While the ideal COP for R-22 and R-134a is increased by about 40% through a 10 K condenser outlet temperature reduction, the effect on the CO₂ cycle COP is nearly twice as high (70%). The close temperature approach that is obtained in CO₂ gas coolers therefore contributes significantly to practical COP improvement.

3.6. Analysis of transcritical system energy efficiency

Comparisons of energy efficiency and/or TEWI (total equivalent warming impact) between baseline systems and CO₂ systems have to account for two important factors:

The effect of climate, i.e. a seasonal data for comparisons of energy consumption, and a system approach, including the effects of supplementary heat and secondary power requirements for fans or pumps.

Most refrigeration, air-conditioning and heat pump systems are operated in a varying climate. Comparisons based on design point operation apply conditions that rarely occur—typically at an extreme ambient temperature. In order to obtain a realistic comparison of annual or seasonal energy consumption, realistic climatic data should

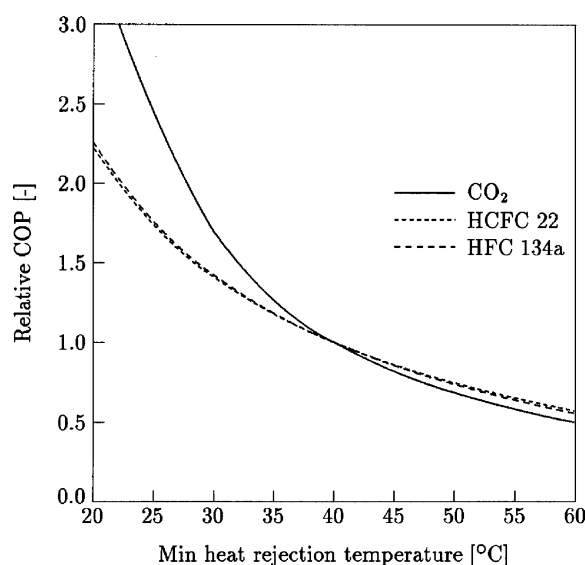


Fig. 23. Relative change in cooling COP for R-22, R-134a and CO₂ at varying refrigerant exit temperature from condenser/gas cooler (i.e. minimum heat rejection temperature). Evaporating temperature 0 °C. Reference point: 40 °C exit temperature. Based on ideal cycle calculations without subcooling or superheating.

be applied, e.g. temperature occurrence data. Even though the COP of the CO₂ system may be somewhat lower at an extreme ambient temperature, the seasonal energy consumption may be reduced compared to a baseline system using conventional refrigerants.

Differences in heating capacity characteristics between CO₂ and conventional refrigerants have to be taken into account in the comparison of CO₂ to baseline systems, since differences in supplementary heating requirements may significantly affect the system energy efficiency. In this respect, the system energy efficiency is calculated as *heating system COP*, i.e. the ratio of heat pump heat output plus supplementary heat, to heat pump energy use plus supplementary heat input. By reducing the need for supplementary heat the *system COP* of a CO₂ heat pump may often be higher than the baseline. The reason is that the baseline system does not maintain its heating capacity at lower heat source temperature, and more supplementary heat is needed.

In general, CO₂ systems may offer more possibilities for efficient and useful heat recovery, since higher temperatures can be provided. In comparisons between different systems, this factor should be taken into account through studies on overall energy requirements for cooling and heating.

Differences in fan and pump power requirements should also be considered, particularly since air-side pressure drops and air flow rates are likely to be different, thus giving differences in fan power. In a comparison with heat pumping systems using secondary fluid circuits, the pumping power should not be overlooked, particularly if a direct-evaporation CO₂ system may offer the same environmental and personal safety.

4. Modified cycles

There are several reasons for modifying the basic single-stage transcritical cycle, including improvement of energy efficiency, increase of capacity for given system and component size, and adaptation of the heat rejection temperature profile to given requirements, e.g. in a heating system. In principle, a large number of possible modifications are possible, including staging of compression and expansion, splitting of flows, use of internal heat exchange, and work-generating expansion instead of throttling. Lorentzen [32] outlined several advanced heat pump cycles and circuits for CO₂, including two-stage cycles, cycles with internal ‘subcooling’ and cycles with expander. In order to reduce the throttling loss and to adapt the heat rejection temperature profile, cycles with two or more compression/throttling stages, internal heat transfer, subcooling, and expansion work recovery can be applied.

The economic viability of the transcritical cycle is enhanced by making use of the high-temperature heat rejected, for example, for domestic hot water in stationary

applications and for reheating/defogging in mobile applications. Theoretically the same options are available in subcritical systems, but the relatively small amount of recoverable high-temperature heat has meant that it is usually wasted. The potential payoff is generally greater in CO₂ systems. Therefore, in transcritical heat pumps many more options exist for reversing flow between heating and cooling modes and for meeting simultaneous loads. Placement of the reversing valves is further complicated by the existence of the internal heat exchanger, where decisions must be made about preferences for counter- vs. parallel flow in heating mode.

4.1. Internal heat exchange cycle

The impacts of liquid-line/suction-line heat exchange on cycle COP have been documented for a wide variety of refrigerants commonly used in subcritical cycles [33]. Two offsetting effects—capacity increase due to subcooling and power increase due to higher suction temperature—combine to produce net thermodynamic benefits for some refrigerants such as R-134a and penalties for others such as R-22. Kim [34] reported that application of the internal heat exchange cycle was beneficial to COPs of all fluids tested (R-22, R-134a, R-407C, R-32/134a), given that the low-pressure refrigerant was superheated in the internal heat exchanger. However, the influences of the internal heat exchange on the system overall efficiency depend on the working fluids and operating conditions. For R-22 and R-134a, the COP was not improved when the heat was transferred to low-pressure two-phase refrigerant (indicated by a low value of superheat leaving the suction-line heat exchanger). For the zeotropic mixtures (R-407C and R-32/134a), COPs were improved even at small values of superheat leaving the suction-line heat exchanger. The benefits of this heat exchange between subcooled high-pressure liquid and two-phase low-pressure refrigerant has been hypothesized in literature [35], but has not been quantified and warrants further investigation. In practical systems there may be some benefits due to improved heat transfer caused by absence of superheating, and higher compressor efficiency due to higher suction temperature.

For CO₂ the benefits are substantial, because the COP-optimizing discharge pressure is lower when an internal heat exchanger is present. Moreover, internal heat exchange brings the capacity- and efficiency-maximizing discharge pressures closer together, creating opportunities for using less precise or simpler control systems and strategies. Second-law analyses of the transcritical cycle demonstrate how the internal heat exchanger increases compressor discharge temperature and consequently the irreversibility of high-side heat rejection from the gas cooler, and introduces a finite temperature difference of its own due to the difference between specific heats of the suction gas and supercritical fluid. However, these inefficiencies are more than offset by the reduction in

throttling loss [36]. In some high-lift applications such as refrigeration or space heating where a highly effective internal heat exchanger may produce compressor discharge temperatures high enough to damage the lubricant, the internal heat exchanger may employ a parallel-flow configuration. In case of given capacity requirement, the reduced high-side pressure needed in a system with internal heat exchanger may give a compressor discharge temperature which is comparable to a system without internal heat exchanger [37].

4.2. Expansion with work recovery

Internal heat exchange is only one option for reducing expansion losses. Another approach is to extract and make use of the work potentially available from the process. Owing to the high throttling loss of CO₂, there is a considerable potential for COP improvement by the introduction of an expander. Several authors have therefore studied this potential.

Regarding cycles and circuits with work-producing expansion, Negishi [38] devised a system based on the Plank cycle [39] where the supplementary pump/compressor is driven by an expander in a self-contained unit. Ikoma et al. [40] suggested another approach that expansion from supercritical state in a single-stage cycle is allowed to continue until near the saturation curve, and a throttling valve controls the remaining pressure reduction down to the evaporator pressure. Thus, the expander operates with a single-phase fluid only.

From a hardware standpoint, the practical challenges are substantial because cooling systems experience a wide range of mass flow rates, requiring a robust design as detailed in Maurer and Zinn [41]. Positive-displacement devices, specifically internal and external gear pumps are theoretically more desirable because of the edge losses inherent in small turbines and even pistons. Research has focused on finding an instantaneous use for the highly variable work output, because of the inevitable losses associated with electric generators and motors. As a result, recent investigations have aimed to explore direct mechanical linkages to the high stage of a two-stage compressor [42–45].

Aside from implementation issues, the recovery of expansion work involves interesting thermodynamic tradeoffs with alternative methods of reducing expansion losses, such as internal heat exchange. A detailed parametric analysis revealed that internal heat exchange could increase cycle COP if the expander efficiency was only 30%, but would substantially decrease COP if the expander isentropic efficiency was 60% [36]. These results were based on a rather large assumed gas cooler outlet approach temperature difference (5 °C), so the impacts would be smaller if the gas cooler were more effective in reducing potential expansion losses (ineffective gas coolers lead to high evaporator inlet quality, hence more potentially

recoverable expansion work). Nevertheless, the results of this parametric analysis reflect a fundamental reality: the large difference in specific heats between the suction gas and supercritical hot stream limit the second-law effectiveness of an internal heat exchanger, even as the first-law effectiveness approaches unity. An expander is subject to no such theoretical limit, only practical ones which have to date made internal heat exchange the technology of choice in prototype and production systems.

Maurer and Zinn [41] conducted a theoretical and experimental study of expanders for CO₂, including axial piston machines and gear machines. Measured energy efficiency reached 40–50% for axial piston machines, and 55% for gear machines. The higher efficiency of gear machines was somewhat unexpected, since these did not have any volume expansion (constant-volume machines). Important reasons for these results were lower friction losses and smaller clearances and leakage losses in the gear machine.

Heyl and Quack [42,46] discussed various cycles with expanders, and showed the design and results of a free-piston expander/compressor concept. The machine had two-double-acting pistons, which were connected by a piston rod. Each piston divided the cylinder into a compression and expansion volumes. In order to achieve a balance of forces over the entire stroke, the expansion was conducted at full pressure, i.e. in a ‘square’ process in the pressure–volume diagram. Thus, only about 78% of the available expansion power could be recovered. The machine was intended as a second-stage compressor (from intermediate to high pressure), driven by the expansion work from high to low pressure.

Nickl et al. [47] proposed the design principle of a rather simple second generation expander–compressor that provided a further 10% increase in COP compared with the first generation machine [42,46] and a 50% improvement over the same system with a throttle valve. They speculated that the discharge pressure of the main compressor could be further reduced.

Hesse and Tiedemann [48] showed the possible use of a pressure wave machine for expansion work recovery in a CO₂ system. The pressure wave machine could compress a part of the vapor from the evaporator outlet by using the expansion energy. Adachi et al. [49] showed a combined axial-piston compressor/expander unit with expansion ratio control means that could keep the high-side pressure at the optimum.

Heidelck and Kruse [50] discussed a conceptual design for a CO₂ expander based on a modified reciprocating (axial piston) machine. The expander needs mechanically controlled valves, and the authors showed a concept using a rotating control disc and slots similar to what is used in hydraulic machines. A design concept for a combined compressor–expander machine in one axial-piston unit was also outlined. Experiments on a modified hydraulic machine gave moderate efficiencies due to internal leakage in

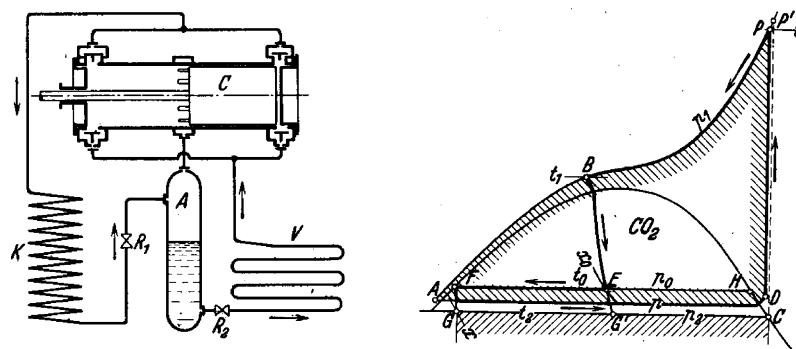


Fig. 24. Voorhees dual-effect compressor circuit (left) and thermodynamic cycle in temperature–entropy diagram (right) [10].

the control disc sealing surfaces. Hesse [51] proposed using a gear machine as expander in CO₂ vehicle air conditioning systems. By using helical gears, acceptable efficiency of the expansion process was predicted.

4.3. Two-stage cycle

The performance deterioration of the basic single-stage cycle can be largely mitigated by using multistage compressors and with intercooling of liquid and vapor refrigerant. In 1905, Voorhees [10] introduced a dual-effect compressor. The principle was that a supplementary suction orifice opened during compression, which allowed the refrigerant to be taken in at two different pressures. Figs. 24 and 25 show Voorhees dual-effect cycle [10], and Plank cycle [39] using an additional ‘pump’ stage near

the expansion valve, respectively. The latter cycle uses two-stage compression, but instead of dividing the pressure rise into two stages, as commonly used, the cycle adds another, higher, pressure level before the compressed refrigerant is cooled. This reduces the enthalpy before throttling, and thus increases the cooling capacity. Due to the high refrigerant density in the second-stage compression, the power requirement is low—almost comparable to a liquid pump. In another publication, Plank [52] found that the intercooling of vapor by evaporation of liquid in a flash intercooler resulted in an increase of COP except for operating conditions near the critical point.

Thiessen [53] devised a two-stage system with single-stage compression, using the intermediate pressure accumulator as a buffer for pressure control. Advantages

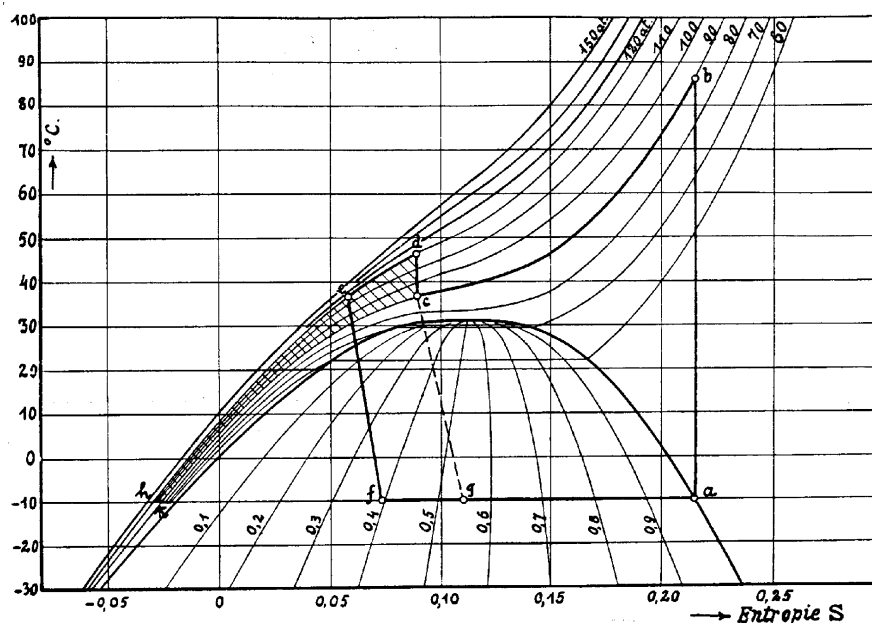


Fig. 25. Plank's two-stage cycle with high-pressure ‘pump’ [39].

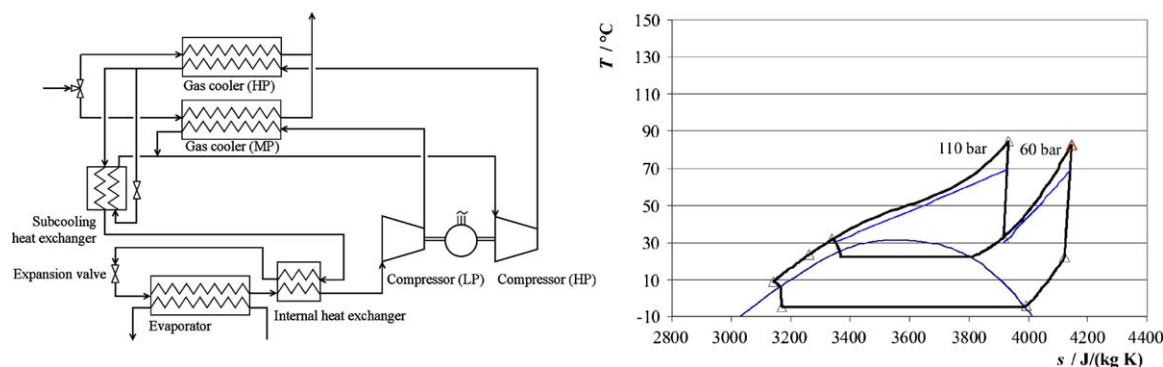


Fig. 26. Two-stage cycle with internal subcooling, internal heat exchange, and parallel heat transfer to heat sink [32,57].

of the concept are claimed to be better liquid distribution to the evaporator, and possibly a better behavior under non-stationary conditions. The need for three control valves is a disadvantage, however.

Ozaki et al. [54] described several circuit arrangements and control principles for cycles having two-stage throttling. By using a 'subcooling' heat exchanger as shown earlier by Lorentzen [32], the COP could be improved while capacity was increased and necessary high-side pressure was reduced. This circuit could have either a low-pressure accumulator or an intermediate-pressure accumulator.

Shunichi and Hiroshi [55] also described some two-stage cycle arrangements, primarily based on conventional circuits for industrial and commercial refrigeration systems. Many similar two-stage concepts are shown by Okaza et al. [56]. Another variant of this two-stage cycle is shown in Fig. 26, in this case with some high-pressure refrigerant being expanded into an internal subcooling heat exchanger operating at intermediate pressure [32,57].

Huff et al. [58] investigated three different variations for a two-stage transcritical CO₂ cycle by using simplified modeling assumptions. A flash cycle, a phase separation cycle, and a split cycle were considered and potential benefits for each cycle with an internal heat exchanger, a suction line heat exchanger, and intermediate

cooling between the compressor stages were studied. They speculated that the split two-stage cycle showed the highest performance improvement (38–63%) over the basic single-stage cycle.

Inagaki et al. [59] also found that the capacity and COP of a CO₂ air-conditioning system were improved significantly by using a two-stage split cycle. The capacity and COP for moderate ambient temperature were improved 35 and 20%, respectively, while the increments of the capacity and COP were 10 and 5%, respectively, for higher ambient temperature conditions.

More advanced two-stage cycles may be of interest both to save compression power but also to adapt the heat rejection temperature glide to a heating system. An example of this concept is shown in Figs. 26 and 27, where compression to 6.0 and 11.0 MPa gives heat rejection temperature profiles that match heating of water from 30 to 70 °C in a hydronic heating network [57]. By using an internal heat exchanger the throttling loss is reduced as discussed above.

4.4. Flash gas bypass

Most prototypes of CO₂ systems have employed small-diameter or flat multiport tubes in evaporators to handle high

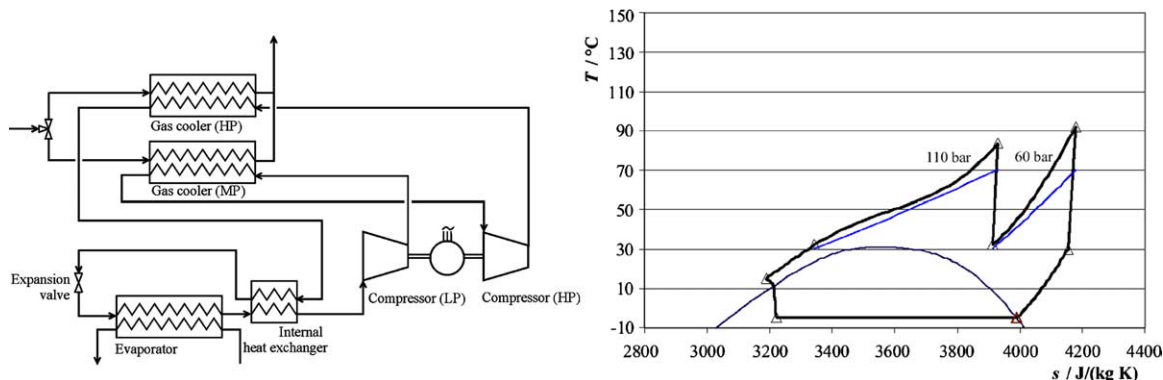


Fig. 27. Two-stage cycle with internal heat exchange and parallel heat transfer to heat sink [57].

pressures without adding weight or bulk. These evaporators face a challenging problem—how to distribute the developing two-phase flow from the header uniformly into so many circuits. Under normal conditions the void fraction at the evaporator inlet exceeds 0.8, and the liquid film and droplets are subject to a complex combination of inertial, gravitational and surface forces inside the header. While this problem is inherent to all microchannel evaporators and is not refrigerant-specific, it is being faced first with CO₂ because its high operating pressures favor the use of small-diameter channels. One approach to dealing with this problem is to install a separator downstream of the expansion device, bypass the vapor around the evaporator, feeding saturated liquid into the evaporator to eliminate altogether the problems of two-phase distribution. This splitting of the flow requires relocating the receiver, for example, from the evaporator outlet where it served to fix the evaporator outlet state to a location upstream of the evaporator where it serves a different purpose. Initial experiments with this approach have proved promising, and are summarized in Section 8.

While these cycle modifications may appear as small changes on a thermodynamic state diagrams, they are nevertheless significant in terms of their effects on improving component performance and increasing the value of services delivered by the system. Often their impacts on control strategies are greater than their impacts on system efficiency. Their benefits and costs tend to be system-specific, as illustrated by many of the prototype systems described in Section 8.

5. Heat transfer and fluid flow

Most studies on heat transfer and pressure drop in CO₂ system have focused on supercritical cooled flow, and flow vaporization, in microchannel tubes and in larger-diameter tubes. The term ‘microchannel’ is used for flowchannels with hydraulic diameter less than 1 mm. Data on condensation of CO₂ are very scarce, and this mode of heat transfer is not discussed here.

5.1. Supercritical-flow heat transfer and pressure drop

Olson [60] measured heat transfer for cooled supercritical CO₂ flow in a 10.9 mm ID (inner diameter) tube. Comparisons were made between the test data and correlations of Gnielinski [61] and a Krasnoshchekov and Protopopov [62] model developed for supercritical fluids. Olson [60] found that the Gnielinski model underpredicted the measured coefficients, and more so when using wall-based property data than bulk-based. The special supercritical model worked well as long as the temperature was above the pseudocritical temperature,

but gave large scattering and overprediction at lower temperatures.

Pitla et al. [63] reviewed the available literature on supercritical CO₂ heat transfer, including:

- Physical factors influencing in-tube forced convection heat transfer
- Deterioration or improvement of heat transfer in the supercritical region
- Effects of buoyancy driven secondary flows on heat transfer in tube flow
- Heat transfer correlations for in-tube flow of a supercritical fluid
- Coefficient of friction of a supercritical fluid, and
- Influence of lubricant on heat transfer

For fully developed flow the supercritical-pressure heat transfer coefficient of CO₂ increases gradually as the flow is cooled, until a peak is reached at the pseudocritical state (maximum isobaric specific heat). Based on the experimental and numerical data of Pitla et al. [63], the use of the Gnielinski heat transfer correlation [61] was suggested, taking the average of calculated coefficient for wall and bulk conditions. Presence of lubricant reduced heat transfer (especially the peak value) and increased the pressure drop.

More extensive investigations of heat transfer in single tubes have been undertaken by several investigators, starting with a thorough literature review [64], to determine whether variations in transport and thermodynamic properties in the vicinity of the critical point have an effect on turbulence and therefore on heat transfer. A detailed model has been developed and verified experimentally for a 5 mm tube [65,66] but at this point there exists insufficient data or reasons to believe that the dependence of heat transfer and pressure drop on fluid properties are not captured adequately by conventional single-phase turbulent flow correlations that have been verified for the appropriate ranges of heat and mass flux and other non-dimensional variables. However, at high heat flux and at conditions close to the pseudocritical state, buoyancy effects and thermophysical property variation may be large, thus making ordinary single-phase correlations incorrect.

Pettersen et al. [67] measured and correlated heat transfer of cooled supercritical CO₂ flow in 0.8 mm microchannel tubes. The standard single-phase correlations such as the widely used Dittus–Boelter model and the Gnielinski correlation [61] gave good correspondence between measured and calculated heat transfer coefficient, and the Colebrook and White correlation reproduced the pressure drop data well.

Recently, Liao and Zhao [27] measured heat transfer coefficients from supercritical CO₂ flowing in horizontal micro/minitubes. Test tubes were stainless steel tubes having inside-diameters of 0.5, 0.7, 1.1, 1.4, 1.55 and 2.16 mm, respectively. A series of test were conducted for

the pressures and temperatures ranging from 7.4 to 12 MPa and 20–110 °C, respectively. The buoyancy force affected supercritical CO₂ flow significantly. The buoyancy effect became smaller as the tube diameter decreased, however. They reported that the existing correlations for larger tubes deviated notably from their test data for the micro/minitubes. Based on the test data, they developed a correlation for the axially averaged Nusselt number with the mean relative error of 9.8%.

5.2. Flow vaporization heat transfer and pressure drop

Bredesen et al. [24] measured heat transfer and pressure drop for flow vaporization of pure CO₂ in a horizontal 7 mm ID (inner diameter) aluminum test tube. The heat transfer test data indicated regimes of convective boiling at high mass flux and low evaporating temperature, and nucleate boiling regimes at lower mass flux and higher temperatures. At most conditions, the local heat transfer coefficient increased up to a vapor fraction of around 0.9, but at the highest evaporating temperature (5 °C), the behavior was quite different, with a decreasing heat transfer coefficient at increasing x . In the latter case ($G = 200 \text{ kg/m}^2 \text{ s}$, $T = 5 \text{ °C}$, $q = 6 \text{ kW/m}^2$), the heat transfer coefficient dropped from about $14,000 \text{ W/m}^2 \text{ K}$ at $x = 0.2$ to about $8000 \text{ W/m}^2 \text{ K}$ at $x = 0.9$. The authors explained this by the high pressure and low liquid/vapor density near the critical point. A comparison to a few common heat transfer correlations gave poor correspondence for all test data, the experimental coefficients being about twice as high as predicted.

Rieberer [14] found that common heat transfer correlations gave considerably higher predicted heat transfer coefficients than his experimental data from a rig where there was some compressor lubricant in the CO₂ flow. Models that gave best fit to the data of Bredesen et al. [24] overpredicted the experimental data of Rieberer [14] by a factor of 3–4. These large differences were probably caused by the presence of lubricant and the data gives some indication of a possible serious impact of lubricant on nucleate boiling heat transfer. Further test data by Rieberer [14] on a 10 mm tube (still including lubricant) shows that the heat transfer coefficient is almost unaffected by a doubling of the heat flux, and that the coefficient increases with mass flux. Both these observations indicate that nucleate boiling is not a dominant mechanism of heat transfer, or that this mechanism is suppressed by a lubricant concentration.

Sun and Groll [68] conducted flow vaporization experiments for pure CO₂ on a horizontal 4.6 mm ID (inner diameter) stainless steel tube. Test data were recorded at CO₂ mass flux between 500 and $1670 \text{ kg/m}^2 \text{ s}$, heat flux $10\text{--}50 \text{ kW/m}^2$ and vapor fraction 0–0.95. Evaporating temperatures were maintained between -2 and $+10 \text{ °C}$. In general, the heat transfer coefficient dropped at increasing x . A more or less abrupt drop in heat transfer above a vapor fraction of 0.4–0.6 was observed in most tests, and was

explained by dryout of the liquid film. The heat transfer was not influenced much by varying mass flux at low vapor fractions, while heat flux variation had significant influence. This was taken as evidence of nucleate boiling as the dominant heat transfer mechanism at lower x . The heat transfer after dryout was influenced by mass flux, indicating a convection-dominated heat transfer.

Hihara and Tanaka [69] conducted measurements on a horizontal stainless steel microchannel test tube with 1 mm internal diameter. The authors measured very high heat transfer coefficients (around $10\text{--}20 \text{ kW/m}^2 \text{ K}$) in the nucleate boiling regime at low vapor fractions. At the onset of dryout the coefficients dropped abruptly to only a small fraction of the nucleate boiling level. Onset of dryout occurred at a vapor fraction of around 0.8 at a mass flux of $360 \text{ kg/m}^2 \text{ s}$, decreasing to 0.4 at a mass flux of $1440 \text{ kg/m}^2 \text{ s}$.

Pettersen [20] conducted extensive studies on flow vaporization in microchannel tubes, using an aluminum test tube with 25 channels having 0.81 mm diameter. Vaporization heat transfer and pressure drop data were recorded over a wide range of conditions, including temperatures (0–25 °C), heat flux ($5\text{--}20 \text{ kW/m}^2$), mass flux ($190\text{--}570 \text{ kg/m}^2 \text{ s}$), and vapor fraction (0.2–0.8). Test results showed that the nucleate boiling mechanism dominated at low/moderate vapor fractions. Dryout effects became very important at higher mass flux and temperature, where heat transfer coefficient (h) dropped rapidly at increasing vapor fraction (x). Heat transfer coefficients were correlated using a combination of models for nucleate boiling, convective evaporation, dryout inception, and post-dryout heat transfer.

Microchannel frictional pressure drop was correlated using the ‘CESNEF-2’ correlation by Lombardi and Carsana [70], with a mean/average deviation of 16.4/–1.1%. Special small-tube correlations from literature did not reproduce the test data well.

5.3. Two-phase flow patterns

Pettersen [20] conducted experiments for two-phase flow patterns at a temperature of 20 °C and for mass flux ranging from 100 to $580 \text{ kg/m}^2 \text{ s}$, using a heated glass tube with 0.98 mm ID. The observations showed a dominance of intermittent (slug) flow at low x , and wavy annular flow with entrainment of droplets at higher x . At high mass flux, the annular/entrained droplet flow pattern could be described as dispersed. The aggravated dryout problem at higher mass flux could be explained by increased entrainment. Stratified flow was not observed in the tests with heat load. Bubble formation and growth could be observed in the liquid film, and the presence of bubbles gave differences in flow pattern compared to adiabatic flow.

The flow pattern observations on CO₂ did not fit any of the generalized maps or transition lines, including the map proposed by Kattan et al. [71]. Only the intermittent–annular

transition prediction of Weisman et al. [72] was close to the observed behavior. Compared to small-diameter observations with air/water at low pressure, the transition into annular flow occurred at much lower superficial vapor velocity (superficial velocity of approximately 0.5 m/s).

6. Issues related to high operating pressure

Pressures in CO₂ systems are typically 5–10 times higher than with conventional refrigerants, and this gives several effects that influence the design of components and their performance, in particular regarding compression and compressor design, and heat transfer and heat exchanger design. In addition, high pressure may create perceived safety problems unless the underlying issues are addressed properly.

6.1. High pressure compression

Compressors in CO₂ systems will operate at high mean effective pressure and with large pressure differentials, but the pressure ratios will be quite low due to operation close to the critical point. Fig. 28 indicates ideal (with 4% clearance volume) pressure/volume diagrams for compression of R-134a and CO₂ with equal cooling capacity at 0 °C [31]. As may be observed, the displacement of the R-134a machine is 6.7 times larger, and the pressure ratio (π) is 5.0 as compared to 3.1 with CO₂. Re-expansion losses are much smaller in CO₂ process. Owing to the higher pressure level and the different shape of the pV -diagram, the negative effect of valve pressure drops tends to be small in CO₂ compressors, thus giving higher efficiency. The compressor for the transcritical CO₂ cycle requires thicker walls to contain the high operating pressure, but since the volumetric capacity of the fluid is large, the compressor itself will

actually be smaller than refrigeration compressors for the same capacity using conventional refrigerants [73].

Internal leakage losses in valves and as piston blow-by were initially expected to be a problem with the large pressure differentials in CO₂ compressors. With appropriate design it has been shown that these losses account for less than 1% difference in cylinder charge compared to a zero leakage model [74], leading to the conclusion that the influence of leakage can be neglected in properly designed lubricated reciprocating compressors. This conclusion is supported by other investigations [75] measuring piston blow-by rates of 1.1–2.8% of the compressed mass flow at 9.0/3.5 MPa discharge/suction pressure.

6.2. High pressure heat transfer

Tolerable pressure drops in heat exchangers become higher as the pressure level increases, and this gives a possibility of improving heat transfer through higher flow velocities in high-pressure systems. This is of particular importance for single-phase heat transfer in the gas cooler of CO₂ systems. High pressure and proximity to the critical point gives increased specific heat, again leading to improved convective heat transfer.

Evaporator pressure drop leads to reduced temperature differences due to the corresponding drop in saturation temperature. Pettersen [31] showed how the relation between pressure drop and temperature loss in evaporators, i.e. the slope of the saturation pressure curve, was very different for CO₂ than for conventional refrigerants, since the pressure level of CO₂ was much higher. Nucleate boiling heat transfer is also affected to a large extent by pressure, since the wall superheat needed to initiate boiling becomes lower as the critical pressure is approached.

Owing to the higher pressures, optimum compact heat exchanger designs for CO₂ generally tend to use small-diameter flow channels, in many cases based on extruded ‘multiport’ tubing with parallel flow of refrigerant in several tubes and flow channels. In some cases it may be more economical to use conventional flat-fin/round-tube heat exchangers with small-diameter tubes. Also in this case, the internal diameter will most likely be smaller than for conventional refrigerants. Pettersen et al. [76] showed some compact heat exchanger concepts for CO₂ air conditioning systems having internal tube diameter of 2 mm.

6.3. Compactness of equipment

Low-side refrigerant line diameters (inner diameter) are typically reduced by 60–70% compared to HFC systems, due to the higher vapor density and flow velocity. High-side piping dimensions will also be reduced. Assuming a wall thickness that is more or less the same as in HFC piping of equal capacity, the pressure capability will be sufficient for CO₂ due to the reduced diameters

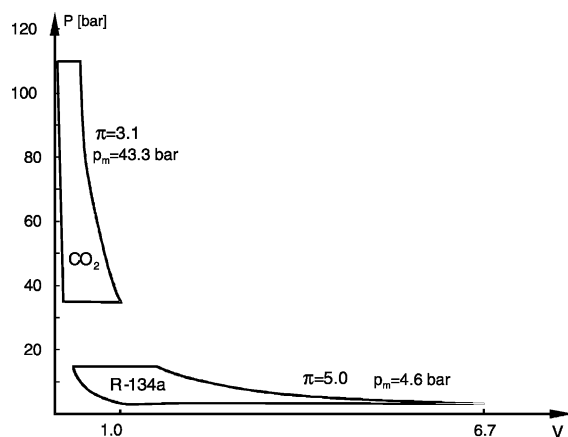


Fig. 28. Compressor pressure/volume diagrams for R-134a and CO₂, assuming equal cooling capacity (π : pressure ratio, p_m : mean effective pressure).

(inner diameter). For the same reasons as above, the compressor displacement is reduced by 80–85% for a given capacity. Compressor and heat exchanger size and weight reductions seem possible due to the reduced refrigerant-side volumes and cross-sections.

6.4. High-pressure safety issues

In general, the hazards of refrigerants and vapor compression systems are associated with the physical and chemical characteristics of the refrigerant as well as with the pressures and temperatures occurring in the system. Factors discussed by Pettersen et al. [77] in relation to CO₂ were

Flammability. CO₂ is non-flammable, and it is even used as a fire-fighting or fire-preventing gas. Thus, flammability is not an issue.

Inhalation safety. Although CO₂ is usually regarded as non-toxic there are physiological effects from breathing air with a CO₂-concentration above a few percent. At 2–3% concentration by volume, the breathing rate will increase, and headache may be experienced after some time. The IDLH (Immediate Danger to Life and Health) concentration is set to 4% [78], and the lowest reported lethal concentration is 10% [79]. In practice, a maximum allowable concentration of about 5% by volume seems to be a reasonable limit [79,80]. In the design and operation of CO₂ systems, this will be the maximum acceptable concentration as a result of sudden release or prolonged leakage of CO₂ into occupied space. The assessment of hazards resulting from accidental leakage of CO₂ into occupied space should consider factors like

- rate of CO₂ outflow at decreasing system pressure,
- formation of dry ice inside system at 0.52 MPa system pressure,
- amount of CO₂ dissolved in lubricant,
- room/cabin ventilation rate, and
- stratification (CO₂ is heavier than air).

Frost burn is probably not a problem with CO₂ since the triple point is at 0.52 MPa, i.e. there will be no boiling refrigerant at atmospheric pressure. Also, the toxic or irritating effects from decomposition products known to occur when fluorocarbon refrigerants contact flames or hot surfaces will not occur with CO₂.

Explosion or rupture of a pressurized component or vessel. The hazards may include blast effects and shocks, as well as flying fragments. Such incidents may be caused by a number of factors, such as malfunctioning safety device, overheating, over-charging, incorrect operation, construction weakness/corrosion, mechanical impact, etc. Low-side pressures in CO₂ systems are typically 3–4 MPa, and high-side pressures may be as high as 12–14 MPa. These pressures are 5–10 times higher than in traditional fluorocarbon systems. High pressure is not a safety issue in

itself, since the equipment will be designed for this. In case of a component rupture, however, the explosion energy (stored energy) may characterize the extent of potential damage. The explosion energy can be estimated based on component (refrigerant-side) volumes, pressures and refrigerant property data. The possible occurrence of a BLEVE (Boiling Liquid Expanding Vapor Explosions) may create a more severe blast effect than by an ordinary refrigerant expansion. The following sections will address the two last issues—explosion energy and BLEVE—based on calculations and experimental data.

6.4.1. Explosion energy

The explosion energy can be estimated as the energy released by expansion of the refrigerant contained in a component or system. The expansion process will be very rapid, with little or no time for heat transfer between the ambient air and the expanding gas, and the explosion energy can therefore be estimated as the reversible adiabatic (isentropic) work of expansion.

A detailed analysis of explosion energies should consider the refrigerant charge inside each component, as well as the local pressure, temperature and vapor fraction. In the current analysis, pressures are assumed to be equalized and temperatures uniform throughout the system. As a consequence, the charge and volume are assumed to reflect the refrigerant condition inside the entire system. When the temperature of the system is varied, the charge/volume ratio will remain constant (constant average specific volume), and pressure will vary either as saturation pressure, or as pressure along a constant-volume (isochoric) line in the gas region.

Pettersen [81] calculated and compared the explosion energies of equal-capacity (7 kW) ductless split residential air conditioning systems with R-22 and CO₂ as refrigerant. The R-22 system was based on flat-fin/round-tube heat exchangers, while the CO₂ prototype system had all-aluminum microchannel heat exchangers. Even though pressures were higher in the CO₂ system, reductions in internal volume and refrigerant charge gave comparable energy levels in the two systems. At room temperature, the CO₂ system energy was higher, while at elevated temperature that may occur in a fire the R-22 energy was highest. For the R-22 system, the total volume occupied by refrigerant was approximately 11.4 l, of which 0.7 l (6%) was in the indoor unit and 8.5 l (75%) in the outdoor unit. The remaining volume was in the 10 m of piping between the two units. The average refrigerant density in the system was then 300 kg/m³ (3.5 kg charge/11.4 l refrigerant volume). Corresponding data for the CO₂ prototype system were: 4.2 l total volume, 0.27 l (6%) in the indoor unit and 3.3 l (78%) in the outdoor unit, and an average charge density of 260 kg/m³ (1.1 kg/4.2 l). Fig. 29 shows the total explosion energies (in kJ) for the two systems at varying initial temperature. The energies are equal around 60 °C,

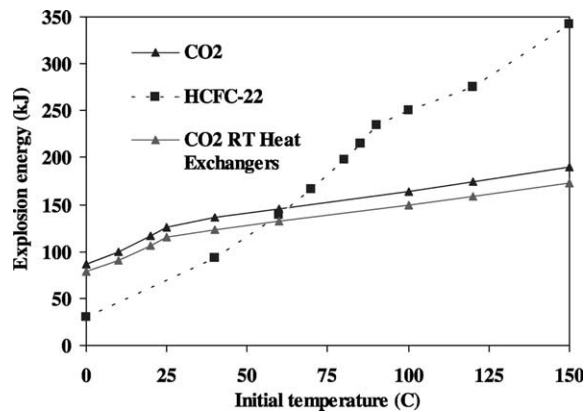


Fig. 29. Calculated total explosion energy for R-22 system and CO₂ system at varying initial temperature. Data for a CO₂ system with optimized round-tube (RT) heat exchangers is also shown [81].

but the R-22 system energy is more sensitive to temperature than the CO₂ system.

The above system data show that owing to the smaller volume and refrigerant charge in a CO₂ system, the actual explosion energies are in the same range. As may be observed from Fig. 29, the ratio of energies (CO₂/R-22) is about 2 at room temperature, and 0.7 at 100 °C. The difference in energy becomes significant at temperatures above 120–130 °C, and in an extreme situation such as a fire, the energy release from a R-22 system is likely to be much higher than from a CO₂ system. In both systems the refrigerant volume in the indoor unit is only about 6% of the total volume, so the largest potential energy release is clearly in the outdoor unit containing the accumulator, receiver (R-22 system) and compressor.

Calculations for R-134a and CO₂ mobile air-conditioning systems showed similar results [82]. The CO₂ system explosion energy typically ranged from 40 to 80 kJ, while the baseline R-134a system ranged from 20 to 80 kJ. Again, the baseline system energy was smaller at normal temperatures, but became higher at elevated temperature. Although, an explosion caused by the combustion of a flammable refrigerant is an entirely different scenario, it may be worthwhile to note that the energy released by combustion of one kilogram of propane (R-290) is 46,000 kJ (lower heating value).

6.4.2. Boiling liquid explosion

The duration of the energy release may be of equal importance as the amount of energy released. An important consequence of a possible explosive vaporization is shorter duration and thereby a more severe blast effect than from ordinary refrigerant expansion, even though the energy is the same. In the assessment of safety issues, the possible occurrence of rapid phase transition phenomena is important. Mechanisms of explosive vaporization discussed in the literature include BLEVE and BLCBE (*Boiling Liquid Collapsed Bubble Explosion*). These phenomena

may occur when a vessel containing a pressurized liquid or supercritical fluid is rapidly depressurized, e.g. due to an initial crack or rupture. The sudden depressurization gives a superheated liquid phase that is suddenly vaporized in an explosive manner. This may give a transient overpressure peak inside the vessel, which again may lead to a powerful burst of the whole vessel, with total loss of content, a resulting blast wave and risk of flying fragments. Pettersen and Hakenjos [83] and Pettersen [84] investigated the possible occurrence of BLEVE/BLCBE in CO₂ vessels.

An important reason for considering the possible occurrence of BLEVE with CO₂ is a paper by Kim-E and Reid [85], which pointed to this possibility. The authors applied a thermodynamic model based on the spinodal fluid state, which represents the limit-of-stability for the liquid phase during expansion. In a rapid expansion process, homogeneous nucleation will occur at this state. The predicted shock effects or pressure spikes did not occur in their experiments on CO₂ using a 7-l tank with a 1.5 in. diameter burst disc, however. Reasons for disagreement between theory and experiments may include factors like vapor bubbles on the wall of the vessel and shock waves or disturbances from the mechanism that ruptured the burst disc of the test vessel. The presence of vapor bubbles before depressurization may have given heterogeneous nucleation instead of the homogeneous nucleation required for a BLEVE.

In the general literature on BLEVE, a majority of publications discuss hydrocarbon (LPG, propane) tank explosions. The key safety issues in such incidents are the ignition and combustion of the flammable content when this is vaporized, creating severe damage due to shock waves and burning. Usually, this situation arises due to a fire near the tank or due to an ignition source that starts an explosion of the escaped gas/vapor cloud. The concept of a ‘cold’ BLEVE is not much focused on, and the few publications that report accidents with CO₂ storage tanks generally do not mention BLEVE effects [86,87].

Pettersen and Hakenjos [83] and Pettersen [84] reported from extensive experiments on a CO₂ test vessel of 1.0 l volume, using burst discs to initiate rapid depressurization. They did not observe significant overpressure spikes in any of their tests at 3.5, 4.5, 6.0 and 10.0 MPa initial pressures with varying liquid fill level and discharge opening, although quite large pressure oscillations in a millisecond-scale occurred in some experiments. The maximum observed pressure amplitude was 0.6 MPa, and the maximum overpressure spike was 0.3 MPa (7% above initial pressure). The authors found that thermal shock effects on the pressure sensors were significant and had to be avoided or corrected for. What initially appeared to be significant overpressure spikes later turned out to be a result of thermal shock caused by the top pressure sensor being contacted by the swelling cold liquid inside the test vessel. It is not clear if similar thermal shock effects have influenced overpressure spikes reported by other authors. Graphs shown by Venart

and Ramier [88] for a 2.4 l R-22 vessel, for instance, have a quite similar shape to graphs from the present tests before the top pressure sensor was insulated. The results have thus not given any reason to expect BLEVE in CO₂ system accumulators or receivers. In real systems the presence of compressor lubricant, particles and contaminants, as well as unstable pressure/temperature, would make homogeneous nucleation even less likely.

Graz and Stenzel [89] outlined a new draft SAE safety standard (J639) for mobile air conditioning and heat pump systems, also including CO₂. Proposed rules for CO₂ (R-744) included:

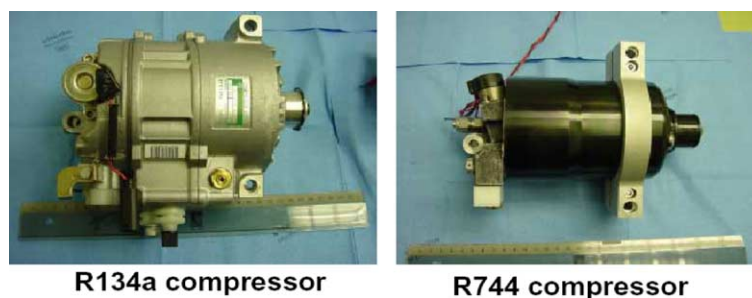
- Carbon dioxide (CO₂) air-conditioning systems and integrated systems for heating and cooling (heat pumps) shall have a pressure blow-out disk as the overpressure relief device on both the high and low-pressure sides of the system when operating in the heating or cooling modes. The blow-out disc on the high-pressure side shall have a maximum allowable release pressure of 16 MPa, when the system is operating in the cooling mode and a maximum allowable release pressure of 12 MPa when the system is operating in the heating mode. The blow-out disc on the low-pressure side shall have a maximum allowable release pressure of 12 MPa, when the system is operating in the heating or cooling modes.
- Components on the high-pressure side of the system shall have an ultimate burst pressure, when tested at the highest temperature reached by said component under typical operating conditions, which is not less than two times the release pressure of the Pressure Relief Device. In addition, components on the high-pressure side of the system shall have an ultimate burst pressure, when tested at the highest temperature reached by said component under typical operating conditions and after appropriate exposure to the system operating conditions (temperature, pressure, pressure cycling, vibration, corrosion), that is not less than 1.5 times the release pressure of the Pressure Relief Device.
- Components on the low-pressure side of the system shall have an ultimate burst pressure, that is not less than two times the release pressure of the Pressure Relief Device.

- For safety relevant pressurized components of air-conditioning systems and integrated systems a proof of integrity shall be carried out (by calculations, experiments or by a combination of both). Basis is the knowledge about the operational loadings and demanded lifetime of the components as well as of the specific behavior of the used structural material and its process treatment. The proof of integrity shall be carried out against (i) bursting, (ii) failure by fatigue, respectively, creep fatigue due to cycling pressure (pressure cycles between the conditions: system ‘in operation’—‘out of operation’, and (iii) failure by cruising vibrations. Creep fatigue instead of fatigue only has to be considered in case of some structural materials (e.g. aluminum alloys) which point out a time and temperature dependent behavior yielding to a decrease in strength over the time at elevated temperatures.

7. Component design

7.1. Compressors

The vapor pressure of CO₂ is higher than conventional refrigerants and the transcritical CO₂ cycle operates at much higher pressures than the conventional vapor compression systems. Higher pressure gives special requirements regarding the design of suitable components, especially compressors for the CO₂ systems. As the compressor is one of major components of air-conditioning and refrigeration systems and has an important effect on the system performance, compressor technology for the CO₂ transcritical systems has reached an advanced level after years of development. Some examples are recent compressor models shown by Parsch [90], and Bullard [91]. Parsch [90] exploited the potential for a compact design with CO₂ as shown in Fig. 30. Fig. 31 shows a 155 cm³ R-134a compressor next to a 21 cm³ CO₂ compressor [91]. The relationship between a compressor's mass and its displacement rate is not an obvious one, and will depend on specific design tradeoffs involving piston diameter and stroke and number, rpm, materials, etc. There is no evidence at the present time to suggest that



R134a compressor

R744 compressor

Fig. 30. Mobile air-conditioning compressors with variable displacement. State-of-the-art R-134a design (left) and a recent design for CO₂ (right) [90].

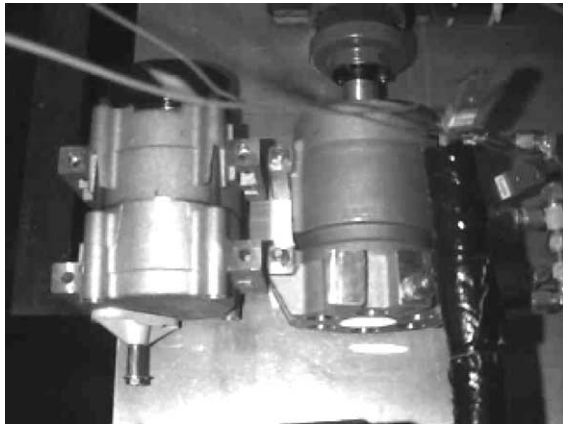


Fig. 31. A 155 cm³ R-134a compressor (left) next to a 21 cm³ CO₂ compressor (right) [91].

switching to higher-pressure refrigerants for their capacity advantages would necessarily entail substantial weight penalties in the compressor.

Fagerli [92] evaluated the possibilities for transcritical compression of CO₂ in small hermetic reciprocating compressors, through a theoretical and experimental study. A single-cylinder 2.6 cm³ hermetic prototype machine with flanged shell was built and instrumented, using some parts from a R-22 machine. Measured isentropic efficiencies for the CO₂ compressor were 9–15% lower than the R-22 machine, while volumetric efficiency was less than 5% lower. These results were considered as promising considering the early stage of development. Theoretical models indicated a potential for higher energy efficiency with CO₂ than with R-22. Lubricant temperatures were acceptable at 15 and 0 °C evaporation, while at –15 °C oil cooling was necessary. Fagerli [92] used mineral oil and had to use a three times higher viscosity grade than for the R-22 machine due to the viscosity reduction caused by dissolved CO₂.

Süss and Kruse [93] reported that high compressor performance could be achieved due to the lower pressure ratio of the transcritical compression process with CO₂. Leakage may have strong influence on the CO₂ compressor performance since the pressure difference is extremely high,

but the effect of leakage on the compressor performance can be reduced to a reasonable amount with an appropriate design of the machine. On the other hand, the pressure losses inside a CO₂ compressor have a small influence on the energetic and volumetric efficiency of the compression process.

Süss [94] was quite concerned about internal leakage losses in CO₂ compressors, and did not leave rotary designs (scroll, rotary vane, and rolling piston) much chance for achieving acceptable efficiency. His primary focus was thus reciprocating compressors with piston rings.

Nekså et al. [95] developed a series of semi-hermetic reciprocating CO₂ compressors in the range of 1.7–10.7 m³/h swept volume. The series comprises single- and two-stage compressors with two cylinders, running at nominal speeds of 1450 and 2900 rpm (50 Hz). This corresponds to cooling capacities in the range of 3–25 kW at –10 °C evaporating temperature. Measurements of compressor efficiencies were presented for a single- and a two-stage compressor in the lower capacity range of the compressor series. The isentropic and volumetric efficiencies were relatively good, taking into consideration that this was a pre-series compressor. At a pressure ratio of 2.6, which was representative for a heat pump water heating application, overall isentropic (including electric motor) and volumetric efficiencies of 0.69 and 0.77 were measured for the single-stage compressor, respectively. There was some leakage in both valves, however, and the stiffness of the discharge reed valves had to be reduced, in order to avoid valve fluttering. Attention should also be given to reduce heat transfer to the suction gas, which may reduce the efficiencies significantly at high pressure ratios.

Measurements on a two-stage version of the compressor [96] showed a potential for 20% COP improvement. This machine was intended for lower-temperature applications, e.g. in commercial refrigeration at freezing temperatures. Two-stage compression may also be of interest in relation to energy saving in air conditioning and heat pump processes, however. Polyolester (POE) lubricant was used in both versions of the compressor.

Suzai et al. [97] and Tadano et al. [98] developed a hermetic two-stage rolling piston compressor (Fig. 32) with a nominal power of 750 W. Compressing in two stages and letting the pressure inside the shell correspond to

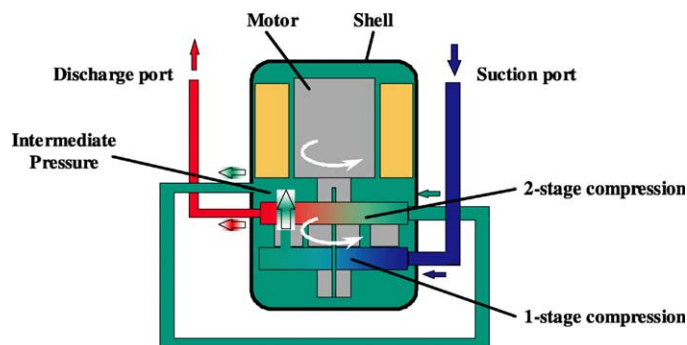


Fig. 32. Schematic of a hermetic two-stage rolling piston CO₂ compressor [98].

Table 2

CO₂ compressor developments in Japan [106]

Companies	Field	System	Compressor	
Denso	Mobile air-conditioning	Direct expansion	Open-type	Swash
Zexel				Swash
MHI				Scroll
Sanyo	Tap water heat pump	Direct expansion	Hermetic	Rotary
TEPCO, Denso and CRIEPI				Scroll
Mayekawa	Commercial	Indirect ice storage	Hermetic	Screw
Matsushita	Residential	Direct expansion	Hermetic	Scroll
Daikin				Swing

the intermediate pressure could reduce internal leakage losses. The machine also became better balanced by having two rolling pistons in 180-degree phase difference. The shell design was comparable to compressors for room air conditioners, and by using high-strength steel the shell could withstand 25 MPa pressure with the same thickness as for R-410A compressors.

Fukuta et al. [99] analyzed the potential for sliding vane machines in CO₂ compression and expansion. Through a mathematical model the influence of various design parameters were analyzed. Leakage flows were the dominant source of losses in the machine, and clearances had to be reduced compared to conventional machines in order to get acceptable efficiency. Vane contact forces and resulting friction losses were high, but could be reduced by pressure equalization on the vane sides. An interesting option was to build a combined compressor/expander unit.

Hiwada and Hokotani [100] and Ohakawa et al. [101] suggested the use of a swing type rotary compressor in what appears to be an air-source heat pump water heater using CO₂ as refrigerant.

Fagerli [102] conducted a theoretical study on scroll compression of CO₂, finding that reduced clearances and axial/radial compliance were needed in order to limit internal leakage flows. Calculations for 134a and CO₂ compressors showed that in order to have equal influence from leakage on energy efficiency the clearances had to be reduced to less than half in the CO₂ machine.

Hasegawa et al. [103] conducted an experimental and theoretical study of a hermetic CO₂ scroll compressor of cooling capacity of 4.3 kW. The compressor displacement was 7.23 cm³. Relatively low energy efficiency (47%) was measured, while the volumetric efficiency (87%) was quite good. A loss analysis showed that the thrust bearing accounted for approximately 40% of the total loss, and the design of this part had to be modified.

Denso Corporation [104] has developed a single-stage semi-hermetic scroll compressor, but any details on this machine have not been published.

Baumann and Konzett [105] has been developing an oil-free four-cylinder reciprocating compressor prototype

with about 500 W power input. Experiments have shown acceptable energy efficiency. A major issue is cost of production due to materials and tolerance requirements.

Süss [106] aims to produce a complete range of machines working with hydrocarbons and CO₂ both for air conditioning and refrigeration. A design study considered a hermetic single-cylinder reciprocating compressor. Süss [106] gave a summary of compressor developments in Japan as shown in Table 2.

The screw compressor by Mayekawa (MYCOM) is a larger machine built for a prototype system of 120 kW cooling capacity. According to Sasaki et al. [107] the compressor is an open-type screw, so the information on a hermetic screw compressor in the table is most likely an error.

The European company Dorin developed the first high-pressure semi-hermetic CO₂ compressor series in the range of 1.7–10.7 m³/h swept volume [108]. The series comprises single- and two-stage compressors with two cylinders, running at nominal speeds of 1450 and 2900 rpm (50 Hz). This corresponds to cooling capacities in the range of 3–25 kW at –10 °C evaporating temperature. Fig. 33 shows a picture of the compressor, and measured overall isentropic and volumetric efficiency figures for medium sized compressors at the current stage of development [108].

7.2. Heat exchangers

Heat exchangers for mobile and unitary equipment are designed with a finned air-side surface and usually have more than 700 m² surface area per m³ core volume. This ratio is the loosely defined limit for a compact heat exchanger. The heat exchangers may be mechanically expanded flat-fin/round-tube units or brazed aluminum cores, in both cases various enhancements are used on the air and refrigerant side as shown in Fig. 34.

The high working pressure and favorable heat transfer properties of CO₂ enable reduced tube diameters and small refrigerant-side surface areas. Since these reductions may give room for more air-side surface per unit core volume, the compactness can be increased. Depending on the heat

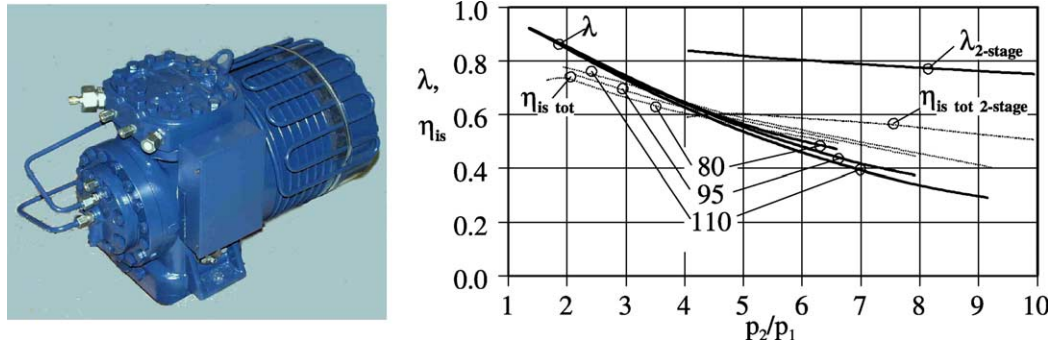


Fig. 33. Compressor design and measured volumetric and isentropic efficiency for a single-stage and a two-stage pre-series CO₂ compressor with a swept volume of 2.7 m³/h, as function of the pressure ratio, for high-pressures of 80, 95 and 110 bar. A constant suction gas superheat of 10 °C was applied. For the two-stage compressor the intermediate pressure gas was cooled to 20 °C [108].

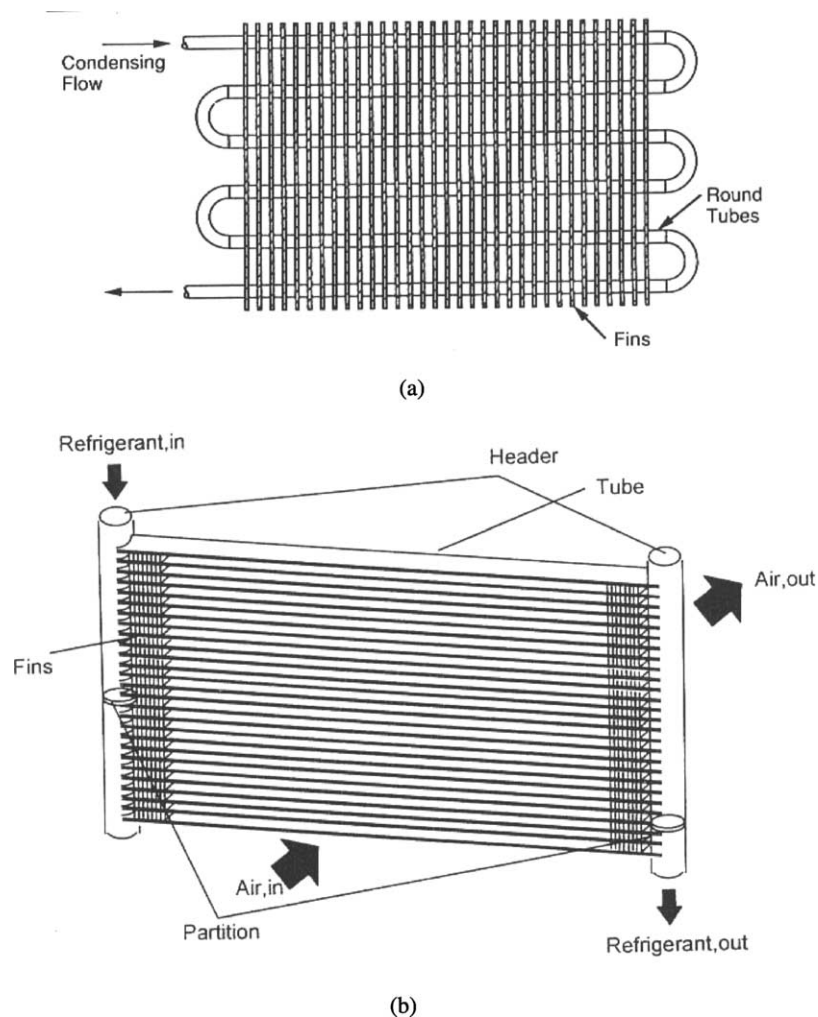


Fig. 34. Fin-and-tube and brazed aluminum microchannel condensers. (a) Serpentine circuited round-tube condenser, (b) parallel flow brazed aluminum automotive air-cooled condenser.

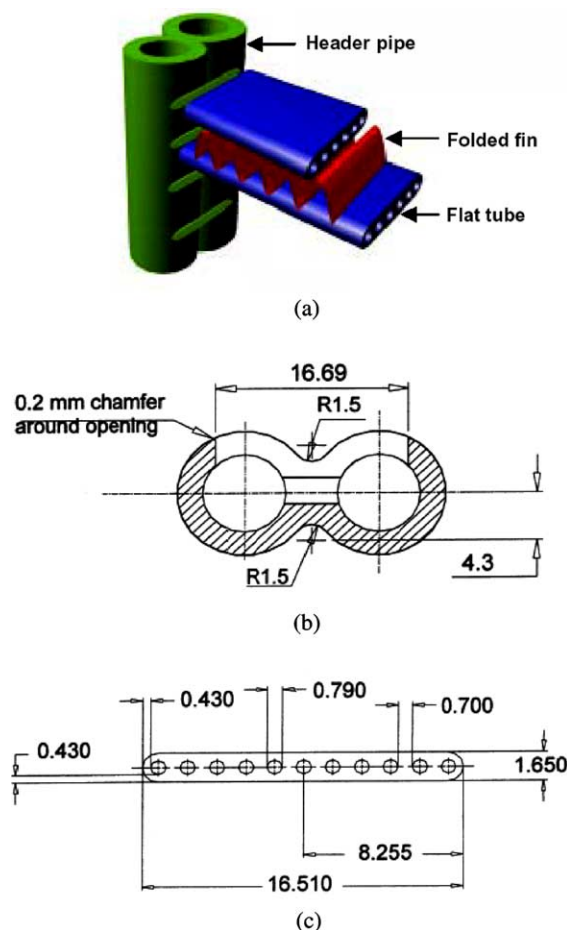


Fig. 35. A prototype microchannel CO₂ gas cooler for a car air-conditioning system [76]. (a) Geometry of heat exchanger, (b) cross-section of header pipe, (c) flat microchannel tube.

exchanger type, the size and mass of high-pressure manifolds or headers may offset some of these advantages. Innovative solutions that benefit from reduced refrigerant-side volume are therefore needed.

Pettersen et al. [76] reported microchannel heat exchangers (gas cooler and evaporator) could be used for CO₂ air-conditioning systems, but several issues remained to be investigated, including frosting formation of outdoor heat exchangers and condensate drainage at low face velocity, for residential systems. Figs. 35 and 36 show gas cooler and evaporator configuration designed by Pettersen et al. [76]. Even though small-diameter round-tube heat exchangers can achieve low weight and compact design for a high-pressure fluid like CO₂, the added performance and compactness of brazed microchannel heat exchangers make these very attractive especially in transport applications.

7.2.1. Gas coolers

To handle the high pressures associated with the CO₂ cycle many CO₂ systems employ heat exchangers with flat multiport (microchannel) tubes as shown in Fig. 35. This technology, with its folded louvered fins, provides additional benefits as a byproduct. Compared to conventional flat-fin/round-tube designs, microchannel heat exchangers increase refrigerant-side area by about a factor of three, and have far less air-side pressure drop due to the streamlined profile presented by the tubes. The flat tubes enable higher face velocities that increase the air-side heat transfer coefficient. Because of high investment costs, microchannel heat exchangers for fluorocarbon refrigerants have appeared first in high-volume applications where compactness is valued.

The flat-fin/round-tube condenser technology for mobile air-conditioning system has now been mostly replaced in automotive applications by flat-tube microchannel condensers as shown in Fig. 34(b). The difference in free flow area

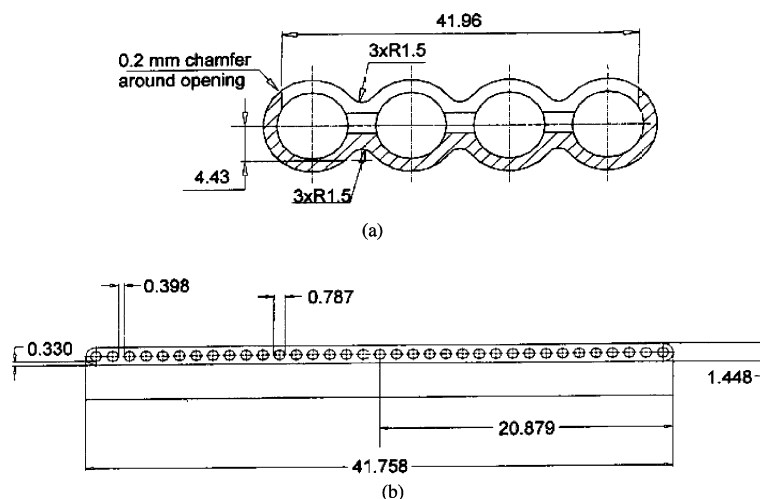


Fig. 36. Cross-section of the header pipe and microchannel tube of a prototype CO₂ evaporator for a car air-conditioning system [76]. (a) Cross-section of header pipe, (b) flat microchannel tube.

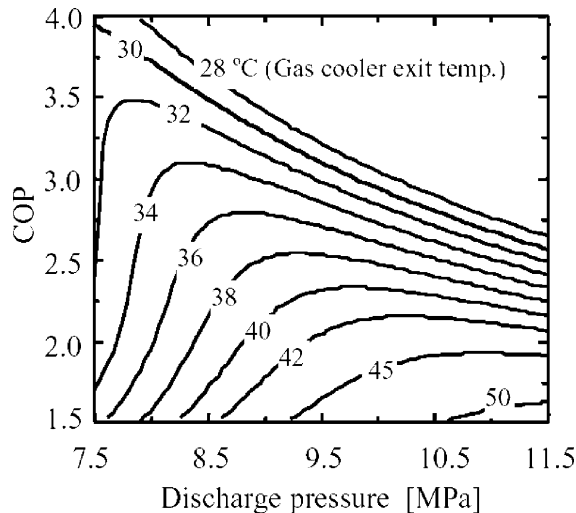


Fig. 37. Effect of gas cooler exit temperature on transcritical cycle COP for realistic high-side pressures.

is obvious, owing to the fact that the flat tubes are usually less than 2-mm thick. What they have in common is their single slab cross-flow configuration that exposes all tubes to the inlet air. Some of the early theoretical analyses of CO₂ system performance assumed that both indoor and outdoor heat exchangers would be of conventional flat-fin/round-tube design [36].

One issue in compact gas cooler design is internal conduction due to large temperature differences across small lengths. As pointed out by Pettersen et al. [76] internal conduction in fins, tubes and manifolds may lead to performance reduction. Solutions to avoid these problems include splitting of fins, use of several heat exchanger sections, and careful design of manifold geometries.

In the transcritical CO₂ cycle, system performance is very sensitive to gas cooler design. A small change in refrigerant exit temperature can produce a large change in gas cooler exit enthalpy (and evaporator inlet enthalpy) because specific heat becomes infinite at the critical point. Fig. 37 shows how COP can be increased 11% and

the COP-optimizing discharge pressure reduced 0.5 MPa by a gas cooler in an automotive air-conditioning system ($T_0 = 3.9$ °C; IHX effectiveness 0.8) that cools the refrigerant exit an additional 2 °C [109]. This indicates that a CO₂ transcritical cycle is so sensitive to the refrigerant exit condition that a counterflow configuration is important for the gas cooler to exploit the large refrigerant-side temperature glide. Moreover, the steep refrigerant temperature glide allows for ideal cycle efficiency to be achieved at finite air flow rate, in contrast to the infinite air flow required to achieve ideal efficiency in the subcritical cycle.

Yin et al. [110] validated a gas cooler simulation model using measured inlet data for a diverse set of 48 operating conditions, predicting refrigerant outlet temperature within ± 0.5 °C for most of the experimental data. They proposed a multislab gas cooler design (Fig. 38(b)), and reported the new design offered better performance than the commonly used multipass design (Fig. 38(a)). For the given heat exchanger volume, they reported that a newly designed cross-counter flow gas cooler could be improved system capacity and COP by 3–4 and 5%, respectively, compared to the old design (Fig. 38(a)). Additional details on the selection of heat transfer and pressure drop correlations may be found in [67,111–113]. The model was used to design the next-generation prototype gas cooler shown in Fig. 38(b), where a multislab overall counterflow configuration concentrates the cool air stream on the exiting refrigerant, because the transcritical cycle is so sensitive to this exit condition [31,113,114]. The new gas cooler design achieves approach temperature differences < 2 °C at most operating conditions because air flowing over the first slab undergoes only a small temperature change, and that ΔT is what places an upper bound on the approach temperature difference [109]. The flat tubes are vertical in this prototype, to facilitate condensate drainage and defrosting in heating mode. Finally, the refrigerant flows in a single pass from the inlet to outlet, with no intermediate headers, to accommodate reversibility and facilitate refrigerant distribution in heating mode. It is clear that flat tubes must be oriented vertically for any air-source heat

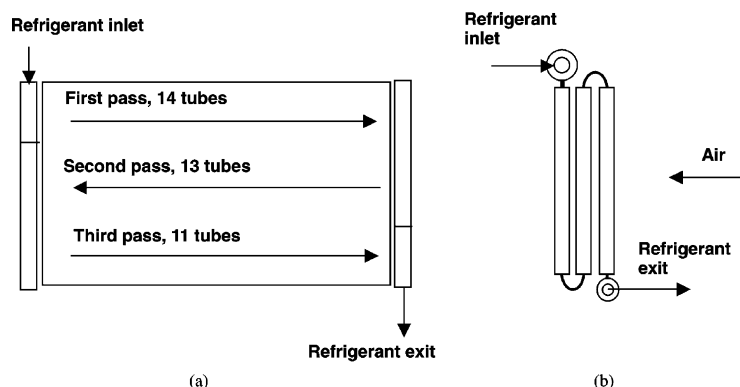


Fig. 38. Gas cooler design for a CO₂ air-conditioning system [110]. (a) One-slab three-pass design, (b) three-slab one-pass design.

pump, for reasons of defrost and condensate drainage, because both indoor and outdoor heat exchangers must function as evaporators as well as gas coolers.

7.2.2. Evaporators

In the auto air-conditioning industry during the 1980s conventional copper tube-aluminum fin evaporators were replaced by lighter, more compact brazed aluminum designs. Refrigerant flows between plates patterned with chevrons or dimples to facilitate refrigerant distribution between the upwind and downwind sides; sets of parallel plates are in cross-flow, usually with several passes between headers, with a variable number of plates per pass to control pressure R-134a pressure drop.

With plate evaporators the auto industry adopted louvered fins, which re-start the boundary every millimeter, increasing air-side heat transfer coefficient by 50–100% over that of plain fins. Condensate retention and blowoff remain a problem, which manufacturers address in a variety of ways to minimize performance degradation and mold growth: e.g. tilting the heat exchanger about 10° off the vertical, optimizing louver angle and spacing; and applying hydrophilic coatings and biocides. Kim et al. [115] reviewed critically the flow structure and its effect on the thermal hydraulic performance of folded louvered fins. They also described air-side heat transfer and pressure drop data and correlations of brazed aluminum heat exchangers under dry and wet conditions.

Microchannel evaporators are currently the subject of research within the automotive air-conditioning industry because of the potential performance improvements obtainable from further increases in refrigerant-side area and higher face velocities. Such prototypes have already been built and tested for CO₂ systems, such as the one shown in Fig. 39, sized for a sport utility vehicle. Next to it is a conventional R-134a evaporator that has less capacity, despite its greater face area, and only slightly shorter depth

in the air flow direction. The fins on each heat exchanger are of the louvered folded type. The enhanced performance is attributable to the fact that microchannel tubes are thinner than the brazed plates, allowing the same air volume to pass with greater face velocity through a deeper heat exchanger, without a pressure drop penalty. In both plate evaporators and microchannel evaporators, the challenge is to distribute the two-phase flow uniformly through the parallel circuits. The current strategy for dealing with this problem is to find ways of eliminating it, such as flash gas bypass as described for the residential system prototype in Section 8. Kim and Bullard [116] developed a detailed finite volume model for a multislab microchannel evaporator and validated the model for a two-slab prototype evaporator. Several correlations for air- and refrigerant-side heat transfer and friction loss were compared before selecting appropriate correlations for the model. They reported their model predicted the experimental data with reasonable accuracy, and could be used for the performance analysis and designing of a microchannel evaporator. Currently, all simulation models of microchannel heat exchangers assume perfect distribution on the refrigerant side [116]. Their main focus is on capturing accurately the important air-side phenomena such as the effects of condensate and inclination angle.

Extremely, high heat transfer coefficients have been reported for flow boiling in microchannel tubes [117], and explored in greater detail by Pettersen [20]. However, only a few experimental studies have been done to measure the effects of condensate retention on the performance of microchannel evaporators. The first study used 30 microchannel heat exchanger samples, and found that the sensible heat transfer coefficient was impaired only slightly by wet surface at low face velocities, but was similar to that for dry a surface at higher face velocities, for fin pitch = 1.4 mm. However, for those with smaller fin pitch, there was clear evidence of performance degradation by condensate bridging across the fins at all operating conditions. Based on these data, j - and f -factor correlations were developed [118]. In another investigation of the effect of inclination angle ($-60 < \theta < 60^\circ$), heat transfer performance for both dry and wet conditions was not influenced significantly, while the pressure drops increased consistently with the inclination angle. The heat transfer coefficients and the pressure drops for the wet conditions revealed the importance of the role of condensate drainage [119].

Also emerging is yet another approach to design of evaporators for automotive applications. That is to use many parallel circuits of small-diameter circular aluminum tubes [76]. The small diameters enable use of higher pressure refrigerants, CO₂ included. Most importantly these heat exchangers use flat fins that can be enhanced with waves or offset strips, which are less susceptible to degradation by condensate retention and are more easily defrosted. In that sense they are taking advantage of all that has been learned through the design of air conditioners and heat pumps for stationary applications. Unlike conventional systems,

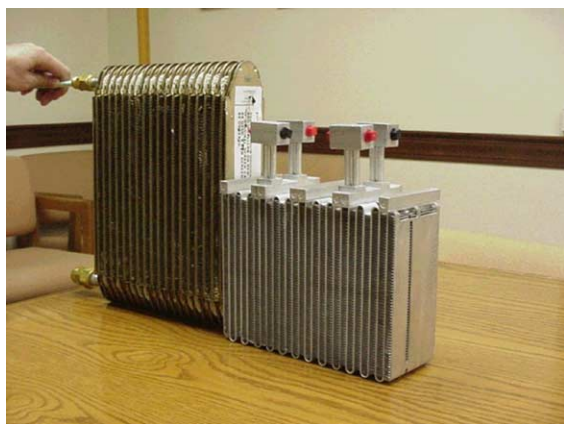


Fig. 39. Conventional (left) and prototype (right) CO₂ evaporator for mobile air-conditioner.

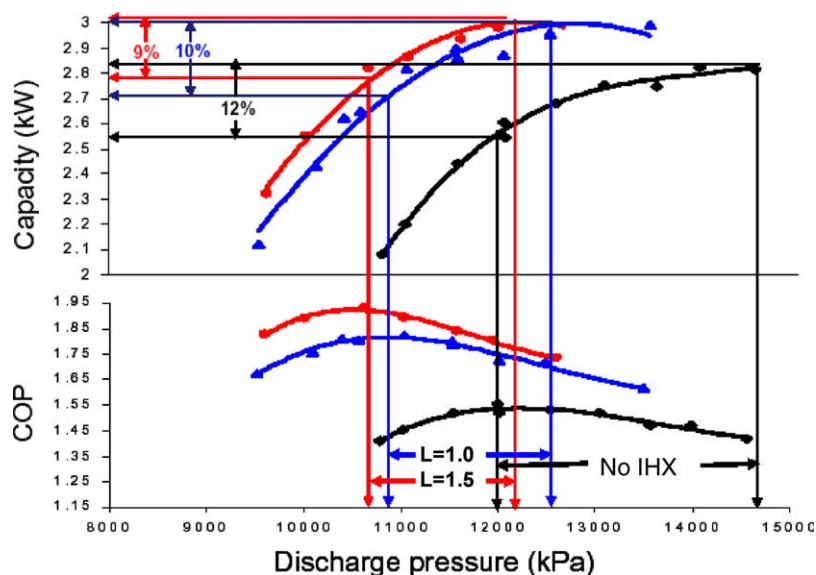


Fig. 40. Effect of internal heat exchanger (IHX) in mobile air-conditioning system at idling speed and 43.3 °C ambient (L is the length of IHX in meter).

however, these heat exchangers have much greater primary surface area. At this time there is relatively little published data that would allow detailed comparisons of these heat exchangers with the microchannel type, because their geometry lies outside the range of many correlations developed for stationary applications.

7.2.3. Internal heat exchangers

The benefits of an internal heat exchanger for transcritical automotive air-conditioning systems have been documented through extensive experiments in CO₂ prototype systems, and subsequent analyses using a validated simulation model. It has been demonstrated [120] that internal heat exchange can increase cycle efficiency up to 25%. Fig. 40 shows experimental results for a base case

automotive air-conditioning system with no internal heat exchanger, and two others of lengths 1.0 and 1.5 m. The longer internal heat exchanger provides the greatest increase in COP and the greatest decrease in the corresponding optimal discharge pressure. In automotive air-conditioning systems, internal heat exchange provides the greatest capacity enhancement when it is needed most, while idling at high ambient temperatures. Boewe et al. [37] showed how three microchannel tubes could be stacked to provide many parallel ports to control pressure drop in the cold suction gas, while forcing the supercritical fluid through smaller ports to maximize heat transfer coefficients and areas upstream of the expansion device where larger pressure drop can be tolerated. Compared to conventional concentric tube designs, the microchannel configuration shown in Fig. 41 reduced

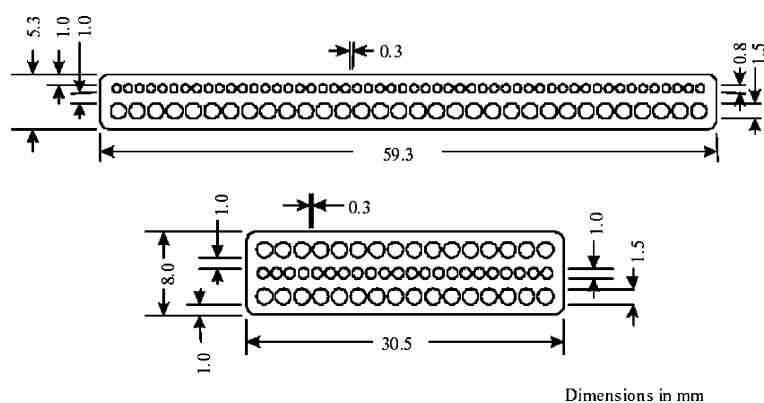


Fig. 41. Illustration of new designs of internal heat exchanger.

material requirements by 50% while eliminating the need for long suction and liquid lines, and increasing effectiveness by 10%.

7.3. Other components

7.3.1. Lubricants

A variety of lubricants can be used for CO₂ applications. In certain systems synthetic hydrocarbons such as poly alpha olefins (PAOs) and alkyl benzenes (ABs) can be still used even though they have poor solubility. The poor solubility of the synthetic hydrocarbons is compensated for by their excellent low temperature flow properties and can be improved still further by blending with more miscible lubricants (e.g. polyalkylene glycols (PAGs), esters, etc.). A range of individual and blends of synthetic lubricants are therefore being evaluated to find the more cost effective solution for a particular application. Quite often lubricant selection will be based on logistic factors, i.e. a lubricant that can work with a variety of refrigerants [121].

Kawaguchi et al. [122] reported that polyalkylene glycol (PAG) was the primary lubricant candidate since it was partially miscible with CO₂. It had excellent lubricity in boundary condition and supercritical condition, and showed good stability under supercritical condition. Other lubricants tested were polyolester (POE), polycarbonate (PC) and polyvinyl ether (PVE).

Li and Rajewski [123] conducted a screening study on various lubricant candidates for CO₂ systems, including mineral oil, polyalphaolefin (PAO), polyolester (POE), polyalkylene glycol (PAG) and alkyl naphthalene (AN). The experimental results raised concern about the compatibility between POE and CO₂ after significant degradation was found for this lubricant. The authors speculated that carbonic acids formed by dissolution of CO₂ into the moisture in the polyolester (POE) lubricant accelerated the degradation. Dissolved aluminum was found in the polyalkylene glycol (PAG) lubricant, and this was probably caused by a phosphate anti-wear additive which had been converted into aluminium-aggressive alkyl phosphates.

Seeton et al. [124] studied solubility, viscosity, boundary lubrication and miscibility of CO₂ and synthetic lubricants. They concluded that the polyalkylene glycol (PAG) lubricant seemed to give the best lubricity for transcritical applications.

Heide and Fahl [125] studied the miscibility in CO₂ of several candidate lubricants for transcritical systems, including alkyl benzene (AB), alkyl naphthalene (AN), polyalkylene glycol (PAG), polyolester (POE), and polymer ester (PME). The POE lubricants showed good miscibility, while the other candidates had large regions of immiscibility. The results indicated a strong influence of chemical structure of lubricant on phase behavior with CO₂. Investigations on thermal stability of lubricants by Fahl et al. [126] showed that PME and aromatic ester derivatives

have a good potential for applications with high temperatures.

7.3.2. Elastomers

Some issues are being studied with respect to elastomer materials for seals and hose connections in CO₂ systems. Permeation rates are quite high, thus giving potential problems regarding desired leakage rates in automobile air conditioning systems. Explosive decompression may occur when CO₂ systems or components are rapidly depressurized, leading to fractured and ruptured sealing elements [127]. A fluorite elastomer, FKM was regarded as promising due to its wide temperature range of application and the negligible impact of explosive decompression.

7.3.3. Valves and controls

Jain et al. [128] has developed components for CO₂ air-conditioning systems, including electronic expansion valves, accumulators, hoses, o-rings and fittings. The expansion valve is a linear proportional solenoid valve. Several manufacturers are working on expansion valves and controls for CO₂ systems. Saginomiya and Fujikoki in Japan are working on valves (especially expansion valves) and controls for transcritical CO₂ systems, especially heat pump water heaters on the market. In Europe, Danfoss AS is working on various concepts, including mechanical (automatic, thermostatic) and electronic (modulating coil) valves. The German company Otto Egelhof GmbH and Co. is working on a step-motor controlled valve, mainly intended for the mobile air-conditioning market. In addition, Obrist Engineering in Austria is offering valves, controls and other components for prototyping purposes.

8. Application areas

Recent research on transcritical CO₂ systems has investigated a variety of possible applications, mostly with funding from the affected industries. While many government-sponsored R&D programs can afford the luxury of starting with basic research, industry-sponsored efforts generally proceed in two stages. The first task is to prove that the technology will work for a specified application, and then in stage two the state of the art is advanced to enable the technology to compete in the market.

From the standpoint of experimental design, first stage is the horseless carriage stage. Any new technology that challenges an existing one must demonstrate that it is workable, usually on the old technology's terms. The first CO₂ prototype systems were therefore built to mimic the conventional technology in size, weight, air flow rates, etc. In the long run, however, that is an unrealistic and non-sensical demand: like requiring Henry Ford's new invention to compete with a horse-drawn carriage on muddy

roads. Ford's technology was not rejected; instead the system boundary was expanded and roads were paved to capture the benefits of the internal combustion engine.

For most of the application areas discussed below, CO₂ technology is now at the second stage where it must demonstrate competitiveness. It is no longer necessary to mimic the old technology. However, many of the existing publications describe experiments conducted under stage-1 constraints. Current research is aimed at identifying the best way to utilize the unique characteristics of the new technology. In the case of CO₂, these characteristics include certain thermophysical (thermodynamic and transport) properties, which increase heat transfer and boost compressor efficiency. Its high heat rejection temperature, a disadvantage for air conditioning, is a potential advantage for heating by delivering instant high-temperature heat quietly due to the need to move less air than existing heat pump technologies.

During this second stage of prototype development the main question is how closely the ideal cycle can be approached at reasonable cost—a question that goes beyond simple thermodynamic cycle comparisons. The air flow rates and heat exchanger circuiting for an optimized CO₂ system will differ greatly from conventional systems. While questions related to cost are being explored on a proprietary basis, papers in the open literature are suggesting ways of approaching ideal cycle efficiency by exploiting the unique characteristics of CO₂, such as the slope of its vapor-pressure curve, boiling behavior near the critical point, high capacity at low temperatures, and its supercritical temperature glide. Other papers suggest ways of altering the transcritical cycle to increase the ideal efficiency, for example, through use of expanders, internal heat exchangers and multistage compression. In all cases, however, the path of technology development is defined by market needs for lightweight and ultra-compact systems (e.g. mobile air-conditioning, and portable air-conditioning units for the military), or the need for high-temperature heat (space and water heating; dryers), and needs for high refrigerating capacity at moderate to low temperatures. Examples are described in the following sections.

8.1. Automotive air conditioning

For several reasons, mobile air conditioning applications were among the first to be considered for application of the transcritical CO₂ cycle. The most obvious was the high leakage rate of R-12 (and later R-134a, both greenhouse gases) through the flexible nylon or butyl rubber hoses needed for vibration protection, and through the compressor shaft seal needed to avoid the additional weight and conversion losses associated with the hermetic electric compressors used in other applications. In automobiles, the chief thermodynamic disadvantage of CO₂—its high temperature of heat rejection—makes it possible to design an ultra-compact gas cooler, which increases energy

efficiency indirectly by enabling more aerodynamically streamlined vehicle design.

The earliest analyses of R-134a and CO₂ for automotive air conditioning began with ideal cycle comparisons [129,130], and rested on assumptions that failed to account properly for the unique thermodynamic and transport properties of CO₂, even though experimental data for a prototype CO₂ system had already shown competitive performance to a state-of-the-art R-12 system [3]. Not surprisingly the theoretical studies concluded that the total global warming impact of CO₂ systems would exceed that of R-134a, considering both direct (leakage) and indirect (fuel combustion) emissions of greenhouse gases. The first experimentally based assessment of TEWI [131] showed that in practice the energy consumption of the systems was comparable, thus giving considerably reduced warming impact due to elimination of the direct effect. Through improvements in system operation and control [28], compressor performance, and heat exchanger performance [76], the CO₂ technology was able to compete even with the improved R-134a systems that were introduced in the mid-1990s.

The European RACE project from 1994 to 1997 [132] focused on development and testing of car-installed prototype systems, with results confirming the potential for CO₂-based mobile air conditioning. Members in the RACE project included five European car manufacturers, two system suppliers, and one compressor manufacturer.

Based on these initially promising results, a rigorous side-by-side test program was undertaken, and conducted in specially designed well-instrumented facilities, using micro-channel heat exchangers built to match closely the weight, heat exchanger dimensions, face velocities and air-side pressure drops of a commercially available clutch-cycling R-134a system for a Ford Escort. Separate environmental chambers were constructed to simulate a very wide range of indoor and outdoor climate conditions. To produce data on both systems and components, each chamber contained a wind tunnel, and had parallel sets of refrigerant piping to facilitate comparisons of CO₂ and other refrigerants. The heavily insulated walls with heat transmission measurement, plus accurate metering of refrigerant and air mass flow rates made it possible to obtain three energy balances for both the indoor and outdoor heat exchangers: air-side, refrigerant-side and room calorimetry. Detailed descriptions of the mobile and residential air conditioning facilities may be found in Refs. [133,134].

Heat exchangers for the CO₂ system were made of flat aluminum extruded multiport tubes to deal with the high-pressure refrigerant, making it possible to maximize air-side heat transfer area within the overall weight constraint. Photographs of the evaporators (top) and condenser/gas cooler (bottom) are shown in Fig. 42. The 21.0 cm³ compressor shown in Fig. 31 was of swash-plate design, and the high-side pressure could be controlled by either a needle valve or a backpressure valve.

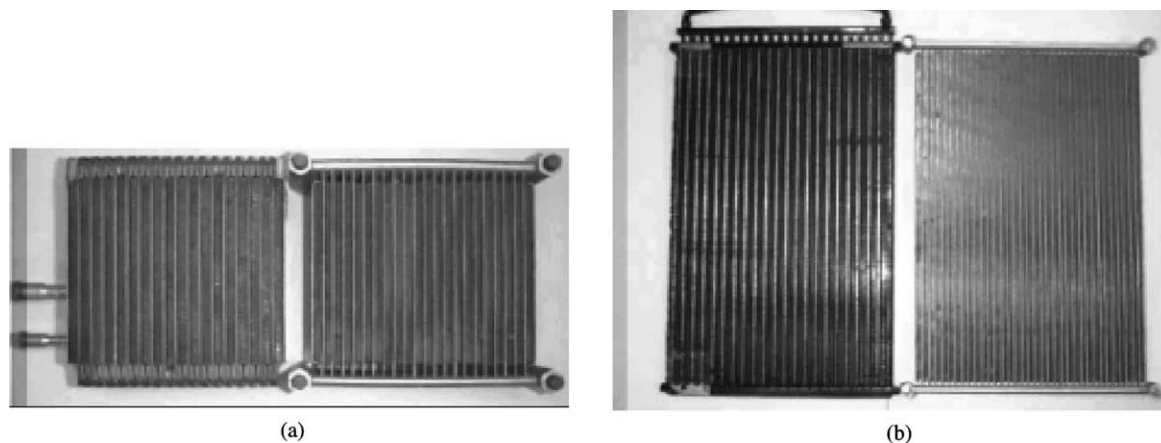


Fig. 42. Heat exchangers of CO₂ mobile air-conditioning system prototype (right) compared to R-134a baseline (left). (a) Evaporator, (b) condenser or gas cooler.

Test matrices were defined for the purpose of developing and validating component and system simulation models, as well as supporting data-to-data comparisons of CO₂ and R-134a at normal, seasonal and extreme operating conditions.

The results demonstrated that comparable cooling COPs could be obtained at most operating conditions (Fig. 43). The CO₂ system was sized to provide approximately equal capacity at the extreme high-temperature (54.4 °C) idling condition, as shown in Fig. 44. However, its COP fell 10% short of the baseline system at that point. At outdoor ambient temperatures below 40 °C where most air-conditioning operation occurs, the CO₂ system COP exceeded that of the baseline R-134a system up to 40%. The lines in Fig. 44 connect points having equal outdoor air flow rates, V_c , while the indoor air temperatures and air flow rates are

shown in boxes. The 22 data points represent only a subset of the conditions investigated. Several factors were found to be responsible for these results: (1) higher real compressor efficiency due to lower compression ratio; (2) higher evaporating temperature due to superior thermophysical properties and greater tolerance of pressure drop due to the slope of the vapor pressure curve; (3) closer approach temperature differences at the gas cooler outlet. More detailed data can be found in Refs. [133,135–137].

Experiments were conducted on both systems in both steady state and cycling modes. Cycling behavior is very sensitive to the type of expansion device used. A fixed orifice is simplest, but is unable to maintain the high-side pressure at its COP-optimizing level during the on-cycle as reflected by the large differences between refrigerant flow rates shown in Fig. 45 [137]. It is also clear that the backpressure valve

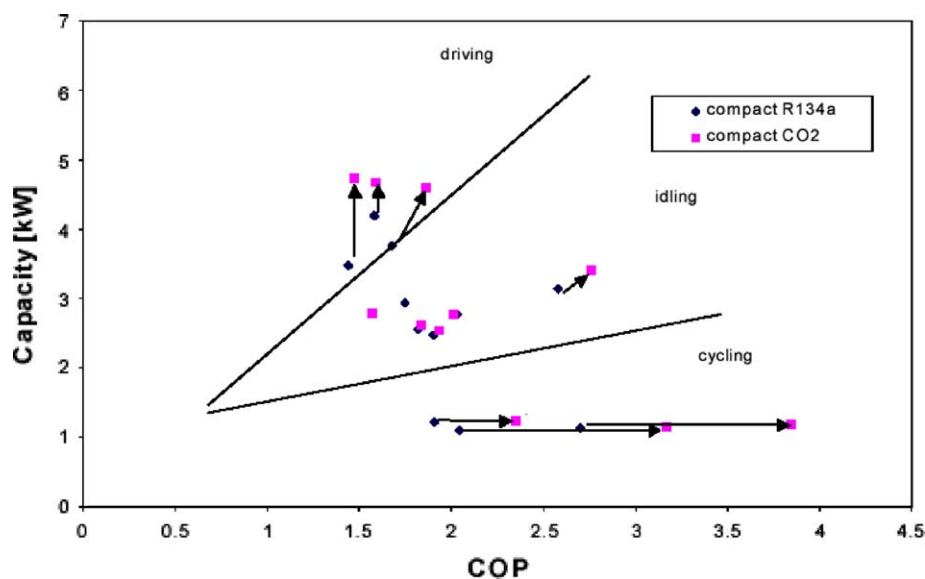


Fig. 43. Measured performance of automotive air-conditioning systems.

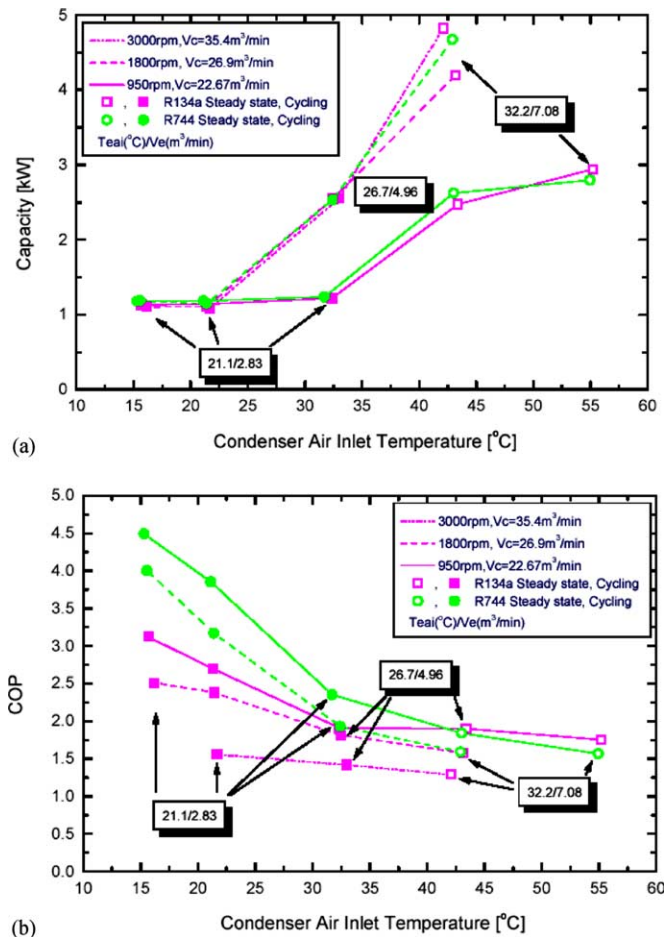


Fig. 44. Comparison of CO₂ mobile air-conditioning system prototype performance to R-134a baseline. (a) Capacity, (b) coefficient of performance.

maintains a steadier compressor torque, F_c , than the fixed orifice (needle valve in fixed position). Control options are discussed in Refs. [138,139]. Additional experimental results and a more detailed investigation of the time averaged COP-maximizing high side pressure strategy is presented in Ref. [140], which found a linear relationship between gas cooler exit temperature and COP maximums over a wide range of operating conditions.

Based on the results of an analysis of a large number of experiments and some new concepts, next-generation prototype systems have been designed and are serving as the focus for current research. Most are equipped with variable-displacement compressors, and heat exchangers configured to exploit the unique transport and thermodynamic properties of CO₂. Some of these design features and model validation results are discussed in Section 7.

Research and development of transcritical CO₂ technology marked a significant departure from mobile air conditioning industry's traditional product development programs, which are dominated by internally funded

proprietary efforts. The involvement of academic research at such an early stage is unprecedented, and illustrates two distinct types of value delivered by the academy to the industry. The first is not new: peer-reviewed research elucidates the fundamental physical processes, and provides a physical basis for discontinuous technological change,

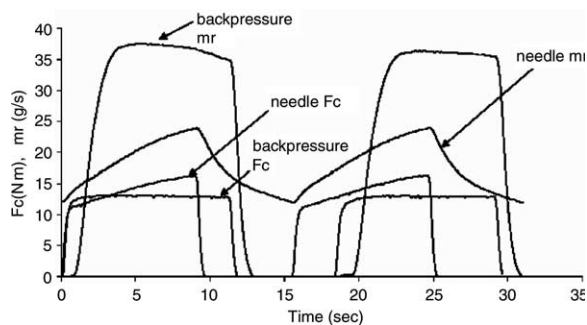


Fig. 45. Characteristic behavior in cycling.

which is less risky than extrapolating empirical data. The second type of value stems from the uncertain timetable for dealing with global warming, which is quite aggressive in some parts of the world and creates a need for detailed, credible peer-reviewed results of carefully designed experiments. In both cases the world auto industry—OEM's and component suppliers—have decided to pool resources and share the cost of producing such information. The results of the European RACE consortium's efforts were produced by member companies and shared internally, and later placed in the public domain [132]. To enhance acceptance, a broader-based cooperative research program is now being undertaken by SAE and conducted at the University of Illinois. That 18-month effort involves a rigorous experimental evaluation of several competing systems, with extensive instrumentation under identical operating conditions [141]. The systems are: baseline production R-134a; advanced R-134a; transcritical CO₂; and propane (R-290) with a secondary loop containing a non-flammable coolant.

Laboratory experiments—carefully designed and documented—are one important step along the path to commercializing any new technology. Designing and retooling to accommodate the high pressures in CO₂ refrigeration systems, and dealing with safety concerns are generic issues to be faced by any companies involved in a transition to CO₂ systems. The auto industry is positioned to benefit from existence of captive vehicle fleets, which can provide test-beds for confirming the conclusions drawn from laboratory experiments. On the other hand the industry is beset with a variety of logistical concerns related to the worldwide service infrastructure: the need for technicians to handle not only the new technology but also its overlap with conventional systems. Maintenance problems are more prominent in vehicles than in stationary applications because of the need for more extensive spatial, mechanical and electrical integration of the air-conditioning unit with other subsystems (severe packaging constraints; compressor mechanical drive; and the need for reheating dehumidified air for defogging). Moreover, the auto industry is accustomed to producing cars capable of operating in almost any climate. Therefore, investigations of advanced cooling applications are being accompanied by experiments in heating mode, because many of today's efficient cars reject too little waste heat to the engine coolant to keep cars comfortable in severe winter conditions.

8.2. Automotive heating

Modern cars with efficient fuel-injection engines often have insufficient waste heat for heating of the passenger compartment in the winter season. The long heating-up period and slow defroster action is unacceptable both in terms of safety and comfort. Supplementary heating is therefore necessary, and one attractive solution may be to operate the air conditioning system as a heat pump. CO₂ systems have special benefits in heat pump mode, since high

capacity and COP can be achieved also at low ambient temperature and with high air supply temperature to the passenger compartment.

The first results of CO₂ heat pump experiments were obtained by running an auto air-conditioning prototype system in reverse [142–144]. Although the cross-counter-flow interior heat exchangers were far from ideal, the data shown in Fig. 46 show the essential features of an automotive heat pump: capacity is highest at startup when it is needed most; the capacity is at least three times higher than what could be obtained from an electric resistance or friction heater due to the high heat pumping efficiency; and capacity and efficiency (heating performance factor, HPF) decline slowly due to reduced volumetric and isentropic compressor efficiencies at higher temperature lift, as the car warms up and heat becomes available from the engine coolant. These initial results have proven quite valuable in guiding the design and development of improved components for next-generation systems. Next-generation prototypes will need to address such operational issues as defogging.

One reason heat pumps are not currently employed in automobiles is that R-134a has disadvantages as a heat pump fluid (e.g. large compressor displacement; air in-leakage in compressor shaft seal at subatmospheric suction pressures). Regardless of the fluid, however, air-to-air heat pumps present substantial technological challenges that have not yet been addressed: the outdoor heat exchanger will accumulate frost, and perhaps ice as water is splashed on it from the road. Very little is known about frosting and condensate drainage from ultra-compact microchannel heat exchangers, and what is known suggests that the difficulties may be substantial [143–146]. Residential heat pumps defrost by switching into air conditioning

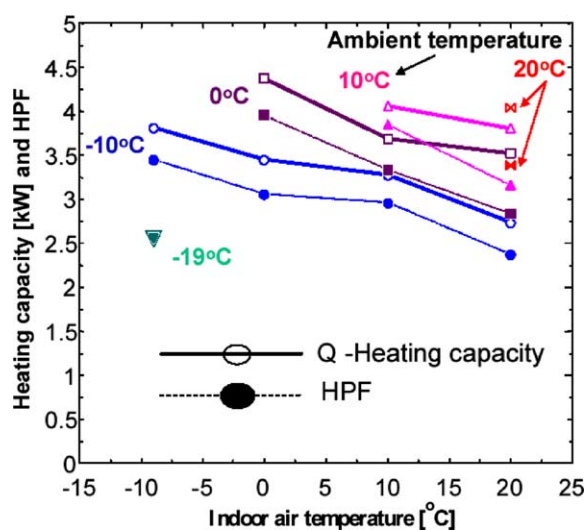


Fig. 46. Automotive heat pump performances at different indoor and outdoor conditions.

mode, but that is not a feasible option for automobiles because the small volume of air in the passenger compartment would cool immediately. Connecting to another heat source for defrosting may also be problematic, especially after a series of short trips during which the engine never reaches normal operating temperature. On the other hand, during normal operation, the heat pump needs only to provide supplemental capacity for a short period after startup, while the engine is warming up. After that, sufficient heat should be available for defrosting; the only problem is how to transfer it. Other options for avoiding frosting, such as obtaining heat from the engine coolant, have their own unique difficulties: for example, causing the engine to operate at suboptimal temperatures and exceed air pollutant emission standards. These difficulties might be avoided through careful design in the future, by integrating and improving thermal management within the engine.

Hammer and Wertenbach [147] showed test data for an Audi A4 car with 1.6l gasoline engine, comparing a standard heater and a CO₂ heat pump system based on engine coolant as heat source. Fig. 47 shows measured air temperatures at foot outlet nozzles and passenger compartment temperatures using standard heater core ('production'), and a heat pump system (without heater core). The more rapid heating up with heat pump is clear, with almost 50% reduction in the heating-up time from -20 to $+20$ °C. Since the heat pump used engine coolant as heat source, the possible risk of extended heating-up time for the engine was of some concern. Measurements showed that owing to the added load on the engine by the heat pump compressor, the heating-up time was in fact slightly reduced even when heat was absorbed from the coolant circuit.

Despite the technical challenges, the ability of a heat pump to provide 'instant heat,' and the capability of a CO₂ heat pump to deliver that heat at higher temperatures while moving less air, create value that may warrant development of more complex automotive climate control systems. This feature, combined with the long-term need for increasing vehicle efficiency, is driving ongoing research in both universities and industry. Moreover, the emergence of electric and hybrid vehicles is causing the scope of the investigations to be expanded to reconsider electrically driven hermetically sealed heat pumps.

8.3. Residential cooling

The first assessment of transcritical CO₂ systems for residential air conditioning was done by simulating operation of an Asian-style ductless minisplit system, comparing CO₂ to a baseline R-22 system [148].

Evaporator temperatures were higher in the CO₂ system, and very small approach temperatures were estimated for the CO₂ gas cooler. The mechanically expanded round-tube heat exchangers were designed within the same core dimensions and air-side pressure drop in both systems. The effects of pressure drop, particularly in the evaporator and suction line of the R-22 system and the superheat characteristics of the expansion valve, gave cooling COPs (summer operation) that were similar in both systems, even at high ambient temperatures.

An extensive set of experiments was conducted on a prototype North American-style ducted split air conditioning system. The baseline R-410A system selected was the most efficient commercially available, and the CO₂

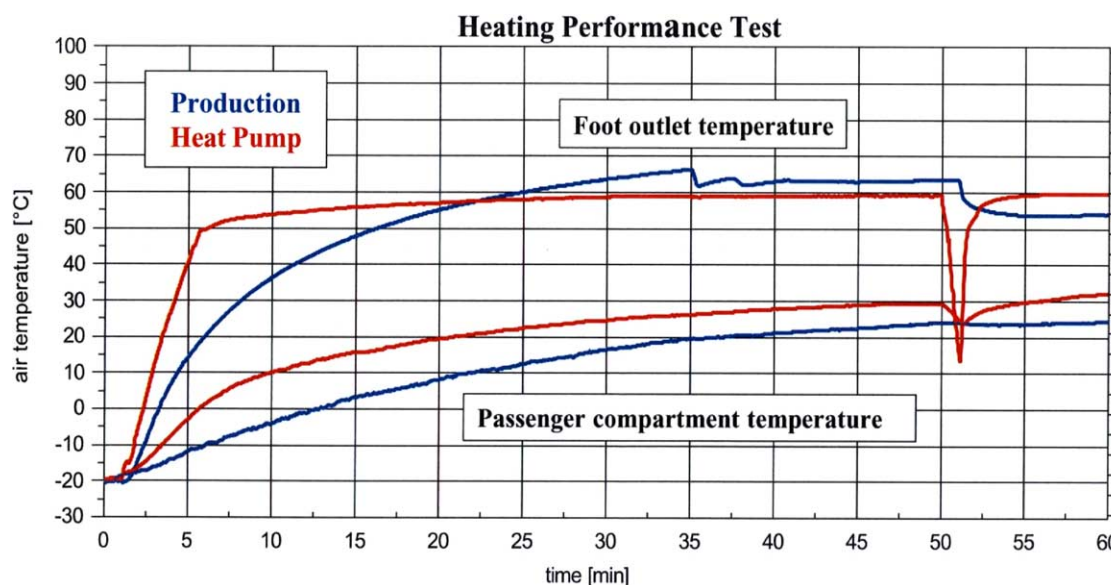


Fig. 47. Measured air temperatures in during start-up of an Audi A4 test vehicle (production) and same car with CO₂ heat pump ('heat pump') [147].



Fig. 48. Heat exchangers of CO₂ residential air-conditioning system prototype (left) compared to R-410A baseline (right) [134]. (a) Indoor heat exchangers, (b) outdoor heat exchangers.

prototype heat exchangers were designed to match as closely as possible its overall package dimensions, as shown in Fig. 48. Detailed experiments were conducted on each system at three standard ARI test conditions, and the prototype CO₂ system achieved approximately the same cycle COP (omitting fan and blower powers) as the baseline R-410A system at ARI test conditions B and C (26.7/27.8 °C) [149]. The raw data in Fig. 49 should be adjusted downward about 10% for comparison with the hermetic R-410A compressor, because the CO₂ prototype compressor was an open automotive prototype where power input could only be measured on the shaft. As expected, the CO₂ exhibited a substantially lower COP at the higher ambient temperature condition A (26.7/35 °C). Results shown in Fig. 49 demonstrated how the lower air-side pressure drop of microchannel heat exchangers enabled the CO₂ system to benefit from greater air flow rate with no penalty in fan or blower power. The test matrix was designed to guide next-generation component designs, for example: as alternatives to increasing air flow rate, direct fan power savings could be realized, or air-side heat transfer area could be increased until pressure drop matched that of the baseline.

The model validation effort was based on these initial experiments, and a large discrepancy was noted between simulation and data for the evaporator. A thermocouple grid

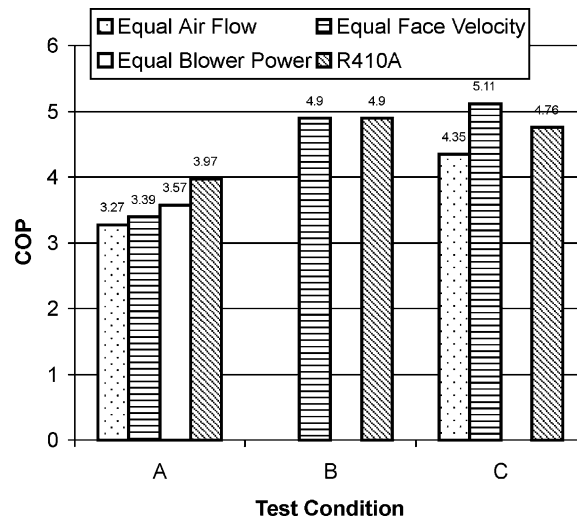


Fig. 49. CO₂ residential air-conditioning system data compared to R-410A baseline.

was then installed downwind of evaporator, and provided evidence of significant refrigerant maldistribution among the parallel microchannel tubes (Fig. 50). As shown in Fig. 50(b), even symmetrical feeding of the header results in the middle tubes receiving excess liquid while the outer ones receive excess vapor. Fig. 50(c) shows how this problem was eliminated through use of controlled flash gas bypass—a new concept to improve distribution and increase heat transfer coefficients while reducing pressure drop in evaporator—increasing heat exchanger effectiveness by 17% and increasing the evaporating temperature by 3.8 °C as described in Ref. [150]. Since compact high-performance heat exchangers such as these are likely to be needed for efficient heat pumps in the future, solving the two-phase refrigerant distribution problem has become a high priority for systems using any kind of refrigerants. Accordingly, a substantial amount of research is now being initiated to understand the behavior of developing two-phase flow in headers, and on schemes for bypassing vapor to minimize degradation of evaporator performance.

8.4. Residential heating

Today's residential heat pumps deliver large amounts of air at temperatures very near that of human skin, causing discomfort via evaporative cooling. On the other hand the transcritical cycle can deliver air at 60 °C, achieving the same level of comfort as a gas forced air furnace while quietly moving substantially less air than conventional heat pumps. Similarly, CO₂ can provide heat via a hydronic secondary loop without the energy penalty that would be incurred in a heat pump operating on a subcritical cycle. Several analytical studies of the global warming implications of alternative heat pumping systems have

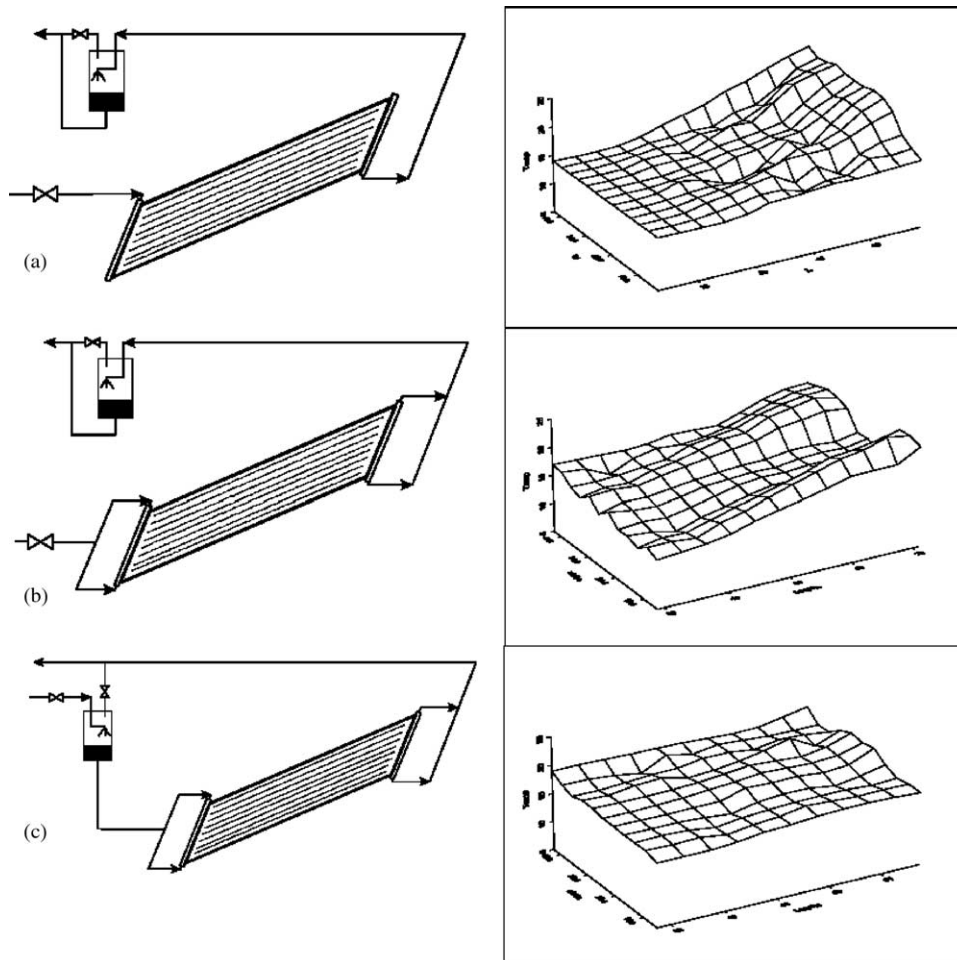


Fig. 50. Effects of flash gas bypass expressed through air exit temperature profiles shown on the right. On the left (a) regular HX configuration with single side inlet, (b) same as (a) just with two inlets and (c) flash gas bypass. All three operations are completed with same evaporator capacity. In both (a) and (b) cases evaporation temperature was 7 °C while in (c) it was 10.8 °C that consequently increased COP by 17%.

concluded that the direct effect of refrigerant emissions is relatively small, compared to the indirect effects associated with differences in energy efficiency [151]. Accordingly, for almost all applications except automotive air-conditioning and supermarket refrigeration, the highest R&D priority is to maximize the efficiency of CO₂ systems.

8.4.1. Direct air heating

Differences in heating capacity characteristics between CO₂ and R-22 are important for the seasonal heating performance (winter operation), since differences in the need for supplementary heating affect the total system energy efficiency. In their model-based study, Pettersen et al. [148] found that the CO₂ system was able to maintain a higher heating capacity than the R-22 system at low ambient temperatures, thereby saving supplementary heat. Even though the heating COPs of the two heat pump circuits were similar, the overall result was a 20% increase

in system energy efficiency (HSPF) for the CO₂ system, due to a lower need for supplementary heat of any kind.

Experimental investigations of transcritical CO₂ systems for residential space heating were conducted on a prototype residential split system, originally designed for cooling only, by simply reversing its operation to study heating performance [152]. Since the original baseline system was obtained before the first R-410A heat pump system became available, the package dimensions for the heating comparisons were no longer equal: the baseline subcritical R-410A system had larger heat exchangers. Nevertheless, system performance was compared for two configurations: first when the CO₂ prototype semi-hermetic compressor speed was set to match heating capacity at 8.2 °C outdoors and 21.1 °C indoors; and second when the air conditioning capacity was matched at 35 °C outdoors and 26.5 °C indoors. The CO₂ system had similar cycle COP in heating mode, but its higher capacity at lower outdoor temperatures increased its heating performance factor (HPF) by reducing

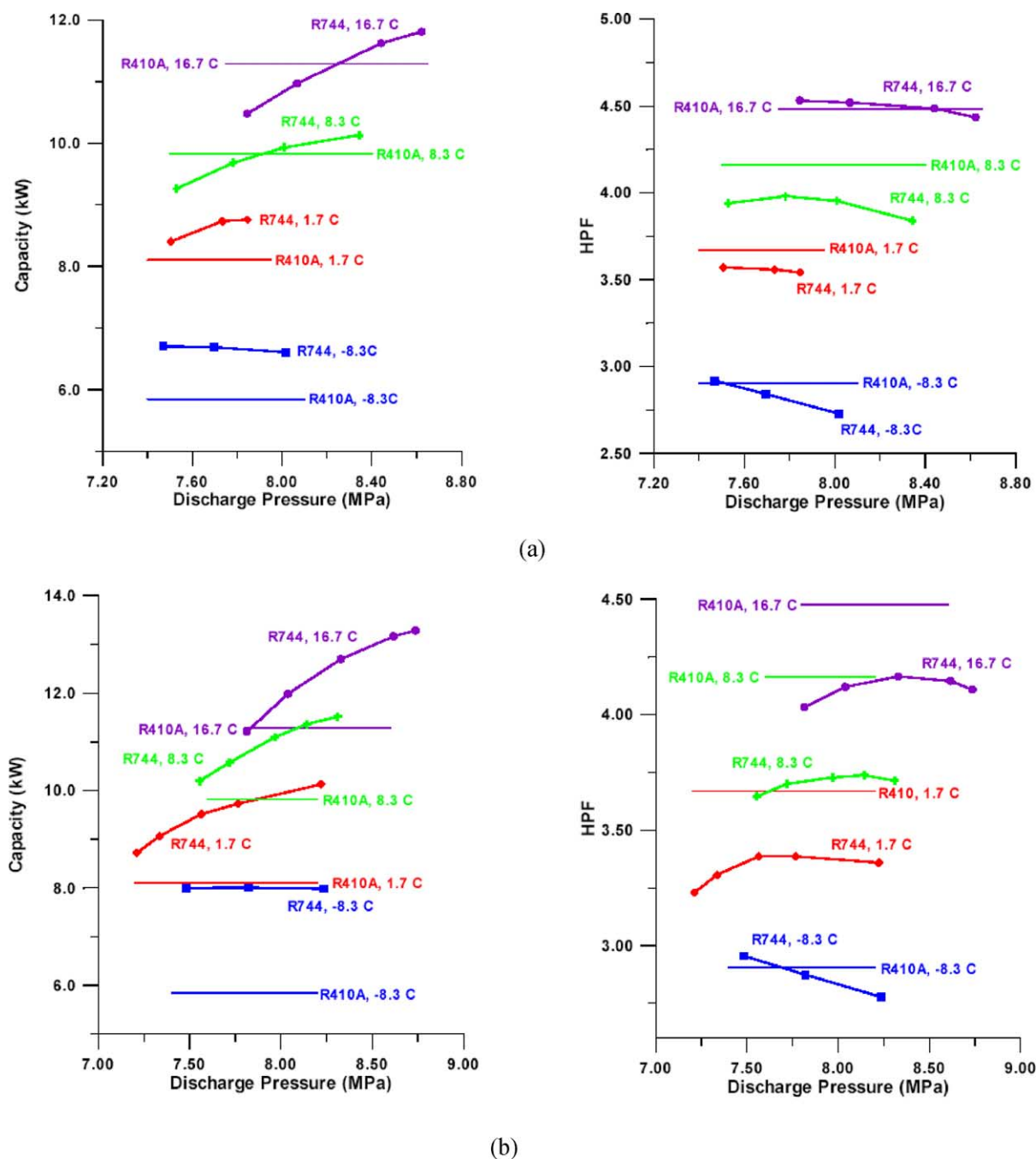


Fig. 51. Residential CO₂ system controls of capacity and efficiency. (a) Heat pump, (b) air-conditioning.

the need for supplemental heat (Fig. 51), which illustrates the CO₂ system's ability to select a compressor discharge pressure that gives it extra capacity or efficiency when needed. These results helped establish priorities for subsequent analyses of the effects of CO₂'s transport properties on heat exchanger temperature differences, and ways to optimize the geometry of the next generation

of reversible heat exchangers for transcritical CO₂ heat pump systems.

To complement the experimental comparisons of competing systems, a parallel analytical effort was undertaken to develop a relatively simple simulation model that could analyze many of the essential differences between transcritical and subcritical systems [153].

To ensure that the comparison was geometry-independent, the air-side heat transfer and pressure drop characteristics were assumed to be identical, and the ‘ideal’ assumption of infinite heat exchanger areas was retained. The analysis began with a simple comparison of ideal thermodynamic cycles, which, as expected, showed R-410A to be more efficient in both heating and cooling modes. Then as constraints and non-ideal considerations (e.g. finite air flow rates required to achieve comfort and limit fan power) were introduced simultaneously for both systems, the efficiency gap narrowed. The results suggest that CO₂ heat pumps could be more efficient than R-410A in cold climates, due to their higher capacity at cold temperatures and correspondingly less need for electric resistance backup heat. In climates dominated by cooling loads, such as the southern US, subcritical R-410A systems have a clear advantage in annual average efficiency, as shown in Fig. 52. The abscissa spans a wide range of climates, indicating the outdoor temperature at which the magnitude of the heating load on an average-insulated house equals the cooling load (normalized to 1 kW) at the 45 °C design condition for which the system was sized. Imposition of finite-area constraints on the heat exchangers would benefit CO₂ preferentially, but probably not enough to reverse the result for warm climates.

Despite its simplicity, the analysis helped quantify the individual differences between the two systems and cycles. The pressure ratio of the CO₂ cycle is lower, real compressor efficiencies are higher. The superior thermophysical properties of CO₂, together with the small slope of the vapor

pressure curve, allow for substantially increased heat transfer coefficients with negligible thermodynamic penalties from the associated pressure drop, enabling CO₂ systems to meet a given dehumidification constraint at a slightly higher evaporating temperature than R-410A. At supply air temperatures greater than 40 °C, the ideal CO₂ cycle is slightly more efficient than R-410A and provides substantially higher capacity at colder outdoor temperatures. This advantage appears not only for air-to-air heat pumps, but also for hydronic heating systems where higher quality heat is required. In hydronic systems water chilling may be a preferred option for the cooling season; it has been investigated experimentally and analytically, and found to have efficiency similar to that of R-22 [154–156].

Rieberer and Halozan [157] and Rieberer et al. [158] made detailed theoretical studies of controlled ventilation air heating systems with an integrated CO₂ heat pump. The results look very promising. The overall system seasonal performance factor for a Graz, Austria climate was calculated to be in the range 6.15–6.5. This corresponds to a seasonal performance factor of the heat pump of above 4 (author’s remark).

8.4.2. Hydronic heating

Schiefloe and Neksa [159] investigated a system design as shown in Fig. 53. In order to achieve a lowest possible return temperature from the heating system, the radiator and air heating are connected in series. Tap water is pre-heated in parallel with the space heating and heat exchange against hot discharge gas is used to achieve the required hot water

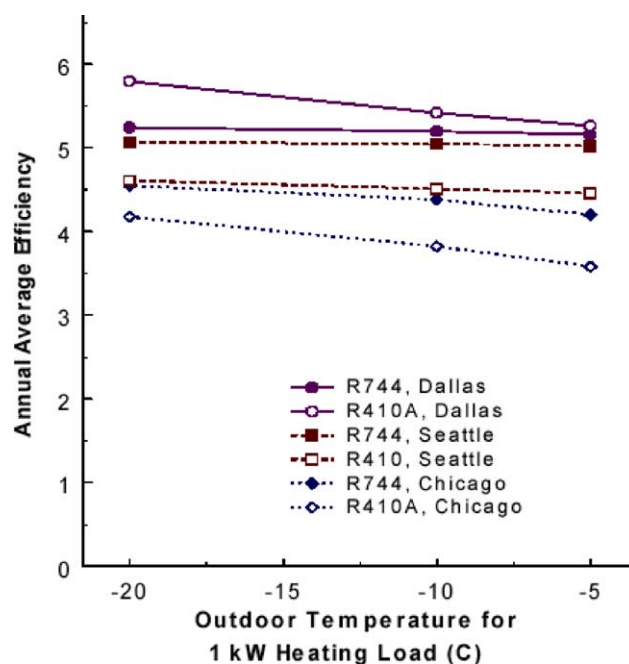


Fig. 52. Annual average efficiency for R-410A and CO₂ systems as function of heating load requirement for 60 °C supply air in heating-model predictions.

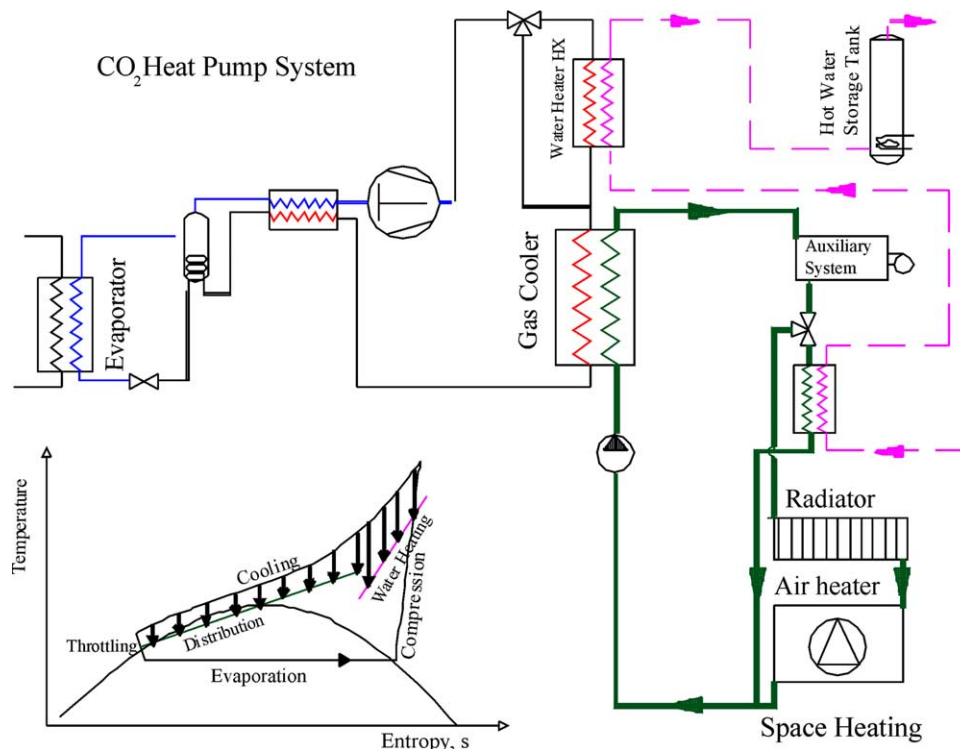


Fig. 53. System design for a combined space and water heating system. The process is also illustrated in the $T-s$ diagram.

temperature. In order to simplify the system design, the tap water heating part could also be implemented as a separate system or covered when space heating is not required.

Compared to a system using R-134a as working fluid the proposed CO₂ system showed favorable seasonal performance when more than 30% of the power demand for space heating was covered by the air heating system. The rest was then covered by the radiator system. A 70/50 °C radiator system and heat recovery efficiency of the balanced ventilation system of 60% was assumed. In larger buildings in Norway typically more than 50% of the heating demand is air heating and this percentage is increasing due to better insulation and increased air quality requirements. This indicates that CO₂ may be a promising candidate for this application.

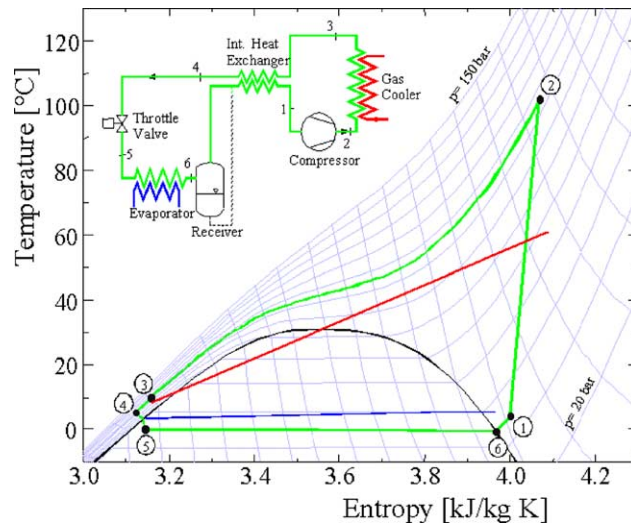
Enkemann et al. [160] made a theoretical study on CO₂ heat pumps for retrofit in typical hydronic heating systems in Western Europe. A system originally designed for temperatures 70/50 °C was modified by reducing the mass flow rate of water to obtain a 93/40 °C system, which should give a corresponding heat output using the existing radiator system. The seasonal performance was then increased from 2.8 to 3.2. In addition, this system will be able to supply hot tap water without any loss in energetic efficiency. Experimental results from two prototype systems for this application are reported in Ref. [161]. Efficiency figures in the same range as the calculated were reported.

Professor Gustav Lorentzen published several papers describing the possibilities of using CO₂ as working fluid in heat pumps and refrigeration systems. Lorentzen [32,162] outlined possible system design of large heat pumps for district heating. This is a high-capacity application where turbo expanders may be possible to realize in a cost efficient manner. Also described is the possibility to combine refrigeration/freezing and tap water heating, which will give very high overall system efficiency.

8.5. Water heating

The first application of CO₂ systems on the market is heat pump water heaters, where the thermodynamic properties are very favorable Fig. 54 shows, in a temperature–entropy diagram, how the temperature characteristics of the transcritical cycle matches the temperature profiles of the heat source and heat sink, giving small heat transfer losses and high efficiency. A pre-condition for high efficiency is a low water inlet temperature, giving a low refrigerant inlet temperature to the throttling device. Thus, the design of the hot water accumulating system for temperature stratification is essential in order to achieve high heating COP.

Studies on CO₂ heat pump water heaters were initiated at SINTEF/NTNU from the late 1980s, and a full-scale prototype system of 50 kW heating capacity was completed in 1996 as shown in Fig. 55 [108]. Results from extensive measurements on this prototype showed that a COP above 4

Fig. 54. T - s diagram showing the transcritical CO₂ cycle used for water heating.

was achievable even for a hot water temperature of 60 °C as shown in Fig. 56 [163]. The high process efficiency is partly due to good adaptation of the process to the application, but also due to efficient compression and the good heat transfer characteristics for CO₂. A CO₂ heat pump water heater may produce hot water with temperatures up to 90 °C without operational problems and with only a small loss in efficiency. Increasing the required hot water temperature from 60 to 80 °C reduces the heating COP only slightly (from 4.3 to 3.6 at an evaporating temperature of 0 °C), and one of the big advantages of this technology is the ability to supply water at high temperature with good COP. Important

application areas for commercial-size systems are in hotels, apartment houses, hospitals, and food industries.

The above heat pump water heater system was included in the European Union (EU) cooperative project ‘COHEPS’ from 1996 to 1998, where research groups in Austria (Graz University of Technology), Norway (SINTEF/NTNU), Germany (University of Hanover, Essen University) and Belgium (Catholic University of Leuven) together with their industrial partners studied various aspects of heat pumping applications for CO₂, including commercial-scale heat pumps, residential heat pumps, systems for hydronic heating circuits, and drying heat pumps. Hwang and Radermacher [164] published data on water heater, and used model to show 10% COP improvement over R-22.



Fig. 55. Fifty kilowatt prototype heat pump water heater in SINTEF/NTNU laboratory [108].

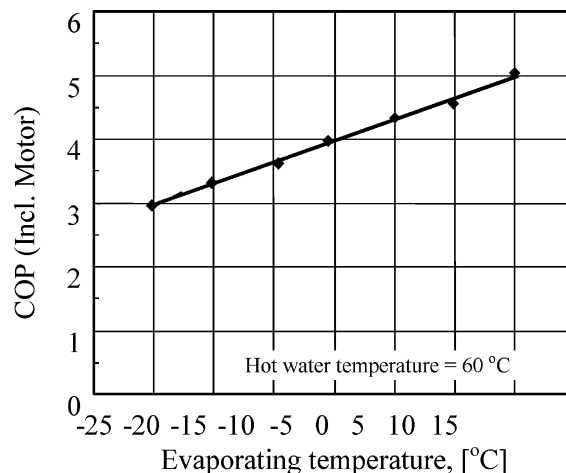
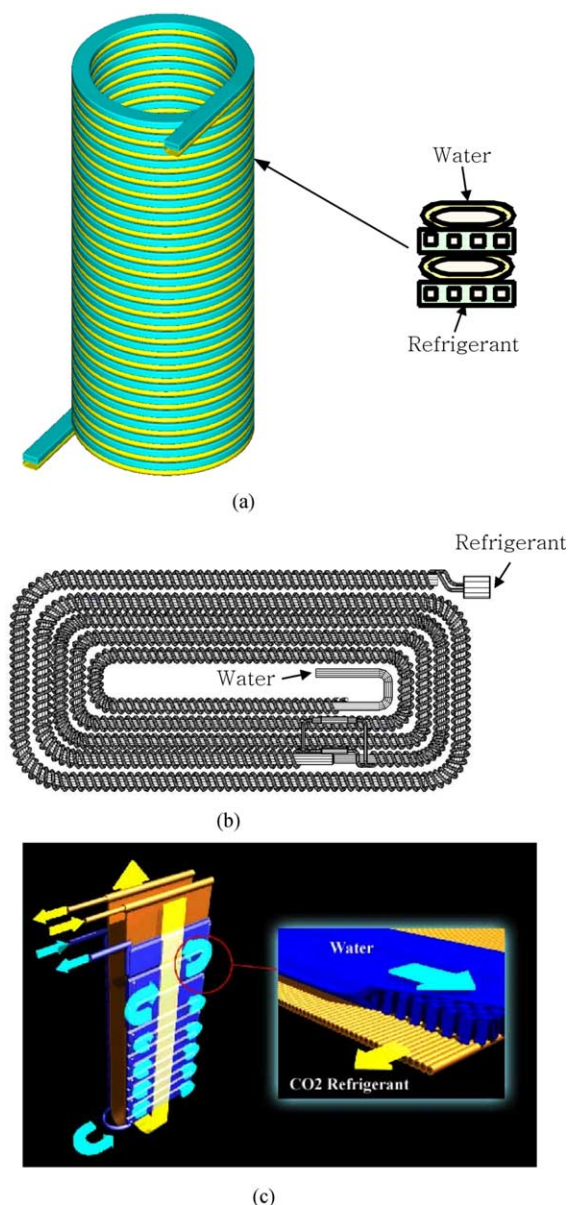


Fig. 56. Measured heating COP of laboratory prototype system, at water inlet temperature 10 °C.

Fig. 57. Gas coolers for CO₂ heat pump water heaters [168].

A 25 kW pilot plant was installed in a food-processing factory in Larvik, Norway in 1999, using waste heat from an industrial NH₃ refrigerating system as a heat source. Performance has exceeded the initial expectations, and the system has proven to be a very profitable investment for the company. A new pilot plant is now under erection in Oslo, Norway.

Several Japanese manufacturers put CO₂ heat pump water heaters on the market in 2001/2002 [165]. The typical rated heating capacity and COP are 4.5 kW and over 3.0, respectively, based on the JRA Standard 4050 [166] which provides test standards and terminologies of small CO₂ heat pump water heaters (capacity, $Q < 11.8$ kW). These water heater systems produce hot water using cheap late-night electric power, and stores hot water in a tank for daytime use [167]. These CO₂ heat pump water heaters used several different types of gas coolers for the cost effective compact systems as shown in Fig. 57 [168].

8.6. Environmental control units

Military needs for space conditioning systems for temporary shelters, command modules, and vehicles have traditionally been met by procurement rather than R&D, using custom-built units based on the same basic technology used for commercial applications. The conventional Mil-Std (Military-Standard) ECU (Environmental Control Unit) consists of a reciprocating compressor, copper tube and aluminum fin coils, scroll cage fan assemblies, and a housing that has been hardened to meet the military unique requirements as shown in Fig. 58 [73]. However, two recent developments have motivated the US military to sponsor research on CO₂ systems to meet its operational requirements for (1) lightweight ultra-compact units for rapid deployment via air transport, and (2) a refrigerant that is globally available and free of the diverse and extensive regulatory requirements and logistical challenges associated with greenhouse gases. That body of research has spanned a relatively wide spectrum, from the first demonstration of space heating operation [152] to investigations of ways to make evaporators more compact: bypassing flash gas [150]; and fundamental investigations of boiling behavior near the critical point [20]. One of the earliest theoretical analyses of



Fig. 58. Military environmental control unit [73].

Table 3
Summary of capacity and COP for the different configurations [169]

		R-22 Mil-Std	CO ₂ Basic	CO ₂ Plus
Average ^a	Capacity (kW)	9.91	7.62	8.20
	COP	1.46	0.96	1.03
Peak ^b	Capacity (kW)	12.9	11.62	11.47
	COP	2.10	1.34	1.54
Design condition ^c	Capacity (kW)	9.60	6.75	8.47
	COP	1.40	0.97	1.03

^a Average values across all sixteen test conditions (indoor: 32 °C/50 and 90% RH, and 26.7 °C/50 and 90% RH, outdoor: 52, 49, 43, and 38 °C).

^b The one test condition out of sixteen where the value was greatest (R-22 Mil-Std: at 26.7 °C/50% RH indoor and 38 °C outdoor, CO₂ Basic: at 32 °C/50% RH indoor and 38 °C outdoor, CO₂ Plus: at 32 °C/90% RH and 38 °C outdoor).

^c It reflects the current military rating point of 32 °C/50% RH indoor and 49 °C outdoor. Future Mil-Std design conditions will be raised to 32 °C/50% RH indoor and 52 °C outdoor.

this type of system compared performance of CO₂ and R-22 and found them roughly equivalent under some conditions, even if the CO₂ unit used conventional fin-and-tube heat exchangers [36].

The first data from a microchannel-based CO₂ prototype ECU were presented in 2002 as shown in Table 3 [169]. The 'CO₂ Basic' unit consists of an automotive reciprocating compressor, microchannel heat exchangers, an accumulator, and an expansion device which was a hand-adjusted metering valve. The system was designed with a safety factor of four times the expected working pressure, which is common for current military systems. The design burst pressure was 62.0 MPa since the high-side system pressure was limited to 15.5 MPa. The CO₂ Basic ECU did not perform as well as the R-22 Mil-Std ECU in terms of capacity and COP. The addition of internal heat exchanger ('CO₂ Plus' unit) improved the capacity and COP but still fell short of the R-22 baseline. They speculated that the system capacity and COP could be further improved by using an appropriate compressor, and a change in fan type. These government-sponsored research efforts have augmented the already substantial industry-funded efforts to identify opportunities for improving system efficiency by developing advanced component technologies for the next generation of prototype residential space conditioning systems.

8.7. Transport refrigeration

Research interest in CO₂ has also been renewed in the area of transport refrigeration for two reasons. The first relates to the relatively high density and capacity of CO₂ at low temperatures, compared to alternatives such as

hydrocarbons or ammonia; the advent of lightweight compact microchannel heat exchangers presents new opportunities for system optimization. Second, the worldwide availability of CO₂ and freedom from HFC-related regulatory uncertainties fits well with the global nature of the transport refrigeration industry. Shipping containers must comply with regulations at all ports, and mass-produced trucks must be capable of operating at the farthest reaches of the 'cold chain' in rural developing countries where fluorocarbon refrigerants and trained recovery technicians may not be available.

Preliminary test results on a prototype CO₂ system for truck refrigeration gave COP data that matched equally sized systems using R-502 and R-507 [170]. A Danish study predicted the performance of refrigerating systems for transport containers, concluding with COP values that were 15–20% below those of R-134a systems, not including the effects of differences in compressor efficiency and refrigerant-side pressure drops [171]. Jakobsen and Neksa [172] conducted more detailed simulations including the effects of capacity control and varying compressor efficiency at varying compression ratio. The results showed very similar COP values in freezing mode for CO₂ and R-134a over the full range of ambient temperature. In cooling mode, the excess capacity was much greater with R-134a than with CO₂ due to differences in refrigerant properties. When the influence on COP by suction throttling or cylinder unloading was included, the estimated COP in freezing mode became slightly (3–10%) higher for the CO₂ system than for the R-134a system. One problem with CO₂ may be very high compressor discharge temperature for freezing operation at high ambient temperature.

8.8. Commercial refrigeration

Commercial refrigeration systems for shops, supermarkets, larger kitchens, etc. have large refrigerant emissions, and the energy use is in many cases high. Thus, there is a need for efficient, safe and environmentally friendly refrigeration systems. New concepts based on CO₂ have been demonstrated for centralized systems using CO₂ as a secondary heat transfer fluid or in a low-temperature cascade stage, and recently decentralized concepts with heat recovery have been shown. Some of these developments are outlined in the following text.

Eggen and Aflekt [173] reviewed the possibilities for CO₂: (i) as secondary refrigerant, (ii) as a primary refrigerant in a low temperature stage in a cascade system, and (iii) in all-CO₂ centralized systems. They also presented a prototype CO₂/NH₃ cascade system built in Norway. A large number of secondary fluid systems are already operating in the Nordic countries using CO₂ as a volatile secondary refrigerant. The safety aspects and good thermophysical properties of CO₂, leading to small pipe dimensions and good heat transfer, make it a preferable

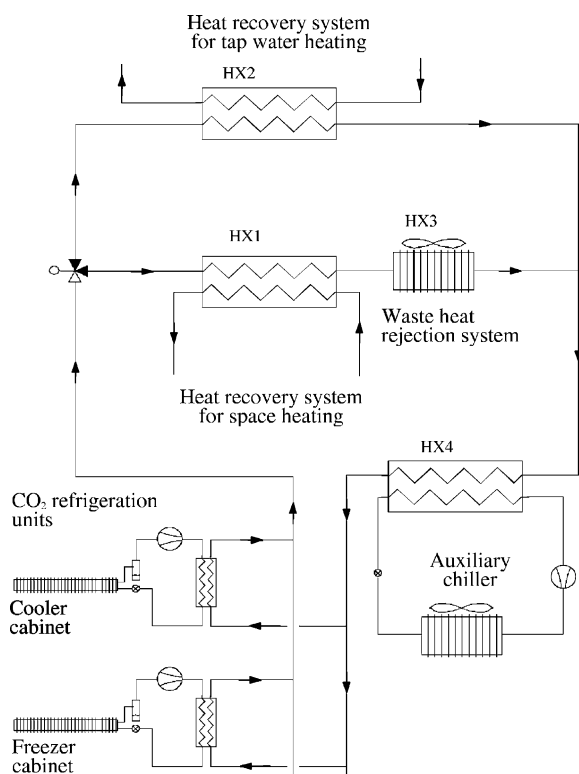


Fig. 59. Distributed CO₂ supermarket refrigeration system with central heat recovery.

fluid in indirect systems. Further advantages of cascade systems include the greatly reduced low-temperature compressor sizes, the absence of a liquid pump, and fewer stages of heat transfer. With heat recovery, centralized all-CO₂ systems may also have an interesting potential.

The decentralized supermarket system described by Neksa et al. [174] uses CO₂ as the only refrigerant in a system with heat recovery. Self-contained display cabinets

each with CO₂ refrigeration units are connected to a hydronic heat recovery circuit that heats service water and buildings (Fig. 59).

By utilizing the transcritical CO₂ process, it is possible to have a large temperature glide in the hydronic circuit, typically 50–60 K, and a correspondingly low volume flow rate and small pipe dimensions. Waste heat with high temperature (70–75 °C) is available for tap water and/or space heating. Excess heat is rejected to the ambient air by direct heat exchange. The system offers a very easy installation and gives the owner of the store a great flexibility in arranging and rearranging the cabinets.

System simulations for a medium size supermarket have been carried out. Optimum hydronic supply and return temperatures to the cooling and freezing cabinets were identified. A comparison between the CO₂ system and a conventional R-22 system with respect to the overall energy consumption of the supermarket for one year of operation in a southern European climate was carried out. The CO₂ system was found to reduce the total energy consumption for refrigeration and heating by 32% compared to the R-22 system. Each CO₂ unit can also be equipped with a condensing unit in order to reject heat directly to the shopping area when space heating is required. In the warm season with a heat surplus, the waste heat recovery circuit removes the heat. This concept reduces the power demand for the refrigeration units to the same level as for the baseline R-22 system, and the resulting overall energy consumption of the supermarket will then be further reduced.

8.9. Dryers

Another interesting application of CO₂ vapor compression cycle is heat pump dryer. One example is the prototype of a commercial size dryer as shown in Fig. 60, which shows the schemes of the heat pump and the hot air circuit [175]. The auxiliary heat exchanger is located

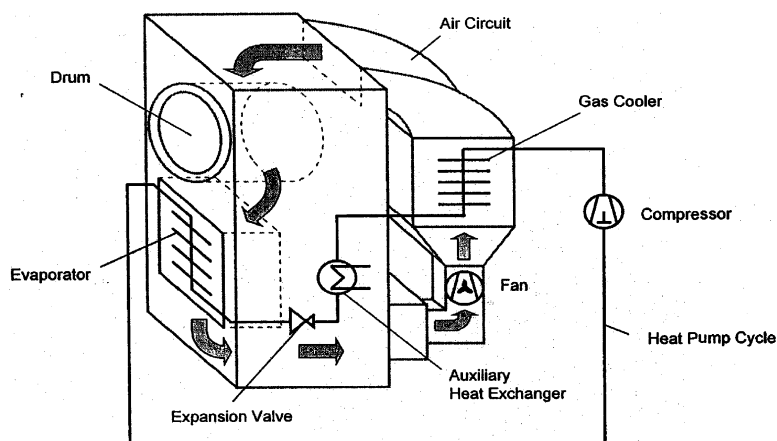


Fig. 60. CO₂ heat pump dryer [175].

between a gas cooler and an expansion valve, thus contributing to additional cooling of the supercritical CO₂. Based on theoretical considerations, Steimle [176] reported that energy saving is possible due to better temperature adaptation in the heat exchangers, compared to subcritical processes. It is also possible to achieve higher air temperatures without loss in efficiency, thus increasing the moisture extraction rate. Schmidt et al. [175,177] compared the thermodynamic behavior of two dehumidification heat pump cycles: the subcritical R-134a process and the transcritical CO₂ process. Experimental results from Schmidt et al. [175] report heat pump COPs in the range 5.5 and 55% reduction in the energy consumption, including fan power, compared to traditional electrically heated clothes dryer. The results were achieved after a first optimization of the prototype system and it was claimed that further improvements still could be realized.

9. Concluding remarks

The state of the art for the transcritical CO₂ cycle technology in various refrigeration, air-conditioning and heat pump applications was critically reviewed. The article covered the history and re-emergence of the natural refrigerant CO₂, its thermodynamic and transport properties, basic CO₂ transcritical cycles and some options of cycle modifications (advanced cycles), heat transfer and pressure drop characteristics in CO₂ systems, and issues and design characteristics related to high operating pressure. It also explored component design issues and possible applications for the earliest markets, and those barriers to be overcome before commercialization.

The prospects for CO₂ and its transcritical cycle are still uncertain, mainly because of the many simultaneous component and system innovations required, e.g. to handle the high pressures, and to develop microchannel evaporators that tolerate frost and condensate while distributing refrigerant uniformly. The greatest obstacle it faces is its high temperature of heat rejection, which explains why its first commercial opportunities are occurring in water heating, and in space heating applications where high delivery temperatures are required. Its inherent advantage—negligible global warming impact—has focused most of the early research on automotive air conditioning applications where direct refrigerant leakage has been a significant contributor to global warming.

The re-emergence of the ‘old refrigerant’ CO₂ provides a historical context for making several important observations about the path of technological innovation in air conditioning and refrigeration systems and components. A century ago, the earliest engineering development efforts focused on the compressor because it was the most costly component, and efficiency improvements accompanied cost reduction. With the advent of CFCs that could operate at low pressures

with reasonable thermodynamic cycle efficiencies and avoid the toxicity or flammability risks of ammonia and hydrocarbons, system costs dropped to the point where mass production became feasible. Declining real energy prices over most of the twentieth century expanded the market for air conditioning, so the industry realized the economies of mass production by (1) focusing on the simple ‘standard’ vapor-compression cycle to minimize the number of components, and (2) optimizing the components to make the actual cycle approach the refrigerant’s ideal thermodynamic efficiency, for example, by taking full advantage of the particular refrigerant’s transport properties.

Over the last decade the situation began to change dramatically as chlorofluorocarbon refrigerants were phased out, and the prospect of global warming signaled higher energy costs and controls on fluorocarbon refrigerants. In parts of the world where energy prices are already high, the simple vapor-compression cycle efficiency has been increased by adding sensors, actuators and controls to allow modulating refrigerant flow rate, thereby minimizing temperature differences across the heat exchangers at all operating conditions. Unfortunately, the maximum efficiency attainable through this approach is refrigerant-specific: the COP of that particular refrigerant on the standard cycle. Today’s research is focusing on ways to modify the standard vapor-compression cycle, for example, through use of multistage compression, intercooling, internal heat exchangers and expanders as is now done routinely in industrial-scale systems where energy costs dominate.

As the cycle is modified by addition of such components and controls, the system COP depends less on the thermodynamic properties of the refrigerant and more on the cost of manufacturing the more complex systems. Therefore, refrigerants will be chosen in the future for their environmental safety and compatibility with various cycle-improving component designs, rather than their simple-cycle ideal efficiency. If the cost of sensors, actuators and microprocessor controls continue to decrease, along with the cost of embedding them in mass produced items, the cost advantage now enjoyed by refrigerants having favorable thermodynamic properties may diminish. Modern manufacturing technologies (e.g. for making small diameter tubes) have already reduced the weight and volume penalties once associated with high-pressure refrigerants like CO₂, and various methods for refrigerant-side area enhancement have further decreased the importance of refrigerant transport properties.

Strictly speaking, the Carnot cycle is not always the ideal because heat sources and sinks are finite in all heat pumping applications. This is especially true in heating mode where substantial increases in air or water temperatures are required; the temperature glide of the transcritical CO₂ cycle provides a distinct advantage in such cases. While such loads are generally met today by direct fossil fuel combustion at COPs less than one, in the future they are

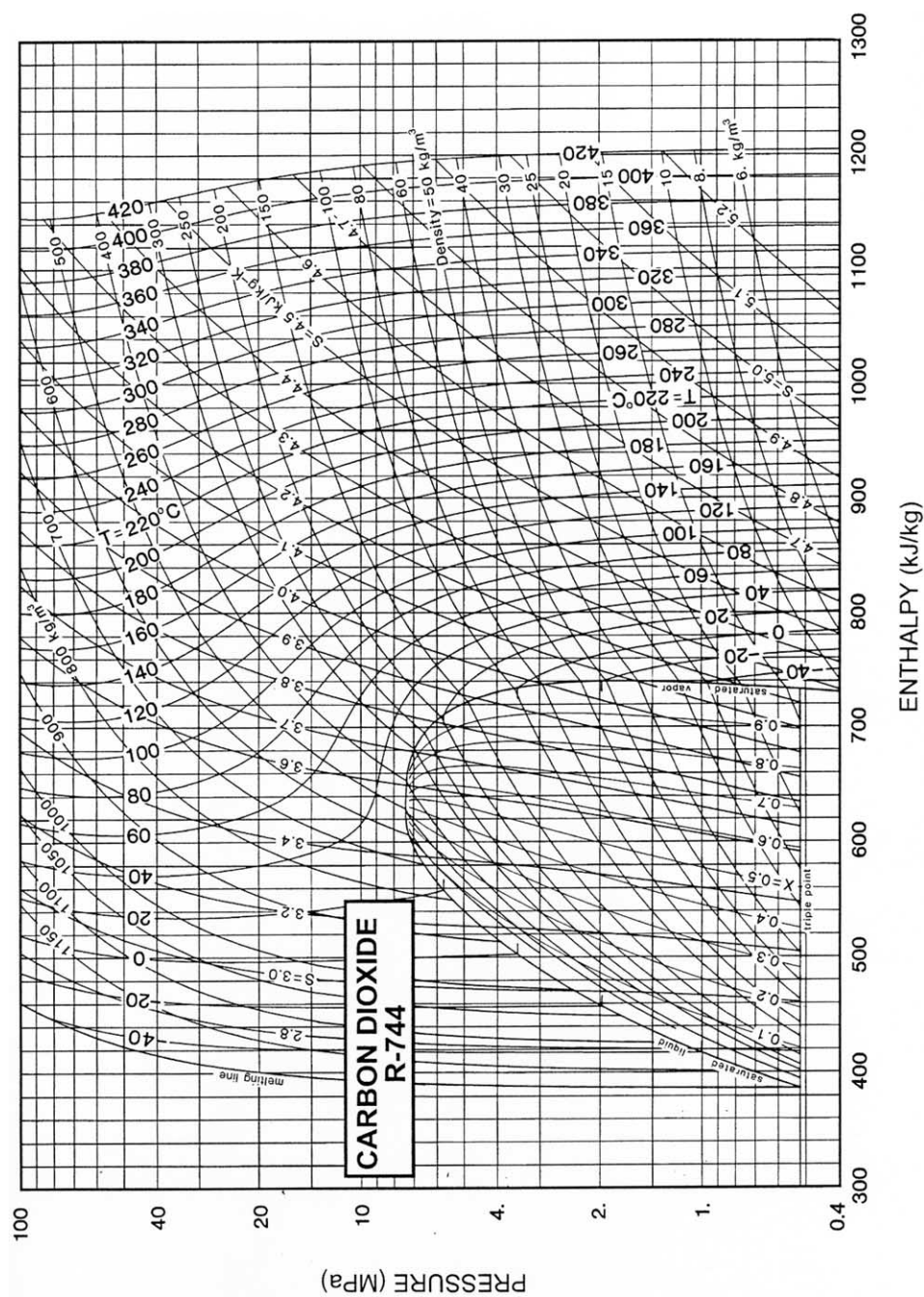
Fig. A1. Pressure-enthalpy diagram of CO₂ [19].

Table A1
Refrigerant CO₂ properties of saturated liquid and vapor [19]

Temperature ^a , °C	Pressure, MPa	Density (liquid), kg/m ³	Volume (Vapour), m ³ /kg	Enthalpy, kJ/kg	Entropy, kJ/(kg K)		Specific heat, c_p , kJ/(kg K)		c_p/c_v		Velocity of sound, m/s		Viscosity, μ Pa s		Thermal conductivity, mW/(m K)		Surface tension, mN/m	Temp., °C
					Liquid	Vapour	Liquid	Vapour	Liquid	Vapour	Liquid	Vapour	Liquid	Vapour	Liquid	Vapour		
-56.56a	0.51796	1178.5	0.07267	80.04	430.42	0.5213	2.1390	1.953	0.909	1.444	976.0	222.8	256.7	10.95	180.6	11.01	17.16	-56.56
-50.00	0.68234	1154.6	0.05579	92.94	432.69	0.5794	2.1018	1.971	0.952	1.468	928.0	223.4	229.3	11.31	172.1	11.58	15.53	-50.00
-48.00	0.73949	1147.1	0.05162	96.90	433.29	0.5968	2.0909	1.978	0.967	1.477	914.0	223.5	221.6	11.42	169.5	11.76	15.04	-48.00
-46.00	0.80015	1139.6	0.04782	100.88	433.86	0.6142	2.0801	1.985	0.982	1.486	900.0	223.6	214.3	11.53	166.9	11.95	14.56	-46.00
-44.00	0.86445	1132.0	0.04435	104.87	434.39	0.6314	2.0694	1.993	0.998	1.496	885.0	223.6	207.2	11.64	164.4	12.14	14.07	-44.00
-42.00	0.93252	1124.2	0.04118	108.88	434.88	0.6486	2.0589	2.002	1.015	1.507	871.0	223.6	200.3	11.75	161.8	12.34	13.60	-42.00
-40.00	1.0045	1116.4	0.03828	112.90	435.32	0.6656	2.0485	2.012	1.033	1.518	856.0	223.5	193.8	11.87	159.3	12.54	13.12	-40.00
-38.00	1.0805	1108.5	0.03562	116.95	435.72	0.6826	2.0382	2.022	1.052	1.530	842.0	223.4	187.4	11.98	156.8	12.75	12.65	-38.00
-36.00	1.1607	1100.5	0.03318	121.01	436.07	0.6995	2.0281	2.033	1.072	1.544	827.0	223.2	181.3	12.10	154.3	12.97	12.18	-36.00
-34.00	1.2452	1092.4	0.03093	125.10	436.37	0.7163	2.0180	2.045	1.094	1.558	813.0	223.1	175.4	12.22	151.8	13.20	11.72	-34.00
-32.00	1.3342	1084.1	0.02886	129.20	436.62	0.7331	2.0079	2.059	1.116	1.573	798.0	222.8	169.7	12.34	149.3	13.43	11.26	-32.00
-30.00	1.4278	1075.7	0.02696	133.34	436.82	0.7498	1.9980	2.073	1.141	1.590	783.0	222.5	164.2	12.46	146.9	13.68	10.80	-30.00
-28.00	1.5261	1067.2	0.02519	137.50	436.96	0.7665	1.9880	2.089	1.166	1.608	768.0	222.2	158.9	12.59	144.4	13.94	10.35	-28.00
-26.00	1.6293	1058.6	0.02356	141.69	437.06	0.7831	1.9781	2.105	1.194	1.627	753.0	221.8	153.8	12.72	141.9	14.20	9.90	-26.00
-24.00	1.7375	1049.8	0.02205	145.91	437.06	0.7997	1.9683	2.124	1.223	1.648	738.0	221.4	148.8	12.85	139.5	14.49	9.46	-24.00
-22.00	1.8509	1040.8	0.02065	150.16	437.01	0.8163	1.9584	2.144	1.255	1.671	723.0	220.9	144.0	12.98	137.1	14.78	9.02	-22.00
-20.00	1.9696	1031.7	0.01934	154.45	436.89	0.8328	1.9485	2.165	1.289	1.696	708.0	220.4	139.3	13.12	134.6	15.09	8.59	-20.00
-19.00	2.0310	1027.0	0.01873	156.61	436.81	0.8411	1.9436	2.177	1.307	1.709	700.0	220.1	137.1	13.18	133.4	15.25	8.37	-19.00
-18.00	2.0938	1017.6	0.01756	158.77	436.70	0.8494	1.9386	2.189	1.326	1.723	684.0	219.5	132.6	13.33	131.0	15.59	7.95	-18.00
-17.00	2.1581	1012.8	0.01700	160.95	436.58	0.8576	1.9337	2.201	1.346	1.738	676.0	219.2	130.4	13.40	129.8	15.77	7.74	-17.00
-16.00	2.2237	1008.0	0.01647	163.14	436.44	0.8659	1.9287	2.215	1.366	1.753	660.0	218.5	128.3	13.47	128.6	15.95	7.53	-16.00
-15.00	2.2908	1003.1	0.01595	165.34	436.27	0.8742	1.9237	2.228	1.388	1.768	643.0	217.7	126.2	13.55	127.4	16.14	7.32	-15.00
-14.00	2.3593	998.1	0.01545	167.55	436.09	0.8825	1.9187	2.243	1.410	1.785	626.0	216.9	124.1	13.63	126.2	16.34	7.11	-14.00
-13.00	2.4294	993.1	0.01497	169.78	435.89	0.8908	1.9137	2.258	1.433	1.802	610.0	216.1	122.0	13.70	125.0	16.54	6.90	-13.00
-12.00	2.5010	988.1	0.01450	172.01	435.66	0.8991	1.9086	2.273	1.457	1.821	600.0	215.6	120.0	13.78	123.8	16.74	6.70	-12.00
-11.00	2.5740	982.9	0.01405	174.26	435.41	0.9074	1.9036	2.290	1.483	1.840	600.0	215.2	118.0	13.86	122.5	16.96	6.50	-11.00
-10.00	2.6487	977.7	0.01361	176.52	435.14	0.9157	1.8985	2.307	1.509	1.860	600.0	214.7	116.1	13.95	121.3	17.18	6.29	-10.00
-9.00	2.7249	972.5	0.01319	178.80	434.84	0.9240	1.8934	2.325	1.537	1.881	600.0	214.2	114.1	14.03	120.1	17.42	6.09	-9.00
-8.00	2.8027	967.1	0.01278	181.09	434.51	0.9324	1.8882	2.345	1.566	1.904	600.0	213.7	112.2	14.12	118.9	17.66	5.89	-8.00
-7.00	2.8821	961.7	0.01238	183.39	434.17	0.9408	1.8830	2.365	1.597	1.927	600.0	213.2	110.3	14.20	117.7	17.91	5.70	-7.00
-6.00	2.9632	956.2	0.01200	185.71	433.78	0.9491	1.8778	2.386	1.629	1.952	591.0	212.6	108.4	14.30	116.5	18.17	5.50	-6.00
-5.00	3.0459	950.6	0.01162	188.05	433.33	0.9576	1.8725	2.408	1.663	1.979	582.0	212.0	106.6	14.39	115.3	18.44	5.30	-5.00
-4.00	3.1303	945.0	0.01126	190.40	432.95	0.9660	1.8672	2.432	1.699	2.007	573.0	211.4	104.8	14.48	114.1	18.73	5.11	-4.00
-3.00	3.2164	939.2	0.01091	192.77	432.48	0.9744	1.8618	2.457	1.737	2.037	564.0	210.8	102.9	14.58	112.9	19.03	4.92	-3.00
-2.00	3.3042	933.4	0.01057	195.16	431.99	0.9829	1.8563	2.484	1.777	2.068	555.0	210.2	101.2	14.68	111.6	19.34	4.73	-2.00
-1.00	3.3938			197.57	431.46	0.9914	1.8509	2.512	1.819	2.102	546.0	212.6						-1.00

(continued on next page)

Table A1 (continued)

Temperature, °C	Pressure, MPa	Density (liquid), kg/m ³	Volume (Vapour), m ³ /kg	Enthalpy, kJ/kg	Entropy, kJ/(kg K)		Specific heat, c_p , kJ/(kg K)	c_p/c_v		Velocity of sound, m/s	Viscosity, μ Pa s		Thermal conductivity, mW/(m K)		Surface tension, mN/m	Temp., °C
					Liquid	Vapour		Liquid	Vapour		Liquid	Vapour	Liquid	Vapour		
0.00	3.4851	927.4	0.01024	200.00	430.89	1.0000	1.8453	2.542	1.865	2.138	99.4	14.79	110.4	19.67	4.54	0.00
1.00	3.5783	921.4	0.00992	202.45	430.29	1.0086	1.8397	2.574	1.913	2.176	97.6	14.89	109.2	20.02	4.35	1.00
2.00	3.6733	915.2	0.00961	204.93	429.65	1.0172	1.8340	2.609	1.965	2.218	95.9	15.00	108.0	20.38	4.17	2.00
3.00	3.7701	909.0	0.00931	207.43	428.97	1.0259	1.8282	2.645	2.020	2.262	94.2	15.12	106.8	20.76	3.99	3.00
4.00	3.8688	902.6	0.00901	209.95	428.25	1.0346	1.8223	2.685	2.080	2.309	92.5	15.24	105.5	21.17	3.80	4.00
5.00	3.9695	896.0	0.00872	212.50	427.48	1.0434	1.8163	2.727	2.144	2.360	90.8	15.36	104.3	21.60	3.62	5.00
6.00	4.0720	889.4	0.00845	215.08	426.67	1.0523	1.8102	2.772	2.213	2.416	89.1	15.49	103.1	22.06	3.45	6.00
7.00	4.1765	882.6	0.00817	217.69	425.81	1.0612	1.8041	2.822	2.289	2.476	87.5	15.62	101.8	22.54	3.27	7.00
8.00	4.2831	875.6	0.00791	220.34	424.89	1.0702	1.7977	2.875	2.370	2.541	85.8	15.76	100.6	23.06	3.10	8.00
9.00	4.3916	868.4	0.00765	223.01	423.92	1.0792	1.7913	2.934	2.460	2.612	84.2	15.91	99.4	23.61	2.93	9.00
10.00	4.5022	861.1	0.00740	225.73	422.88	1.0884	1.7847	2.998	2.558	2.690	82.6	16.06	98.1	24.21	2.76	10.00
11.00	4.6149	853.6	0.00715	228.49	421.79	1.0976	1.7779	3.068	2.666	2.776	80.9	16.22	96.9	24.84	2.59	11.00
12.00	4.7297	845.9	0.00691	231.29	420.62	1.1070	1.7710	3.145	2.786	2.871	79.3	16.39	95.6	25.53	2.42	12.00
13.00	4.8466	837.9	0.00668	234.13	419.37	1.1165	1.7638	3.232	2.919	2.977	77.7	16.56	94.4	26.27	2.26	13.00
14.00	4.9658	829.7	0.00645	237.03	418.05	1.1261	1.7565	3.328	3.068	3.095	76.1	16.75	93.1	27.08	2.10	14.00
15.00	5.0871	821.2	0.00622	239.99	416.64	1.1359	1.7489	3.436	3.237	3.228	74.4	16.95	91.9	27.96	1.95	15.00
16.00	5.2108	812.4	0.00600	243.01	415.12	1.1458	1.7411	3.558	3.429	3.378	72.8	17.16	90.6	28.93	1.79	16.00
17.00	5.3368	803.3	0.00578	246.10	413.50	1.1559	1.7329	3.698	3.649	3.550	71.2	17.39	89.4	29.99	1.64	17.00
18.00	5.4651	793.8	0.00557	249.26	411.76	1.1663	1.7244	3.858	3.905	3.748	69.5	17.64	88.1	31.16	1.49	18.00
19.00	5.5958	783.8	0.00536	252.52	409.89	1.1769	1.7155	4.044	4.204	3.979	67.8	17.90	86.9	32.47	1.35	19.00
20.00	5.7291	773.4	0.00515	255.87	407.87	1.1877	1.7062	4.264	4.560	4.252	66.1	18.19	85.7	33.94	1.20	20.00
21.00	5.8648	762.4	0.00494	259.33	405.67	1.1989	1.6964	4.526	4.990	4.578	64.4	18.50	84.5	35.61	1.06	21.00
22.00	6.0031	750.8	0.00474	262.93	403.26	1.2105	1.6860	4.846	5.519	4.976	62.7	18.85	83.4	37.52	0.93	22.00
23.00	6.1440	738.4	0.00453	266.68	400.63	1.2225	1.6749	5.248	6.185	5.472	60.9	19.23	82.4	39.74	0.80	23.00
24.00	6.2877	725.0	0.00433	270.61	397.70	1.2352	1.6629	5.767	7.049	6.107	59.0	19.66	81.5	42.35	0.67	24.00
25.00	6.4342	710.5	0.00412	274.78	394.43	1.2485	1.6498	6.467	8.212	6.949	57.0	20.16	80.8	45.51	0.55	25.00
26.00	6.5837	694.5	0.00391	279.26	391.71	1.2627	1.6353	7.460	9.862	8.121	55.0	20.73	80.5	49.44	0.44	26.00
27.00	6.7361	676.4	0.00369	284.14	386.39	1.2783	1.6189	8.97	12.38	9.87	52.8	21.42	80.7	54.56	0.33	27.00
28.00	6.8918	655.3	0.00346	289.62	381.20	1.2958	1.5999	11.55	16.69	12.78	50.3	22.27	81.9	61.73	0.23	28.00
29.00	7.0509	629.4	0.00320	296.07	374.61	1.3163	1.5763	16.95	25.74	18.63	47.5	23.41	85.2	73.19	0.13	29.00
30.00	7.2137	593.3	0.00290	304.55	365.13	1.3435	1.5433	35.34	55.82	36.66	43.8	25.17	95.4	98.02	0.02	30.00
30.98c	7.3773	467.6	0.00214	332.25	332.25	1.4336	1.4336	∞	∞	∞	—	—	∞	∞	0.00	30.98

^a Temperatures are on the ITS-90 scale. a, triple point; c, critical point.

likely to be met by heat pumps at $COP \gg 1$ as regulation of greenhouse gas emissions requires that fossil fuels be used more efficiently. The early introduction of transcritical CO₂ systems into the Asian domestic water heating market is providing the first test of this hypothesis, since earlier attempts to introduce subcritical systems have failed.

Research on alternative refrigerants is continuing on many parallel paths, including explorations of the use of hydrocarbons or ammonia by minimizing charge or using secondary refrigerant loops. Each of these paths efforts is yielding surprising results, as illustrated by this review for the case of CO₂. What these efforts have in common is that they are bring fundamental research to bear on a technology whose development has been driven for decades by reliability concerns, and therefore characterized by incremental improvements built on a massive empirical database. After the Montreal and Kyoto Protocols rendered much of this data useless, the industry entered an era of discontinuous technological change that required development of new technology within the industry, as well as importing technology from outside.

Acknowledgements

This work was partly supported by the Brain Korea 21 Program, by Shecco Technology, and by the member companies of the Air Conditioning and Refrigeration Center at the University of Illinois at Urbana-Champaign.

Appendix A. Pressure–enthalpy diagram and saturation properties for CO₂

See Fig. A1 and Table A1.

References

- [1] The Kyoto Protocol to the United Nations Framework Convention on Climate Change, 1997.
- [2] Billiard F. Refrigeration and air conditioning: what's new at regulatory level. The Ninth European Conference on Technological Innovations in Refrigeration, Air Conditioning and in the Food Industry, Politecnico di Milano; 2001.
- [3] Lorentzen G, Pettersen J. New possibilities for non-CFC refrigeration. In: Pettersen J, editor. IIR International Symposium on Refrigeration, Energy and Environment, Trondheim, Norway. 1992. p. 147–63.
- [4] Bodinus WS. The rise and fall of carbon dioxide systems. In: Will HM, editor. The first century of air conditioning. Atlanta, GA: ASHRAE; 1999. p. 29–34.
- [5] Thevenot R. A history of refrigeration throughout the world. Paris: IIR; 1979. [Fidler JC, Trans.].
- [6] Donaldson B, Nagengast B. Heat and cold: mastering the great indoors. Atlanta, GA: ASHRAE; 1994.
- [7] Kohlendioxid. Besonderheiten und Einsatzchancen als Kältemittel. Statusbericht des Deutschen Kälte- und Klimatechnischen Vereins. Nr 20. DKV, Stuttgart; 1998.
- [8] Stera A. Ammonia refrigerating plant on reefer ships. Introduction to ammonia as a marine refrigerant. Lloyd's Register Technical Seminar, London; 1992.
- [9] Plank R. Amerikanische Kältetechnik. Berlin: VDI-Verlag; 1929.
- [10] Voorhees G. Improvements relating to systems of fluid compression and to compressors thereof. British Patent 4448; 1905.
- [11] Lorentzen G. Trans-critical vapour compression cycle device. International Patent Publication WO 90/07683; 1990.
- [12] Morley J, Bivens D. Trends in environmental issues and implications for automotive air conditioning. Vehicle Thermal Management Systems Conference, London; 1995. p. 405–12.
- [13] Bhatti M. A critical look at R-744 and R-134a mobile air conditioning systems. SAE Paper No. 970527; 1997.
- [14] Rieberer R. CO₂ as working fluid for heat pump. PhD Thesis. Institute of Thermal Engineering, Graz University, Austria; 1998.
- [15] Lorentzen G. The use of natural refrigerants: a complete solution to the CFC/HCFC predicament. Int J Refrig 1995; 18(3):190–7.
- [16] Vesovic V, Wakeham WA, Olchowy GA, Sengers JV, Watson JTR, Millat J. The transport properties of carbon dioxide. J Phys Chem Ref Data 1990;19:763–808.
- [17] Fenghour A, Wakeham W, Vesovic V. The viscosity of carbon dioxide. J Phys Chem Ref Data 1998;27(1):31–44.
- [18] VDI, VDI Wärmeatlas: Berechnungsblätter für den Wärmeübergang. Düsseldorf, Germany: VDI Verlag; 1994.
- [19] ASHRAE, ASHRAE handbook: fundamentals. Atlanta, GA: American Society of Heating, Refrigerating and Air-Conditioning Engineers; 2001.
- [20] Pettersen J. Flow vaporization of CO₂ in microchannel tubes. PhD Thesis, Norwegian University of Science and Technology, Norway; 2002.
- [21] Liley P, Desai P. Thermophysical properties of refrigerants, SI ed. ASHRAE; 1993. p. 259–67.
- [22] Klein S, Alvarado F. Engineering equation solver, version 6.242. F-Chart Software; 2001.
- [23] Span R, Wagner W. A new equation of state for carbon dioxide covering the fluid region from the triple-point temperature to 1100 K at pressure up to 800 MPa. J Phys Chem Ref Data 1996;26:1509–96.
- [24] Bredeesen A, Hafner A, Pettersen J, Aflekt K. Heat transfer and pressure drop for in-tube evaporation of CO₂. International Conference on Heat Transfer Issues in Natural Refrigerants, College Park, MD; 1997. p. 1–15.
- [25] Rathjen W, Straub J. Temperature dependence of surface tension, coexistence curve, and vapor pressure of CO₂, CClF₃, CBrF₃, and SF₆. Heat transfer in boiling, New York: Academic Press; 1977 [chapter 18].
- [26] Estrada-Alexanders AF, Trusler JPM. Speed of sound in carbon dioxide at temperatures between (220 and 450) K and pressures up to 14 MPa. J Chem Thermodyn 1998;30(12):1589–601.
- [27] Liao S, Zhao T. Measurements of heat transfer coefficients from supercritical carbon dioxide flowing in horizontal mini/meso channels. J Heat Transfer 2002;124:413–20.

- [28] Pettersen J, Skaugen G. Operation of trans-critical CO₂ vapour compression systems in vehicle air conditioning. IIR International Conference on New Applications of Natural Working Fluids in Refrigeration and Air Conditioning, Hanover, Germany; 1994. p. 495–505.
- [29] Inokuty H. Graphical method of finding compression pressure of CO₂ refrigerating machine for maximum coefficient of performance. The Fifth International Congress of Refrigeration, Rome; 1928. p. 185–92.
- [30] Pettersen J. Process with high-pressure control. Kohlendioxid: Besonderheiten und Einsatzchancen als Kältemittel, Statusbericht des DKV, No. 20, German Association of Refrigeration and Air Conditioning; 1998. p. 64–74.
- [31] Pettersen J. Experimental results of carbon dioxide in compression systems. ASHRAE/NIST Conference Refrigerants for the 21st Century, Gaithersburg, MD; 1997. p. 27–37.
- [32] Lorentzen G. Revival of carbon dioxide as a refrigerant. Int J Refrig 1993;17(5):292–301.
- [33] Domanski P, Didion D, Doyle J. Evaluation of suction-line/liquid-line heat exchange in the refrigeration cycle. Int J Refrig 1994;17(7):487–93.
- [34] Kim M-H. Performance evaluation of R-22 alternative mixtures in a heat pump with pure cross-flow condenser and counter-flow evaporator. Energy 2002;27(2):167–81.
- [35] Vakili H. Thermodynamics of heat exchange in refrigeration cycles with non-azeotropic mixtures. Part II. Suction line heat exchange and evaporative cooling of capillary. Proceedings of the International Congress of Refrigeration, Paris, France: IIR; 1983. p. 533–8.
- [36] Robinson D, Groll E. Efficiencies of transcritical CO₂ cycles with and without an expansion turbine. Int J Refrig 1998; 21(7):577–89.
- [37] Boewe D, Yin J, Park Y, Bullard C, Hrnjak P. The role of suction line heat exchanger in transcritical R744 mobile A/C systems. SAE Paper No. 1999-01-0583; 1999.
- [38] Negishi M. Refrigeration air conditioner. Japan No. JP11094379; 1997.
- [39] Plank R. Arbeitsverfahren an Kompressionskältemaschinen, insbesondere für Kälteüberträger mit tiefer kritischer Temperatur. German Patent No. DE278095; 1912.
- [40] Ikoma M, Hasegawa H, Shintaku H. Refrigeration cycle device and its control method. Japan Patent No. JP2002022298; 2000.
- [41] Maurer T, Zinn T. Untersuchung von Entspannungsmaschinen mit mechanischer Leistungsauskopplung für die transkritische CO₂-Kältemaschine. DKV-Tagungsbericht 26, Berlin; 1999. p. 264–77.
- [42] Heyl P, Quack H. Transcritical CO₂ cycle with expander–compressor. In: Groll EA, Robinson DM, editors. The Fourth IIR-Gustav Lorentzen Conference on Natural Working Fluids, West Lafayette, IN. 2000. p. 471–80.
- [43] Stosic N, Smith I, Kovacevic A. A twin screw combined compressor and expander for CO₂ refrigeration systems. In: Soedel W, editor. Proceedings of the International Compressor Engineering Conference at Purdue, West Lafayette, IN. Paper No. C21-2; 2002. p. 703–10.
- [44] Huff H-J, Lindsay D, Radermacher R. Positive displacement compressor and expander simulation. In: Soedel W, editor. Proceedings of the International Compressor Engineering Conference at Purdue, West Lafayette, IN. Paper No. C9-2; 2002. p. 209–16.
- [45] Baek J, Groll E, Lawless P. Development of a piston-cylinder expansion device for the transcritical carbon dioxide cycle. In: Groll EA, editor. Proceedings of the International Refrigeration and Air Conditioning Conference at Purdue, West Lafayette, IN, Paper No. R11-8. 2002.
- [46] Heyl P, Quack H. Free piston expander–compressor for CO₂: design, applications and results. The 20th International Congress of Refrigeration, Sydney, Australia; 1999.
- [47] Nickl J, Will G, Kraus W, Quack H. Design considerations for a second generation CO₂-expander. In: Xu Z, Fan J, Huang W, editors. The Fifth IIR-Gustav Lorentzen Conference on Natural Working Fluids. Guangzhou, China. 2002. p. 189–96.
- [48] Hess U, Tiedemann T. Klimaanlage für Kraftfahrzeuge und Verfahren zum Betreiben einer Klimaanlage für Kraftfahrzeuge. German Patent No. DE19959439, 1999.
- [49] Adachi Y, Kazuo K, Masahiro I. Vapor compression type refrigerator. Japan Patent No. JP2000241033; 1999.
- [50] Heidelck R, Kruse H. Expansion machines for carbon dioxide based on modified reciprocating machines. In: Groll EA, Robinson DM, editors. The Fourth IIR-Gustav Lorentzen Conference on Natural Working Fluids, West Lafayette, IN. 2000. p. 455–62.
- [51] Hesse U. Klimaanlage, insbesondere für Kraftfahrzeuge und Verfahren zum Betreiben einer Klimaanlage, insbesondere für Kraftfahrzeuge. German Patent No. DE10013191; 2000.
- [52] Plank R. Ueber den Ideal-Prozess von Kältemaschinen bei Verbund-Kompression. Zeitschrift für die gesamte Kälte-Industrie 1928;35:17–24.
- [53] Thiessen H. Verfahren zum Betrieb einer Kompressionskälteanlage. German Patent No. DE19522884; 1995.
- [54] Ozaki Y, Sakajo Y, Sakakibara H, Uchida, K. Vapor compression type refrigerating system. European Patent No. EP0837291; 1997.
- [55] Shunichi F, Hiroshi K. Refrigerating cycle. European Patent No. EP0976991; 1999.
- [56] Okaza N, Nishiwaki F, Fukunara S, Matsuo M, Yoshida Y. Refrigeration cycle. Japan Patent No. JP2001133058; 1999.
- [57] Pettersen J. Cycle options for CO₂. Workshop on Vapor Compression with the Critical Point in Mind, College Park, MD; 2000.
- [58] Huff H-J, Hwang Y, Radermacher R. Options for a two-stage transcritical carbon dioxide cycle. In: Xu Z, Fan J, Huang W, editors. The Fifth IIR-Gustav Lorentzen Conference on Natural Working Fluids, Guangzhou, China. 2002. p. 143–9.
- [59] Inagaki M, Sasaya H, Ozakli Y. Pointing to the future: two-stage CO₂ compression. Heat transfer issues in natural refrigerants, International Institute of Refrigeration; 1997. p. 131–40.
- [60] Olson D. Heat transfer of supercritical carbon dioxide flowing in a cooled horizontal tube. In: Groll EA, Robinson DM, editors. The Fourth IIR-Gustav Lorentzen Conference on Natural Working Fluids, West Lafayette, IN. 2000. p. 251–8.
- [61] Gnielinski V. New equations for heat and mass transfer in turbulent pipe and channel flow. Int Chem Engng 1976;16(2): 359–68.
- [62] Krasnoshchekov E, Protopopov V. A generalized relationship for calculation of heat transfer to carbon dioxide at

- supercritical pressure. *Telofizika Vysokikh Temperatur* 1972;9(6):1314.
- [63] Pitla S, Robinson D, Zingerli A, Groll E, Ramadhyani S. Heat transfer and pressure drop characteristics during in-tube gas cooling of supercritical carbon dioxide. ASHRAE 913-RP, report HL 2000-10 No. 3613-1, Herrick Laboratories, Purdue University; 2000.
- [64] Pitla S, Robinson D, Groll E, Ramadhyani S. Heat transfer from supercritical carbon dioxide in tube flow: a critical review. *Int J HVAC&R Res* 1998;4(3):281–301.
- [65] Pitla S, Groll E, Ramadhyani S. Convective heat transfer from in-tube flow of turbulent supercritical carbon dioxide. Part 1. Numerical analysis. *Int J HVAC&R Res* 2001;7(4):345–66.
- [66] Pitla S, Groll E, Ramadhyani S. Convective heat transfer from in-tube cooling of turbulent supercritical carbon dioxide. Part 2. Experimental data and numerical predictions. *Int J HVAC&R Res* 2001;7(4):367–82.
- [67] Pettersen J, Rieberer R, Leister A. Heat transfer and pressure drop characteristics of supercritical carbon dioxide in microchannel tubes under cooling. In: Groll EA, Robinson DM, editors. *The Fourth IIR-Gustav Lorentzen Conference on Natural Working Fluids*, West Lafayette, IN. 2000. p. 99–106.
- [68] Sun Z, Groll E. CO₂ flow boiling in horizontal tubes. Internal report No. HL-2001-8, Ray W. Herrick Laboratories, Purdue University; 2000.
- [69] Hihara E, Tanaka S. Boiling heat transfer of carbon dioxide in horizontal tubes. In: Groll EA, Robinson DM, editors. *The Fourth IIR-Gustav Lorentzen Conference on Natural Working Fluids*, West Lafayette, IN. 2000. p. 279–84.
- [70] Lombardi C, Carsana C. A dimensionless pressure drop correlation for two-phase mixtures flowing upflow in vertical ducts covering wide parameter range. *Heat Technol* 1992;10(1-2):125–41.
- [71] Kattan N, Thome J, Favrat D. Flow boiling in horizontal tubes. Part 1. Development of a diabatic two-phase flow pattern map. *J Heat Transfer* 1998;120:140–7.
- [72] Weisman J, Duncan D, Gibson J, Crawford T. Effect of fluid properties and pipe diameter on two-phase flow pattern in horizontal lines. *Int J Multiphase Flow* 1979;5:437–62.
- [73] Groll E, Cohen R. Review of recent research on the use of CO₂ for air conditioning and refrigeration. CLIMA 2000, The Seventh Rehva World Congress, Naples, Italy; 2000.
- [74] Süss J, Kruse H. Einfluss von Leckage auf die Effizienz von Verdichtern für Kohlendioxid. *Ki Luft- und Kältetechnik* 1997;173–6.
- [75] Fagerli B. CO₂ compressor development. IEA/IIR Workshop on CO₂ Technologies in Refrigeration, Heat Pump and Air Conditioning Systems, Trondheim, Norway 1997;13–14.
- [76] Pettersen J, Hafner A, Skaugen G, Rekstad H. Development of compact heat exchangers for CO₂ air-conditioning systems. *Int J Refrig* 1998;21(3):180–93.
- [77] Pettersen J, Brånäs M, Hafner A. Some safety aspects of CO₂ vapor compression systems. IEA Annex 27 Workshop Proceedings: Selected Issues on CO₂ as Working Fluid in Compression Systems, Trondheim, Norway 2000; p. 61–75.
- [78] NIOSH. US National Institute for Occupational Safety and Health; 1996. <http://www.cdc.gov/niosh/idlh/124389.html>.
- [79] Berghmans J, Duprez H. Safety aspects of CO₂ heat pumps. IEA/IZWe.V./IIR Workshop on CO₂ Technology in Refrigeration, Heat Pump and Air Conditioning Systems, Mainz, Germany; 1999.
- [80] Amin J, Dienhart B, Wertenbach J. Safety aspects of an A/C system with carbon dioxide as refrigerant. The SAE Automotive Alternate Refrigerants Systems Symposium, Scottsdale, AZ; 1999.
- [81] Pettersen J. Comparison of explosion energies in residential air-conditioning systems based on HCFC-22 and CO₂. Proceedings of the 20th International Congress of Refrigeration (IIR), Sydney, Australia; 1999.
- [82] Pettersen J. Refrigerant R-744 fundamentals. VDA Alternate Refrigerant Winter Meeting, Saalfelden, Austria; 2002.
- [83] Pettersen J, Hakenjos J. Boiling liquid expanding vapor explosions (BLEVE) in CO₂ vessels: initial experiments. In: Groll EA, Robinson DM, editors. *The Fourth IIR-Gustav Lorentzen Conference on Natural Working Fluids*, West Lafayette, IN. 2000. p. 216–24.
- [84] Pettersen J. Experimental study on boiling liquid expansion in a CO₂ vessel. In: Xu Z, Fan J, Huang W, editors. *The Fifth IIR-Gustav Lorentzen Conference on Natural Working Fluids*. Guangzhou, China. 2002. p. 92–9.
- [85] Kim-E M, Reid R. The rapid depressurization of hot, high pressure liquids or supercritical fluids. Chemical engineering at supercritical fluid conditions, Michigan: Ann Arbor Science; 1983.
- [86] Clayton W, Griffin M. Catastrophic failure of a liquid carbon dioxide storage vessel. *Process Safety Prog* 1994;13(4):202–9.
- [87] Vörös M, Honti G. Explosion of a liquid CO₂ storage vessel in a carbon dioxide plant. The First International Loss Prevention Symposium, The Hague/Delft, the Netherlands; 1974. p. 337–46.
- [88] Venart J, Ramier S. Boiling liquid expanding vapor explosions (BLEVE): the influence of dynamic re-pressurization and two-phase discharge. PVP-vol. 377-2, Computational technologies for fluid/thermal/structural/chemical systems with industrial application, vol. II.; 1998. p. 249–54.
- [89] Graz M, Stenzel A. Overview of the proposed J639 working draft about safety and containment of refrigerant for mechanical vapor compression systems used for mobile air conditioning systems. VDA Alternate Refrigerant Winter Meeting, Saalfelden, Austria; 2002.
- [90] Parsch W. Status of compressor development for R-744 systems. VDA Alternative Refrigerant Winter Meeting, Saalfelden, Austria; 2002.
- [91] Bullard C, Hrnjak P. Advanced technologies for auto a/c components. The Seventh IEA Conference on Heat Pumping Technologies, Beijing, China; 2002. p. 112–24.
- [92] Fagerli B. On the feasibility of compressing CO₂ as working fluid in hermetic reciprocating compressors. Dr Ing Thesis. Department of Refrigeration and Air Conditioning, Norwegian University of Science and Technology, Norway; 1997.
- [93] Süss J, Kruse H. Efficiency of the indicated process of CO₂ compressors. *Int J Refrig* 1998;21(3):194–205.
- [94] Fagerli B. On the feasibility of compressing CO₂ as working fluid in hermetic reciprocating compressors. Dr Ing Thesis. Department of Refrigeration and Air Conditioning, Norwegian University of Science and Technology, Norway; 1997.
- [95] Nekså P, Rekstad H, Zakeri G, Schiefloe P, Svensson M. Commercial heat pumps for water heating and heat recovery. IEA/IZWe.V./IIR Workshop on CO₂ Technology in

- Refrigeration, Heat Pump and Air Conditioning Systems, Mainz, Germany; 1999.
- [96] Nekså P, Dorin F, Rekstad M, Bredesen A. Development of two-stage semi-hermetic CO₂-compressors. In: Groll EA, Robinson DM, editors. The Fourth IIR-Gustav Lorentzen Conference on Natural Working Fluids, West Lafayette, IN. 2000. p. 355–62.
 - [97] Suzai T, Sato A, Tadano M, Komatsubara T, Ebara T, Oda A. Development of a carbon dioxide compressor for refrigerators and air conditioners. Conference of the Japan Society of Refrigerating and Air Conditioning Engineers, Tokyo; 1999.
 - [98] Tadano M, Ebara T, Oda A, Susai T, Kikuo T, Izaki H, Komatsubara T. Development of the CO₂ hermetic compressor. In: Groll EA, Robinson DM, editors. The Fourth IIR-Gustav Lorentzen Conference on Natural Working Fluids, West Lafayette, IN. 2000. p. 323–30.
 - [99] Fukuta M, Radermacher R, Lindsay D, Yanagisawa T. Performance of vane compressor for CO₂ cycle. In: Groll EA, Robinson DM, editors. The Fourth IIR-Gustav Lorentzen Conference on Natural Working Fluids, West Lafayette, IN. 2000. p. 339–46.
 - [100] Hiwada T, Hokotani K. Carbon dioxide refrigerating machine. Japan Patent No. JP2001065888; 1999.
 - [101] Ohakawa T, Kumakura E, Saitani K, Higuchi M, Taniwa H, Ozawa H. Development of hermetic swing compressors for CO₂ refrigerant. In: Soedel W, editor. Proceedings of the International compressor engineering conference at Purdue, West Lafayette, IN, Paper No. C25-1. 2002. p. 841–52.
 - [102] Fagerli B. Theoretical analysis of compressing CO₂ in scroll compressors. Proceedings of the Third IIR-Gustav Lorentzen Conference on Natural Working Fluids, Oslo, Norway; 1998. p. 249–59.
 - [103] Hasegawa H, Ikoma M, Nishawaki F, Shintaku H, Yakumaru Y. Experimental and theoretical study of hermetic CO₂ scroll compressor. In: Groll EA, Robinson DM, editors. The Fourth IIR-Gustav Lorentzen Conference on Natural Working Fluids, West Lafayette, IN. 2000. p. 347–53.
 - [104] Hihara E. R&D on heat pumps with natural working fluids in Japan. The Seventh International Energy Agency Conference on Heat Pump Technologies, Beijing, China; 2002. p. 272–9.
 - [105] Baumann H, Conzett M. Small oil free piston type compressor for CO₂. In: Soedel W, editor. Proceedings of International Compressor Engineering Conference at Purdue, West Lafayette, IN, Paper No. C25-3. 2002. p. 861–8.
 - [106] Süß J. Kompressoren und Expansionsorgane für das Kältemittel CO₂. Seminar Stand und Anwendung natürlicher Kältemittel, Mainz, Germany; 2002.
 - [107] Sasaki M, Koyatsu M, Yoshikawa C, Fujima K, Mizuno T, Kawai S, Hashizume T. The effectiveness of a refrigeration system using CO₂ as a working fluid in the trans-critical region. ASHRAE Trans 2002;108(1):413–8.
 - [108] Pettersen J, Nekså P. CO₂ refrigeration, air conditioning and heat pump technology development in Europe. Mag Soc Air-Conditioning Refrig Engrs Korea 2002;31(7):53–64.
 - [109] Bullard C, Yin M, Hrnjak P. Compact counterflow gas cooler for R-744. ASHRAE Trans 2002;108(1):487–91.
 - [110] Yin J, Bullard C, Hrnjak P. R-7.4.4. gas cooler model development and validation. Int J Refrig 2001;24:652–9.
 - [111] Fang X, Bullard C, Hrnjak P. Heat transfer and pressure drop of gas coolers. ASHRAE Trans 2001;107(1):255–66.
 - [112] Fang X, Bullard C, Hrnjak P. Modeling and analysis of gas coolers. ASHRAE Trans 2001;107(1):4–13.
 - [113] Yin J, Bullard C, Hrnjak P. Single-phase pressure drop measurements in a microchannel heat exchanger. Heat Transfer Engng 2002;23(4):3–12.
 - [114] Yin J, Bullard C, Hrnjak P. Design strategies for R744 gas coolers. Proceedings of the International Refrigeration Conference at Purdue, West Lafayette, IN; 2002. p. 315–22.
 - [115] Kim M-H, Lee S, Mehendale S, Webb R. Microchannel heat exchanger design for evaporator and condenser applications. Adv Heat Transfer 2003;37:297–429.
 - [116] Kim M-H, Bullard C. Development of a microchannel evaporator model for a carbon dioxide air conditioning system. Energy 2001;26(10):931–48.
 - [117] Zhao Y, Molki M, Ohadi M, Dessiatoun S. Flow boiling of CO₂ in microchannels. ASHRAE Trans 2000;106(1):437–45.
 - [118] Kim M-H, Youn B, Bullard C. Effect of inclination on air side performance of a brazed aluminum heat exchanger under dry and wet conditions. Int J Heat Mass Transfer 2001;44:4613–23.
 - [119] Kim M-H, Bullard C. Air-side thermal hydraulic performance of multi-louvered aluminum heat exchangers. Int J Refrig 2002;25(3):390–400.
 - [120] Boewe D, Bullard C, Yin J, Hrnjak P. Contribution of internal heat exchanger to transcritical R744 cycle performance. Int J HVAC&R Res 2001;7(2):155–68.
 - [121] Randles S, Pasquin S, Gibb P. A critical assessment of synthetic lubricant technologies for alternative refrigerants. The 10th European Conference on Technological Innovations in Air-Conditioning and Refrigeration Industry, Milan; 2003.
 - [122] Kawaguchi Y, Takesue M, Kaneko M, Tazaki T. Performance study of refrigerating oils with CO₂. The SAE Automotive Alternate Refrigerants Systems Symposium, Scottsdale, AZ; 2000.
 - [123] Li H, Rajewski T. Experimental study of lubricant candidates for the CO₂ refrigeration system. In: Groll EA, Robinson DM, editors. The Fourth IIR-Gustav Lorentzen Conference on Natural Working Fluids, West Lafayette, IN. 2000. p. 409–16.
 - [124] Seeton C, Fahl J, Henderson D. Solubility, viscosity, boundary lubrication and miscibility of CO₂ and synthetic lubricants. In: Groll EA, Robinson DM, editors. The Fourth IIR-Gustav Lorentzen Conference on Natural Working Fluids, West Lafayette, IN. 2000. p. 417–24.
 - [125] Heide R, Fahl J. Mischbarkeit von Schmierölen mit Kohlendioxid. KI Luft- und Kältetechnik 2001;No. 10: 456–70.
 - [126] Fahl J, Bruns B, Langenberg E, Pötke W. Thermoanalyse synthetischer Schmieröle mit DSC und TGA. KI Luft- und Kältetechnik 2001;No. 7:309–13.
 - [127] Leisenheimer B, Fritz T. Interaction between CO₂ and elastomers with respect to permeation and explosive decompression. In: Groll EA, Robinson DM, editors. The Fourth IIR-Gustav Lorentzen Conference on Natural Working Fluids, West Lafayette, IN. 2000. p. 201–8.
 - [128] Jain V, Haramoto C, Shilad I, Pfister J. Components for CO₂ A/C systems. The SAE Automotive Alternate Refrigerants Systems Symposium, Scottsdale, AZ; 2000.

- [129] Bhatti M. A critical look at R-744 and R-134a mobile air conditioning systems. SAE Paper No. 970527; 1997.
- [130] Fischer S, Sand J. Total Environmental Impact (TEWI) calculations for alternative automotive air-conditioning systems. SAE Paper No. 970526; 1997.
- [131] Pettersen J, Hafner A. Energetischer Wirkungsgrad und TEWI von CO₂-Fahrzeug-Klimaanlagen. Seminar: Fahrzeugklimatisierung mit Naturlichen Kaetlemitteln, Karlsruhe, C.F. Mueller Verlag; March 8, 1997.
- [132] Gentner H. Passenger car air conditioning using carbon dioxide as refrigerant. Proceedings of the Third IIR-Gustav Lorentzen Conference on Natural Working Fluids, Oslo, Norway; 1998. p. 303–13.
- [133] Boewe D, McEnaney R, Park Y, Yin J, Bullard C, Hrnjak P. Comparative experimental study of subcritical R134a and transcritical R744 refrigeration systems for mobile applications. ACRC report CR-17. University of Illinois at Urbana-Champaign, Illinois; 1999.
- [134] Beaver A, Yin J, Bullard C. An experimental investigation of transcritical carbon dioxide systems for residential air conditioning. ACRC report CR-18. University of Illinois at Urbana-Champaign, Illinois; 1999.
- [135] Yin J, Park Y, Boewe D, McEnaney R, Beaver A, Bullard C, Hrnjak P. Experimental and model comparison of transcritical CO₂ versus R134a and R410 system performance. Proceedings of the Third IIR-Gustav Lorentzen Conference on Natural Working Fluids, Oslo, Norway; 1998. p. 331–40.
- [136] McEnaney R, Boewe D, Yin J, Park Y, Bullard C, Hrnjak P. Experimental comparison of mobile A/C systems when operated with transcritical CO₂ versus conventional R134a. Proceedings of the Third IIR-Gustav Lorentzen Conference on Natural Working Fluids, Oslo, Norway; 1998. p. 145–50.
- [137] McEnaney R, Park Y, Yin J, Bullard C, Hrnjak P. Performance of the prototype of a transcritical R744 mobile A/C system. SAE Paper No. 99PC-6-7; 1999.
- [138] McEnaney R, Hrnjak P. Control strategies for transcritical R744 systems. SAE Paper No. 2000-01-1272; 2000.
- [139] McEnaney R, Yin J, Bullard C, Hrnjak P. An investigation of control-related issues in transcritical R744 and subcritical R134a mobile air conditioning systems. ACRC report CR-19. University of Illinois at Urbana-Champaign, Illinois; 1999.
- [140] Park Y, Yin J, Bullard C, Hrnjak P. Experimental and model analysis of control and operating parameters of transcritical CO₂ mobile A/C system. Proceedings of VTMS-4 Conference, London, England; 1999. p. 163–70.
- [141] Hrnjak P. Some lessons learned from SAE AR CRP. The SAE Automotive Alternative Refrigerant Systems Symposium, Scottsdale, AZ; 2002.
- [142] Giannavola M, Murphy R, Yin J, Kim M-H, Bullard C, Hrnjak P. Experimental investigations of an automotive heat pump prototype for military, SUV and compact cars. In: Groll EA, Robinson DM, editors. The Fourth IIR-Gustav Lorentzen Conference on Natural Working Fluids, West Lafayette, IN. 2000. p. 115–22.
- [143] Hafner A. Experimental study on heat pump operation of prototype CO₂ mobile air conditioning system. In: Groll EA, Robinson DM, editors. The Fourth IIR-Gustav Lorentzen Conference on Natural Working Fluids, West Lafayette, IN. 2000. p. 183–90.
- [144] Giannavola M. Experimental study of system performance improvements in transcritical R744 systems for mobile air-conditioning and heat pumping. MS Thesis. University of Illinois at Urbana-Champaign, Illinois; 2002.
- [145] Itoh M, Kogure H, Yoshinaga S, Hoshino R, Wakabayashi N, Kudoh M, Kusumoto H. Study on parallel-flow-type heat exchangers for residential heat pump systems. Proceedings of the JAR Annual Conference; 1996. p. 73–6.
- [146] Song S, Bullard C, Hrnjak P. Frost deposition and refrigerant distribution in microchannel heat exchangers. ASHRAE Trans 2002;108(2):944–53.
- [147] Hammer H, Wertenbach J. Carbon dioxide (R-744) as supplementary heating device. The SAE Automotive Alternate Refrigerants Systems Symposium, Scottsdale, AZ; 2000.
- [148] Pettersen J, Aarlien R, Nekså P, Skaugen G, Aflekt K. A comparative evaluation of CO₂ and HCFC-22 residential air-conditioning systems in a Japanese climate. IEA/IIR Workshop on CO₂ Technologies in Refrigeration, Heat Pump and Air Conditioning Systems, Trondheim, Norway; 1997.
- [149] ARI, Standard 210/240, Standard for air-conditioning and air-source heat pump. Arlington, VA: Air-conditioning and Refrigeration Institute; 1994.
- [150] Beaver A, Hrnjak P, Yin J, Bullard C. Effects of distribution in headers of microchannel evaporators on transcritical CO₂ heat pump performance. In: Garimella S, Von Spakovsky M, Somasundaram S, editors. The ASME advanced energy systems division, AES-vol. 40. New York: ASME; 2000. p. 55–64.
- [151] Sand J, Fischer S, Baxter V. Comparison of TEWI for fluorocarbon alternative refrigerants and technologies in residential heat pumps and air-conditionings. ASHRAE Trans 1999;105(1):1209–18.
- [152] Richter M, Song S, Yin J, Kim M-H, Bullard C, Hrnjak P. Experimental results of transcritical CO₂ heat pump for residential application. Energy 2003;28:1005–19.
- [153] Richter M, Bullard C, Hrnjak P. Effect of comfort constraints on cycle efficiencies. In: Hernandez-Guerrero A, editor. The ASME advanced energy systems division, AES-vol. 41. New York: ASME; 2001. p. 275–86.
- [154] Nekså P, Zakeri G, Aarlien R, Jakobsen A. Carbon dioxide as working fluid in air conditioning and heat pump systems. The Earth Technologies Forum, Washington, DC; 1998.
- [155] Hwang Y, Radermacher R. Theoretical evaluation of carbon dioxide refrigeration cycle. Int J HVAC&R Res 1998;4(3): 245–63.
- [156] Hwang Y, Radermacher R. Experimental investigation of the CO₂ refrigeration cycle. ASHRAE Trans 1999;105(1): 1219–27.
- [157] Rieberer R, Halozan H. CO₂ heat pumps in controlled ventilation systems. Proceedings of the Third IIR-Gustav Lorentzen Conference on Natural Working Fluids, Oslo, Norway; 1998. p. 212–22.
- [158] Rieberer R, Kasper G, Halozan H. CO₂: a chance for once-through heat pump heaters. CO₂ technology in refrigeration, heat pumps and air conditioning systems, Trondheim, Norway; 1997.
- [159] Schiefloe P, Nekså P. CO₂ varmpumpe for bygningsoppvarming. forprosjekt (Project report, in Norwegian). Trondheim, Norway: SINTEF Energy Research; 1999.
- [160] Enkemann T, Kruse H, Oostendorp P. CO₂ as a heat pump working fluid for retrofitting hydronic heating systems in

- western Europe. IEA/IIR Workshop on CO₂ Technologies in Refrigeration, Heat Pump and Air Conditioning Systems, Trondheim, Norway; 1997.
- [161] Brandes H. Energy efficient and environmentally friendly heat pumping systems using CO₂ as working fluid. IEA/IZWe.V./IIR Workshop on CO₂ Technology in Refrigeration, Heat Pump and Air Conditioning Systems, Mainz, Germany; 1999.
- [162] Lorentzen G. Large heat pumps using CO₂ refrigerant. Energy efficiency in refrigeration and global warming impact, Gent, Belgium: IIR; 1993.
- [163] Neksa P, Rekstad H, Zakeri G, Schiefloe P. CO₂-heat pump water heater: characteristics, system design and experimental results. *Int J Refrig* 1998;21:172–9.
- [164] Hwang Y, Radermacher R. Experimental evaluation of CO₂ water heater. Proceedings of the Third IIR-Gustav Lorentzen Conference on Natural Working Fluids, Oslo, Norway; 1998. p. 368–75.
- [165] Kim M-H. Research and development trends of CO₂ heat pump water heaters in Japan. *Mag Soc Air-Conditioning Refrig Engrs Korea* 2002;31(7):65–70.
- [166] JRAIA, JRA Standard 4050: heat pump water heaters using carbon dioxide refrigerant. The Japan Refrigeration and Air Conditioning Industry Association; 2001.
- [167] Hihara E. R&D on heat pumps with natural working fluids in Japan. The Seventh International Energy Agency Conference on Heat Pump Technologies, Beijing, China; 2002. p. 272–9.
- [168] Kim M-H. Unpublished technical report. Samsung Electronics, Co., Ltd; 2002.
- [169] Manzione J, Calkins F. Evaluation of transcritical CO₂ using an automotive compressor in a packaged-unitary military ECU. *ASHRAE Trans* 2002;108(2):937–43.
- [170] Sonnekalb M, Köhler J. Transport refrigeration with a transcritical refrigeration cycle using carbon dioxide as refrigerant. Proceedings of the International Conference on Ozone Protection Technologies, Washington DC; 1997. p. 124–33.
- [171] Kauffeld M, Christensen K. REEFER: a new energy-efficient reefer container concept using carbon dioxide as refrigerant. Proceedings of the Third IIR: Gustav Lorentzen Conference on Natural Working Fluids, Oslo, Norway; 1998. p. 399–410.
- [172] Jakobsen A, Neksa P. Carbon dioxide in marine refrigeration applications. Earth Technologies Forum Conference, Washington, DC; 1998. p. 153–62.
- [173] Eggen G, Aflekt K. Commercial refrigeration with ammonia and CO₂ as working fluids. Proceedings of the Third IIR: Gustav Lorentzen Conference on Natural Working Fluids, Oslo, Norway; 1998. p. 281–92.
- [174] Neksa P, Giroto S, Schiefloe P. Commercial refrigeration using CO₂ as refrigerant: system design and experimental results. Proceedings of the Third IIR: Gustav Lorentzen Conference on Natural Working Fluids, Oslo, Norway; 1998. p. 270–80.
- [175] Schmidt E, Klöcker K, Flacke N. Heat pumps for dehumidification and drying processes in residential and commercial applications. IEA/IZWe.V./IIR Workshop on CO₂ Technology in Refrigeration, Heat Pump and Air Conditioning Systems, Mainz, Germany; 1999.
- [176] Steimle F. CO₂-drying heat pumps. CO₂ Technology in Refrigeration, Heat Pump and Air Conditioning Systems, Trondheim, Norway; 1997.
- [177] Schmidt E, Klöcker K, Flacke N, Steimle F. Applying the transcritical CO₂ process to a drying heat pump. *Int J Refrig* 1998;21(3):202–11.

Reprinted from *Progress in Energy and Combustion Science*, Vol 30 (2004), p. 119-174
 Man-Hoe Kim, Jostein Pettersen, Clark W. Bullard,
 "Fundamental process and system design issues
 in CO₂ vapor compression systems"

Copyright (c) 2004, with permission from Elsevier

6 Annex Projects

6.1 Systems

6.1.1 Feasibility of transcritical R744 systems for mobile space conditioning applications

**US Army Communications - Electronics Command
RDEC C2 South
AMSEL-RD-C2-PS-E**

Feasibility of transcritical R744 systems for mobile space conditioning applications

**Research performed for
US Army Communications - Electronics Command
RDEC C2 South
AMSEL-RD-C2-PS-E**

by
University of Illinois at Urbana-Champaign
Air Conditioning & Refrigeration Center

Predrag S. Hrnjak
Clark W. Bullard

INTRODUCTION

The objective of the project is to explore the feasibility of transcritical CO₂ (R744) systems for mobile space air conditioning. This project focused on three major areas: 1) combining validated component submodels into a system simulation model; 2) validating the system model; and 3) using the validated model to design a truly reversible transcritical CO₂ heat pump system.

ACCOMPLISHMENTS TASK-BY-TASK

Estimate potential tradeoff of a/c performance, if any, in the event that next-generation systems would be designed with reversing valve to operate in heat pump mode.

Our modeling and design efforts showed how to approach ideal performance through single-pass counterflow designs and Modine developed the manufacturing technology needed to realize it. The result, embodied in the MAC2 (mid-sized car) prototype gas cooler now in the initial stages of testing, shows performance data remarkably close to simulation model predictions. Details are presented in Appendix A. More complete results and analyses will be published as the experimental program continues. At this point it appears that research may have eliminated microchannel heat exchanger design as a source of a/c performance degradation in transcritical R744 heat pump systems. The remaining sources of possible degradation will be associated with the 4-way reversing valve (common to all systems) and the refrigerant distributors – losses common to all heat pumps. Contributions from these sources in the MAC 2 design were estimated to be less than or equal to those in conventional HFC heat pumps because the transcritical R744 cycle is much more tolerant of pressure drops than the subcritical HFC cycles, due to differences in thermodynamic properties of the refrigerants.

Based on the analysis of detailed component-level data conducted earlier, estimate maximum potential performance improvements obtainable in a next generation design. Propose design changes that would be likely to achieve such performance. Quantify tradeoffs between system performance and compactness.

Analysis of the MAC1 (Ford Escort-sized) system, operating in heating and cooling modes, led to identification and validation of equations describing the underlying physical processes occurring in each of the components. Those equations were used to simulate hundreds of possible design improvements, leading to the MAC2 system design. Close interaction with component manufacturers limited the design space to configurations that could be realized using existing or improved manufacturing techniques. Key system design parameters and performance characteristics are detailed in Appendix B. The results of MAC1 system simulations, and comparisons with experimental data, are shown in Appendix C. The same simulation model was then used to design the MAC2 system. Data obtained from MAC2 experiments are included in Appendix A.

Address control strategies for maximizing Q and COP while reducing high side pressure and limiting discharge temperature.

The extensive set of a/c and heat pump experiments using the MAC1 system confirmed that optimizing high-side pressure is the best approach for maximizing transcritical cycle energy efficiency with R744. Thus energy efficiency can be optimized for any level of comfort desired by the passengers (indoor temperature and humidity). Optimal strategies are described in Appendix D, and practical ways of implementation are discussed. The optimization allows

for sacrificing energy efficiency briefly after startup when the car is very hot, to achieve extra capacity at the expense of COP. For the transcritical cycle in heat pump mode, energy efficiency is maximized subject to a comfort constraint, namely the desired warm air supply temperature. That constraint in turn sets the high side pressure and determines the energy efficiency. The heating mode also differs from cooling, because maximum capacity is achieved exactly when it is needed most: immediately after startup when the passenger compartment is coldest. Our experiments have confirmed this fact, and demonstrated that no sacrifice of efficiency is needed to achieve maximum heating capacity during the critical pulldown period. COP is highest during that pulldown period. After the passenger compartment warms up and adequate heat is available from the conventional system using engine coolant, the heat pump is shut off.

Address and analyze the risks that are related to CO₂ effects to vehicle occupants: system charge, size of passenger compartment, tolerable CO₂ concentrations, etc.

There are several ways to prevent CO₂ levels from reaching unsafe levels inside the vehicle. A variety of active approaches are being explored by the industry, including valves to isolate part of the charge outside the passenger compartment, ventilation controls activated by CO₂ sensors, etc. Our approach has been to explore the limits of passive safety measures, namely system charge minimization, to see whether it could actually eliminate the need for active safety systems.

Based on our experience with the MAC1 prototype, we designed the MAC2 system to use less charge – less than 210 grams when charged for 90F indoor/110F outdoor. This counts the charge present in the all components except the accumulator, which needs to hold additional charge to offset leakage anticipated between recharges. The MAC2 design, however, could be improved to reduce the charge in the headers by making them smaller, the microchannel tubes by using fewer or smaller ports, and by reducing the size of the connecting lines. Because MAC2 is a breadboard system with long lines between indoor/outdoor environmental chambers, approximately 40% of its charge is in the connecting lines. Clearly it should be possible to reduce system charge requirements below the 210 grams required by the MAC2 prototype, which was sized for a mid-to-large car or SUV.

Figure 1 shows the CO₂ concentrations that would result from a sudden release of the full refrigerant charge into the vehicle. The vertical line indicates the internal volume of the GMC Jimmy SUV (136 cu ft). The symbols shown along the line represent the volume definitions of mini-compact (< 85 cu ft), subcompact, compact, midsize, and large cars (> 120 cu ft), and station wagons (small < 130; large > 160). Smaller cars contain less air to dilute a leak, but on the other hand they require smaller a/c systems than large cars or SUV's. For reference, the 200 g charge for the MAC2 prototype is shown, along with the 400 g typical of some of the prototype systems developed for the SAE Phoenix competitions, and a 600 g level that probably represents the largest conceivable system charge.

A 5% CO₂ limit is being discussed by SAE as an appropriate limit for shorter exposure periods of the type caused by a sudden release of charge. The assumption of instantaneous release of charge, of course, is very conservative in the sense that it assumes zero ventilation of the passenger compartment. Industry sources have indicated to us that HVAC systems at the “full recirculation” setting are designed to provide 20-30 cfm fresh air supply to accommodate

occupant respiration and minimize odor problems. At the 100% outside air setting, ventilation rates range from 200-300 cfm, or more than one air change per minute.

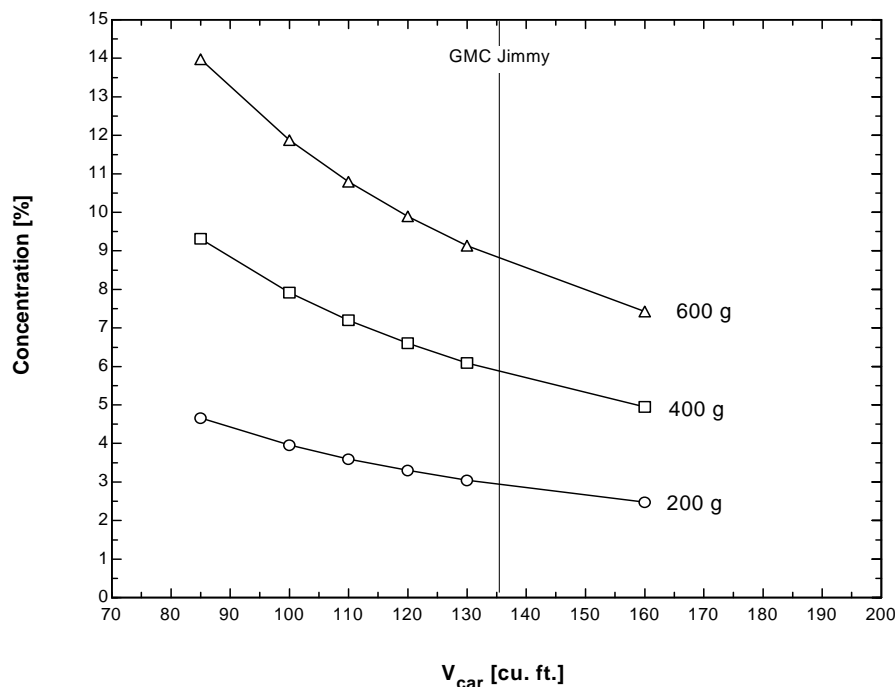


Figure 1. Concentration resulting from sudden release of full charge

ASHRAE standard SSPC34 sets refrigerant concentration limits (RCL) for all refrigerants, based on reviews of toxicological studies and public comments during a consensus standard-setting process. One of the source documents is published by DoE with the assistance of the industry-based Air Conditioning and Refrigeration Technology Institute is: *Toxicity data to determine refrigerant concentration limits*, DOE/CE/23810-110, September, 2000. Table 4 of that report lists the following RCL's for R134a (50,000 ppmv) and for R744 (40,000 ppmv). These limits, 5% and 4% by volume, respectively are based on 30 minute exposure periods.

Since the molecular weights of CO₂ and R134a are different, it takes about twice the mass of R134a to produce the same % volume concentration as CO₂. Therefore in the GMC Jimmy, immediate release of its 1000 gram charge into the passenger compartment would produce the same % volume concentration as 500 g CO₂. Accounting for the different refrigerant concentration limits (RCL's), release of 1000 g of 134a would be equivalent to release of 400 g CO₂. In that respect, production R134a vehicles with 1000 g charge may pose risks similar to existing prototype CO₂ vehicles which have 400 g charge. The potential for future CO₂ charge reductions has been discussed above.

The vehicle volumes shown in Figure 1 are those used to define size classes in the annual EPA Fuel Economy Guide; they include both passenger and cargo volume. EPA does not require reporting of light truck volumes, so the internal volume of the Jimmy was estimated as follows. The General Motors website reports front and back seat headroom, legroom and shoulder room; the product of those dimensions for the mid-sized Malibu yields 99 cu. ft. (the exact

number reported by EPA for passenger volume) and it matches exactly the product of the same three dimensions provided for the GMC Jimmy. An inquiry to a GMC dealer yielded a report of 16 cu. ft. for the Jimmy's cargo volume "below the top of the back seat", coincidentally the same figure reported for the Malibu's trunk. Thus the 115 cu. ft. total for the Malibu places it in the middle of the "midsize" car category. The total for the Jimmy, including the additional 21 cu. ft. of "cargo volume" above the back seat, yields the 136 cu. ft. total shown in Figure 1.

Appendix A

NEW GAS COOLER DESIGN FOR TRANSCRITICAL CO₂ CYCLE

ABSTRACT

Exit temperature from the gas cooler is an extremely important parameter affecting the efficiency of the transcritical a/c and heat pump cycle. Interest in carbon dioxide as a refrigerant has recently led to development and testing of several prototypes, all of cross flow design. This article employs a validated simulation model to analyze tradeoffs involved in approaching counter flow configuration through multi-slab configurations. It also presents the first experimental confirmation of the concept.

INTRODUCTION

As a natural and environmentally benign refrigerant, CO₂ (R-744) has gained more attentions recently. In addition to its environmental advantages, R-744 offers certain attractive thermophysical property characteristics such as low surface tension and low liquid viscosity. Compared with conventional mobile air-conditioning systems, the major difference is that R-744 cycle operates in the transcritical region, where the heat rejection process occurs in the region above the refrigerant's critical temperature and pressure. Compressor suction and discharge pressures (30-120bar) are far greater than for conventional hydrofluorocarbon (HFC) refrigerants, which means that higher pressure drops may be tolerated in the heat exchangers without significantly impairing cycle performance. Moreover because of the low pressure ratio, higher compressor efficiencies can be achieved. More detailed discussions and experimental results from prototype systems can be found in Pettersen et al. (1994), Yin et al.(1997).

Thermodynamically one of the most interesting feature of the transcritical R-744 cycle is the existence of a COP-optimizing high-side pressure (Pettersen et al, 1994 and Boewe et al, 1999, McEnaney et al.,1999). In experiments with a prototype mobile a/c system, results showed that if the exit temperature from gas cooler could be reduced, the optimum high-side pressure would also be reduced, and the COP will be increased because of the reduced compressor power. This paper is motivated by those experimental results, which included more than 350 experimental data points and served as the basis for the development and validation of the simulation model used here (Yin et al. 2000).

This paper will discuss the importance of refrigerant temperature at gas cooler exit, and then investigate quantitatively two distinct gas cooler design concepts: the multi-pass single-slab designs used in existing prototypes; and the single-pass multi-slab counter-flow configurations proposed here. To the best of our knowledge this is the first proposal of this kind in the open literature. The idea for using a multi-slab counterflow arrangement for the transcritical R-744 system was conceived in 1998 during our earlier experiments with a conventional multi-pass single-slab crossflow heat exchanger.

IMPORTANCE OF GAS COOLER EXIT TEMPERATURE

Figure 1 shows the predicted relationship between COP and discharge pressure for different gas cooler exit temperatures, and illustrates the benefits obtainable from a closer approach to ambient air temperature. The evaporation temperature was set at 3.9°C (corresponding to evaporation pressure 3851kPa) and the suction line internal heat exchanger effectiveness was 0.8. Pressure drop is neglected to simplify the presentation. The compressor efficiency used in the calculation was fitted from one of our previous experiments (Boewe et al. 1999) at 2000rpm:

$$\eta_m = 0.734 - 0.01048 \times P_r \quad (1)$$

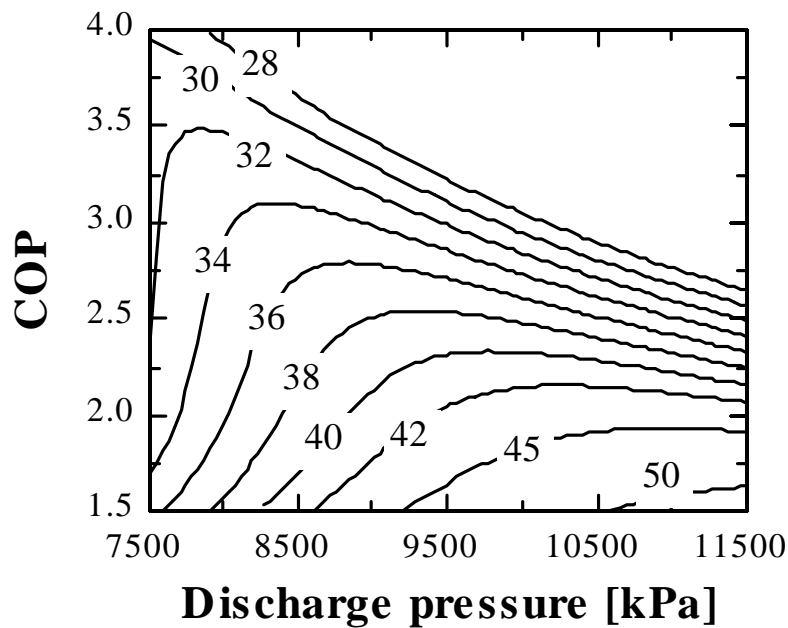


Figure 1. Effect of refrigerant exit temperature on COP-maximizing high-side pressure

Despite the assumptions underlying Figure 1, several conclusions can be drawn from it. First, when the air inlet temperature entering the gas cooler increases, and the R744 exit temperature also increases, the operating pressure needs to be increased in order to achieve an optimum cycle COP. This COP decreases as the gas cooler exit temperature increases. Second, the COP curve tends to be flatter when the temperature at the gas cooler exit is higher. Third, the COP curve is not symmetric along the pressure axis. At lower exit temperatures, the COP drops more steeply on the low-pressure side than on the high-pressure side. Also, accurate high-side pressure control is more important for maximizing COP on cool days than for the case of higher inlet air temperature. And fourth, when the refrigerant temperature at gas cooler exit is lower than the critical temperature (31°C), there is no local optimum COP.

Prototype R-744 system performance tests by Boewe et al. (1999) showed that for a single slab, three passes gas cooler, the approach temperature difference between refrigerant exit and ambient air ranged from 2 to 9°C. If that difference could be reduced by redesigning the gas cooler without violating packaging constraints, system performance could be improved based on the conclusions from Figure 1. For example, suppose the air inlet temperature is 34°C, if the refrigerant exit temperature from gas cooler is 38°C, from Figure 1 the optimized COP is

about 2.54, and the corresponding discharge pressure is 9278kPa. If the discharge temperature can be reduced to 36 °C, the corresponding COP and pressure will be 2.79 and 8833kPa, respectively, this means that a 2°C reduction in refrigerant exit temperature could increase COP by as much as 10%.

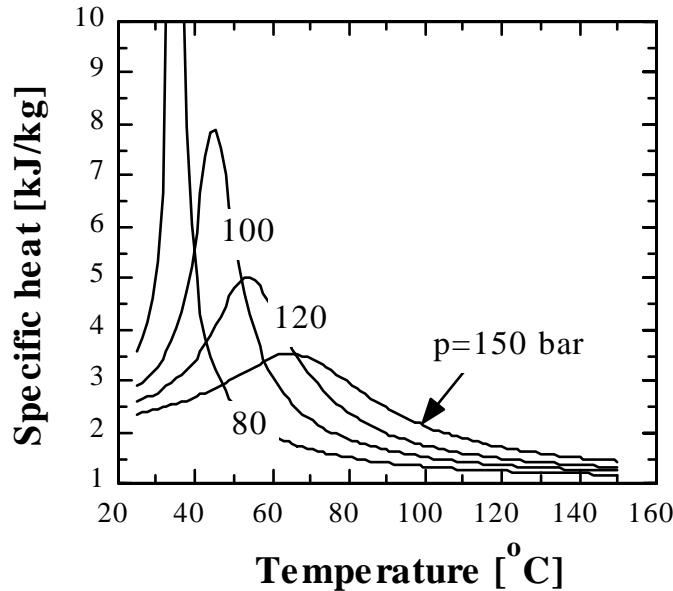


Figure 2 Specific heat of R744 in the transcritical region

Figure 2 shows how the specific heat changes with temperature at different pressures. Specific heat of the refrigerant in the gas cooler will gradually increase downstream, then go through a peak region when close to the critical point and then decrease again as it approaches the ambient air temperature. As the C_p changes along the gas cooler, so also does the temperature difference between refrigerant and air along the heat exchanger tube. Due to high refrigerant-air temperature difference in the inlet region and lower C_p , the refrigerant temperature falls quickly. Then as the fluid enters the peak C_p region, even at the same heat transfer rate, the refrigerant temperature tends to be flat for two reasons: higher C_p and lower refrigerant-air temperature difference.

DIMENSIONS OF THE GAS COOLER, TUBE AND FINS

This paper will focus on two designs, multi-pass vs multi-slab (counter-flow), using available fin dimensions. In order to have a reasonable in-tube pressure drop on the refrigerant side, the port number and diameter will be simulated. The gas cooler packaging constraints were specified as a rectangular box of 607mm length, 355mm height and 18mm depth.

Table 1 shows the geometric parameters, including those constrained the design; dimensions of available fins, and packaging constraints.

Table 1 MAC gas cooler dimensions

Face Area (m ²)	0.179	Number of tubes	66	Louver angle (°)	27
Volume (m ³)	0.0039	Fin thickness (mm)	0.102	Louver pitch (mm)	1.016
Airside area (m ²)	6.86	Fin pitch (mm)	1.155	Fin height (mm)	7.925
Ref side area (m ²)	0.76	Number of fins per meter	866	Louver length (mm)	6.6

The number of tubes was determined by the width of the given rectangular box, the height of the fins and tube thickness. Tube lengths were determined from the height of the given rectangular box and system performance for different slab number. Based on the results from simulation model, three slab is closer to the optimum design, because three slab is much better than two slab, but not too bad than four slabs. Too many slabs could also be linked to the manufacturing difficulties because it reduces the slab thickness. Figure 3 shows the schematics of a three slabs arrangement. The tube depth (major) was limited by the coil depth. In order to avoid the conduction between tubes in each slab, the tube major needs to be shorter than 1/3 of the coil depth. For a given tube depth, the number of ports and their diameter could have many combinations, for a given design condition. The allowable range of port diameters and numbers are not very sensitive to the system performance if the pressure drops are constrained within a reasonable range; a large number of small ports can provide the same mass flux as a smaller number of large ones. Due to surface friction effects, there is a slight advantage to having smaller ports for larger mass fluxes.

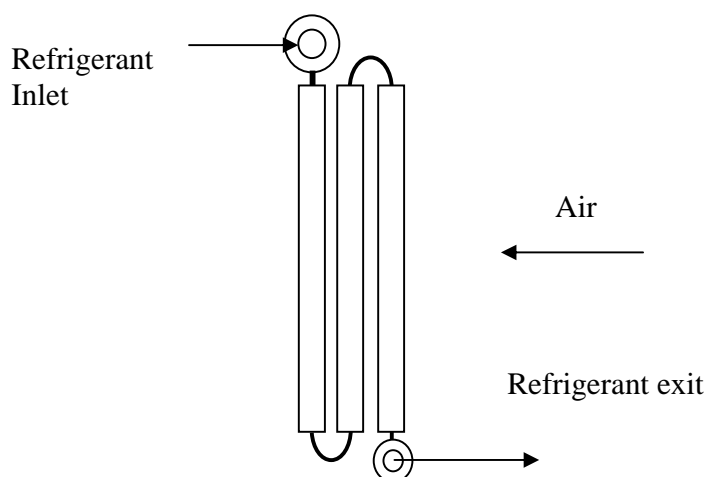


Figure 3 Multi-slab arrangement

Optimizing a gas cooler for a given design point is a relatively simple task. The following analysis must address the more complex tradeoffs associated with the heat pump

operating mode, when the a/c gas cooler serves as an evaporator. Pressure drops are larger for two-phase operation, so the critical port sizing condition shifts to heating mode. System charge is a safety consideration in automotive applications; a criterion that favors strategies that minimize internal volume.

Table 2 shows the selected operating conditions at which the port dimensions are simulated, and Table 3 shows the simulation results. These results show how optimal tube dimensions differ among operating conditions. If a/c operation is optimized for the most typical operating condition A, then the optimal tube diameters could be from 0.7 to 0.47mm, depending on the number of ports per tube.

Table 3 Four different operating conditions:

Condition	Teai (°C)	Rhea (%)	Tcai (°C)	AFRe (scfm)	AFRc (scfm)	Rpm
A	32	50	49	175	2100	1800
B	32	50	49	300	950	950
C	32	50	49	175	950	950
D	26	50	35	175	950	950*

* Variable displacement for this condition, Tero was set to be 0.5 °C

In Table 2, Teai is the air inlet temperature to evaporator; Rhea is the air relative humidity inlet to evaporator; Tcai is the air temperature at the inlet of gas cooler; AFRe and AFRc are the air flow rates through evaporator and gas cooler, respectively and Tero is the evaporation temperature at evaporator exit. Oil effects on heat transfer and pressure drop were neglected in the analyses underlying Table 3.

Table 3 Number of ports and port diameter:

Number of ports	2	3	4	5	6	7	8
Condition A							
Diameter (mm)	0.705	0.6	0.57	0.52	0.5	0.49	0.47
COP	1.352	1.355	1.356	1.357	1.358	1.358	1.359
Condition B							
Diameter (mm)	0.64	0.57	0.54	0.47	0.47	0.44	0.44
COP	1.929	1.938	1.944	1.948	1.95	1.953	1.954
Condition C							
Diameter (mm)	0.602	0.535	0.502	0.468	0.468	0.435	0.435
COP	1.696	1.701	1.704	1.707	1.708	1.709	1.71
Condition D							
Diameter (mm)	0.51	0.45	0.43	0.39	0.37	0.33	0.33
COP	2.213	2.227	2.236	2.242	2.246	2.249	2.251

In order to keep the inner volume of the heat exchanger as small as possible, fewer larger ports have the advantage, but larger port diameters require a thicker wall for structural reasons, increasing tube cost and also increase pressure drop in heat pump operation. Shown in Figure 4, for example, is a near-optimal tube with 5 ports, and a port diameter of 0.5mm, shown. Figure 5 shows the resulting relations between port number, port diameter and tube cross-section area.

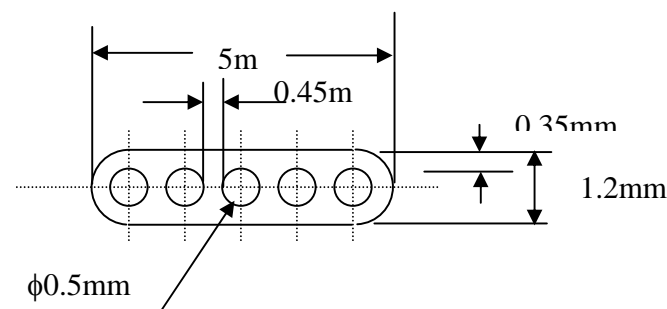


Figure 4. Microchannel tube dimensions

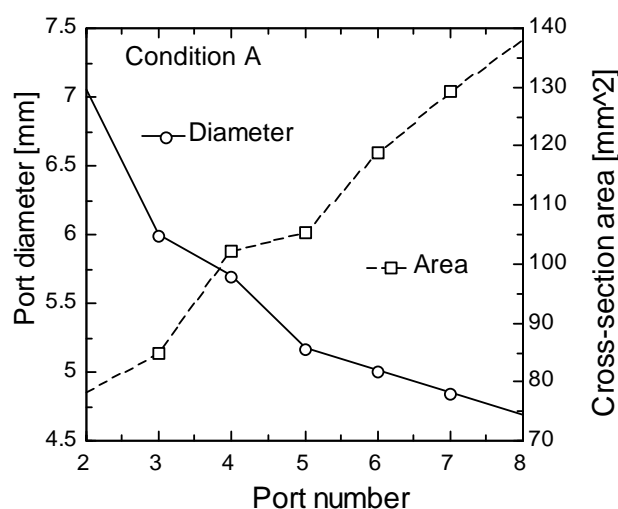


Figure 5. Port number, diameter and cross-section area

MULTI-SLAB COUNTERFLOW ARRANGEMENT

The counter flow configuration is more important for the gas cooler than for an evaporator or condenser because of the large temperature gradient on the refrigerant side. One effective way to accomplish this within a rectangular package constraint is to use a multi-slab arrangement as shown in Figure 3, in which the third slab will always feel the coolest air. When refrigerant flow is reversed in heating mode, the now-parallel configuration imposes no penalty because of the gas cooler serves as evaporator, and the presence of a low-side receiver commonly used in prototype transcritical systems will always make the evaporation in two-phase region if the system has enough charge.

Figures 6 and 7 compares the experimental results to the model prediction for a prototype gas cooler having tubes similar to that shown in Figure 4. Simulation results are shown for predicted refrigerant (T_r) and surface (T_s) temperatures along the tube at two different operating conditions: high temperature/low air flow rate/low capacity; and high temperature/high air flow rate/high capacity. Measured surface temperatures along three of the 64 parallel tubes (tube #8 tube from left, close to the header inlet; #32 near the middle; and #8 from right, farther away from the header inlet). The slightly cooler surface temperature for the

tube located farthest from the header inlet suggests the presence of moderate flow maldistribution among the 64 parallel circuits. The detailed comparisons are shown in Table 4, along with gas cooler performance indicators.

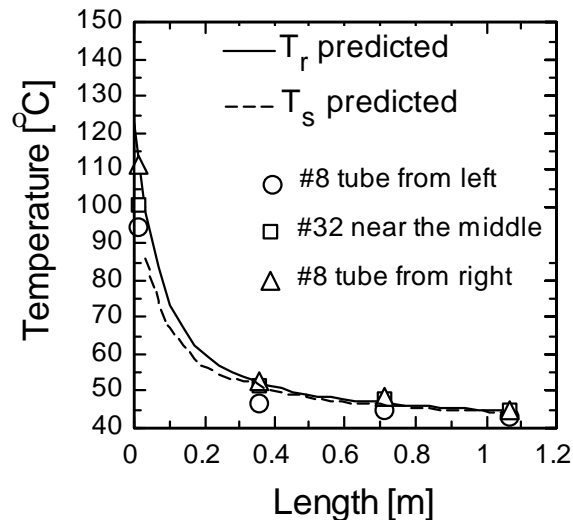


Figure 6 Result for idle condition

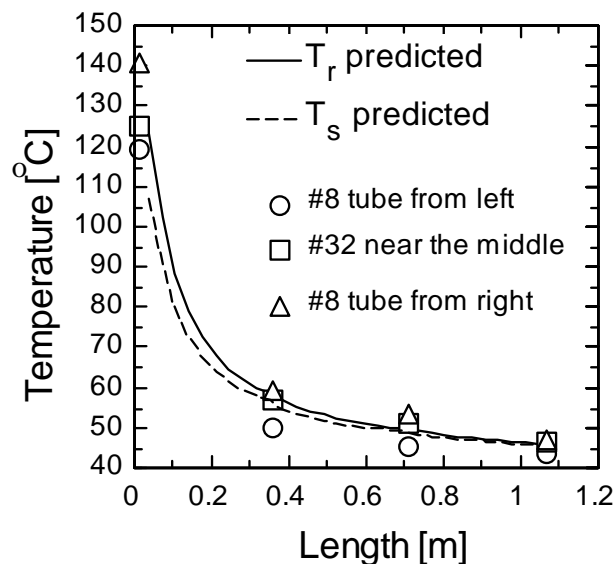


Figure 6 Result for driving condition

Table 4 Measured and predicted gas cooler performance data

Conditions	Idle	Driving
Air inlet temperature (°C)	43	43.4
Air flow rate (kg/s / scfm)	0.439/775	0.708/1250
R744 inlet pressure (kPa)	9793	10327
R744 inlet temperature (°C)	122.7	155.5
R744 flow rate (g/s)	27.7	45.0
R744 exit temperature (°C)	44.7	46.5
Predicted R744 exit temperature (°C)	44.7	46.0
R744 pressure drop(kPa)	72	147
Predicted R744 pressure drop (kPa)	20	48
Capacity (kW)	5.04	10.52
Predicted capacity (kW)	5.09	10.78

MULTIPLE PASS ARRANGEMENT

Figure 7 shows the arrangement of a typical multi-pass microchannel heat exchanger, of the crossflow design used for automotive a/c condensers. The following analysis begins with the same packaging constraints and fin characteristics, and uses the same simulation model to optimize gas cooler performance. Since the tubes are horizontal in this conventional design, only 38 are needed. Since it is a crossflow design, the tube depth is three times that of the tube shown in Figure 4. In order to minimize overall pressure drop, different numbers of tubes are used in each pass as shown in Figure 7.

No comparisons with experimental data are shown here, because the multi-slab prototype gas cooler has a different air side area compared with the multi-pass prototype that was used to validate the simulation model (see Yin et al., 2001 for detailed comparisons of the multipass crossflow prototype with data from more than 350 operating conditions). Table 5 therefore shows the simulation model predictions for a hypothetical multi-pass crossflow gas cooler having the same air side area as the multi-slab counterflow prototype described above. The two operating conditions are the same as shown in Table 4.

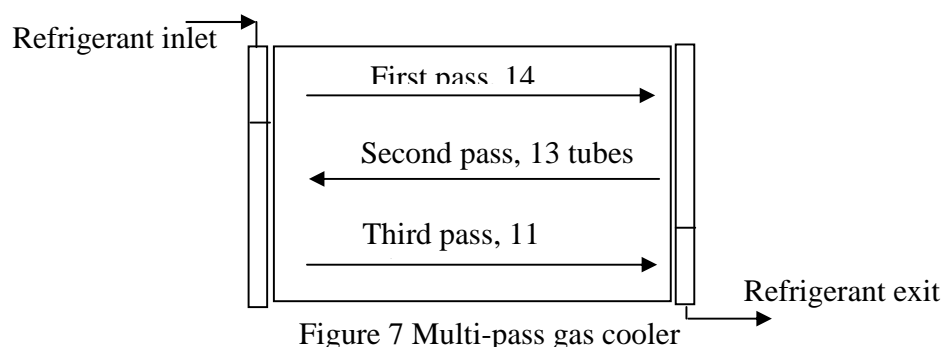


Figure 7 Multi-pass gas cooler

Table 5 Simulation of 3-pass crossflow gas cooler and 3-slab counterflow

Conditions	Idle	Driving
Predicted R744 exit temperature (°C)	46.4	48.6
Predicted R744 exit temperature for 3-slab (°C)	44.7	46.0
Temperature difference between two arrangement (°C)	1.7	26
Predicted capacity (kW)	4.7	9.9
Predicted capacity for 3-slab (kW)	5.1	10.8
Capacity difference (%)	8.7	9

CONCLUSION

A multi-slab counterflow gas cooler design was proposed in this paper, as conceived in 1998 during some earlier experiments with a multi-pass crossflow design. Simulation results suggested, and experimental results confirmed, that this new design offers better performance than the single-slab multi-pass crossflow designs traditionally employed in microchannel heat exchangers. The results showed, for the given gas cooler volume constraints and available fin material, the new design can achieve 8 to 9% higher capacity than the old one. The approach temperature difference is reduced by about 2°C. The results also confirmed that the model developed and validated based on experiments conducted with a single-slab crossflow gas cooler could accurately predict the performance of a substantially different multi-slab counterflow design.

REFERENCES

- Boewe, D., J., Bullard, C. W. and Hrnjak, P. S.: An experimental investigation of transcritical carbon dioxide systems for residential air conditioning. University of Illinois at Urbana-Champaign, ACRC CR-18, 1999.
- Boewe, D., Yin, J. M., Park, Y. C., Bullard, C. W. and Hrnjak, P. S.: The role of the suction line heat exchanger in transcritical R744 mobile a/c systems. SAE paper 1999-01-0583, 1999.
- McEnaney, R., Park, Y. C., Yin, J. M., Bullard, C. W. and Hrnjak, P. S.: Performance of the prototype of a transcritical R744 mobile a/c system. SAE paper 1999-01-0872, 1999.
- McEnaney, R. P., Boewe, D. E., Yin, J. M., Park, Y. C., Bullard, C. W. and Hrnjak, P. S.: Experimental comparison of mobile a/c systems when operated with transcritical CO₂ versus conventional R134a. 1998 International Refrigeration Conference at Purdue, pp.145-150.
- Park, Y. C., Yin, J. M., Bullard, C. W. and Hrnjak, P. S. Hrnjak.: Experimental and model analysis of control and operating parameters of transcritical CO₂ mobile A/C system. VTMS, London, May 1999.
- Pettersen, J., Aarli, R., Neksa, P., Skaugen, G. and Aflekt, K.: A comparative evaluation of CO₂ and R22 residential air-conditioning systems in a Japanese climate. IIR/IEA Workshop in CO₂ technology in refrigeration, heat pumps and air conditioning systems, Trondheim, Norway, 1997.

Yin, J. M., Bullard, C. W. and Hrnjak, P. S.: Model development for R744 gas cooler. University of Illinois at Urbana-Champaign, ACRC CR-29, 2000.

Yin, J. M., Park, Y. C., McEnaney, R. P., Boewe, D. E., Beaver, A., Bullard, C. W. and Hrnjak, P. S.: Experimental and model comparison of transcritical CO₂ versus R134a and R410A system performance. IIR conference Gustav Lorentzen, Oslo, Proceedings, Preprints, pp. 331-340, 1998.

Appendix B

Prototype system geometry and performance

The following Table summarizes relevant characteristics of two off-the-shelf R134a baseline systems, and their CO₂ prototype counterparts, MAC1 and MAC2. Note that the baseline systems were optimized for air conditioning only, as was MAC1. However MAC1 was operated in heating mode to obtain data and validate simulation models, which were later used to design a truly reversible system, MAC2, which was designed from the outset to operate in both cooling and heating modes.

Heat exchanger dimensions for four systems

Outdoor coil:

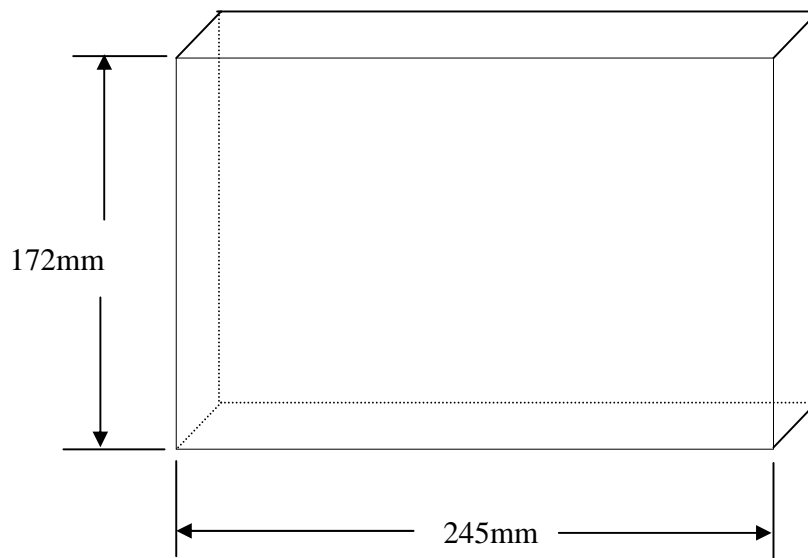
System	Escort	MAC1	Jimmy	MAC2
Louver angle (°)		23		27
Louver pitch (mm)		0.99		1.06
Fin pitch (mm)		1.155		1.155
Fin thickness (mm)		0.1		0.1
Tube thickness (mm)		1.65		1.524
Fin density (fpi)		22	18	22
Core volume (cm ³)	4477	3446	7547	4456
Core depth (mm)	22	16.5	31	21.1
Core width (mm)	553	523	667	608
Core height (mm)	368	366.5	365	349
Face area (cm ²)	2035	1950	2435	2122
Air side area (m ²)	7.2	5.35	8.4	7.09
Refrigerant side area (m ²)	0.4	0.49		0.5347
Free flow cross-section area (m ²)		0.1467		0.1617
Measured D _{pca} (Pa) @2100scfm	170	100	50-97	140

Indoor coil:

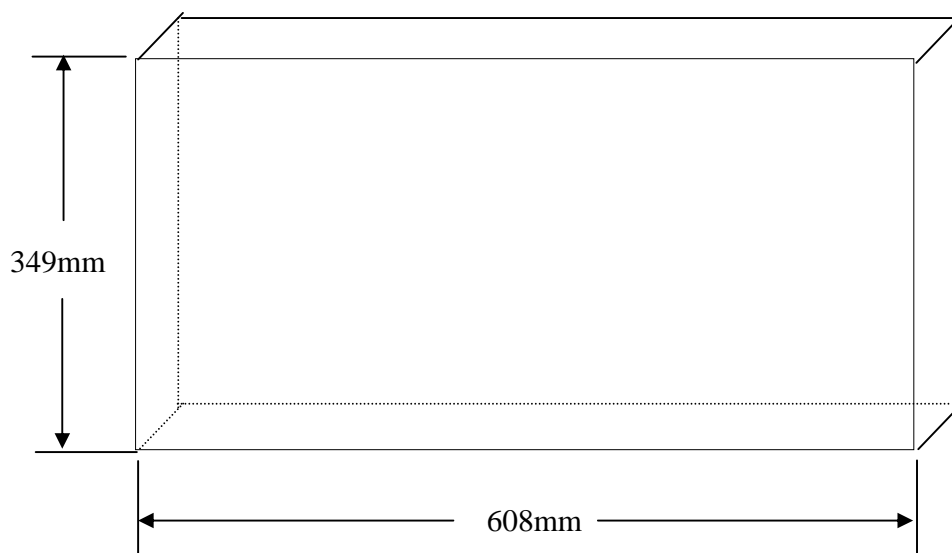
System	Escort	MAC1	Jimmy	MAC2
Louver angle (°)		30		27
Louver pitch (mm)		1.55		1.397
Fin pitch (mm)		1.494		1.494
Fin thickness (mm)		0.1		0.1
Tube thickness (mm)		1.448		1.905
Fin density (fpi)		17	14	17
Core Volume (cm)	3649	3250	4462	3666
Core depth (mm)	90	83	72	87.3
Face area (cm ²)	406	391.5	620	421.4
Core width (mm)	218	225	255	245
Core height (mm)	186	174	243	172
Air side area (m ²)	3.5	4.36	4.4	4.584
Refrigerant side area (m ²)	0.55	0.67		0.9198
Free flow cross-section area (m ²)		0.03133		0.03133
Measured D _{pca} (Pa) @300scfm	220	180	130-160	185

Actual heat exchanger size for MAC2 system (finned core)

Indoor coil core depth: 87.3mm; Tube depth: $3 \times 25.91 = 77.7\text{mm}$



Outdoor coil core depth: 21mm; Tube depth: $3 \times 4.763 = 14.3\text{mm}$



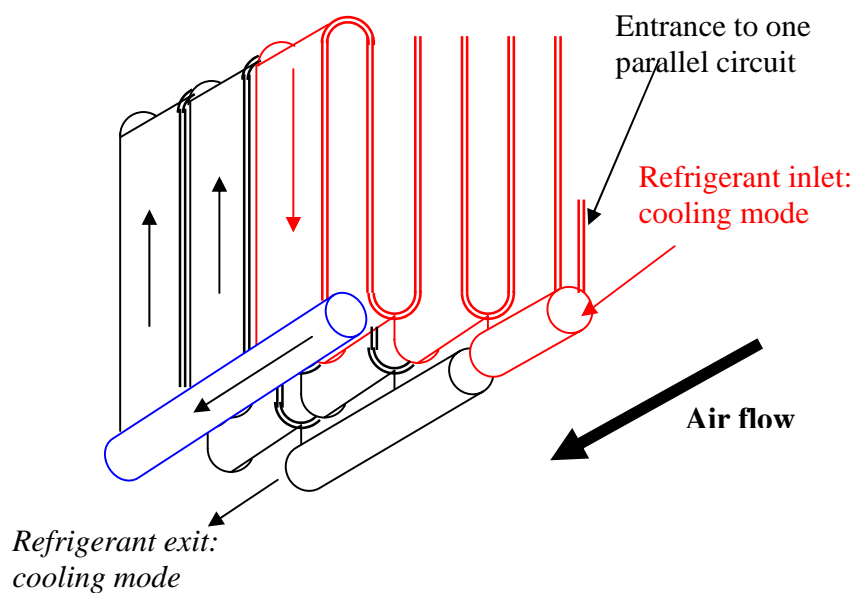
Internal heat exchanger for MAC2 system

Length: 355mm

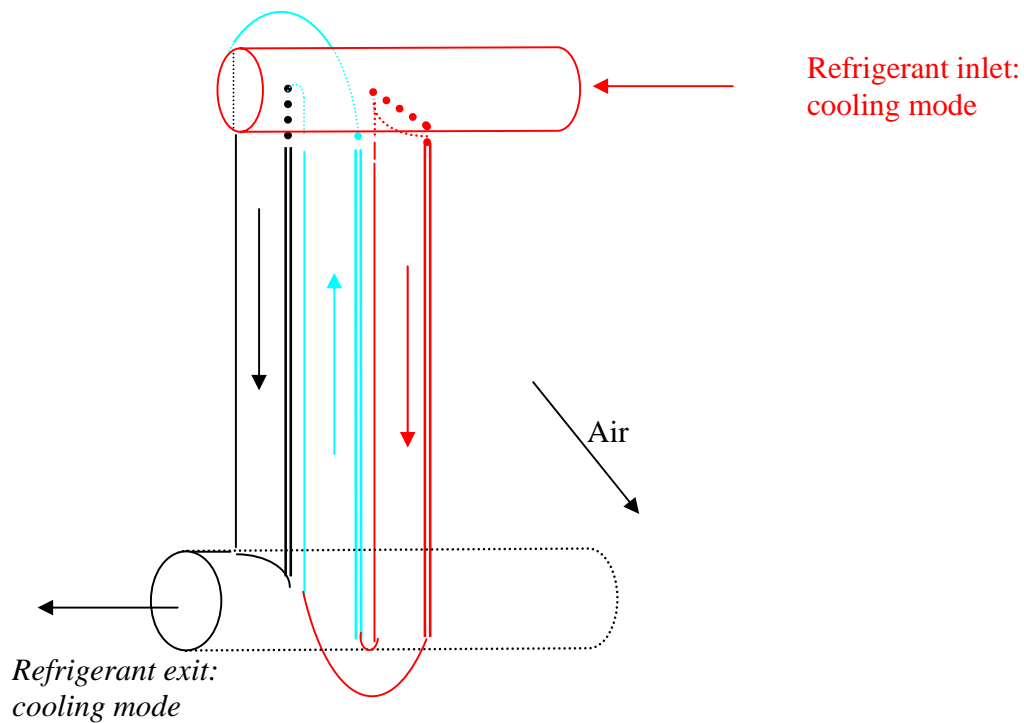
Four parallel tubes for suction side, each tube has 17/1.09mm square ports.

Two parallel tubes for liquid side, each tube has 11/1.27mm square ports.

Indoor heat exchanger serpentine details



Outdoor heat exchanger circuiting (single tube)



MAC2 system simulation results

Army design condition

Indoor air temperature: 32.2°C

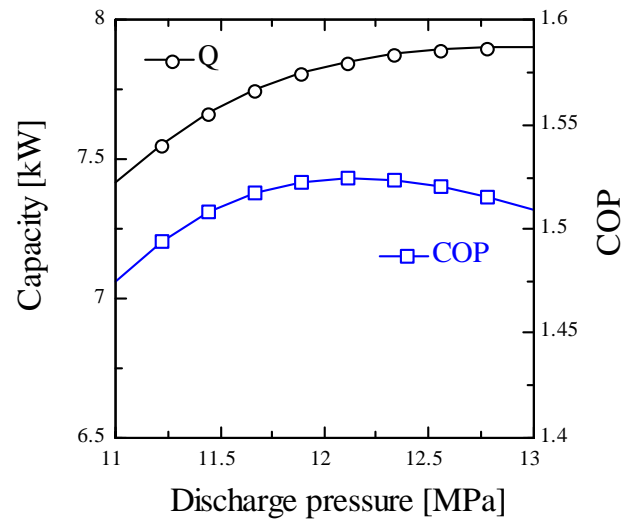
Indoor air relative humidity: 50%

Air flow rate across indoor coil: 300scfm

Outdoor air temperature: 48.9°C

Air flow rate across outdoor coil: 2100scfm

Compressor rpm: 2000



GM design condition

Indoor air temperature: 37.8°C

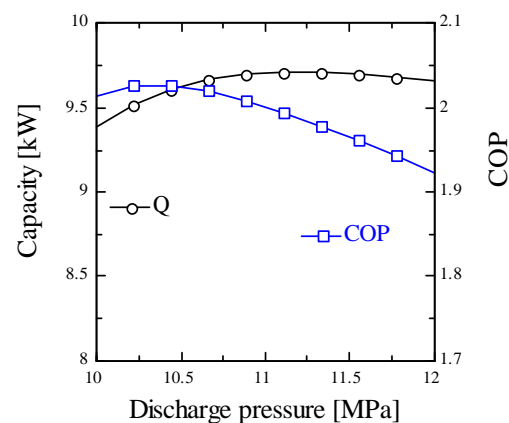
Indoor air relative humidity: 40%

Air flow rate across indoor coil: 300scfm

Outdoor air temperature: 37.8°C

Air flow rate across outdoor coil: 2100scfm

Compressor rpm: 2000



Appendix C

Simulation of MAC1 system in heating and cooling modes

The system

For simulation purposes, the system is defined by the schematic shown in Figure 1, which shows the components configured for cooling mode. The models were developed and validated using data obtained from the MAC1 prototype system described by Yin et al. (1998) and Park et al. (1999).

The system model was composed of several component models that have been described elsewhere: gas cooler (Yin et al., 2000); evaporator (Kim et al., 2000); internal heat exchanger (Boewe et al., 2001); compressor; and other additional equations including experimentally-determined pressure drop correlations for the accumulator and oil separator. For the MAC1 prototype system shown in Figure 1, all the component models were verified by comparison with data obtained at more than 300 operating points. Agreement was quite good, as indicated by the results shown in the following sections.

For the prototype system tested, there were three valves: one is the expansion valve between internal heat exchanger and evaporator; the second is an oil flow control metering valve between oil separator and suction line; the third is on the accumulator, which controls the liquid/oil mixture flow rate from accumulator to internal heat exchanger. In a production system the oil separator would probably be internal to the compressor, and the suction accumulator valve replaced by a fixed orifice. For research purposes, however, these valves provided important flexibility and ability to achieve desired operating states.

There were also three mass flow rate meters used to measure flow rates and densities. Oil density measurement on the oil return line was used during some experiments as the basis for flow rate control. Another density measurement at the accumulator exit serves as an indicator of evaporator exit quality during flooded conditions. For each component, pressure and temperature were measured at upstream and downstream locations.

Compressor model

Details of the compressor model have not been published elsewhere, so they are described here. The compressor model used isentropic and volumetric efficiencies, expressed as a function of pressure ratio, determined from the experimental data.

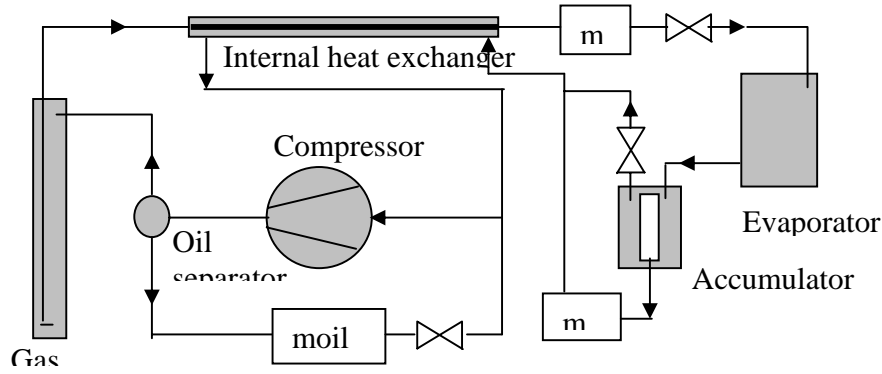


Figure 1 CO2 air conditioning system schematic

Figure 2 shows the energy balance for compressor. For this particular system, the energy balance equations can be expressed as:

$$h_{shro} = h_{rcpi} - moil \left[cp0 * (Toil - Trcpi) + cp1 * (Toil^2 - Trcpi^2) / 2 \right] / (mr - moilC) \quad (1)$$

$$- moilC \left[cp0 * (Tshro - Trcpi) + cp1 * (Tshro^2 - Trcpi^2) / 2 \right] / (mr - moilC)$$

$$W_{comp} = (h_{rcpo} - h_{rcpi}) * (mr - moilC) + Q_{conv} \quad (2)$$

$$+ (moil + moilC) * \left[cp0 * (Trcpi - Trcpi) + cp1 * (Trcpi^2 - Trcpi^2) / 2 \right]$$

where cp0 and cp1 are the coefficients of the linear specific heat equation of oil; moil is the oil flow rate from oil separator back to compressor suction; Toil is the oil temperature after oil control metering valve; moilC is the oil flow rate circulating with CO2 and Q_{conv} is the convective heat transfer between compressor surface and its surroundings.

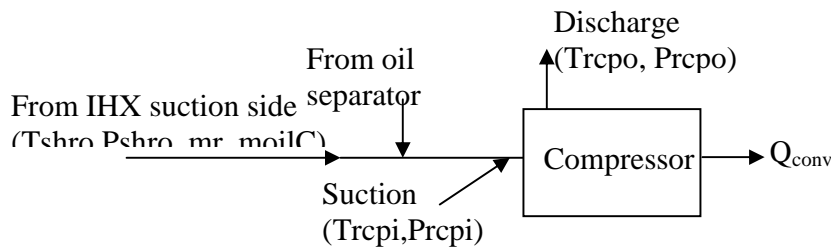


Figure 2 Compressor energy balance schematics

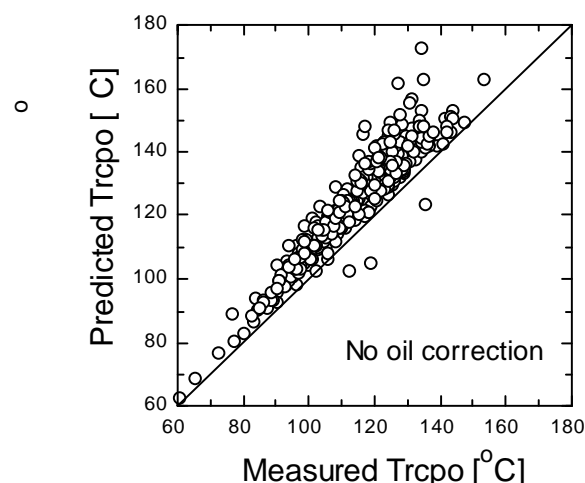


Figure 3 Compressor discharge temperature prediction with no oil correction

Figure 3 shows that compressor discharge temperature is overpredicted if all oil effects are neglected. Shell heat transfer was accounted for, so clearly some other effect is responsible for the overprediction.

Figure 4 shows the effect of accounting properly for the heat capacity of the oil returning from the separator to the crankcase, as detailed in Equations 1 and 2. Figure 5 shows the same result, assuming that oil in circulation is equal to 3% of the refrigerant mass flow rate (a reasonable assumption based on sampling data taken at several operating conditions).

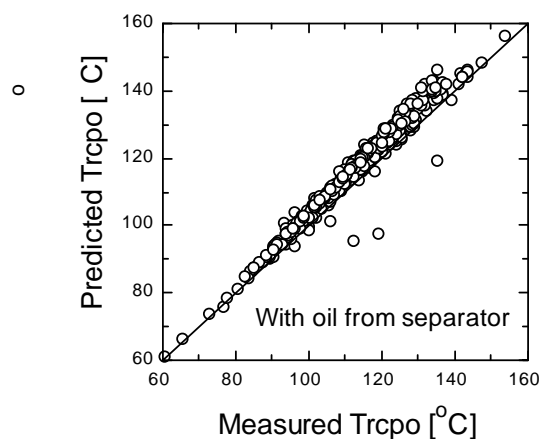


Figure 4 Discharge temperature prediction accounting for oil from separator

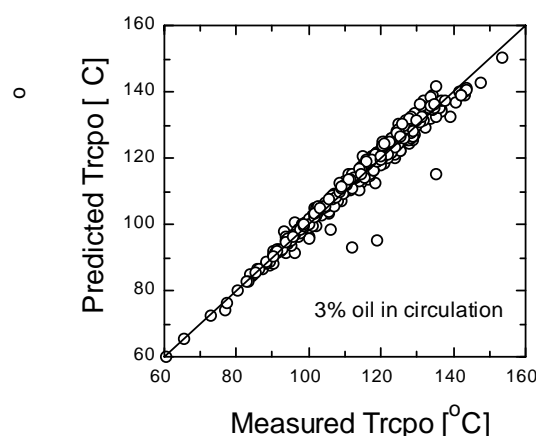


Figure 5 Discharge temperature prediction accounting for oil from separator and in circulation

Table 1 shows the connecting tube dimensions for the prototype CO₂ system. Suction and liquid line lengths exclude the length of the internal heat exchanger. With this information the component models were connected to simulate the system.

Table 1 Tubing dimensions

	Suction line	Discharge line	Liquid line
Length (m)	4.45	2.99	3.5
Inner diameter (mm)	7.9	6.3	6.3

Oil separator and accumulator equations

Two other very important components had significant impacts on the prototype system's performance: the accumulator the oil separator. These two components produced larger pressure drops in the prototype than would be expected in production components, but our research was not focused on them at this time. Because no reliable coefficients exist for such unique geometries, empirical correlations were developed from over 300 experimental data. The pressure drop for accumulator and oil separator were correlated to the simple relation as:

$$\Delta P = k_{loss} \frac{\rho v^2}{2} \quad (3)$$

Here k_{loss} is the pressure drop coefficient; ρ and v are refrigerant density and velocity, respectively. The pressure drop coefficient for the accumulator is about 100 and for the oil separator, the coefficient is about 80.

Experimental data and model prediction comparison for a/c condition

Table 2 shows the data selected from more than 300 experiments. They were selected because they were taken at steady state with same indoor air temperature.

Table 2: a/c system performance data

Test point	I11	I19	I44	M5	M10
Tea [°C]	26.4	26.5	26.5	26.3	26.6
mea [g/s]	143	141	143	143	140
RH [%]	40	40	40	40	40
Tca [°C]	43.1	32.4	27.0	42.9	32.4
mca [g/s]	453	452	447	537	538
mr [g/s]	22.29	23.44	22.90	34.0	35.4
ρ_r [kg/m ³]	0.725	0.717	0.770	0.702	0.716
rpm	951	950	951	1801	1802
Q [kW]	2.654	2.986	3.508	3.942	4.274
W [kW]	1.532	1.238	1.209	2.918	2.377
COP	1.732	2.411	2.901	1.351	1.798
DG [g/s]	0.2099	0.2886	0.4041	0.4949	0.5173
Prcpi [kPa]	4149	4015	3851	3552	3390
Prcpo [kPa]	10888	8987	8570	11052	9559
Trcpi [°C]	38.5	32.8	24.2	38.5	29.5
Trcpo [°C]	111.8	93.7	88.4	111.8	118.2
Peri [kPa]	4262	4137	3983	3838	3655
Pero [kPa]	4211	4083	3926	3721	3552
Teri [°C]	9.5	8.2	6.7	9.5	3.3
Tero [°C]	9.1	7.8	6.2	9.1	2.2
Pcri [kPa]	10732	8835	8413	10789	9192
Pcro [kPa]	10687	8789	8382	10654	9128
Tcri [°C]	108.1	90.4	85.5	108.1	114.6
Tcro [°C]	46.6	37.9	33.7	46.6	40.2
DP_evap [Pa]	171	181	198	188	204
DP_gc [Pa]	37	37	31	37	36
η_m	0.72	0.74	0.70	0.71	0.71
η_v	0.77	0.81	0.78	0.75	0.75
moil [g/s]	2.5	2.3	1.4	2.3	2.0
ML [g/s]	0.18	0.11	0.30	0.47	1.0
Toil [°C]	87	71	65	87	87
Tshro [°C]	27.3	26.1	20.0	29.5	24.4
Tori [°C]	38.5	33.3	27.9	38.5	32.9
X_in	0.38	0.36	0.27	0.44	0.37
X_out	0.96	0.97	0.98	0.97	0.97
IHX length [m]	1.5	1.5	1.5	1.5	1.5
IHX direction	PF	PF	PF	PF	PF
Compressor #	2	2	3	2	3

Figure 2 compares measured and predicted system performance data at driving conditions (1800 rpm). Figure 3 shows the results for idling conditions. Because the exact oil circulation rate in the system was unknown, a 3 percent oil circulation rate was assumed for the model predictions.

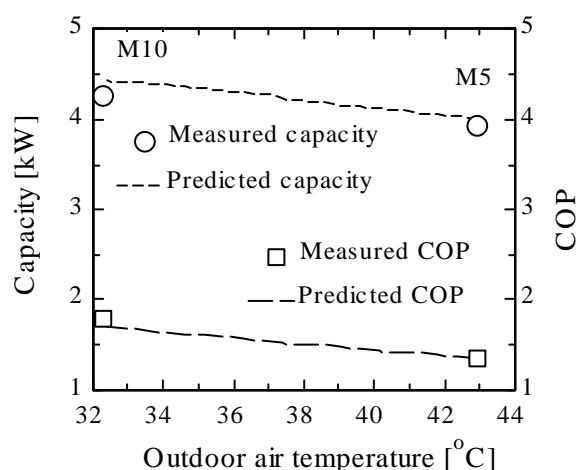


Figure 2 Measured and predicted system performance data

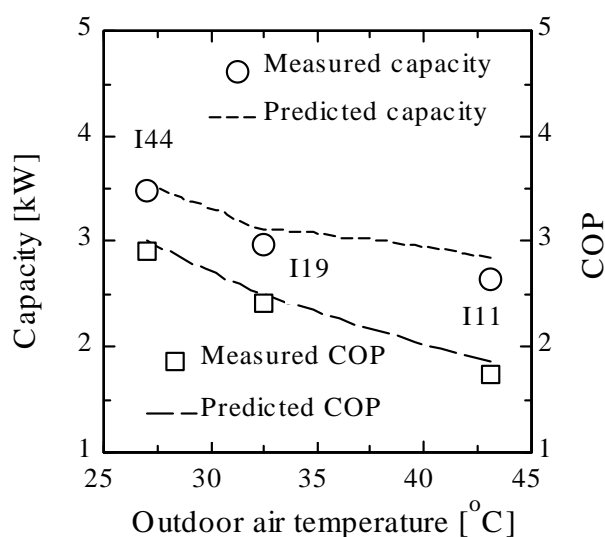


Figure 3 Measured and predicted system performance data

As shown in Figures 2 and 3, the model can predict the system performance very accurately. Of course this reflects the fact that these data points are taken from the same prototype system and data set used to validate the model. However the model is based on first principles, plus heat transfer and pressure drop correlations taken from the literature and based on studies of a wide range of geometries and operating conditions. Therefore we expect the model to provide similarly accurate results for very different components and system configurations.

Operation in heat pump mode

The MAC1 heat pump was composed of the same components as the a/c system. The indoor coil became the gas cooler and the outdoor coil operated as an evaporator in heating mode. The same 1.5m counterflow internal heat exchanger was installed in the system. The test were done at “dry” outdoor coil conditions, to minimize complications due to frost formation. However due to the high ambient humidity conditions in the laboratory during the test, some of the air-side pressure drop data suggested the presence of a small amount of frost on the surface, due to the water vapor in the air at the time the outdoor chamber was sealed.

Tables 3 and 4 show the data for different indoor/outdoor temperature conditions. In order to protect the compressor, higher liquid/oil mixture flow rates from accumulator to internal heat exchanger were allowed, to guarantee sufficient oil return to compressor. The oil used in these experiments was designed for air conditioning only, not for heating mode, so the amount of CO₂ dissolved in the returning oil was excessive. As a result, the exit quality from the evaporator was lower than desired. We have re-tested some of the similar conditions with lower liquid/oil flow rate, the results shows that the exit quality from evaporator increased, but the system performance changed very little, suggesting that the data given below may represent the actual condition.

Table 3: Heat pump system performance data

Test point	HP1	HP2	HP3	HP4
Tea [°C]	20.0	9.9	0.0	-10.3
mea [g/s]	541	538	532	544
RH [%]	39	56	33	43
Tca [°C]	20.6	20.0	20.0	20.0
mca [g/s]	142	142	142	142
mr [g/s]	35.4	24.7	17.3	12.0
ρ_r [kg/m ³]	0.785	0.886	0.959	1.012
Rpm	946	947	945	943
Q [kW]	3.797	3.591	3.336	2.740
W [kW]	1.126	1.138	1.178	1.155
COP_HP	3.37	3.16	2.83	2.37
Prcpi [kPa]	4570	3631	2854	2228
Prepo [kPa]	8623	8126	8108	8055
Trcpi [°C]	19.1	16.3	16.6	8.7
Trcpo [°C]	63.2	72.4	81.2	87.5
Peri [kPa]	4825	3812	2975	2313
Pero [kPa]	4672	3703	2910	2270
Teri [°C]	12.7	3.5	-5.7	-14.5
Tero [°C]	11.5	2.5	-6.3	-14.9
Pcri [kPa]	8474	8037	8041	8001
Pcro [kPa]	8393	7996	8022	7991
Tcri [°C]	62.9	72.2	80.8	85.9
Tcro [°C]	38.4	35.8	33.1	26.6
DP_gc [Pa]	123	119	120	118
DP_evap [Pa]	32	30	28	27
η_m	0.81	0.79	0.77	0.70
η_v	0.89	0.86	0.84	0.75
mL [g/s]	4.8	3.9	5.4	5.2
Toil [°C]	52.1	60.6	69.3	71.8
Tshro [°C]	14.9	8.3	-6.1	-14.7
Tori [°C]	28.5	16.5	3.6	-6.6
X_in	0.20	0.14	0.08	0.06
X_out	0.64	0.57	0.54	0.44

Table 4: Heat pump system performance data

Test point	HP5	HP6	HP7	HP8	HP9	HP10
Tea [°C]	9.8	0.1	-10	0	-10.1	-10
mea [g/s]	525	532	527	529	533	534
RH [%]	61	33	46	37	58	60
Tca [°C]	10.0	10.2	10.0	0.2	0	-8.4
mca [g/s]	142	141	142	143	142	144
mr [g/s]	23.7	18.1	13.6	17.9	12.6	12.7
ρ_r [kg/m ³]	0.931	0.986	1.024	1.006	1.034	1.041
Rpm	943	946	946	945	944	947
Q [kW]	4.356	3.857	3.314	4.451	3.449	3.811
W [kW]	1.169	1.213	1.189	1.196	1.162	1.104
COP_HP	3.73	3.18	2.79	3.72	2.97	3.45
Prcpi [kPa]	3398	2733	2173	2634	2150	2056
Prcpo [kPa]	8161	8312	8260	8206	8068	7571
Trcpi [°C]	7.8	-0.4	-11.8	-7.8	-5.4	-13.4
Trcpo [°C]	63.7	65.7	73.2	65.3	73.7	77.4
Peri [kPa]	3575	2872	2274	2776	2247	2170
Pero [kPa]	3473	2793	2216	2693	2196	2099
Teri [°C]	0.9	-7.1	-15.0	-8.0	-15.2	-16.4
Tero [°C]	0	-7.8	-15.6	-8.9	-15.8	-17.3
Pcri [kPa]	8091	8264	8221	8166	8028	7541
Pcro [kPa]	8060	8247	8211	8154	8021	7533
Tcri [°C]	63.7	65.6	72.5	65.5	73.1	76.4
Tcro [°C]	29.6	20.3	14.7	7.7	3.9	-4.2
DP_gc [Pa]	116	113	111	108	103	102
DP_evap [Pa]	69	42	29	30	28	30
η_m	0.77	0.75	0.70	0.73	0.69	0.69
η_v	0.85	0.81	0.76	0.79	0.75	0.75
mL [g/s]	5.8	5.9	3.3	3.3	5.1	1.93
Toil [°C]	50.3	50.4	56.3	48.6	56.4	60.2
Tshro [°C]	0.2	-7.7	-15.6	-9.2	-16.0	-17.5
Tori [°C]	8.6	-1.3	-9.4	-5.2	-11.8	-14.1
X_in	0.07	0.05	0.05	0.03	0.03	0.03
X_out	0.64	0.64	0.49	0.65	0.55	0.66

Figures 4-6 show the model prediction compared to the experimental data for different indoor and outdoor air temperature conditions. Because the oil flow rate was not measured for this data during the test, but an in-line sight glass was used to visually determine the oil flow condition from the oil separator, and later similar conditions were repeated and oil flow rate were measured, the predictions were based on the following approximations: 3g/s of oil flow rate from oil separator; and 2% oil in circulation. Condensation and frosting on the outdoor heat exchanger was also neglected, resulting in overestimation of system performance by a small but unknown amount.

The model generally predicted very well except for very high indoor/outdoor air temperature conditions shown in Figure 4, where the frost effects would have been greatest.

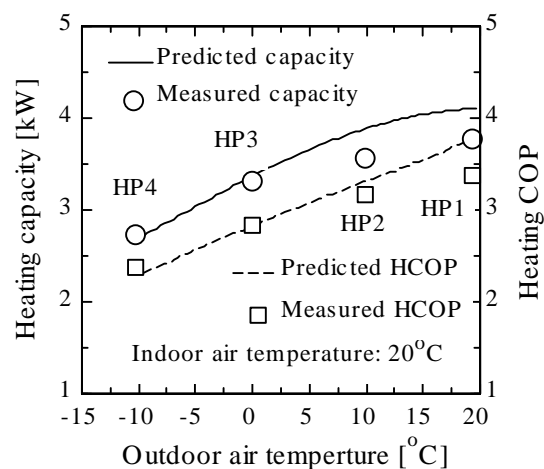


Figure 4 Measured and predicted heat pump performance data

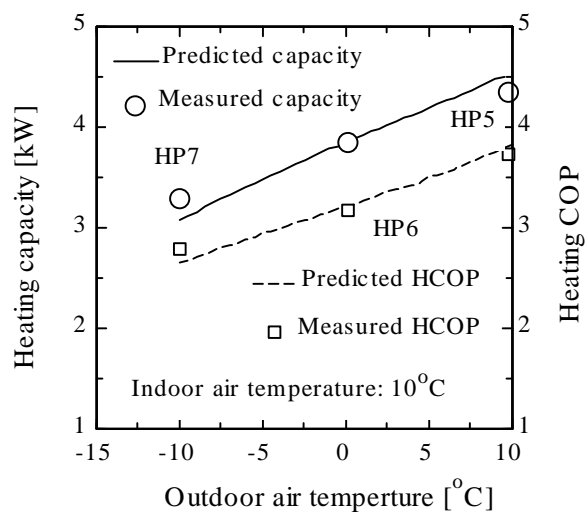


Figure 5 Measured and predicted heat pump performance data

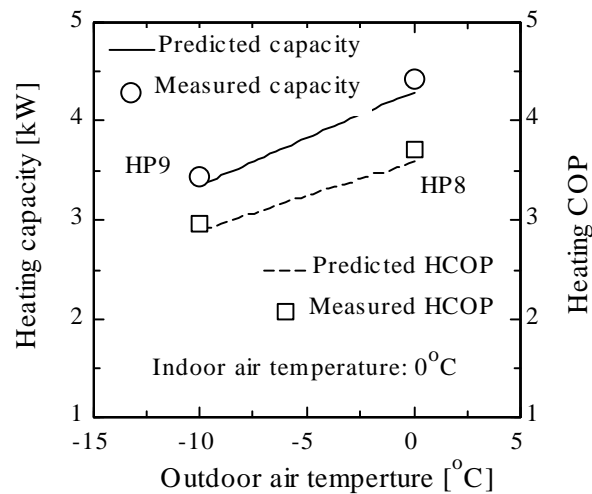


Figure 6 Measured and predicted heat pump performance data

System performance at steady state

Figure 7 shows simulation results over a wide range of heating and cooling conditions. The compartment air temperature was set at 21.1°C for both a/c and heat pump modes. For the heat pump, there are two curves corresponding to two different compressor rpm (1800 and 950), while air flow rates over the indoor and outdoor heat exchangers were 250scfm and 950scfm, respectively). At the 1800rpm driving condition, the heating capacity is much higher than for idling. To maximize vehicle fuel economy, the heat pump will be shut off after the engine warms up, so the issue of compressor cycling or displacement control is not addressed for heating mode.

In cooling mode four curves are shown; the two solid lines represent full compressor displacement operation at two different compressor rpm and air flow rates (250scfm for 1800rpm, 175scfm for 950rpm). Because the system capacities exceed typical loads for most of the temperatures shown, the actual compressor will start cycling or its displacement must be reduced. The two dashed lines on this figure represent the variable displacement performance, assuming no compressor efficiency degradation.

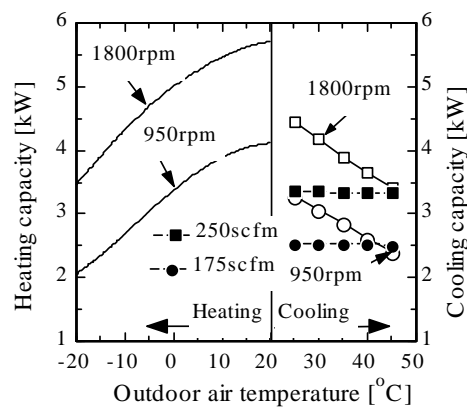


Figure 7 Capacity curve for a/c and heat pump conditions

Figure 8 shows the system energy efficiencies in heating and cooling modes. Clearly higher capacity at heat pump and a/c conditions is obtained at the cost of lower efficiency. In cooling mode, the COP at 1800 rpm for a system with a variable displacement compressor is much higher than for fixed compressor. However, requirements for dehumidification may limit the magnitude of savings actually achieved by variable displacement operation.

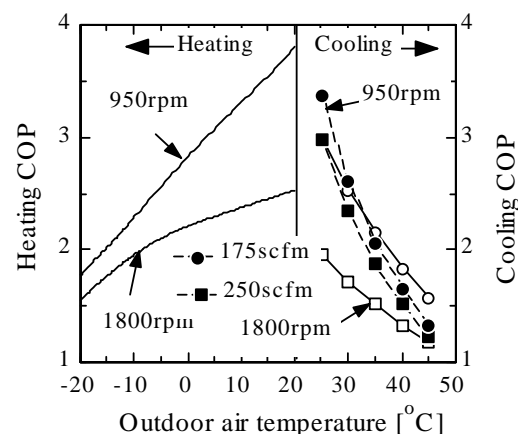


Figure 8 Performance curve for a/c and heat pump conditions

Warmup performance

Figure 9 shows the simulated performance of the prototype system at different ambient temperature conditions with comfort constrain and without indoor air recirculation. In the latter case indoor coil air inlet temperature is set equal to the outdoor coil air inlet temperature. The results are for the conditions with 35°C supply air to the passenger compartment (gas cooler air outlet temperature), with indoor and outdoor air flow rates (250 and 950 scfm, respectively), discharge pressure (80 bar) and compressor rpm (950) held constant. Only compressor displacement was varied, to achieve the mass flow rates and heating capacities shown in the Figures.

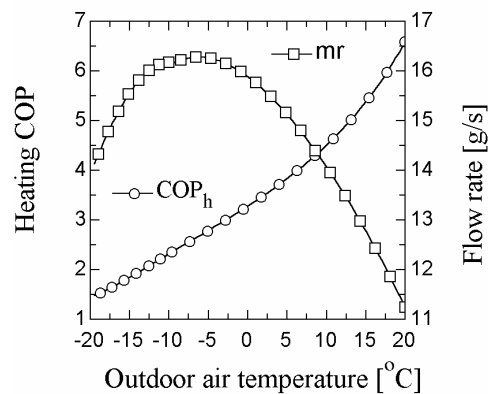


Figure 9 Heat Pump performance with 35°C comfort constraint

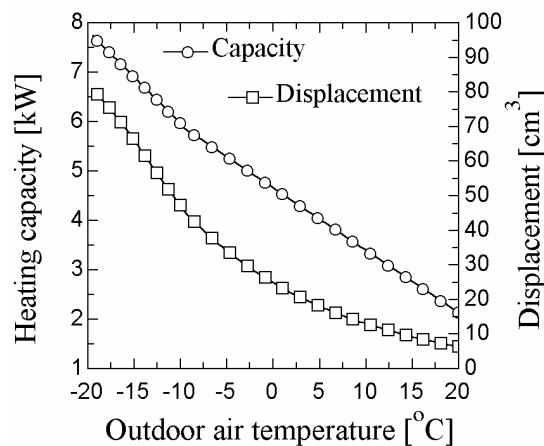


Figure 10 Heating capacity and compressor displacement

As shown in Figure 10, to supply 35°C hot air from -20°C to 20°C, the required compressor displacement ranged from 7 to 80 cm³.

In many vehicles, the indoor air recirculation rate is set by the occupants. In winter, it is used to ensure adequate defrosting. With zero recirculation, commonly used after warmup and steady state has been reached, air infiltration amounts to about 10-15% of the evaporator air flow rate. During warmup, however, the fraction would generally be larger, especially when relative humidity is high. Therefore in the following analysis it is assumed conservatively that the recirculation fraction is set at a level that results in indoor air inlet temperature to indoor coil is always 5°C higher than the outdoor air. All other conditions are kept the same as for the no recirculation case analyzed above. Figures 11 and 12 show the results.

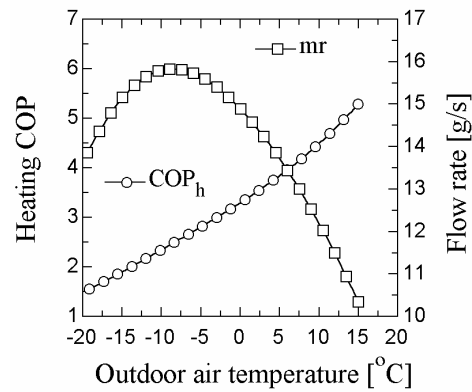


Figure 11 Heat Pump performance with comfort constrain

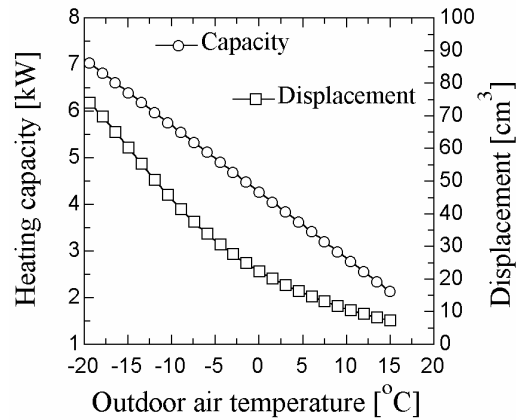


Figure 12 Heating capacity and compressor displacement

The results show that system performance is affected very little by small changes in the evaporator inlet air temperature. Note, however, that the heating capacity is very high when the outdoor air temperature is lowest: heat is available when it is needed most. Once the air warms up to comfortable indoor temperatures and defogging is accomplished, capacity needs would be met by the engine coolant in the most energy-efficient strategy, and the heat pump would be shut off.

References

- Boewe, D. E., C. W. Bullard, J. M. Yin, and P. S. Hrnjak, "Contribution of Internal Heat Exchanger to Transcritical R744 Cycle Performance" *International Journal of HVAC&R Research*, April 2001, in press
- Kim, M.-H., J.M. Yin, C.W. Bullard, P.S. Hrnjak, "Development of a Micro-Channel Evaporator Model for a CO₂ Mobile Air-Conditioner", *Proceedings of the ASME, AES-Vol. 40, Advanced Energy Systems Division*, pp. 47-54, 2000.
- Park, Y. C., J. M. Yin, C. W. Bullard, and P. S. Hrnjak, "Experimental and Model Analysis of Control and Operating Parameters of Transcritical CO₂ Mobile A/C System," *VTMS-4 Conference*, London, England, 163-170, May 1999.
- Yin, J. M., C. W. Bullard, and P. S. Hrnjak, 2000, "Design Strategies for R744 Gas Coolers," *Proceedings of the IIF-IIR Commission B1, B2, E1, and E2*, Purdue University, W. Lafayette, IN, 315-322, July.
- Yin, J., Y. C. Park, D. Boewe, R. McEnaney, A. Beaver, C. W. Bullard, and P. S. Hrnjak, "Experimental and Model Comparison of Transcritical CO₂ Versus R134a and R410 System Performance," *Proceedings of the International Institute of Refrigeration Conference on Natural Working Fluids 1998*, Oslo, Norway, 376-387, June, 1998, 10 pp.

Appendix D

Control of Transcritical R744 Cycle

Introduction

Carbon dioxide (R744, CO₂) is a natural refrigerant whose higher operating pressure (over 100 bar) has limited its application. However with the development of microchannel heat exchanger technology in recent years, it is much easier to handle the high pressure without increasing the component and system weight.

Because CO₂ operates in a transcritical thermodynamic cycle at normal air conditioning mode, it is very important to take the advantage of CO₂ properties in different operating conditions. In the case of CO₂, this can be achieved by controlling the system discharge pressure to maximize COP.

Recent research on CO₂ systems for mobile a/c applications have been limited mainly to laboratory prototype tests. There are several prototype cars with R744 a/c system installed, but there is no indication that any have a proper control system. Because of the many variables that could affect the COP-maximizing discharge pressures for a given a/c system, finding a simple control logic for the CO₂ mobile a/c system becomes an urgent issue.

One very direct way to solve this problem is by building many prototype systems and testing them at many different operating conditions, but the cost would be prohibitive because of huge amount of experimental works involve. By analyzing our test results from a prototype system, we have found a simple way to control the discharge pressure by using the CO₂ temperature at gas cooler exit to control the pressure at the same location. In this paper, a system model will be used to first check with the experimental data, and then to develop the control logic for other conditions.

Experimental results for COP-maximizing discharge pressure

Figure 1 shows a schematic of the prototype CO₂ a/c system. It includes all the components in a conventional mobile a/c system except the added oil separator and internal heat exchanger. The internal heat exchanger is very important for R744 cycle, because it can improve the system performance by increase COP and lower the discharge pressure, especially at high ambient temperature conditions. The low-pressure accumulator is needed in order to have enough charge when the operating condition changes, as in conventional systems. Because the R744 system has a maximum COP for a given indoor/outdoor operating condition, which also corresponds to a given discharge pressure, so it is very important to understand how the maximum COP changes with system component and operating conditions. More importantly, it is necessary to understand how to control the high-side pressure in a practical system.

The prototype system was tested at different operating conditions, with internal heat exchangers of three different lengths (1m, 1.5m and 2m) and with no internal heat exchanger. Each was configured first for counterflow and then for parallel flow. For a given operating condition and internal heat exchanger length, experiments were conducted at several different discharge pressures to locate the maximum COP range.

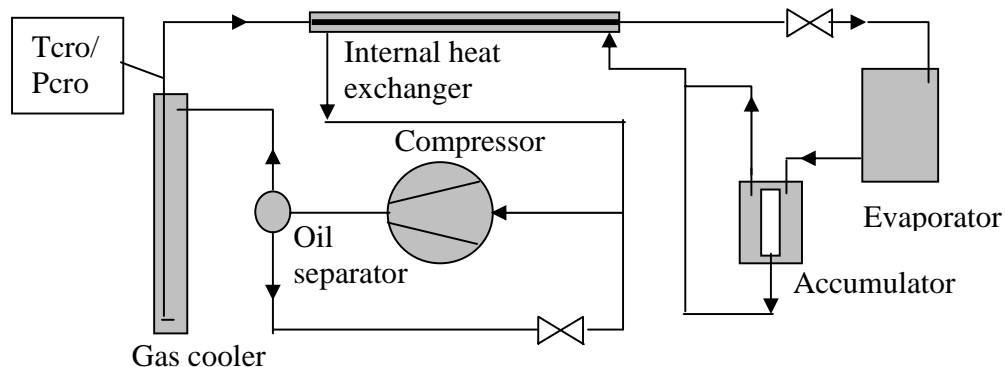
Figure 1 CO₂ air conditioning system schematic

Figure 2 shows the resulting R744 pressure and temperature at gas cooler exit location for different internal heat exchanger length and operating conditions. The data was scattered in this plot, it is because many other factors affected discharge pressure at the maximum COP condition. Moreover the tested discharge pressure was only “close” to the maximum COP discharge pressure. Nevertheless it is clear in this Figure that the R744 pressure at gas cooler exit condition is linked mainly to R744 temperature at the same location.

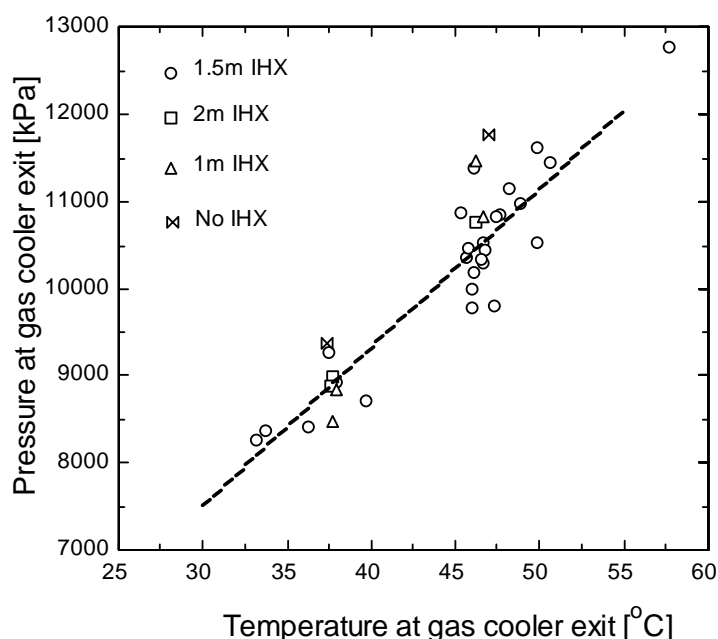


Figure 2 MAC1 Optimum pressure vs temperature at gas cooler exit condition

Figure 3 shows the result for the system with 1.5m counterflow internal heat exchanger at similar airflow rates and compressor rpm conditions (only one data has higher air flow rate across gas cooler).

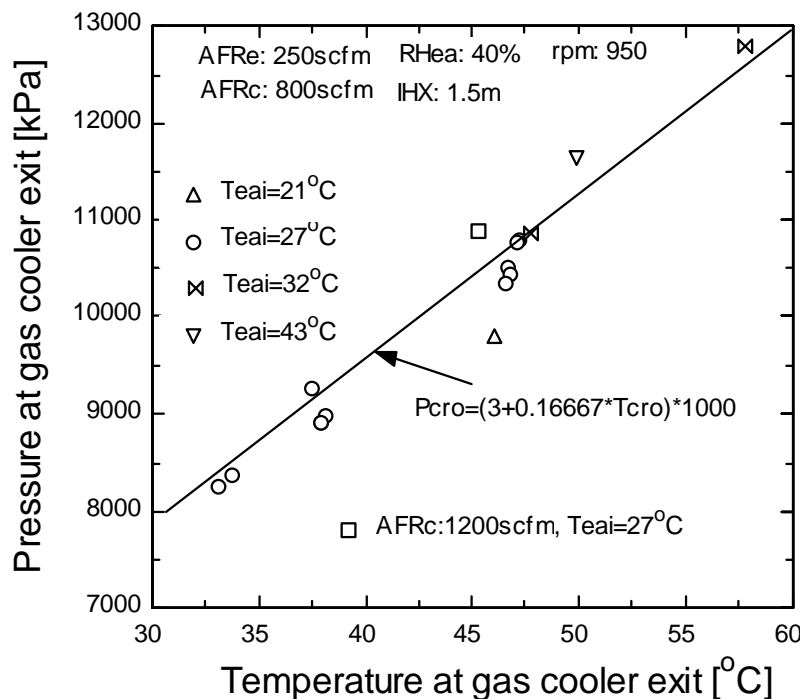


Figure 3 Optimum pressure vs temperature at gas cooler exit for given condition

As shown in Figure 3, for most of the test points, the relation between R744 pressure and temperature at gas cooler exit location is very close to linear. Therefore a temperature sensor measuring the R744 temperature at gas cooler exit location could be used to control the R744 pressure at the same location.

Discharge pressure at maximum COP condition

As suggested by the foregoing experimental results, is very difficult to experimentally determine exactly the COP-maximizing discharge pressure across the entire range of operating conditions. On the other hand, it is only necessary to control the system to operate at its maximum COP at those conditions where the system is used most. An alternative would be to divide the operating conditions into several groups, each group having a unique set of control parameters. For example, the a/c operating conditions could be divided into two modes, one for driving in the city (low rpm and gas cooler air flow) and another for driving on the highway (high rpm and gas cooler air flow).

The following model results are for the tested prototype MAC1 system configuration. Two kinds of driving patterns were simulated, one is typical pulldown performance and another is lower airflow rate driving condition.

For the pull down operation (city driving), the compressor is in lower rpm range (950 rpm); airflow rate across gas cooler is limited by the vehicle moving speed or the blower capacity (950 scfm). The airflow rate across evaporator, regulated by changing the indoor blower speed, is assumed to operate in higher position during the pulldown process (250 scfm). The air inlet temperature to evaporator is assumed to span the range from outdoor ambient to 20°C.

For the highway driving condition, the compressor is in the higher rpm range (2000 rpm), air flow rate across gas cooler higher due to vehicle speed (1500 scfm) and air flow rate across evaporator is assumed to be lower than pull down condition (175scfm). Because of the high compressor rpm, conventional mobile a/c systems will operate in cycling condition to ensure that evaporating temperature remains above zero. If the system is equipped with a variable displacement compressor; the conventional system will operate at a reduced displacement conditions, with the compressor displacement controlled to maintain the evaporation temperature. In the following calculations, the R744 temperature at evaporator exit was set at 0°C. For the highway driving condition, a constant 25°C temperature was assumed for the evaporator inlet condition. For both operating modes, the indoor air inlet relative humidity was assumed to be 40%.

Figure 4 shows the simulation results. The model prediction is very close to the test results, and for the highway driving condition, the optimum discharge pressure is a little higher than for the pulldown condition. This result was based on the assumption that the compressor efficiency will not degrade when the displacement was reduced.

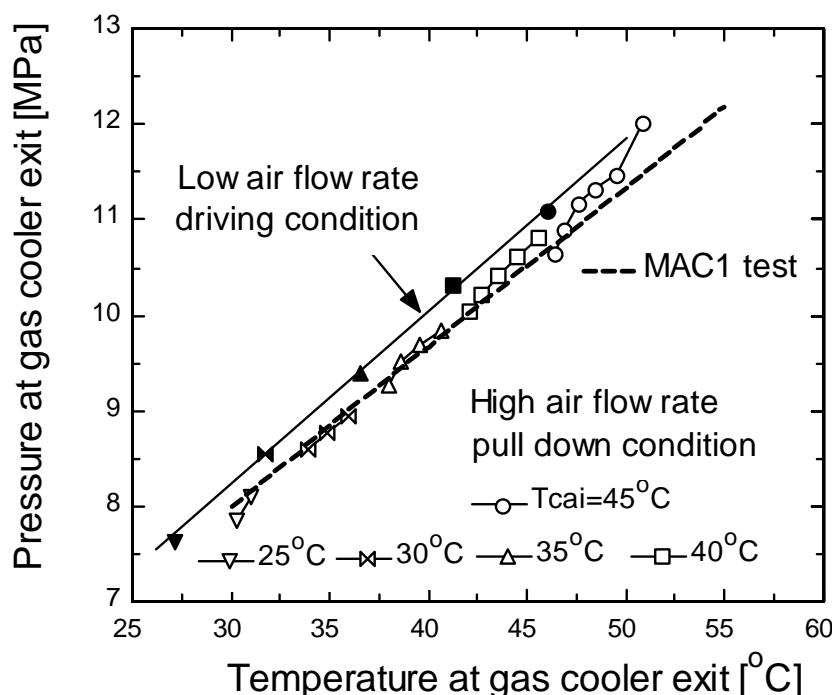


Figure 4 Optimum pressure vs temperature at gas cooler exit condition (model prediction)

COP penalty if system is not controlled to the optimal discharge pressure

In order to maximize system efficiency at different operating conditions, the discharge pressure needs to be controlled. Lower than optimum discharge pressure will cause lower COP and cooling capacity; higher than optimum discharge pressure will have higher cooling capacity but much lower COP.

Figure 5 shows the model prediction results for low air flow rate driving conditions by assuming the system is controlled rather crudely: operating at either a low (9000 kPa) or a high (11000 kPa) discharge pressure. It is clear for both cases that the COP penalty is very high.

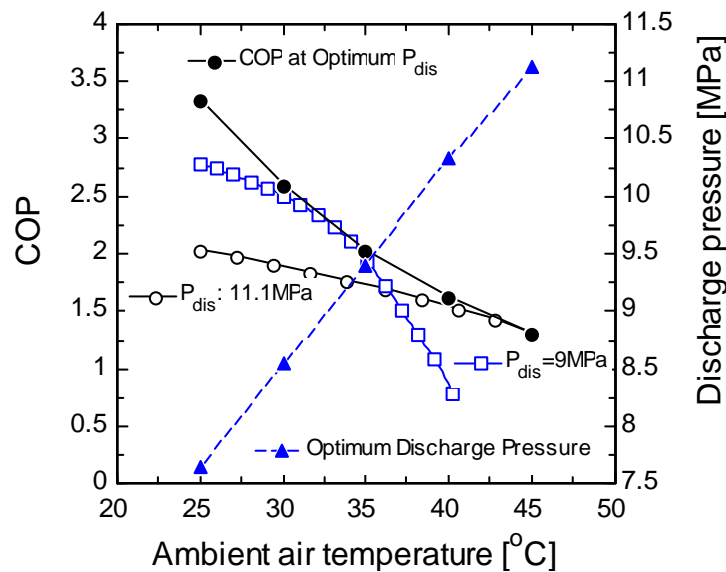


Figure 5 COP at different discharge pressures

Using TXV for system with no low side accumulator

For systems having no low side accumulator the evaporator exit state must be controlled in a different way. Thermostatic expansion valves are the most common; they control the superheat at some positive value. In conventional subcritical systems a receiver can be located downstream of the condenser, and used to store excess charge while controlling the condenser outlet quality at $x=0$ to maximize condenser performance. However this is not possible in the transcritical cycle, because the gas cooler and its exit are single phase. Therefore in a transcritical system without a low-side receiver/accumulator, the discharge pressure of the system at different operating conditions will be determined by the system charge distribution.

Figure 6 shows the results predicted by the simulation model. Although TXV controlled system usually has some finite superheat, it was assumed in the model that the TXV was ideal, controlling superheat at zero, and that the system was charged to maximize efficiency at the most common low-ambient temperature conditions. Figure 6 shows, for the system having no low side accumulator, at high ambient temperature conditions, that the extra charge will move to gas cooler and cause the discharge pressure to exceed the COP maximizing discharge pressure. Because the system COP is not as sensitive to discharge pressure in the high ambient/high discharge region, the COP penalty is not too high. This results shows that it is possible to control the system with no low side accumulator by a TXV, as has been done in several of the early prototype R744 systems in vehicles. Practically, however, this option may cause the system to operate nearer to high pressure limit, and the extra high discharge pressure will cause system to have excessive cooling capacity that will increase the need for cycling or variable displacement control.

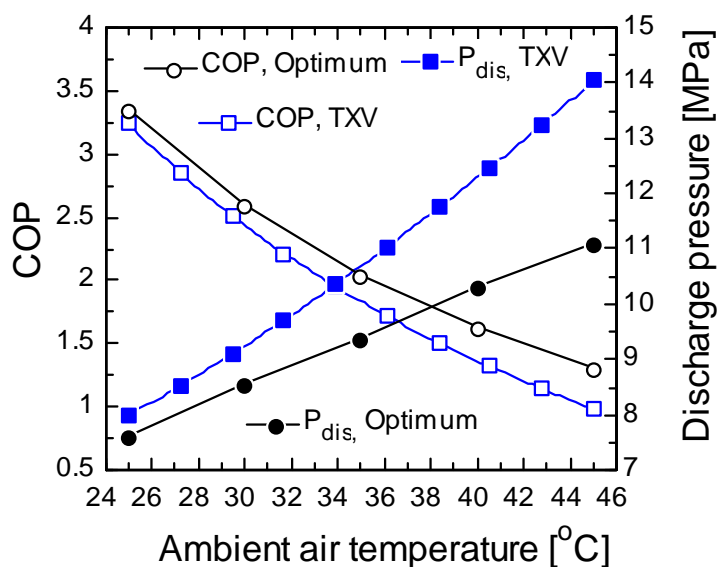


Figure 6 COP and discharge pressure

Basically, any system without a high- or low-side receiver containing a two-phase mixture will always have too much or too little of charge at almost every operating conditions; if it is properly charged at driving condition, its performance will be suboptimal at other operating conditions. Figure 7 shows the simulation model results for the city driving operation as defined before, but at a fixed evaporator inlet air temperature of 25°C. Again the discharge pressure is much higher than the optimized pressure, and COP is slightly lower.

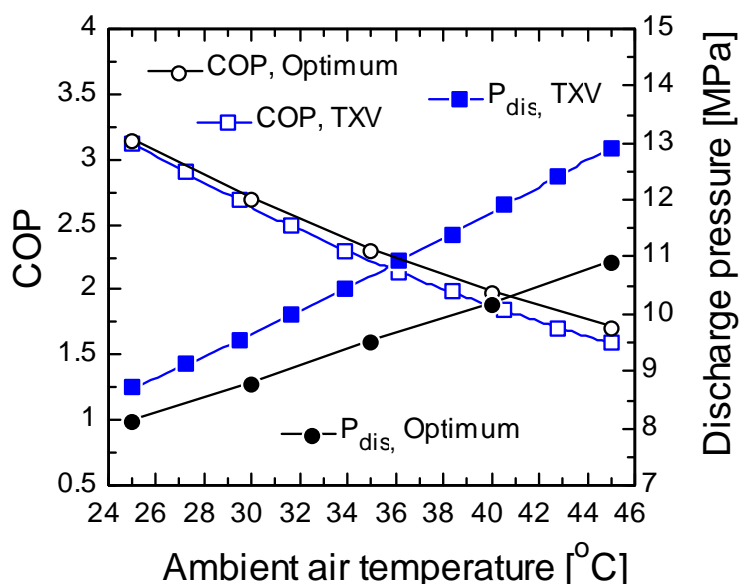


Figure 7 COP and discharge pressure at pull down conditions

One possible way to reduce the overcharge problem at high ambient temperature conditions is to add a high side receiver. Several variations of this option were explored using the simulation model. The problem is that the receiver needs to store more refrigerant at high

ambient temperatures than at low ambients. There are three possible locations for install this high side accumulator: 1) between the compressor and gas cooler, 2) after gas cooler and before internal heat exchanger, or 3) after the internal heat exchanger and before expansion valve.

After extensive simulations it was found that the only feasible location for the high side receiver is between compressor and gas cooler exit. At the other two locations the vessel would hold less charge at high ambient conditions than at lower temperatures.

Figure 8 shows the model prediction results for the city driving conditions. There are two configurations shown: one with no high side receiver; the other with a 400 cc receiver installed between compressor discharge and gas cooler inlet. As shown in the Figure, even this very large receiver was rather ineffective in reducing the discharge pressure. Such a large receiver would introduce safety problems because it would increase the total system charge so much.

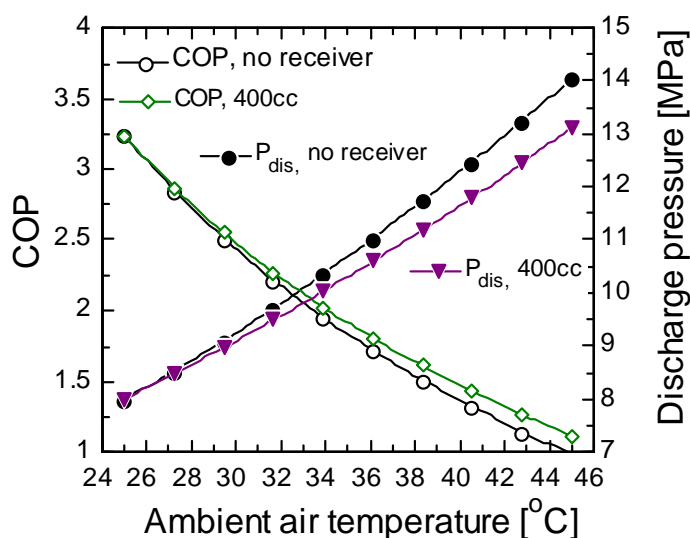


Figure 8 COP and discharge pressure for systems with and without high side receiver

Conclusion

Based on the extensive set of experiments conducted with the MAC1 prototype transcritical a/c system (more than 300 operating conditions), it was possible to validate a system simulation model. That model was then used to explore hundreds of additional operating conditions, testing a variety of control strategies. It was found that it is simplest and easiest to install a low-side receiver for the purpose of storing excess charge not needed by the system at a given operating condition, plus extra charge to compensate for leakage. Locating this receiver downstream of the evaporator ensures that the evaporator is always fully utilized, having saturated vapor at the outlet, and maximizing system efficiency by maintaining the highest possible evaporating pressure. Then, to maximize efficiency of the transcritical cycle, a refrigerant temperature sensor at the gas cooler outlet is used to control pressure at the same location by modulating the expansion valve. This algorithm is quite simple, and can be made even more robust by using different coefficients in the linear P-T relationship for different categories of operating conditions.

6.1.2 Use of CO₂- and Propane- Thermosyphons in Combination with Compact Cooler in Domestic Freezer

Excerpts from a student project report by
Anders Larsson, P-O Nilsson and Per Holmlund,
 Edited by **Björn Palm**

Department of Energy Technology
 Div. of Applied Thermodynamics and Refrigeration
 Royal Institute of Technology,
 Stockholm, Sweden

Abstract

This report is an evaluation of the use of a compact cooler in a standard freezer. Previous attempts using secondary, liquid loops on the cold and the hot side have been done in an earlier project but there were problems keeping an acceptable efficiency because of the energy demand of the pumps in these loops.

The objective of this project is to design systems for both evaporator and condenser that are driven by density difference, so called thermosyphons. The intention is that at least the cold side should have CO₂ as refrigerant.

The appliance for this test was a standard freezer. Before the modifications were made, the cabinet was tested according to the standard test procedure to receive reference values. After testing was finished, all of the standard equipment except the cabinet was removed, things as: compressor, condenser, evaporator and all shelves. The cabinet was finally turned upside down.

Two thermosyphon systems were designed. The first system is for cooling the compact cooler's warm side. This cooling system uses propane as refrigerant. The other thermosyphon system is used for heat extraction from the cabinet. It uses CO₂ as refrigerant.

The tests show at first that the output capacity of the cooler is smaller than expected. Only 70 % of expected output could be reached and that was not sufficient to reach the desired cabinet temperature of -18°C. A lowest cabinet temperature of -11°C was reached, while the saturation temperature in the CO₂ thermosyphon was -18 and the surface temperature of the compact cooler was -37°C.

The tests definitely shows a potential to use the compact cooler as a replacement for the standard compressor system. Both thermosyphon systems are only prototypes and much more can be done to reduce the temperature differences.

1. Background

The major driving force of developing new products for households is saving of energy. From both a government regulation, and the price of energy, point of view. The development of a replacement for compressor technology would probably give the inventors an advance in the next generation of refrigeration products.

In an internal report from Ericsson, a compact cooler for domestic freezer applications has been investigated. The results show a need for improvement in the heat distribution if the cooler is placed outside the freezer. To beat the conventional system, a low energy system like a thermosyphon should be used if the aim is to reduce power consumption. The results from previous tests show 15 % higher power consumption, compared to a conventional system, in best case for the compact cooler. This is with the use of brine-loops driven by vibration pumps. The larger power consumption is due mainly to the high temperature difference between the cold spot on the compact cooler and the heat exchanger for the evaporator brine-loop in this particular test.

2. Outline of present study

The major aim in this work is to improve heat distribution efficiency to and from the compact cooler with the intention to reduce power consumption. In order to achieve this, thermosyphons were

designed for both the hot and the cold side of the compact cooler. CO₂ was used as refrigerant on the cold side while propane was used on the hot side. The reason for using different fluids is that the pressure levels would be very different in the two systems if one fluid was used. However, both systems are designed to withstand the pressures at +60°C.

3. Design of the cold side thermosyphon

3.1 Design criteria

The criteria for the dimensioning of the evaporator for the freezer is the geometry of the freezer and the capacity of the compact cooler combined with the desired air temperature in the freezer and the heat leakage from the ambient. In this case, the expected capacity of the cooler is 60 W and the heat leakage is about 30 W for the desired inside air temperature of -18°C, according to the reference measurements of the original set-up.

The geometry of the freezer limits the dimensioning of the evaporator in terms of the level of the compact cooler or more precisely the level of the condenser, mounted on the cooler. The level of the condenser gives the driving force for the refrigerant due to gravity. This force is needed to compensate for the pressure loss in piping and evaporator. Furthermore, the inner dimension of the freezer restricts the outer dimensions of the evaporator.

The demand that the freezer should be able to resist an ambient temperature of 60°C puts some serious demands on the material, as the internal pressure will reach 150 bars at this temperature. This calls for small inner dimensions and/or thick walls of the evaporator. Large wall thickness will affect the capacity because of the thermal resistance in the material.

3.2 Design

The position of the cooler will have a large effect on the system design. At a first glance on the emptied freezer, a large empty space was recognized in the bottom of the freezer (former compressor compartment). This space was of no use for this application and the first decision was to turn the freezer upside down. This resulted in a suitable space to put the compact cooler at a higher level than the evaporator. The inner dimensions of the freezer are given in figure 1. They are the same as before the freezer was emptied.

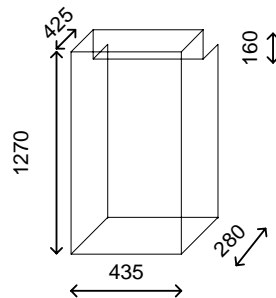


Figure 1: Inner dimensions of freezer cabinet turned upside down

Special software acquired from SINTEF [6] was used to assist in the design of the geometry of the evaporator. This program also calculated the expected suitable CO₂ filling.

Tests were done with different evaporator designs but only the final, best working one will be presented here. This evaporator consisted of ten vertical tubes, connected in parallel, going from the bottom of the cabinet and up to the top. The tubes were 1.24 m in length and made of stainless steel with 8 mm outer and 6 mm inner diameter. The maximum allowed pressure for these tubes was 170 bars and for the used T-connectors 1500 bar. The final construction is shown schematically in figure 2.

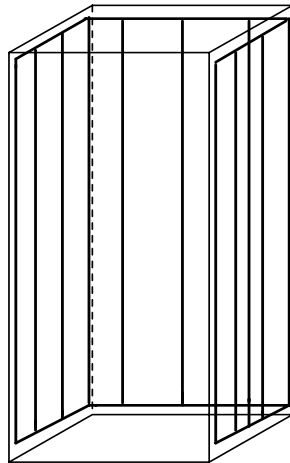


Figure 2: Model of evaporator in freeze

The outside surface area of the evaporator was calculated as:

$$A_{air} = (10 \cdot 1.24 + 2 \cdot 0.4 \cdot 3) \cdot \pi \cdot 0.008 = 0.372 m^2$$

The condenser was made of a 1.5 m long ¼ “ outer diameter copper pipe. This pipe was bent over a “dummy” having the same diameter as the cold side of the compact cooler (see fig 3). The cross pipe was to by-pass, liquid that comes with the vapor, past the condenser. The coil was molded in a tin/lead alloy (Woods metal). During the casting of the condenser, a plug with correct outer diameter was put in the melted metal. The difference in thermal expansion between the Woods metal and the copper in the cooler helped to tighten the fit between the cooler and the condenser.



Figure 3: Picture of condenser tubing before casting

The condenser and the evaporator were connected by a downcomer and a return line made of stainless steel.

4. Design of the hot side thermosyphon

4.1 Design criteria

The criteria for the compact cooler's warm side are the ambient temperature, the maximum temperature of the cooler allowed by the manufacturer, the area of the hot side on the cooler and the power output. In this case t_{ambient} was 25°C and $t_{\text{hot side}}$ 60°C . The power dissipated by the cooler depends on COP. Earlier evaluations had shown a COP of approximately 1 and a cooling capacity of 40 W at this temperature lift. This means that at least $q = 40 + 40 = 80\text{W}$ must be rejected from the rather small warm side of the compact cooler.

Propane was chosen at an early stage as refrigerant in the hot side thermosyphon.

4.2 Design

The final design of the thermosyphon had a finned coil condenser rejecting heat to ambient. This condenser was placed at the highest possible level, above the compact cooler.

The evaporator was designed like a cylinder with a hole fitting the warm side of the compact cooler with a tight fit (fig. 4).

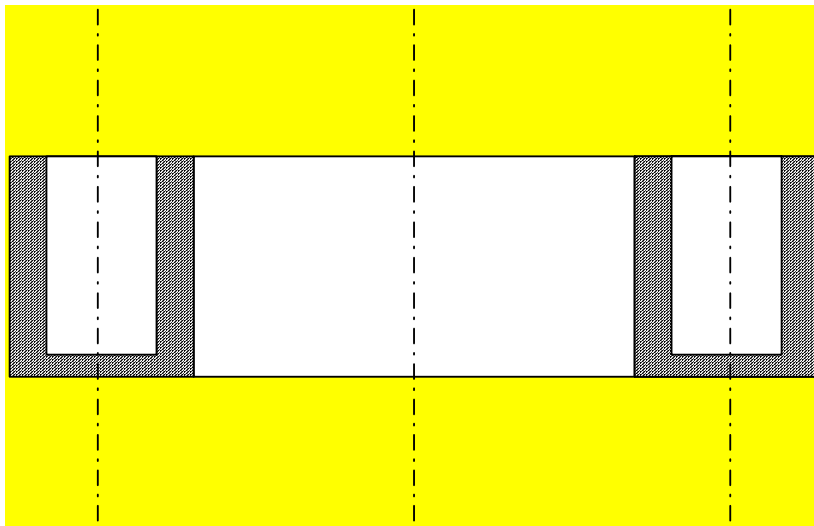


Figure 4: Cut view of evaporator of hot side thermosyphon

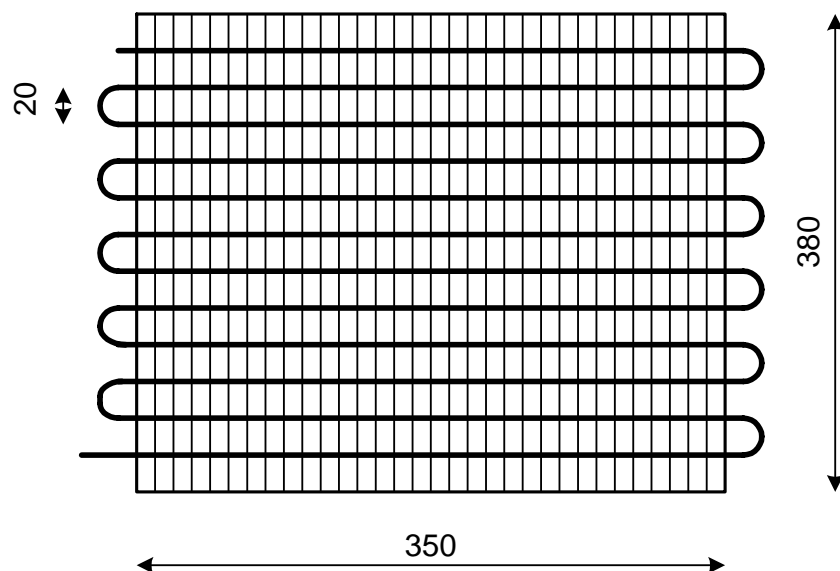


Figure 5: Condenser coil layout

The cylinder was hollow to allow a space for the evaporating refrigerant. The condenser and evaporator were connected by flexible hoses.

The evaporator was manufactured in two pieces, a body and a top. Both parts were made of copper, just like the warm side of the compact cooler. This means that it should be possible to keep a sufficient heat transfer between the surfaces due to the identical thermal expansion coefficients.

The condenser used for the hot side thermosyphon consisted of two finned coil condensers, made of construction steel, connected in parallel (see figure 5). The total surface area of the coil's air side was 6.5 m² and the fin efficiency was calculated to be 87%.

5. Experimental tests

5.1 Test set-up

The tests were made in a climatic chamber where the temperature was held constant at 25 C. To achieve this steady condition the air was circulated with a fan and with a heating element with a built in fan. One thermostat relay was used together with a PT100 temperature sensor. Reference tests were done with the original vapor compression system at three different temperatures in the freezer, -15, -18 and -24 C. The energy consumption was measured during 24 h at stable temperatures.

The temperature of the freezer air was measured by thermocouples placed in small "meat" packs (t11, t12, t13, t14). The meat packs were placed on the shelves on top of an isolating piece of plastic.

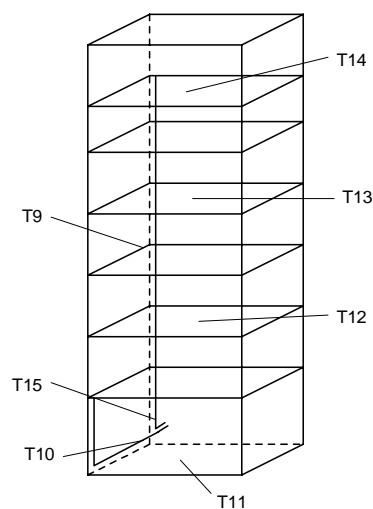


Figure 6: Position of thermocouples in “meatpacks”

In the reference measurements the evaporation temperatures and the condensation temperatures were measured by thermocouples placed on the surface of the tubes.

Only one test with the compact cooler will be shown here as the cooling capacity turned out to be too low to achieve the desired air temperatures in the freezer. During this test temperature measurements were done at several locations on the cold and hot side thermosyphons as well as in the “meatpacks” in the freezer.

5.2 Test results, reference measurements

For the case with the freezer set at -18°C the energy consumption was 30.9 W averaged over 24 hours. The diagram (fig. 7) shows the temperatures at different locations in the freezer. In the center, there is a variance of up to 0.6°C due to the compressor cycles.

Inside temperature set at -18

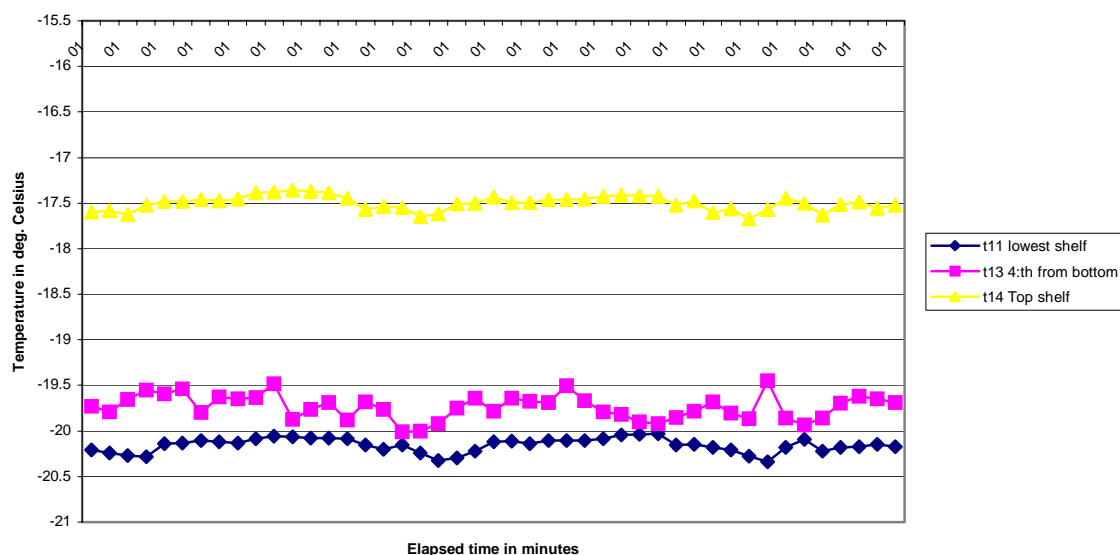


Figure 7: Temperatures inside freezer during reference tests @ -18°C .

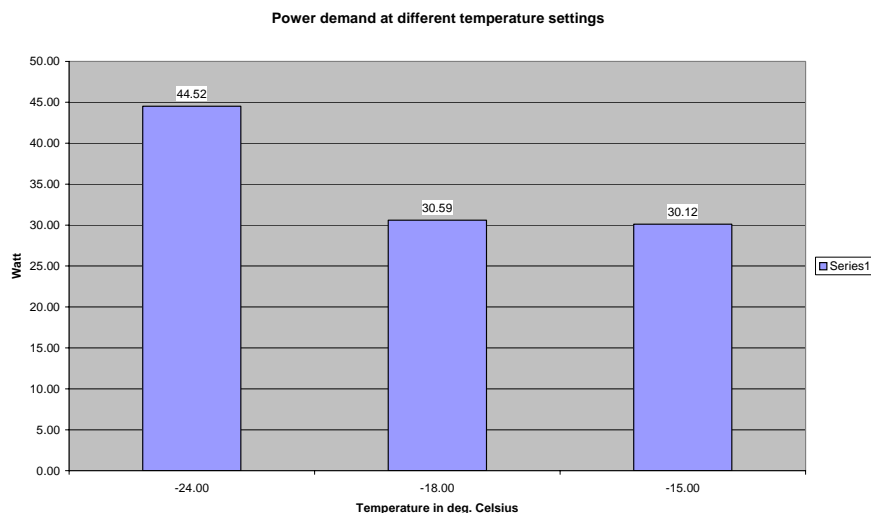


Figure 8: The power demand variation for different temperature settings during reference measurements.

The comparison regarding power consumption for the different temperature settings are shown in fig. 8.

5.3 Test results, compact cooler with thermosyphons

Several tests were done, with different amounts of CO₂ in the cold side thermosyphon. All tests showed that the compact cooler had problems reaching lower temperatures in the cabinet than -10°C. This limits the interesting tests to a *maximum performance* test.

When the lowest possible temperature was reached and the system was in equilibrium there was very little variation in the temperature inside the cabinet with time (fig. 9). However, the temperature at the top shelf is at least 8°C higher than at the middle and bottom.

The saturation temperature, as measured by the surface temperature of the evaporator or condenser tubes, was about -17°C, while the cold surface of the compact cooler had a temperature of approximately -37°C.

On the hot side, the temperature at the condenser outlet was about +28°C, the condenser inlet +38°C, the evaporator wall temperature was +40°C and the surface of the compact cooler was about +48°C (fig. 10).

Finally, an average power demand of 41.4 W was noticed during the maximum performance test.

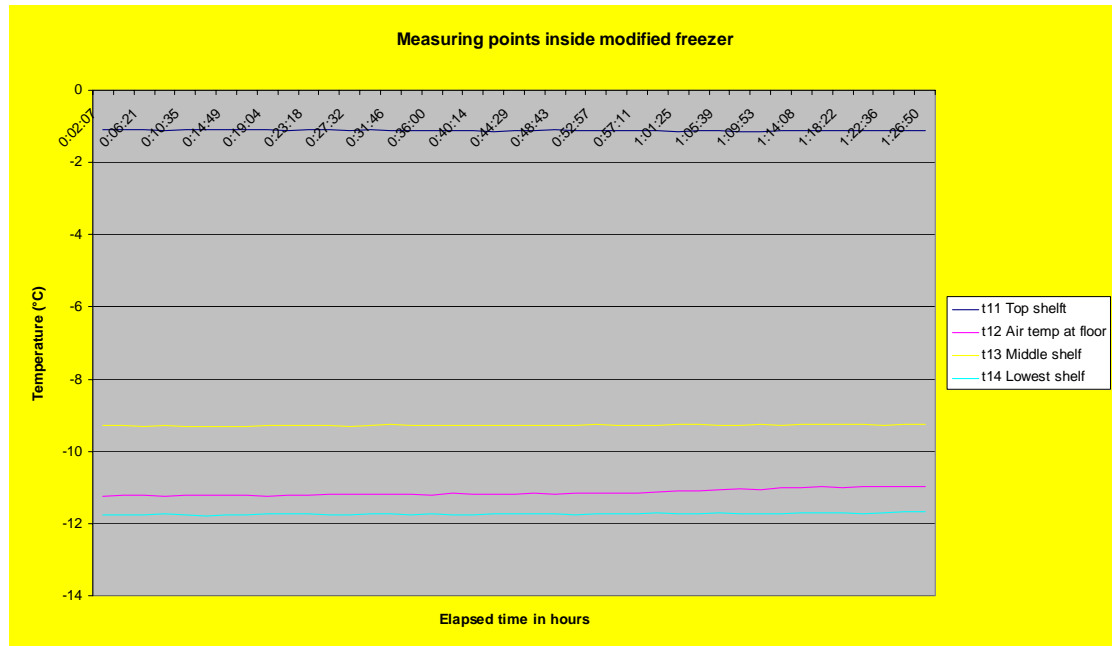


Figure 9: Temperatures at different levels in freezer with compact cooler and thermosyphons

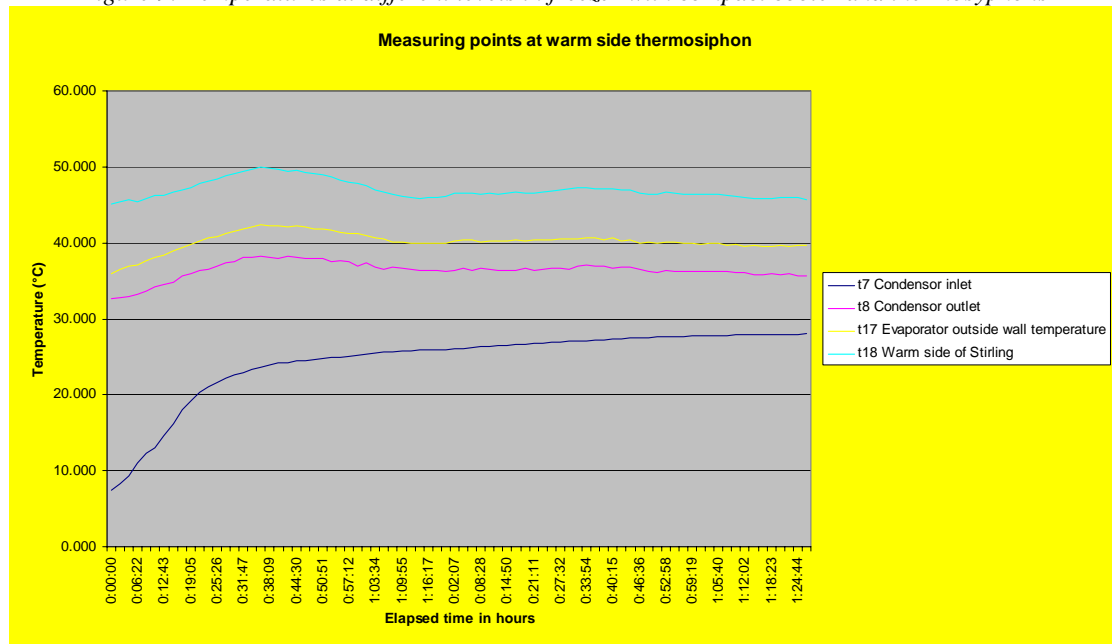


Figure 10: Temperatures in hot side thermosyphon

6. Discussion and conclusions

The project objective to design two fully operating separate thermosyphon systems for a compact cooler that was mounted on a standard freezer was reached. The aim to have a completely comparable modified system was not reached because a temperature of -18°C could not be reached inside the cabinet. There are several explanations for this and the main causes are:

- Lack of capacity of the compact cooler
- Low total COP due to the high temperature differences in both hot and cold side thermosyphons.
- Heat losses into the system from the ambient.

REFERENCES

1. **Granryd, E et al:** Refrigerating engineering. KTH, 1999
2. **Arkestein, K et al:** The design of a PV-Refrigerator, 1999

6.2 Heat Transfer

6.2.1 HEAT TRANSFER OF CARBON DIOXIDE IN AN EVAPORATOR

Eiji Hihara

Institute of Environmental Studies, School of Frontier Sciences, The University of Tokyo
7-3-1 Hongo, Bunkyo-ku, Tokyo 113-0033, Japan

ABSTRACT

An experimental apparatus for carbon dioxide was constructed for measurement of boiling heat transfer characteristics inside horizontal tubes. The test sections were horizontally placed smooth tubes of which inner diameter was 0.7, 1, 2 and 4mm. Experimental conditions were as following; evaporating temperature was 15°C, quality was from 0.1 to 0.9, heat flux was between 9 and 36kW/m² and mass flux was between 360 and 1440kg/m²s. The heat flux mainly affected the heat transfer, and mass velocity mainly affected the quality at onset of dryout. The experimental results of boiling heat transfer and pressure drop in tubes were compared with those of fluorocarbons, but they were not fitted very much. Then a new correlation of heat transfer coefficient was proposed.

INTRODUCTION

The objective of this study is to investigate of boiling heat transfer characteristic and pressure drop of carbon dioxide in tubes. Carbon dioxide is a kind of natural working fluid, and is expected for a new working fluid for automotive air conditioners and for water heaters. Because the operating pressure of the carbon dioxide heat pumps is higher than that of fluorocarbon heat pumps, carbon dioxide has advantageous characteristics for working fluids such as high density and low viscosity. For a development of highly efficient heat pumps, it is necessary to develop high-performance heat exchangers. But information of heat transfer and pressure drop of carbon dioxide in tubes is not adequate.

NOMENCLATURE

Bo :	Boiling number
C_p :	Isobaric specific heat
D :	Tube diameter
G :	Mass velocity
g :	Gravity
h :	Heat transfer coefficient
λ :	Thermal conductivity
L :	Length of test section
q :	Heat flux
T_S :	Saturation temperature
T_w :	Inside wall temperature
x :	Quality

X_{tt} :	Lockhart-Martinelli parameter
μ :	Viscosity
ρ :	Density
ν :	Specific volume
σ :	Surface tension
Subscript:	l : Liquid g : Vapor tp : Two-phase

1. EXPERIMENT

A schematic diagram of the experimental apparatus is drawn in Fig. 1. The experimental apparatus consisted of a main refrigerant loop and a test loop because the capacity of the compressor was too large for the experimental condition. The main loop was a simple heat pump cycle, and was composed of a compressor, a gas cooler, an expansion valve, and an evaporator. The oil separator removes lubricating oil from the circulating refrigerant. In order to ensure stable separation of refrigerant flow at the junction, the carbon dioxide was separated in liquid phase. The test loop was composed of a mass flow meter, a subcooler, a needle valve, the test evaporator tube, and a super heater. The subcooler was made of stainless steel tube and the super heater was made of copper tube. Both tubes were bended spirally and immersed in a constant-temperature water bath.

The test evaporator was a horizontally placed stainless steel tube and was directly heated by direct current electricity. The length of heated section was varied in accordance with the test conditions of heat flux. The outside wall temperature of test evaporator tube was measured by T-type thermocouples, which were attached to outside wall of tube. The number of measurement point was ten and thermocouples were placed at equal intervals in the heated section between two electrodes. The thermocouples were electrically insulated from the tube by thin Teflon film. The flow rate of the refrigerant that entered the test evaporator was measured by a mass flow meter. The local pressures and temperatures at the key points of the cycle were measured using strain gauge type pressure transducers and K-type thermocouples. Especially, the pressure drop in the test evaporator tube between its inlet and outlet was measured by a quartz type precision pressure gauge using switching valves. The strains of the pressure transducers were converted to voltages by dynamic strain amplifiers. The dynamic strain amplifiers and the data acquisition equipment were placed in a constant-temperature-air box to ensure highly stable measurements.

The pressure of gas cooler was adjusted by controlling the compressor speed and the gas cooler capacity. Mass flow rate of the test evaporator tube was controlled by the needle valve. The refrigerant vapor quality at the test evaporator inlet was adjusted by the subcool of the refrigerant at the needle valve inlet, which was set by the constant temperature water bath. The local heat transfer coefficient was calculated by

$$h = q / (T_w - T_s).$$

The heat flux, q , was calculated from the measured electrical power applied to the test evaporator tube. In order to minimize the heat loss or gain to/from the air, the test evaporator was placed in a constant-temperature-air box, of which temperature was kept close to that of the outside wall of test tube. The inside wall temperature, T_w , was calculated from measured outside wall temperature by solving the equation of radial heat conduction. The saturation temperature, T_s , was calculated from measured pressure using thermodynamic property data of carbon dioxide at saturation state. The measurement

was executed about four times to ensure the repeatability of the results.

The experimental conditions are showed in Table 1. The range of mass velocity was quite higher than conventional range of fluorocarbons, because the pressure drop of carbon dioxide in tubes was considerably small. According to boiling heat transfer theory, the boiling temperature affects the heat transfer coefficient only through the temperature dependence of thermal properties, and its effect is not so large. Therefore the evaporating temperature was arbitrarily determined at 15°C, which was closer to the room temperature than practical evaporating temperature.

2. EXPERIMENTAL RESULTS

2.1 Heat transfer coefficient

Heat transfer coefficient increased as heat flux increased. But the larger the inner diameter of tube was, the smaller the increase of heat transfer became. Generally nucleate boiling is promoted if heat flux increases, and then smaller diameter may be more effective to heat transfer.

The heat transfer coefficient before dryout did not depend on the mass velocity and quality very much. But for 0.7mm I.D. tube the heat transfer coefficient decreased as mass velocity increased, while for 4mm I.D. tube the heat transfer coefficient increased as mass velocity increased slightly. That may be the effect of tube diameter on flow patterns, but the mechanism is not well known so far.

The refrigerant includes some oil even if it passes an oil separator after the compressor. It is known that oil contamination causes deterioration in heat transfer of refrigerant. The effect of oil concentration on heat transfer for 2mm I.D. tube was measured changing the oil concentration at the inlet of evaporation tube. The results are shown in Fig. 2. The heat transfer coefficient drastically decreased when the oil concentration at the tube inlet was over 0.3%. So all of the heat transfer data was taken under the condition that oil concentration at the inlet was below 0.3% in this study.

Furthermore the heat transfer coefficient was arranged by local oil concentration in liquid phase.

$$\psi_l = \frac{\psi_p}{\psi_p + (1 - \psi_p)(1 - x)} \approx \frac{\psi_p}{1 - x},$$

where ψ_l and ψ_p are local oil concentration and overall oil concentration, respectively. The arranged results are shown in Fig. 3. From this result, heat transfer coefficient decreased drastically if the local oil concentration is above 0.7%.

Generally speaking, forced convective boiling consists of two heat transfer mechanisms including nucleate boiling and forced convective vaporization. For a low quality flow, most of the heat transfers from the wall by nucleate boiling. In this situation, heat transfer coefficient is kept almost constant independent of quality. For a high quality flow, nucleate boiling is suppressed due to convective effect, and most of the heat transfers through a thin liquid film and the liquid evaporates at the gas-liquid interface. In this situation, heat transfer coefficient increases with quality because liquid film velocity is raised due to expansion of specific volume by liquid evaporation. From the experimental results of this study, forced convection seems not to contribute to the heat transfer, because the heat transfer coefficient is independent of mass velocity and quality. The evaporating temperature of this experimental condition

is close to the critical point of carbon dioxide, and thus the ratio of specific volumes of vapor to liquid is smaller than that of usual fluorocarbons as showed in Table 2. Therefore, the refrigerant velocity is not accelerated so much by evaporation, and thus the contribution of forced convective vaporization in boiling heat transfer is negligible.

2.2 Quality at dryout

The vapor quality at the onset of dryout decreased as the mass velocity increased. The higher the mass velocity was, the smaller the quality at onset of dryout became. Large mass velocity may induce mist flow rapidly, so dryout may occur earlier.

For all diameter tubes the qualities at the onset of dryout were independent of mass velocity. Those were about 0.4 at mass velocity 1440kg/m²s, 0.6 at mass velocity 720kg/m²s, and 0.8 at mass velocity 360kg/m²s. Generally the qualities at the onset and completion of dryout were accorded. But for 4mm I.D. tube, difference between onset and completion qualities was ranged between 0.1 and 0.15. The dryout characteristics are influenced by the flow patterns of fluid, which are also influenced by the tube diameter.

3. COMPARISON BETWEEN EXPERIMENTAL RESULTS AND CORRELATION

3.1 Heat transfer coefficient

Experimental results were compared with the following type of correlation, which is frequently used for fluorocarbons.

$$\alpha = F\alpha_l + S\alpha_b,$$

where α_l is Dittus-Boelter equation which presumes liquid phase flow, F is the heat transfer enhancement factor by convection of two-phase flow, α_b is Stephan-Abdelsalam equation which is proposed for pool nucleate boiling of fluorocarbons, and S is the suppression factor of nucleate boiling. Each parameter is expressed as follows:

$$\alpha_l = 0.023 \frac{\lambda_l}{D} \left[\frac{G(1-x)D}{\mu_l} \right]^{0.8} Pr^{0.4},$$

$$\alpha_b = 207 \frac{\lambda_l}{D_b} \left(\frac{qD_b}{\lambda_l T_b} \right)^{0.745} \left(\frac{\rho_v}{\rho_l} \right)^{0.581} Pr_l^{0.533},$$

where D_b is the diameter of bubble in nucleate boiling and Re_{tp} is the two-phase Reynolds number:

$$D_b = 0.51 \left[\frac{2\sigma}{g(\rho_l - \rho_v)} \right]^{0.5}, \quad Re_{tp} = \left[\frac{G(1-x)D}{\mu_l} \right] F^{1.25}.$$

Based on the experimental results, a new correlation is proposed.

$$F = 1 + \left(\frac{1}{X_{tt}} \right)^{1.2}, \quad S = \frac{1}{1 + K_1 \frac{(Re_{tp} \times 10^{-4})^2}{(Bo \times 10^4)^{K_2}}},$$

where $K_1 = 15$, $K_2 = 4$ for 0.7mm I.D. tube and $K_1 = 0.5$, $K_2 = 0$ for 1, 2, 4mm I.D. tubes.

The comparison between the new correlation and the experimental data are shown in Figs. 4 to 7. For 0.7mm I.D. tube, the results of correlation are smaller than experimental data as the heat flux decreases. So the parameters in correlation for 0.7mm tube are different from others. The experimental data can be correlated within 30% deviation, but the deviation of 4mm I.D. tube is about 40%. More revision of correlation is necessary for a practical use.

3.2 Pressure drop

3.2.1 Ueda's equation

Firstly frictional pressure drop was compared with Ueda's equation⁽¹⁾ that was an approximation formula of Martinelli-Nelson chart⁽²⁾ assuming homogeneous flow for the estimation of acceleration loss. Ueda's correlation is

$$\frac{\Delta p_{tp}}{\Delta p_l} = 1 + 1.20 x_{outlet}^{\frac{3}{4} \left(1 + 0.01 \sqrt{\frac{v_g}{v_l}} \right)} \left\{ \left(\frac{v_g}{v_l} \right)^{0.8} - 1 \right\},$$

$$\Delta p_l = \frac{2 f_l G^2}{D \rho_l} L, \quad f_l = \frac{0.046}{Re_l^{0.2}},$$

where x_{outlet} is the quality at the test section outlet assuming that the quality at the inlet is zero, Δp_l is frictional pressure drop when all fluid is flowing as liquid, f_l is estimated by Colburn's equation. The comparison between the calculation and the experimental data is shown in Fig. 8. From this figure, it is found that the correlation is higher than experimental result as the mass velocity increases and the tube diameter decreases.

3.2.2 Thome's correlation

Thome's correlation⁽³⁾ was compared with the experimental results. In Thome's correlation frictional pressure drop is given by Friedel equation.

$$\left(\frac{\partial p}{\partial l} \right)_f = \left[\frac{2 \xi_{l,0} G^2 v_l}{D} \right] \phi_{l,0}^2$$

where parameters are expressed as follows:

$$\phi_{l,0}^2 = I + \frac{3.24 F H}{Fr_h^{0.09} We_h^{0.035}},$$

$$I = (1-x)^2 + x^2 \frac{v_g \xi_{g,0}}{v_l \xi_{l,0}}, \quad F = x^{0.78} (1-x)^{0.224}, \quad H = \left(\frac{\rho_l}{\rho_g} \right)^{0.91} \left(\frac{\mu_g}{\mu_l} \right)^{0.19} \left(1 - \frac{\mu_g}{\mu_l} \right)^{0.7},$$

ξ is Fanning's friction parameter defined by

$$\xi = 0.079 Re^{-\frac{1}{4}}.$$

Froude number, Fr_h , Weber number, We_h , and density of homogeneous fluid, ρ_h , are defined as

$$Fr_h = \frac{G}{\rho_h \sqrt{gD}}, \quad We_h = \frac{G^2 D}{\sigma \rho_h}, \quad \frac{1}{\rho_h} = \left(\frac{x}{\rho_g} + \frac{1-x}{\rho_l} \right),$$

where subscript 0 means that mass velocity G is assumed that all fluid is flowing as gas or liquid. Acceleration loss is expressed by momentum equation as follows using void fraction ε .

$$\Delta p_a = G^2 \left[\frac{x^2}{\rho_g \varepsilon} + \frac{(1-x)^2}{\rho_l (1-\varepsilon)} \right]_{inlet}^{outlet},$$

$$\varepsilon = \frac{1}{1 + \left(S \frac{1-x}{x} \frac{\rho_g}{\rho_l} \right)},$$

S is slip ratio, and the other parameters are as follows:

$$S = 1 + E_1 \left(\frac{y}{1 + yE_2} - yE_2 \right)^{0.5},$$

$$y = \frac{\beta}{1 - \beta}, \quad E_1 = 1.578 Re_{l,0}^{-0.19} \left(\frac{\rho_l}{\rho_g} \right)^{0.22}, \quad E_2 = 0.0273 We Re_{l,0}^{-0.51} \left(\frac{\rho_l}{\rho_g} \right)^{-0.08},$$

where β is volumetric flow rate

$$\beta = \frac{\rho_l x}{\rho_l x + \rho_g (1-x)},$$

$Re_{l,0}$ is Reynolds number assuming that all fluid is flowing as liquid.

$$Re_{l,0} = \frac{GD}{\mu_l},$$

We is Weber number defined by

$$We = \frac{G^2 D}{\sigma \rho_l}.$$

The comparison between the calculation and the experimental data is shown in Fig. 9. Though the deviation is smaller than Ueda's correlation, it has similar tendency. But for 4mm I.D. tube deviation is within 20%. So it could be said that this correlation is more suitable for larger diameter tubes.

4. CONCLUSION

The boiling heat transfer coefficient and pressure drop of carbon dioxide were measured inside horizontal smooth tubes and the following important information was obtained.

Heat transfer coefficient is dependent on heat flux. The diameter of tubes affects the rate of increase of heat transfer coefficient.

Mass velocity generally does not affect the heat transfer coefficient very much.

Oil contamination in refrigerant depresses pre-dryout heat transfer coefficient, particularly when its local concentration was above 0.7%.

The quality at the onset of dryout is dependent only on mass velocity.

In this experimental condition, the heat transfer coefficient and the pressure drop did not agree with existing correlations. A new correlation for heat transfer coefficient was proposed.

REFERENCES

- (1) Ueda, T., "A flow in evaporation tubes of a flowing-through boiler," Thermal power generation, 11-4, pp325-332, 1960.
- (2) Martinelli, R. C. and Nelson, D.B., "Prediction of pressure drop during forced-circulation boiling of water," Trans. ASME, 70, pp695-702, 1948.
- (3) Thome, J. R., "Refrigeration Heat Transfer" (Course notes), GRETh/CEA, Grenoble, France, 1997

Table 1 Experimental conditions

Material of tube	SUS316
Inner diameter [mm]	1
Heat flux [kW/m ²]	9, 18, 36
Mass velocity [kg/m ² s]	360, 720, 1440
Evaporating temperature [°C]	15
Quality	0.1 – 0.9

Table 2 Comparison of ratio of vapor specific volume to liquid one at 15°C.

Refrigerant	v_g / v_l
R113	670
R134a	53
R22	37
CO ₂	5

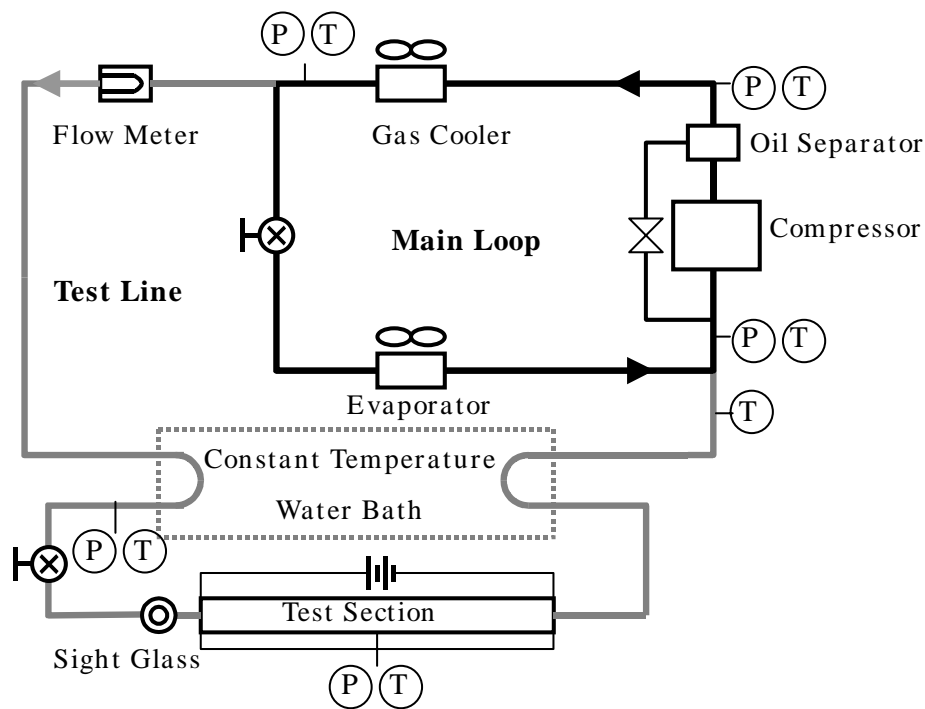


Fig. 1 Schematic diagram of experimental apparatus

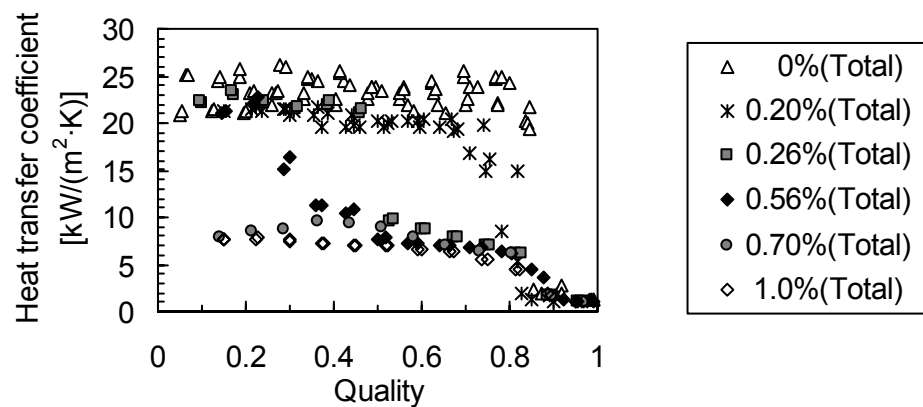


Fig. 2 Heat transfer coefficient at different oil concentration (1mm I.D. tube, mass velocity $360 \text{ kg}/(\text{m}^2 \cdot \text{s})$, heat flux $36 \text{ kW}/\text{m}^2$)

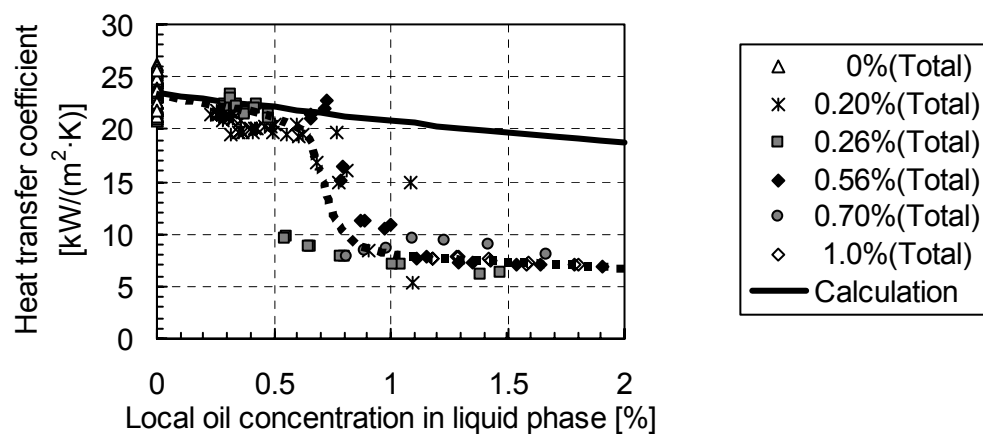


Fig. 3 Heat transfer coefficient versus local oil concentration in liquid phase at different oil concentration (1mm I.D. tube, mass velocity $360 \text{ kg}/(\text{m}^2 \cdot \text{s})$, heat flux $36 \text{ kW}/\text{m}^2$)

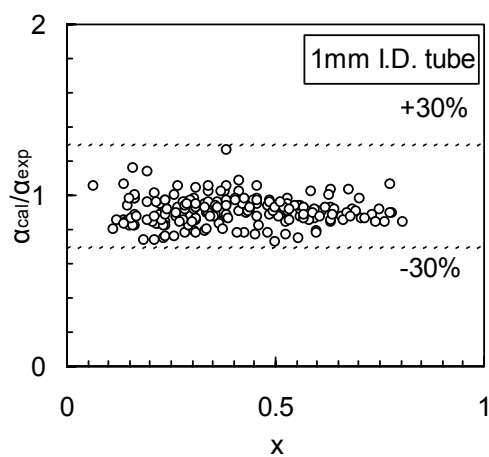
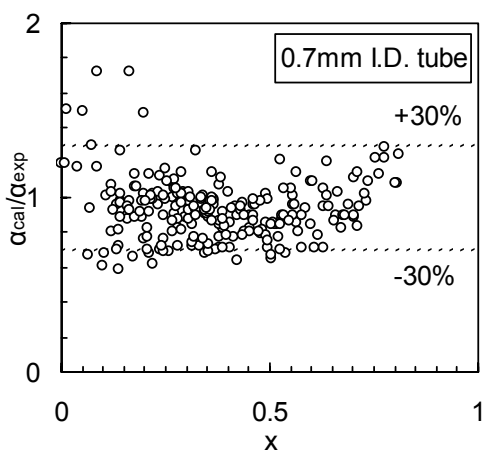
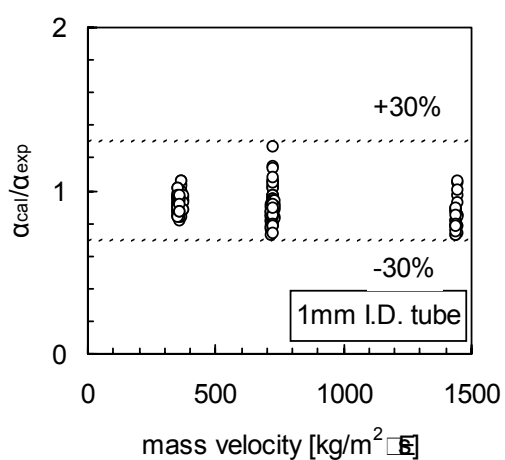
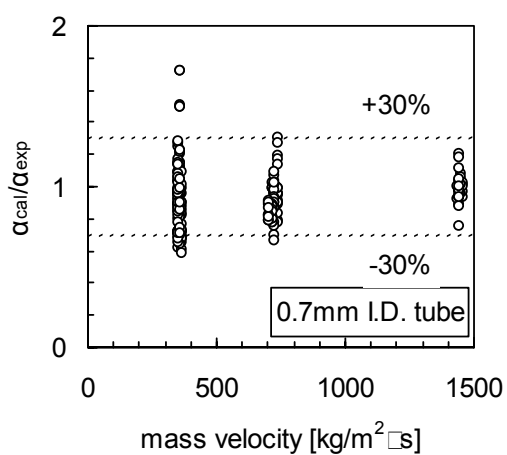
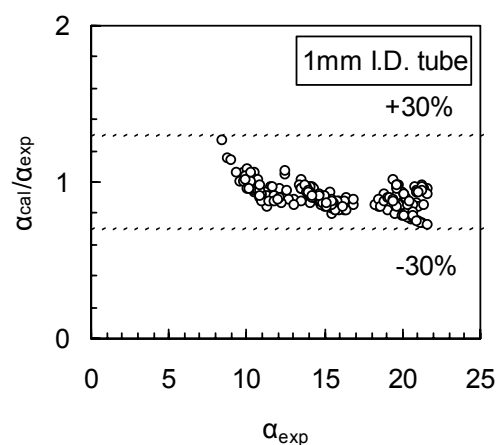
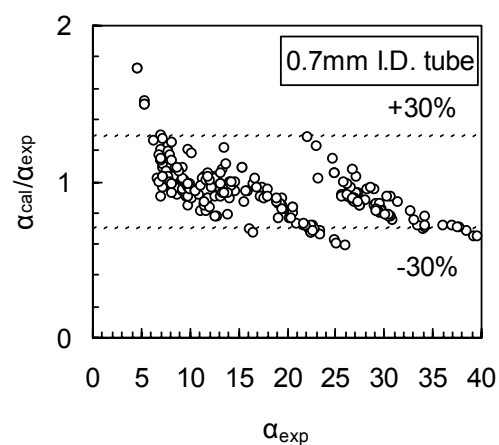


Fig. 4 Comparison of heat transfer coefficient between present correlation and experiment for 0.7mm I.D. tube

Fig. 5 Comparison of heat transfer coefficient between present correlation and experiment for 1mm I.D. tube

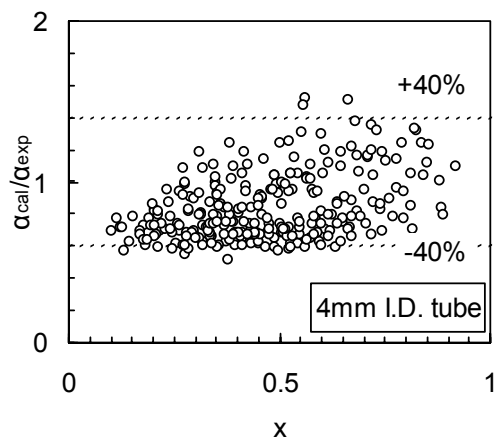
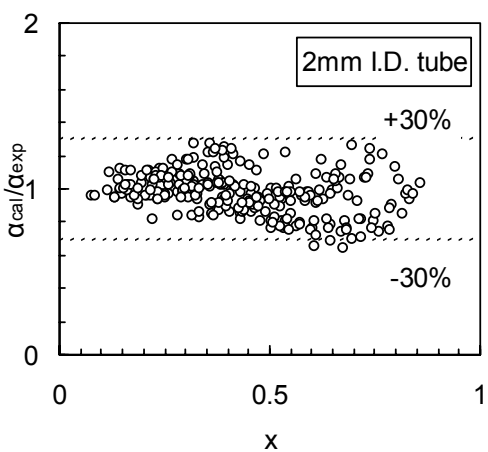
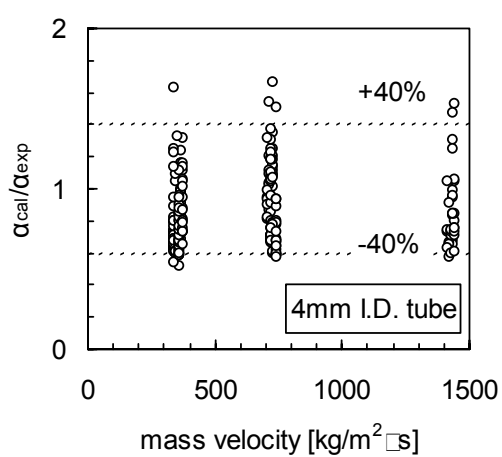
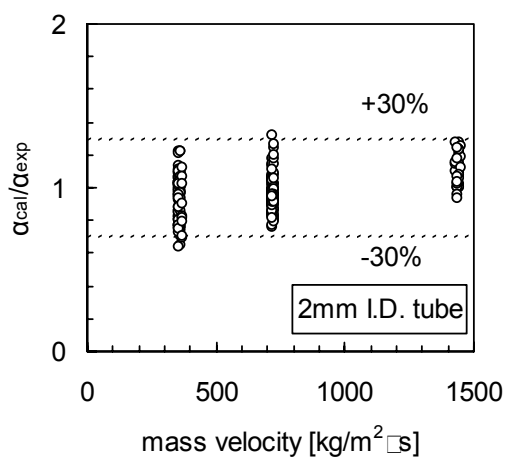
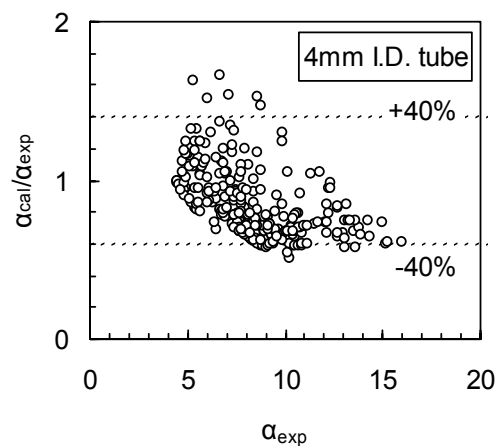
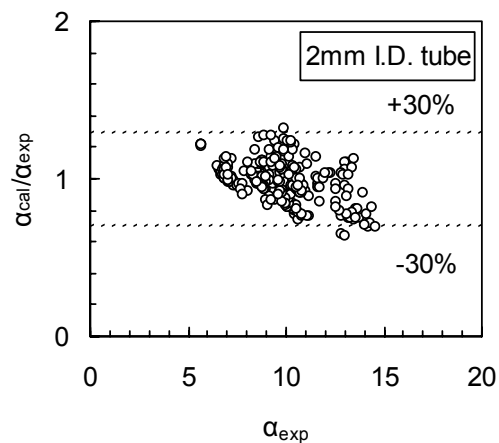


Fig. 6 Comparison of heat transfer coefficient between present correlation and experiment for 2mm I.D. tube

Fig. 7 Comparison of heat transfer coefficient between present correlation and experiment for 4mm I.D. tube

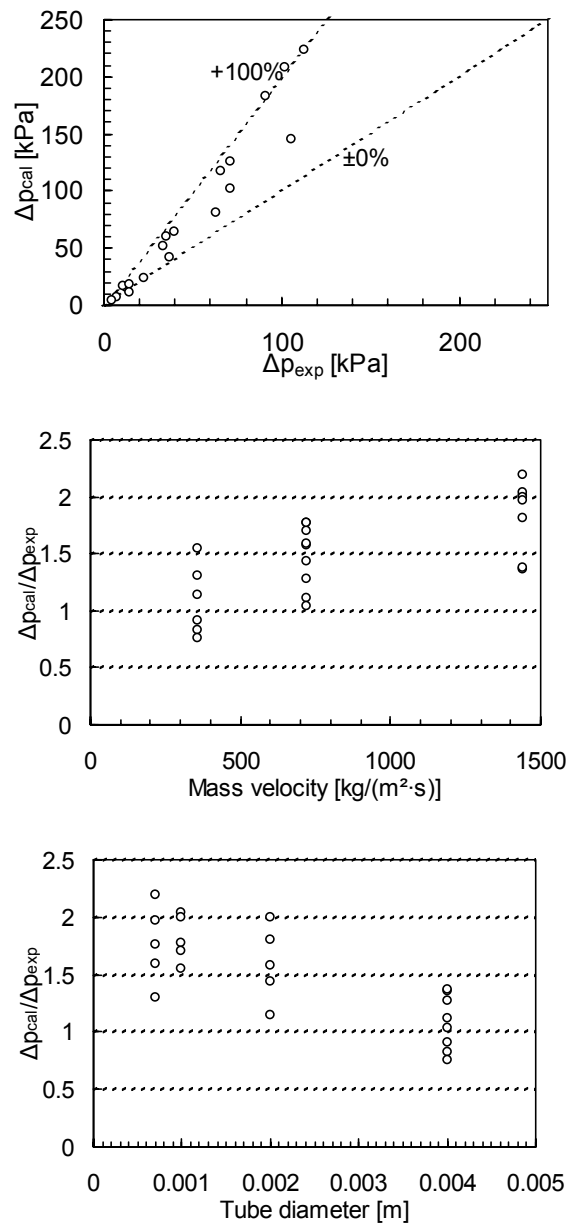


Fig. 8 Comparison of pressure drop between Ueda's equation and experiment

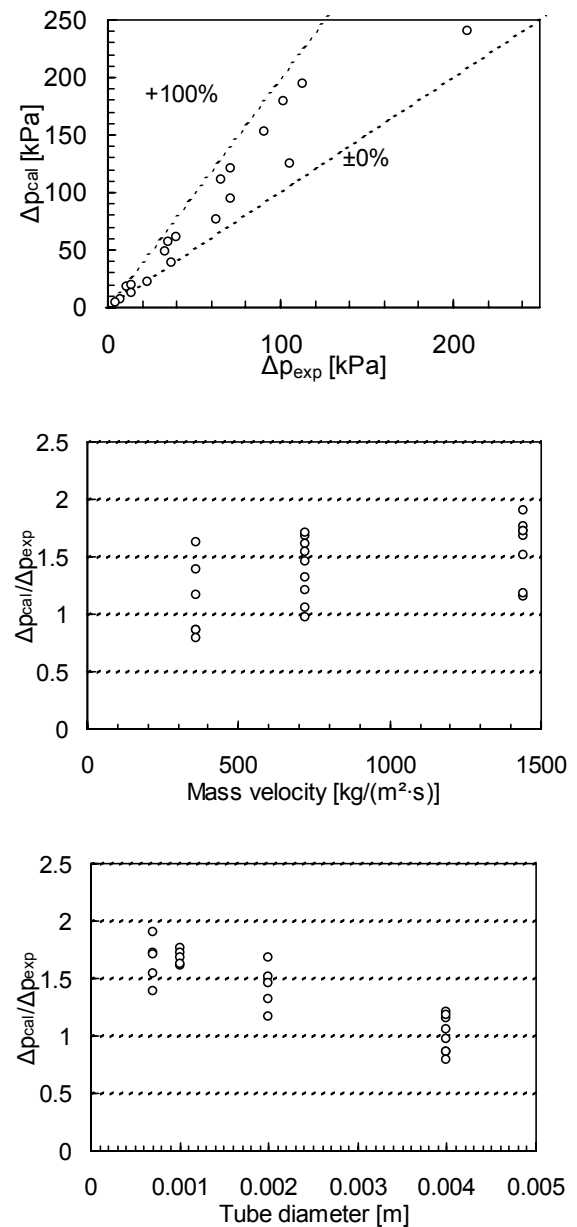


Fig. 9 Comparison of pressure drop between Thome's correlation and experiment

6.2.2 CORRELATING THE HEAT TRANSFER COEFFICIENT DURING IN-TUBE COOLING OF TURBULENT SUPERCRITICAL CARBON DIOXIDE

Srinivas S. Pitla⁺, Eckhard A. Groll, Satish Ramadhyani

Purdue University
Ray W. Herrick Laboratories
West Lafayette, IN 47907, USA

⁺Visteon Climate Control Systems
Plymouth, MI 48170, USA

ABSTRACT

An extensive study of the heat transfer and pressure drop characteristics of supercritical carbon dioxide during in tube cooling was carried out by the authors as part of ASHRAE RP-913. Within this study, a new correlation to predict the heat transfer coefficient of supercritical carbon dioxide during in-tube cooling was developed based on the numerical predictions and experimental data. The new correlation is presented in this paper. It is based on a mean Nusselt number that is calculated using the Gnielinsky correlation, which is determined using the thermophysical properties at the wall and the bulk temperatures, respectively. It was seen that the majority of the numerical and experimental values predicted by the new correlation were within $\pm 20\%$.

NOMENCLATURE

ρ = Density
 c_p = Specific heat
 D = Diameter of the tube
 k = Thermal conductivity
 Nu = Nusselt number
 Pr = Prandtl number
 Re = Reynolds number

INTRODUCTION

A comparison of the transcritical carbon dioxide cycle to conventional vapor compression technology shows that the heat rejection process from the supercritical carbon dioxide is of particular interest. This process occurs along an isobar that is close to the critical isobar. The heat exchanger in which the process occurs is called a “gas cooler,” instead of a condenser, because the process occurs at a supercritical pressure and a phase change does not take place. However, the thermophysical properties of the fluid change drastically during the

process. While a great deal of research has been performed to determine the heat transfer characteristics during condensation of CFC, HCFC, and HFC refrigerants, comparatively few investigations have been conducted on the in-tube heat transfer of a supercritical fluid.

The investigation presented in this paper was concerned with developing a suitable heat transfer correlation for carbon dioxide flow in the supercritical region during in-tube cooling. The correlation was developed based on the numerical and experimental work carried out by the authors. A detailed description of the numerical model, the experimental apparatus, and a literature review of heat transfer in the supercritical region can be found in Pitla et al. (2000a), Pitla et al. (2000b), and Pitla et al. (1998), respectively.

NUMERICAL MODEL

The geometry under consideration is a tube-in-tube heat exchanger, as shown in Figure 1. Water is flowing in the annulus, while carbon dioxide flows in the inner tube in counterflow. The inlet conditions of the carbon dioxide (State 1) were well in the supercritical region as typically seen for compressor outlet conditions. The water entering the heat exchanger was at a temperature below the critical temperature of carbon dioxide (State 2).

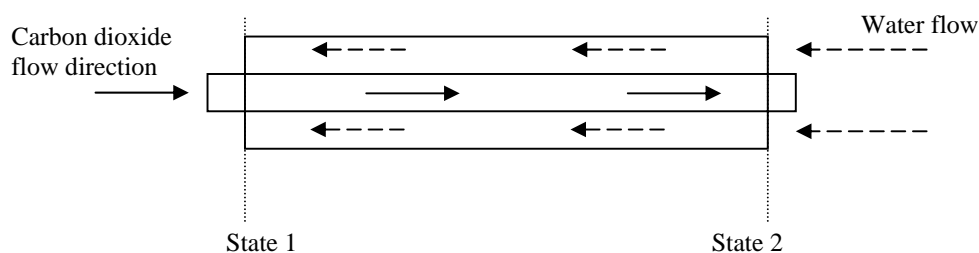


Figure 1: Schematic of the tube-in-tube counter flow heat exchanger

For the given geometry, a detailed numerical model based on the governing equations of mass, momentum and energy was developed. The numerical model of the complex turbulent flow was solved by two independent methods: Favre-averaging, also referred to as density-weighted averaging, and time averaging. Favre averaging has an advantage over time averaging the governing equations, as there are fewer assumptions in the former, to achieve closure. The two different methods of achieving closure were studied using various turbulence models. In particular, the time averaged equations were investigated using the Bellmore and Reid [BRMLH] (1983) mixing length model, Lee and Howell [L&H] (1998) modification to BRMLH, and Nikuradse's mixing length with damping function (NMLH). The Favre averaged equations were studied using Nikuradse's mixing length model and the k-equation turbulence model. Model validation revealed that the Favre averaging technique using the k-equation turbulence model produced the most accurate results and thus, was used for further analysis and comparison to experimental results.

In addition, a grid independence study was conducted to make certain that the solution was grid independent. The study showed that a compressed grid near the near-wall region was necessary to investigate the flow. The size of the grid in the axial direction of the grid is not as critical as in the radial direction. By studying the flow in the near-wall region it was observed

that the superficial profiles of the velocity and the temperature look very similar to constant property turbulent flows. However, upon close examination it was seen that the velocity and temperature law of the wall that were derived for constant property flows are not valid here.

EXPERIMENTAL TEST FACILITY

Figure 2 shows a schematic diagram of the experimental test facility. Since the operating pressure of the apparatus is between 8.0 MPa to 12.0 MPa, special safety procedures were observed, such as thick-walled stainless steel tubes. The test apparatus consists of a closed carbon dioxide loop, an open water loop, and a closed water-glycol loop. The carbon dioxide loop consists of four main components: a sub-cooler/receiver assembly, a magnetically coupled, sealed, gear pump, a heater, and the test-section. In addition, a mass flow meter, pressure transducers, probe thermocouples, and a pressure relief valve are installed in the loop.

Carbon dioxide enters the test section in the supercritical state at about 120°C. In passing through the test section, the CO₂ is cooled by water to approximately 25°C, which is below the thermodynamic critical temperature of carbon dioxide. The fluid enters the sub-cooler/receiver assembly where it is further cooled to increase its density. The fluid leaves this assembly at about 5°C and is then pumped by the variable speed internal gear pump. The function of the pump is to maintain a certain mass flow rate and overcome the pressure drop throughout the CO₂ piping. The cool liquid carbon dioxide then enters the heater, where it is heated to the supercritical inlet conditions of the test section.

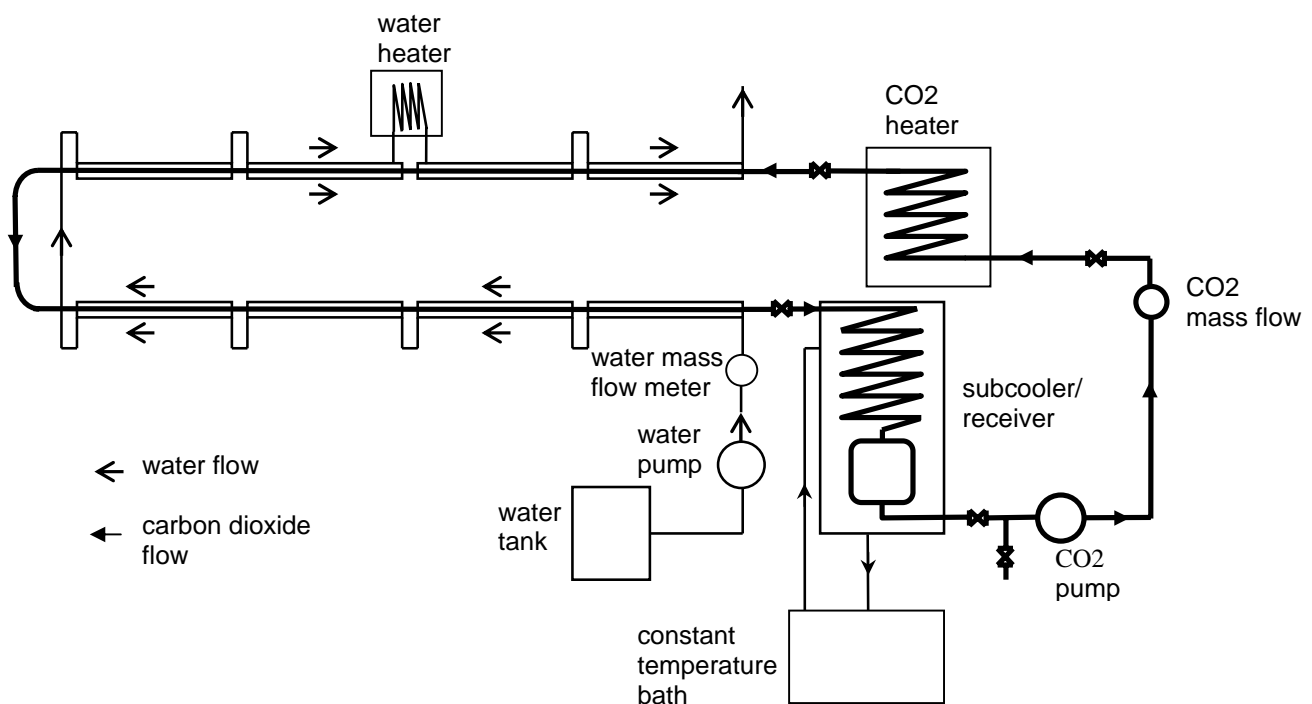


Figure 2: Schematic diagram of the test facility

The pump is a custom-designed, variable speed internal gear pump, which is magnetically coupled to a 1-hp motor. It is designed to work at pressures up to 136 bar (2000 psig). Flow into the test section is controlled by the variable speed drive of the motor. The mass-flow meter measures the flow and the drive can be adjusted accordingly. All the tubes are connected with compression fittings.

The test section consists of eight subsections. Each subsection is a tube-in-tube counter-flow heat exchanger. Carbon dioxide flows in the center and water flows in the annulus. Five subsections are 1.8 m long and three subsections are 1.3 m long. The tubing of the carbon dioxide loop is made of stainless steel with a nominal OD of 6.35 mm and a thickness of 1.8 mm. To minimize the heat transfer to the environment, the test sections were heavily insulated.

RESULTS

Numerical simulations were conducted corresponding to the conditions of twelve experimental runs that are described in detail by Pitla et al. (2000c). In each case, the measured carbon dioxide inlet temperature and the measured water outlet temperature were provided as inputs to the model. The experimental data and the numerical predictions were compared for each test run. For three runs, detailed comparisons are provided here. The experimental test conditions of the three runs are summarized in Table 1. The selected test runs represent three different supercritical pressures as well as three different mass flow rates. The selected pressures span the expected pressure range seen during gas cooler operation. The selected mass flow rates are representative of cooling capacities from 3 to 7 kW.

Table 1: Run matrix of the experimental test runs used in the comparative study

Test Run	Pressure, Mpa	Temperature, °C	Mass flow rate, kg/s
1	10.8	124 ... 27	0.029
2	9.4	121 ... 34	0.020
3	13.4	101 ... 20	0.039

Figures 3, 4, and 5 show the variations of the heat transfer coefficient along the tube length. It can be observed that the heat transfer coefficient is not constant, as would be the case in constant property fluids. The peak in the heat transfer coefficient occurs in the pseudocritical region. Experimental data was used to compute the average heat transfer coefficient of each subsection. These values can be seen as the horizontal lines in the plots. Figure 4 and more prominently, Figure 5, display a discontinuity. This is accounted for by the water heater, which is placed after the first two heat exchangers. Thus, the “entrance effect” is felt in the third heat exchanger. This is observed from the plots by the heat transfer rapidly diminishing for a small axial distance along the tube. Experimental measurements give an average value of the heat transfer coefficient over a heat exchanger. The average heat transfer predicted by the numerical program was calculated and compared with that of the experimental measured value. The results are shown in Table 2.

Figures 6, 7, and 8 show a comparison of the numerically predicted and the experimentally measured water temperature. The experimental measurements agree within $\pm 3\%$ of the numerical prediction.

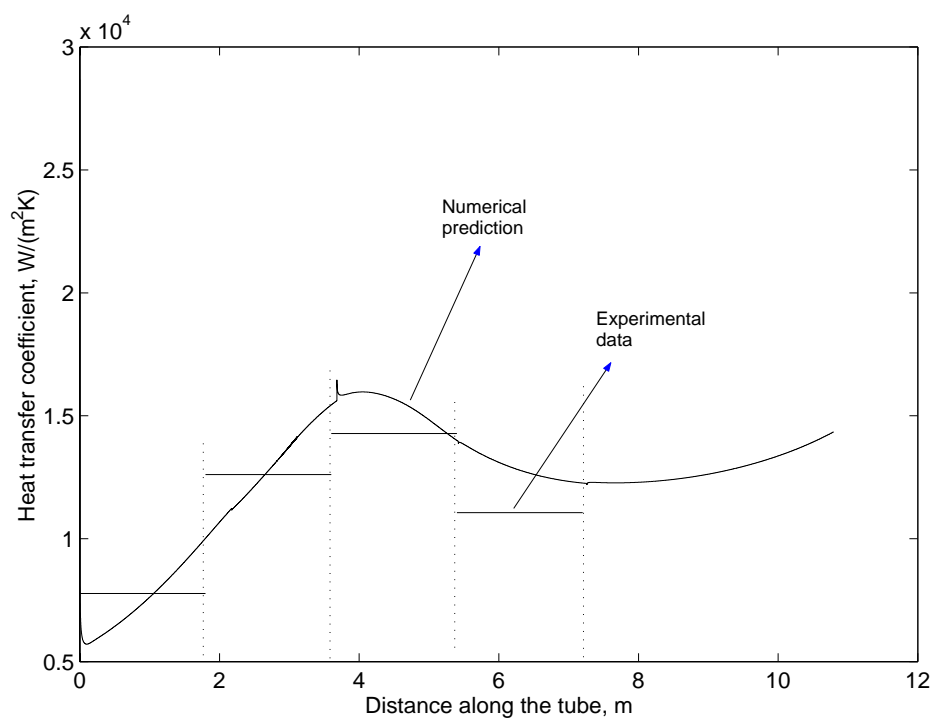


Figure 3: Variation of the heat transfer along the length of the tube (Run 1)

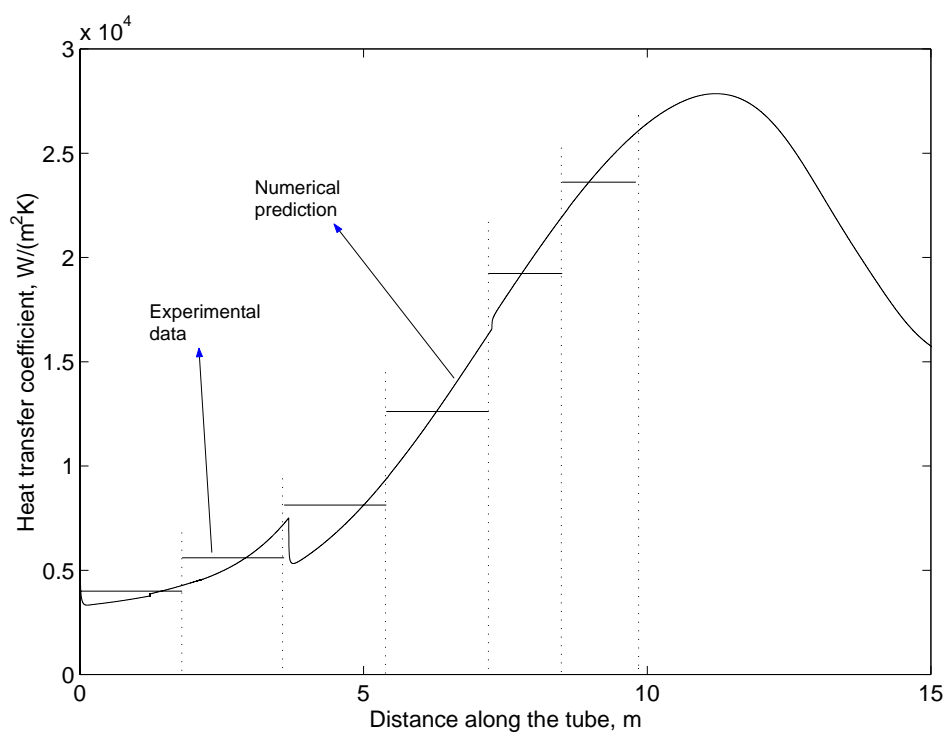


Figure 4: Variation of the heat transfer along the length of the tube (Run 2)

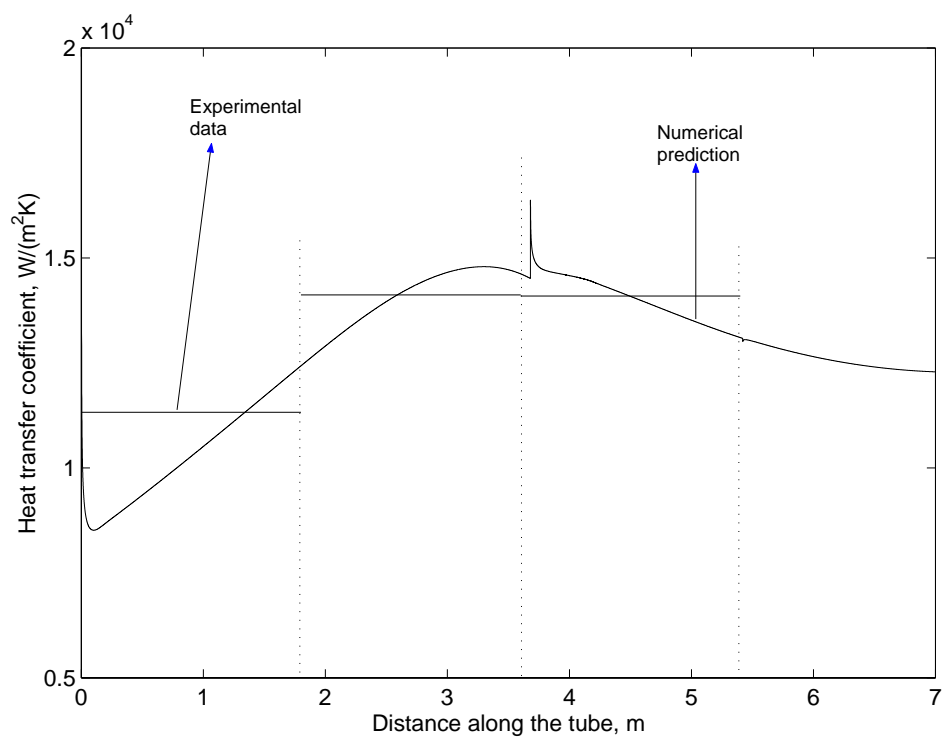


Figure 5: Variation of the heat transfer coefficient along the tube (Run 3).

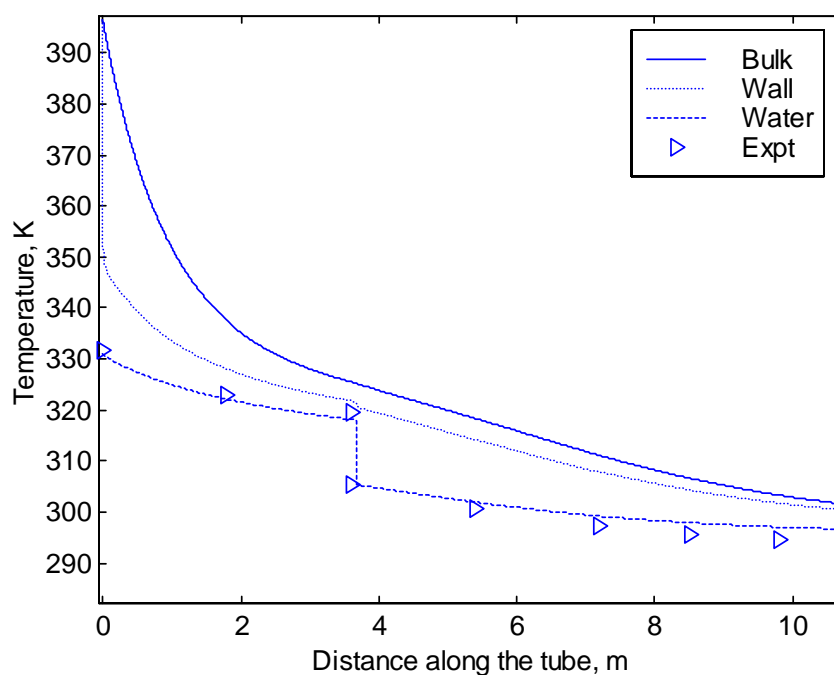


Figure 6: The variation of the temperature along the length of the tube (Run 1).

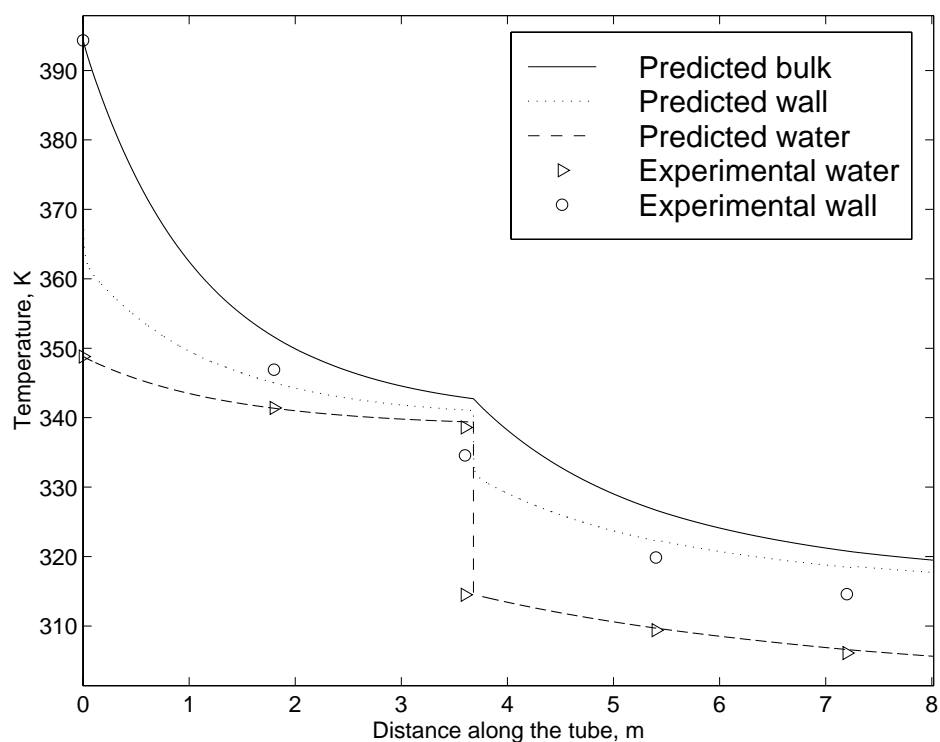


Figure 7: The variation of the temperature along the length of the tube (Run 2).

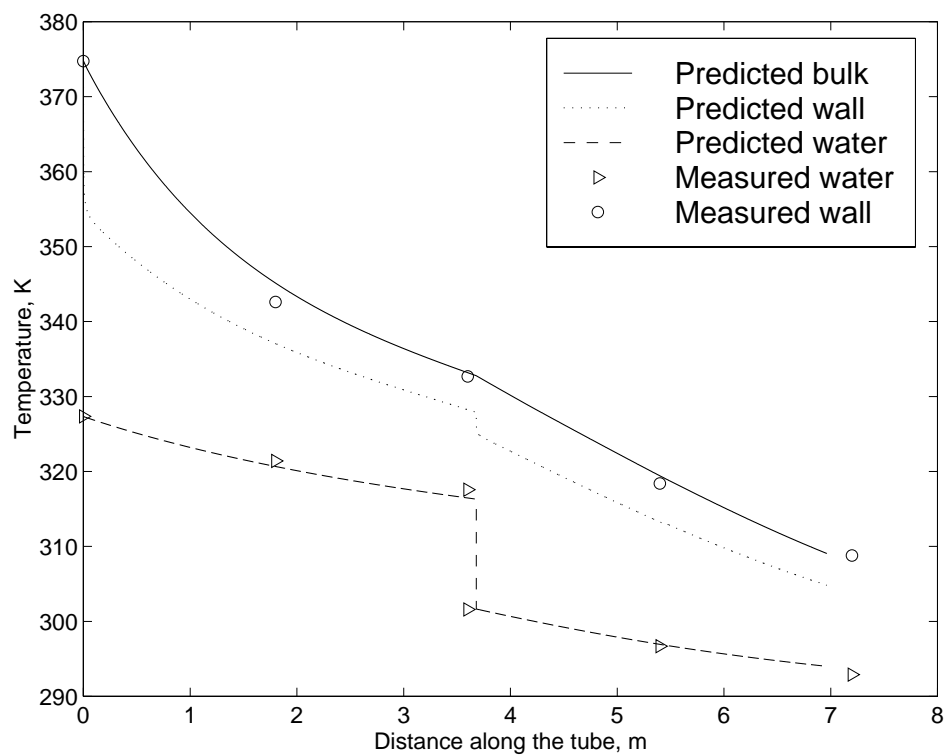


Figure 8: Variation of temperature along the length of the tube (Run 3).

Table 2: Comparison between the experimentally measured and the numerically predicted heat transfer coefficient.

(Heat transfer coefficient) times (length), W/mK (Numerical prediction)	(Heat transfer coefficient) times (length), W/mK (Experimental measurement)	Percentage error
<u>Run 1</u>		
1. 13568	13991.4	3.0
2. 23031	22694.4	1.0
3. 27689	25702.2	7.0
4. 23228	19909.8	14.0
<u>Run 2</u>		
1. 6683.9	6851.7	2.5
2. 9725.5	10080	3.5
3. 12653	14625	15.5
4. 22923	22696.2	1.0
5. 25255	25004.2	1.0
6. 31346	30695.6	2.0
<u>Run 3</u>		
5. 18619	20383.2	8.0
6. 25280	25417.8	0.5
7. 25285	25371	0.5

CORRELATION FOR THE HEAT TRANSFER COEFFICIENT

Several investigators attempted to correlate the heat transfer of supercritical carbon dioxide during in-tube heating. Relatively fewer attempts were made to correlate the heat transfer for in-tube cooling of supercritical carbon dioxide. In particular, Krasnoshechekov et al. (1970), Baskov et al. (1977) and Petrov and Popov (1985) attempted to correlate the heat transfer of supercritical carbon dioxide during in-tube cooling. The correlations were complex and were not very accurate, especially in the pseudocritical region. Lee and Howell (1997) stated that it was not possible to develop a generalized correlation for the heat transfer coefficient in the pseudocritical region and a detailed numerical analysis is necessary to predict the heat transfer in this region.

Based on the numerical predictions of the heat exchanger problem defined in Figure 1, it was attempted to develop a new correlation for the Nusselt number in terms of other dimensionless parameters. For this purpose, the numerically predicted Nusselt numbers were correlated. The final outcome was a new correlation that is based on the “mean Nusselt number” and is defined as shown in Equation (1):

$$Nu = \left(\frac{Nu_{wall} + Nu_{bulk}}{2} \right) \frac{k_{wall}}{k_{bulk}} \quad (1)$$

where Nu_{wall} and Nu_{bulk} are Nusselt numbers that are evaluated based on the thermophysical properties at the wall and the bulk temperatures, respectively. In each case, the Gnielinski correlation, as shown in Equation (2), is used to calculate the respective Nusselt number. The inlet velocity was used in computation of the Reynolds number at the wall and the mean velocity was used in computation of the bulk Reynolds number.

$$Nu_o = \frac{\xi / 8(Re - 1000) Pr}{12.7 \sqrt{\xi / 8} (Pr^{2/3} - 1) + 1.07} \quad (2)$$

Once the mean Nusselt number has been obtained, the heat transfer coefficient can be computed as shown in Equation (3):

$$h = \frac{Nu}{D} k_{bulk} \quad (3)$$

In the following section, the numerical computed values and the experimental data of the heat transfer coefficient are compared with the ones obtained with the proposed correlation.

Figures 9, 10, and 11 compare the accuracy of the proposed correlation with the numerical prediction for Runs 1, 2, and 3, respectively. In each figure, the heat transfer coefficient computed using the proposed correlation is plotted together with the numerical prediction (N) and the experimental data versus the tube length. To observe the accuracy of the new correlation, two help lines have been plotted. The first line, 1.2 N, denotes a +20% value of the numerically predicted heat transfer coefficient, and the second line, 0.8 N, represents a -20% value of the numerically predicted heat transfer coefficient. It is seen from Figures 9, 10, and 11 that the proposed correlation agrees within the range of $\pm 20\%$ for most of the tube length of the three test runs, except for two deviations. In Run 1, the new correlation overpredicts the heat transfer coefficient after the pseudocritical region. The pseudocritical region is defined as the region where the specific heat has a peak and coincides with the region where the heat transfer coefficient has a maximum (Pitla et al., 1998). In Run 2, the new correlation underpredicts the heat transfer coefficient far out in the vapor region.

Figures 12, 13, and 14 show the variation of the mean Nusselt number computed using the proposed correlation together with the numerically predicted Nusselt number (N) versus the bulk temperature for Runs 1, 2, and 3, respectively. As in Figures 9, 10, and 11, the $\pm 20\%$ curves (1.2 N and 0.8 N, respectively) are also plotted in the figures. It is seen that the Nusselt numbers calculated using the proposed correlation agree to within $\pm 20\%$ for all test runs, except for Run 1 at lower temperatures (after the pseudocritical temperature), where there is a sharp change in the thermophysical properties.

From this comparison it can be seen that the new correlation is most accurate for the data obtain during Run 3, where the pressure is the highest (13.4 MPa). As the pressure is increased from the critical point, the variation in the thermophysical properties is less severe. It is thus possible to correlate the heat transfer coefficient of supercritical carbon dioxide more accurately at pressures away from the critical point.

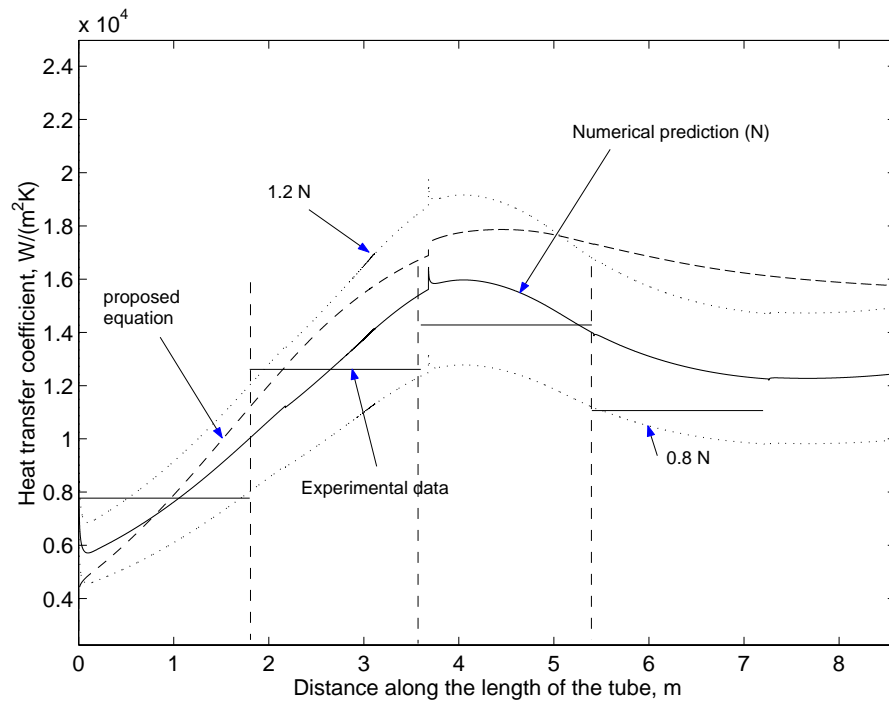


Figure 9: Comparison of the proposed correlation with the numerical prediction and experimental data along the length of the tube (Run 1).

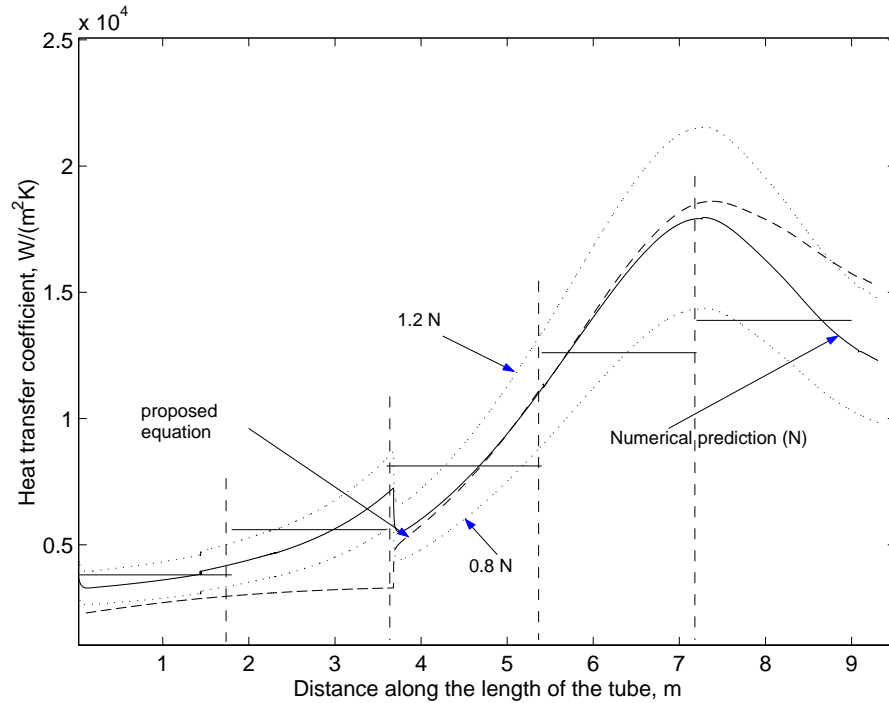


Figure 10: Comparison of the proposed correlation with the numerical prediction and experimental data along the length of the tube (Run 2).

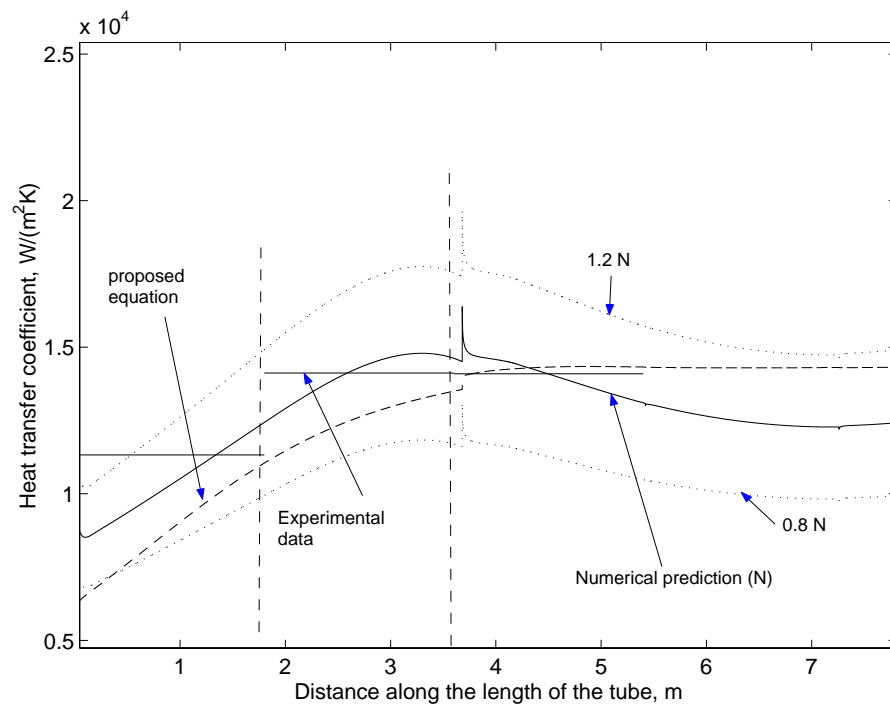


Figure 11: Comparison of the proposed correlation with the numerical prediction and experimental data, along the length of the tube. (Run 3)

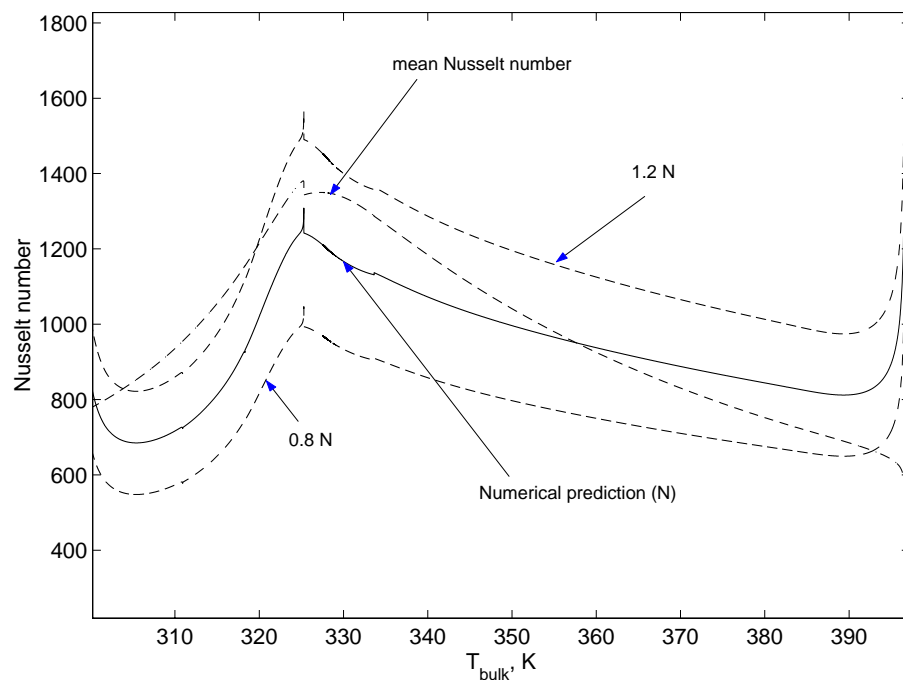


Figure 12: Comparison of the proposed correlation with the numerical prediction versus the temperature (Run 1).

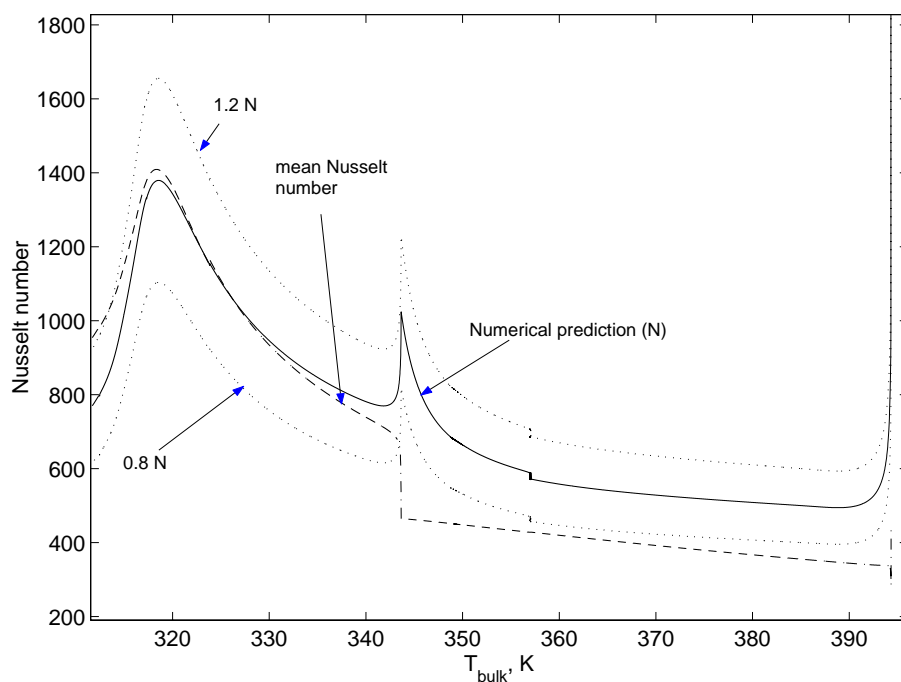


Figure 13: Comparison of the proposed correlation with the numerical prediction versus the temperature (Run 2).

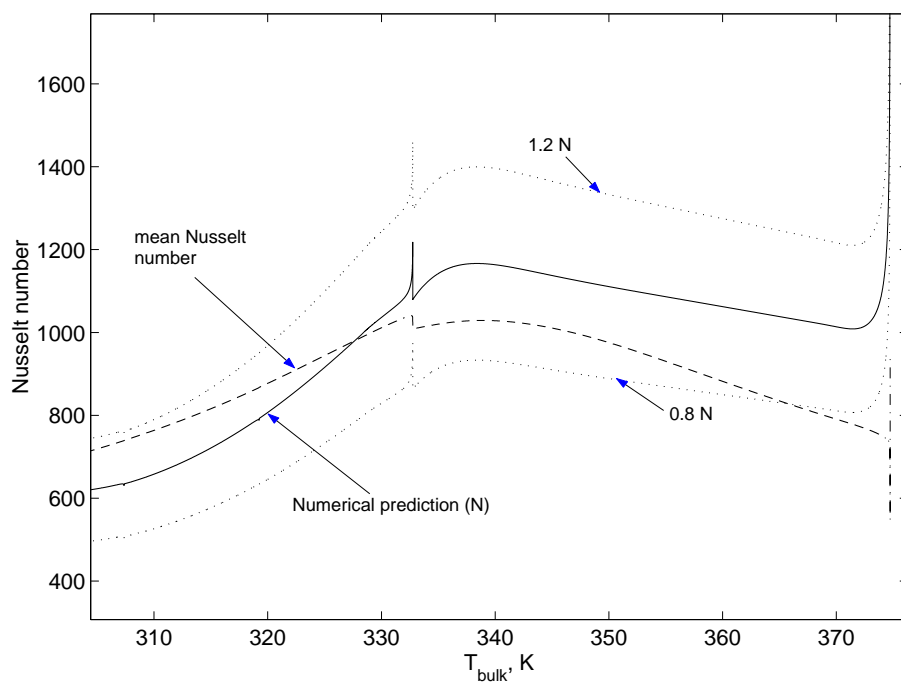


Figure 14: Comparison of the proposed correlation with the numerical prediction versus the temperature (Run 3).

The proposed correlation was also compared to the existing correlations for the supercritical heat transfer coefficient (Krasnoshchekov et al., 1970; Baskov et al., 1977), which are given in Equations (4) and (5), respectively. Figures 15, 16, and 17 show the heat transfer coefficient computed with the new proposed correlation and with the two existing correlations together with the numerically predicted heat transfer coefficient versus the bulk temperature for Runs 1, 2, and 3, respectively. It is seen from Figures 15, 16, and 17 that the new correlation matches the numerical prediction better than the ones proposed by Krasnoshchekov et al. (1970) and Baskov et al. (1977), especially in the pseudocritical region.

$$Nu_{bulk} = Nu_{PKP,wall} \left(\frac{\rho_{wall}}{\rho_{bulk}} \right)^n \left(\frac{\bar{c}_p}{c_{pwall}} \right)^m \quad (4)$$

$$Nu_{wall} = Nu_{PKP,wall} \left(\frac{\bar{c}_p}{c_{pwall}} \right)^m \left(\frac{\rho_b}{\rho_{wall}} \right)^n \quad (5)$$

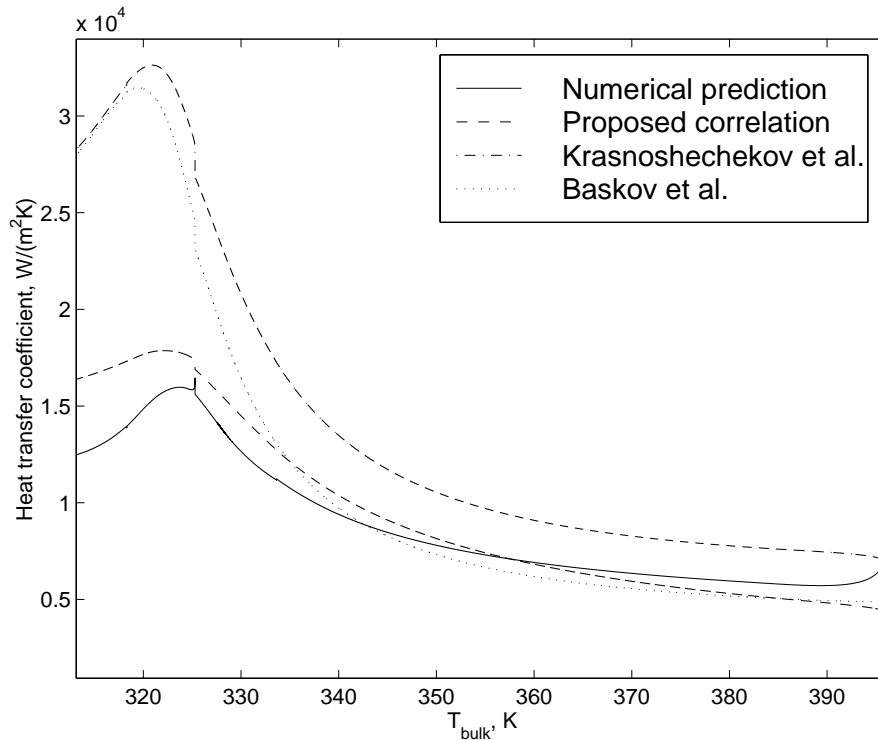


Figure 15: Comparison of the heat transfer coefficient predicted by various correlations (Run 1).

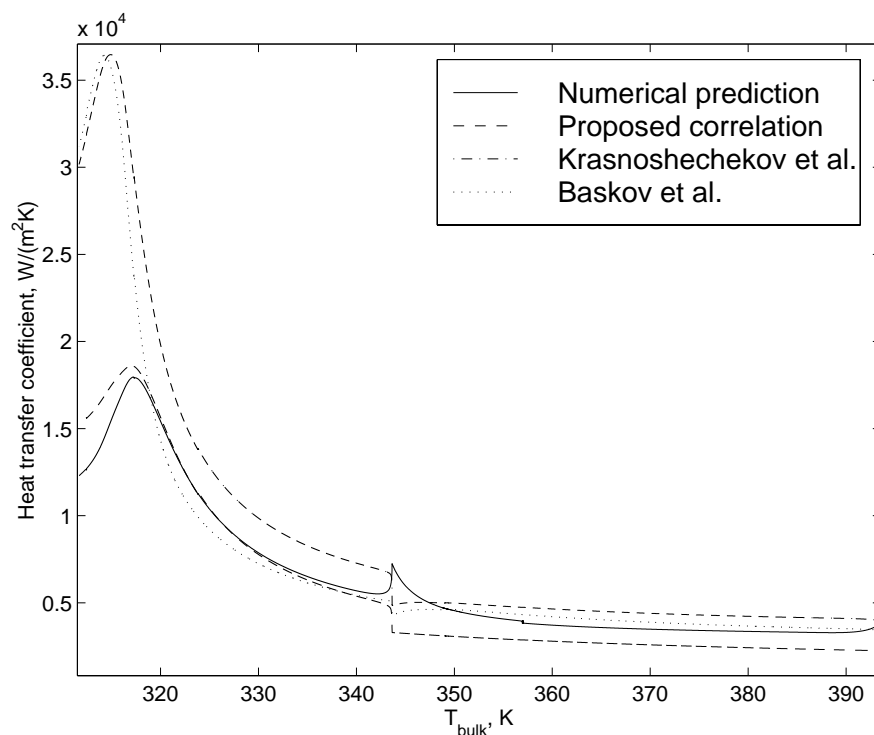


Figure 16: Comparison of the heat transfer coefficient predicted by various correlations (Run 2).

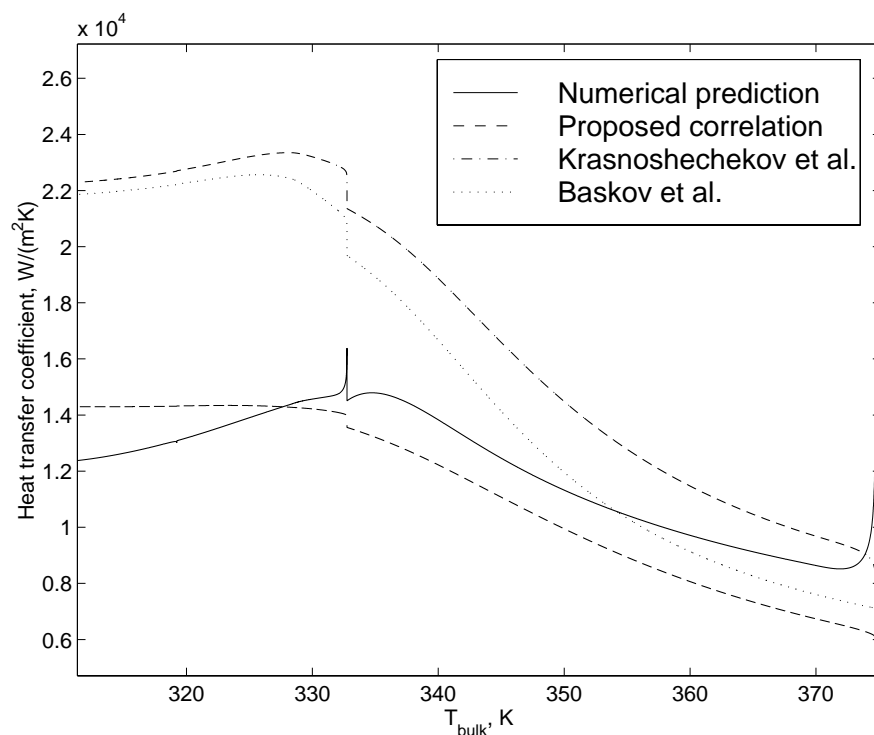


Figure 17: Comparison of the heat transfer coefficient predicted by various correlations (Run 3).

CONCLUSIONS

The heat transfer coefficient in supercritical fluids is not constant and varies as both the wall temperatures and the bulk temperatures of the fluid vary. It was seen that there is a spike in the heat transfer coefficient in the pseudocritical region. The correlation to predict the heat transfer coefficient has been developed based on curve fit of the numerically predicted and experimentally obtained data and is shown below:

$$Nu = \left(\frac{Nu_{wall} + Nu_{bulk}}{2} \right) \frac{k_{wall}}{k_{bulk}} \quad (6)$$

where Nu_{wall} and Nu_{bulk} are calculated using the Gnielinsky correlation evaluated based on the thermophysical properties at the wall and the bulk temperatures, respectively. It was seen that the 85% of the heat transfer coefficient values predicted by the new correlation were accurate to within $\pm 20\%$. A comparison of the heat transfer coefficient calculated using the new correlation and two existing correlations found in the literature showed that the accuracy in predicting the heat transfer coefficient with the new correlation was greatly increased, especially in the pseudocritical region.

ACKNOWLEDGEMENTS

The study presented in this paper was funded by ASHRAE RP-913. The authors would like to thank ASHRAE for the sponsorship.

REFERENCES

- Baskov, V.L., Kuraeva, I.V., and Protopopov, V.S., 1977, "Heat Transfer with the Turbulent Flow of a Liquid at Supercritical Pressure in Tubes Under Cooling Conditions," *Teplofizika Vysokikh Temperatur*, Vol. 15, No. 1, pp. 96-102.
- Bellmore, C.P., and Reid, R.L., 1983, "Numerical Prediction of Wall Temperatures for Near-Critical Para-Hydrogen in Turbulent Upflow Inside Vertical Tubes," *Transactions of the ASME*, Vol. 105, pp. 536-541.
- Gnielinski, V., 1976, "New Equation for Heat and Mass Transfer in Turbulent Pipe and Channel Flow," *Int. Chemical Engineering*, Vol. 16, pp. 359-368.
- Krasnoshechekov, E.A., Kuraeva, I.V., and Protopopov, V.S., 1970, "Local Heat transfer of Carbon Dioxide at Supercritical Pressure Under Cooling Conditions," *Teplofizika Vysokikh Temperatur*, Vol. 7, No5, pp. 922-930.
- Krasnoshechekov, E.A., and Protopopov, V.S., 1972, "A Generalized Relationship for Calculation of Heat Transfer to Carbon Dioxide at Supercritical Pressure," *Teplofizika Vysokikh Temperatur*, Vol. 9, No. 6, pp. 1314.
- Lee, S.H., and Howell, J.R., 1997, "Turbulent Developing Convective Heat Transfer in a Tube for Fluids Near the Critical Point," *International Journal Heat Mass Transfer*, Vol. 41 No. 10, pp. 1205-1218.
- Petrov, N.E., and Popov, V.N., 1985, "Heat Transfer and Resistance of Carbon Dioxide Being Cooled in the Supercritical Region," *Thermal Engineering*, Vol. 32, No. 3, pp. 131-134.

- Pitla, S.S., Robinson, D.M., Groll, E.A., and Ramadhyani, S., 1998, "Heat Transfer from Supercritical Carbon Dioxide in Tube Flow: A Critical Review," *Int'l J. HVAC&R Research*, Vol. 4, No. 3, pp. 281 –301.
- Pitla, S.S., Ramadhyani, S., and Groll, E.A., 2000a, "Convective heat transfer from in-tube flow of turbulent supercritical carbon dioxide: Part 1 – numerical analysis," *Int'l J. HVAC&R Research*, in review.
- Pitla, S.S., Groll, E.A., and Ramadhyani, S., 2000b, "Convective heat transfer from in-tube cooling of turbulent supercritical carbon dioxide: Part 2 – experimental data and numerical predictions," *Int'l J. HVAC&R Research*, in review.
- Pitla, S.S., Robinson, D.M., Zingerli, A., Groll, E.A., and Ramadhyani, S., 2000c, "Heat Transfer and Pressure Drop Characteristics During In-Tube Gas Cooling of Supercritical Carbon Dioxide," Final Report ASHRAE 913-RP, American Society of Heating, Refrigerating, and Air Conditioning Engineers, Inc., Atlanta, GA, August 2000.

6.2.3 HEAT TRANSFER AND PRESSURE DROP CHARACTERISTICS OF SUPER-CRITICAL CARBON DIOXIDE IN MICROCHANNEL TUBES UNDER COOLING

J. PETTERSEN¹, R. RIEBERER², A. LEISTER³

¹Norwegian University of Science and Technology (NTNU)
Dept. of Refrigeration and Air Conditioning, N-7491 Trondheim, Norway

²Graz University of Technology (present affiliation)

³BEHR GmbH & Co (present affiliation)

Contact e-mail: Jostein.Pettersen@kkt.ntnu.no

ABSTRACT

This paper provides heat transfer and pressure drop data for carbon dioxide (CO₂) at supercritical pressures in a multiport extruded (MPE) aluminium tube. The tube had 25 circular ports/channels with 0.79 mm inner diameter. Data are presented for the following range of variables: Mass flux 600 - 1200 kg/(m²s), pressure 81 - 101 bar and heat flux 10 - 20 kW/m². The temperature range investigated was 15 to 70°C. The measured heat transfer coefficients were in the range of 5,000 to 17,500 W/(m²K) and the measured pressure drop in the range of 0.05 to 0.32 bar corresponding to a mean pressure gradient of 10,000 to 64,000 Pa/m. In addition, the measured values were compared to correlations available in literature. Gnielinski's correlation for the single-phase heat transfer coefficient and Colebrook & White's correlation for the pressure drop showed a satisfactory correspondence.

An accompanying paper (Pettersen et al., 2000a) presents the results of two-phase heat transfer and pressure-drop experiments.

1. NOMENCLATURE

c_p	specific isobaric heat capacity [J/(kg K)]	t	Temperature [°C]
\dot{m}	Mass flux [kg/(m ² s)]	α	Heat transfer coefficient [W/(m ² K)]
p	Pressure [Pa, bar]	.	Difference [-]
Pr	Prandtl number [-]	.	Density [kg/m ³]
\dot{q}	Heat flux [kW/m ²]	σ	Deviation [-]

2. INTRODUCTION

Since the re-introduction of carbon dioxide (CO₂, R-744) as a working fluid (Lorentzen and Pettersen, 1992), it has been shown to have several favourable applications, for instance in heat pump water heaters (Nekså et al., 1998), laundry dryers (Schmidt et al., 1998), mobile air conditioners and heat pumps (Hafner et al., 1998), residential air conditioners (Pettersen et al., 1997), as well as in military environmental control units (Patil and Manzione, 1999).

The motivation of the present study was to obtain heat transfer and pressure drop data for heat exchangers to be used for the transcritical CO₂ process, as well as to examine the applicability of common engineering correlations. This paper focuses on heat transfer and pressure drop at super-critical pressures under cooling in multiport extruded (MPE) aluminium tubes. A cross-sectional sketch of the tested tube is shown in Figure 1. The dimensions are in millimetres.

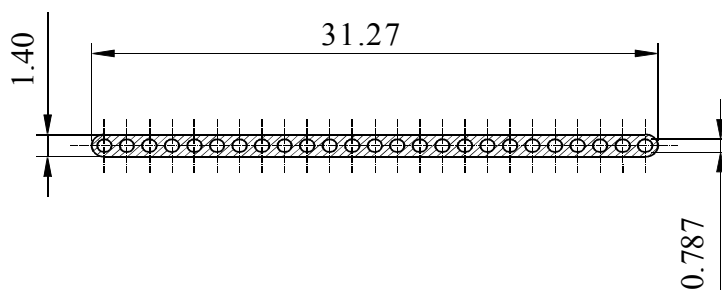


Figure 1: Cross-section of the multiport extruded (MPE) tube (Dimensions in mm)

IIF-IIR – Commission B1, B2, E1, and E2 – Purdue University, USA – 2000

As most single-phase engineering correlations were not developed for supercritical fluids, they cannot necessarily be expected to give accurate results for CO₂. The reasons for this are the differences in thermophysical and thermodynamic properties, such as thermal conductivity and isobaric heat capacity. In particular, CO₂ heat pumping units usually operate close to the critical point (73.8 bar, 31.1°C). The main difference between the supercritical and the subcritical region is that - in case of an isobaric change of state - at supercritical pressures all properties of the single-phase fluid change continuously with temperature, Figure 2.

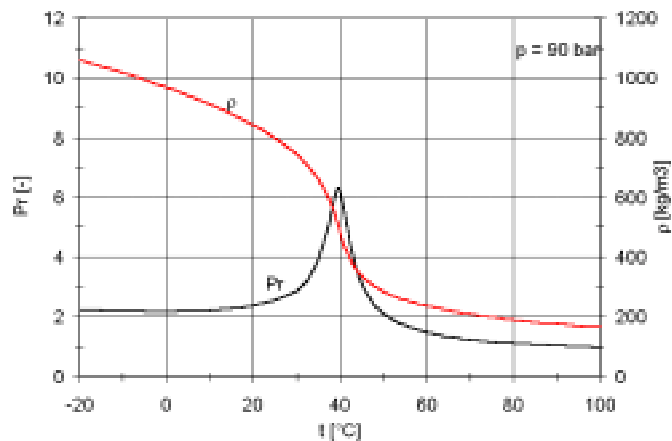


Figure 2: Prandtl number (Pr) and density (ρ) of CO₂ at 90 bar and varying temperature

As one can see, the density of the fluid decreases continuously from approximately 970 kg/m³ at 0°C to 165 kg/m³ at 100°C, while the Prandtl (Pr) number has a maximum at the pseudocritical temperature. This is caused by the maximum of the isobaric heat capacity. In the low-temperature quasi-liquid region Pr is between 2.2 and 2.9, the maximum value is 6.3, and it decreases to approximately 1 at 100°C. The temperature-dependency of the Prandtl number is different at other pressures. These facts lead to a strongly varying heat transfer coefficient.

3. TEST FACILITIES, DATA ACQUISITION AND REDUCTION

In this section, the test facility at SINTEF Energy Research, Trondheim (Norway) is briefly explained. The investigated MPE tube (Figure 1) had an overall length of 540 mm. It was placed inside a PTFE (Teflon) jacket, where channels were milled out. These channels were shaped like an edgy double helix around the MPE tube. A photograph of the MPE tube in the (opened) PTFE jacket is shown in Figure 3. De-ionised water – used as heat-sink (cooling tests) as well as heat-source (evaporation tests, see accompanying paper) – flowed through these channels, i.e. on the outside of the MPE tube.

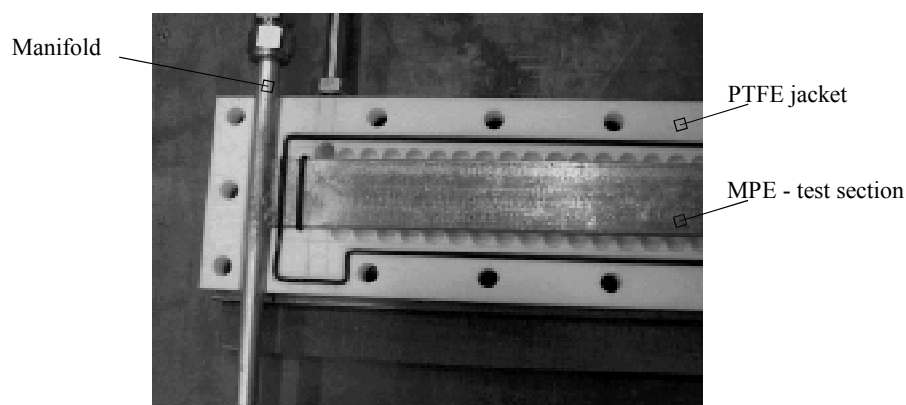


Figure 3: MPE test section in the PTFE jacket

Important temperatures in the test rig were measured with Pt-100 sensors, and the mass flow rate and pressures were measured with electronic transmitters. The data were electronically logged, and processed on a PC.

The overall heat transfer coefficient was determined by means of the measured mass flow rates, pressures, and temperatures assuming a linear CO₂-side pressure profile along the test section. Then, the CO₂-side heat transfer coefficient (α_{CO_2}) was re-calculated using "calibrated" equations for the water-side heat transfer coefficient. These equations were found by means of a modified Wilson plot technique. The test rig, the calibration procedure, and the test results are described in full detail in an open technical report (Pettersen et al., 2000b).

4. EXPERIMENTAL RESULTS AND DISCUSSION

4.1 Heat Transfer

In order to determine the influence of the mass flux on the heat transfer coefficient, certain tests were carried out. The test points were taken at mass fluxes of 600, 900 and 1,200 kg/(m²s), while the (inlet-) pressure was kept constant at 91 bar. The heat flux was about 20 kW/m². Each test series consisted of five test points with different mean temperature. These mean temperatures were chosen in such a way that one point was close to the pseudocritical temperature - where c_p shows its maximum - and at least two points were above and below this point. The choice of the test points below and above the pseudocritical temperature aimed at keeping the enthalpy difference between the points constant. Some of the points did not follow this principle, however, because of constraints given by the test rig.

Results from the measurements at varying mass flux are shown in Figure 4. The legend contains information on the pressure, mass flux, and heat flux applied: E.g. "p91 m600 q20" means that the tests were carried out at a pressure of 91 bar, a mass flux of 600 kg/(m²s) and a heat flux of 20 kW/m². It should be noticed that the horizontal lines in the charts are not error bars, they indicate the temperature glide of the CO₂ inside the test section. The data points indicate the length-averaged value, where the temperature profile along the tube has been calculated assuming a constant overall heat transfer coefficient U . In addition, the charts show calculated results of the heat transfer coefficient according to Gnielinski's correlation.

The influence of the mass flux on the heat transfer coefficient of CO₂ is significant. Of course, a higher mass flux results in a higher heat transfer coefficient. If the mass flux is increased from 600 to 900 kg/(m²s) the calculation as well as the measurement show a rise in the heat transfer coefficient of about 40%, and a rise of about 80% if the mass flow is increased to 1200 kg/(m²s). The peak in the graph indicates the pseudocritical temperature. At 91 bar the maximum c_p is located at 40.6°C.

The agreement between calculation and measurement was quite satisfactory. Only at high temperatures a moderate deviation can be seen.

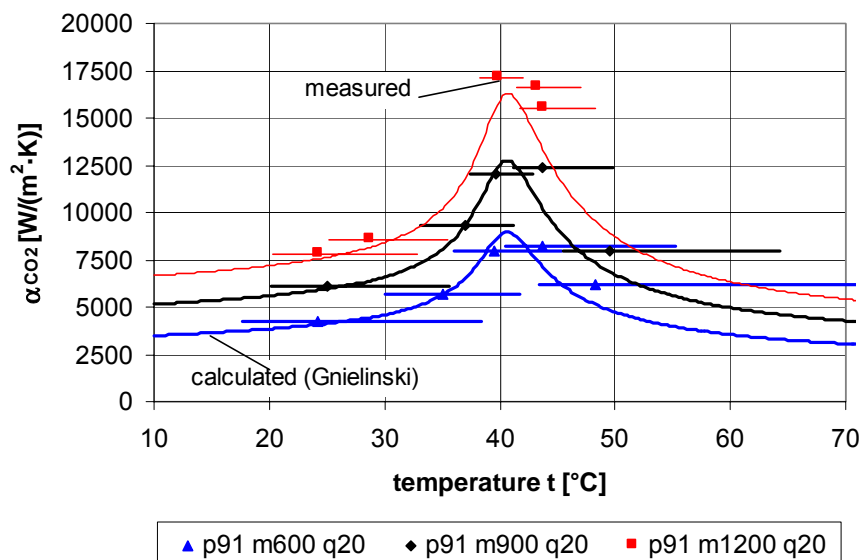


Figure 4: Influence of the mass flux on the heat transfer coefficient

As can be seen from Figure 5, the influence of varying heat flux on the heat transfer coefficient was rather small. In this test series, the heat flux was either 10 or 20 kW/m². The heat transfer coefficient varied less than 1 to 2% as a result of varying heat flux. The measured values show a high accuracy compared with the calculated results. From Gnielinski's correlation one can find an explanation of the (negligible) influence of the heat flux on the heat transfer coefficient; The influence is taken into account by means of the correction factor $(Pr/Pr_w)^{0.11}$. Since the wall temperature changes with the heat flux, the Prandtl number at the wall temperature (Pr_w) changes as well. However, due to the small exponent of 0.11 the correction factor is almost 1 for the test conditions applied.

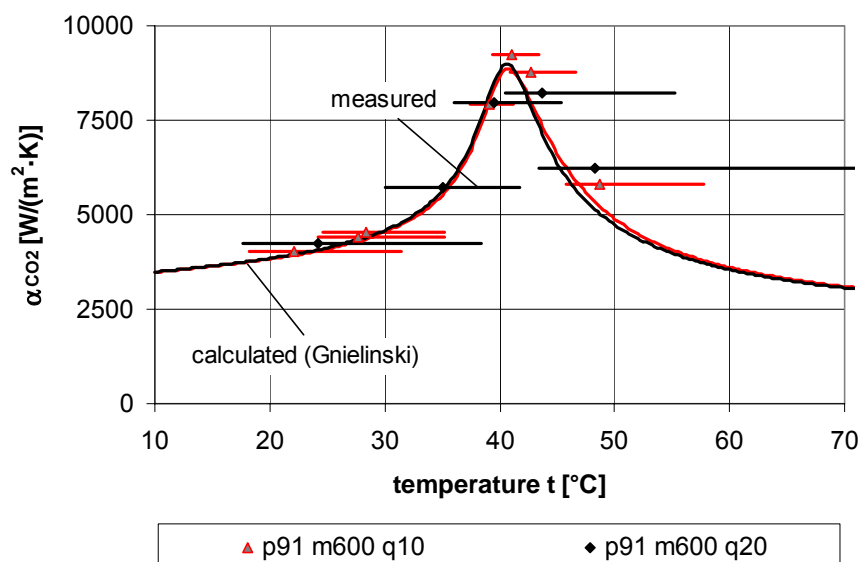


Figure 5: Influence of the heat flux on the heat transfer coefficient

The influence of varying pressure on the heat transfer coefficient is of considerable interest. Since the heat transfer coefficient reaches a maximum at the pseudocritical temperature, this maximum will change with varying pressure. Figure 6 shows the results. As may be observed, the maximum heat transfer coefficient increases when the pressure approaches the critical pressure of CO₂ (73.8 bar).

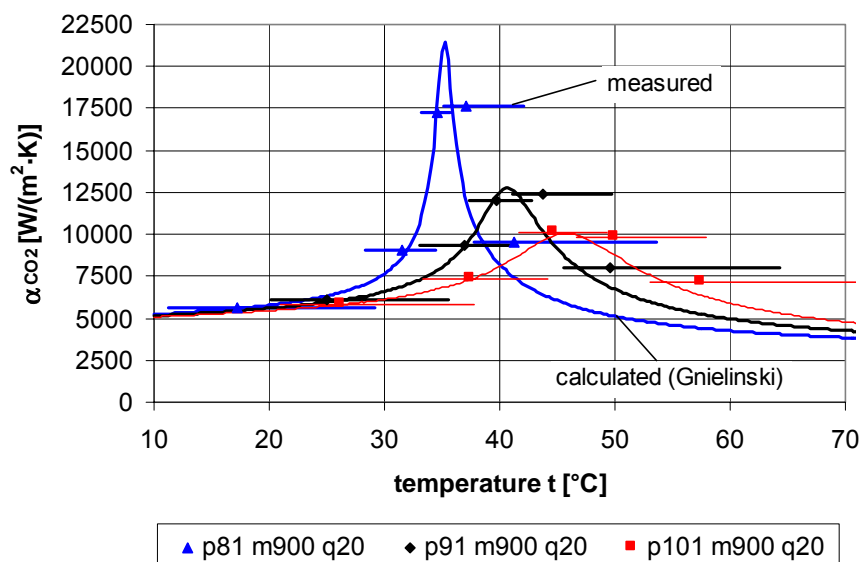


Figure 6: Influence of the pressure on the heat transfer coefficient

For a mass flux of 900 kg/(m²·s) and a heat flux of 20 kW/m², the peak heat transfer coefficient is about 21,000 W/(m²·K) for a pressure of 81 bar, and about 10,000 W/(m²·K) at 101 bar. This corresponds to a more than 100% rise IIF-IIR – Commission B1, B2, E1, and E2 – Purdue University, USA – 2000

when the pressure is decreased from 101 to 81 bar. An increase of the pressure from 91 to 101 bar leads to a drop of the maximum heat transfer coefficient of about 20%. A more or less negligible influence of the pressure on the heat transfer coefficient can be seen in case of temperatures "far away" from the pseudocritical value, i.e. at rather low or high temperatures. This is visualised by the asymptotic approach of the curves below 25°C and above 70°C. Again, the deviation between measurement and calculation was small.

Finally, all measured single-phase heat transfer coefficients were compared to different calculation models. For this, two different deviation data were used:

$$\sigma_{avg} = \frac{1}{n} \sum_n \frac{(\alpha_{calc} - \alpha_{meas})}{\alpha_{meas}} \quad \dots \text{average deviation} \quad \text{Eq 1}$$

$$\sigma_{mean} = \frac{1}{n} \sum_n \left| \frac{(\alpha_{calc} - \alpha_{meas})}{\alpha_{meas}} \right| \quad \dots \text{mean deviation} \quad \text{Eq 2}$$

As can be seen from Table 1, three different forms of Gnielinski's correlation, the 'special' models for supercritical heat transfer proposed by Polyakov (1991) and Ghajar & Asadi (1986), as well as the Dittus-Boelter correlation with two different Prandtl-exponents were used for the comparisons.

Here, "simple Gnielinski" means Gnielinski's correlation for the Nusselt number using the Haaland (1983) friction factor and neglecting the influence of the wall temperature (see above). The other variant of the original Gnielinski correlation was "Gnielinski (VDI)" where the Filonenko (1954) friction factor was used.

Table 1: Deviation between measured heat transfer coefficients and calculation models

	σ_{avg} [%]	σ_{mean} [%]
simple Gnielinski	-3	4
Gnielinski	-1	4
Gnielinski (VDI)	-7	8
Polyakov	19	19
Ghajar & Asadi	1	8
Dittus-Boelter ($n = 1/3$)	-18	18
Dittus-Boelter ($n = 0.4$)	-7	9

All in all, the comparison showed a quite good correspondence. Gnielinski's model in combination with Haaland's friction factor as well as the model proposed by Ghajar & Asadi predict very well the supercritical heat transfer coefficient of CO₂ under cooling within the temperature region investigated. A mean deviation of about 4% was determined for Gnielinski's model. The fit of the rather sophisticated model proposed by Polyakov was worse than the values according to the standard textbook correlation of Dittus-Boelter. However, the fit of the Dittus-Boelter correlation using a Prandtl-exponent n of 0.4 – which is normally used for heated flow – was much better compared to the fit with $n = 1/3$, which should be used here since the CO₂ was cooled in the test section.

4.2 Pressure drop

In addition to measuring heat transfer coefficients, the pressure drop along the multiport tube was also recorded as part of the measurements. Again, the influence of the mass flux, heat flux and pressure will be discussed briefly. The test results are shown in Figure 7 to Figure 9. In addition, calculated values - according to Colebrook & White (VDI, 1994) - are indicated (C&W). In these figures the absolute pressure drop in the test section in *bar* is shown. Considering the heat transfer length of 503 mm, the given numbers must be multiplied by a factor of about $2 \cdot 10^5$ in order to obtain the mean pressure gradient in *Pa/m*.

As expected the mass flow rate influences the pressure drop considerably (Figure 7). In case of an increase of the mass flux from 600 to 900 kg/(m²s) and from 600 to 1200 kg/(m²s), the measured pressure drop increased by about

100% and 240%, respectively. As stated above, the heat transfer coefficient increased by about 40% and 80%, respectively, at the same conditions.

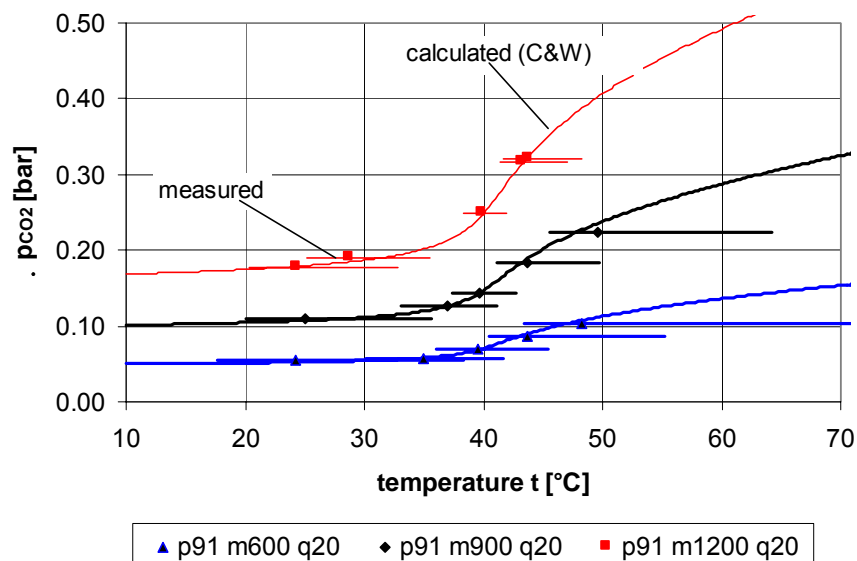


Figure 7: Influence of the mass flux on the pressure drop ($l = 503$ mm)

As can be seen from Figure 8, there was no noticeable influence by varying heat flux on the pressure drop. In general, the influence of varying temperature on pressure drop changes significantly close to the pseudocritical temperature. The steep gradient is caused by the rapid change in CO₂-density in this region, as may be observed in Figure 2.

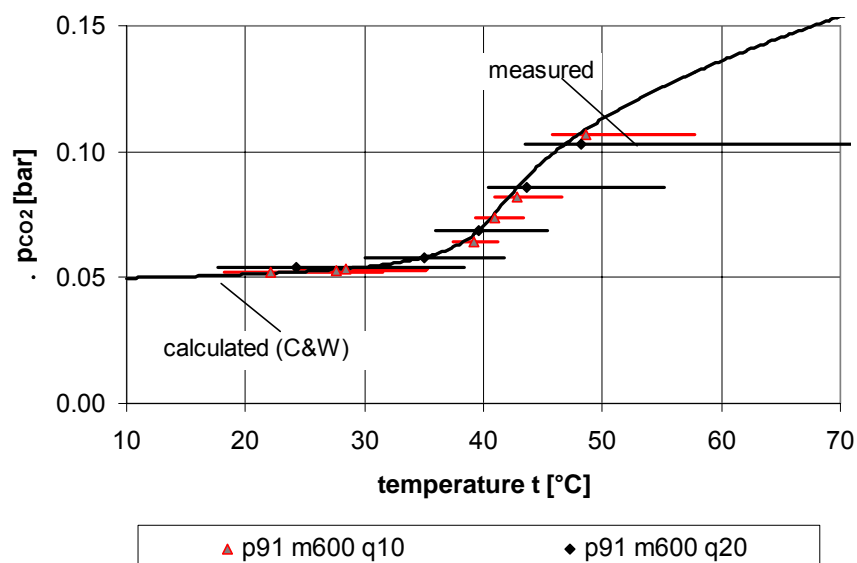
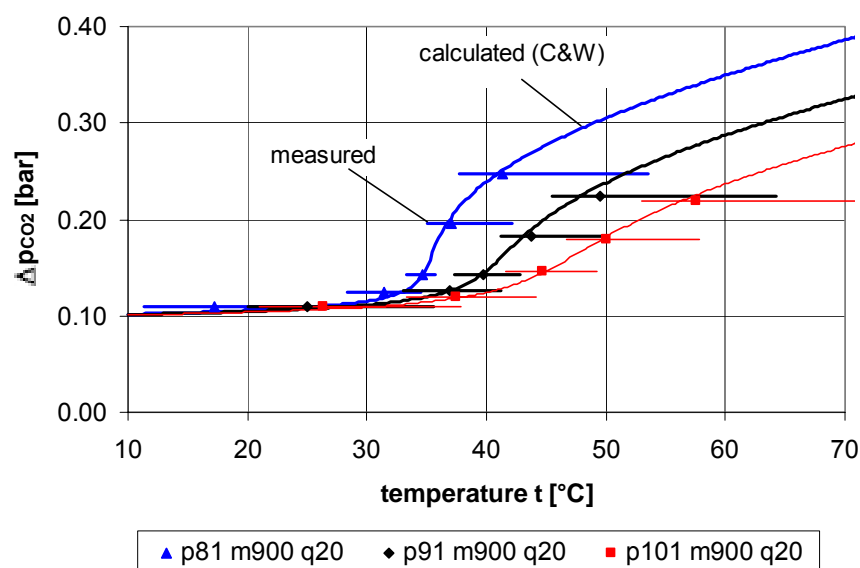


Figure 8: Influence of the heat flux on the pressure drop ($l = 503$ mm)

Since the pressure has a large influence on the pseudocritical temperature, the pressure-drop characteristics change with the absolute value of the pressure (Figure 9). If the pressure changes from 91 to 81 bar and from 91 to 101 bar, the mean pressure drop changes about +17% and -13%, respectively, in the temperature range 10 to 80°C. The corresponding change of the heat transfer coefficient was +68 and -20%, respectively.

Figure 9: Influence of the pressure on the pressure drop ($l = 503 \text{ mm}$)

Again, the measured results were compared to correlations from the literature. Firstly, a comparison was made with the well-known Blasius correlation (VDI, 1994), which is used for estimating the pressure drop in a smooth tube and turbulent flow regime. The next was the Colebrook & White correlation (VDI, 1994), which is an implicit form for the friction factor based on the Moody-diagram. The third was an explicit form of the Colebrook & White friction factor published by Swamee et al. (1975). The results of the comparisons - i.e. the average and the mean deviations of Equations 1 and 2 - are listed in Table 2.

Table 2: Deviation of the measured pressure drop to calculation models

	$\sigma_{avg} (\%)$	$\sigma_{mean} (\%)$
Blasius	-6	6
Colebrook & White	1	2
Swamee	1	2

As one can see, the models predict the pressure drop quite accurately. The mean deviation was 2% for both the Colebrook & White and the Swamee model. Only the Blasius correlation underestimated the pressure drop slightly. But this can be expected, because the MPE tube was made of extruded aluminium with a certain roughness.

5. CONCLUSION

In a transcritical cycle, the refrigerant is cooled down at a supercritical pressure. In this region the influence of the critical point on the properties is large. This fact leads to conditions in CO₂ equipment differing considerably from in systems using conventional refrigerants.

The experimental results confirm that CO₂ offers high heat transfer coefficients at supercritical pressures. A comparison between experimental data and common correlations showed an acceptable correspondence. Especially the Nusselt number based on Gnielinski's correlation in combination with Haaland's friction factor correlated the experimental heat transfer data well.

The expected pressure drop of CO₂ in a refrigerant cooler is rather high, but due to the high pressure level, the effect on temperature loss is moderate (Rieberer, 1998). A comparison between experimental data and calculated results according to the Colebrook & White correlation showed a satisfactory agreement.

ACKNOWLEDGEMENT

Most of the presented data were recorded by Andreas Leister as part of his diploma work (Leister, 1999). The project was sponsored jointly by the U.S. Army European Research Office, London, and the CECOM Research, Development, and Engineering Center of the U.S. Army at Ft. Belvoir, Virginia.

6. REFERENCES

- Filonenko, G. K., 1954, *Teploenergetika*, 4
- Ghajar A. T., Asadi, A., 1986, Improved Forced Convective Heat Transfer Correlation for Liquids in the Near Critical Region, *AIJA Journal*, Vol.24, p. 2030-2037
- Haaland, S.E., 1983, Simple and Explicit Formulas for the Friction Factor in Turbulent Pipe Flow, *J. Fluids Eng.*, March, p. 89-90
- Hafner, A., Pettersen, J., Skaugen, G. and Neksa, P., 1998, An automobile HVAC system with CO₂ as the refrigerant, *In: Proceedings, Natural Working Fluids '98 -- IIR Gustav Lorentzen Conference*, IIF-IIR, Oslo, Norway, p. 335-345.
- Leister, A., 1999, Experimental Study on Heat Transfer and Pressure Drop in Extruded and Drawn Tubes for Compact Heat Exchangers, Diplomarbeit Nr. 99-29, Fachhochschule Karlsruhe, Germany, Fachbereich Maschinenbau, Work carried out at SINTEF Energy Research, Trondheim, Norway.
- Lorentzen, G. and Pettersen, J., 1992, New Possibilities for Non-CFC Refrigeration, *Proc. IIR International Symposium on Refrigeration, Energy and Environment*, Trondheim, Norway, June 22-24, p.147-163..
- Neksa, P., Rekstad, H., Zakeri, G.R. and Schiefloe, P.A., 1998, CO₂-heat pump water heater: characteristics, system design and experimental results, *International Journal of Refrigeration*, vol. 21, no. 3: p. 172-179.
- Patil, A.S. and Manzione, J.A., 1999, US Army CO₂ Development Program, *In: 20th International Congress of Refrigeration*, IIF-IIR, Sydney, Australia.
- Pettersen, J., Aarli, R., Neksa, P., Skaugen, G. and Aflekt, K., 1997, A comparative evaluation of CO₂ and R-22 residential air-conditioning systems in a Japanese climate, *In: IEA/IIR Workshop on CO₂ Technologies in Refrigeration, Heat Pump and Air Conditioning Systems*, Trondheim, Norway.
- Pettersen, J., Rieberer, R. and Munkejord, S.T., 2000a, Heat transfer and pressure drop characteristics of evaporating carbon dioxide in microchannel tubes, *4th IIR Gustav Lorentzen Conference on Natural Working Fluids*, Purdue, IN, USA, July
- Pettersen, J., Rieberer, R. and Munkejord, S.T., 2000b, Heat transfer and pressure drop for flow of supercritical and subcritical CO₂ in microchannel tubes, Technical report, TR A5127, SINTEF Energy Research, Refrigeration and Air Conditioning, Trondheim, Norway.
- Polyakov, A. F., 1991, Heat Transfer under Supercritical Pressures. *Adv. in Heat Trans.*, Acad. Press, p. 1-51.
- Rieberer, R., 1998, CO₂ as Working Fluid for Heat Pumps, Doctoral thesis, Graz University of Technology, Institute of Thermal Engineering.
- Schmidt, E.L., Klöcker, K., Flacke, N. and Steimle, F., 1998, Applying the transcritical CO₂ process to a drying heat pump, *International Journal of Refrigeration*, vol. 21
- Swamee, P. K., Jain A. K., 1975, Explicit Equations for Pipe-Flow Problems. *Journal of the hydraulic division, Proc. of the American Society of Civil Engineers*, Vol. 102, No. HY5, p. 657-664
- VDI, 1994, VDI-Wärmeatlas, Düsseldorf, Germany, VDI-Verlag.

IIF-IIR – Commission B1, B2, E1, and E2 – Purdue University, USA – 2000

CARACTÉRISTIQUES DES TRANSFERTS THERMIQUES ET PERTES DE CHARGE POUR LE DIOXIDE DE CARBONE SUPERCRITIQUE DANS LES TUBES MICROCONDUITS SOUS REFROIDISSEMENT

Cet article fournit les données en transfert thermique et pertes de charge pour le dioxyde de carbone (CO₂) à des pressions super-critiques dans un tube en aluminium extrudé (MPE) plat et à multi-conduits. Le tube dispose de 25 conduits circulaires de 0.79 mm de diamètre intérieur. Les données sont présentées pour les variables suivantes : flux massique de 600 à 1200 kg/(m²s), pression de 81 à 101 bar et flux thermique de 10 à 20 kW/m². L'intervalle de température étudié est de 15 - 70 °C. Les coefficients de transfert thermique mesurés se situent entre 5,000 et 17,500 W/(m²K) et la perte de charge mesurée entre 0.05 et 0.32 bar correspondant à un gradient moyen de pression de 10,000 à 64,000 Pa/m. En outre, les valeurs mesurées ont été comparées à des corrélations disponibles dans la littérature. La corrélation de Gnielinski pour le coefficient de transfert thermique pour une seule phase et la corrélation de Colebrook & White pour la perte de charge ont montré une similitude satisfaisante. Un article d'accompagnement (Pettersen et al., 2000a) présente les résultats des expériences de transfert thermique et perte de charge pour un écoulement à deux phases.

6.2.4 FLOW VAPORIZATION OF CO₂ IN MICROCHANNEL TUBES

Jostein Pettersen

Norwegian University of Science and Technology
Department of Refrigeration and Air Conditioning
NO-7491 Trondheim, Norway
email: Jostein.Pettersen@kkt.ntnu.no

ABSTRACT

Flow vaporization heat transfer coefficient and pressure drop of carbon dioxide was measured in an extruded microchannel tube with 25 flowchannels of 0.8 mm ID and 0.5 m length. The test tube was heated by a water jacket, and the internal heat transfer coefficient was derived based on measured overall heat transfer and a regression-based expression for water-side heat transfer. Test principles are discussed and special emphasis is given to measurement uncertainties, including the propagation of uncertainty through the water-side regression. Studies of two-phase flow pattern were conducted in a separate test rig, using a 0.98 mm heated glass tube and a high-speed digital camera. Heat transfer and pressure drop measurements were conducted at varying vapour fraction for temperatures 0-25°C, mass flux 190-570 kgm⁻²s⁻¹, and heat flux 5-20 kWm⁻². Heat transfer results show significant influence of dryout, particularly at high mass flux and high temperature. Nucleate boiling dominates prior to dryout. Two-phase flow observations show increasing entrainment at higher mass flux, and a dominance of annular flow. Heat transfer data can be correlated reasonably well with a combination of models for nucleate boiling, convective evaporation, dryout incipience, and post-dryout heat transfer.

INTRODUCTION

Carbon dioxide (CO₂ – R-744) is receiving renewed interest as an efficient and environmentally safe refrigerant in a number of applications, including mobile and stationary air conditioning and heat pump systems, and hot water heat pumps. Compact heat exchangers for CO₂ systems are designed with small-diameter tubing [1]. Geometries using flat extruded microchannel tubes with flow through a number of parallel channels give compact and lightweight heat exchangers even with a high-pressure fluid like CO₂, Figure 1.

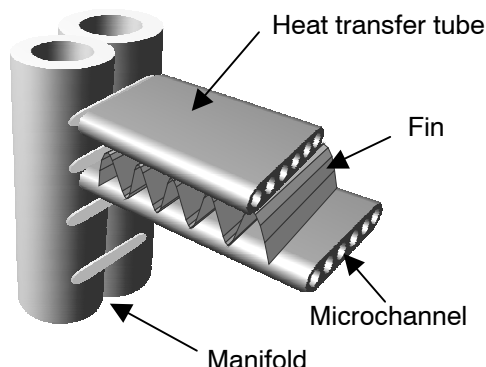


Figure 1 - Principles of CO₂ heat exchanger geometry using “multi-port” extruded tubes with microchannels, folded fins, and a compact “double barrel” manifold [1]. The heat exchanger is assembled by brazing in a furnace

Studies on two-phase flow and heat transfer in microchannel geometries have mostly been focused on low-pressure refrigerants and air/water flow at atmospheric pressure. Even for conventional fluids, the knowledge on

microchannel flow and heat transfer is limited, and very few results have been published on CO₂. Owing to the low critical temperature (31°C), CO₂ vaporization takes place at near-critical pressure. At 0°C, for instance, reduced pressure with CO₂ is 0.47, while for HFC-134a it is 0.07. The resulting “unusual” properties of carbon dioxide give heat transfer and two-phase flow characteristics that are very different from those of conventional refrigerants. Examples of such differences are a much higher pressure, a resulting high vapour density, a very low surface tension, and a low liquid viscosity. High pressure and low surface tension has a major effect on nucleate boiling characteristics, and earlier test data have shown a clear dominance of nucleate boiling even at very high mass flux. Two-phase flow patterns are also greatly affected by these fluid properties

The present paper outlines experimental methods, and shows results from two-phase flow pattern observations and heat transfer and pressure drop measurements for microchannel flow vaporization of CO₂. Results are analysed, and models for correlating the data are developed. Finally, some consequences of the results and findings are discussed.

EXPERIMENTAL METHODS

Heat transfer and pressure drop tests were conducted in a flat, extruded aluminium microchannel tube of 540 mm length with 25 circular channels of 0.81 mm diameter. The tube was installed in a instrumented test section connected to CO₂ and water circuits that controlled flow rates, pressures, temperatures and fluid conditions in the test section. A cross-sectional drawing and enlarged photo of the tube geometry is shown in Figure 2.

The horizontal test tube was heated by a water jacket in order to get representative boundary conditions for air-to-

refrigerant heat transfer (“fluid heating”). Constant heat flux conditions do not simulate these boundary conditions well, and may give unrealistic behaviour especially in relation to dryout and post-dryout heat transfer. The water jacket had flowchannels of hydraulic diameter 5.6 mm that led the water in a spiral flow pattern around the test tube at a pitch of 16.5°.

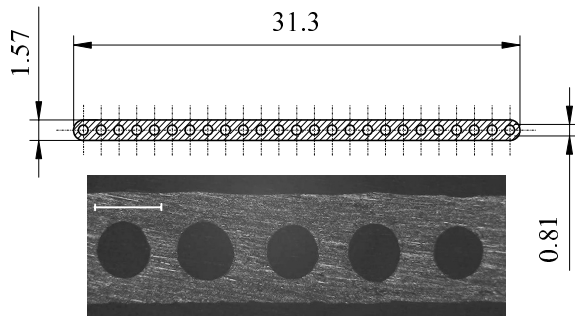


Figure 2 - Cross-section drawing and enlarged photo of the multiport extruded (MPE) test tube (1 mm scale in upper left corner of photo)

Instrumentation and Data Reduction

Important temperatures in the test rig were measured with calibrated Pt-100 sensors, and mass flow rates and pressures were measured with electronic transmitters. Test section heat transfer rate was determined from a water-side heat balance.

The evaporating temperature changed through the test section due to pressure drop, and the water properties were not constant due to temperature and pressure change. A logarithmic mean temperature difference could therefore not be used in finding the overall heat transfer coefficient U of the test section. Pressure changes on the water-side were in fact large enough to influence the water enthalpy significantly. The determination of U was therefore based on a procedure where the test section was divided numerically into $N=60$ elements having equal heat load. Each cell was regarded as small enough to have approximately constant CO₂ temperature and constant water properties. Local refrigerant pressure was assumed to drop linearly with exchanged heat along the test section and a corresponding saturation temperature profile could thus be found. A similar approach was used on the water side, thereby obtaining local water pressures. On this basis, the logarithmic mean temperature difference $\Delta T_{lm,n}$ could be calculated for each cell, and the overall heat transfer coefficient U for the entire test section could be calculated as

$$U = \frac{1}{A_i} \sum_{n=1}^N U_n A_{i,n} = \frac{1}{A_i} \sum_{n=1}^N \frac{\dot{Q}_n}{\Delta T_{lm,n}} \quad (1)$$

It was inherent in the design of the experiment that the overall heat transfer coefficient U was assumed to be constant, and equal in all cells. This assumption is reasonable as long as the change in x from inlet to outlet is small, and as long as the local heat transfer coefficient does not change too much. This assumption may be doubtful in some experiments where dryout occurred inside the test section. In the absence of local data, however, the above method is in fact the only viable solution in order to account for temperature- and pressure variation along the test section.

Data Regression to Correlate Water-Side Heat Transfer

Systematic tests at constant heat flux and with constant liquid CO₂ flow at low temperature inside the tube gave

calibration data that constituted the basis for finding the water-side heat transfer. A regression based on these calibration data gave an equation for water-side heat transfer on the form $Nu = Nu(Re, Pr)$. This equation was then used in the flow vaporization experiments to subtract water-side thermal resistance from the measured overall resistance ($1/UA$), thereby finding the internal heat transfer coefficient. The test section overall heat transfer coefficient U can be expressed as:

$$\frac{1}{U} = \frac{1}{h} + R_{cf} + \frac{1}{h_w} \left(\frac{A_i}{A_o} \right) \quad (2)$$

where the water-side heat transfer coefficient (h_w) can be correlated by

$$Nu = \frac{h_w D}{k} = C \cdot Re^m Pr^n \quad (3)$$

Inserting Eq. (3) into Eq. (2), and reorganizing, we get

$$\left(\frac{1}{U} - R_{cf} \right) \frac{A_o}{A_i} = \frac{1}{C} \cdot Re^{-m} Pr^{-n/3} \cdot \frac{D}{k} + \frac{1}{h} \frac{A_o}{A_i} \quad (4)$$

This is an equation on the form

$$Y = a \cdot X_1^b \cdot X_2 + K \cdot c \quad (5)$$

where the dependent variable is

$$Y = \left(\frac{1}{U} - R_{cf} \right) \cdot \frac{A_o}{A_i} \quad (6)$$

the independent variables are

$$X_1 = Re \quad X_2 = Pr^{-1/3} \cdot \frac{D}{k} \quad (7)$$

and the parameters to be fitted are

$$a = \frac{1}{C} \quad b = -m \quad c = \frac{1}{h} \quad (8)$$

The constant is $K = A_o/A_i = 0.852$. The commercial software package *DataFit* v. 7.1.44 was used to conduct a non-linear least-squares data regression based on the 20 calibration data points. The program used a Levenberg-Marquardt (iterative) method to find the optimum solution. Convergence was obtained with the following results:

$$C = 0.1820, \quad m = 0.6352, \quad h = 9840$$

The water-side heat transfer coefficient could thus be calculated as:

$$Nu = 0.182 \cdot Re^{0.635} Pr^{1/3} \quad (9)$$

A Reynolds number exponent m of 0.635 is significantly lower than the usual value of 0.8 for fully developed turbulent tube flow. The range of water-side Re was generally in the transition region, and fully developed flow could not be expected in the short water channels of the test section. A somewhat lower value therefore seems plausible.

Figure 3 shows results from a comparison of measured U in the calibration tests, and calculated U using the derived correlation and the regression-based CO₂-side single-phase heat transfer coefficient of $9840 \text{ W m}^{-2} \text{ K}^{-1}$. The latter was checked against single-phase models and found to be reasonable. The mean (absolute) deviation between calculated and measured U is 0.29%.

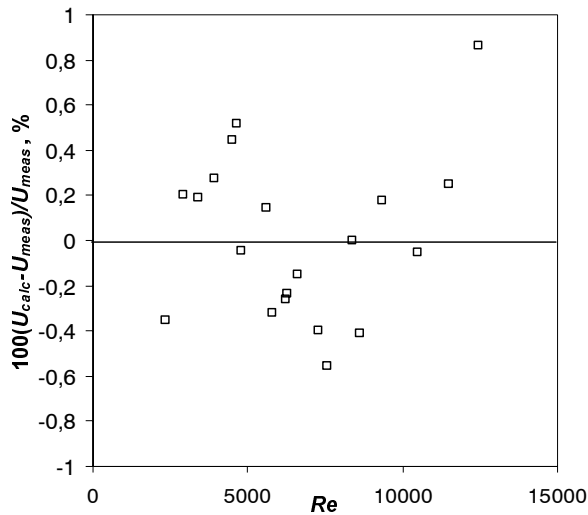


Figure 3 – Deviation between measured test section U and calculated U using Eq. (9), Eq. (2), $h_{co2} = 9840 \text{ Wm}^{-2}\text{K}^{-1}$, and $R_q = 10^{-5} \text{ m}^2\text{KW}^{-1}$

Experimental Uncertainties

Based on uncertainties of temperature, pressure and mass flow measurements, plus uncertainties in geometry parameters, the uncertainties of results could be calculated using propagation analysis [2]. Key uncertainty data are summarized in Table 1.

Table 1 – Uncertainty of main test data

Parameter	Uncertainty
Evaporating temperature, T	$\pm(0.08-0.13) \text{ K}$
Refrigerant mass flux, G	$\pm(2.6-2.8) \%$
Heat flux, q	$\pm(1.8-8.5) \%$
Mean vapour fraction, x	$\pm(0.028-0.137)$
Overall heat transfer coefficient, U	$\pm(2.5-10) \%$

The uncertainty of measured heat transfer coefficient (h) depended on uncertainty of U and h_w . Since h_w was derived based on regression, its uncertainty had to be determined by a propagation analysis through the data regression scheme. A modified procedure based on [3] was used, with perturbations of Re , U and fixed resistance. Details of the scheme are reported in [4]. Resulting uncertainty in h is shown in Figure 4 at $q=20 \text{ kWm}^{-2}$. The relative uncertainty ($\delta h/h$) becomes significant when measuring high heat transfer coefficients, due to the increased influence of water-side resistance ($1/h_w$) and its uncertainty, plus the effect of increased relative uncertainty of the temperature difference between water and CO₂.

Test methods with wall temperature measurement is not likely to give much lower uncertainty, considering the small difference in temperature between tube wall and fluid. In addition, it would be difficult to measure a representative temperature on the surface of a multi-channel tube

Two Phase Flow Visualization Rig

A special rig was built in order to observe two-phase flow patterns. A horizontal quartz glass tube with ID 0.98 mm was coated by transparent resistive coating of indium tin oxide (ITO), and connected to an open fluid circuit where liquid CO₂ was taken from a heated storage cylinder, its pressure reduced and mass flow adjusted by valves before a preheater section that gave the desired x into the observation tube. Heat flux was

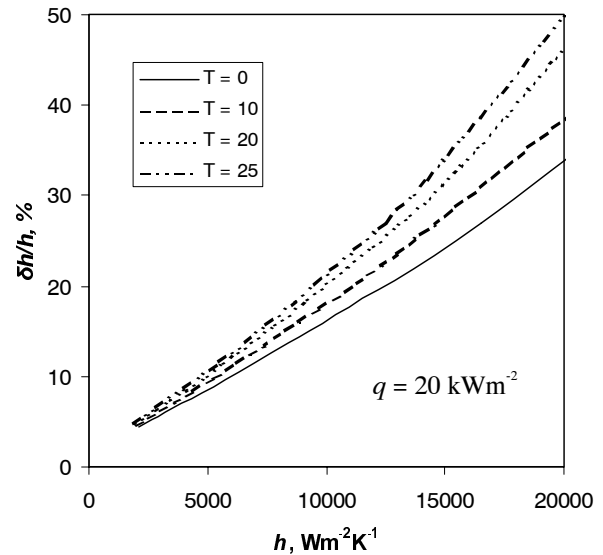


Figure 4 – Relative uncertainty of CO₂ vaporization heat transfer coefficient at varying h and evaporating temperature (T), for a heat flux (q) of 20 kWm^{-2}

obtained by applying DC power to the ITO film, and flow patterns were recorded at 4000-8000 frames per second by a digital video camera. Vapour fraction was measured by heat balance, and mass flow rate by recording the weight of the CO₂ storage cylinder. Compared to “standard” test arrangements, the use of a transparent heated tube enabled flow pattern visualization in the heated zone, and not in an adiabatic observation tube installed after or between heated tubes. In heat transfer dominated by nucleate boiling this makes quite a difference.

FLOW VISUALIZATION RESULTS

Two-phase flow patterns were visualized mainly at a temperature of 20°C, and for CO₂ mass flux ranging from 100 to $580 \text{ kgm}^{-2}\text{s}^{-1}$. Figure 5 shows still photos of flow patterns at a nominal mass flux of $375 \text{ kgm}^{-2}\text{s}^{-1}$ and (equilibrium) x varying from 0.12 to 0.99. Direction of flow was towards left. The camera was normal to the test tube, but pictures were taken from an angle of 28° above horizontal.

Flow was mainly in the wavy annular regime, with considerable entrainment of liquid drops in the core flow. The liquid film on the tube wall was very irregular, and due to the amount of entrained droplets, the film was becoming thin even at moderate vapour fractions. At the lowest vapour fraction, flow was in the dispersed bubble regime, and nucleate boiling could be clearly observed. At $x=0.99$ there was still a notable amount of entrained liquid droplets, indicating a non-equilibrium situation where the vapour phase was becoming superheated. At lower mass flux, intermittent flow regimes were observed at low/moderate vapour fraction. Stratified flow was not observed in any of the tests with heat load.

Figure 6 shows some photos taken at other mass fluxes. The picture at $G=260 \text{ kgm}^{-2}\text{s}^{-1}$ and $x=0.27$ shows a slug flow pattern, where liquid at the front of a slug created an oblong “nose” that protruded into the core. Larger drops detached from this nose and moved in the core flow, and such a drop may be observed in the left part of the picture. This mechanism seemed to be an important source of entrainment, while shear-induced entrainment from wave crests seemed to be less important. The latter type of mechanism can be seen in the picture taken at $x=0.63$.

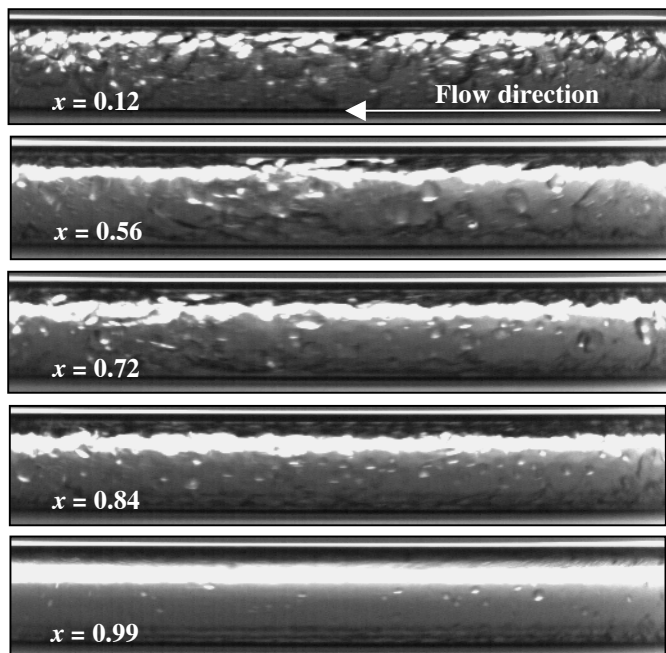


Figure 5 – Two-phase flow patterns in horizontal 0.98 mm ID tube at $T = 20^\circ\text{C}$, $q = 13 \text{ kWm}^{-2}$, $G = 375 \text{ kgm}^{-2}\text{s}^{-1}$, and varying vapour fraction x

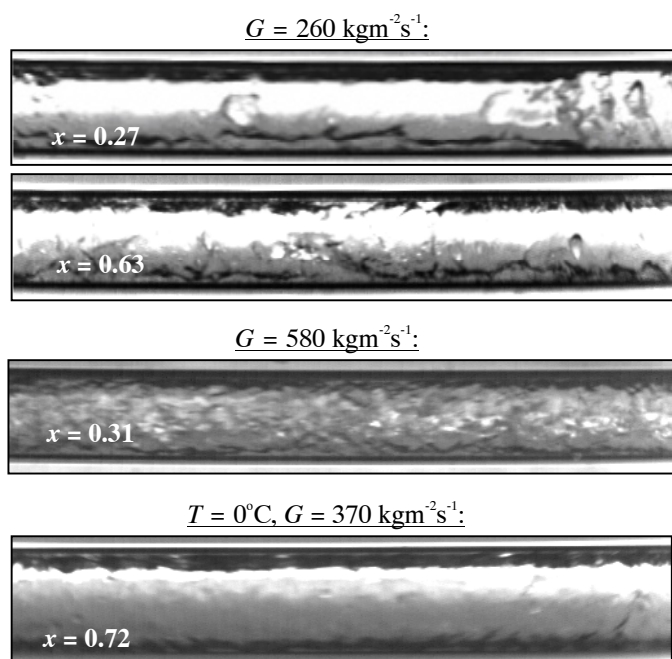


Figure 6 – Flow patterns at mass flux 260 and $580 \text{ kgm}^{-2}\text{s}^{-1}$, $T = 20^\circ\text{C}$, $q = 13 \text{ kWm}^{-2}$, and one observation at $T = 0^\circ\text{C}$ ($G = 370 \text{ kgm}^{-2}\text{s}^{-1}$, $q = 13 \text{ kWm}^{-2}$)

At the higher mass flux. of $580 \text{ kgm}^{-2}\text{s}^{-1}$, the observed flow was annular and with a “mist” flow of liquid droplets in the core. Even though the vapour fraction was moderate, the liquid film appeared to be very thin, and there was a notable difference in velocity between the film and the mist.

The final photo in Figure 6 was taken at a temperature of 0°C , with other conditions similar to the middle picture in Figure 5 ($x = 0.72$). The reduced temperature gave a much smoother liquid film, and the entrainment was considerably lower. Droplet size was smaller than at the higher temperature. Higher liquid surface tension reduced the entrainment and gave a more stable film even though the vapour velocity was much higher at this lower temperature.

Flow Pattern Maps

Figure 7 shows all flow pattern observations at $T = 20^\circ\text{C}$ and $q = 13 \text{ kWm}^{-2}$ in maps using superficial vapour and liquid coordinates (top) and x/G coordinates (bottom). Intermittent flow includes slug, bubble and elongated bubble flow regimes. Approximate lines of transition are indicated. These lines are of course uncertain since the number of data points is limited

From the x/G diagram, the dominance of intermittent flow at low G and the dominance of annular flow at higher G can be observed. The droplet flow regime becomes more important at higher G , a fact that may help explaining the observed dryout problems in heat transfer at higher G , as discussed in the following text.

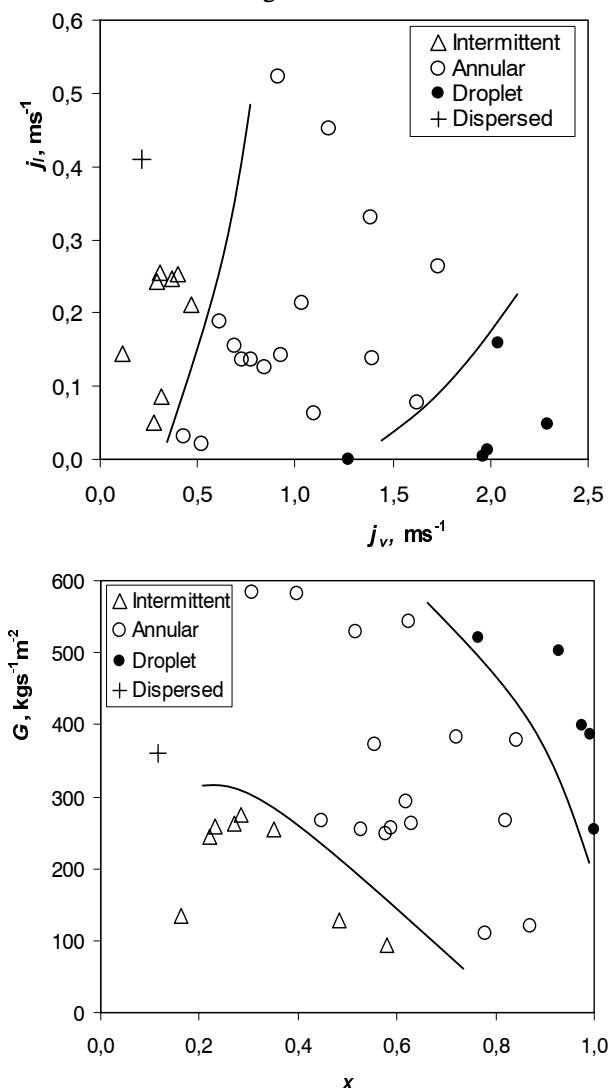


Figure 7 - Flow pattern observations plotted against vapour and liquid superficial velocities in linear scale (top), and against x/G (bottom). Conditions: $D = 0.98 \text{ mm}$, $T = 20^\circ\text{C}$, $q = 13 \text{ kWm}^{-2}$

The flow pattern observations did not fit any generalized maps or transition lines reported in the literature, including the generalized map recently proposed in [5]. Only the intermittent-to-annular transition prediction in [6] was close to the observed behaviour. Compared to small-diameter observations with air/water at low pressure, the transition into annular flow occurred at much lower superficial vapour velocity (superficial velocity of approximately 0.5 ms^{-1}).

HEAT TRANSFER DATA

Flow vaporization heat transfer and pressure drop data were recorded over a wide range of conditions, including temperatures from 0 to 25°C, heat flux from 5 to 20 kWm⁻², mass flux from 190 to 570 kgm⁻²s⁻¹, and vapour fraction between 0.2 and 0.8. The experimental method did not enable measurement of local h and x inside the tube, and the results are therefore mean values over the length of the test section.

Figure 8 shows the effects of varying heat flux on the heat transfer coefficient, at a temperature of $T=10^\circ\text{C}$ and a mass flux G of 280 (top) and 570 kgm⁻²s⁻¹ (bottom diagram).

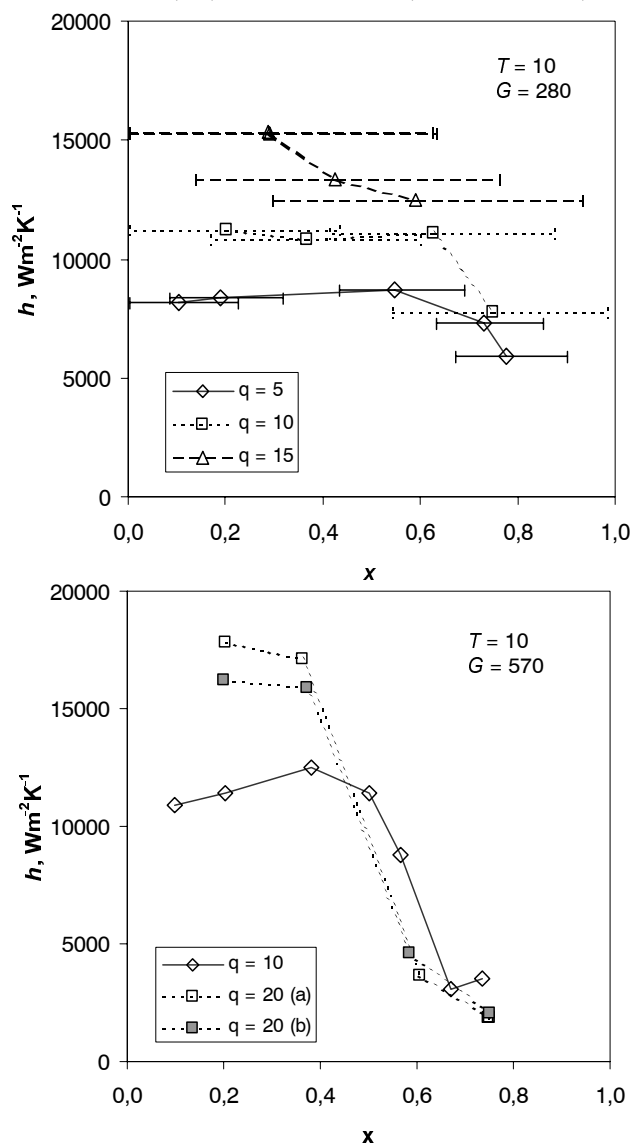


Figure 8 - Measured heat transfer coefficient (h) at varying vapour fraction (x), for heat fluxes (q) 5, 10, 15 and 20 kWm⁻². Evaporating temperature is 10°C and mass flux is $G=280$ (top) and 570 kgm⁻²s⁻¹ (bottom). (a) and (b) are different test series.

The horizontal bars in the top diagram show the change in x through the test section. In the remaining diagrams only the mean points are shown, to avoid problems of reading the data. Varying heat flux has a major effect on heat transfer at low/moderate x , while the data fall together at higher x . A sudden drop in heat transfer at increasing x can be observed in both diagrams, with more extreme variation at high mass flux and heat flux. This drop in heat transfer is probably caused by dryout. The heat transfer coefficient at $q=10$ kWm⁻² is similar

for both mass fluxes at low x . This fact and the heat flux influence indicate nucleate boiling domination at low x .

Figure 9 shows the effects of varying mass flux, at a heat flux of $q=10$ kWm⁻² and temperatures $T=0^\circ\text{C}$ (top) and 10°C (bottom). Again, the drop in heat transfer at increasing x is noticeable, especially at the higher temperature and mass flux. Another important observation from these diagrams is that varying mass flux and vapour fraction (both being related to flow velocity) has almost no influence on heat transfer over a wide range of x . This clearly shows that nucleate boiling is the dominant heat transfer mechanism. The increased heat transfer coefficient at higher temperature is also an indication of nucleate boiling, which becomes more effective at higher satu-

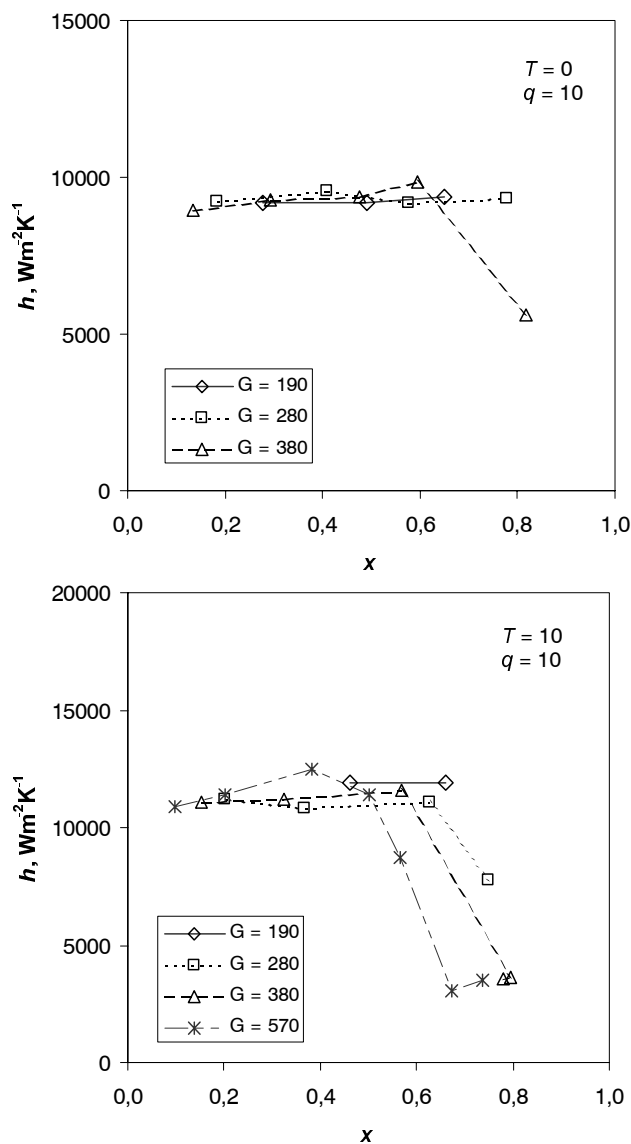


Figure 9 - Measured heat transfer coefficient (h) at varying vapour fraction (x), for mass fluxes (G) 190, 280, 380 and 570 kgm⁻²s⁻¹. Heat flux is $q=10$ kWm⁻² and evaporating temperature is 0°C (top) and 10°C (bottom). Note different scales on h -axis

ration pressure. Finally, some results at varying evaporating temperature are shown in Figure 10, at $G=280$ kgm⁻²s⁻¹ and $q=10$ kWm⁻².

The heat transfer is a strong function of temperature, with almost constant h at 0°C and rising pre-dryout heat transfer coefficients at higher temperatures. The reduction in h with T at higher vapour fraction may be due to reduced flow velocity caused by higher vapour density, possibly in combination with

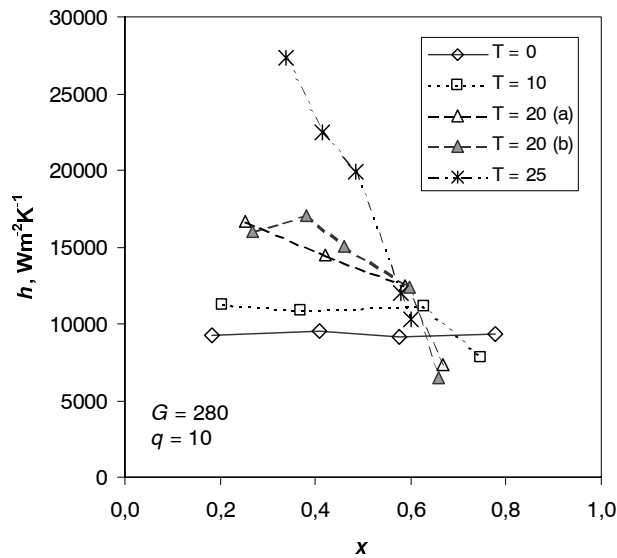


Figure 10 - Measured heat transfer coefficient (h) at varying vapour fraction (x), for evaporating temperatures (T) of 0, 10, 20 and 25°C. $G=280 \text{ kgm}^{-2}\text{s}^{-1}$, and $q=10 \text{ kWm}^{-2}$. Results (a) and (b) are from different test series

non-equilibrium effects due to poor heat transfer between vapour and liquid droplets

DISCUSSION AND CORRELATION OF HEAT TRANSFER DATA

The test results showed that nucleate boiling is important at low/moderate x , while convective evaporation seems to be of minor importance, at least at low/moderate x prior to dryout. Only at a mass flux of $570 \text{ kgm}^{-2}\text{s}^{-1}$ there is some increase in heat transfer with x in Figures 8 and 9. Flow pattern observations showed that flow-induced entrainment became important at higher mass flux, and dryout of the liquid film may occur at these conditions. The flow pattern chart in x/G -coordinates (Figure 7) shows how droplet (post-dryout) flow becomes more dominant at higher G . Post-dryout heat transfer may be affected by non-equilibrium effects, and some of the test data indicate that such effects are present. Local heat transfer data published by others also show significant non-equilibrium effects [7].

Thus, in order to correlate the test data, fundamental models for nucleate boiling, convective evaporation, dryout, and post-dryout heat transfer must be considered. Most “general” heat transfer correlations from the literature lack the necessary mechanistic foundation and fail to reproduce the observed trends in these experiments with the extreme variation in heat transfer caused by dryout/post-dryout [4].

Heat transfer data in the low- x region was compared to various nucleate boiling correlations from the literature. The nucleate (pool) boiling correlation of Cooper [8] predicted 20-30% lower heat transfer coefficient than measured, while the best fit was obtained with the correlation of Gorenflo [9] which gave values 8% above the present test data on average (using a reference coefficient of $4170 \text{ Wm}^{-2}\text{K}^{-1}$). The special small-tube nucleate flow boiling correlation of Tran et al. [10] failed to reproduce the level and trend of the test data at varying temperature, probably since this model does not account for the effects of saturation pressure on boiling heat transfer.

Convective evaporation could maybe have been neglected, at least for moderate/low mass fluxes, but the model proposed by Kattan et al. [11] was included for the sake of

completeness. Nucleate and convective terms were combined using an asymptotic model:

$$h = \left[(h_{nb})^3 + (h_{ce})^3 \right]^{1/3} \quad (10)$$

Onset of dryout (x_{cr}) could be estimated using water dryout data [12] scaled to CO₂ by the method of Ahmad [13], even though we are well outside the limits of applicability in terms of tube diameter, scaling parameter, and tube inlet conditions. The method of Ahmad is a fluid-to-fluid scaling model based on dimensional analysis. A mass flux scaling/modelling parameter ψ is used, based on the Weber number and liquid/vapour superficial Reynolds numbers. Parameters for the fluid concerned (in this case CO₂) must be converted into equivalent values for water, using ψ that should have the same value for both fluids:

$$\psi = \left[\frac{GD}{\mu_l} \right] \left[\frac{\mu_l^2}{\sigma D \rho_l} \right]^{2/3} \left[\frac{\mu_l}{\mu_v} \right]^{-1/5} \quad (11)$$

The second dimensionless group in the above expression may be termed a *Weber-Reynolds* number. Hydraulic diameter (D) is the same for both fluids. If surface tension data are unavailable or inaccurate, it has been suggested to replace the We-Re group and convert the above expression to

$$\psi = \left[\frac{GD}{\mu_l} \right] \left[\frac{\gamma^{0.5} \mu_l}{D \rho_l^{0.5}} \right]^{2/3} \left[\frac{\mu_l}{\mu_v} \right]^{1/8}, \quad \gamma = \left| \frac{\partial(\rho_l / \rho_v)_{sat}}{\partial p} \right| \quad (12)$$

where the second dimensionless group in the expression for ψ is called *Barnett* number. Property data for water should be evaluated at a saturation pressure giving the same density ratio as for the fluid concerned, in this case CO₂, and the heat flux need to be scaled so that the Boiling number is the same for both fluids. Since the present tests did not give local h measurements, a comparison between estimated and measured onset of dryout was done based on the data of Hihara and Tanaka [7], Figure 11. The estimated critical x is correct at higher mass flux, using the We-Re model (Eq.11), while the level is not correct at lower G , and the trend is not reproduced well. Data from the present study indicate earlier onset of dryout than in [7], a fact that may be explained by flow oscillation between parallel flowchannels in the present tests. Such oscillations may reduce critical heat flux considerably [14]. In fact, the Barnett number scaling parameter (Eq.12) seems to give better correspondence to the range of x where the heat transfer coefficient suddenly drops in the present tests.

Non-equilibrium effects during post-dryout heat transfer can be accounted for by using special correlations. The correlation of Shah and Siddiqui [15] seems to reproduce test data well, including the local data of Hihara and Tanaka [7], while the much-quoted model of Groeneveld and Delorme [16] gave larger deviation and incorrect trends at varying x . Table 2 shows a summary of the selected combination of models that gave best correlation of heat transfer test data [4].

In order to get a correct comparison between measured and correlated data, the mean heat transfer coefficient for the range of x in the test section had to be calculated. A special procedure was applied in calculation of the mean coefficient, using the measured G , q , and T . Based on the measured inlet and outlet x to the test section, the mean heat transfer coefficient was calculated for ten “sub-sections” using the following scheme, where x_{in}/x_{out} was the measured inlet and outlet vapour fraction in the test section in each test.

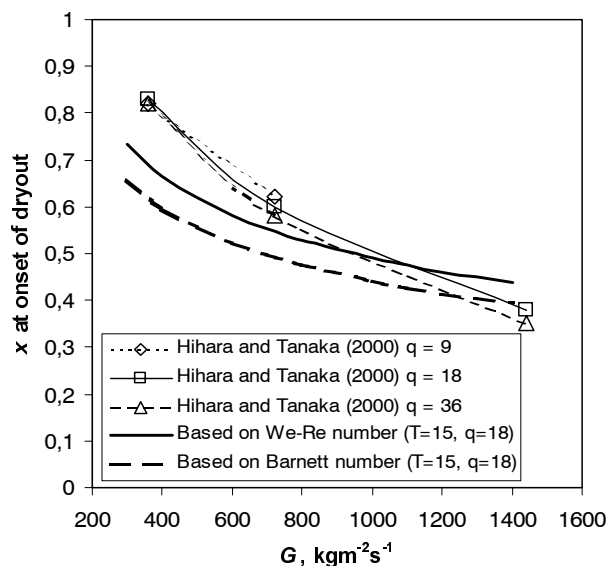


Figure 11 - Predicted dryout x for flow at varying mass flux at 15°C in a 1 mm ID tube, using [12] and [13], compared to experimental local dryout data from Hihara and Tanaka [7]

Table 2 - Models that constitute the basis for correlating CO₂ heat transfer test data

Mechanism	Model	Comment
Nucleate boiling	Cooper [8]	
Convective evaporation	Kattan et al. [11]	Based on estimated film thickness and flow velocity
Model for combining nucleate and convective heat transfer	Asymptotic model,	Eq. (10)
Dryout inception	Kon'kov [12] data scaled from H ₂ O to CO ₂ using Ahmad [13]	Using Barnett number, Eq. (12)
Post-dryout heat transfer	Shah and Siddiqui [15]	

$$h_{calc} = \frac{1}{10} \sum_{i=1}^{10} h(x_i) \quad x_i = x_{in} + \frac{i-0,5}{10} (x_{out} - x_{in}) \quad (13)$$

Figure 12 compares all the 140 test data points to calculated heat transfer coefficients. Average deviation is +7.7% and mean deviation is 35.1 %. Two notable trends can be observed; overprediction at low h which may be caused by too large convective contribution and dryout predicted at too high x , and a general tendency of underprediction due to the nucleate boiling correlation [8] which underpredicts the test data.

One example of measured data points and correlated data are shown in Figure 13, using data from Figure 8. The underprediction of nucleate boiling heat transfer and the “delayed” predicted onset of dryout can be observed in the diagram. Replacing the Cooper [8] nucleate boiling model with the Gorenflo [9] model did not improve correspondence, since low- x data then became significantly overpredicted. Considering the extreme variation in heat transfer, the above fit is quite good, even though the introduction of empirical factors could have given even better correspondence

PRESSURE DROP

Figure 14 shows some pressure drop test data at varying mass flux (top), at a temperature of $T=0^\circ\text{C}$ and heat flux $q=10$

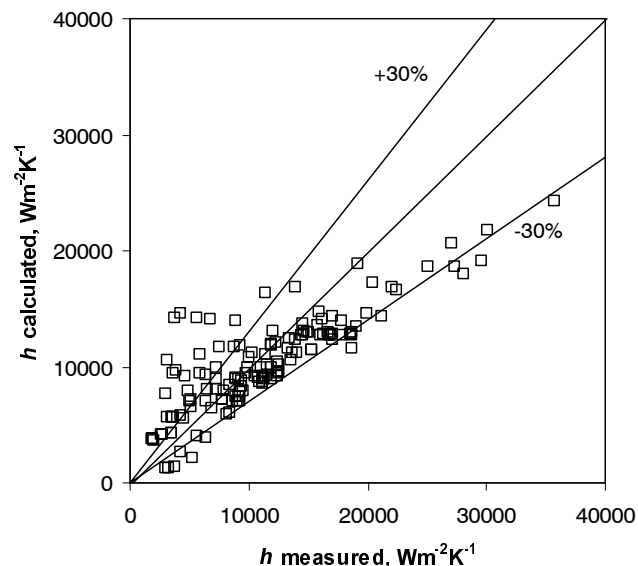


Figure 12 - Comparison of measured and calculated heat transfer coefficients using a combination of models as given in Table 2

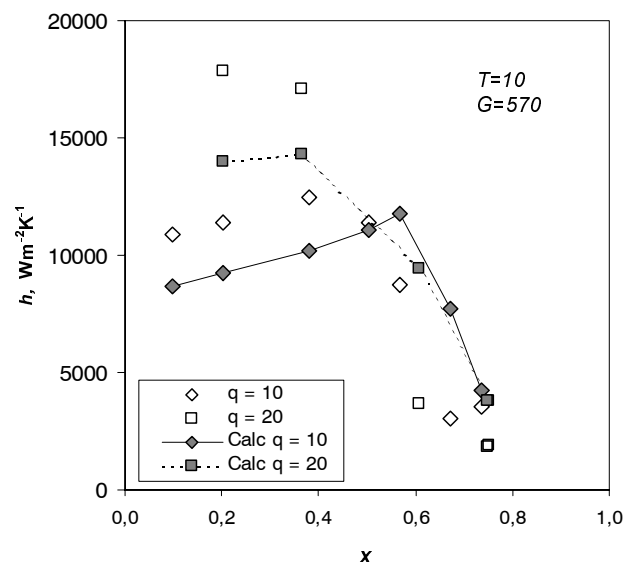


Figure 13 - Measured and calculated (“calc”, using models in Table 1) heat transfer coefficients at $q=10$ and 20 kWm^{-2} , $G=570 \text{ kgm}^{-2}\text{s}^{-1}$ and $T=10^\circ\text{C}$

kWm^{-2} , and at varying temperature (bottom) at mass flux of $G=280 \text{ kgm}^{-2}\text{s}^{-1}$. As expected, the pressure drop is a strong function of mass flux and vapour fraction – both parameters that characterize flow velocity. Larger pressure drop at lower temperature is also as expected, due to the lower vapour density giving higher flow velocity.

Comparing the pressure drop data at $T=0^\circ\text{C}/q=10 \text{ kWm}^{-2}$ to the heat transfer data in Figure 9, it is interesting to note how increased mass flux gives higher pressure drop while heat transfer remains unchanged. As a consequence of nucleate boiling domination, added mass flux does not improve heat transfer much, while added pressure drop may give reduced local temperature difference in a heat exchanger. Measured pressure drops do not increase linearly with x , and this may be due to changes in two-phase flow patterns.

Frictional pressure drop was correlated with a mean/average deviation of 22.3/-17.4% using the Friedel [17] correlation with liquid property data. The underprediction was significant at low pressure drop (low mass flux), and at low temperature. The “CESNEF-2” correlation by Lombardi and

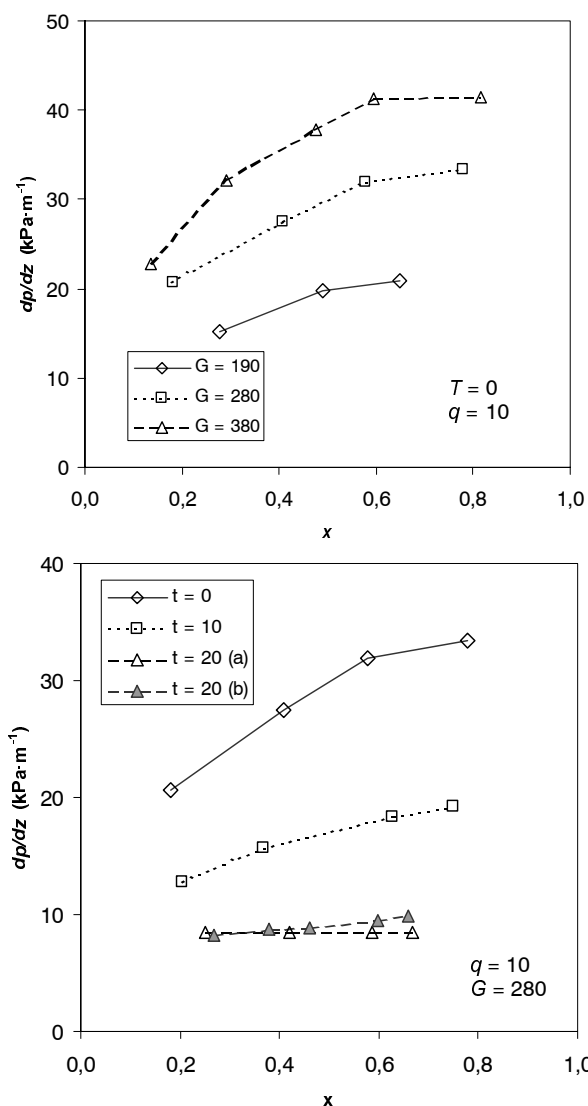


Figure 14 - Pressure drop (dp/dz) at varying vapour fraction (x), for mass flux 190, 280 and 380 $\text{kgm}^{-2}\text{s}^{-1}$ (top) and evaporating temperatures (T) 0, 10 and 20 °C (bottom). Heat flux is 10 kWm^{-2} . Results (a) and (b) are from different test series.

Carsana [18] gave much better accuracy, with a mean/average deviation of 16.4/-1.1%. Comparisons between test data and these correlations are shown in Figure 15. The special small-tube correlations of Tran et al. [19] and Zhang and Webb [20] gave poor correspondence, with mean/average deviation of 80.4/74.5% and 40.5/-40.5%, respectively. The latter model is actually a modified Friedel correlation, but the intended improvement for small-diameter flow did apparently not work well with CO₂.

CONCLUSION

A number of conclusions can be drawn from this investigation on heat transfer, pressure drop and flow patterns in microchannel flow vaporization of CO₂.

Analysis of experimental uncertainties has demonstrated the accuracy of measured heat transfer coefficients using a heat exchanger regression (“Wilson plot”) method. The accuracy of this method has been widely discussed, and very little systematic work has been done on documenting the real uncertainties involved. Results from the present study show that the uncertainty of measured heat transfer coefficients is

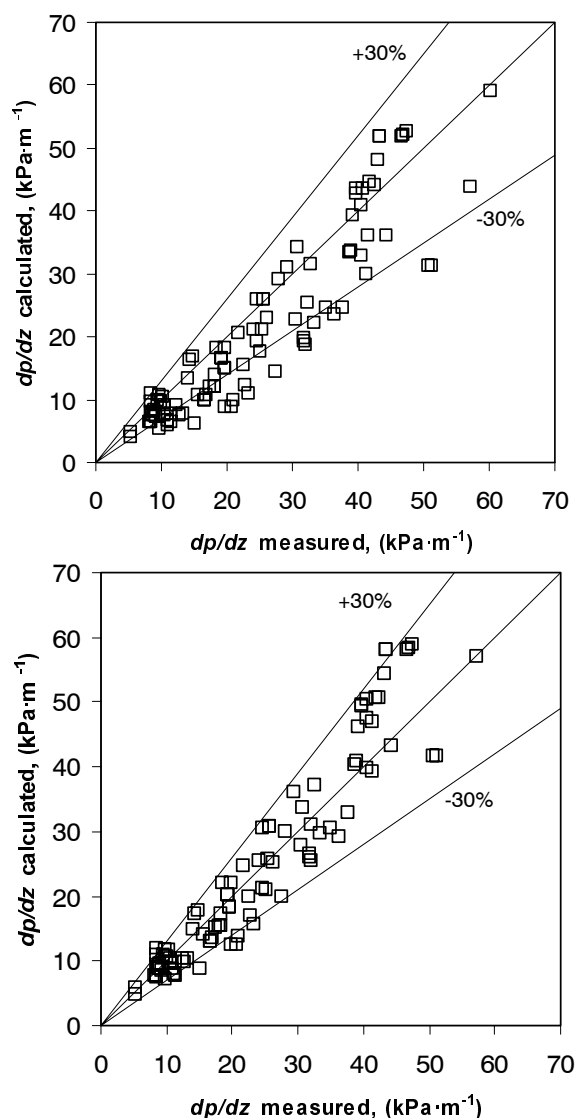


Figure 15 – Comparison between measured and calculated pressure drop data using the Friedel [17] correlation (top) and the “CESNEF-2” correlation by Lombardi and Carsana [18] (bottom)

comparable to what can be obtained by direct measurement of tube wall temperature, provided that the water-side heat transfer coefficient is high enough

Two-phase flow pattern observations have shown a dominance of intermittent and annular flow regimes, the latter becoming more important at high mass flux. Entrainment increases at higher mass flux, and this, together with a very irregular liquid film, may give dryout and reduced heat transfer at moderate vapour fractions. Test results showed that nucleate boiling dominated at low/moderate vapour fractions, where h increased with heat flux and temperature but was less affected by varying mass flux and vapour fraction. Dryout effects became very important at higher mass flux and temperature, where h dropped rapidly at increasing x .

An important consequence of the test results is that efficient compact CO₂ evaporators for mobile or unitary applications can be designed with low mass flux. Increased G does not improve heat transfer while added pressure drop acts negatively by reducing the local temperature difference. Another reason for selecting low mass flux is the increased critical vapour fraction. Thus, dryout can be avoided by reducing G . It follows from this that the evaporator preferably should be fed with liquid only or with a low vapour fraction, and if possible, the evaporator outlet condition should be kept

in the wet region. A secondary advantage of liquid feeding is that flow distribution between parallel channels can be improved, especially at low mass flux.

Further studies in this area should extend the range of test conditions and flow observations, e.g. to lower temperature and lower mass flux, and to other tube diameters. The effects of lubricant on heat transfer and pressure drop also need to be investigated. Lubricant may have considerable influence on nucleate boiling heat transfer.

NOMENCLATURE

A	Area	m^2
C	Constant	-
D	Hydraulic diameter	m
G	Mass flux	$\text{kgm}^{-2}\text{s}^{-1}$
h	Heat transfer coefficient	$\text{Wm}^{-2}\text{K}^{-1}$
j	Superficial velocity	ms^{-1}
k	Thermal conductivity	$\text{Wm}^{-1}\text{K}^{-1}$
p	Pressure	Pa
\dot{Q}	Heat transfer rate	W
T	Temperature	$^{\circ}\text{C}$
R_{cf}	Conduction and fouling resistance	m^2KW^{-1}
q	Heat flux	Wm^{-2}
U	Overall heat transfer coefficient	$\text{Wm}^{-2}\text{K}^{-1}$
x	Vapour mass fraction (quality)	-

Greek symbols

ρ	Density	kgm^{-3}
μ	Dynamic viscosity	Nsm^{-2}
σ	Surface tension	Nm^{-1}

Subscripts

i	inside
l	liquid
lm	logarithmic
o	outside
v	vapour
w	water-side

REFERENCES

- Pettersen, J., Hafner, A., Skaugen, G., and Rekstad, H. 1998. Development of Compact Heat Exchangers for CO₂ Air-Conditioning Systems. *Int. J. Refrig.*, vol. 21, no 3, pp. 180-193, 1998
- Moffat, R. J. Describing the Uncertainties in Experimental Results. *Experimental Thermal and Fluid Science*, vol. 1, pp. 3-17, 1988
- Khartabil, H. F., and Christensen, R. N., An Improved Scheme for Determining Heat Transfer Correlations from Heat Exchanger Regression Models with Three Unknowns. *Experimental Thermal and Fluid Science*, vol. 5, pp. 808-819, 1992.
- Pettersen, J, Flow Vaporization of CO₂ in Microchannel Tubes. Dr. techn. thesis, Norwegian University of Science and Technology, 2002
- Kattan, N., Thome, J. R., Favrat, D., Flow Boiling in Horizontal Tubes : Part 1 – Development of a Diabatic Two-Phase Flow Pattern Map. *Trans. ASME, J. Heat Transfer*, Vol 120, pp. 140-147, 1998
- Weisman, J., Duncan, D., Gibson, J., and Crawford, T., Effect of Fluid Properties and Pipe Diameter on Two-Phase Flow Pattern in Horizontal Lines, *Int. J. Multiphase Flow*, Vol 5, 1979, pp. 437-462, 1979
- Hihara, E., and Tanaka, S. Boiling Heat Transfer of Carbon Dioxide in Horizontal Tubes. Preliminary Proceedings of the *IIR Gustav Lorentzen Conference on Natural Working Fluids*, Purdue University, W. Lafayette, IN, USA, July. pp. 279-284, 2000
- Cooper, M. G., Heat flow rates in saturated nucleate pool boiling – a wide-ranging examination using reduced properties, *Advances in Heat Transfer*, Vol 16, pp. 157-239, 1984
- Gorenflo, D., Pool Boiling. Chapter Ha in *VDI Heat Atlas*, English translation of VDI –Wärmeatlas, 6. auflage. Edited by VDI Gesellschaft Verfahrenstechnik und Chemieingenieurwesen. VDI-Verlag, 1993
- Tran, T. N., Wambsganss, M. W., Chyu, M.-C. and France, D. M., A Correlation for Flow Boiling in Small Channels. Proc. *International Conference on Compact Heat Exchangers for the Process Industries*, Snowbird, Utah, USA, June 22-27, pp. 353-363, 1997
- Kattan, N., Thome, J. R., Favrat, D., Flow Boiling in Horizontal Tubes : Part 3 – Development of a New Heat Transfer Model Based on Flow Pattern. *Trans. ASME, J. Heat Transfer*, Vol 120, pp. 156-165, 1998
- Kon'kov, A. S., Experimental Study on the Conditions under which Heat Exchange Deteriorates when a Steam-Water Mixture Flows in heated Tubes. *Teploenergetika*, Vol 13, No 12, pp. 77, 1965
- Ahmad, S. Y., Fluid to fluid modeling of critical heat flux: A compensated distortion model. *Int. J. Heat Mass Transfer*. Vol 16, pp. 641-662, 1973
- Umekawa, H., Ozawa, M., Mitsunaga, T., Mishima, K., Hibiki, T., and Saito, Y., Scaling Parameter of CHF under Oscillatory Flow Conditions, *Heat Transfer – Asian Research*, Vol 28 No 6, pp. 541-550, 1999
- Shah, M.M., and Siddiqui, M.A., A General Correlation for Heat Transfer During Dispersed-Flow Film Boiling in Tubes, *Heat Transfer Engineering*, Vol 21 No 4, pp. 18-32, 2000
- Groeneveld, D. C., and Delorme, G. G. J., Prediction of Thermal Non-Equilibrium in the Post-Dryout Regime. *Nuclear Engineering and Design*, Vol 36, pp. 17-26, 1976
- Friedel, L., Improved friction pressure drop correlations for horizontal and vertical two-phase pipe flow, Presented at the *European Two-phase Flow Group Meeting*, Ispra, Italy, paper E2, June, 1979
- Lombardi, C., and Carsana, C. G., A dimensionless pressure drop correlation for two-phase mixtures flowing upflow in vertical ducts covering wide parameter range, *Int. J. Heat and Technology*, Vol 10, No 1-2, pp. 125-141, 1992
- Tran, T. N., Wambsganss, M. W., and France, D. M., 1999, Two-phase Pressure Drop of Refrigerants During Flow Boiling in Small Channels: An Experimental Investigation and Correlation Development. *Int. Conference On Compact Heat Exchangers and Enhancement Technology for the Process Industry*, Banff, Canada, July 18-23, pp 293-302, 1999
- Zhang, M., and Webb, R. L., Correlation of two-phase friction for refrigerants in small-diameter tubes, *Experimental Thermal and Fluid Science*, Vol 25, pp. 131-139, 2001

KEYNOTE LECTURE

6.2.5 TWO-PHASE FLOW PATTERNS DURING MICROCHANNEL VAPORIZATION OF CO₂ AT NEAR-CRITICAL PRESSURES

Jostein Pettersen

Jostein.Pettersen@kkt.ntnu.no

Norwegian University of Science and Technology
Department of Energy and Process Engineering
NO-7491 Trondheim, NORWAY

ABSTRACT

Carbon dioxide (CO₂ / R-744) is receiving renewed interest as a refrigerant, in many cases based on systems with microchannel heat exchangers that have high pressure capability, efficient heat transfer, and compact design. A good understanding of two-phase flow of evaporating CO₂ in microchannels is needed to analyze and predict heat transfer. A special test rig was built in order to observe two-phase flow patterns, using a horizontal quartz glass tube with ID 0.98 mm, externally coated by a transparent resistive film. Heat flux was obtained by applying DC power to the film, and flow patterns were recorded at 4000 or 8000 frames per second by a digital video camera. Flow patterns were recorded for temperatures 20°C and 0°C, and for mass flux ranging from 100 to 580 kgm⁻²s⁻¹. The observations showed a dominance of intermittent (slug) flow at low x , and wavy annular flow with entrainment of droplets at higher x . At high mass flux, the annular/entrained flow pattern could be described as dispersed. The aggravated dryout problem reported from heat transfer experiments at high mass flux could be explained by increased entrainment. Stratified flow was not observed in the tests with heat load. Bubble formation and growth could be observed in the liquid film, and the presence of bubbles gave differences in flow pattern compared to adiabatic flow. The flow pattern observations did not fit generalized maps or transition lines showed in the literature.

INTRODUCTION

Thanks to its environmental and personal safety features, carbon dioxide (CO₂ – R744) is receiving renewed interest as a refrigerant in a number of applications, including mobile and stationary air conditioning and heat pump

systems, and hot water heat pumps. In many heat pump applications, CO₂ systems can offer improved efficiency and capacity, as well as high output temperature. Compact heat exchangers for CO₂ systems can be designed with small-diameter tubing (Pettersen et al. 1998). Geometries using flat extruded microchannel tubes with flow through a number of parallel small-diameter channels give compact and lightweight heat exchangers even with a high-pressure fluid like CO₂.

Studies on two-phase flow and heat transfer in microchannel geometries have mostly been focused on low-pressure refrigerants and air/water flow at atmospheric pressure. Even for conventional fluids, the knowledge on microchannel two-phase flow and heat transfer is limited, and very few results have been published on CO₂.

Owing to the low critical temperature (31°C), CO₂ vaporization takes place at near-critical pressure. At 0°C, for instance, reduced pressure of CO₂ is 0.47, while for a more conventional fluid like HFC-134a it is 0.07. The resulting “unusual” properties of carbon dioxide give heat transfer and two-phase flow characteristics that are very different from those of conventional refrigerants. A high boiling pressure gives high vapor density, low surface tension, and low liquid viscosity.

CO₂ vapor and liquid densities, and liquid surface tension, are shown in Fig. 1 and 2, respectively. Two-phase flow patterns are influenced to a large extent by these fluid properties, and high pressure and low surface tension also has a major effect on nucleate boiling characteristics.

Earlier heat transfer test data have shown a dominance of nucleate boiling even at very high mass flux conditions for CO₂. The local experimental data of Hihara and Tanaka (2000) showed dramatic and abrupt changes in local heat transfer coefficient at moderate to high vapor mass fraction (x), a behavior that was probably caused by dryout. The onset of dryout occurred at lower x when the mass flux was increased.

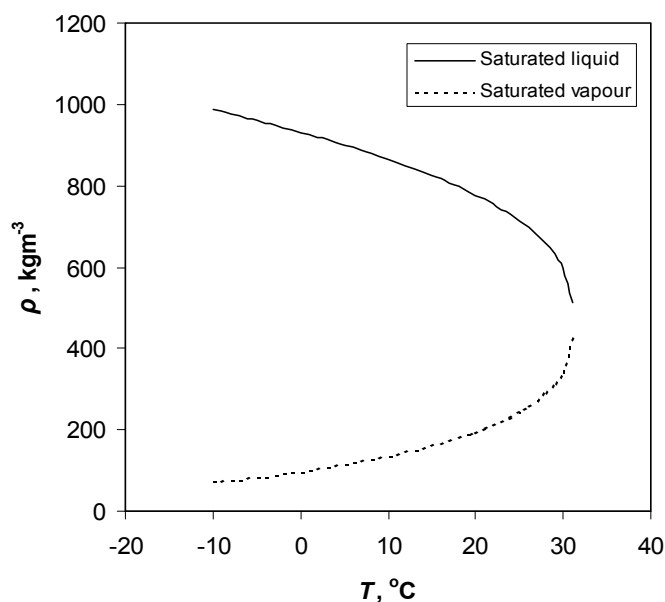


Figure 1 Saturated liquid and vapor density for CO₂

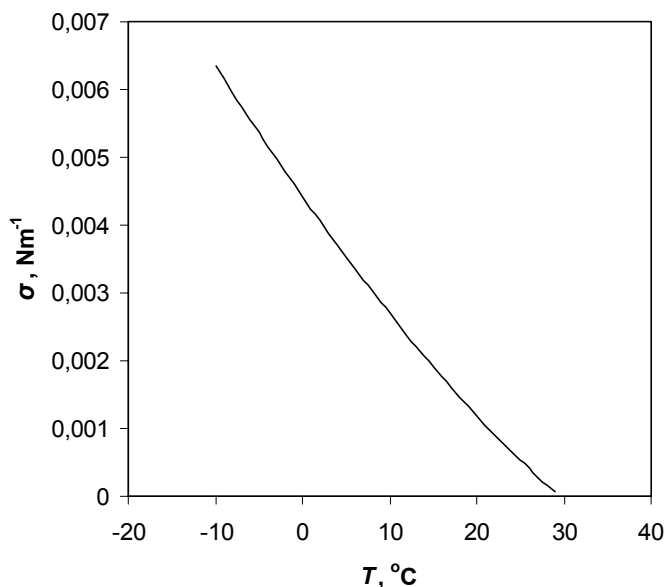


Figure 2 Surface tension of saturated CO₂ liquid

The test data also showed significant non-equilibrium effects in post-dryout heat transfer, i.e. superheated vapor with entrained liquid droplets. Since two-phase flow patterns inside the test tube was not observed by Hihara and Tanaka (2000), the dryout theory could not be confirmed. Furthermore, their measurements were conducted in a single stainless-steel tube under constant heat-flux conditions (electric heating).

The present study was initiated in order to visualize and evaluate the two-phase flow conditions during microchannel flow vaporization of CO₂. After outlining the experimental methods and test program, the paper shows results from two-phase flow pattern observations. The observations are analyzed in relation to generalized charts and prediction

methods for flow patterns, and conclusions are drawn with respect to consequences of the results.

EXPERIMENTAL RIG

In the design of an experimental rig to observe flow patterns in microchannels during vaporization of CO₂, a number of challenges had to be coped with:

- Owing to the small tube diameter and high flow velocity, a magnified, high-speed recording was needed.
- Owing to the high saturation pressure, special care was needed in the preparation of the test section to meet safety requirements without seriously impairing observation possibilities.
- The phenomena to be observed were related to diabatic flow conditions, and the addition of heat flux to the observation tube was thus desired (again without impairing the observation possibilities).

A combination of a glass tube with sufficient wall thickness and a high-speed camera with magnifying optics was chosen. A “standard” quartz glass tube of ID/OD 0.98/6.35 mm was pressure tested and found capable of withstanding 25 MPa without breaking. It was thus decided to use this type of tube in the flow observations. Two different options for applying heat load to the observation tube were evaluated; a water jacket in a transparent outer tube, and a transparent resistive film coating on the glass tube. The last option gave the least effect on transparency, and was thus selected. In contrast to most earlier studies on flow pattern in evaporator tubes, where glass tube sections are installed after or between heated sections, this arrangement gives flow pattern observation inside the heated zone. This may not be of great importance in larger tubes and at conditions where the vaporization is dominated by convective effects, where the flow pattern is maintained through the adiabatic section. In microchannel flow, and especially when the heat transfer is dominated by nucleate-boiling, however, the use of an unheated observation section that is very long compared to the tube diameter is not acceptable.

Since the refrigerant mass flow rate in a single tube would be quite small, it was decided to use an open circuit where CO₂ was taken from the liquid phase of a storage cylinder, metered through a control valve, preheated to reach the desired vapor fraction at the observation section, and finally expanded to atmospheric pressure and discharged from the circuit after passing through the observation tube. The circuiting of the test system, and its instrumentation and components is shown in Fig. 3

A commercial CO₂ storage cylinder with internal riser tube was placed on a scale to measure average mass flow rate during the test period. A heater blanket wrapped around the cylinder controlled the temperature and maintained a slightly higher pressure than in the test section.

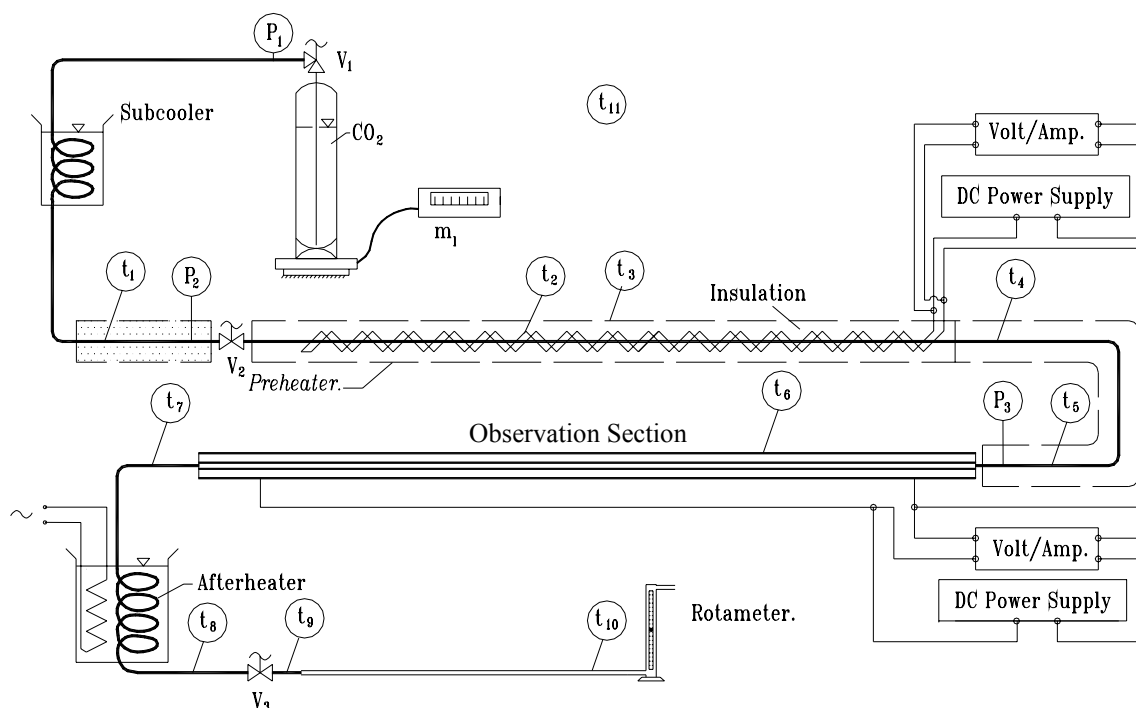


Figure 3 Flow circuit and instrumentation of experimental rig

A subcooling coil on the line from the CO₂ cylinder was submerged in ice/water to control the temperature at the inlet of the manual metering valve (V_2), which expanded the liquid CO₂ down to the evaporating pressure/temperature. The CO₂ flow then entered the preheater section, which consisted of a stainless steel tube with heating wires, all coated by thermal insulation. Heat load in the preheater was controlled by regulating the DC voltage and current applied to the heating wires.

After the test section, the refrigerant flow was taken through a coil submerged in heated water. This was done in order to evaporate any remaining liquid which otherwise could form dry ice in the final expansion valve (V_3) that reduced the pressure down to atmospheric pressure. Finally, a rotameter was used to monitor refrigerant flow rate during adjustment of conditions.

The instrumentation consisted of surface thermocouples at the locations shown in Fig. 3, and manometers at p_1 , p_2 and p_3 . CO₂ mass flow rate was measured by a scale with a resolution of 1 g, and voltage/current to the preheater section and observation section were measured by volt/ampere meters.

Observation tube and camera equipment

The horizontal quartz glass observation tube was installed in a steel frame that supported the glass tube. Sealing between the glass tube and the steel frame was obtained by threaded packing glands. Main specifications of the observation tube are given in Table 1. Heating of

the observation tube was achieved by applying DC voltage to a resistive coating film of transparent Indium Tin Oxide (ITO). Wires were strapped around the tube perimeter at each end of the ITO film to serve as electrical connectors.

A high-speed digital camera recorded flow-patterns inside the observation tube at a location 65 mm downstream from the start of the heated part of the test section. A relatively short distance (but still corresponding to 66 tube diameters) was chosen to reduce the uncertainty in local x caused by heat loss to/from the observation tube.

The camera had an observation angle 28 degrees above the horizontal, i.e. the images were taken slightly from above. Images were recorded for a test period of 1 second, and downloaded from the camera to a PC. For a recording rate of 4000 frames per second (fps), the recording image was 512x128 pixels. In some of the tests at higher mass flux, a recording rate of 8000 fps was used and only 50% of the image size could be recorded. The shutter speed was typically 15 microseconds.

Camera Software was used in the processing of the images, including generation of still images, video clips, and measurements of dimensions and velocities.

Test principles

Most of the flow-pattern recordings were taken at 20°C evaporating temperature, to reduce the uncertainties due to heat losses to/from the test section and the preheater, and to be able to focus on the temperature

range where the dryout effects were of greatest importance.

Tests were conducted in series at constant mass flux, and increasing heat load in the preheater, thereby giving points of increasing vapor fraction in the observation tube. Once stable operating conditions were reached, temperatures, pressures, heat loads and mass flow data were recorded, and a flow pattern recording was made.

Table 1 Test section data

Tube inside/outside diameter	0.98 / 6.5	mm
Tube length	570	mm
Length of heated section	442	mm
Electrical resistance of film	237	Ohm

EXPERIMENTAL PROGRAM

In order to separate between the different flow patterns that were observed, a classification system was used, as shown in Table 2. The degree of detail that can be illustrated in flow regime charts is limited, and only the major flow regimes are identified in the charts. In the list of test data and observation shown in the Appendix, however, the patterns in most flow situations are characterized in some more detail, using the flow pattern terminology of Table 3. The term “droplet” flow could have been replaced by “mist” flow, but since the liquid droplets were quite large compared to the tube diameter, the pattern did not associate well with “mist” even though the droplets had a diameter only of a fraction of a millimetre.

Table 2 Classification of flow regimes

Major flow regime	Flow pattern
<i>Stratified</i>	<i>Smooth</i>
	<i>Wavy</i>
<i>Intermittent</i>	<i>Bubble</i>
	<i>Elongated bubble</i>
	<i>Slug</i>
<i>Annular</i>	<i>Smooth</i>
	<i>Wavy</i>
	<i>(E) - With entrainment</i>
<i>Dispersed</i>	<i>Bubble</i>
<i>Droplet</i>	

RESULTS

Fig. 4 shows still photos of flow patterns at four different nominal mass fluxes and varying (equilibrium) vapor fraction x . Direction of flow was towards left. At a mass flux of $100 \text{ kgm}^{-2}\text{s}^{-1}$, the flow regime changed from

intermittent to annular flow as the vapor fraction was increased. Observed flow patterns included elongated bubble flow at $x=0.16$, slug flow at $x=0.48$ and 0.58 , and annular (smooth) flow at $x=0.78$ and 0.87 . Nucleation and growth of vapor bubbles could be observed in the low- x recordings, showing heat transfer dominated by nucleate boiling. Entrainment of liquid droplets in the vapor phase was generally not observed at this mass flux. In the annular flow observations, flow was quite unstable, with varying amounts of bubbles in the film depending on the flow velocity. The latter effect could indicate some suppression of nucleate boiling. The row of drops on the tube wall at $x=0.87$ could not be easily explained; one possible reason may be “rivulet flow” as observed by Barajas and Panton (1993) for liquid/surface combinations giving large contact angle.

At $G=250 \text{ kgm}^{-2}\text{s}^{-1}$, the change from intermittent (elongated bubble or liquid slug flow pattern) to annular flow regime occurred at a vapor fraction of about 0.4. The annular patterns were of a wavy character with irregular liquid film, and there was considerable entrainment of liquid drops/droplets in the vapor core flow. Nucleate boiling could be observed in the liquid slugs at lower vapor fraction. In many cases the front of an advancing slug developed a liquid “nose” that protruded into the vapor core. This seemed to be a significant source of entrainment when liquid drops detached from the “nose”. In some cases, drops were sheared off from waves in the liquid film. Thickness of the liquid film was reduced at higher x , and almost no film was left at $x=0.82$. Entrained droplets could still be observed, however. Similar tendencies could be observed at $G=380 \text{ kgm}^{-2}\text{s}^{-1}$, although the lowest vapor fraction ($x=0.12$) now gave a dispersed bubble flow pattern. The annular-flow liquid films were quite irregular/unstable. The number of entrained droplets seemed to be higher at $G=380 \text{ kgm}^{-2}\text{s}^{-1}$ than at $G=250 \text{ kgm}^{-2}\text{s}^{-1}$, and drops were still present in the core at $x=0.99$, thus indicating a non-equilibrium situation where the vapor was becoming superheated.

At a mass flux of $550 \text{ kgm}^{-2}\text{s}^{-1}$, the picture size (number of pixels) had to be reduced since the recording rate was increased from 4000 to 8000 frames per second. The photo at $x=0.40$ is reduced vertically, while the photos at higher x are reduced horizontally. Flow patterns at this mass flux was quite different from the lower mass flux recordings, with an apparent “dispersed” core flow and a thin unstable liquid film which could be seen flowing at lower velocity than the core. For $x=0.77$, there seems to be only minor amounts of liquid left in the bottom of the tube, while the entrained amount seems to be quite large. Reduced film thickness and disruptions in the liquid layer due to instability could cause dryout in this situation.

The effects of evaporating temperature are illustrated by results from two experiments (Test 21 and 41), conducted at a nominal temperature of 0°C instead of 20°C . The nominal mass flux was $250 \text{ kgm}^{-2}\text{s}^{-1}$ in Test

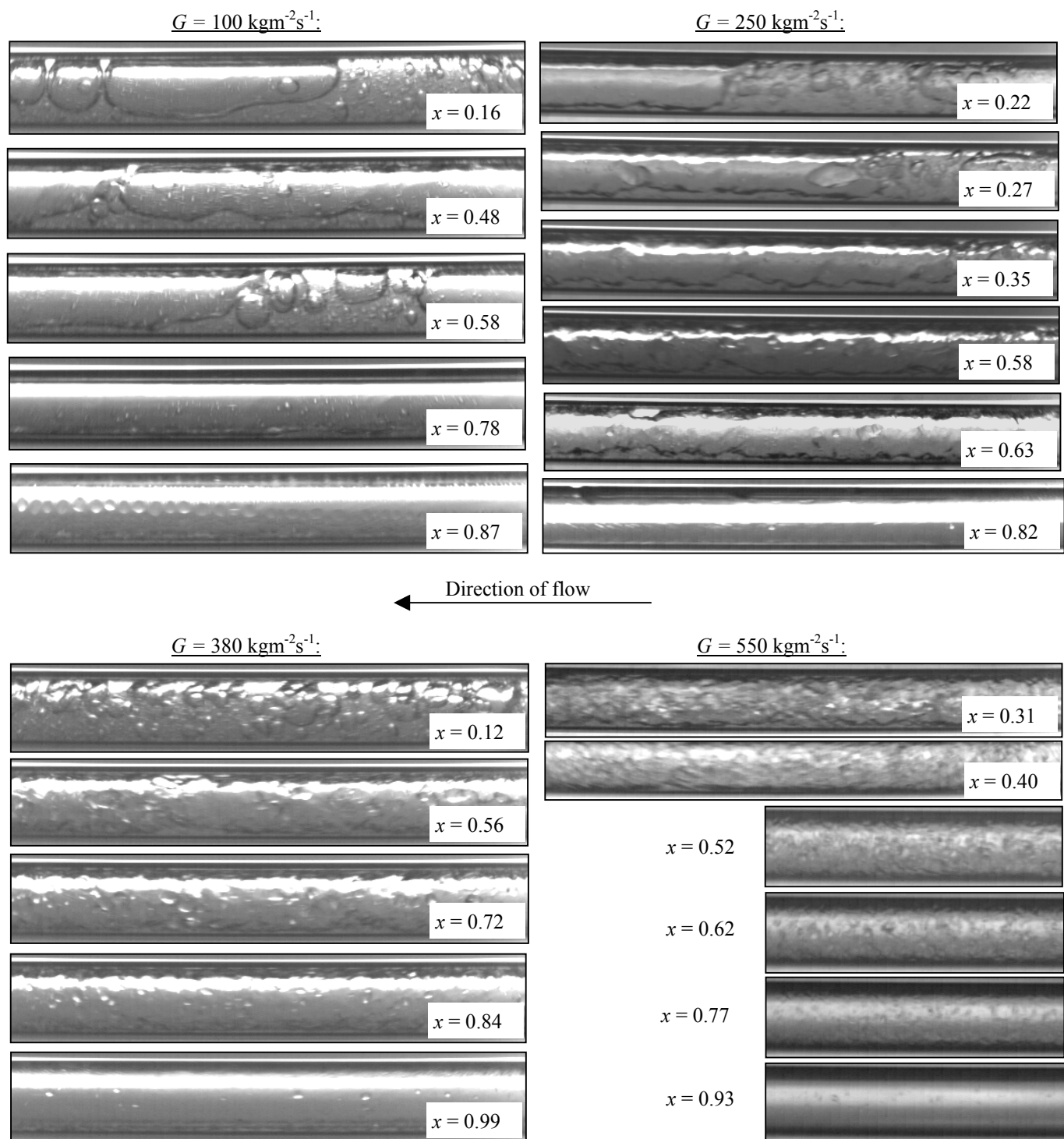


Figure 4 Two-phase flow patterns in horizontal 0.98 mm ID tube at $T = 20^\circ\text{C}$ and $q = 13 \text{ kWm}^{-2}$, for varying mass flux G and vapor fraction x

21, i.e. at conditions comparable to Test 7 at 20°C , and the mass flux was $400 \text{ kgm}^{-2}\text{s}^{-1}$ in test 41, i.e. at conditions comparable to Test 35. An image from Test 21 is shown in Fig. 5, in comparison to the Test 7 image. As may be observed, the flow was annular, with a quite smooth liquid film having only small waves. A few small

entrained drops could be observed at 0°C . The flow pattern fluctuated quite a bit over the one-second recording time, with a large variation in film thickness, and fronts of liquid occurred intermittently. This could have been caused by flow instabilities in the test rig. The occurrence of liquid droplets was also intermittent.

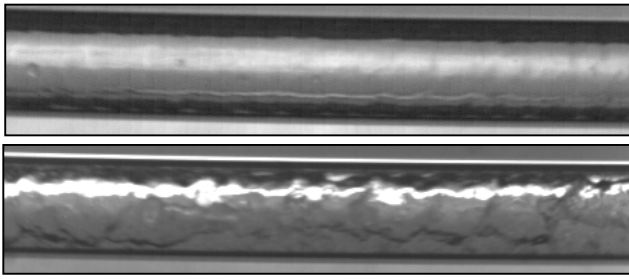


Figure 5 Flow pattern in Test 21(top) at conditions $T=-1^{\circ}\text{C}$, $G=229\text{ kgm}^{-2}\text{s}^{-1}$, $x=0.42$. The lower image is from Test 7, at comparable conditions but a temperature of 20°C .

Compared to the flow pattern in Tests 6, 7 and 8 at similar x and G but at higher temperature, the pattern was quite different. While the higher-temperature recordings showed very unstable liquid/vapor interface, and large entrained drops, the reduced-temperature test had a much more stable smooth wavy interface even though the vapor velocity and the slip velocity was more than twice as high.

A similar comparison at higher mass flux gave the same tendencies. Fig. 6 shows an image from Test 41 with a mass flux of $379\text{ kgm}^{-2}\text{s}^{-1}$ at a temperature of 0°C ($x=0.72$), compared to the flow pattern at the same G and x at 20°C (Test 35). The liquid surface was smoother at the lower temperature, the vapor core contained much less entrained drops/droplets, and the droplets were generally smaller.

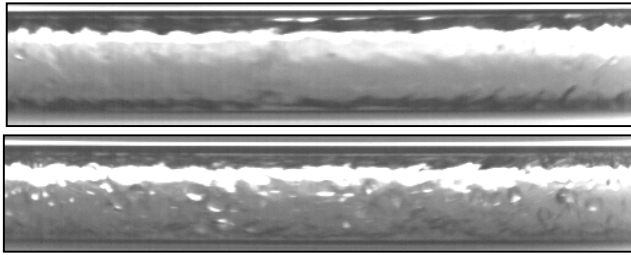


Figure 6 Flow pattern in Test 41(top) at conditions $T=0^{\circ}\text{C}$, $G=379\text{ kgm}^{-2}\text{s}^{-1}$, $x=0.72$. The lower image is from Test 35, at comparable conditions but a temperature of 20°C .

DISCUSSION

In analyzing the flow pattern observations, a key question is whether the transitions between flow regimes can be predicted by generalized chart types and transition lines discussed in the literature. In addition, the observations can be compared to published charts based on experiments in small-diameter air/water flow.

Fig. 7 shows two of the transition lines proposed by Weisman et al. (1979); for transition between intermittent

and annular flow, and for transition into the dispersed flow regime at increasing liquid superficial velocity.

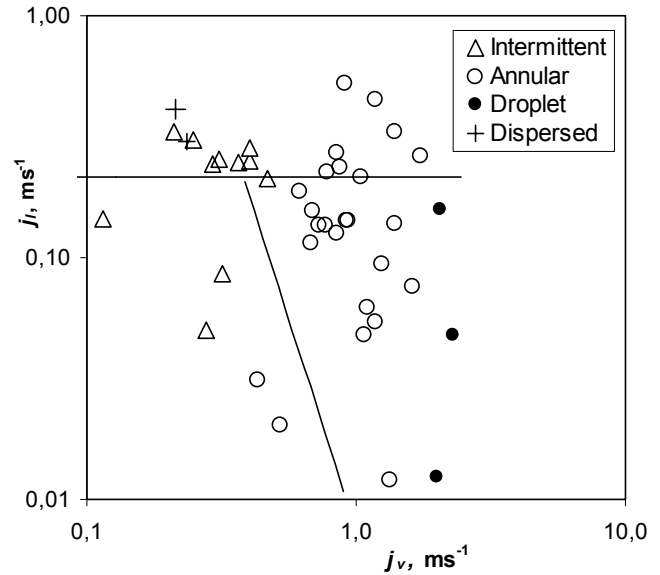


Figure 7 Flow pattern observations for CO₂ at 20°C in relation to transition lines proposed by Weisman et al., (1979) (regime names in CAPITAL ITALICS).

The intermittent/annular transition line of Weisman et al. (1979) is close to predicting the observed behavior, even though a few points fall on the “wrong” side of the line and the slope apparently should have been in the opposite direction. This line is given by:

$$1.9 \left(\frac{j_v}{j_l} \right)^{1/8} = \left(\frac{j_v \rho_v^{1/2}}{[g(\rho_l - \rho_v)\sigma]^{1/4}} \right)^{0.2} \left(\frac{j_v^2}{gD} \right)^{0.18} \quad (1)$$

Coleman and Garimella (1999) also noted that this transition line was close to their experimental air/water observations in a 1.3 mm ID tube. The Weisman transition line into dispersed flow does not fit the data, however, predicting transition at a moderate liquid superficial velocity (0.22 ms^{-1}). Coleman and Garimella (1999) observed the opposite tendency, so this transition prediction seems questionable as a general tool.

Weisman et al. (1979) also gives a transition line into stratified flow, giving a horizontal line at a liquid superficial velocity of 0.00006 ms^{-1} , corresponding to a liquid flow rate that probably cannot be observed in practice. The possible occurrence of stratified flow below this j_l has no practical significance, since x will be equal to 1.0. Stratified flow was not observed in the experiments with $q>0$.

Compared to the observed transitions of Damianides and Westwater (1988), and Coleman and Garimella (1999), the present observations show some important differences. The air–water two-phase flow map of

Damianides and Westwater (1988) show transition from intermittent (slug) flow to annular flow at vapor superficial velocity of 20–40 ms⁻¹, i.e. almost two decades higher than in the present study. Stratified flow was not observed by Damianides and Westwater (1988).

Coleman and Garimella (1999) observed transition from intermittent to wavy annular flow at about $j_v = 6$ ms⁻¹ in a 1.3 mm ID tube with air/water flow, and transition to annular flow at about 20 ms⁻¹ for a wide range of liquid superficial velocity. Stratified flow was not observed. The absence of stratified flow and the transition to dispersed flow show some similarities to the present observations on CO₂, while transition to annular flow occurs at much lower vapor velocity with CO₂ than with air/water at low pressure. Another difference is the absence of droplet or mist flow patterns in the air/water tests. Several authors have claimed that surface tension effects were responsible for absence of stratified flow, but this factor should not play an important role with CO₂ considering the much lower surface tension than of water.

Observations of CO₂ flow were made also at 0°C and zero heat flux, to see the effects of temperature and heat flux on the flow pattern. Results from these observations are shown as gray markers in Fig. 8. At a temperature of 0°C, annular flow was maintained up to a much higher superficial vapor velocity. This confirms that the entrained amount of liquid is smaller at low temperature, thus leaving more liquid in the annular film. At $q=0$, one observation of stratified flow was made, at conditions that gave annular flow when heat flux was added. The other observations at $q=0$ gave flow patterns that matched observation with positive heat flux (intermittent or annular flow), even though transition from intermittent into annular flow seems to occur at lower vapor superficial velocity.

The stratified flow observation at zero heat flux is quite interesting, indicating an influence of heat flux in determining the flow pattern. It is not clear what mechanism that gives annular flow when heat is added, but the presence of small vapor bubbles may alter the flow characteristics of the liquid phase by changing the effective density and viscosity.

Vapor fraction / mass flux chart

Based on the equations and procedures for drawing transition lines in the flow pattern chart of Kattan et al. (1998), a chart for CO₂ flow in a 0.98 mm diameter tube at 20°C was generated. Fig. 9 shows the resulting chart, with the present observations plotted into the coordinate system. The generalized transition lines give a poor prediction of the actual situation, with droplet (“mist”) flow observations in the predicted annular regime, and a majority of the annular observations in the predicted intermittent regime.

The transition into bubbly flow is predicted to occur at mass flux around 600 kgm⁻²s⁻¹, while transition into mist flow is predicted from a mass flux of 1500 kgm⁻²s⁻¹

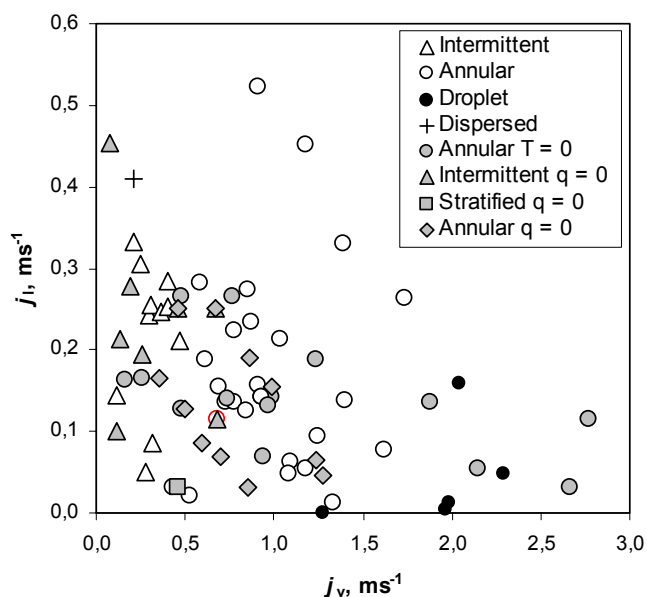


Figure 8 Flow pattern observations for CO₂ including points at 0°C and at zero heat flux.

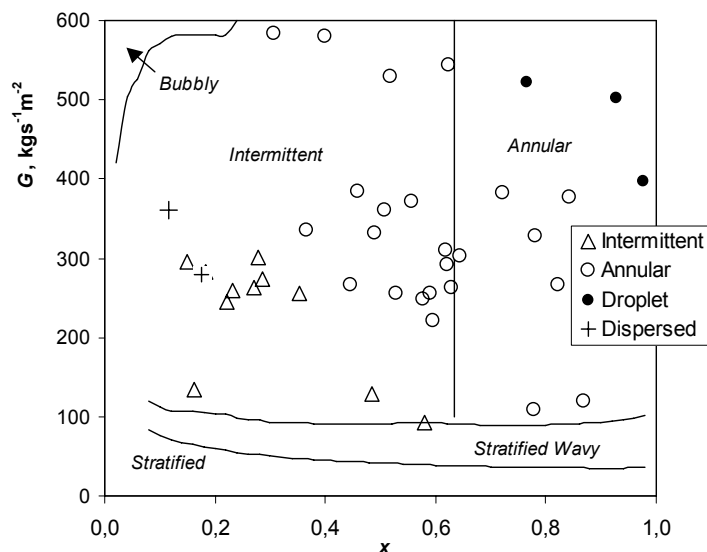


Figure 9 Flow pattern observations for CO₂ at 20°C in relation to transition lines proposed by Kattan et al. (1998). Predicted flow chart regimes are shown in *Italics*

and upwards, which is well above the range where mist flow (entrained droplet flow) was observed in the present tests. It is clear that the concept of the transition lines in this map does not match the present data. The flow chart of Kattan et al. (1998) was based on earlier charts by Taitel and Dukler (1976) and Steiner (1993), all of which were adapted to larger diameter flow and quite different fluid properties than of CO₂.

Onset of partial dryout in the flow pattern map of Kattan et al. (1998) was based on identifying the conditions that would give a transition from annular flow

to stratified-wavy flow. By modifying the Weber- and Froude number influence on the stratified-wavy flow boundary in the Steiner (1993) flow map, transition to partial dryout could be accounted for.

In the present tests, the dryout mechanism is not related to stratification of the flow, and liquid entrainment seems to have much more influence on the dryout occurrence. In the experiments that constitute the basis for the Kattan et al. (1998) flow map, annular to mist flow transitions occurred only at very high mass flux, due to the properties of the refrigerants studied, and the relatively low pressures. Entrainment effects and models were not considered by Kattan et al. (1998). In the present system, however, the annular to mist transition and liquid entrainment effects on dryout are of great importance, and have to be accounted for.

Inception of entrainment

Droplet entrainment into the vapor flow field starts when the retaining force of surface tension is exceeded by the interfacial shear force by vapor flow. An entrainment inception criterion for turbulent liquid film (film Reynolds number above 1635) is given by the critical superficial vapor flow velocity j_{vc} defined by Utsuno and Kaminaga (1998):

$$\frac{\mu_l j_{vc}}{\sigma} \left(\frac{\rho_v}{\rho_l} \right)^{1/2} = N_\mu^{0.8} \text{ for } N_\mu < 1/15 \quad (2)$$

$$\frac{\mu_l j_{vc}}{\sigma} \left(\frac{\rho_v}{\rho_l} \right)^{1/2} = 0.1146 \text{ for } N_\mu > 1/15 \quad (3)$$

where N_μ is the viscosity number given by

$$N_\mu = \frac{\mu_l}{\left(\rho_l \sigma \sqrt{\frac{\sigma}{g(\rho_l - \rho_v)}} \right)^{1/2}} \quad (4)$$

For CO₂ in a 1 mm ID tube, the above model predicts inception of entrainment at a superficial vapor flow velocity of about 0.4 ms⁻¹ at a temperature of 20°C.

Table 3 shows results from flow pattern observations that indicate conditions when entrainment could/could not be observed in the video recordings. Superficial velocity data are based on measured mass flux and vapor fraction.

Table 3 Entrainment observations in tests at 20°C

Test	G , kgm ⁻² s ⁻¹	x	j_v , ms ⁻¹	$j_{l,v}$, ms ⁻¹	En- trainment
29	109	0.78	0.43	0.03	no
30	119	0.87	0.53	0.02	no
7	266	0.45	0.62	0.19	yes
11	263	0.63	0.85	0.13	yes
13	266	0.82	1.10	0.06	yes

From these observations, the inception of entrainment seems to occur at a superficial vapor velocity between 0.5 and 0.6, thus indicating that the inception criterion of Utsuno and Kaminaga (1998) is close to the actual situation. The thicker liquid film in tests 7 and 11 than in tests 29 and 30 also contributes to onset of entrainment, since higher film Reynolds number is known to increase entrainment.

Entrained liquid fraction

Ishii and Mishima (1981) and Kataoka et al. (2000) developed correlations for entrainment rate and equilibrium entrainment fraction (the fraction of the liquid phase flowing as droplets) in vertical adiabatic annular two-phase flow. The basis was a mechanistic model of shearing-off of a roll wave crest by a streaming gas. They found that equilibrium entrainment fraction as well as the entrainment rate, could be correlated by the superficial liquid Reynolds number, and a Weber number defined as

$$We = \frac{\rho_v j_v^2 D}{\sigma} \left(\frac{\rho_l - \rho_v}{\rho_v} \right)^{1/3} \quad (5)$$

Even though the superficial Reynolds number is quite high in CO₂ flow vaporization due to the low viscosity and low liquid density, the Weber number is quite moderate due to very low vapor superficial velocity. In the model, the Weber number is the dominating parameter, characterizing the relation between flow-induced force causing entrainment, and stabilizing force due to liquid surface tension. Based on this model, the predicted entrained liquid fraction in the above tests is always below 3%, which is obviously much lower than observed. Thus, the above model seems to not reflect the situation in CO₂ microchannel flow.

CONCLUSION

The flow pattern observations were dominated by intermittent (slug) flow at low x , and wavy annular flow with entrainment of droplets at higher x .

The aggravated dryout problem reported from heat transfer experiments with CO₂ at high mass flux could be explained by increased entrainment. Stratified flow was not observed in the tests with heat load. Bubble formation and growth could be observed in the liquid film, and the presence of bubbles gave differences in flow pattern compared to adiabatic flow.

The flow pattern observations on CO₂ did not fit any of the generalized maps or transition lines, including the map proposed by Kattan et al. (1998). Only the intermittent-annular transition prediction of Weisman et al. (1979) was close to the observed behavior.

Compared to small-diameter observations with air/water at low pressure, the transition into annular flow occurred at much lower superficial vapor velocity (superficial velocity of approximately 0.5 ms^{-1}). Observed inception of entrainment at $0.5\text{--}0.6 \text{ ms}^{-1}$ superficial vapor flow velocity was close to the predicted onset at 0.4 ms^{-1} .

REFERENCES

- Barajas, A. M., and Panton, R. L., 1993. The effects of contact angle on two-phase flow in capillary tubes, *Int. J. Multiphase Flow*, Vol. 19 No. 2, pp. 337-346.
- Coleman, J. W., and Garimella, S., 1999. Characterisation of two phase flow patterns in small diameter round and rectangular tubes. *Int. J. Heat Mass Trans.*, Vol. 42, pp. 2869-2881
- Damianides, C. A., and Westwater, J. W., 1988. Two-phase flow patterns in a compact heat exchanger and in small tubes, Proceedings of 2nd UK National Conference on Heat Transfer, Glasgow, Scotland, Vol. II, pp. 1257-1268.
- Hihara, E., and Tanaka, S., 2000. Boiling Heat Transfer of Carbon Dioxide in Horizontal Tubes. Preliminary Proceedings of the IIR Gustav Lorentzen Conference on Natural Working Fluids, Purdue University, W. Lafayette, IN, USA, July. pp. 279-284.
- Ishii, M., and Mishima, K., 1981. Correlation for liquid entrainment in annular two-phase flow of low viscous fluid. Argonne National Laboratory Report, ANL/RAS/LWR 81-2.
- Kataoka, I., Ishii, M., and Nakayama, A. 2000. Entrainment and deposition rates of droplets in annular two-phase flow, *Int J Heat Mass Trans*, Vol 43, pp. 1573-1589
- Kattan, N., Thome, J. R., Favrat, D., 1998. Flow Boiling in Horizontal Tubes : Part 1 – Development of a Diabatic Two-Phase Flow Pattern Map. *Trans. ASME, J. Heat Transfer*, Vol. 120, pp. 140-147
- Pettersen, J., Hafner, A., Skaugen, G., and Rekstad, H. 1998. Development of Compact Heat Exchangers for CO₂ Air-Conditioning Systems. *Int. J. Refrig.*, Vol. 21, no 3, pp. 180-193.
- Steiner, D. 1993. Heat transfer to boiling saturated liquids. Chapter Hbb in *VDI Heat Atlas*, English translation of VDI –Wärmeatlas, 6. auflage. Edited by VDI Gesellschaft Verfahrenstechnik und Chemieingenieurwesen. VDI-Verlag.
- Taitel, Y., and Dukler, A. E., 1976. A model for predicting flow regime transitions in horizontal and near-horizontal gas-liquid flow. *AIChE J.* Vol 22, pp. 47-55.
- Utsuno, H., and Kaminaga, F., 1998. Prediction of Liquid Film Dryout in Two-Phase Annular-Mist Flow in a Uniformly Heated Narrow Tube – Development of Analytical Method under BWR Conditions. *J. Nuclear Science and Tech.*, Vol 35, No 9, pp. 643-653.
- Weisman, J., Duncan, D., Gibson, J., and Crawford, T., 1979. Effect of Fluid Properties and Pipe Diameter on Two-Phase Flow Pattern in Horizontal Lines, *Int J. Multiphase Flow*, Vol 5, pp. 437-462.

NOMENCLATURE

D	Hydraulic diameter	m	ρ	Density	kgm^{-3}
G	Mass flux	$\text{kgm}^{-2}\text{s}^{-1}$	μ	Dynamic viscosity	$\text{Pa}\cdot\text{s}$
j	Superficial velocity	ms^{-1}	σ	Surface tension	Nm^{-1}
q	Heat flux	Wm^{-2}	Subscripts		
T	Temperature	$^{\circ}\text{C}$	v, l	vapor, liquid	
x	Vapor fraction (quality)	-			

APPENDIX – TEST DATA AND OBSERVATIONS

(E) : Entrained droplets observed

Test	$G, \text{kgm}^{-2}\text{s}^{-1}$	Superficial velocity, ms^{-1}		q, kWm^{-2}	$T, ^{\circ}\text{C}$	x	Flow regime	Flow pattern
		liquid	vapor					
1	252	0,278	0,177	0	19	0,13	Intermittent	Elongated bubble
2	244	0,243	0,284	13	19	0,22	Intermittent	Elongated bubble
3	259	0,255	0,310	13	20	0,23	Intermittent	Elongated bubble
4	263	0,246	0,366	13	20	0,27	Intermittent	Slug
5	274	0,252	0,401	13	20	0,28	Intermittent	Slug
6	255	0,212	0,466	13	20	0,35	Intermittent	Slug
7	266	0,189	0,616	13	20	0,45	Annular	Wavy (E)
8	255	0,155	0,693	13	20	0,53	Annular	Wavy (E)
9	248	0,135	0,731	13	20	0,58	Annular	Wavy (E)
10	256	0,136	0,772	13	20	0,59	Annular	Wavy (E)
11	263	0,125	0,845	13	20	0,63	Annular	Wavy (E)
12	292	0,143	0,929	13	20	0,62	Annular	Wavy (E)

13	266	0,062	1,095	13	21	0,82	Annular	Smooth (E)
15	584	0,523	0,913	12	20	0,31	Annular	Wavy (E)
16	581	0,451	1,176	12	20	0,40	Annular	Wavy (E)
17	529	0,330	1,392	12	20	0,52	Annular	Wavy (E)
18	544	0,264	1,736	12	20	0,62	Annular	Wavy (E)
19	522	0,158	2,039	12	20	0,76	Droplet	
20	502	0,048	2,290	13	21	0,93	Droplet	
21	229	0,143	0,992	12	-1	0,42	Annular	Smooth (E)
25	99	0,100	0,113	0	20	0,23	Intermittent	Elongated bubble
26	135	0,145	0,114	13	20	0,16	Intermittent	Elongated bubble
27	93	0,050	0,277	13	20	0,58	Intermittent	Slug
28	128	0,085	0,317	13	20	0,48	Intermittent	Slug
29	109	0,031	0,432	13	20	0,78	Annular	Smooth
30	119	0,020	0,525	13	20	0,87	Annular	Smooth
31	115	0,032	0,457	0	20	0,78	Stratified	Smooth
32	367	0,453	0,081	0	20	0,04	Intermittent	Bubbly
33	360	0,410	0,213	13	20	0,12	Dispersed	Bubble
34	371	0,214	1,035	13	21	0,56	Annular	Wavy (E)
35	382	0,137	1,399	13	20	0,72	Annular	Wavy (E)
36	378	0,076	1,623	13	20	0,84	Annular	Wavy (E)
37	387	0,005	1,951	13	20	0,99	Droplet	
38	398	0,012	1,989	13	20	0,98	Droplet	
39	253	0,000	1,276	13	21	1,00	Droplet	
40	557	(-0,059)	2,966	13	21	1,08	Droplet	
41	379	0,115	2,767	12	0	0,72	Annular	Wavy (E)
45	323	0,334	0,328	0	21	0,20	Intermittent	Slug
46	221	0,114	0,682	13	20	0,60	Annular	Wavy
48	283	0,305	0,249	14	22	0,18	Intermittent	Slug
49	296	0,332	0,211	13	22	0,15	Intermittent	Slug
50	301	0,285	0,403	13	21	0,28	Intermittent	Slug
51	336	0,282	0,584	13	22	0,36	Annular	Wavy (E)
52	331	0,224	0,780	13	22	0,49	Annular	Wavy (E)
53	360	0,235	0,868	13	22	0,51	Annular	Wavy (E)
54	384	0,273	0,853	13	22	0,46	Annular	Wavy (E)
55	259	0,048	1,078	13	21	0,86	Annular	Wavy (E)
57	302	0,142	0,925	13	22	0,64	Annular	Wavy (E)
58	285	0,054	1,178	13	22	0,86	Annular	Wavy (E)
59	328	0,094	1,247	13	21	0,78	Annular	Wavy (E)
60	281	0,012	1,330	13	21	0,97	Annular	Wavy (E)
61	318	0,358	0,219	0	21	0,14	Intermittent	Elongated bubble
62	327	0,339	0,332	0	21	0,21	Intermittent	Elongated bubble
64	285	0,250	0,462	0	21	0,33	Annular	Wavy
65	330	0,250	0,670	0	22	0,42	Annular	Wavy (E)
66	326	0,190	0,867	0	22	0,56	Annular	Wavy (E)
67	309	0,065	1,238	0	22	0,84	Annular	Wavy (E)
68	304	0,045	1,277	0	22	0,89	Annular	Wavy (E)
69	320	0,154	0,987	0	21	0,63	Annular	Wavy (E)
70	284	0,274	0,294	0	1	0,10	Intermittent	Slug
71	294	0,265	0,476	13	0	0,16	Annular	Wavy (E)
72	323	0,265	0,769	13	1	0,24	Annular	Wavy (E)
73	297	0,188	1,234	13	0	0,41	Annular	Wavy (E)
74	313	0,164	0,162	13	0	0,51	Annular	Smooth
75	311	0,135	1,879	13	0	0,60	Annular	(E?)
76	268	0,055	2,145	13	1	0,81	Annular	(E)
77	299	0,032	2,665	13	1	0,90	Annular	Smooth
78	189	0,212	0,136	0	22	0,15	Intermittent	Elongated bubble
79	201	0,195	0,255	0	21	0,26	Intermittent	Elongated bubble
80	199	0,165	0,357	0	21	0,37	Annular	
81	201	0,128	0,498	0	22	0,51	Annular	Wavy
82	186	0,085	0,593	0	21	0,65	Annular	Wavy
83	199	0,070	0,700	0	22	0,73	Annular	Smooth
84	201	0,031	0,857	0	21	0,88	Annular	Smooth
85	280	0,304	0,234	13	22	0,18	Dispersed	Bubble
86	309	0,156	0,907	13	22	0,62	Annular	Wavy (E)
87	276	(-0,026)	1,402	13	22	1,07	Annular	Wavy (E)
88	178	0,165	0,256	13	1	0,15	Annular	
89	167	0,127	0,483	13	1	0,29	Annular	(E?)
90	207	0,140	0,739	13	3	0,38	Annular	(E)
91	162	0,070	0,938	13	2	0,60	Annular	Smooth
92	223	0,131	0,971	13	2	0,46	Annular	(E)

6.3 Compressors/machinery

6.3.1 Small oilfree piston type compressor for CO₂

Heinz Baumann, CH-8400 Winterthur, Switzerland; E-mail: hpbaumann@bluewin.ch
 Martin Conzett, Zurich University of Applied Sciences (ZHAW), CH-8401 Winterthur;
 E-mail: martin.conzett@zhwin.ch

Abstract

The objective of this project is to prove the feasibility of a small oilfree semi hermetic piston type CO₂ compressor for supercritical heatpump applications with large temperature spans. These processes involve high pressures like 35 bar suction pressure and 80 to 150 bar delivery pressure.

The compressor design is based on two key elements which are :

- clearance seal piston/cylinder combination and
- PEEK-plate valves with flat valve springs

The feasibility study covers :

- design and manufacturing of a functional model
- performance tests over the full range of speed and pressure
- manufacturing cost estimate for a modified serial model design.

The compressor was designed for domestic water heating applications and has therefore no external cooling. The cooling of the motor is effected by the suction CO₂-gas flow through the motor, crankcase and cylinder head to the suction valves.

The tests confirmed the feasibility of the technology for the use in small oilfree compressors. The compressor which has a scotch yoke drive operates very quietly and without vibrations. It is able to handle outlet pressures up to 150 bar and outlet temperatures up to 200 °C .

Two kinds of cylinder-heads from stainless steel and from plastic were tested in order to find out the influence of heat exchange and heat conduction. The stainless steel cylinder-heads conduct a lot of heat to the compressor housing which results in a considerable preheating of the suction gas (see Diagr.4). The process of preheating and compression follows different courses for the two cylinder head materials (see Diagr.5). However, the characteristic values of compression are practically the same for both (see Diagr.8-12).

The Isentropic Efficiency (see Diagr.10) is comparable to the efficiency of oil-lubricated compressors on the market, despite the very small cylinder volume of 1.25 cm³. The Volumetric Efficiency (see Diagr.12) is rather low due to the large design-related dead volume of 18%.

This CO₂ compressor technology is a possible alternative to oil lubricated compression systems in

- automotive air conditioning (heating and cooling)
- domestic water heating
- applications in the food industry where oilfree compression is a must.

Precondition for most of the applications however are competitive costs in comparison to oil-lubricated systems. In order to reach this target further development steps will be needed.

This work was done on behalf of the Swiss Federal Office of Energy. The author alone is responsible for the content and the conclusion of this report.

Content	page
1 Introduction	3
2 Objectives of the project	3
3 Procedure	3
4 Design	4
4.1 Data of the compressor	4
4.2 Design features	4
4.3 Functional model	6
4.4 Serial model	6
4.5 Motor	6
5 Motor measurements	6
6 Compressor testloop	8
7 Compressor test results	9
7.1 Functionality	9
7.2 Test results	10
7.3 Efficiencies	13
8 Manufacturing costs of Serial Model	15
9 Conclusions	16
10 Definition of the compressor efficiencies	17
11 Symbols	18
12 Acknowledgement	18
13 References	18
Pictures of teststands	19

1 Introduction

The synthetic refrigerants HCFC will be phased out in the near future due to their ozone depletion effect. The substitutes HFC are not less problematic due to their Global Warming Potential.

The real substitutes for these synthetic refrigerants are Natural Working Fluids like :

Ammonia
Air
Water
Hydrocarbons (for example Isobutane, Propane, Butane etc.)
Carbon dioxide

The Carbon dioxide is interesting for applications like

Automotive air conditioning (heating and cooling)
Domestic water heating and
Drink refrigeration

because it is neutral to the environment, has no smell, is non-toxic, non-flammable and is not limited in nature, and furthermore has interesting thermodynamic properties.

These applications require supercritical processes with high pressures.

The problem is the handling of the high pressures with oil-lubricated compressors and the interaction between the oil and the CO₂-gas.

The use of oilfree compressors is proposed in order to overcome these problems.

2 Objectives of the project

The objective of this project is to proof the feasibility of a small oilfree semi hermetic piston type CO₂ compressor for supercritical heat pump applications with large temperature spans.

3 Procedure

A Functional Model was designed and manufactured, with the use of two serial proven key elements which are

- high pressure clearance seal piston/cylinder combination and
- PEEK-plate valves with flat valve springs

The Functional Model was tested and its performance characteristics evaluated over a wide range of speed and pressure.

The project concludes with a Manufacturing Cost Estimate for a modified Serial Model.

4 Design

The compressor was designed as a heat pump for domestic water heating applications. In order to use all the available heat for the heat pump process the CO₂ gas was used to cool the motor. The CO₂ gas enters at the bottom end of the motor and flows through the motor and crankcase into the cylinder heads. A high efficiency motor should guarantee a high overall efficiency of the compressor and keep the preheating of the suction gas as low as possible.

4.1 Data of the compressor :

- | | |
|---------------------------------|------------------|
| • Number of stages | 1 |
| • Number of cylinders | 4 |
| • Cylinder diameter | 10 mm |
| • Stroke | 16 mm |
| • Suction pressure | 35 bar |
| • Delivery pressure | 80 – 150 bar |
| • Speed variabel | 500 – 3000 U/min |
| • Power consumption at 1500 RPM | ca. 500 W |
| • Dead volume | 18 % |

4.2 Design features of the Functional Model and the Serial-Model :

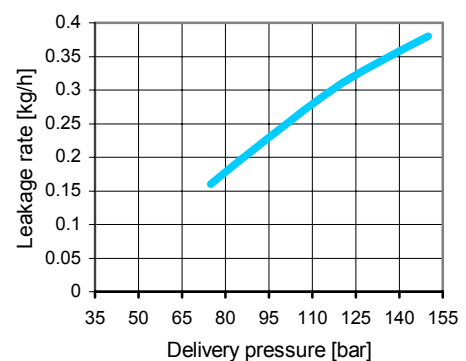
- Semihermetic compressor with integrated motor
- 4 cylinders in cross arrangement
- Scotch yoke drive with complete mass balance, no vibrations
- Simple shaft with one crank pin; arranged on two sealed ball bearings
- Piston/cylinder: Clearance seal
- Valves: Plastic-plate valves with flat spring
- Driven by Permanent Magnet Synchron Motor
- Cooling effected by working media CO₂

The cross section of the Functional Model is shown in Fig. 1.

The following design features deserve particular attention:

➤ **High pressure clearance seal**

The clearance seal seals with a minimal gap between piston and cylinder of $4\pm6\ \mu\text{m}$ in diameter. The leakage flow through the gap is laminar and according to pressure a few percent of the flowrate (see Diagr. 1). The piston moves practically frictionless back and forth and does therefore not wear. (In similar applications with other gases the service period of piston/cylinder used to reach 10`000 hours)



Diagr. 1: Estimated clearance seal losses

➤ **Valves**

The compressor valves are flat sealing plates from PEEK, pushed against the metallic seat by a flat spring. The sealing plates have good sealing qualities, are light and operate quietly without any wear. The service period of the valves exceeds the one of the clearance seal.

➤ **Scotch yoke drive**

This well known drive configuration produces sinusoidal movements. Advantageous is a combination with 4 cylinders in cross arrangement with the two opposed pistons coupled together by a yoke. The addition of the two 90° phase shifted mass forces of the first order results in a rotating force which can be completely balanced by two rotating counterweights on the shaft. Machines with this drive configuration operate very quietly and without vibrations.

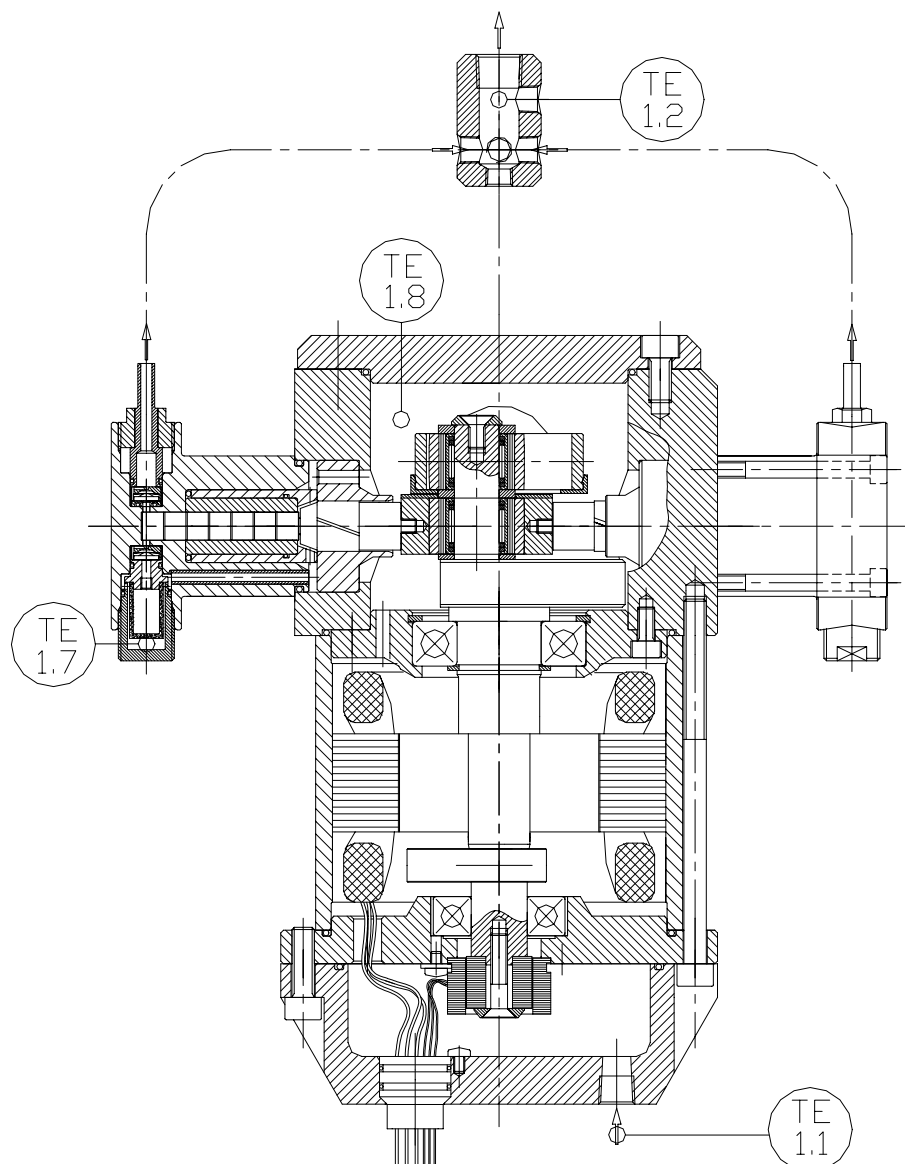


Fig. 1 : CO₂-Compressor, Functional Model
Temperature measuring points on the compressor
(Measuring points list see Tab.1)

4.3 Functional Model (see Fig.1)

The compressor housing parts are all manufactured in aluminium. The cylinder-heads are from stainless steel in order to keep the heat conduction losses low. Cylinder-heads from a temperature resistant plastic were manufactured too in order to investigate the influence of heat conduction.

The resolver on the motor side shaft end serves the control of speed.

4.4 Serial Model

The Serial Model is different from the Functional Model in shape and manufacturing method of the housing parts which are aluminium castings.

4.5 Motor

A Permanent Magnet Synchron Motor was chosen for highest efficiency over a wide range of speed and torque. The speed can be varied by a frequency converter between 500 and 3000 RPM.

5 Motor measurements

For a detailed analysis of the compressor efficiency it was necessary to know the efficiency of the drive train <frequency converter – motor – shaft> at the respective operating conditions. The performance of the motor together with the frequency converter was measured on a motor teststand (see Fig.2 below and Pict.1 page 19). For this the cylinder heads and the scotch yokes were removed and a shaft extension piece was fixed onto the crank pin of the shaft. An elastic coupling connected it to the torque transmitter and the motor brake.

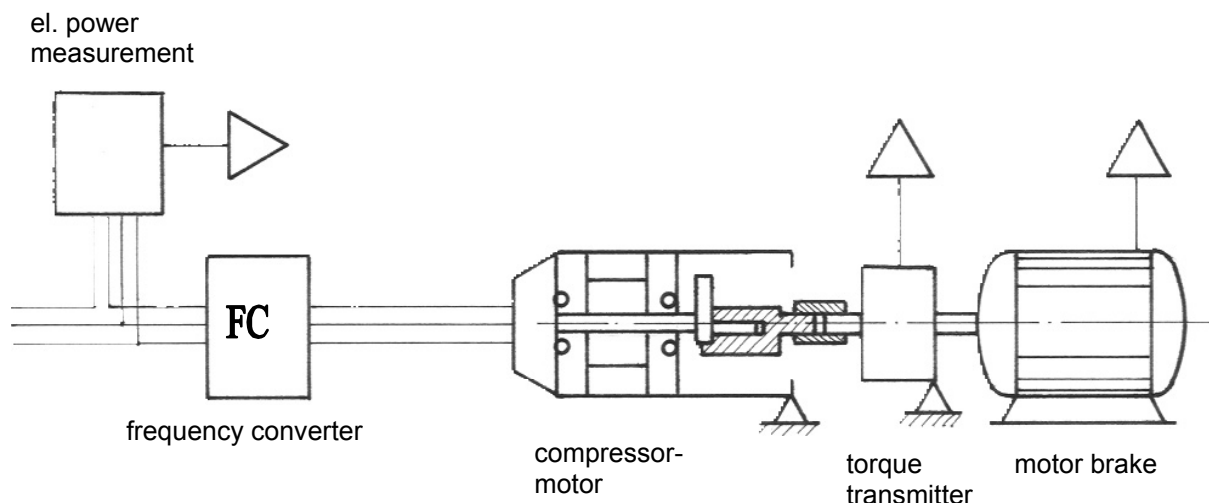
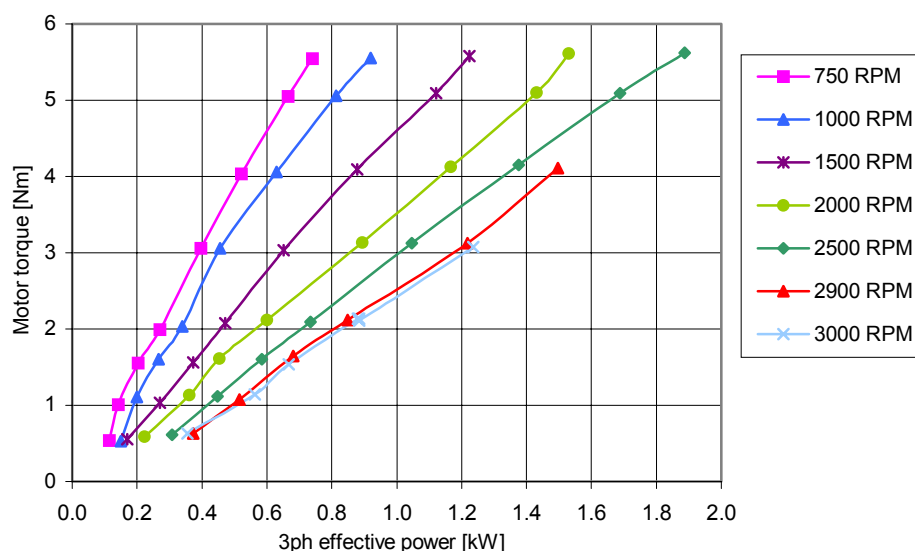
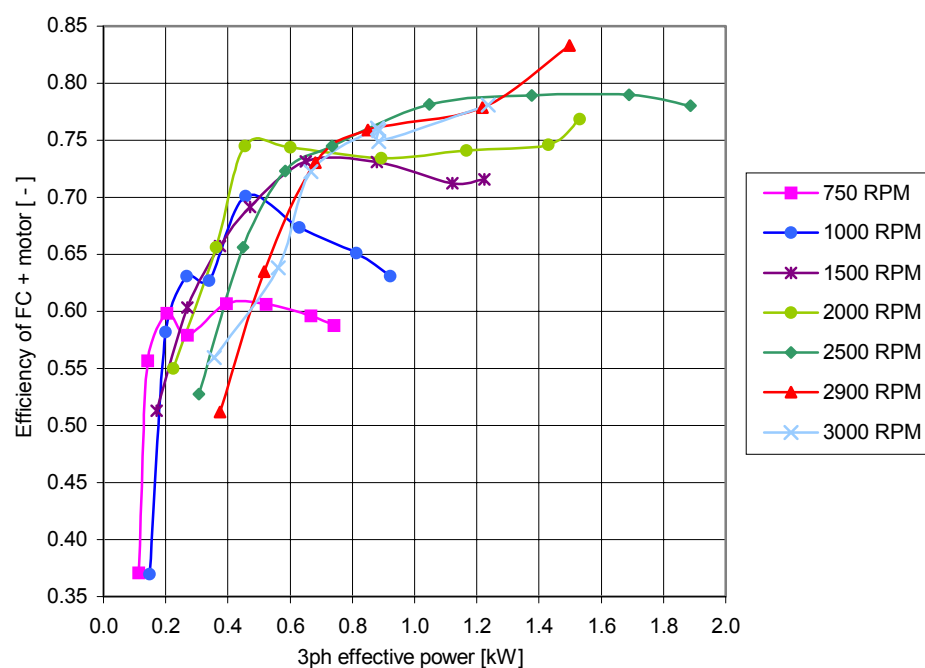


Fig.2 : Motor measuring arrangement

The data were stored on a PC and afterwards converted into the torque and efficiency curves in the following diagrams 2 und 3:



Diagr.2 : Motor measurements; Torque on compressor shaft



Diagr. 3 : Motor measurements; Efficiency of Frequency Converter + Motor

The motor efficiency was not as good as expected; especially at part load and at low speeds the efficiency was rather low.
(The compressor testruns covered the power range between 160 and 950 Watt)

6 Compressor testloop

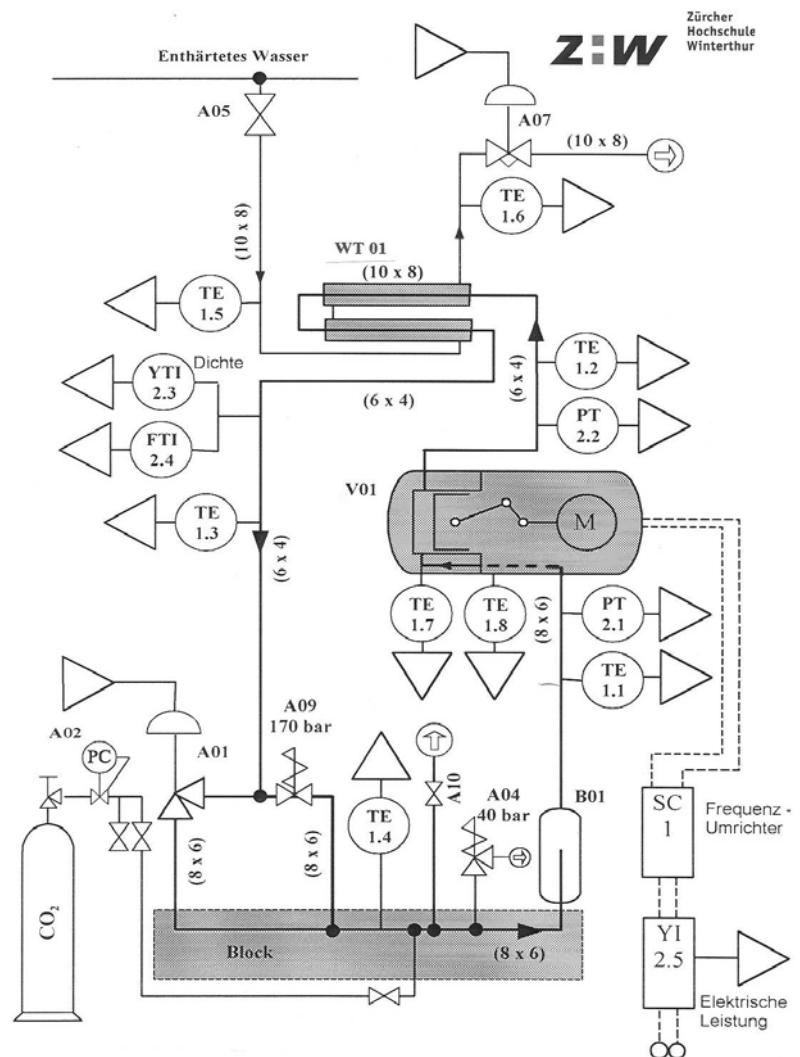
The testloop (see Pict. 2 page 19) was planned as a so called Hot Gas Loop, which was more practical for performance measurements on the compressor than a complete heatpump process with condensation and evaporation.

Figure 3 shows the (P+I) - diagram of the testloop.

The measuring data were all conducted to the PC. The monitoring and the storage of the measuring data and the control of the process was done with the software program DASYLab32. The following variables were adjusted or controlled:

- The suction pressure was set to 35 bar for all the test runs. (Reason: 35 bar is the vapour pressure of CO₂ at 0°C which is the evaporation temperature of the assumed domestic water heat pump process)
- The motor speed and the position of the expansion valve A01 were adjusted to a preset value for each measurement.
- The process was controlled only by the cooling water metering valve A07; the cooling water flowrate was controlled in this way, that the gas temperature reached +5°C after the expansion valve, which corresponds to a superheating of 5°C. (i.e. the controlled variable was the gas temperature TE1.4 after the expansion valve).

Fig.3 : (P+I) – diagram of the testloop



Tab.1 Measuring points list

Measuring point	Measured variable				Principle of Measurement	Channel assignment	
	Sym-bol	Unit	Description	Signal			
TE 1.1	T	°C	Gas-temperature compressor inlet		Thermocouple	1	Analog inputs Board DS-16-8-TC-AO
TE 1.2	T	°C	Gas-temperature compressor outlet		Thermocouple	2	
TE1.3	T	°C	Gas-temperature expansion valve in		Thermocouple	3	
TE1.4	T	°C	Gas-temperature expansion valve out		Thermocouple	4	
TE1.5	T	°C	Cooling water heat exchanger in		Thermocouple	5	
TE 1.6	T	°C	Cooling water heat exchanger out		Thermocouple	6	
TE 1.7	T	°C	Gas-temperature at suction valve		Thermocouple	7	
TE 1.8	T	°C	Gas-temperature in crankcase		Thermocouple	8	
PT 2.1	p	bar g	Suction pressure	mA	Pressure transmitter	1	Analog inputs Board DS-16-8-GP-AO
PT 2.2	p	bar g	Delivery pressure	mA	Pressure transmitter	2	
YTI 2.3	ρ	kg/m ³	Density of gas	mA	Coriolis-flowmeter	3	
FTI 2.4	m	kg/h	Massflow of gas	mA		4	
YI 2.5	P _{el}	W	Electric power consumption	V	el. power measurement	5	

Tab.2 Equipment list

Designation	Description	Channel assignment		
A01	Expansion valve	V	2	Analog outputs Board DS-16-8-GP-AO
A07	Cooling water metering valve	mA	1	
A02	Gas cylinder pressure control valve			
A04	Low-pressure relief valve 40 bar			
A05	Cooling water shut-off valve			
A09	High-pressure relief valve 170 bar			
B01	Vessel 300 cm ³			
WT01	Double-pipe heat exchanger			
V01	Compressor			

7 Compressor test results

7.1 Functionality

The key components piston/cylinder and the valves show no sign of wear or fatigue after approx. 300 hours of operation. These components are excellent for the use in CO₂ compressors at high pressures.

We did not run any endurance tests so far, but from experience with other applications and gases, we expect these components to last several thousand hours of operation with CO₂.

7.2 Test results

The compressor performance test results are presented in diverse diagrams. The compressor measurements were carried out both with cylinder-heads from stainless steel and with cylinder-heads from plastic.

The basic course of a testloop process with its process points is shown in Fig.4 .

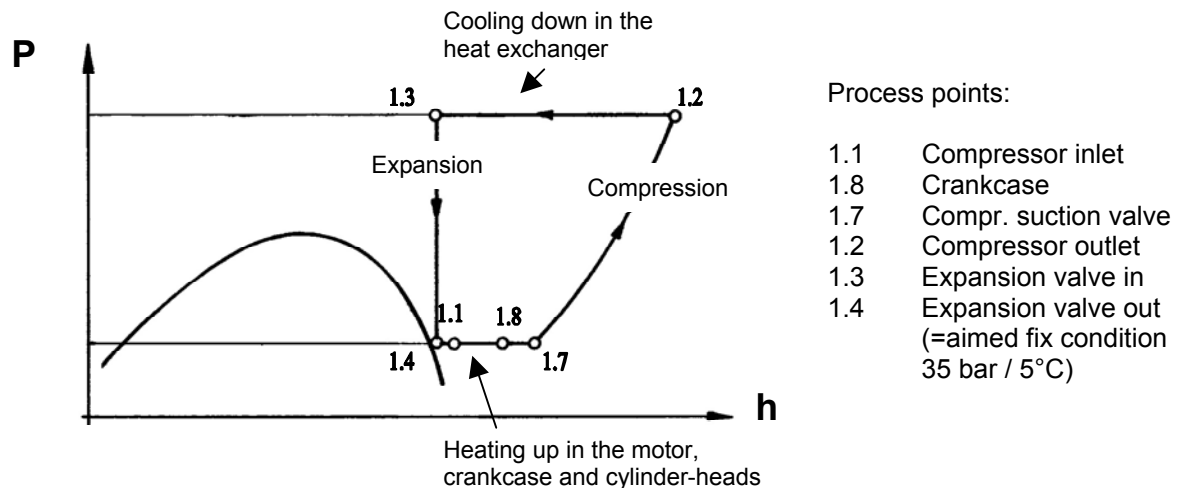
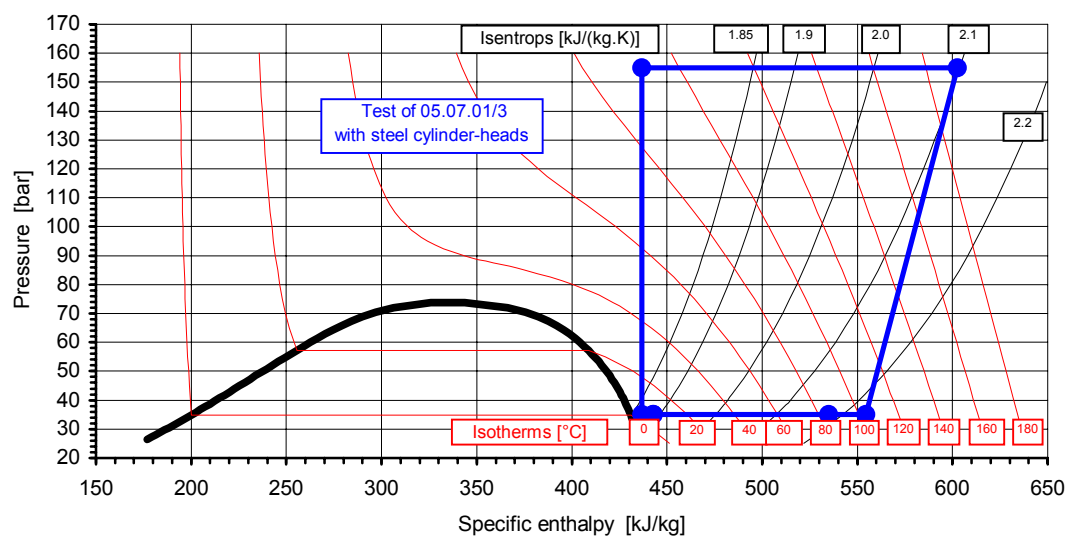


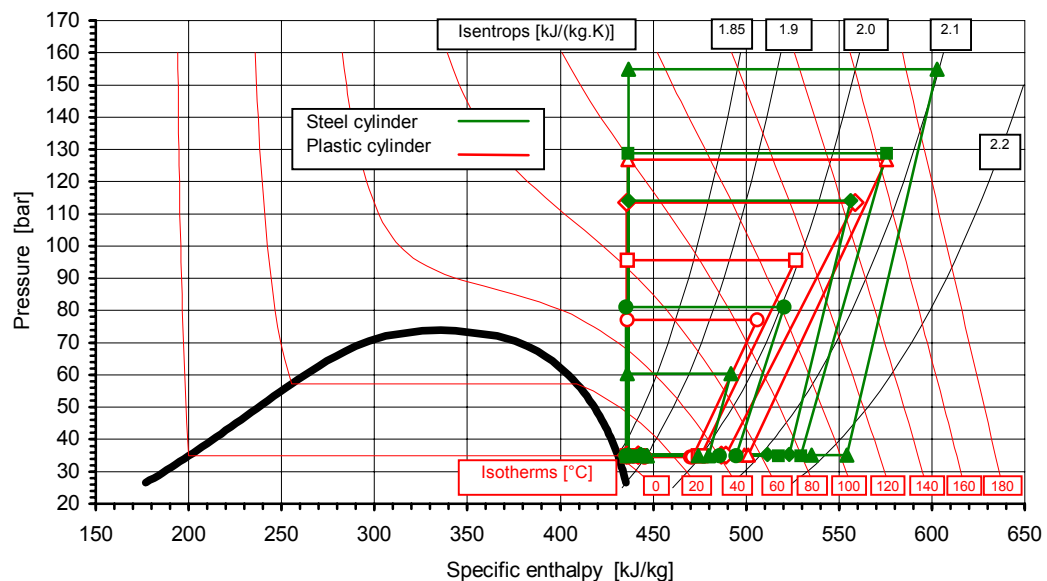
Fig.4 : Basic course of a testloop-process in the (p-h)-diagram

A typical course of a process is shown in diagram 4. It represents a measurement with steel cylinder-heads. The suction gas is heated up in the motor and in the crankcase quite strongly by about 70°C and in the cylinder-head again almost 20°C ! The reason for this is the high crankcase temperature of about 85°C which is caused by the heat conduction from the steel cylinder-heads to the compressor housing. (The compressor is not cooled externally!).



Diagr.4 : Typical course of a process in the (p-h)-diagram (with steel cylinder-heads)

Diagram 5 shows a comparison of a few process-courses with steel cylinder-heads against courses with plastic cylinder-heads.



Diagr.5 : Comparison of process-courses with steel cylinder-heads and with plastic cylinder-heads in the (p-h)-diagram

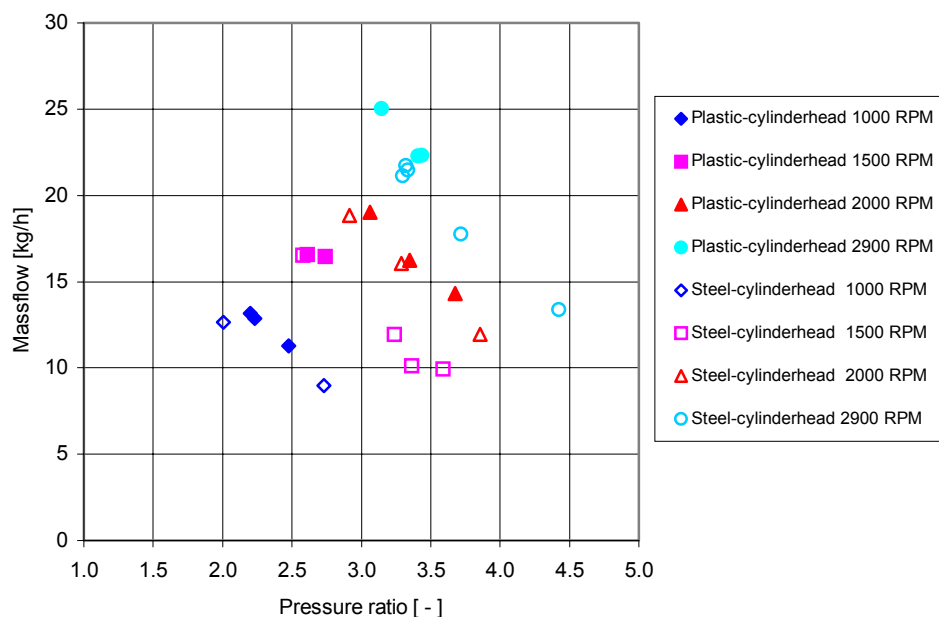
The remarkable difference between the two cylinder-material executions can be recognized in the process-courses:

- The compressor with steel-cylinderheads shows a considerable heating up of the gas before it enters the cylinder, but compresses the gas with heat rejection.
- The plastic-cylinders prevent the heat exchange and the heat conduction to the compressor housing, which shows in lower housing temperatures and less heating up of the gas before the compression. The compression itself is almost isentropic which means there is less heat exchange with the cylinders.
- **The result at the end stays the same!** The compressor outlet temperatures are approximately the same, independent of cylinder-head material. All the characteristic values of compression, presented in the diagrams 8 – 12 show only very small differences between the two executions of cylinder-head material. It seems that above effects are compensating each other.

The evaluation of the numerous measurements are shown in the following diagrams 6 – 12, diagrams 6 and 7 with the speed as parameter.

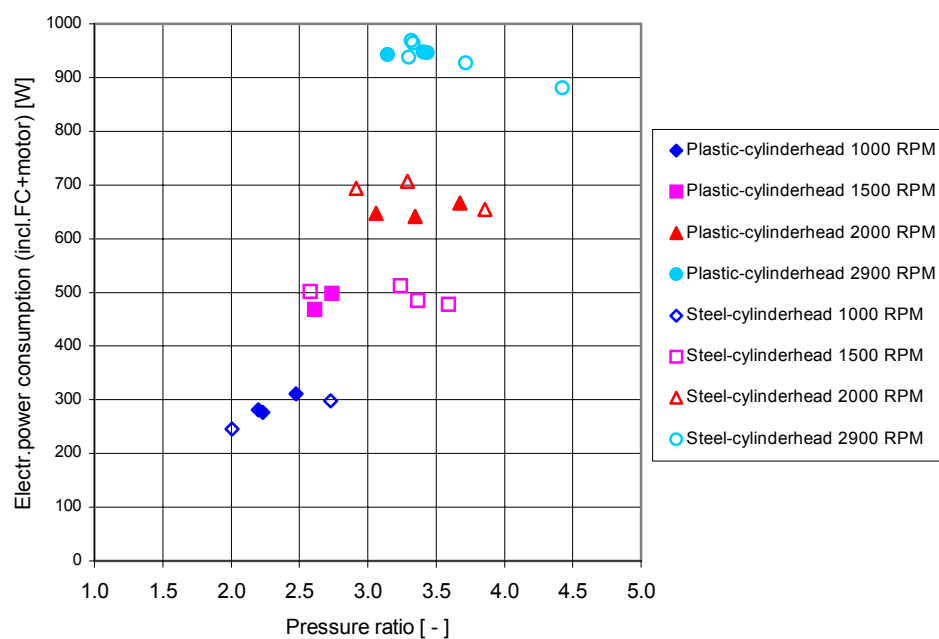
The diagrams 8 –12 apply for the whole range of speed from 750 to 2900 RPM. The speed has practically no influence on the compression specific values, i.e. the valve losses do not weight within our range of operation.

Diagram 6 shows the massflow of CO₂ in function of the pressure ratio, with the speed as parameter.



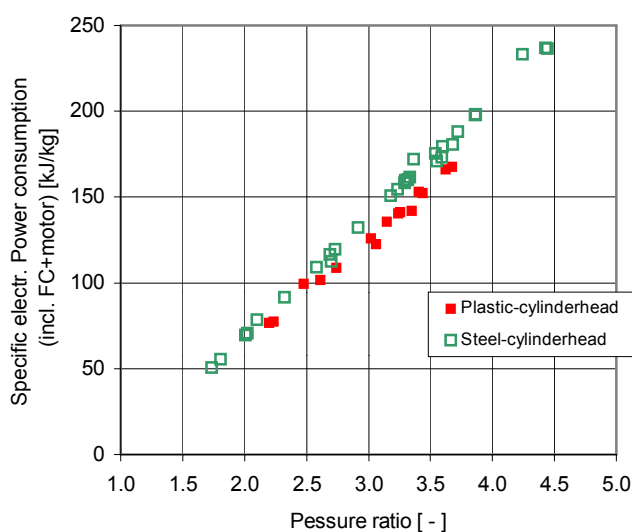
Diagr. 6 : Massflow of CO₂

Diagram 7 shows the electrical power consumption measured at the input of the frequency converter, in function of the pressure ratio, with the speed as parameter.



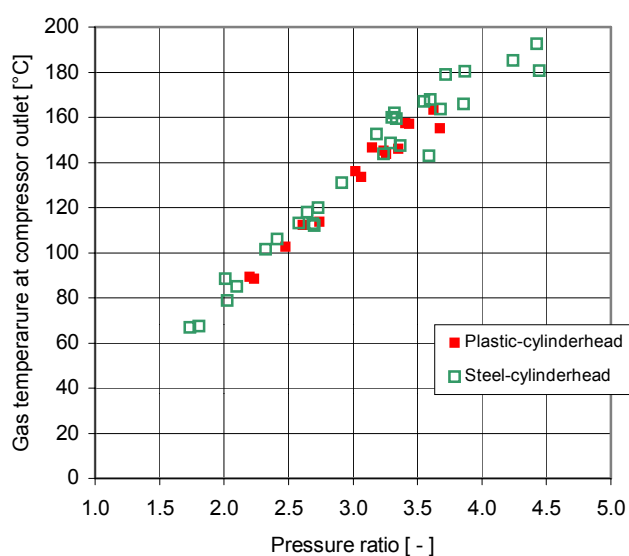
Diagr. 7 : Electrical power consumption (inclusive frequency converter + motor)

Diagram 8 shows the specific electrical power consumption measured at the input of the frequency converter, in function of the pressure ratio.



Diagr. 8 : Specific electr. power consumption inclusive frequency converter + motor

Diagram 9 shows the gas temperatures on the compressor outlet in function of the pressure ratio.



Diagr. 9 : Gas temperature at compressor outlet (TE1.2)

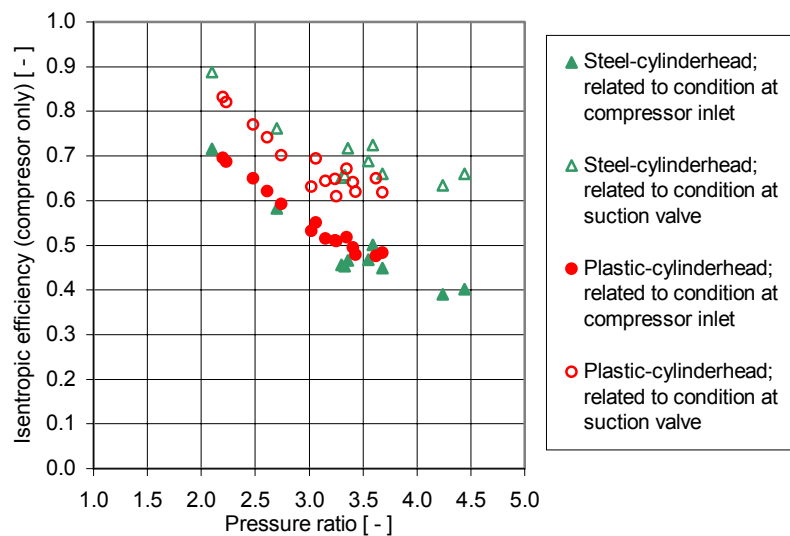
7.3 Efficiencies

The various efficiencies of the compression are defined in chapter 10, page 16.

In order to be able to compare the "quality" of the compression with values of compressors on the market, the Volumetric Efficiency as well as the Isentropic Efficiency were each related to the condition at **compressor inlet** and to the condition at the **suction valve**. With the latter the negative effect of the heating up of the suction gas in the motor and crankcase is excluded.

Diagram 10 shows the Isentropic Efficiency of the compressor without frequency converter and motor, in function of the pressure ratio.

(The Isentropic Efficiency compares the theoretical isentropic compression power with the shaft power).

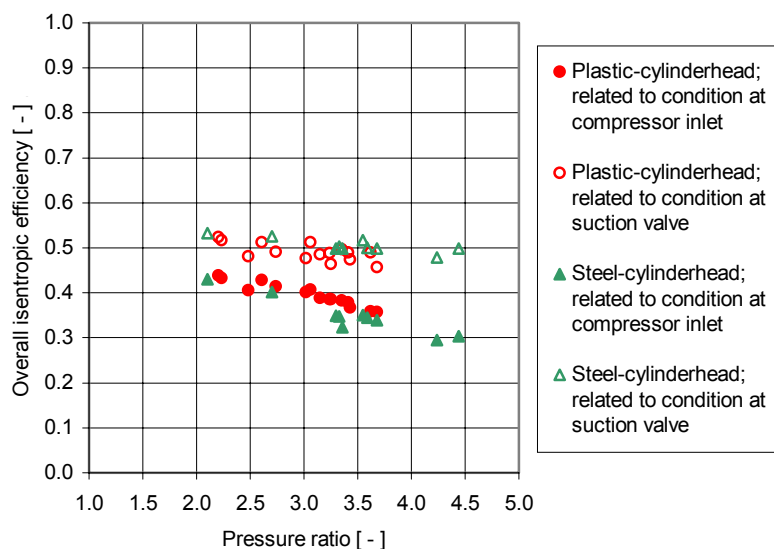


Diagr. 10 : Isentropic efficiency (compressor only)

Diagram 11 shows the Overall Isentropic Efficiency (incl. motor + frequency converter), in function of the pressure ratio.

(The Overall Isentropic Efficiency compares the theoretical isentropic compression power with the electric power input).

The Overall Isentropic Efficiency is low due to the low motor efficiency (see Diagr.3, page 8), especially at low pressure ratios.



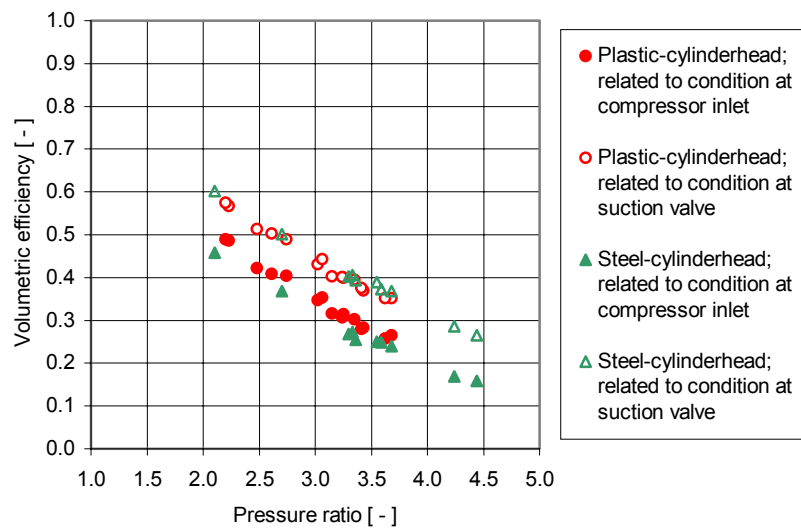
Diagr. 11 : Overall isentropic efficiency (inclusive motor+FC)

Comparison with compressors on the market:

The few CO₂-compressor-reports found in Literature [1;2] give an Isentropic Efficiency of about 0.7 (for lubricated compressors) in the pressure-ratio range of 3÷4.

As in Diagr.10 the Isentropic Efficiencies of our oilfree CO₂ compressor in the same pressure-ratio range varies between 0.6 and 0.72, related to the condition at the suction valves, which compares to compressors with the suction line directly into the cylinder. This is quite a remarkable result for a small compressor with 1.25 cm³ cylinder volume.

Diagram 12 shows the Volumetric Efficiency in function of the pressure ratio.



Diagr. 12 : Volumetric efficiency

The Volumetric Efficiency is rather low due to the large dead volume of 18%. The dead volume could not be reduced any further for design reasons. It is large in relation to the very small cylinder volume of only 1.25 cm³.

Comparison with compressors on the market:

In Literature [3] a Volumetric Efficiency of 0.6 is given for a lubricated CO₂ compressor with 10% dead volume and a pressure ratio of 3. This compares to a Volumetric Efficiency of 0.45 for our compressor. The influence of the larger dead volume makes at least 0.1 from the total difference of 0.15 .

8 Manufacturing costs for a small series of the Serial Model

The manufacturing costs for a small series of 5000 pieces of the Serial Model was evaluated. (The tooling costs for the castings and the Injection moulds are not included.)

Low Cost execution:

Compressor with Asynchronmotor, motor efficiency 78%,
fix speed; assembled and tested

CHF 1320.-

High Tech execution:

Compressor with Permanentmagnet-Synchronmotor of highest efficiency of
88%, variable speed; with Frequency Converter and Netfilter;
assembled and tested

CHF 1860.-

(The Frequency Converter without housing, only as board, integrated in an external control box would reduce the price by approx. CHF 150.-)

The reasons for the relatively high manufacturing costs are:

- The size of the series of 5000 is relatively small.
- Although it is called the Serial Model it is still more or less based on conventional mechanical engineering technics. For large series a redesign would be needed focused on cheap manufacturing methods.
- The manufacturing costs of the 4 Piston/Cylinder combinations alone makes almost 40% of the total manufacturing costs. A cheaper material combination suitable for dryrun should be evaluated. The reduction of the amount of cylinders would have a positive effect on the costs but would cause disadvantages like stronger vibrations, higher pressure pulsations and higher bearing loads.

9 Conclusion and outlook

The test series proved the feasibility of the used technology for small oilfree high-pressure CO₂-compressors. The Efficiencies and the Functionality show that there is a lot of potential in this technology.

A redesign should concentrate on a more compact design and lower production costs.

Where the main focus of future developments will be is dependent on the kind of application.

Future development areas could be:

- Development of cheaper material combinations for the dryrunning Piston/Cylinders.
- Detailed analysis of the thermodynamic processes and energy flows in the cylinders. The concept with the cooling of the unit by the gasflow alone is to be questioned and according to the application possibly another gasflow direction to choose.
- Design study and development of a dryrunning multi-axialpiston-compressor for compact arrangements.
- Redesign focused on cheap mass manufacturing methods.

10 Definition of the compressor efficiencies

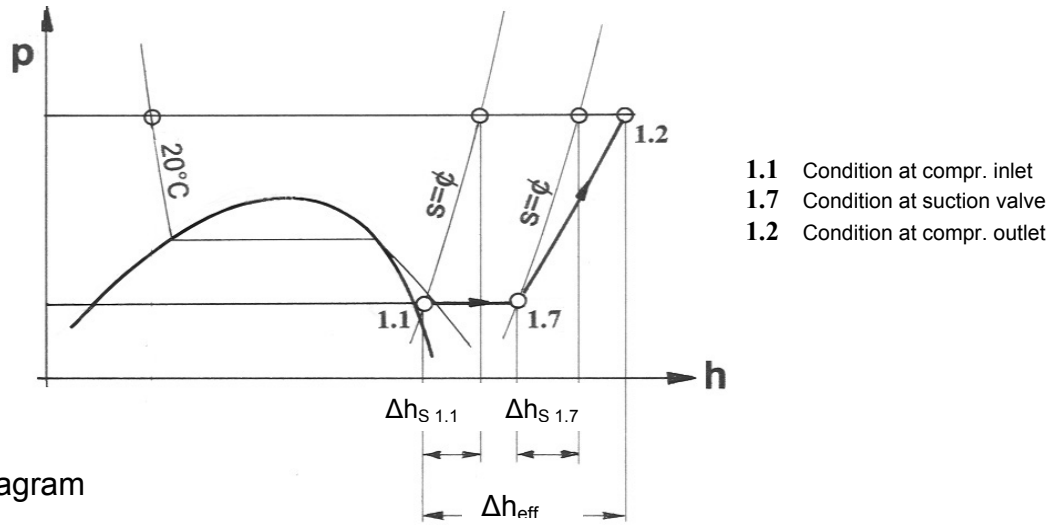


Fig.6 : p-h-Diagram

Isentropic Efficiency (without motor) (Diagram 10)

related to condition at compressor inlet

$$\eta_{is\ 1.1\ Compr} = \frac{\Delta h_{S\ 1.1}}{w_{el} \cdot \eta_{Motor}} \quad (\text{Eq.1})$$

related to condition at suction valve

$$\eta_{is\ 1.7\ Compr} = \frac{\Delta h_{S\ 1.7}}{w_{el} \cdot \eta_{Motor}} \quad (\text{Eq.2})$$

Overall Isentropic Efficiency (incl. FC+motor) (Diagram 11)

related to condition at compressor inlet

$$\eta_{is\ 1.1\ overall} = \frac{\Delta h_{S\ 1.1}}{w_{el}} \quad (\text{Eq.3})$$

related to condition at suction valve

$$\eta_{is\ 1.7\ overall} = \frac{\Delta h_{S\ 1.7}}{w_{el}} \quad (\text{Eq.4})$$

Volumetric Efficiency (Diagram 12)

related to condition at compressor inlet

$$\eta_{Vol\ 1.1} = \frac{\dot{V}_{eff\ 1.1}}{\dot{V}_H} = \frac{\dot{m}}{\rho_{1.1} \cdot \dot{V}_H} \quad (\text{Eq.5})$$

related to condition at suction valve

$$\eta_{Vol\ 1.7} = \frac{\dot{V}_{eff\ 1.7}}{\dot{V}_H} = \frac{\dot{m}}{\rho_{1.7} \cdot \dot{V}_H} \quad (\text{Eq.6})$$

$$\begin{aligned} \dot{V}_H &= \text{theoretically displaced volume-flow} \\ &= \frac{D^2 \cdot \pi \cdot H \cdot n \cdot 4}{4 \cdot 60} \end{aligned}$$

11 Symbols

p	pressure
T	absolut temperature
ρ	density
h	specific enthalpy
h_s	specific enthalpy difference at isentropic compression
h_{eff}	real specific enthalpy difference in the compressor
s	specific entropy
w_{el}	specific electrical energy consumption measured at the input of the FC
η_{Motor}	efficiency of motor+FC
η_{is}	isentropic efficiency
η_{Vol}	volumetric efficiency
\dot{V}_H	theoretically displaced volume-flow
\dot{V}_{eff}	effective flowrate
z_s	dead volume (= 0.18)
\dot{m}	massflow
D	cylinder diameter
H	stroke
n	speed

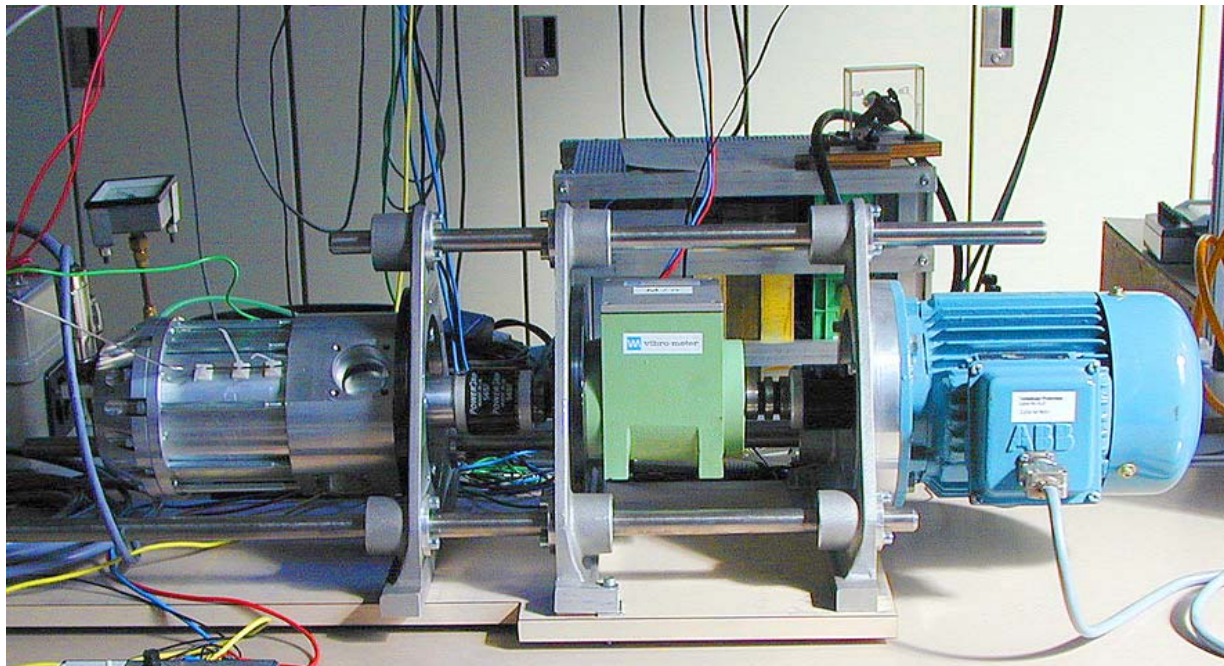
12 Acknowledgement

We are grateful for the funding of this work by the Swiss Federal Office of Energy .

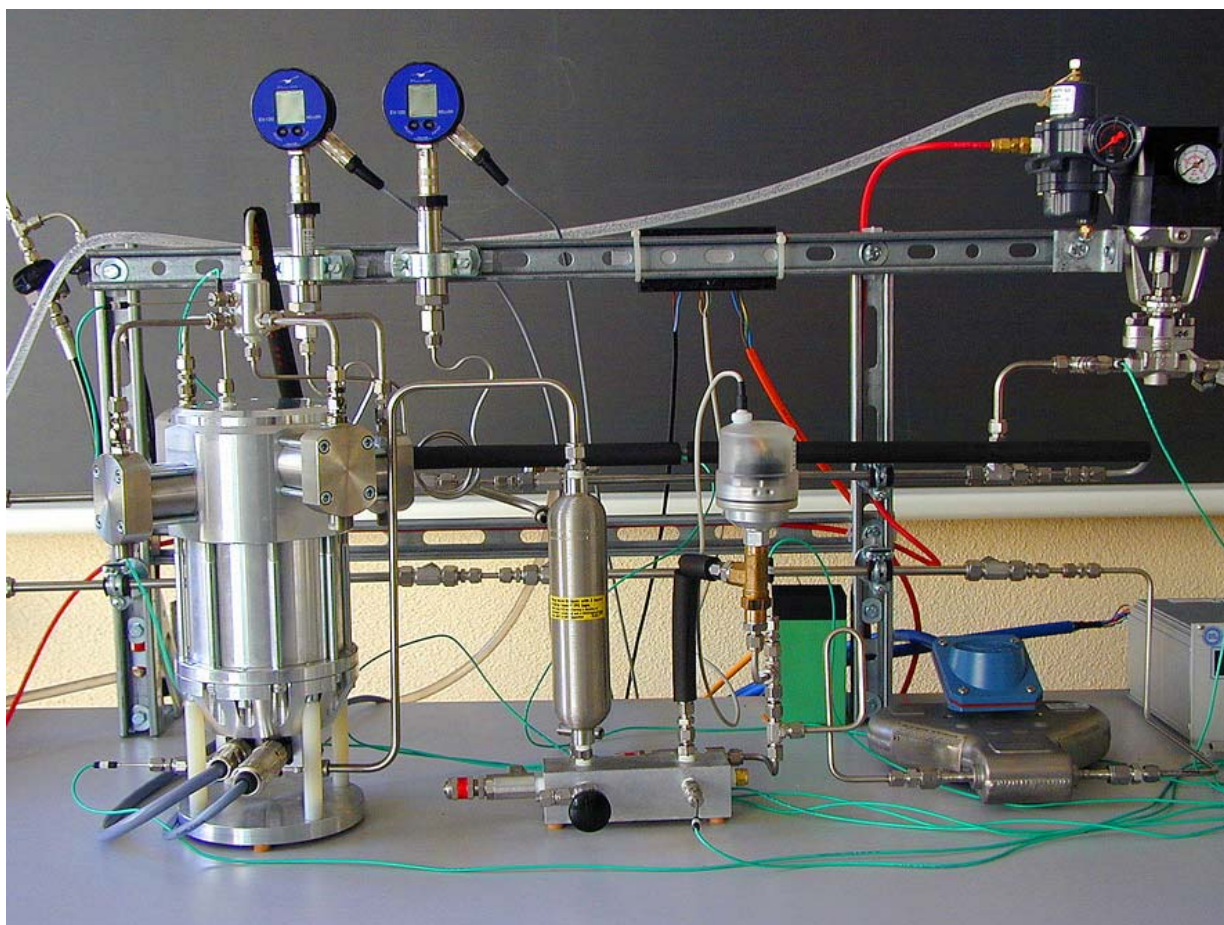
13 References

- [1] Pettersen, J.,G. Lorentzen: Eine neue, effiziente und umweltfreundliche Pkw-Klimaanlage mit CO₂ als Kältemittel. Luft- und Kältetechnik, 29 (1993), H.3,S.105-111
- [2] P.S.Hrnjak et al., University of Illinois, USA
Experimental Investigation of an Automotive Heat Pump prototype for Military, SUV and compact cars.
Proceedings of the 4th IIR-Gustav Lorentzen Conference on Natural Working Fluids at Purdue, July 2000, Page 115-122
- [3] Werthenbach, J., J. Maue: Klimakälteanlagen mit CO₂ im Pkw.
Fahrzeugklimatisierung mit natürlichen Kältemitteln – auf Strasse und Schiene. Karlsruhe, 8.3.96
- [4] Baumann, H. : Design features of a small oilfree, reciprocating, high pressure compressor. Proceedings of the 1994 International Compressor Engineering Conference at Purdue, Purdue University, West Lafayette, Indiana, USA

Annex



Pict. 1 Motor measuring set up with torque transmitter and motor brake



Pict. 2 Compressor testloop

6.4 Safety Issues

6.4.1 SOME SAFETY ASPECTS OF CO₂ VAPOUR COMPRESSION SYSTEMS

Jostein PETTERSEN¹, Armin HAFNER², Marit BRÅNÅS²

¹Norwegian University of Science and Technology (NTNU)

Dept. of Refrigeration and Air Conditioning, NO-7491 Trondheim, Norway

²SINTEF Energy Research, Refrigeration and Air Conditioning

NO-7465 Trondheim, Norway

Contact e-mail: Jostein.Pettersen@kkt.ntnu.no

ABSTRACT

Since CO₂ is a non-toxic and non-flammable refrigerant, the major safety issues for CO₂ systems are related to the high operating pressure. In case of a component rupture, the explosion energy (stored energy) may characterise the extent of potential damage. The explosion energy can be estimated based on component (refrigerant-side) volumes, pressures and refrigerant property data. The explosion (stored) energies of baseline systems and CO₂ systems are calculated and compared. Results show that the explosion energies are not as different as the large difference in pressure would indicate. It has been suggested that a Boiling Liquid Expanding Vapour Explosion (BLEVE) may occur when a vessel containing pressurised liquid or supercritical fluid is rapidly depressurised, e.g. due to a crack or a rupture. The overpressure from a BLEVE may be high enough to rupture the whole vessel, with a resulting blast wave and risk of flying fragments. Some tests on CO₂ have been conducted at varying initial conditions and liquid fill levels, and with varying vent areas. No significant overpressure peaks above the initial pressure has been observed in the current test programme.

1. INTRODUCTION

With increasing focus on the use of carbon dioxide (CO₂ or R-744) as a refrigerant, the safety characteristics of CO₂ vapour compression systems are being discussed. Due to the unusual properties of CO₂ compared to conventional refrigerants, there are a few safety-related factors that need to be addressed.

In general, the hazards of refrigerants and vapour compression systems are associated with the physical and chemical characteristics of the refrigerant as well as with the pressures and temperatures occurring in the system. These factors are commented in relation to CO₂ in the following text.

Flammability: Carbon dioxide is non-flammable, and it is even used as a fire-fighting or fire-preventing gas. Thus, flammability is not an issue.

Inhalation safety: Although carbon dioxide is usually regarded as non-toxic (DKV, 1998), there are physiological effects from breathing air with a CO₂-concentration above a few percent. At 2-3 % concentration by volume, the breathing rate will increase, and headache may be experienced after some time. The IDLH (Immediate Danger to Life and Health) concentration is set to 4% (NIOSH, 1996), and the lowest reported lethal concentration is 10% (Berghmans and Duprez, 1999). In practice, a maximum allowable concentration of about 5% by volume seems to be a reasonable limit (Berghmans and Duprez, 1999), (Amin, Dienhart and Wertenbach, 1999). In the design and operation of CO₂ systems, this will be the maximum acceptable concentration as a result of sudden release or prolonged leakage of CO₂ into occupied

space. The assessment of hazards resulting from accidental leakage of CO₂ into occupied space should consider factors like

- rate of CO₂ outflow at decreasing system pressure,
- formation of dry ice inside system at 5.2 bar system pressure,
- amount of CO₂ dissolved in lubricant,
- room/cabin ventilation rate, and
- stratification (CO₂ is heavier than air).

Frost burn is probably not a problem with CO₂ since the triple point is at 5.2 bar, i.e. there will be no boiling refrigerant at atmospheric pressure. Also, the toxic or irritating effects from decomposition products known to occur when fluorocarbon refrigerants contact flames or hot surfaces will not occur with CO₂.

Explosion or rupture of a pressurized component or vessel: The hazards may include blast effects and shocks, as well as flying fragments. Such incidents may be caused by a number of factors, such as malfunctioning safety device, overheating, over-charging, incorrect operation, construction weakness/corrosion, mechanical impact etc. Low-side pressures in CO₂ systems are typically 30-40 bar, and high-side pressures may be as high as 120-140 bar. These pressures are 5-10 times higher than in traditional fluorocarbon systems. High pressure is not a safety issue in itself, since the equipment will be designed for this. In case of a component rupture, however, the explosion energy (stored energy) may characterise the extent of potential damage. The explosion energy can be estimated based on component (refrigerant-side) volumes, pressures and refrigerant property data. The possible occurrence of a BLEVE (Boiling Liquid Expanding Vapour Explosions), may create a more severe blast effect than by an ordinary refrigerant expansion. This paper will address the two last issues – explosion energy and BLEVE – based on calculations and experimental data.

2. EXPLOSION ENERGY COMPARISONS

2.1 Estimation of explosion energy

The explosion energy can be estimated as the energy released by expansion of the refrigerant contained in a component or system. The expansion process will be very rapid, with little or no time for heat transfer between the ambient air and the expanding gas, and the explosion energy can therefore be estimated as the reversible adiabatic (isentropic) work of expansion. A closed-system model can be used, with a system boundary containing the mass of expanding refrigerant (m). The energy release (E) can be estimated as the difference in internal energy (u) between the initial state of the refrigerant inside the system (1), and the final state after the expansion (2):

$$E = m (u_2 - u_1)_{s=\text{const}}$$

The final state will be at the atmospheric pressure, with a final temperature corresponding to isentropic expansion. A more advanced model would consider effects of heat transfer between ambient air and the expanding gas or two-phase mixture, but this is outside the scope of the present paper.

Equations of state and tabulated thermodynamic data for the refrigerants are used to estimate the explosion energies. For HCFC-22, the equations of state by Chan and Haselden (1981) was used, and for HFC-134a, the equation by Tillner-Roth and Baehr (1994). For CO₂ a combination of data from Angus et al. (1976), Pitzer and Schreiber (1988) and Kuprianoff (1953) were used. The Kuprianoff (1953) data were used to obtain property data below the triple point of CO₂.

A detailed analysis of explosion energies should consider the refrigerant charge inside each component, as well as the local pressure, temperature and vapour fraction. In the current analysis, pressures are assumed to be equalized and temperatures uniform throughout the system. As a consequence, the charge/volume are assumed to reflect the refrigerant condition inside the entire system. When the temperature of the system is varied, the charge/volume ratio will remain constant (constant average specific volume), and pressure will vary either as saturation pressure, or as pressure along a constant-volume (isochoric) line in the gas region.

2.2 Comparison of split ductless residential AC systems

The data in this Section are based on a standard R-22 ductless split heat pump/air conditioning system, and a laboratory prototype CO₂ system with equal heat exchanger dimensions and cooling capacity (Pettersen, 1999). R-22 system data were taken from a standard 7 kW ductless split system, that served as a baseline, and a prototype CO₂ system with equal capacity and heat exchanger sizes (Aarlién and Frivik, 1998). The HCFC-22 system was based on round-tube heat exchangers, while the CO₂ prototype system had all-aluminium microchannel heat exchangers. A change over to optimised round-tube heat exchangers in the CO₂ system would reduce the internal volume and the explosion energy.

For the HCFC-22 system, the total volume occupied by refrigerant was approximately 11.4 liters, of which 0.7 liter (6%) was in the indoor unit and 8.5 liter (75%) in the outdoor unit. The remaining volume was in the 10 meters of piping between the two units. The average refrigerant density in the system was then 300 kg/m³ (3.5 kg charge / 11.4 liter refrigerant volume). The HCFC-22 refrigerant charge was specified by the system manufacturer. Corresponding data for the CO₂ prototype system were: 4.2 liter total volume, 0.27 liter (6%) in the indoor unit and 3.3 liter (78%) in the outdoor unit, and an average charge density of 260 kg/m³ (1.1 kg / 4.2 liter). A receiver was not needed in the CO₂ system, since this operated in a transcritical cycle, i.e. with supercritical high-side pressure.

Figures 1 and 2 show pressures and calculated specific explosion energy (per kg refrigerant) for HCFC-22 and CO₂, respectively. The diagrams were based on charge/volume ratios for the actual systems.

At initial temperatures below the saturated vapour state, the location and shape of the graphs are determined by the saturation pressure curve of the refrigerant. The saturation state represents the intersection of the given constant-density line and the saturated vapour line. At temperatures above the saturation state, the system is gas-filled, and the slope of the curve depends on the charge/volume ratio. Owing to the low critical temperature of CO₂ (31.1°C), a large part of the curve is in the vapour (gas) region.

On the basis of Figures 1 and 2, the total explosion energies (in kJ) for the two systems may be calculated, Fig. 3. As may be observed from the diagram, the energies

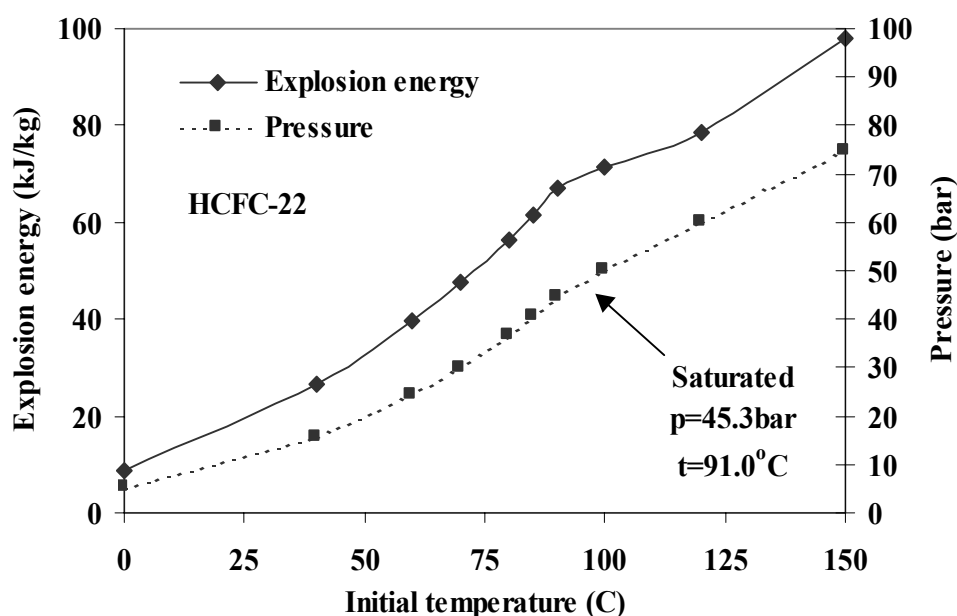


Figure 1: Pressure and calculated specific explosion energy for HCFC-22 at varying initial temperature for a density of $\rho=300 \text{ kg/m}^3$ (3.5 kg refrigerant in 11.4 liter volume)

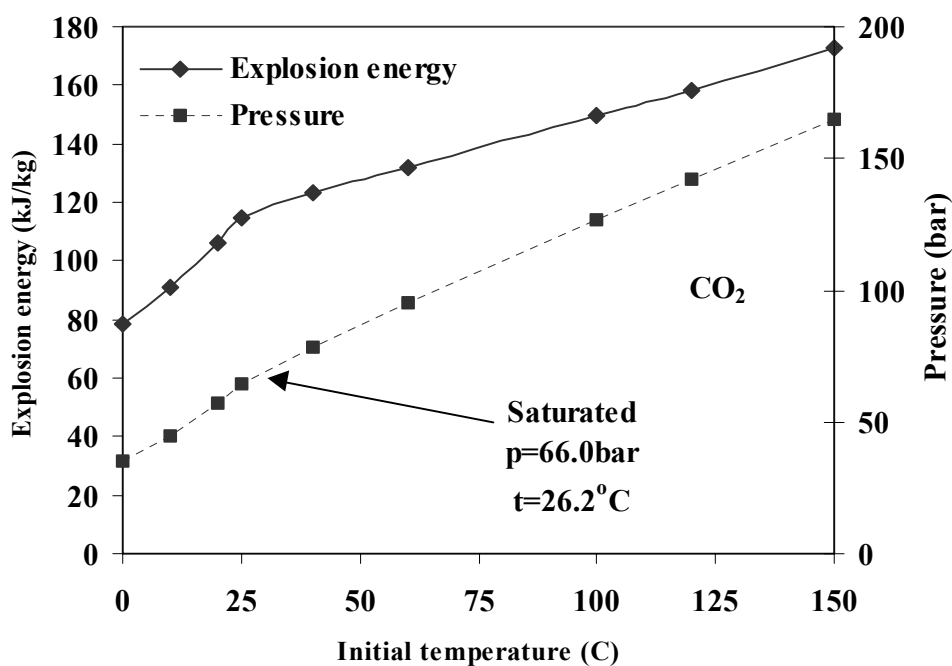


Figure 2: Pressure and calculated specific explosion energy for CO₂ at varying initial temperature for a density of $\rho=260 \text{ kg/m}^3$ (1.1 kg refrigerant in 4.2 liter volume)

are equal around 60°C, but the HCFC-22 system energy is more sensitive to temperature than the CO₂ system.

These calculations have shown that for realistic charge/volume ratios, the specific (per kg refrigerant charge) explosion energy of CO₂ is higher than of HCFC-22,

particularly at low and moderate temperatures. At room temperature (20°C), the CO₂ specific energy is about 6 times higher than the HCFC-22 specific energy, while at 100°C, the ratio is about 2.

In practice, however, the comparison should not be made between systems with equal charge, but with equal cooling or heating capacity, and similar efficiency. The above system data show that owing to the smaller volume and refrigerant charge in a CO₂ system, the actual explosion energies are in the same range. As may be observed from Figure 3, the ratio of energies (CO₂/HCFC-22) is about 2 at room temperature, and 0.7 at 100°C. The difference in energy becomes significant at temperatures above 120-130°C, and in an extreme situation such as a fire, the energy release from a HCFC-22 system is likely to be much higher than from a CO₂ system. In both systems the refrigerant volume in the indoor unit is only about 6% of the total volume, so the largest potential energy release is clearly in the outdoor unit containing the accumulator, receiver (HCFC-22 system) and compressor.

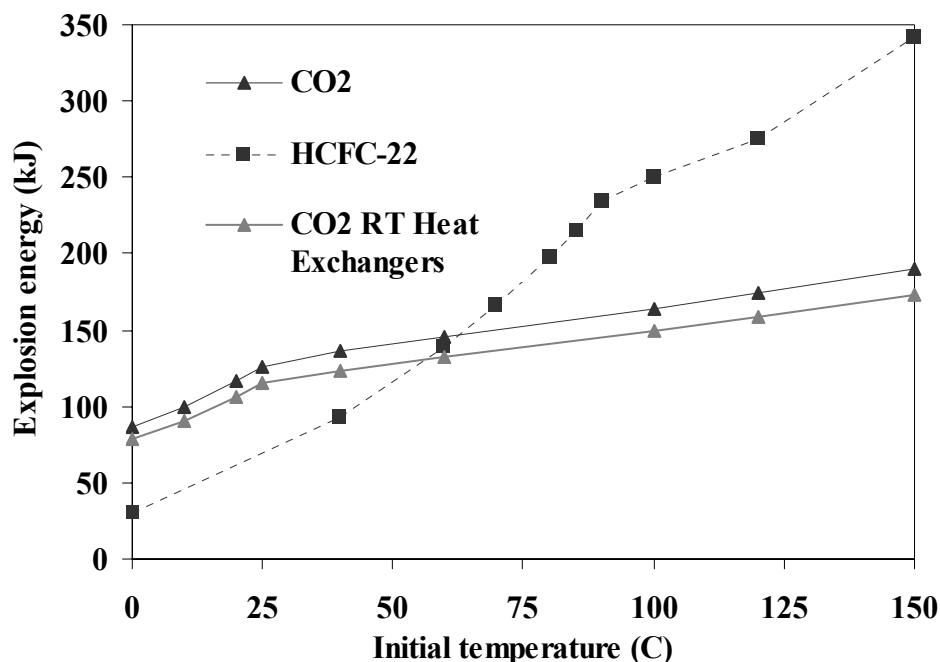


Figure 3: Calculated total explosion energy for HCFC-22 system and CO₂ system at varying initial temperature. Data for a CO₂ system with optimised round-tube (RT) heat exchangers is also shown.

2.3 Car air conditioning systems

Similar calculations as in Section 2.2 were made for car air-conditioning systems. Based on data from the industry, an internal volume of 4 liter was assumed for a state-of-the-art HFC-134a system, and 1.5 liter for a current prototype CO₂ system.

Results are summarized in Figures 4 and 5 (Hakenjos, 2000), showing total explosion energy (in kJ) at varying system charge. A realistic charge for a CO₂ system will be about 0.4 kg, while a HFC-134a system typically has a charge of about 1.0 kg,

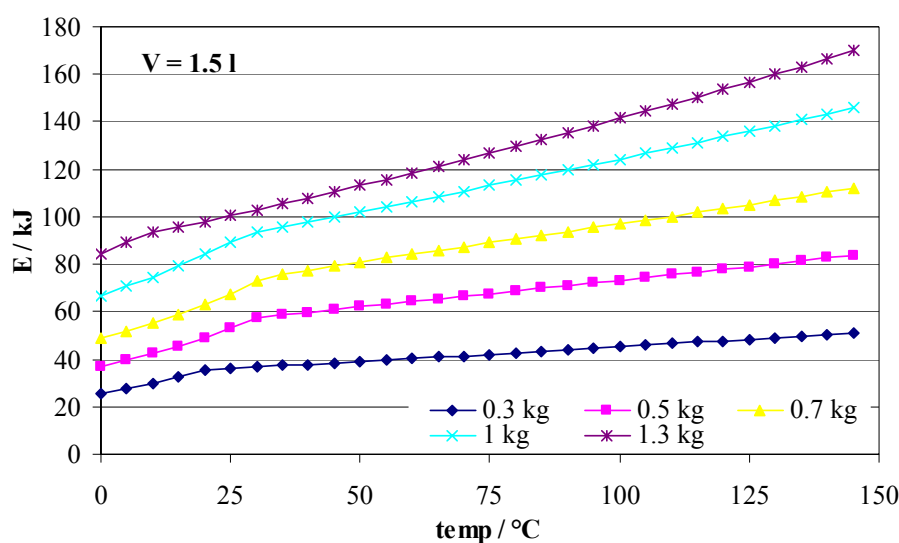


Figure 4: Calculated explosion energy of CO₂ system at varying initial temperature with a system volume of 1.5 l and several different charges

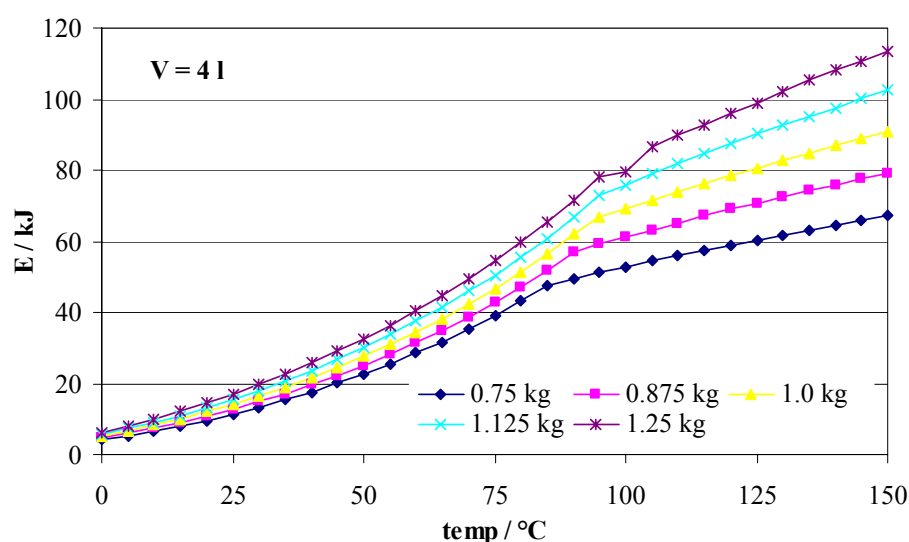


Figure 5: Calculated explosion energy for R-134a system at varying initial temperature with a system volume of 4 l and several different charges

As may be observed from the diagrams, the CO₂ system will have an explosion energy typically ranging from 40 to 80 kJ, while the baseline HFC-134a system ranges from 20 to 80 kJ. Again, the baseline system energy is smaller at normal temperatures, but becomes higher at elevated temperature.

2.4 Discussion of explosion energy results

The explosion energy for the above systems range from around 20 kJ to a few hundred kJ for a refrigerant charge of 0.4 to 3.5 kg. Although an explosion caused by the combustion of a flammable refrigerant is an entirely different scenario, it may be

worth while to note that the energy released by combustion of one kg of propane (R-290) is 46,000 kJ (lower heating value).

It has already been pointed out that a thorough analysis of explosion energies would have to consider the amounts of liquid and vapour in each component and part of the system, as well as the pressure distribution between the different components. In order to simplify the analysis, an average temperature has been applied for the entire system, and it has been assumed that the pressure is equal in all parts. This corresponds to a situation where the system is not operating, and the indoor and outdoor units are exposed to equal temperatures.

3. BLEVE IN CO₂ SYSTEMS

A BLEVE may occur when a vessel containing a pressurised liquid or supercritical fluid is rapidly depressurised, e.g. due to a crack or a rupture. The sudden depressurisation leads to an explosive vaporisation that may give a transient overpressure peak inside the vessel. The overpressure peak may lead to a powerful burst of the whole vessel, with total loss of content, a resulting blast wave and risk of flying fragments. Such a scenario can occur with any liquefied gas or supercritical fluid, and there are numerous reports in the literature about LPG and propane tanks where BLEVE has occurred. With a flammable fluid, there is also the additional risk of an explosion due to combustion of the vessel contents.

A number of theories have been suggested as explanations for this phenomenon, but at present no reliable method can predict BLEVE occurrence. The present Section outlines some results from an experimental study on BLEVE in CO₂ vessels. A major objective of the study is to identify possible regimes of BLEVE occurrence, and to provide a better understanding of the relevance of this phenomenon in CO₂ vapour compression systems.

3.1 Earlier BLEVE studies

The term BLEVE (Boiling Liquid Expanding Vapour Explosion) was introduced in 1957 by J. B. Smith, W. S. Marsh and W. L. Walls, while investigating the causes of a steel vessel explosion at a phenolic resin plant. When a high-pressure liquid or supercritical fluid is very rapidly depressurised as a result of an accident, normal flashing may be delayed and a superheated liquid is formed. Homogeneous nucleation may occur in this metastable liquid, leading to strong and damaging shock waves. Other transient flow effects and shock waves may also contribute to the development of a BLEVE. The BLEVE term is usually associated with combustible fluids like propane or LPG, where ignition of the gas also contributes to the damage.

Kim-E and Reid (1983) discussed a thermodynamic model based on the spinodal fluid state, which represents the limit-of-stability for the liquid phase during expansion. In a rapid expansion process, homogeneous nucleation will occur at this state. The authors were not able to demonstrate the predicted shock effects or pressure spikes in their experiments on CO₂ using a 7-liter tank with a 1.5 inch diameter burst disc. Reasons for poor agreement between theory and experiments may include factors like formation of vapour bubbles on the wall of the vessel, and shock waves or disturbances from the mechanism that ruptured the burst disc of the test vessel (Kim-E and Reid, 1983). The presence of vapour bubbles before depressurisation may have given

heterogeneous nucleation instead of the homogeneous nucleation required for a BLEVE.

McDevitt et al. (1990) conducted experiments with R-22 at 65°C / 27 bar in a one-litre tank, using a rifle bullet shot through the tank to trigger a BLEVE. A transient pressure of 35 bar was recorded (an overpressure of 8 bar or 30%), probably including significant effects of the rifle bullet. Later tests in a shock-tube with a mechanically triggered burst disc gave considerably lower pressure spikes.

Venart and Ramier (1998), and Venart et al. (1993) investigated additional aspects of BLEVEs, including dynamic re-pressurisation, cavitation, and two-phase discharge effects. With top venting, the initial depressurisation is expected to create a rising two-phase swell inside the vessel. When the two-phase flow impacts the top of the vessel, a shock may be created, and re-pressurisation may occur. This re-pressurisation may be large enough to cause cavitation, giving additional shock effects in the liquid and the vessel walls. The latter phenomenon is termed BLCBE (Boiling Liquid Compressed Bubble Explosion). In contrast to the other studies mentioned above, where time-scales typically were a few milliseconds, the time-scale of re-pressurization reported by Venart and Ramier (1998) were in the hundred millisecond regime.

No reliable method exists for prediction BLEVE occurrence and the magnitude of pressure peaks in CO₂ vessels.

In an earlier report from the present study at SINTEF/NTNU by Pettersen and Hakenjos (2000), very moderate maximum pressure spikes were observed within a few milliseconds after rupture disc cracking at 35 and 45 bar. Maximum overpressure spikes were less than 3 bar, and the amplitude of pressure oscillations were less than 6 bar. The maximum pressure spikes occurred for a moderate vent area. Re-pressurisation to higher-than-initial pressure in a 100-300 ms time-scale as reported by Venart and Ramier (1998) were not observed. Such results may be caused by instrumentation errors due to thermal shock effects when the expanding liquid contacts the transient pressure transducer.

3.2 Experimental set-up

The test set-up at NTNU/SINTEF included an instrumented cylindrical test vessel with an internal volume of 1 litre, and a high-speed data recording system. In order to avoid any disturbance caused by a mechanical piercing device, the burst discs were allowed to crack open by internal pressure only, and an electric trigger mechanism initiated data recording. The vessel was positioned with a vertical axis.

A design pressure of 200 bar was used for the vessel, which was made from stainless steel. It consisted of a cylindrical tube of 250 mm length and 73 mm ID, with end plates of 30 mm thickness. The inner surfaces were polished to suppress bubble nucleation. The rupture disc was installed in a holder at the top of the vessel, Figure 6. Piezoelectric pressure sensors were installed in the top and bottom of the vessel, and a static pressure sensor was installed in the bottom.

Data from the pressure transducers were logged by a 100 kHz PC card, giving a sample rate of 33 per millisecond (ms) per channel. In some tests, the static transducer was disconnected, and a sample rate of 50 per millisecond could be achieved. The card was equipped with integrated memory, storing 3 ms of data preceding the trigger signal.

Before each test, the vessel was purged with CO₂ gas, cooled and filled with the specified amount of liquid CO₂. The vessel was then allowed to slowly warm to

approach the specified burst pressure. Depressurisation was initiated when the rupture disc cracked open, leaving a reasonably well-defined cross section, Figure 7. The discs break at a given specific burst pressure with an accuracy of $\pm 5\%$. The vent (outlet) area can be varied by installing adapters with restricted cross-section on the disc holder on the outlet or inlet side (or both sides).

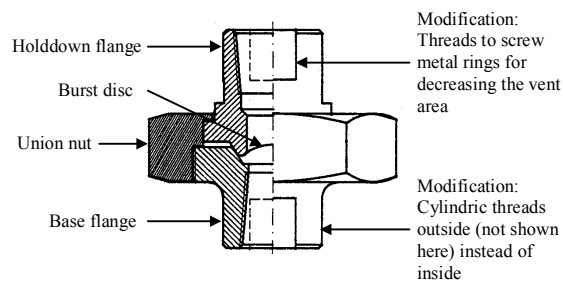


Figure 6: Union holder for rupture disc



Figure 7: 0.5 inch (13 mm) standard type rupture disc with 30° seat

3.3 BLEVE results

Table 1 outlines the test programme for some of the experiments that have been completed so far. A total of 17 tests have been completed, from which some results were presented by Pettersen and Hakenjos (2000). Rupture pressures 35, 45 and 60 bar corresponds to saturation temperatures of 0°C, 10°C and 22°C, respectively. These conditions reflect possible low-side accumulator pressures in AC/HP systems during operation and start-up. A vent area of 124.7 mm² corresponds to full opening, i.e. no restriction adapter on the outlet.

Table 1: Selected test points

Test	Rupture pressure, bar	Liquid CO ₂ charge, g	Fill level, %	Vent area, mm ² restriction location
7	45	450	50	3.1 (outlet restriction)
9	45	456	50	3.1 (inlet restriction)
2	35	485	50	124.7 (no restriction)
11	60	639	80	19.6 (inlet restriction)
16	60	406	50	124.7 (no restriction)
17 ^a	60	400	50	124.7 (no restriction)

a: vessel turned upside down, i.e. with venting downwards

In the initial test set-up, the vent area was adjusted by screwing an “orifice tube” into the outlet of the burst disc holder (Pettersen and Hakenjos, 2000). In later tests, the restriction was moved to the inlet side of the disc holder, and this turned out to have a major influence on the results. Figure 8 shows transient pressure recordings for the top and bottom sensors in tests 7, and 9, focusing on the first five milliseconds after disc rupture. In these tests, all conditions are equal apart from the location of the restriction.

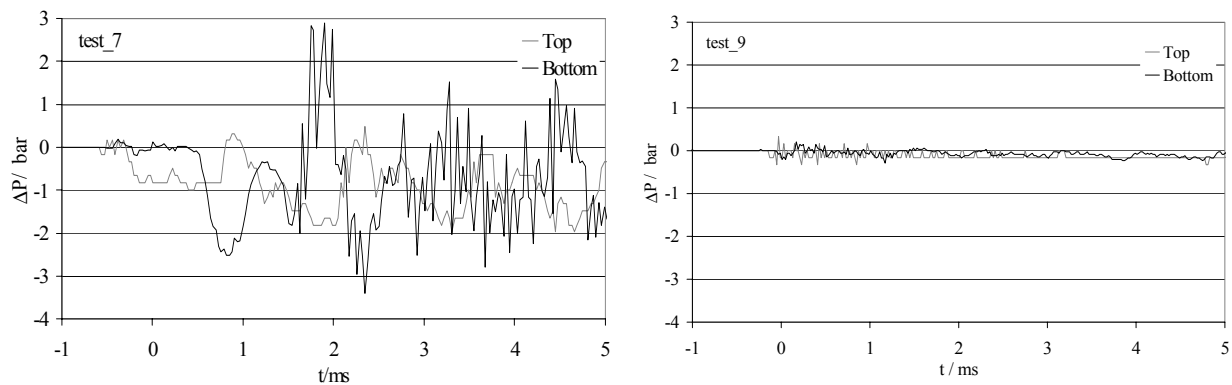


Figure 8: Transient pressure recordings in test 7 (left) and 9 (right). In test 7 the restriction was placed at the inlet of the burst disc holder, and in test 9 at the outlet.

As may be observed from the diagrams, the relocation of the restriction completely changed the transient pressure pattern inside the vessel after disc rupture. In test 7 there were pressure spikes with amplitude 6 bar at the bottom of the vessel, but in test 9, there is only a small ripple on the pressure curve. This means that the dynamic pressure inside the vessel after rupture is greatly affected by the geometry of and flow conditions through the rupture disc unit.

In tests without any restrictions besides the rupture disc itself, pressure oscillations have been measured, Figure 9. In this case the initial pressure was 35 bar, and the cross-section of the rupture disc was 124.7 mm. The oscillations did not give pressure spikes above the initial pressure, however.

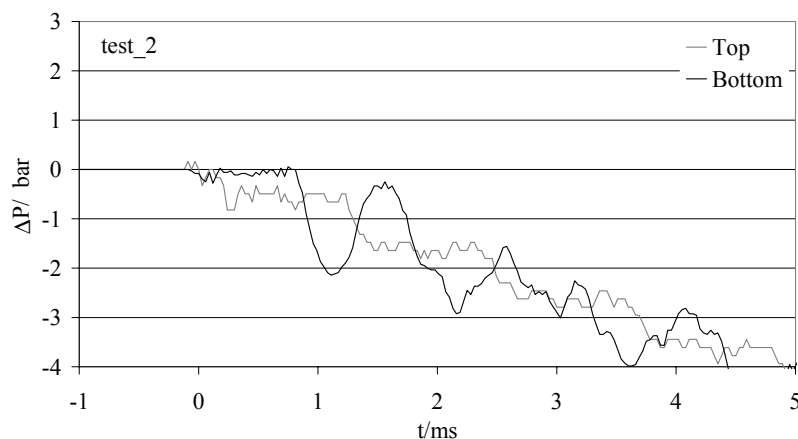


Figure 9: Transient pressure recordings for test 2 (top and bottom transducers)

In test 11, the initial pressure was increased to 60 bar, and the fill level was 80%. This is the only test with “inlet restriction” where a measurable pressure spike above the initial pressure was recorded, Figure 10. The spike was less than 1 bar, however, and was recorded for the top transducer. As shown in the extended-time recording (right diagram), there was also an indication of “pressure recovery” after about 20-30 ms for the top transducer, even though the peak pressure was not higher than the initial pressure. The recordings after 200-300 ms are questionable due to thermal effects on the transducers.

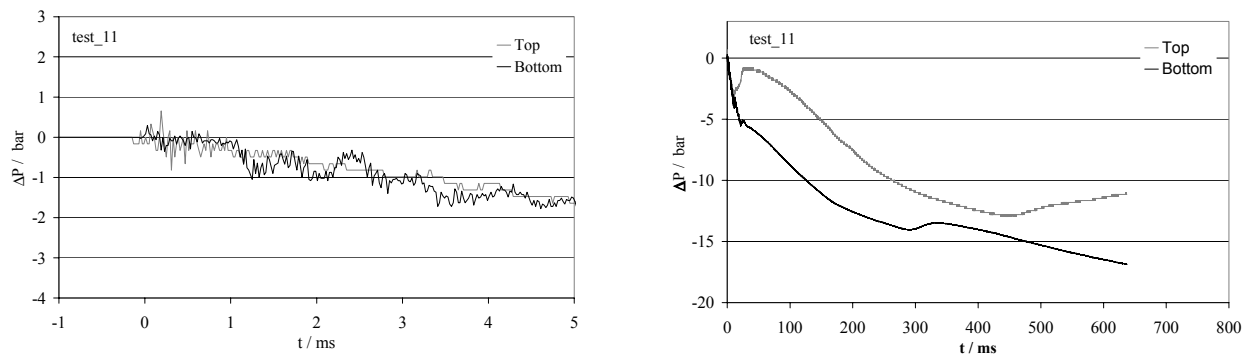


Figure 10: Transient pressure recordings (top and bottom transducers) in test 11
Left: initial 5ms; right: initial 800 ms.

Test 16 was conducted with 60 bar initial pressure, 50% fill level and no restrictions in the burst disc holder, Figure 11. Significant pressure oscillations were recorded, especially for the bottom transducer, but pressure above the initial were not recorded, neither in the short nor long time span.

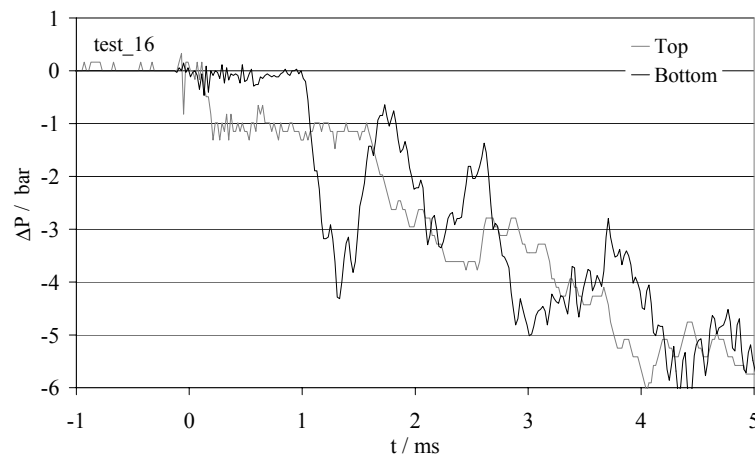


Figure 11: Transient pressure recordings (top and bottom transducers) in test 16

Finally, test 17 was conducted at the same conditions as test 16, but this time with the vessel turned upside down, i.e. with venting downwards. Results are shown in Figure 12. The “top” transducer is still the one that is located near the rupture disc. As may be observed by comparing Figures 16 and 17, the oscillations were smaller with bottom venting, and the larger oscillations occurred near the vent in test 17, and at the bottom (far from the vent) in test 16. As expected, the pressure release occurred faster with bottom venting, when the vapour pressure contributes in pressing the liquid out of the vessel

3.4 Discussion of BLEVE results

The maximum overpressure observed in any of the tests conducted so far was about 3 bar (7% above the initial pressure), and the maximum amplitude of pressure oscillations was 6 bar in the same test (Figure 4). A clear definition of how large overpressure is needed to qualify as a BLEVE does not exist, but the present results would probably not fall into this category. The accumulated results so far indicate that

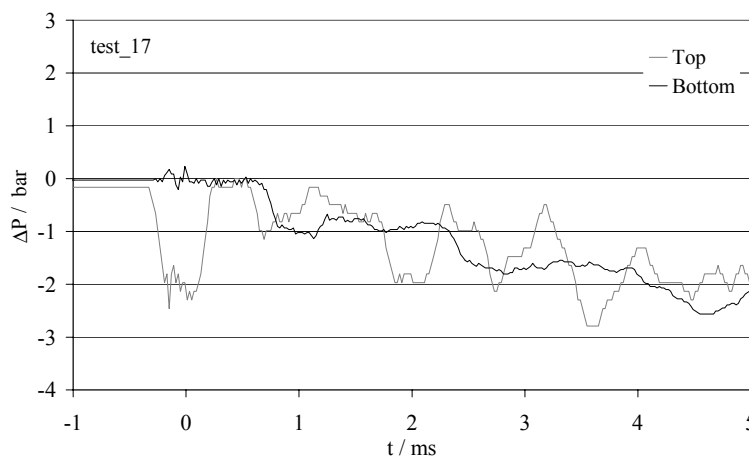


Figure 12: Transient pressure recordings (top and bottom transducers) in test 17, where the vessel is turned upside down. The “top” transducer is still located near the rupture disc, which is now at the bottom of the vessel.

the transient pressure behaviour inside the vessel was determined by the flow conditions in the rupture unit and not by any BLEVE effects.

According to the theory discussed by Kim-E and Reid (1983), the initial state before rupture has to be within a certain domain to reach a spinodal state during expansion, thereby causing a BLEVE. Other authors have shown that BLEVE may occur outside this domain, and may not occur inside this domain (Birk and Cunningham, 1994). The current experiments were based on typical low-pressure receiver conditions during AC system operation and start-up. The tests at 35 and 45 bar initial pressure are outside the calculated domain for CO₂, but the experiments at 60 bar initial pressure are inside, Figure 13. The figure also shows the initial states in the experiments by Kim-E and Reid (1983).

In the current tests, the peak overpressures occurred during the first five milliseconds of expansion, while the work of Venart and Ramier (1998) showed pressure recovery and a significant overpressure peak for the top sensor after 100-250 ms. In some of the early experiments with the current set-up, similar curves were recorded, but the main reason for the apparent overpressure peak turned out to be thermal shock effects in the pressure sensor. When the sensor was hit by the expanding/swelling cold liquid, the thermal distortion of the membrane gave a pressure reading. In separate experiments at atmospheric pressure “overpressure peaks” of 10-30 bar were recorded just by dipping the sensor face into cold liquid. After insulating the sensor face with a layer of PE tape, this effect was reduced/delayed. This experience is discussed in some more detail by Pettersen and Hakenjos (1983).

4. CONCLUSION

Since CO₂ is a non-toxic and non-flammable refrigerant, the major safety issues for CO₂ systems are related to the high operating pressure. In case of a component rupture, the explosion energy (stored energy) may characterise the extent of potential damage. The explosion energy can be estimated based on component (refrigerant-side) volumes, pressures and refrigerant property data.

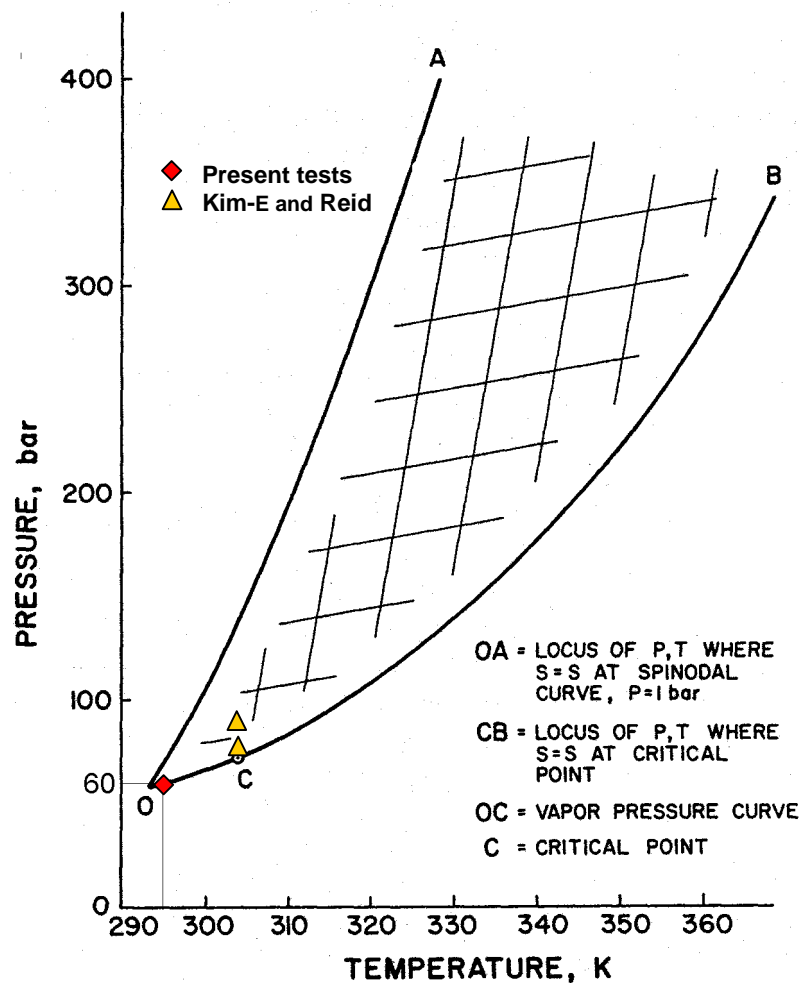


Figure 13: CO₂ p-T Domain, which, according to Kim-E and Reid (1983) could give a spinodal state upon rapid, isentropic depressurization. Figure taken from Kim-E and Reid (1983)

Pressures in CO₂ systems are much higher than with conventional refrigerants, but results from the present study show that for actual systems of equal capacity, reductions in internal volume and refrigerant charge makes the explosion energies comparable. At room temperature, the explosion energy of a CO₂ system may be higher than the HCFC/HFC baseline, but at elevated temperatures the energy of a HCFC/HFC system may exceed that of a CO₂ system.

Regarding the possible occurrence of BLEVE in CO₂ vessels, the maximum observed pressure spikes in the present tests were only a few bar above the initial pressure. These spikes occurred within a few milliseconds of the disc rupture. Transient pressure oscillations inside the test vessel are mainly caused by (two-phase) flow conditions through the rupture disc unit and inlet/outlet restrictions.

Re-pressurisation to higher-than-initial pressure in a longer time-scale as reported by Venart and Ramier (1998) has not been observed in the present tests.

Initial pressures above 60 bar, including supercritical conditions, may give higher probability of BLEVE occurrence, and larger pressure spikes. Further tests will include these conditions, reflecting accumulator, separator or receiver conditions during stillstand or high-temperature pull-down conditions in a vapour compression system.

ACKNOWLEDGEMENTS

Funding for the BLEVE-part of this work was kindly provided by Hydro Aluminium, Visteon Automotive Systems and DaimlerChrysler. The present study is one of the Norwegian projects within IEA Annex 27: Selected Issues on CO₂ as Working Fluid in Compression Systems.

REFERENCES

- Amin, J, Dienhart, B., and Wertenbach, J. 1999. Safety Aspects of an A/C System with Carbon Dioxide as Refrigerant. *SAE Automotive Alternate Refrigerants Symposium*, June 28 – July 1, 1999, Scottsdale, Arizona, USA
- Angus, S., Armstrong, B., and deReuck, D.R., 1976. International Thermodynamic Tables of the fluid State: Carbon Dioxide, International Union of Pure and Applied Chemistry, Pergamon Press, Oxford.
- Berghmans, J., Duprez, H., 1999, Safety Aspects of CO₂ Heat Pumps. *IEA / IZWe.V . /IIR Workshop on CO₂ Technology in Refrigeration, Heat Pump and Air Conditioning Systems*, Mainz, Germany, March 18.
- Birk, A. M., and Cunningham, M. H., 1994. The boiling liquid expanding vapour explosion. *J. Loss Prev. Process Ind.*, Vol 7 No 6, pp 474-480.
- Chan, C.Y., and Haselden, G.G., 1981, Computer-based refrigerant properties. Part 1: Basic Equations, *Int. J. Refrig.* Vol 4, No 1, p.7-12.
- DKV, 1998. Kohlendioxid – Besonderheiten und Einsatzchancen als Kältemittel. Statusbericht des Deutschen Kälte- und Klimatechnischen Vereins (DKV). Nr 20, November 1998.
- Hakenjos, J., 2000. Investigation of BLEVE. A report from project work at SINTEF Energy Research as Exchange Student from FH Karlsruhe, July
- Kim-E, M. E., and Reid, R. C. 1983. The Rapid Depressurization of Hot, High Pressure Liquids or Supercritical Fluids. *Chemical Engineering at Supercritical Fluid Conditions*. Ann Arbor Science, Michigan, USA
- Kuprianoff, J., 1953, Die feste Kohlensäure (Trockeneis) – Herstellung und Verwendung, Sammlung chemischer und chemisch-technischer Vorträge. Neue Folge Heft 52. Zweite umgearbeitete und erweiterte Auflage. Ferdinand Enke Verlag Stuttgart.
- McDevitt, C.A., Chan, C.K., Steward, F.R., Tennankore, K.N. 1990. Initiation Step of Boiling Liquid Expanding Vapour Explosion. *J. Hazardous Materials*, Vol. 25, p. 169-180, 1990
- NIOSH, 1996. US National Institute for Occupational Safety and Health. <http://www.cdc.gov/niosh/idlh/124389.html>
- Pettersen, J., 1999. Comparison of explosion energies in residential air-conditioning systems based on HCFC-22 and CO₂. *20th International Congress of Refrigeration (IIR)*, Sydney, Australia, September 19-24, 1999
- Pettersen, J. and Hakenjos, J, 2000. Boiling Liquid Expanding Vapour Explosions in CO₂ Vessels: Initial Experiments. *4th IIR Gustav Lorentzen Conference on Natural Working Fluids*, Purdue University, IN, USA, July.
- Pitzer, K.S and Schreiber, D., 1988, Improving EOS accuracy in the critical region - Equations for Carbon Dioxide and Neopentane as examples, *Fluid Phase Equilibra*, 41 p.1-17

- Tang, Hoi Ki, 1999. Safety Aspects in CO₂ Vapour Compression Systems - Investigation of BLEVE. External Diploma Work of the University of Dortmund, Germany. Carried out at SINTEF Energy Research, Trondheim, Norway
- Tillner-Roth and Baehr, H.D. 1994. An international standard formulation of the thermodynamic properties of 1,1,1,2-tetrafluoroethane (HFC-134a) covering temperatures from 170 K to 455 K at pressures up to 70 MPa. *J. Phys. Chem. Ref. Data* 23, 657-729
- Venart, J. E. S., Rutledge, G. A., Sumathipala, K., and Sollows, K. 1993. To BLEVE or Not to BLEVE: Anatomy of a Boiling Liquid Expanding Vapour Explosion. *Process Safety Progress*, Vol 12, No 2, April, pp 67-70
- Venart, J. E. S. and Ramier, S. A. 1998 Boiling Liquid Expanding Vapour Explosions (BLEVE): the influence of dynamic re-pressurization and two-phase discharge. PVP-Vol 377-2, *Computational Technologies for Fluid/Thermal/Structural/Chemical Systems With Industrial Applications*, Volume II, ASME, pp. 249-254.
- Aarlien R., and Frivik, P.E. 1998, Comparison of practical performance between CO₂ and R-22 reversible heat pumps for residential use. *Natural Working Fluids '98* Oslo, Norway June 2-5. Proceedings, p.388-398.

6.4.2 BOILING LIQUID EXPANDING VAPOUR EXPLOSIONS (BLEVE) IN CO₂ VESSELS: INITIAL EXPERIMENTS

J. PETTERSEN¹, J. HAKENJOS²

¹Norwegian University of Science and Technology (NTNU)
Dept. of Refrigeration and Air Conditioning, N-7491 Trondheim, Norway

²Fachhochschule Karlsruhe, Germany (Project work at SINTEF/NTNU)

Contact e-mail: Jostein.Pettersen@kkt.ntnu.no

ABSTRACT

A Boiling Liquid Expanding Vapour Explosion (BLEVE) may occur when a vessel containing pressurised liquid or supercritical fluid is rapidly depressurised, e.g. due to a crack or a rupture. The sudden depressurisation leads to instant vaporisation that may give a transient overpressure peak. In some cases the overpressure can be high enough to rupture the whole vessel, with a resulting blast wave and risk of flying fragments. An experimental study at NTNU/SINTEF aims at improving the understanding of BLEVE in CO₂ systems. A test vessel has been built in order to measure transient pressures during initial depressurisation and possible subsequent overpressure peak(s). Some tests have been conducted at varying initial conditions and liquid fill levels, and with varying vent areas. The paper shows typical transient pressure recordings, and provides a discussion of practical relevance of the results. A maximum overpressure peak of 3 bar above the initial pressure has been observed in the current test programme.

1. INTRODUCTION

With increasing focus on the use of carbon dioxide (CO₂ or R-744) as a refrigerant, the safety characteristics of CO₂ vapour compression systems are being discussed. Although carbon dioxide is usually regarded as non-toxic (DKV, 1998), there are physiological effects from breathing air with a CO₂-concentration above a few percent. At 2-3 % concentration by volume, the breathing rate will increase, and headache may be experienced after some time. The IDLH (Immediate Danger to Life and Health) concentration is set to 4%, and the lowest reported lethal concentration is 10% (Berghmans and Duprez, 1999). In practice, a maximum allowable concentration of about 5% by volume seems to be a reasonable limit (Berghmans and Duprez, 1999), (Amin, Dienhart and Wertenbach, 1999). In the design and operation of CO₂ systems, this will be the maximum acceptable concentration as a result of sudden release or prolonged leakage of CO₂ into an occupied space.

Another safety concern with CO₂ is the effect of high operating pressure. Low-side pressures are typically 20-50 bar, and high-side pressures may be as high as 120-140 bar. These pressures are 5-10 times higher than in traditional fluorocarbon systems. High pressure is not a safety issue in itself, since the equipment will be designed for this. In case of a component rupture, however, the explosion energy (stored energy) may characterise the extent of potential damage. The explosion energy can be estimated based on component (refrigerant-side) volumes, pressures and refrigerant property data. Owing to small internal volumes, the energy release from a CO₂ system explosion is not necessarily higher than from a baseline system using a conventional refrigerant (Pettersen, 1999). One important factor related to this is the possible occurrence of a BLEVE (Boiling Liquid Expanding Vapour Explosion), that may create a more severe blast effect than from an ordinary refrigerant expansion. A BLEVE may occur when a vessel containing a pressurised liquid or supercritical fluid is rapidly depressurised, e.g. due to a crack or a rupture. The sudden depressurisation leads to an explosive vaporisation that may give a transient overpressure peak inside the vessel. The overpressure peak may lead to a powerful burst of the whole vessel, with total loss of content, a resulting blast wave and risk of flying fragments. Such a scenario can

occur with any liquefied gas or supercritical fluid, and there are numerous reports in the literature about LPG and propane tanks where BLEVE has occurred. With a flammable fluid, there is also the additional risk of an explosion due to combustion of the vessel contents.

A number of theories have been suggested as explanations for this phenomenon, but at present no reliable method can predict BLEVE occurrence. The present paper outlines some initial results from an experimental study on BLEVE in CO₂ vessels. A major objective of the study is to identify possible regimes of BLEVE occurrence, and to provide a better understanding of the relevance of this phenomenon in CO₂ vapour compression systems. Section 2 of the paper briefly outlines the current status of BLEVE understanding, based on published literature. Experimental arrangements and results from the present study are outlined in Sections 3 and 4. In Section 4 the results and their significance are discussed, and some conclusions are listed in Section 5.

2. EARLIER BLEVE STUDIES

The term BLEVE (Boiling Liquid Expanding Vapour Explosion) was introduced in 1957 by J. B. Smith, W. S. Marsh and W. L. Walls, while investigating the causes of a steel vessel explosion at a phenolic resin plant. When a high-pressure liquid or supercritical fluid is very rapidly depressurised as a result of an accident, normal flashing may be delayed and a superheated liquid is formed. Homogeneous nucleation may occur in this metastable liquid, leading to strong and damaging shock waves. Other transient flow effects and shock waves may also contribute to the development of a BLEVE.

Kim-E and Reid (1983) discussed a thermodynamic model based on the spinodal fluid state, which represents the limit-of-stability for the liquid phase during expansion. In a rapid expansion process, homogeneous nucleation will occur at this state. The authors were not able to demonstrate the predicted shock effects or pressure spikes in their experiments on CO₂ using a 7-liter tank with a 1.5 inch diameter burst disc. Reasons for poor agreement between theory and experiments may include factors like formation of vapour bubbles on the wall of the vessel, and shock waves or disturbances from the mechanism that ruptured the burst disc of the test vessel (Kim-E and Reid, 1983). The presence of vapour bubbles before depressurisation may have given heterogeneous nucleation instead of the homogeneous nucleation required for a BLEVE.

McDevitt et al. (1990) conducted experiments with R-22 at 65°C / 27 bar in a one-litre tank, using a rifle bullet shot through the tank to trigger a BLEVE. A transient pressure of 35 bar was recorded (an overpressure of 8 bar or 30%), probably including significant effects of the rifle bullet. Later tests in a shock-tube with a mechanically triggered burst disc gave considerably lower pressure peaks.

Venart and Ramier (1998), and Venart et al. (1993) investigated additional aspects of BLEVEs, including dynamic re-pressurisation, cavitation, and two-phase discharge effects. With top venting, the initial depressurisation is expected to create a rising two-phase swell inside the vessel. When the two-phase flow impacts the top of the vessel, a shock may be created, and re-pressurisation may occur. This re-pressurisation may be large enough to cause cavitation, giving additional shock effects in the liquid and the vessel walls. The latter phenomenon is termed BLCBE (Boiling Liquid Compressed Bubble Explosion). In contrast to the other studies mentioned above, where time-scales typically were a few milliseconds, the time-scale of re-pressurization reported by Venart and Ramier (1998) were in the hundred millisecond regime.

No reliable method exists for prediction BLEVE occurrence and the magnitude of pressure peaks in CO₂ vessels.

3. EXPERIMENTAL SET-UP

The test set-up included an instrumented cylindrical test vessel with an internal volume of 1 litre, and a high-speed data recording system. In order to avoid any disturbance caused by a mechanical piercing

device, the burst discs were allowed to crack open by internal pressure only, and an electric trigger mechanism initiated data recording. The vessel was positioned with a vertical axis.

A design pressure of 200 bar was used for the vessel, which was made from stainless steel. It consisted of a cylindrical tube of 250 mm length and 73 mm ID, with end plates of 30 mm thickness. The inner surfaces were polished to suppress bubble nucleation. The rupture disc was installed in a holder at the top of the vessel, Figure 1. Piezoelectric pressure sensors were installed in the top and bottom of the vessel, and a static pressure sensor was installed in the bottom.

Data from the pressure transducers were logged by a 100 kHz PC card, giving a sample rate of 33 per millisecond (ms) per channel. The card was equipped with integrated memory, storing 3 ms of data preceding the trigger signal.

Before each test, the vessel was purged with CO₂ gas, cooled and filled with the specified amount of liquid CO₂. The vessel was then allowed to slowly warm to approach the specified burst pressure. Depressurisation was initiated when the rupture disc cracked open, leaving a reasonably well-defined cross section, Figure 2. The discs break at a given specific burst pressure with an accuracy of $\pm 5\%$. The vent (outlet) area can be varied by installing adapters on the disc holder on the outlet side.

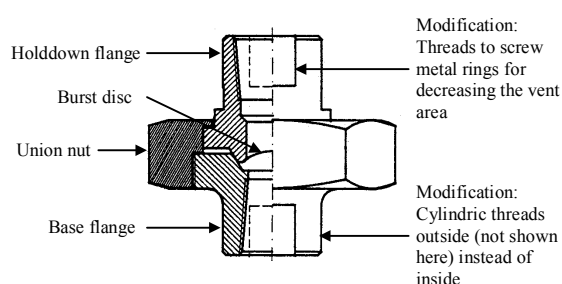


Figure 1 Union holder for rupture disc



Figure 2 0.5 inch (13 mm) standard type rupture disc with 30° seat

4. PRELIMINARY RESULTS

Table 1 outlines the test programme for experiments that have been completed so far. Rupture pressures 35 and 45 bar corresponds to saturation temperatures of 0°C and 10°C, respectively. These conditions reflect typical low-side accumulator pressures in AC systems during operation. A vent area of 113.1 mm² corresponds to full opening, i.e. no restriction adapter on the outlet.

Transient pressure recordings for the top and bottom sensor in tests 3, 1, 5 and 2 are shown in Figure 3a and 3b, focusing on the first five milliseconds after disc rupture. Similar recordings from tests 6 and 7 are shown in Figure 4.

Table 1 Test programme

Test	Rupture pressure, bar	Liquid CO ₂ charge, g	Fill level, %	Vent area, mm ²
3	35	485	50	3.1
1	35	485	50	7.1
5	35	486	50	50.3
2	35	485	50	113.1
6	35	777	80	3.1
7	45	450	50	3.1

By comparing data from tests 3, 1, 5, and 2, the effects of increasing the vent area can be observed. The liquid level (50%) and rupture pressure (35 bar) are kept constant in these tests. Tests 6 and 7 shows the effects of increasing liquid level and rupture pressure, respectively.

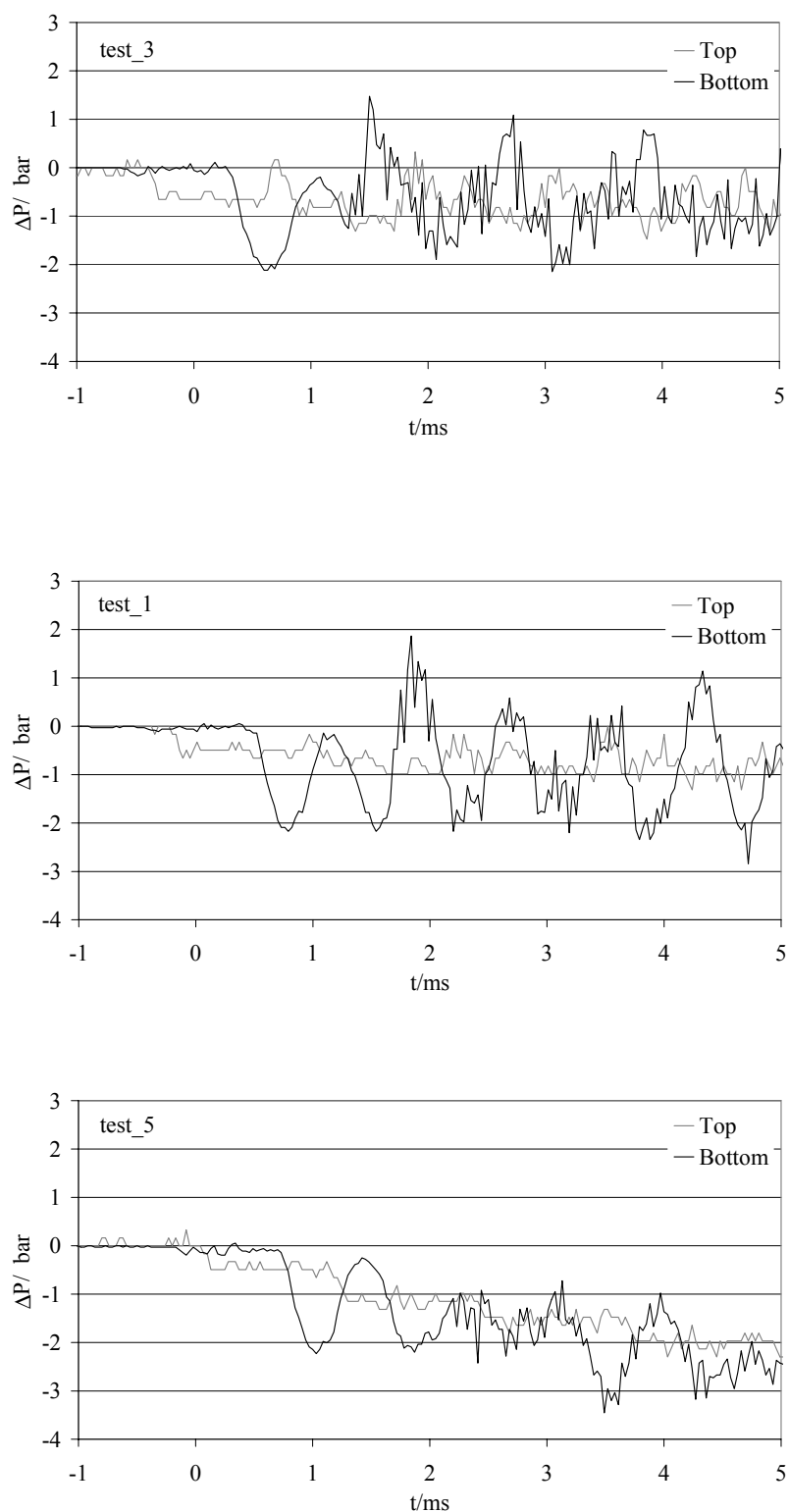


Figure 3a Transient pressure recordings for tests 3, 1 and 5 (top and bottom transducers)

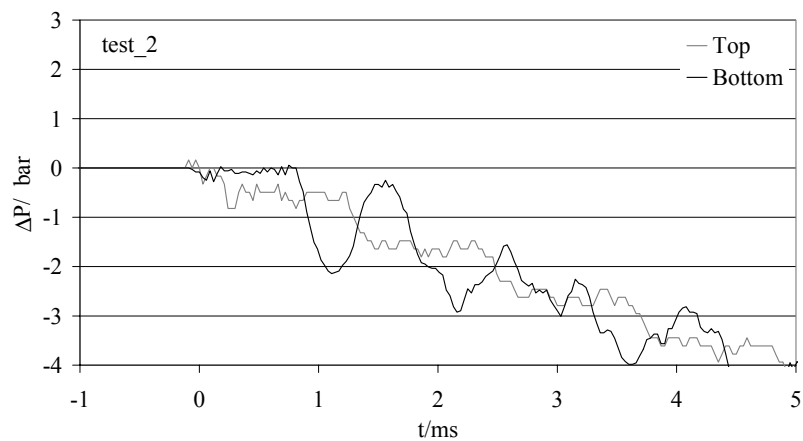


Figure 3b Transient pressure recordings for test 2 (top and bottom transducers)

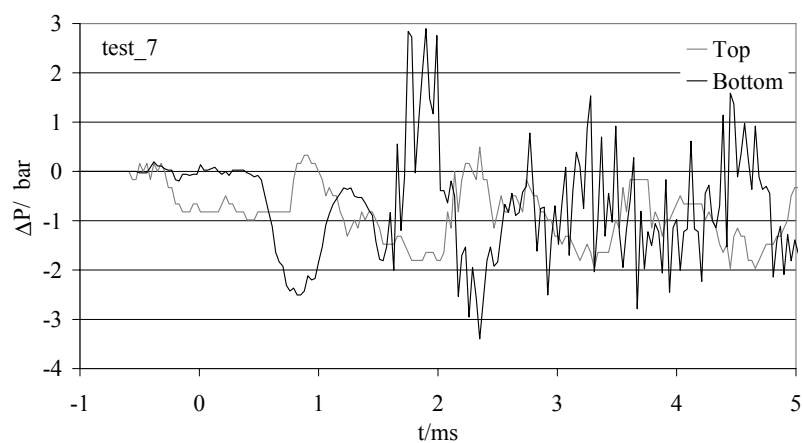
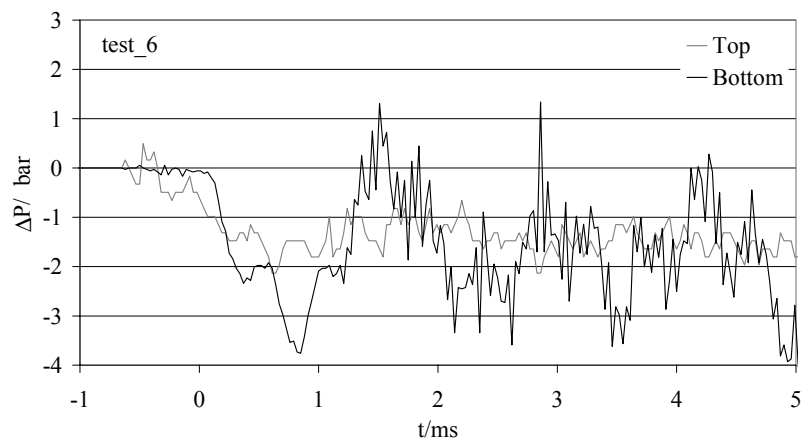


Figure 4 Transient pressure recordings for tests 6 and 7 (top and bottom transducers)

All tests gave much larger pressure amplitudes for the bottom sensor than for the top sensor. In some cases (e.g. test 7) it seems like the two signals are in opposite phases, a fact that may indicate that the liquid phase experienced some kind of oscillation inside the vessel.

In all the tests with 50% fill level (tests 3, 1, 5 and 2), the bottom sensor signal gave a quite distinct and similarly shaped curve during the initial 1-2 ms. During this initial period, the pressure dropped to about 2 bar (5.7%) below the initial pressure, and then increased to about initial pressure. After the first milliseconds, the signal became more rippled and with more rapid oscillations than in the initial period. The maximum amplitude of the “main” oscillation was about 4 bar in test 1, with a peak at about 2 bar above the initial pressure. The top transducer showed less change in signal type during the observed time span.

With a fill level of 80% (test 6), both the initial part of the curve and the shape of subsequent oscillations for the bottom transducer looked somewhat different. With 45 bar rupture pressure (test 7), the amplitude of the oscillations were larger, reaching a maximum of 6 bar, causing an overpressure of almost 3 bar about 2ms after rupture.

5. DISCUSSION

The maximum overpressure observed in any of the current tests was about 3 bar (7% above the initial pressure), and the maximum amplitude of pressure oscillations was 6 bar in the same test (Figure 4). A clear definition of how large overpressure is needed to qualify as a BLEVE does not exist, but a pressure oscillation of 6 bar may in some cases be sufficient to rupture a pressure vessel that has already developed a crack or has been mechanically damaged.

According to the theory discussed by Kim-E and Reid (1983), the initial state before rupture has to be within a certain domain to reach a spinodal state during expansion, thereby causing a BLEVE. Other authors have shown that BLEVE may occur outside this domain, and may not occur inside this domain, however (Birk and Cunningham, 1994). The current experiments were based on typical low-pressure receiver conditions during AC system operation, which are outside the calculated domain for CO₂. Later experiments will include supercritical pressures and saturated conditions above 56 bar, which in theory would give a spinodal state during isentropic expansion (Kim-E and Reid, 1983).

In the current tests, the peak overpressures occurred during the first five milliseconds of expansion, while the work of Venart and Ramier (1998) showed pressure recovery and a significant overpressure peak for the top sensor after 100-250 ms. In some of the early experiments with the current set-up, similar curves were recorded, but the main reason for the apparent overpressure peak turned out to be thermal shock effects in the pressure sensor. When the sensor was hit by the expanding/swelling cold liquid, the thermal distortion of the membrane gave a pressure reading. In separate experiments at atmospheric pressure “overpressure peaks” of 10-30 bar were recorded just by dipping the sensor face into cold liquid. After insulating the sensor face with a layer of PE tape, this effect was reduced/delayed. The upper diagram in Figure 5 shows the sensor signals before thermal insulation was applied on the top sensor, at conditions corresponding to test 2. In the lower diagram, insulation has been applied on the top sensor. The drift away from zero signal for the upper sensor after about 200-300ms was probably caused by thermal stress in the vessel end-plate and the sensor mounting bushing.

One design-related consequence of the present tests is that the opening of a top-mounted pressure relief device may cause significant pressure oscillations, particularly in the bottom of the vessel. In test 7, for instance, the vent area was just 3.1 mm² (diameter 2.0 mm), which could be a relevant cross section for a pressure relief valve.

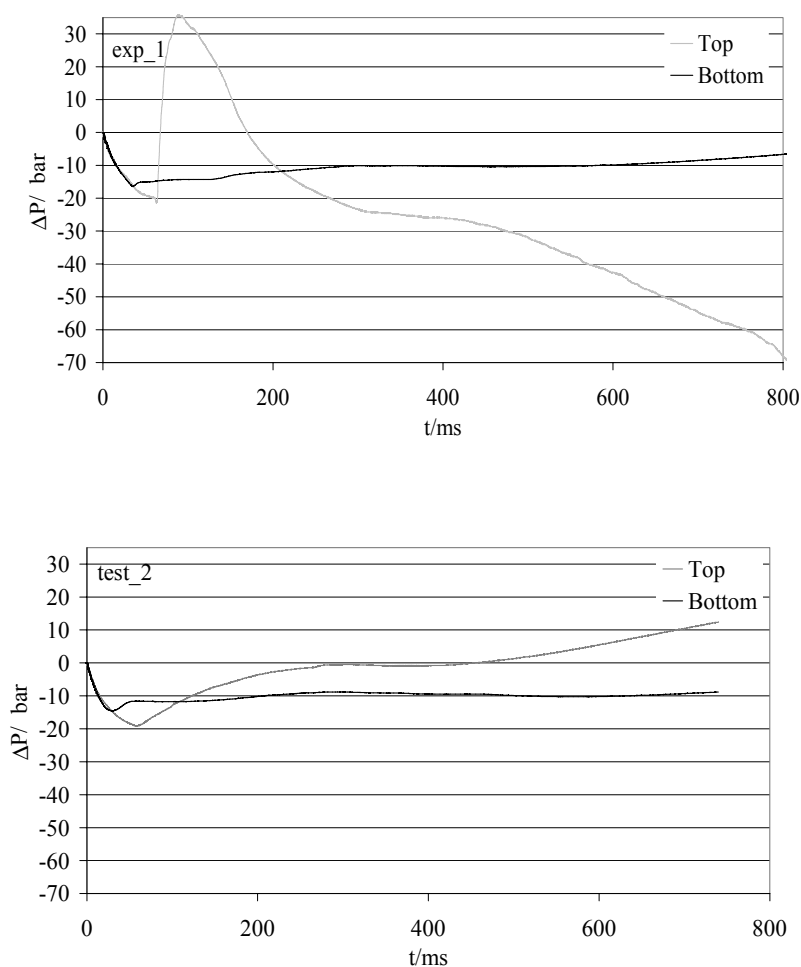


Figure 5 Apparent pressure recovery during 800 ms period. Upper diagram: Without thermal insulation of top sensor. Lower diagram: After insulating the top sensor. Conditions corresponding to test 2.

6. CONCLUSION

Based on the results and findings from the study so far, the following conclusions may be drawn:

- Depressurisation tests with varying vent areas have been completed with a 1-litre test vessel at initial conditions typical of low-pressure accumulators in CO₂ AC systems during operation.
- The maximum observed pressure spikes occurred within a few milliseconds after rupture disc cracking. Maximum overpressure spikes have been less than 3 bar, and the amplitude of pressure oscillations have been less than 6 bar.
- Maximum pressure spikes occurred for a moderate vent area, and in the test with the highest initial pressure.
- Re-pressurisation to higher-than-initial pressure in a longer time-scale as reported by Venart and Ramier (1998) has not been observed in the present tests.

- Higher initial pressures, including supercritical conditions, may give higher probability of BLEVE occurrence, and larger pressure spikes. Further tests will include these conditions, reflecting accumulator, separator or receiver conditions during stillstand or pull-down conditions in a vapour compression system.

7. ACKNOWLEDGEMENTS

Funding for this work was kindly provided by Hydro Aluminium, Visteon Automotive Systems and DaimlerChrysler. The present study is one of the Norwegian projects within IEA Annex 27: Selected Issues on CO₂ as Working Fluid in Compression Systems.

8. REFERENCES

- Amin, J, Dienhart, B., and Wertenbach, J. 1999. Safety Aspects of an A/C System with Carbon Dioxide as Refrigerant. *SAE Automotive Alternate Refrigerants Symposium*, June 28 – July 1, 1999, Scottsdale, Arizona, USA
- Berghmans, J., Duprez, H., 1999, Safety Aspects of CO₂ Heat Pumps. *IEA / IZWe.V . /IIR Workshop on CO₂ Technology in Refrigeration, Heat Pump and Air Conditioning Systems*, Mainz, Germany, March.
- Birk, A. M., and Cunningham, M. H., 1994. The boiling liquid expanding vapour explosion. *J. Loss Prev. Process Ind.*, Vol 7 No 6, pp 474-480.
- DKV, 1998. Kohlendioxid – Besonderheiten und Einsatzchancen als Kältemittel. Statusbericht des Deutschen Kälte- und Klimatechnischen Vereins (DKV). Nr 20, November 1998.
- Kim-E, M. E., and Reid, R. C. 1983. The Rapid Depressurization of Hot, High Pressure Liquids or Supercritical Fluids. *Chemical Engineering at Supercritical Fluid Conditions*. Ann Arbor Science, Michigan, USA
- McDevitt, C.A., Chan, C.K., Steward, F.R., Tennankore, K.N. 1990. Initiation Step of Boiling Liquid Expanding Vapour Explosion. *J. Hazardous Materials*, Vol. 25, p. 169-180, 1990
- Pettersen, J., 1999. Comparison of explosion energies in residential air-conditioning systems based on HCFC-22 and CO₂. *20th International Congress of Refrigeration (IIR)*, Sydney, Australia, September 19-24, 1999
- Tang, Hoi Ki, 1999. Safety Aspects in CO₂ Vapour Compression Systems - Investigation of BLEVE. External Diploma Work of the University of Dortmund, Germany. Carried out at SINTEF Energy Research, Trondheim, Norway
- Venart, J. E. S., Rutledge, G. A., Sumathipala, K., and Sollows, K. 1993. To BLEVE or Not to BLEVE: Anatomy of a Boiling Liquid Expanding Vapour Explosion. *Process Safety Progress*, Vol 12, No 2, April, pp 67-70
- Venart, J. E. S. and Ramier, S. A. 1998 Boiling Liquid Expanding Vapour Explosions (BLEVE): the influence of dynamic re-pressurization and two-phase discharge. PVP-Vol 377-2, *Computational Technologies for Fluid/Thermal/Structural/Chemical Systems With Industrial Applications*, Volume II, ASME, pp. 249-254.

6.4.3 EXPERIMENTAL STUDY ON BOILING LIQUID EXPANSION IN A CO₂ VESSEL

J. PETTERSEN

Norwegian University of Science and Technology
Department of Refrigeration and Air Conditioning
NO-7491 Trondheim, NORWAY
Jostein.Pettersen@kkt.ntnu.no

ABSTRACT

Theory predicts that a Boiling Liquid Expanding Vapour Explosion (BLEVE) or Boiling Liquid Collapsed Bubble Explosion (BLCBE) may occur when a vessel containing pressurised saturated liquid is rapidly depressurised, e.g. due to a crack or initial rupture. The sudden depressurisation leads to explosive vaporisation and a transient overpressure peak that may burst the vessel. The paper provides results from an experimental study aimed at clarifying the possible occurrence of BLEVE/BLCBE in CO₂ systems. A test vessel was built and instrumented in order to measure transient pressures during initial depressurisation, and to record possible subsequent overpressure peak(s). A test program was conducted at varying initial conditions and liquid fill levels, and with varying vent areas. The paper shows typical transient pressure recordings, and provides a discussion of practical relevance of the results. No signs of BLEVE/BLCBE were recorded during this study.

INTRODUCTION

With increasing focus on the use of carbon dioxide (CO₂ or R-744) as a refrigerant, the safety characteristics of CO₂ vapour compression systems are being discussed. The high operating pressures in CO₂ system may be considered a risk factor, although elevated pressure does not pose any risk in itself since components and systems will be designed for this. Low-side pressures in CO₂ systems are typically 2-5 MPa, and high-side pressures may be as high as 10-14 MPa. These pressures are 5-10 times higher than in traditional fluorocarbon systems.

In case of a component rupture, the explosion energy (stored energy) may characterise the extent of potential damage, and this is a function of initial pressure, as well as internal volume. The explosion energy can be estimated based on internal volumes, initial refrigerant conditions, and refrigerant property data. Owing to the small volumes, the energy released from a CO₂ system explosion is not necessarily higher than from a baseline system using a conventional refrigerant. This has been demonstrated by calculations for a typical residential air-conditioning system, and for mobile air conditioning systems (Pettersen et al., 2000). In both cases, the CO₂ explosion energy was comparable to the energy of the baseline fluorocarbon system, with a slightly higher energy in the baseline system at elevated temperature, and the opposite situation at moderate/low temperature.

The duration of the energy release may be of equal importance as the amount of energy released. An important consequence of explosive vaporization is shorter duration and thereby a more severe blast effect than from ordinary refrigerant expansion, even though the energy is the same. In the assessment of safety issues, the possible occurrence of rapid phase transition phenomena is important. Mechanisms of explosive vaporization discussed in the literature include BLEVE (*Boiling Liquid Expanding Vapour Explosion*) and BLCBE (*Boiling Liquid Collapsed Bubble Explosion*). These phenomena may occur when a vessel containing a pressurised liquid or supercritical fluid is rapidly depressurised, e.g. due to an initial crack or rupture. The sudden depressurisation gives a superheated liquid phase that is suddenly vaporized in an explosive manner. This may give a transient overpressure peak inside the vessel, which again may lead to a powerful burst of the whole vessel, with total loss of content, a resulting blast wave and risk of

flying fragments. Such a scenario can occur with any liquefied gas or supercritical fluid, and there are numerous reports in the literature about LPG and propane tanks where BLEVE has occurred. With a flammable fluid, there is also the even more serious risk of an explosion due to combustion of the vaporized vessel contents.

A number of theories have been suggested to explain these phenomena, but no fully reliable method can predict BLEVE or BLCBE occurrence. The present paper outlines the results from an experimental study on explosive vaporization in CO₂ vessels. A major objective of the study was to identify possible occurrence of overpressure peaks, and to provide a better understanding of the relevance of this phenomenon in CO₂ vapour compression systems. The two key questions were to determine if BLEVE/BLCBE occurred, and if so – under which conditions.

1 SUMMARY OF EARLIER STUDIES ON BOILING LIQUID EXPANSION

When a high-pressure saturated liquid or supercritical fluid is very rapidly depressurised as a result of an accident (crack, rupture, puncture etc.), normal flashing may be delayed, thus creating a superheated liquid state. Homogeneous nucleation and explosive vaporization may occur in this metastable liquid, leading to strong and damaging shock waves - a BLEVE. Other transient flow effects and shock waves may also contribute to the development of a BLEVE.

An important reason for considering the possible occurrence of BLEVE in CO₂ vessels is a paper by Kim-E and Reid (1983), which pointed to this possibility. The authors applied a thermodynamic model based on the spinodal fluid state, which represents the limit-of-stability for the liquid phase during expansion. In a rapid expansion process, homogeneous nucleation will occur at this state. The predicted shock effects or pressure spikes did not occur in their experiments on CO₂ using a 7-liter tank with a 1.5 inch diameter burst disc, however. Reasons for disagreement between theory and experiments may include factors like vapour bubbles on the wall of the vessel, and shock waves or disturbances from the mechanism that ruptured the burst disc of the test vessel. The presence of vapour bubbles before depressurisation may have given heterogeneous nucleation instead of the homogeneous nucleation required for a BLEVE.

The general literature on BLEVE is dominated by publications that discuss hydrocarbon (LPG, propane) tank explosions. The key safety issues in such incidents are the ignition and combustion of the flammable content when this is vaporized, creating severe damage due to shock waves and burning. Usually, this situation arises due to a fire near the tank or due to an ignition source that starts an explosion of the escaped gas/vapour cloud. The concept of a “cold” BLEVE is not much focused on, and the few publications that report accidents with CO₂ storage tanks generally do not mention BLEVE effects (Clayton and Griffin, 1994), (Vörös and Honti, 1974). In a recent study on risks with CO₂ as fire suppressant, issues like BLEVE or tank explosions were not considered at all (EPA, 2000), even though such systems may include large storage vessels.

Venart and Ramier (1998), and Venart et al. (1993) investigated additional aspects of BLEVEs, including dynamic re-pressurisation, cavitation, and two-phase discharge effects. With top venting, the initial depressurisation due to a crack or puncture creates a rising two-phase swell inside the vessel. When the two-phase swell impacts the top of the vessel, a shock may be created, and re-pressurisation may occur. In addition to physical constraints, the expanding two-phase flow may be constrained by acoustic or inertial limitations. Re-pressurisation may cause bubbles to collapse (cavitation), giving additional damaging shock effects in the liquid and the vessel walls. This multi-step mechanism is termed BLCBE (Boiling Liquid Compressed Bubble Explosion). In contrast to other studies, where time-scales typically are a few milliseconds, the time-scale of re-pressurization reported by Venart and Ramier (1998) were in the hundred-millisecond regime.

Pettersen and Hakenjos (2000) reported initial experiments from the present project on CO₂. They did not observe significant overpressure spikes in any of their tests at 3.5 and 4.5 MPa initial pressure with varying liquid fill level and discharge opening, although quite large pressure oscillations in a milliseconds-scale occurred in some experiments. The maximum observed pressure amplitude was 0.6 MPa, and the maximum overpressure spike was 0.3 MPa (7% above initial pressure). The authors found that thermal shock effects on the pressure sensors were significant and had to be avoided or corrected for. What initially appeared to be significant overpressure peaks later turned out to be a result of thermal shock caused by the top sensor being contacted by the swelling cold liquid inside the test vessel. Dipping the pressure sensor into hot or cold water/refrigerant at atmospheric pressure gave the same dynamic effect (Hakenjos, 2000). After coating the pressure sensor face with a layer of thermal insulation, repeated experiments always gave transient pressures lower than the initial. An example of transient pressure recordings without and with sensor insulation is shown in Figure 1

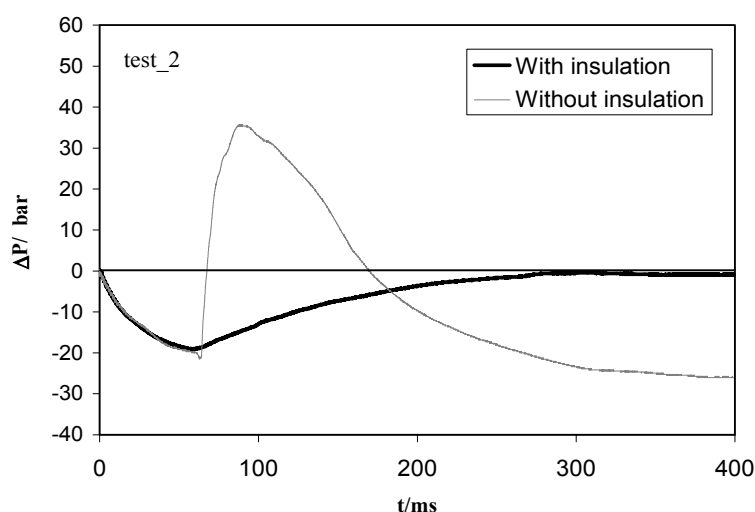


Figure 1 – Comparison of pressure sensor signal before and after applying thermal insulation on top sensor, at conditions corresponding Test 2.

It is not clear if thermal shock effects have influenced overpressure spikes reported in the literature. The graphs shown by Venart and Ramier (1998) for a 2.4 litre R-22 vessel, for instance, have a quite similar shape to graphs from the present tests before the top sensor was insulated, Figure 2.

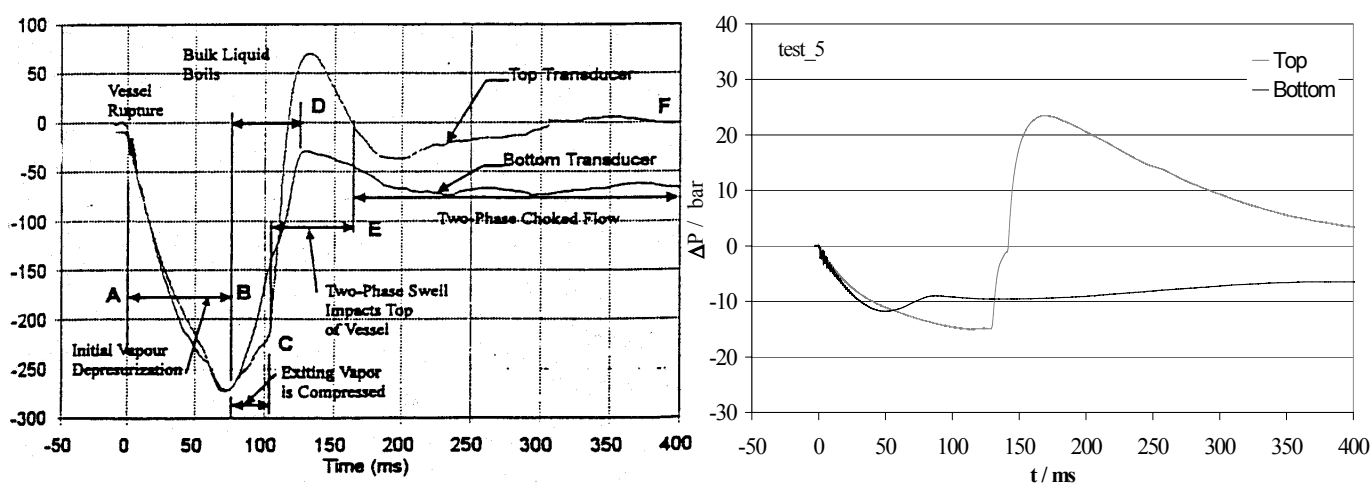


Figure 2 – Examples of dynamic pressure traces for R-22 from Venart and Ramier (1998) (left), and from the present experiments on CO₂ (Test 5) (right). The CO₂ top sensor trace (right diagram) is incorrect due to thermal shock effects.

2 EXPERIMENTAL METHODS

The test rig included an instrumented cylindrical test vessel with an internal volume of 1 litre, and a high-speed data recording system. In order to avoid disturbances caused by a mechanical piercing device or triggering mechanism, burst discs were used. These were cracked open by the slowly rising internal pressure, and an electronic trigger mechanism initiated data recording when the gas flow blew away a copper wire located across the venting outlet. The vessel was positioned with vertical axis, and the test set-up and the burst disc design is shown in Figure 3.

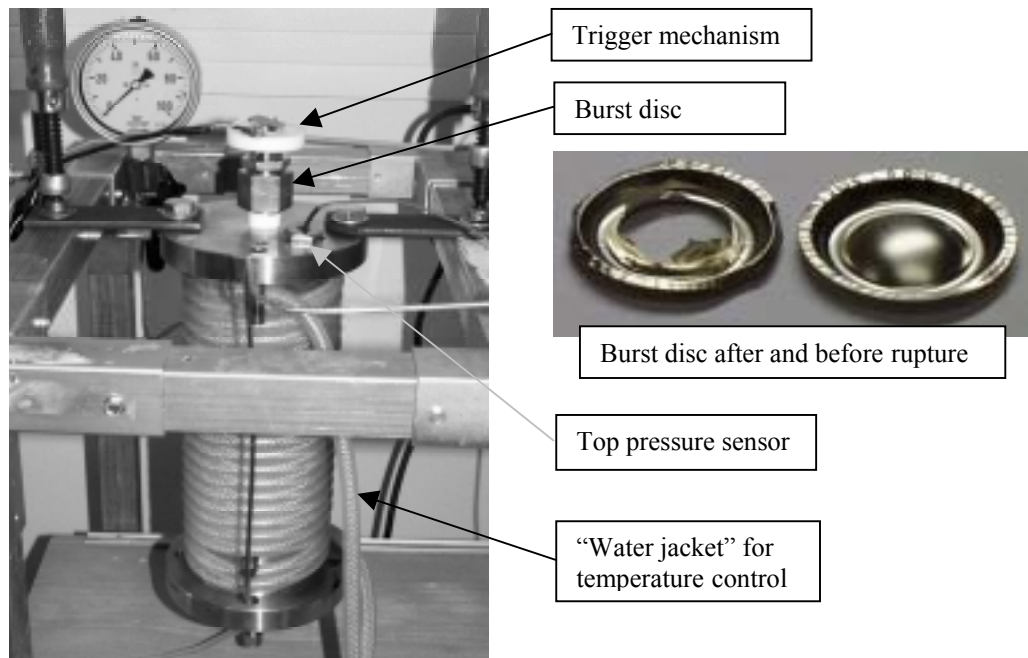


Figure 3 – Test vessel (left) with instrumentation, burst disc holder, trigger mechanism and water jacketing for temperature control. Height of vessel is 250 mm and internal diameter is 73 mm. Detail of burst disc to the right. Diameter of the burst disc is 13 mm

A design pressure of 20 MPa was used for the vessel, which was manufactured from stainless steel parts. It consisted of a cylindrical tube of 250 mm length and 73 mm ID, with end plates of 30 mm thickness. The inner surfaces were polished to suppress bubble nucleation. The rupture disc was installed in a holder at the top. Piezoelectric pressure sensors were installed in the top and bottom of the vessel, and a static pressure sensor was installed in the bottom. Data from the three pressure transducers were logged by a 100 kHz PC card, giving a sample rate of 33 per millisecond (ms) per channel. The card was equipped with integrated memory, storing 3 ms of data preceding the trigger signal. Thus, the pressure trace started right before cracking of the burst disc.

Before each test, the vessel was purged with CO₂ gas, cooled and filled with the specified amount of liquid CO₂. The vessel was then allowed to slowly warm to approach the specified burst pressure. In order to avoid bubble formation on the inner walls, the final degrees of temperature rise up to the burst level was done very slowly, typically over 1-2 hours. Depressurisation occurred when the rupture disc cracked open, leaving a reasonably well-defined cross section, as may be observed in Figure 3. This type of disc break at a given specific burst pressure with an accuracy of $\pm 5\%$. The vent (outlet) flow area could be varied by installing flow-restricting adapters into the disc holder on the inlet or outlet side. Three types of flow restrictions were used; two of these being tubes with restrictions downstream of the burst disc, and one having a short restrictor tube screwed into the disc holder close to the burst disc on the upstream side. The latter type was used in most tests. In some experiments, the static pressure sensor was disconnected, to enable a 50 kHz sample rate for the dynamic sensors.

3 TEST PROGRAM

Table 1 outlines the complete test program. Rupture pressures 3.5, 4.5 and 6.0 MPa correspond to saturation temperatures of 0°C, 10°C and 22°C, respectively. These conditions may reflect typical accumulator pressures in air-conditioning or heat pump systems during operation and standstill. According to the model of Kim-E and Reid (1983), only saturation pressures above 5.7 MPa give initial conditions that result in a spinodal state during rapid isentropic depressurisation to 0.1 MPa. Furthermore, the initial entropy has to be higher than the entropy of the intersection of the spinodal curve and the 0.1 MPa-isobar, Figure 4 (left). As a result, a region of initial conditions that could give a spinodal state can be identified, Figure 4 (right). Tests with 10 MPa initial pressure (supercritical) were included to make sure that conditions were well inside the required domain. Such conditions could occur in a heated receiver for instance in the engine compartment of a car.

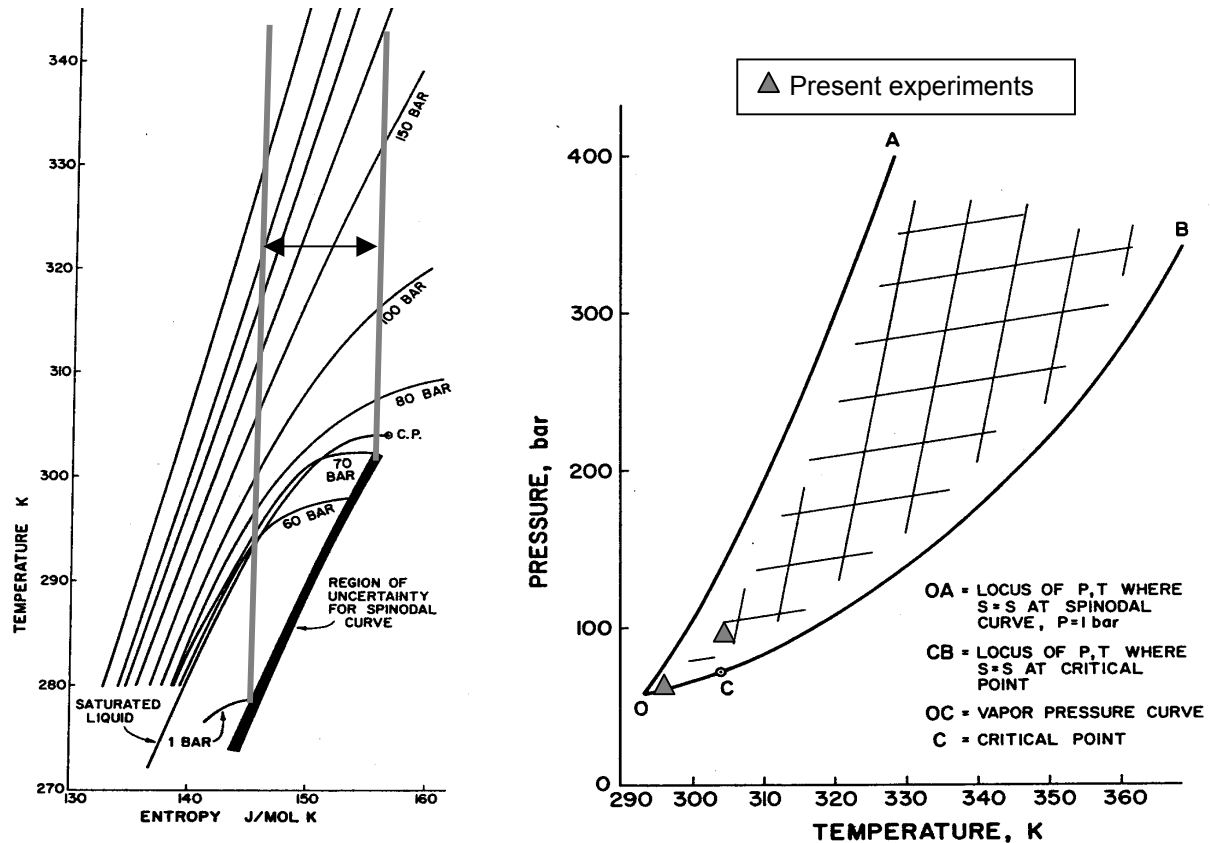


Figure 4 – Regimes giving a spinodal state during rapid isentropic depressurisation of CO₂, reproduced from Kim-E and Reid (1983). Region between vertical lines in left diagram give intersection with spinodal curve at pressures above 0.1 MPa. Right diagram shows resulting domain, including initial conditions in present tests.

Liquid fill levels were varied, and cross section and geometry of the venting opening was varied, as shown in Table 1. Finally, some experiments were conducted with the vessel turned upside down, i.e. with bottom venting. A vent area of 124.7 mm² corresponds to full opening, i.e. no restriction adapter on the outlet.

4 SUMMARY OF TEST RESULTS AND FINDINGS

Figure 5 shows dynamic pressure recordings from some of the tests, in each case using two different time scales; 5 ms and 800 ms. Tests 2, 16 and 22 all have full opening of the burst disc and initial pressures 3.5, 6.0 and 10.0 MPa, respectively. The latter two tests are within the domain

Table 1 - Test program

Test	Rupture pressure, MPa	Initial temperature, °C	Liquid CO ₂ charge, g	Fill level %	Vent area mm ²	Direction of venting
3	3.5	0	485	50	3.1 ^a	up
1	3.5	0	485	50	7.1 ^a	up
5	3.5	0	486	50	19.6 ^b	up
2	3.5	0	485	50	124.7 ^d	up
6	3.5	0	777	80	3.1 ^a	up
7	4.5	10	450	50	3.1 ^a	up
14	4.5	10	460	50	3.1 ^c	up
9	4.5	10	454	50	7.1 ^c	up
12	4.5	10	454	50	19.6 ^c	up
8	4.5	10	721	80	3.1 ^a	up
16	6.0	22	406	50	124.7 ^d	up
17	6.0	22	400	50	124.7 ^d	down
10	6.0	22	634	80	3.1 ^c	up
11	6.0	22	639	80	19.6 ^c	up
15	6.0	22	644	80	124.7 ^d	up
13	6.0	13	860	100	19.6 ^c	up
21	10.0	32	e	supercrit.	3.1 ^c	up
20	10.0	32	e	supercrit.	7.1 ^c	up
19	10.0	32	e	supercrit.	19.6 ^c	up
18	10.0	32	e	supercrit.	124.7 ^d	up
22	10.0	32	e	supercrit.	124.7 ^d	up
26	10.0	32	e	supercrit.	3.1 ^c	down
25	10.0	32	e	supercrit.	7.1 ^c	down
24	10.0	32	e	supercrit.	19.6 ^c	down
23	10.0	32	e	supercrit.	124.7 ^c	down

^a Venting through a 150 mm long tube downstream of burst disc, with flow restriction 60 mm from burst disc

^b Venting through a 50 mm long tube downstream of burst disc, with flow restriction 40 mm from burst disc

^c Bushing installed right upstream of burst disc ^d No restriction ^e Total charge approx. 790 g.

given in Figure 4, but pressure spikes above the initial pressure cannot be observed, although there are noticeable oscillations in the ms time scale. In test 2 there are some indications of re-pressurisation from about 40-60 ms, but there are probably significant effects of thermal stress in the end plate and sensor mounting, as reported by Pettersen and Hakenjos (2000). Test 1 and 9 were conducted at similar conditions, the only difference being initial pressures of 3.5 and 4.5 MPa, respectively, and the flow geometry. The results show the decisive influence of different geometry, where two-phase flow through the downstream restriction in Test 1 generated significant pressure oscillation inside the vessel, especially in the bottom sensor. Pressure traces in the 800 ms diagrams are similar, however. Tests 11 and 13 in Figure 6 were both conducted at initial pressure 6 MPa and with varying fill level, the latter test with 100% liquid charge. As may be observed the pressure decreased more rapidly in the latter test, and the slight re-pressurisation after 10-20 ms seen in Test 11 could not be observed. More rapid depressurisation could be explained by liquid-phase inlet to the burst disc in the initial expansion period. None of the tests conducted gave significant overpressure spikes, apart from the flow-induced pressure oscillation mentioned in Section 1. Tests with the vessel turned upside down did not give significant differences in pressure recordings.

CONCLUSIONS

Based on the results and findings from this study, the following conclusions may be drawn:

- None of the experiments, which were conducted over a wide range of initial conditions, have shown signs of BLEVE or BLCBE, which would be characterized by a sudden re-pressurisation to a level significantly above the initial pressure.

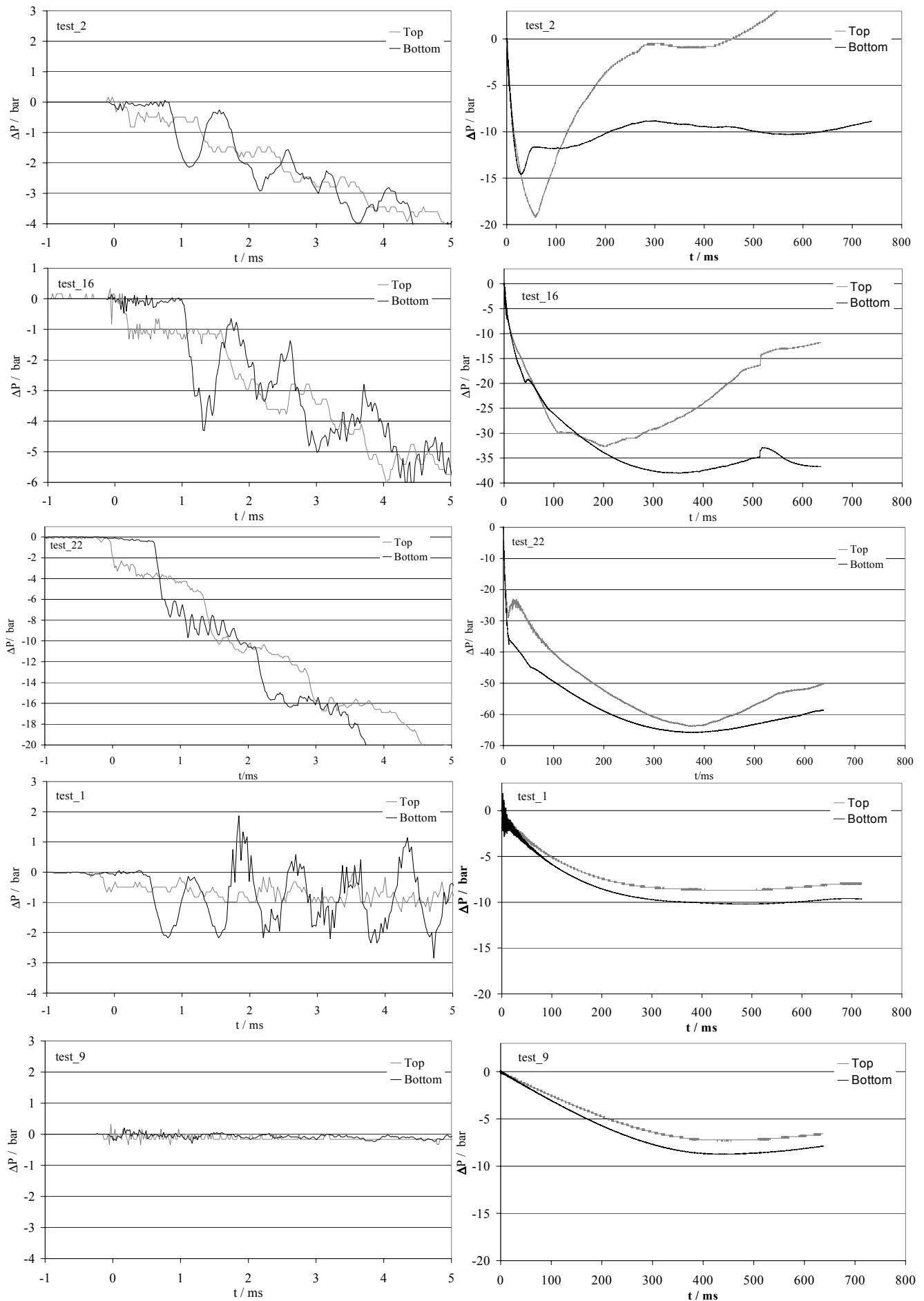


Figure 5 – Dynamic pressure recordings in tests 2, 16, 22, 1 and 9

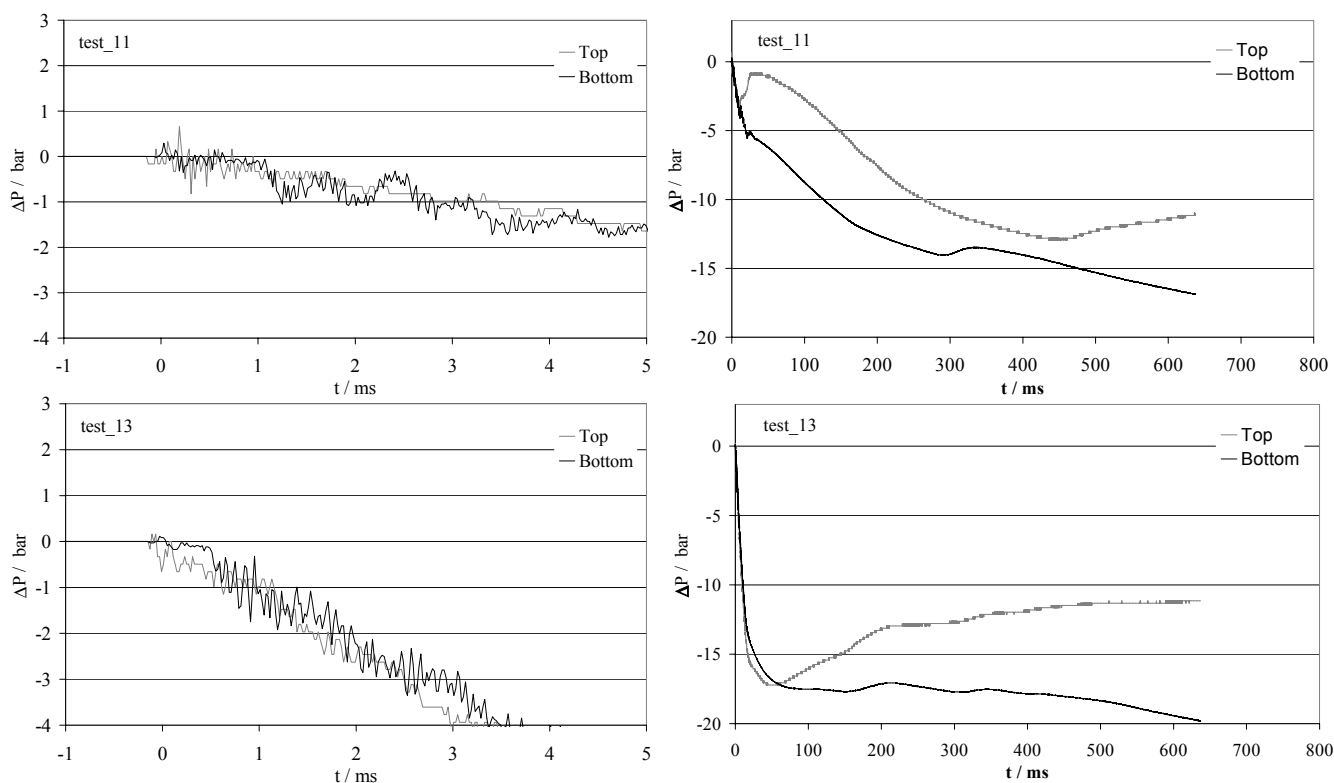


Figure 6 – Dynamic pressure recordings in Test 11 and 13

- Possible internal pressure oscillation, e.g. caused by the opening of a pressure relief device, may have to be considered in the design and sizing of CO₂ liquid accumulators.
- The present results have not given any reason to expect BLEVE in CO₂ system accumulators or receivers. In real systems the presence of compressor lubricant, particles and contaminants, as well as unstable pressure/temperature, would make homogeneous nucleation even less likely.

REFERENCES

1. Clayton, W. E., and Griffin, M. L., 1994, Catastrophic Failure of A Liquid Carbon Dioxide Storage Vessel, *Process Safety Progress*, vol 13 No 4, pp. 202-209.
2. EPA, 2000, Carbon Dioxide as a Fire Suppressant: Examining the Risks, US Environmental Protection Agency, Office of Air and Radiation, February. Report EPA430-R-00-002.
3. Hakenjos, J., 2000. Investigation of BLEVE, Internship Report, SINTEF Energy Research, Norway.
4. Kim-E, M. E., and Reid, R. C. 1983. The Rapid Depressurization of Hot, High Pressure Liquids or Supercritical Fluids. *Chemical Engineering at Supercritical Fluid Conditions*. Ann Arbor Science
5. Pettersen, J., and Hakenjos, J., 2000, Boiling Liquid Expanding Vapour Explosions (BLEVE) in CO₂ Vessels: Initial Experiments, Final Proceedings of the 4th IIR Gustav Lorentzen Conference on Natural Working Fluids, Purdue University, USA, July 25-28, pp. 216-224.
6. Pettersen, J., Hafner, A., and Brånås, M., 2000, Some Safety Aspects of CO₂ Vapour Compression Systems, Workshop Proceedings *Selected Issues on CO₂ as Working Fluid in Compression Systems*, Trondheim, Norway, 18-19 September. Report No HPP-AN27-1, PP. 61-75.
7. Venart, J. E. S., Rutledge, G. A., Sumathipala, K., and Sollows, K. 1993. To BLEVE or Not to BLEVE: Anatomy of a Boiling Liquid Expanding Vapour Explosion. *Process Safety Progress*, Vol 12, No 2, April, pp 67-70
8. Venart, J. E. S. and Ramier, S. A. 1998 Boiling Liquid Expanding Vapour Explosions (BLEVE): the influence of dynamic re-pressurization and two-phase discharge. PVP-Vol 377-2, *Computational Technologies for Fluid/Thermal/Structural/Chemical Systems With Ind. Appl*, Vol II, pp. 249-254.
9. Vörös, M., and Honti, G., 1974, Explosion of a Liquid CO₂ Storage Vessel in a Carbon Dioxide Plant, Proceedings of the 1st International Loss Prevention Symposium, the Hague/Delft, the Netherlands, 28-30 May, pp. 337-346.

6.5 Other Issues

6.5.1 CO₂ as Secondary Refrigerant

S. Sawalha¹, B. Palm¹, L. Rolfsman²

¹Royal Institute of Technology, Stockholm, Sweden

²York Refrigeration, Norrköping, Sweden

1. Introduction

According to 1991 statistics (DOE/AFEAS 1991), worldwide consumption of refrigerants in the applications of commercial refrigeration and cold storage accounts for 28% (135576 tons/year), it is the second largest consuming application after the mobile air conditioning, which accounts for 31%. In commercial refrigeration, including systems used in supermarkets, long refrigerant lines and big charges are used, which make the leakage rate high.

In Sweden, as well as many other countries, the typical refrigerants used in commercial refrigeration plants were R12 or R22 for cooling purposes and R502 for freezing applications, with direct expansion (DX) system that requires big amounts of refrigerants. The leakage rate in such systems was estimated as 30% per year (significantly improved during the 90s due to strict regulations). This situation disagreed with the recent regulations concerning the phase out of the environmentally harmful synthetic refrigerants. According to Montreal protocol, CFC's should be phased out already in the developed countries. In Sweden, CFC's were prohibited completely for refill by the end of the year 1997. HCFC's are a short-term solution due to its effect on the environment, this will lead to phase out of the HCFC's by the year 2020, in Sweden this date was set to be 2001. HFC's are not promising solution due to their Global Warming Potential (GWP).

The most logical and acceptable replacement solution worldwide is to use natural working fluids which occur naturally in the environment and do not have an unforeseen future impact, as artificial refrigerants may have.

CO₂ is unique among the natural refrigerants due to its excellent safety characteristics; it is non-flammable, non-explosive, inexpensive, and relatively non-toxic, which make it almost an ideal fluid to be used in the refrigerated space with relatively big quantities. Owing to the high working pressure, CO₂ as a phase change secondary refrigerant has a high volumetric refrigeration capacity, which equates to approximately 5 times or more than R22 and NH₃. Small equipment and small diameter pipes can be used. Considering its environmental friendly characteristics, one does not need to recover, reclaim, or recycle the CO₂ refrigerant.

2. The system

CO₂ can be applied in the supermarket refrigeration through three main technologies, trans-critical cycle, cascade system, and secondary cycle. In Sweden, the choice was to build plants with central refrigeration system in the machine room away from the refrigerated space, working with ammonia, R404A, propane, or Care50 (ethane-propane mixture). The secondary circuit works with CO₂ as the phase change secondary refrigerant in the refrigerated space.

The heat from the plant is either rejected to the environment or supplied to a heat recovery system and utilized for heating purposes. The expanded primary refrigerant evaporates through one side of a heat exchanger, where CO₂ condenses on the other side within a secondary cycle, figure 1.

An intermediate working fluid (usually glycol) can be used for cooling purposes at intermediate stage, and at the same time to be an intermediate medium to transfer the heat between the two primary refrigerant cycles (two-stage plants). In this case, the CO₂ vapour rejects heat in the low stage cycle evaporator, figure 2.

As shown in figures 1 and 2, CO₂ is circulated via pumping of the liquid CO₂ into its evaporators (freezers), consequently; the CO₂ vapour is sucked into its condenser. Evaporation and condensation of CO₂ occur almost at the same pressure.

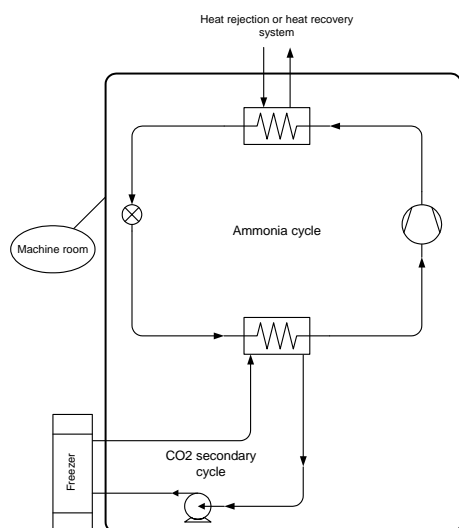


Figure 1: Schematic of a single stage NH₃/CO₂ secondary cycle plant.

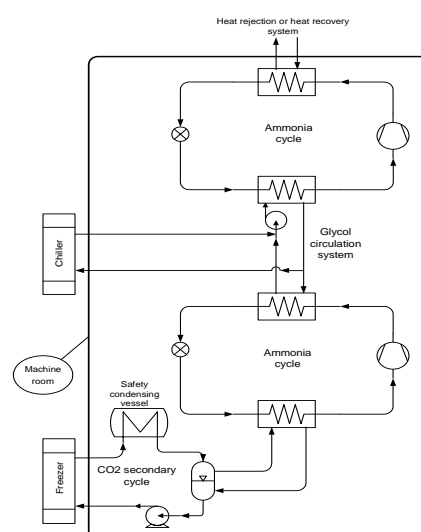


Figure 2: Schematic of a two-stage NH₃/CO₂ secondary cycle plant.

3. Components

Under the conditions in the CO₂ secondary cycle, standard refrigeration devices can efficiently handle CO₂. The main requirements in this cycle can be summarized in the following:

The pressure within the CO₂ secondary cycle was designed to be around 25 bars. This pressure level and the fact that CO₂ is chemically non-reactive made it possible to use standard refrigeration components to handle CO₂. In some cases, heat exchangers are not especially designed for CO₂; this is mainly due to the fact that some plants are converted from old existing systems to the CO₂ secondary cycle. The heat exchangers are of that type that exists on the market and satisfies the required operating conditions. It was also possible to keep the valves from the old plants, except for solenoids that cannot work without lubricant.

In at least one system the pressure level was around 40 bars. In this case special components to handle the fluid at this pressure were selected, e.g., heat exchangers was selected with smaller pipes and thicker walls.

Another important requirement was that within the CO₂ secondary cycle no lubricant exists. The valves and the pumps were selected to satisfy the requirement of handling an oil free working fluid.

4. The current systems in Sweden

The first plant was implemented in 1995 with financial support from the government through the Swedish State Department of Environment Protection; it was helpful to test the technology since no consumer could risk his investment. The successful operation of the first plant encouraged the investors and the owners to build and convert their plants to the new environmentally harmless technology. By the year 2002, around 60 plants are running with capacities ranging from 10 to 280 kW. The following table is a detailed list of some of the plants that were installed up till the year 1998.

Table 1: List of the CO₂ as secondary refrigerant plants in Sweden by the year 1998

#	Customer	Location	Refrigerant	Capacity (kW)	Comments
1	ICA-Focus	Lund	NH ₃	38	----
2	ICA-Maxi	Helsingborg			----
3	ICA-Maxi	Haninge	R404	2*40	----
4	ICA-Maxi	Botkyrka	R404	2*28	----
5	ICA-Maxi	Umeå			----
6	ICA-Maxi	Uppsala			----
7	ICA-Metro	Brommaplan	R404	2*16	----
8	ICA-Kniven	Knivsta	R404	2*10	----
9	ICA-Supermarket	Partille			----
10	ICA-Sparkop	Borås			----
11	ICA-Maxi	Skövde			----
12	AG-Favor	Lund	Care50	2*25	----
13	AG-Favor	Simrishamn	R404	2*20	----
14	AG-Favor	Staffanstorps	R404	2*16	----
15	AG-Favor	Malmö	R404	2*20	----

16	AG-Favor	Örkelljunga			----
17	AG-Favor	Vaxsjö			----
18	AG-Favor	Ljungby	R404	2*16	----
19	AG-Favor	Vala Helsinborg	Care50	4*35	----
20	AG-Favor	Landskrona	Care50	25	----
21	Domus	Visby	Care50	2*20	----
22	DAGAB	Jönköping	NH ₃	26	Cold store converted from R502
23	Bergendahl	Hassleholm	R404	45	Cold store
24	KF fryslager	Karlstad	NH ₃	170	Cold store
25	DAGAB	Becka	NH ₃	280	Cold store

Some of the plants are converted from the old systems running with artificial refrigerants, mainly R12 or R502. The machine room is completely changed due to the change of the working fluid. In case of ammonia in the machine room, additional equipment for the increased safety requirements were required to avoid risk for the workers and neighbouring areas in case of leakage.

Many reasons make the number of installations of such systems in Sweden tends to increase, some of these reasons are:

- Successful operation of the running systems.
- The strict regulations on the leakage from the systems running with environmentally harmful refrigerants.
- Phase out of CFC's and HCFC's those were used in the old installations.
- According to the Swedish laws, R134a can be used in direct systems only if the charge is ≤ 10 kg.
- This technology targets the supermarkets and cold stores, which is a large industry in Sweden and in Europe as well.

5. Operational experience-problems and solutions

Owing to the simplicity of the installed systems, there was no problem in finding refrigeration technicians and engineers to run the systems and perform the maintenance in a proper and safe way.

When working with CO₂ it is important to know that CO₂ should not be trapped between closed valves. In the plants where ammonia is used, if leakage occurs in the heat exchanger, mixing of ammonia and CO₂ forms ammonium carbonate (baking powder), which is safe and can be washed with water. Any such leakage problem should be solved and detected immediately, because the accumulation of the ammonium carbonate powder inside the evaporator could cause blockage of the evaporator, subsequently it could damage the compressor.

The two major problems that were carefully considered during the design are, defrosting and downtime.

Electrical defrosting choice was implemented in all installations up till now. CO₂ is boiled dry inside the evaporator and, as mentioned earlier, carbon dioxide should not be trapped between two closed valves. The pump should be stopped and two approximately identical defrosting periods start. The first one is with closed evaporator inlet, without heating while the ventilators are on, and the second period is with stopped ventilators and heating is on. Without the first defrosting period a lot of electricity would be used to boil liquid CO₂ owing to its relatively high latent heat.

In the pioneer plants, using a cooling vessel to condense the CO₂ by passing the CO₂ return line inside the cooling vessel solved the downtime problem. The vessel is filled with brine at the working temperature of the liquid CO₂. The size of the vessel and the receiver should be large enough to handle all the charge of CO₂ in the secondary cycle. This vessel is kept in the machine room and shown in the schematic diagram in figure 2.

In the first installation (Rolfman 1996), 200 liters of propylene glycol is filled into a drum, which contains the CO₂ return line inside. The glycol is kept at -33, which is the working temperature of the freezer. In case of a failing refrigeration system and temperature rise, the capacity of the cooling vessel should condense the CO₂, which is then kept in the receiver. The power needed for such system is only for the charging of the cooling vessel. Such technique performs effectively in permitting the pressure to rise inside the system in case of rising temperature, which could result from switching off the unit, stopped compressor, or power failure.

Due to the high initial cost of the vessel and the heavy insulation required for the system, other solutions for this problem were looked at.

The most preferable solution that was considered in most of the installations is to install bleed valve, which is controlled by a pressostat. The idea is to prevent the opening of the safety valves and keeping the temperature of CO₂ below a critical value, which corresponds to the critical pressure that the devices and the system can handle. The pressostat is set at a pressure just below that of the safety valves. The blown off CO₂ cools down the CO₂ within the system, thus keeping the fluid pressure inside the system below the pressure of the safety valves. All valves must be selected to handle the relief of the pressure inside the system and to prevent the sublimation of the CO₂, which could plug it. This technique is cheaper than the one described earlier when taking into account that some times small charge of the cheap CO₂ should be added to the system.

Another option could be by using solvent with the CO₂ within a secondary fluid mixture. The secondary fluid mixture should have a saturation pressure less than the pure CO₂. This option was not used in any of the

installations due to the large drawbacks in the energetic behaviour noticed by Enkemann (1994); he used acetone as a solvent.

In all cases safety valves were used to protect the system from an elevated pressure.

6. Economy

6.1 Installation cost

In the cases where ammonia was used as the refrigerant in the machine room, it was more expensive when compared with other systems with relatively safe refrigerants; this is due to the risk accompanying the usage of ammonia. The ammonia compartment should be effectively vented to the atmosphere. The small ammonia leakage gives an objectionable smell and may cause anxiety. This requires special safety equipment and varies from case to another, depends on the place and the surrounding where the plant is installed. It is also important to mention that it was difficult to find ammonia components for low capacity installations.

Comparison between the CO₂ phase change secondary system and other single-phase secondary systems; ends with smaller piping for CO₂ system, smaller pumps are required, and due to the better heat transfer coefficient the heat exchanger size is smaller. This is mainly because of the fact that the energy content in the working fluids without phase change is based only on the sensible heat.

While performing the comparison between CO₂ secondary system and other systems working with HFC's with DX techniques, different parameters should be the base of the comparison. The HFC's charge should be compared to the CO₂ charge, pump, bleed valve, and pressostat costs, plus the cost of an additional CO₂ condenser within the CO₂ cycle. The CO₂ is cheap and the whole system can be cheaper than the HFC for large fillings, where the cost of the HFC filling exceeds the prices of the CO₂ charge, additional CO₂ condenser, pumping unit, bleed valve, and pressostat.

If the plant is converted to the CO₂ system, the pipes could be used; the insulation is usually in bad condition and should be replaced. The CO₂ liquid line should be insulated because it is cold. The supply and return lines of the CO₂ evaporator are almost at the same temperature owing to the phase change heat transfer process inside the evaporator, this means that the two lines can be insulated together as one pipe.

6.2 Running cost

As discussed earlier, the secondary systems without phase change have higher installation cost than CO₂ secondary system, or a phase change system in general. In such systems, without phase change, the amount of circulated fluid is larger; therefore, the pump capacity should be higher. At very low temperatures, the working fluids in these systems have much higher viscosity than the CO₂ has, when combined with the high flow rate required for a certain capacity, the pumping power should be much higher than that needed to operate the CO₂ systems.

Even when CO₂ is compared with some of the other phase change secondary systems, e.g. mixture of ice, water, and ethanol, it has a superior performance. Kauffeld (1995) showed in his study that CO₂ has higher enthalpy change than different mixtures of water, ethanol, and ice. It was also shown that it requires less pumping power, less piping, and has lower viscosity especially at low temperatures.

In general, when comparing the running cost of a secondary system against a DX-system, figures 3 and 4 respectively, it is expected that the energy consumption of the secondary system will be higher due to the temperature difference that exists in the additional heat exchanger in the secondary cycle. This will result in additional temperature lift in the primary refrigerant cycle leading to an increase of the compressor power. Moreover, the power needed to operate the secondary refrigerant circulation pump will add to the running cost of the secondary system. In the specific application of supermarkets the long refrigerant suction and CO₂ return lines must be considered in the energy consumption comparison, where the pressure drops in these lines result in saturation temperature drops that will further increase the temperature lifts and the running cost of the systems.

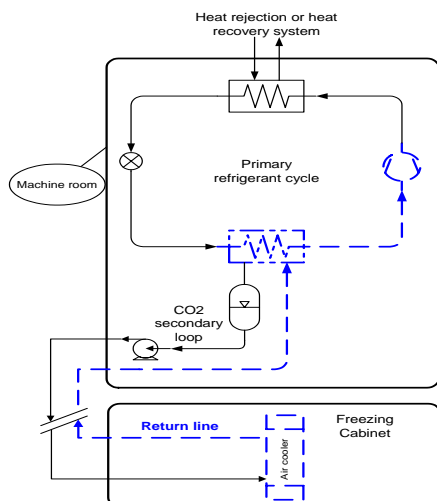


Figure 3: Schematic of a single-stage CO₂ secondary system plant.

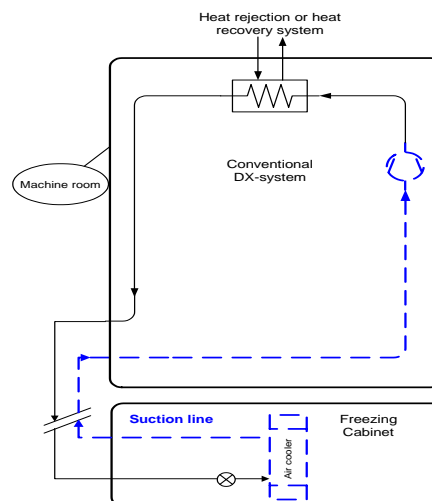


Figure 4: Schematic of a conventional DX-system plant.

In order to verify the effect of the long refrigerant suction and CO₂ return lines, the CO₂ pressure drop and the corresponding saturation temperature drop in low temperature applications are calculated and compared to R404A, which is an alternative for the phased out refrigerant R502 that was intensively used for freezing needs in DX-systems.

For a selected 40 kW freezing capacity supermarket with 40 m-long suction line, the temperature in the freezing cabinet is assumed to be -30°C, condensing temperature is 35°C, and 5°C are assumed for superheating and sub-cooling. CO₂ leaves the flooded evaporator with 0.67 vapour content based on a 1.5 circulation ratio. For the evaporator inlet, R404A enters with a vapour content of approximately 0.45, while CO₂ enters in the saturated liquid phase. The isentropic efficiency of the compressor is assumed to be 0.8. In the 40 m suction/return line, 50% was added to the pipe length to account for the pressure drop in fittings (Dossat 1991). The Friedel correlation of two-phase multiplier (Hewitt 1998) is used to calculate the pressure drop in the two-phase flow in the CO₂ return line. Rieberer (1998) compared a few correlations and concluded that the Friedel correlation gives the best approximation for CO₂ pressure drop in two-phase flow.

Values of the saturation temperature drop in the suction/return line for different pipe diameters are plotted in figure 5. It is clear from the figure that the saturation temperature drop of CO₂ is much less than that for R404A for the same pipe diameters. This indicates that for the same allowable temperature drop in the suction line, CO₂ will require much smaller size than R404A, thus small pipes and compact heat exchangers can be used with CO₂.

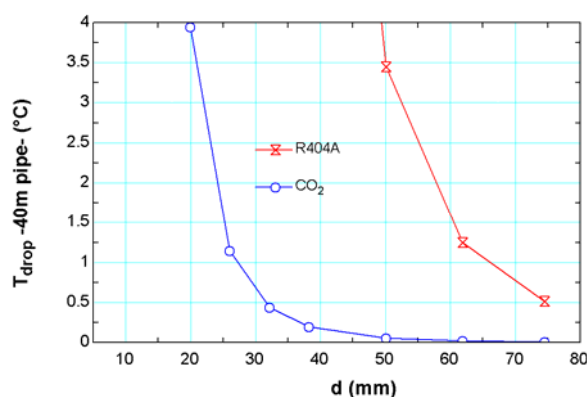


Figure 5: Temperature drop in the suction/return line for R404A and CO₂ for different pipe dimensions

The size of the R404A suction line is selected based on an allowable temperature drop of 3-4°C. According to figure 5, a 2 1/8" suction line is used, which results in a 3.5°C temperature drop in the 40-meter-long pipe. For the same pipe size, the temperature drop in the CO₂ return line is 0.057°C (almost 60 times less). These calculations give an indication of the real case when the plant is converted to CO₂ from originally being operated with R404A or R502. In this case the pipes from the original plant are used to build the CO₂ secondary loop.

Via the temperature and pressure drops obtained in the suction, return lines and the heat exchangers, temperature and pressure profiles can be established as in figures 6 and 7, for R404A-DX and R404A/CO₂

secondary systems respectively. Only the sections of the loops that are denoted in figures 3 and 4 by dashed lines are included in the temperature and pressure profiles. The logarithmic mean temperature difference in the air cooler is assumed to be 5°C. The air inlet temperature is assumed to be -20°C and cooled down to -30°C. The maximum allowable temperature drop for the refrigerant side in the air cooler was estimated to be 1°C (Downing 1988). In order to ensure the proper superheat of the primary refrigerant, the minimum temperature difference in the CO₂ condenser (R404A evaporator) was estimated to be 2°C. For simplicity, the temperature and pressure drops for the CO₂ condenser were assumed to be identical to the values in the CO₂ evaporator.

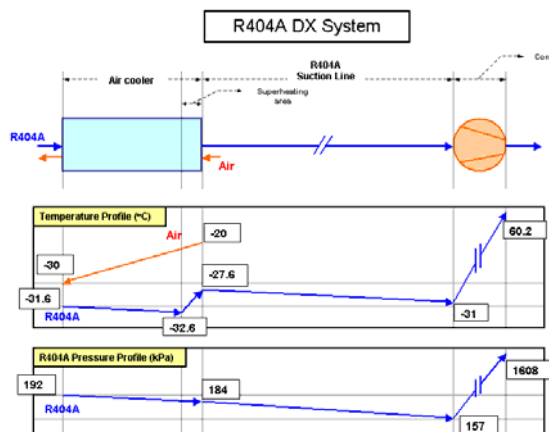


Figure 6: Temperature and pressure profiles for R404A DX-system (2 1/8" suction line)

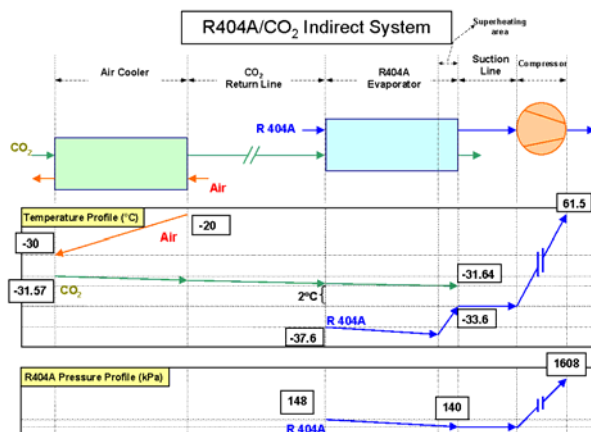


Figure 7: Temperature and pressure profiles for R404A/CO₂ Secondary system (2 1/8" return line)*

As shown in the temperature profile, the compressor inlet temperature is -31°C and -33.64°C for DX and secondary systems respectively. The inlet pressure is 157 and 140 kPa respectively. The excellent temperature and pressure drop characteristics of CO₂ in the return line and in the heat exchangers absorbed almost 60% of the temperature difference that exists in the CO₂ condenser. The logarithmic mean temperature difference in the CO₂ condenser equals 6°C and the total CO₂ temperature drop (air cooler + return line + CO₂ condenser) is less than 0.1°C.

For the 40 kW freezing capacity, the compressor power that is required to provide the needed temperature lift to operate the system is 23.1 kW for R404A DX-system while R404A/CO₂ secondary system requires 24.6 kW. Any taxes and fees that are levied on the charge and leakage of R404A should be considered which would reduce or bridge the gap in the running cost between the two systems. Moreover, conventional DX-systems in the supermarket applications usually have the problem of the poor performance of the thermal expansion valves control and dry evaporator as a result, which is not a problem with CO₂ secondary system.

In the same way we can calculate the power consumption for different refrigerants in the DX and secondary systems. Table 2 summarizes the results of power consumption calculations for different refrigerants in the two systems. The isentropic efficiency of the compressor is assumed to be 0.8 for all the refrigerants under comparison.

Table 2: Calculated power consumption for different primary refrigerants in conventional DX and CO₂ secondary systems.

	DX-system		CO ₂ secondary system		
Primary refrigerant	R404A	R502	R404A	Ammonia	Propane
Power consumption (kW)	23.1	21.1	24.6	20.6	21.1

As shown in table 2, when ammonia or propane is used instead of R404A in the secondary system, the energy consumption becomes less than that of the R404A DX-system, and it is less than or equal to the conventional direct DX-system with R502. Ammonia is the best solution with the lowest power consumption value of 20.6 kW.

If the plant was originally constructed with an ammonia/CO₂ secondary system then it would be possible to have smaller pipes, which would compensate for the cost of the additional equipment needed for the secondary loop and the safety devices needed due to the use of ammonia.

* R404A flow direction in the CO₂ condenser/R404A evaporator is reversed in the figure for explanatory reasons, but the calculations are based on counter-flow conditions.

The power needed to operate the CO₂ pump is calculated based on the assumption that the plant was originally operated with R404A in a DX-system, and when changed to a CO₂ secondary system the same liquid lines were used for the liquid CO₂ in the secondary loop.

The R404A liquid pipe in the DX-system is sized based on the results presented in figure 8, where the allowed velocity must be in the range of 1-2.5 m/s (Stecker 1988), which gave a pressure drop of around 70 kPa. This value is also acceptable according to Dossat (1991) where it is recommended that 70 kPa should not be exceeded.

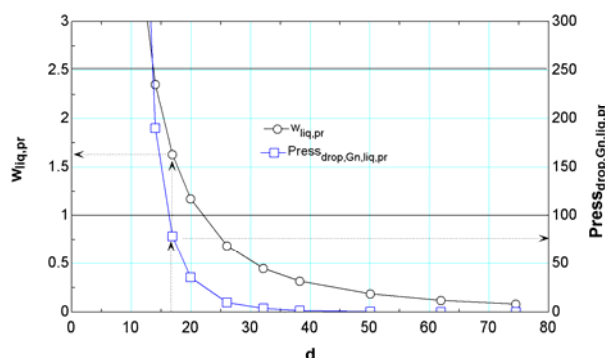


Figure 8: Velocity and pressure drop in the liquid line for R404A in different pipe dimensions

The power required for the CO₂ pump is calculated based on the assumption that the flow in 50% of the CO₂ loop is in the liquid phase and in the other 50% is a two-phase flow. Pump efficiency is assumed to be 50%. The results show that the pumping power required is around 11 W, which is very small, compared to the compressor power.

7. Safety

Leakage is one of the main concerns in applying CO₂ secondary cycle in the commercial refrigeration. CO₂ leakage may occur due to failure of one of the components in the cycle due to the relatively high working pressure of CO₂ in the secondary circuit (12 bars at -35°C). Furthermore, controlled discharge of CO₂ from the plant is performed during downtime as an efficient way to reduce the pressure inside the system.

From safety point of view, CO₂ is classified in group A1, according to ASHRAE Handbook (1997), which is the group that contains the refrigerants that are least hazardous and without an identified toxicity at concentrations below 400 ppm. Naturally, CO₂ exists in the atmosphere at concentrations around 350 ppm and it has been observed that CO₂ concentration between 300 and 600 ppm are adequate and normally people do not feel the difference.

According to ASHRAE Standard 62 (1989), a CO₂ concentration of 1000 ppm is the recommended limit to satisfy comfort for the occupants, where in a CO₂ controlled ventilation system fresh air should be supplied so that the CO₂ concentration level will not exceed this value. This is the case of an application when a small CO₂ generation rate is expected due to different human activities. However, in the case of high leakage rate that might occur in supermarket space or in the machine room, the consequences of serious health hazards, such as suffocation, must be taken into account.

The following table is a list of selected concentration levels of CO₂ and expected effects on the human health.

Table 3: Different Concentrations of CO₂ and the expected health consequences

PPM	Effect on health	Reference
350	Normal value in the atmosphere	[Bearg, 1993]
1,000	Recommended not to be exceeded for human comfort	[ASHRAE, 1989]
5,000 ⁽¹⁾	TLV-TWA ⁽²⁾	(Rieberer 1998)
20,000	Can affect the respiration function and cause excitation followed by depression of the central nervous system. 50% increase in breathing rate	(Berghmans and Duprez 1999)
30,000 ⁽³⁾	100% increase in breathing rate after short time exposure	(Amin et al. 1999)
50,000 (40,000) ⁽⁴⁾	IDLH ⁽⁵⁾ value	(Rieberer, 1998)
100,000	Lowest lethal concentration	(Berghmans and Duprez 1999)
	Few minutes of exposure produces unconsciousness	(Hunter 1975)
200,000	Death accidents have been reported	(Berghmans and Duprez 1999)
300,000	Quickly results in an unconsciousness and convulsions	(Berghmans and Duprez 1999)

⁽¹⁾ OSHA revised permissible exposure limit (PEL): time-weighted average (TWA) concentration that must not be exceeded during any 8 h per day 40 h per week

⁽²⁾ Threshold limit value: time-weighted average (TWA) concentration to which one may be repeatedly exposed for 8 h pre day 40 h per week without adverse effect.

⁽³⁾ Short term exposure limit (STEL): a 15-minute TWA exposure that should not be exceeded at any time during a workday

⁽⁴⁾ NIOSH revised IDLH value

⁽⁵⁾ Immediately dangerous to life or health concentration: maximum level for which one could escape within 30 minutes without any escape-impairing symptoms or any irreversible health effects.

Most of the symptoms accompanying the exposure to high CO₂ concentrations are related to the fact that oxygen concentration in the air becomes less because CO₂ gas replaces it.

In order to perform calculations and discuss the risk of using CO₂ in supermarket refrigeration, the case of an average size supermarket (relative to the CO₂ installations in Sweden) was selected as the base for the calculations. The dimensions of the shopping area are around 40x30x5 m and the machine room's dimensions are 10x10x3 m. The capacity of the plant is around 30 kW and the CO₂ charge in this installation is estimated to be approximately 100 kg.

The concentration of CO₂ is calculated in different accident scenarios, which differ depending on two main parameters: Where the leakage takes place? And how much is the flow rate of the leaking CO₂ into the space?

Wherever the leakage might take place along the CO₂ secondary circuit it will be either in the machine room or in the shopping area. The risk analysis is performed for these two places with different leakage flow rates. The refrigerant is assumed to leak with different flow rates which start with the hypothetical case that the refrigerant escapes instantaneously and completely from the plant resulting in the highest concentration possible. The lowest flow rate used in the calculations was based on two hours of leakage time.

It is assumed in the CO₂ concentration calculations that good mixing occur and that the refrigerant leaks with constant flow rate until all the charge escapes from the plant. The value of 365 ppm was used for the CO₂ concentration in the fresh air supply and as the initial value in the room.

7.1 Risk Analysis in the Shopping Area

Based on the dimensions of the selected supermarket, if the CO₂ is assumed to escape completely within the shopping area in a very short time, then the maximum concentration of CO₂ will be around 9,270 ppm. This concentration level far exceeds the accepted levels for occupants in non-industrial facilities, the value of 1000 ppm in table 3. However, until 1989 the Occupational Safety and Health Administration (OSHA) set the concentration value of 10,000 ppm to be the PEL. Most of the agencies, National Institute for Occupational Safety and Health (NIOSH), American Conference of Governmental Industrial Hygienists (ACGIH), and MAK-commission in Germany, that set the occupational safety standards used the TLV-TWA of 5000 that should be considered in the design of the safety requirements in CO₂ plants. The value of TLV-TWA is usually combined with the STEL value of 30,000 ppm which is much higher than the highest concentration possible in the shopping area (9,270 ppm). Therefore, leakage accident within the shopping area is not expected to result in any health hazard to the occupants.

When the fresh air supply is taken into account, the CO₂ concentration in the space will drop after one hour of ventilation according to equation 1, which is represented by the curve in figure 9. For the shopping area, ASHRAE Standard 62 (1989) recommends almost 0.5 air changes per hour (ACH), which accounts for approximately 40% reduction in the initial CO₂ concentration after one hour of ventilation.

$$\frac{C}{C_{\max}} = \exp^{(-N)} \quad (1)$$

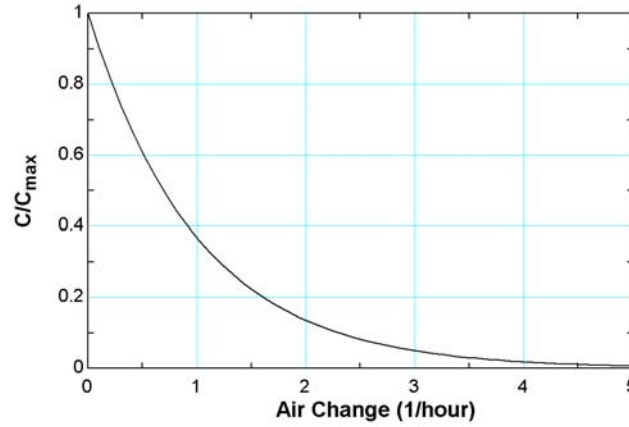


Figure 9: The influence of the ventilation rate on the CO₂ concentration

If the CO₂ charge is assumed to escape with a constant flow rate then the CO₂ concentration, in kg/m³, is calculated as a function of time according to equation 2 and the results, in ppm, are plotted in figure 10 for the shopping area. It was assumed that the CO₂ charge escapes with constant flow rate during different durations of 15 minutes, 30 minutes, 1 hour, and 2 hours. CO₂ generation from the occupants was ignored in the calculations.

$$C_{(kg/m^3)} = \frac{\dot{m}_{CO_2}}{N \times V} + C_{air} - \left\{ \frac{\dot{m}_{CO_2}}{N \times V} + C_{air} - C_0 \right\} \cdot \exp^{(-N.t)} \quad (2)$$

In a CO₂ controlled ventilation, the ventilation rate in the shopping area must be increased when the concentration reaches a value close to 1000 ppm in order to bring the CO₂ concentration down to normal level. In these calculations the ventilation system was assumed to have constant value of 0.5 ACH regardless of the CO₂ concentration level.

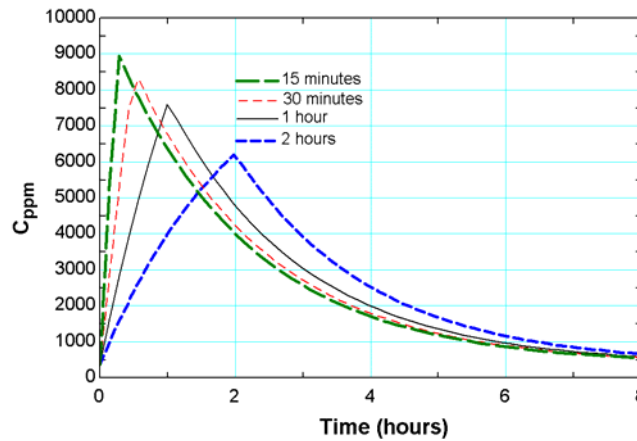


Figure 10: CO₂ concentration versus time in the shopping area for 15 minutes, 30 minutes, 1 hour, and 2 hours of leakage durations.

The results in figure 10 shows that the CO₂ concentration sharply increases during the assumed leakage times. This is due to the fact that the CO₂ leakage rate is higher than the rate of replacement of CO₂ contaminated air by fresh air supply via the ventilation. At the end of the leakage period (after 15, 30, 60, and 120 minutes) the CO₂ concentration reaches the peak because at that point the CO₂ charge escaped completely from the plant into the shopping area. Afterward, the CO₂ concentration decrease in an exponential manner as a result of the solo effect of the ventilation and the replacement of CO₂ contaminated air by fresh air supply.

If we take the accident scenario with the highest peak concentration, almost 9000 ppm at 15 minutes leakage duration, we find out that the CO₂ concentration level in the shopping area does not enclose any health risk to the customers and the workers in the supermarket. In this specific application and based on the calculations, it is not necessary to have alarm system to evacuate the occupants from the accident area, but an alarm is necessary to warn the operator of the plant about the leakage problem to perform the proper maintenance.

7.2 Risk Analysis in the Machine Room

If the same scenario, that the charge escapes completely and instantaneously, is applied in the machine room then the concentration will be around 185,300 ppm. It is very high if compared to the value of 200,000 ppm, listed in table 3 at which death accidents have been reported. Therefore, protective measures of a proper alarm system based on CO₂ detectors and efficient CO₂-controlled ventilation system must be implemented.

According to the Swedish design codes (Svensk kylnorm 2000), a minimum ventilation rate of 2 air changes per hour (ACH) is recommended in the machine room. This value results in 86% drop in the initial CO₂ concentration after one hour of fresh air supply, clarified in figure 9.

The ventilation system in the machine room must be a CO₂ controlled one; therefore, according to the Swedish safety codes when the concentration level in the machine room reaches the TLV, 5000 ppm, the fresh air supply flow rate must be increased according to the formula:

$$V\&= 50\sqrt[3]{G^2} \quad (3)$$

The increase in the ventilation rate is accompanied with a low-alert alarm system, visual and acoustic, in the machine room and in a visible place from outside the room. When the concentration level reaches 50,000 ppm (the IDLH value) high-alert alarm system is triggered and the workers must leave the machine room immediately (Svensk Kylnorm 2000).

Figure 11 indicates that for the leakage duration of 2 hours there are no health consequences for the workers, since the IDLH value is not reached (the maximum value is approximately 26,150 ppm). The concentration curve levels off close to the value of 25,000 ppm due to the fact that the extraction rate of CO₂ is almost equal to the leakage rate. In the case of 1 hour of leakage time, the highest value reached is approximately 50,500 ppm and the high-alert alarm will be triggered for only 4 minutes, when the IDLH value is exceeded.

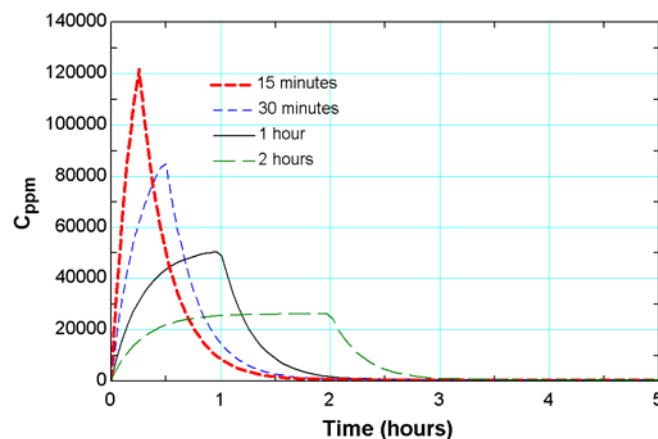


Figure 11: CO₂ concentration versus time in the machine room for 15 minutes, 30 minutes, 1 hour, and 2 hours of leakage durations.

The concern is high in the case of short leakage time of the whole CO₂ charge, for 30 minutes of leakage time the value of 86,000 ppm is reached. According to the settings of the alarm system installed in the machine room, the low-alert alarm will be triggered after less than one minute from the moment that the leakage starts, and it will last for almost 12 minutes until the high-alert alarm is triggered. Which means that the workers have at least 12 minutes to leave the place before the critical CO₂ concentration levels are reached.

In case of 15 minutes of leakage time, the low-alert alarm will be activated for at least 5 minutes before the high-alert alarm will start. This makes the time to escape from the machine room shorter, but it should be also noticed that the period where the IDLH value is exceeded is 25 minutes, which means that the exposure time for the high concentration levels of CO₂ is also short.

The high concentrations reached in the machine room imply that specific safety procedures must be implemented. CO₂ is a colourless odourless gas, which is disadvantageous from the safety point of view thus proper detector should be placed to determine the increase in gas concentration. The detector identifies CO₂ by its infrared absorption capacity; it is important that the detector and the exhaust fan are placed at low level in the space because CO₂ is heavier than air and tends to accumulate close to the floor. Figure 12 clarifies the safety equipment that should be placed in the machine room; it is shown in the figure that acoustic and flashing light alarm devices must be provided in a visible place from inside and outside the room.

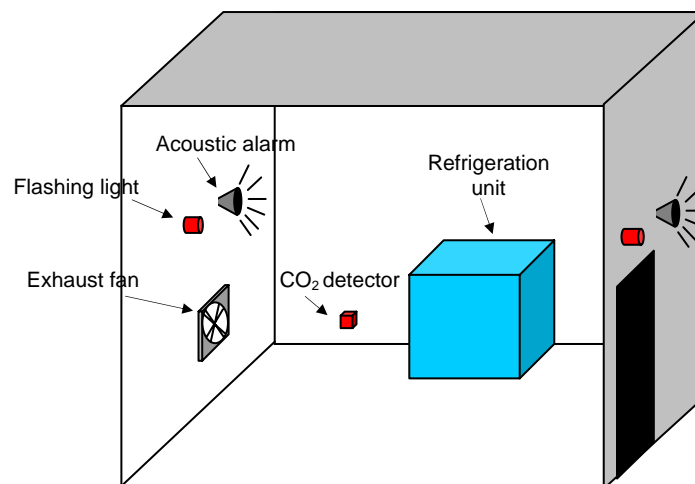


Figure 12: Simplified drawing of the machine room and the required safety equipment

7.3 Discussion of the Assumptions and the Results

The results presented in this safety analysis are based on simplified assumptions and aimed to give an indication of the situation in a practical case. It was assumed that the refrigerant leaks with constant flow rate, which is not the case in practice, where the flow rate is expected to be higher in the first stages of the leakage and then it will decay due to the reduction of the pressure in the system. Also the refrigerant was assumed to escape completely from the system, it should be taken into account that when the pressure in the system drops to 5.2 bars then dry ice will be formed inside the system and will slowly sublime. Furthermore, when the pressure inside the system drops to the ambient pressure, part of the refrigerant will be left in the volume of the system's components and distribution lines.

Due to the fact that CO₂ is 1.5 times heavier than air, stratification will occur and its concentration will be higher at low levels close to the floor. Therefore, CO₂ concentration distribution in air will not be homogenous as assumed in these calculations. An idea for further analysis is to study the concentration distribution of CO₂ at different heights in the room to see if the concentration at an average height of human body will be higher or lower than the calculated value using the good mixing assumption.

Based on the above discussion, it can be concluded that this model over predicts the CO₂ concentration in the machine room and the shopping area.

8. Competitive Technologies

Technique suggested by Lorentzen (1994), is to use the advantages of CO₂ trans-critical cycle for heating purposes of the tap water, and at the same time, to use the low temperature side of the cycle for the chilling and freezing purposes inside the supermarket. This cycle follows the same concept of the typical DX cycles used in old commercial refrigeration systems, with the exception that the high-pressure side in the CO₂ cycle is higher than the critical pressure. This implements the advantage of the excellent heat transfer characteristics in the vicinity of the critical point. Some studies, Eggen, G., et al, 1998 and Neksa, P., et al, 1998, concluded that such system has superior performance over the conventional commercial systems.

By using CO₂ as the working fluid in the low stage of a cascade system there is no need to operate CO₂ at high-pressure levels above the critical value of 74 bars. In this case the operation conditions are always sub-critical where already existing components can be matched. The low pressure-ratation in the CO₂ stage improves the CO₂ compressor efficiency. Other refrigerants with thermo-physical properties that match the high stage boundaries in the cascade system can be used, e.g., ammonia.

These two technologies could have a breakthrough with the availability of the newly developed components that can efficiently handle CO₂.

9. Conclusion

The operation and the analysis of the existing plants proved that CO₂ could be successfully used as an alternative for the artificial refrigerants within the application of refrigeration in supermarkets. In addition to the obvious environmental advantages by using such systems, an extra economical gain was observed during the installation and running of the plants.

The power consumption in the CO₂ secondary system is very close to that of the DX-system with the same refrigerant in the primary loop. The secondary system allows the use of refrigerants that cannot be used in a DX-system. Ammonia and propane cannot be used in DX-systems for safety reasons, but can be used in secondary systems, and the calculations show that the power consumption of such systems is less than that of the R404A DX-system. In the power consumption calculations the focus was on plants with conventional technologies which are converted to a CO₂ secondary system. If the plant was originally constructed with a CO₂ secondary system then smaller pipes could be used for the return and liquid lines, which would compensate for the cost of the additional equipment in the secondary loop and the safety devices needed for the use of ammonia or propane. The power needed for the CO₂ pump is very small compared to the compressor power.

From the analysis of the safety calculations' results, it is clear that using CO₂ in supermarket refrigeration does not enclose health risks for the customers and the workers in the shopping area. Yet, CO₂ detectors are recommended to be installed in the shopping area, especially in places where CO₂ leakage is probable and high local concentrations of CO₂ is expected. We would like to point out that even if the CO₂ charge and the size of the supermarket's shopping area and machine room are identical to the modelled case in this report, the individual case of every supermarket must be considered separately taking into consideration the geometrical variations and the locations of the distribution lines. Apparently, safety requirements such as proper ventilation and alarm system are a must in the machine room.

In the future all three CO₂ systems (secondary, cascade, and trans-critical systems) will exist, each finding its niche.

References

- Amin J., Dienhart B., and Wertenbach J.**, 1999, Safety Aspects of an A/C System with Carbon Dioxide as Refrigerant, SAE Automotive Alternate Refrigerant Systems Symposium, Arizona, USA.
- ASHRAE Handbook, Fundamentals**, 1997. ISBN: 1-883413-45-1.
- ASHRAE Standard 62**, 1989, Ventilation for Acceptable Indoor Quality. ISSN: 1041-2336
- Bearg D. W.**, 1993, Indoor Air Quality and HVAC Systems, Lewis Publisher, USA. ISBN: 0-87371-574-8.
- Berghmans J., and Duprez H.**, 1999, Safety Aspects of CO₂ Heat Pumps, 6th IEA International Energy Agency Heat Pump Conference, Berlin, Germany.
- Bitzer International**, September 1999, Refrigerant Report, Sindelfingen, Germany., http://www.bitzer.de/home/index_e.html, 2000-08-28.
- Christensen, K., G.**, 1999, Use of CO₂ as Primary and Secondary Refrigerant in Supermarket Applications. 20th International Congress of Refrigeration, IIR/IIF, Sydney, Australia.
- Dossat, R. J.**, 1991, Principles of Refrigeration, 3ed edition, Prentice Hall, cop., Englewood Cliffs, N.J., ISBN: 0-13-717687-2
- Downing, R.C.**, 1988, Fluorocarbon Refrigeration Handbook, Prentice Hall, NJ, ISBN: 0-13-32204-6
- Eggen, G., and Aflekt, K.**, 1998, Commercial Refrigeration with Ammonia and CO₂ as The Working Fluids. IIR-Gustav Lorentzen Conference, Oslo, Norway.
- Enkemann, T., and Arnemann, M.**, 1994, Investigation of CO₂ as a Secondary Refrigerant. IIR-New Applications of Natural Working Fluids in Refrigeration and Air Conditioning, Hannover, Germany.
- Gosney, W.B.**, 1982, Principles of Refrigeration, Press Syndicate of the University of Cambridge, NY, ISBN: 0-521-23671-1
- Granryd, E., Ekroth, I., Lundqvist, P., Melinder, Å., Palm, B., Rohlin, P.**, 1999, Refrigeration Engineering. Department of Energy Engineering, Division of Applied Thermodynamics and Refrigeration, Royal Institute of Technology, KTH, S-10044 Stockholm, Sweden.
- Heinsohn R. J.**, 1991, Industrial Ventilation Engineering Principles, Wiley-Interscience Publication, John Wiley & Sons, Inc. USA. ISBN: 0-471-63703-3.
- Hewitt, G. F.**, 1998, Heat Exchanger Design Handbook, Part 2, Begell House, Inc., NY, ISBN: 1-56700-094-0
- Horvath, A. L.**, 1992, Molecular Design-Chemical Structure Generation from the Properties of Pure Organic Compounds, Elsevier Science Publishers B.V., NY, ISBN: 0-444-8917-6
- Hunter D.**, 1975, The Diseases of Occupants. 5th edition, Hodder and Stoughton, London, England.
- IIR**, February 2000, 15th Information Note on Refrigerants: Carbon Dioxide as a Refrigerant.
- Kauffeld, M.**, 5/1995, Ammonia, Carbon Dioxide and Water-the Commercial Refrigerants of Future? Die Kälte und Klimatechnik (KK) 48.

Kylbranschens Samarbetsstiftelse, Svensk Kylnorm, Stockholm, Sweden, 2000.

Lorentzen, G., 1990, Trans-critical Vapour Compression Cycle Devise, International Patent Publication WO 90/07683.

Lorentzen, G., 1994, Use of CO₂ in Commercial Refrigeration an Energy Efficient Solution, IIR-New Applications of Natural Working Fluids in Refrigeration and Air Conditioning, Hannover, Germany.

McAdams, W. H., 1942, Vaporization Inside Horizontal Tubes-II- Benzen-Oil Mixtures, ASME Transactions, Vol. 64, p. 193.

Montreal protocol, 1991, Assessment Report of the Refrigeration, Air-Conditioning and Heat Pump Technical Options Committee.

Nekså, P., Girotto, S., and Schiefloe, P. A., 1998, Commercial Refrigeration Using CO₂ as Refrigerant-System Design and Experimental Results. IIR-Gustav Lorentzen Conference, Oslo, Norway.

Ridge National Laboratory, December 1991, DOE/AFEAS GW Project: Energy and Global Warming of CFC Alternative Technologies, Executive Summary, Oak.

Rieberer, R., 1998, CO₂ as Working Fluid for Heat Pumps, Doctoral Thesis at the Faculty of Mechanical Engineering, Graz University of Technology, Graz, December.

Rolfsman, L., 1996, CO₂ and NH₃ in Supermarket ICA-FOCUS, IIR/IIF, Aarhus, Denmark.

Rolfsman, L., 1999, Plant Design Considerations for Cascade Systems Using CO₂, IIR/IIF, Sydney, Australia.

Sax N. I., and Lewis R. J., 1989, Dangerous Properties of Industrial Materials, 7th edition, Van Nostrand Reinhold, Ontario, Canada. ISBN: 0-442-28020-3.

SCANREF, June 2001, Air-conditioning: Industry in Alarm Over Refrigerants, SCANREF-Scandinavian Refrigeration, ISSN: 0284-0758

Secker, W. F., 1988, Industrial Refrigeration, Basines News Publishing Company, USA, ISBN: 0- 912524-42-1

Sonntag, R. E., Van Wylen, G. J., 1997, Introduction to Thermodynamics: Classical and Statistical, 3rd Edition, John Wiley & Sons, Inc., ISSN: 0-471-61427-0

Whalley, P. B., 1996, Two-Phase Flow and Heat Transfer, Oxford Science Publications, USA, ISBN: 0-19-856444-9

Nomenclatures

C	: Concentration after 1 hour	(ppm)
C_{\max}	: Maximum (initial) concentration	(ppm)
$C_{(kg/m^3)}$: Concentration	(kg/m ³)
C_{ppm}	: Concentration	(ppm)
C_{air}	: Concentration in fresh air	(ppm)
C_0	: Initial concentration	(ppm)
G	: Refrigerant charge	(kg)
\dot{m}_{CO_2}	: CO ₂ mass flow rate	(kg/h)
N	: Air change per hour	(1/hour)
t	: Time	(hour)
\dot{V}	: Fresh air volumetric flow rate	(m ³ /h)
V	: Volume	(m ³)